

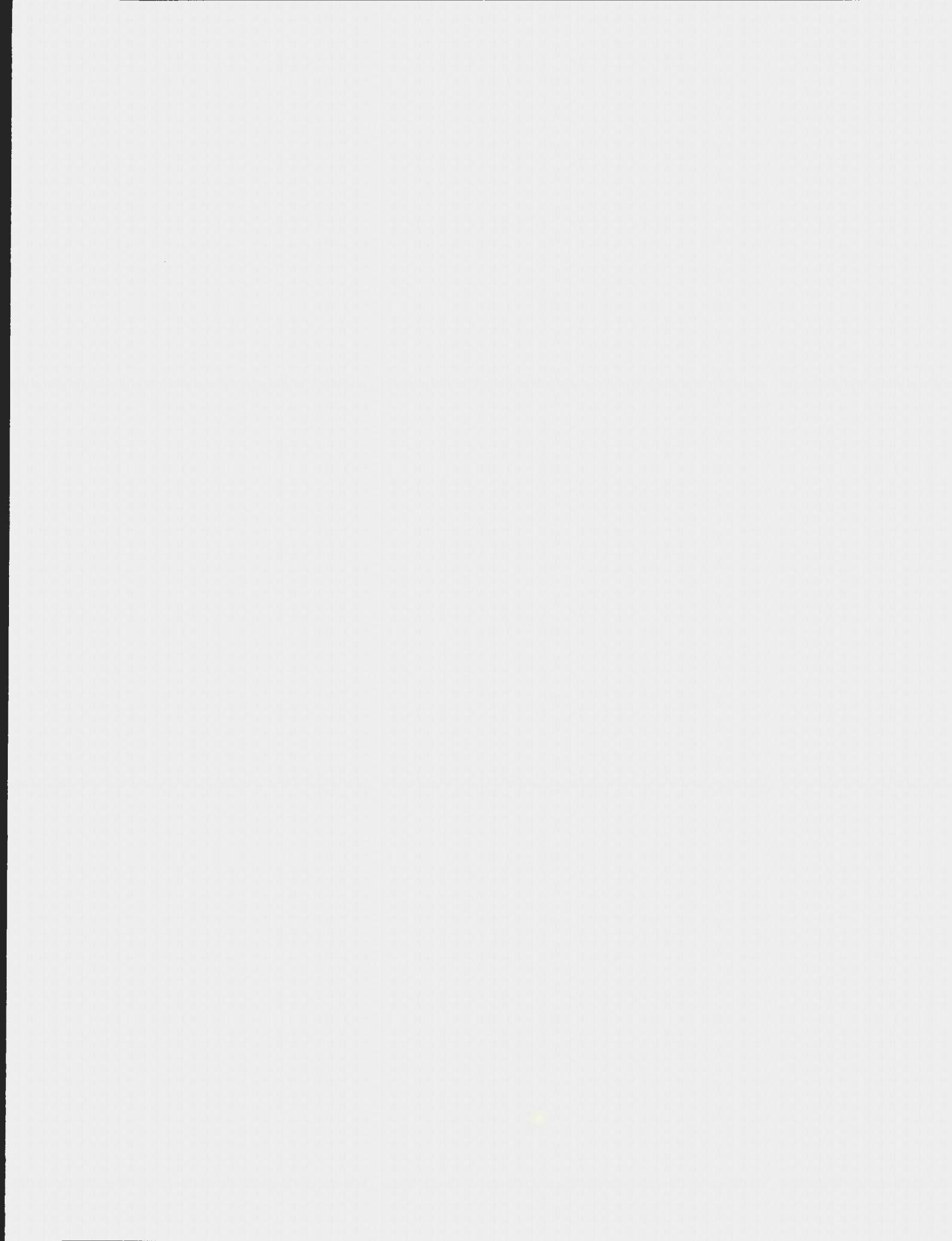
THE GRENVILLE FRONT FORELAND FOLD-AND-THRUST  
BELT IN SOUTHWESTERN LABRADOR:  
MID-CRUSTAL STRUCTURAL AND METAMORPHIC  
CONFIGURATION OF A PROTEROZOIC OROGENIC  
THRUST WEDGE

CENTRE FOR NEWFOUNDLAND STUDIES

TOTAL OF 10 PAGES ONLY  
MAY BE XEROXED

(Without Author's Permission)

JEROEN ANTONIUS MARIA VAN GOOL





National Library  
of Canada

Acquisitions and  
Bibliographic Services Branch

395 Wellington Street  
Ottawa, Ontario  
K1A 0N4

Bibliothèque nationale  
du Canada

Direction des acquisitions et  
des services bibliographiques

395, rue Wellington  
Ottawa (Ontario)  
K1A 0N4

Your file    Votre référence

Our file    Notre référence

## NOTICE

The quality of this microform is heavily dependent upon the quality of the original thesis submitted for microfilming. Every effort has been made to ensure the highest quality of reproduction possible.

If pages are missing, contact the university which granted the degree.

Some pages may have indistinct print especially if the original pages were typed with a poor typewriter ribbon or if the university sent us an inferior photocopy.

Reproduction in full or in part of this microform is governed by the Canadian Copyright Act, R.S.C. 1970, c. C-30, and subsequent amendments.

## AVIS

La qualité de cette microforme dépend grandement de la qualité de la thèse soumise au microfilmage. Nous avons tout fait pour assurer une qualité supérieure de reproduction.

S'il manque des pages, veuillez communiquer avec l'université qui a conféré le grade.

La qualité d'impression de certaines pages peut laisser à désirer, surtout si les pages originales ont été dactylographiées à l'aide d'un ruban usé ou si l'université nous a fait parvenir une photocopie de qualité inférieure.

La reproduction, même partielle, de cette microforme est soumise à la Loi canadienne sur le droit d'auteur, SRC 1970, c. C-30, et ses amendements subséquents.

**THE GRENVILLE FRONT FORELAND FOLD-AND-THRUST BELT  
IN SOUTHWESTERN LABRADOR:  
MID-CRUSTAL STRUCTURAL AND METAMORPHIC CONFIGURATION  
OF A PROTEROZOIC OROGENIC THRUST WEDGE**

**BY**

**© JEROEN ANTONIUS MARIA VAN GOOL, M.Sc.**

**A thesis submitted to the School of Graduate Studies  
in partial fulfilment of the requirements for  
the degree of Doctor of Philosophy**

**Department of Earth Sciences  
Memorial University of Newfoundland**

**1992**

**St. John's**

**Newfoundland**



National Library  
of Canada

Acquisitions and  
Bibliographic Services Branch

395 Wellington Street  
Ottawa, Ontario  
K1A 0N4

Bibliothèque nationale  
du Canada

Direction des acquisitions et  
des services bibliographiques

395, rue Wellington  
Ottawa (Ontario)  
K1A 0N4

Your file Votre référence

Our file Notre référence

**The author has granted an irrevocable non-exclusive licence allowing the National Library of Canada to reproduce, loan, distribute or sell copies of his/her thesis by any means and in any form or format, making this thesis available to interested persons.**

**L'auteur a accordé une licence irrévocable et non exclusive permettant à la Bibliothèque nationale du Canada de reproduire, prêter, distribuer ou vendre des copies de sa thèse de quelque manière et sous quelque forme que ce soit pour mettre des exemplaires de cette thèse à la disposition des personnes intéressées.**

**The author retains ownership of the copyright in his/her thesis. Neither the thesis nor substantial extracts from it may be printed or otherwise reproduced without his/her permission.**

**L'auteur conserve la propriété du droit d'auteur qui protège sa thèse. Ni la thèse ni des extraits substantiels de celle-ci ne doivent être imprimés ou autrement reproduits sans son autorisation.**

ISBN 0-315-82624-X

**National Library  
of Canada**

**Canadian Theses Service**

**Bibliothèque nationale  
du Canada**

**Service des thèses canadiennes**

**NOTICE**

**THE QUALITY OF THIS MICROFICHE  
IS HEAVILY DEPENDENT UPON THE  
QUALITY OF THE THESIS SUBMITTED  
FOR MICROFILMING.**

**UNFORTUNATELY THE COLOURED  
ILLUSTRATIONS OF THIS THESIS  
CAN ONLY YIELD DIFFERENT TONES  
OF GREY.**

**AVIS**

**LA QUALITE DE CETTE MICROFICHE  
DEPEND GRANDEMENT DE LA QUALITE DE LA  
THESE SOUMISE AU MICROFILMAGE.**

**MALHEUREUSEMENT, LES DIFFERENTES  
ILLUSTRATIONS EN COULEURS DE CETTE  
THESE NE PEUVENT DONNER QUE DES  
TEINTES DE GRIS.**

## ABSTRACT

Gagnon terrane in the Parautochthonous Belt of the Grenville Province in southwestern Labrador is a metamorphic foreland fold-and-thrust belt which carried Lower Proterozoic metasediments and their Archean crystalline basement in a north-northwest-directed thrust movement onto the Superior Province foreland. It is separated from the foreland in the northwest by the Grenville Front and overlain by the Parautochthonous Molson Lake terrane to the southeast.

Metasediments in Gagnon terrane are part of the Knob Lake Group and were deposited in the Early Proterozoic on the passive continental margin of the Superior Craton. They form the southern extension of the Labrador Trough into the Grenville Province. The basement rocks are predominantly granulite-facies gneisses, migmatites and amphibolites, which form part of the Ashuanipi Metamorphic Complex of the Superior Province. A system of linked extensional faults presumably existed in the basement at the time of sediment deposition as a result of crustal thinning.

Deformation and metamorphism in Gagnon terrane were a result of the thrust emplacement of Molson Lake terrane over Gagnon terrane along a major ductile shear zone, during the Grenvillian orogeny. Molson Lake terrane formed a thrust wedge which tapered to the northwest and which progressively incorporated thrust sheets of the underlying metasediments of Gagnon terrane. The angle between the Superior continental margin and the front of the advancing Molson Lake terrane placed the belt in a transpressive setting, and resulted in an oblique orientation of the structures and the metamorphic zonation in the area, with respect to the trend of the belt in southwestern Labrador.

Gagnon terrane in the map area consists of two thrust systems, a lower, basement-dominated system and an upper, metasediment-dominated system. Thrust

sheets in the lower system, are separated by steeply east-southeast-dipping, narrow, ductile shear zones, are several kilometers thick and weakly deformed internally. In contrast, the upper, thin-skinned thrust system consists of an imbricate stack of pervasively, ductilely deformed thrust sheets which vary in thickness from about 200 m in the northwest, to several kilometers in the southeast. Thrusting in Gagnon terrane was initiated in the upper thrust system and progressed in a regular sequence towards the foreland. Thrusting in the lower system occurred in a similar foreland-directed sequence, but postdated the thrust activity in the upper system and caused out-of-sequence thrusting in the latter, where basement thrusts breached the metasediments. The thrusts in the basement formed by reactivation under oblique compression of the pre-existing extensional faults.

A pervasive southeast-dipping simple-shear foliation ( $S_1$ ) and south-southeast-plunging elongation lineation ( $L_1$ ) characterize the fabric in the upper thrust system and in the shear zones of the lower thrust system. The thrusts in both systems are formed by southeast-dipping ductile shear zones.  $D_1$  deformation occurred in the footwall of the thrust wedge and during accretion of the rocks into the wedge. During progressive thrusting,  $D_1$  structures inside the thrust wedge were folded into northwest-verging  $F_2$  folds and were affected by northwest-directed out-of-sequence thrusts.  $D_2$  structures reflect changes in the shape of the thrust wedge during the thrust movement. The southeastern part of the map area is dominated by late, kilometer-size  $F_3$  cross-folds that developed as a result of the oblique convergence of the belt. Although the geometry of the stacked thrust sheets resembles that of thrust belts at high crustal levels, all Grenvillian deformation was ductile, typical for rocks of mid-crustal levels.

Grenvillian metamorphic grade of the rocks increases towards the structurally higher thrust sheets in the southeast, and also along the strike of the belt towards the southwest. It ranges from sub-greenschist facies in the north, at the Grenville Front, to upper amphibolite facies (700°C and 11 kbar) in the southeast, near Molson Lake

terrane. Thrusting in Gagnon terrane caused a telescoping and inversion of the metamorphic gradient, with discontinuities in the metamorphic field gradient across thrust faults. P-T paths derived from zoned garnets in metapelites have a "hairpin shape" and suggest rapid cooling and decompression of the rocks after attainment of the "peak" metamorphic conditions. Incorporation of thrust sheets into the thrust wedge caused the switch from prograde to retrograde metamorphism and from predominantly mylonitic deformation ( $S_1$ ), near the base of the thrust wedge, to folding and out-of-sequence thrusting ( $D_2$ ), in the remainder of the thrust wedge.

Metasedimentary thrust sheets were incorporated in the thrust wedge by underplating, rather than by accretion at the toe, after they were buried underneath Molson Lake terrane down to a depth of about 30 km. Underplating as mode of accretion of material to the thrust wedge may be the mechanism that causes inversion of the metamorphic gradient in this and other thrust belts.

## ACKNOWLEDGEMENTS

I wish to acknowledge all the people who have directly or indirectly contributed to the completion of this thesis and to my studies at Memorial University.

First of all I want to thank my supervisors, Toby Rivers and Tom Calon, for introducing me to Grenvillian geology and for their support over the course of the project and for full cooperation in accelerating the completion of the thesis over the final few weeks. Their advice and encouragement have significantly contributed to the successful completion of the work.

I am indebted to Peter Cawood, for showing patience beyond the call of duty during the extended finishing stages of the thesis and for his friendly support and advice during the years of my studies.

Tyson Birkett's role in my introduction to life in the Labrador Bush, his excellent organization of the logistics of the first two field seasons and his daily radio conversations in the field are gratefully acknowledged.

This project has benefitted significantly from discussions with Dennis Brown, Peter Cawood, Jim Connelly, Aphrodite Indares and Gunter Suhr.

I want to thank George Blackwood, Dennis Brown, Brian Davis, Mary Scott and Terry Wiseman, for their friendly and often ingenious assistance in the field and in the camps. Part of the mapping was carried out independently by Dennis Brown. I appreciate the help of Liz Planje and Rob Taylor with colouring the many figures and maps and assembling the final copy of the thesis.

Flemming Mengel is acknowledged for providing the computer program PTCALC for the geothermometric calculations and also for allowing me to change the program to

adapt it to my requirements. I want to thank David van Everdingen for his cooperation in the writing and endless debugging of the computer program QUICKPLOT for the plotting and manipulation of the structural orientation data.

Pilots and staff of Ashuanipi Aviation in Labrador City are acknowledged for their skilful and friendly transportation and expediting services. I wish to thank Wayne Tuttle and Ken O'Quinn of the Newfoundland Department of Mines and Energy for providing radio contact with civilization during the field seasons. Dick Wardle of the Newfoundland Department of Mines is kindly acknowledged for lending Toby Rivers and me two field assistants and a truck for several weeks in the summer of 1989.

The administrative and technical staff of the Department of Earth Sciences has been very helpful during the course of my studies. I specifically want to thank Pat Browne and Foster Thornhill for their friendly cooperation.

I want to thank all my friends for making my stay in St John's enjoyable, especially Adam, David, Dennis, Flemming, Gee-Woong, Günter, Jamie, Jim, John, Kathy, Kaustuv, Rob, Sheila, Sherry and Steve.

The main part of this work was carried out under contract with the Geological Survey of Canada. Further funding of the field work and laboratory work was provided by an NSERC research grant to Toby Rivers, an NSTP grant awarded to Tom Calon and a Sealand Helicopter fellowship awarded to Dennis Brown. My studies were partially funded by a Government of Canada Award to Foreign Nationals and a graduate fellowship from the School of Graduate Studies of Memorial University of Newfoundland.

## TABLE OF CONTENTS

ABSTRACT .....	ii
ACKNOWLEDGEMENTS .....	v
LIST OF TABLES .....	xii
LIST OF FIGURES .....	xiii
LIST OF PLATES .....	xviii
CHAPTER 1 INTRODUCTION .....	1
1.1 GRENVILLIAN TECTONICS .....	3
1.2 THRUST TECTONICS .....	4
1.3 PURPOSE AND SCOPE OF THE THESIS .....	5
1.4 METHODS OF RESEARCH .....	6
1.5 GEOGRAPHICAL DESCRIPTION OF THE MAP AREA .....	8
1.6 ORGANIZATION OF THE THESIS .....	10
CHAPTER 2 GRENVILLE GEOLOGY AND TECTONIC SETTING OF THE MAP AREA .....	11
2.1 THE GRENVILLE FRONT .....	11
2.2 TECTONIC SUBDIVISION OF THE GRENVILLE PROVINCE .....	14
2.3 THE PARAUTOCHTHONOUS BELT IN EASTERN QUEBEC AND WESTERN LABRADOR .....	16
2.4 PREVIOUS WORK IN THE MAP AREA .....	19
CHAPTER 3 STRATIGRAPHY AND LITHOLOGY OF THE MAP AREA ....	21
3.1 GAGNON TERRANE .....	21
3.1.1 LITHOLOGICAL DESCRIPTIONS .....	21
3.1.2 SIMILARITIES IN APPEARANCE OF SOME STRATIGRAPHIC UNITS .....	25
3.2 MOLSON LAKE TERRANE .....	27
3.3 RESTORATION OF THE SEDIMENTARY BASIN .....	28
3.3.1 VARIATIONS IN THE STRATIGRAPHIC SEQUENCE .....	28
3.3.2 PALINSPASTIC RECONSTRUCTION OF THE BASIN .....	32
CHAPTER 4 THRUST BELT GEOMETRY OF GAGNON TERRANE IN THE LABRADOR CITY / WABUSH AREA .....	35
4.1 LITHOTECTONIC DOMAINS IN THE MAP AREA .....	39
4.2 SUBDIVISION OF GAGNON TERRANE INTO THRUST SHEETS ...	41
4.2.1 DOMAIN I .....	44
4.2.2 DOMAIN II .....	44
4.2.3 DOMAIN III .....	46

4.2.4	DOMAIN IV .....	46
4.2.5	DOMAIN V .....	48
4.2.6	LARGE SCALE FAULT ZONES .....	49
4.3	METAMORPHISM IN THE MAP AREA .....	51
4.4	THREE-DIMENSIONAL GEOMETRY OF THE FOLD-AND-THRUST BELT .....	52
<b>CHAPTER 5 STRUCTURAL DEVELOPMENT OF THE FOLD-AND-THRUST BELT .....</b>		<b>55</b>
5.1	DETAILED DESCRIPTIONS OF THE STRUCTURES IN GAGNON TERRANE .....	56
5.1.1	NOMENCLATURE AND AGE RELATIONSHIPS OF THE STRUCTURES .....	58
5.1.2	PRE-GRENVILLIAN STRUCTURES .....	61
5.1.3	THE GRENVILLE FRONT .....	62
5.1.4	STRUCTURES IN THE LOWER THRUST SHEETS, DOMAINS I, II, III AND IV .....	66
5.1.5	BRUCE LAKE AREA .....	67
5.1.5.1	Basement rocks .....	68
5.1.5.2	Bruce Lake shear zone .....	68
5.1.5.3	Corinne Lake and Flatrock Lake thrust sheets .....	69
5.1.5.4	Sickle Lake shear zone .....	84
5.1.5.5	Wide Valley area .....	85
5.1.5.6	Elmer Lake thrust sheet .....	86
5.1.5.7	Goethite Bay area .....	89
5.1.5.8	Mont Bondurant area .....	90
5.1.6	RIVIERE AUX FRAISES AREA .....	92
5.1.7	EMMA LAKE AREA .....	96
5.1.8	LAC VIROT AREA .....	101
5.1.9	CAROL LAKE THRUST SHEET .....	102
5.1.10	LORRAINE LAKE THRUST SHEET .....	103
5.1.11	STRUCTURES IN THE HIGHEST THRUST SHEETS, DOMAIN V .....	104
5.1.11.1	Wabush Lake thrust sheet .....	105
5.1.11.2	Flora Lake shear zone .....	108
5.1.11.3	Duley Lake thrust sheet .....	109
5.1.12	THE FLOOR THRUST OF MOLSON LAKE TERRANE .....	110
5.2	SUMMARY OF THE STRUCTURAL ORIENTATION DATA .....	111
5.3	EVALUATION OF THE STRUCTURES .....	114
5.3.1	VARIATIONS OF THE STRUCTURES THROUGH THE BELT .	115
5.3.2	INFLUENCE OF EARLY PROTEROZOIC EXTENSIONAL FAULTS ON THE DEVELOPMENT OF THE THRUST BELT .	118

5.3.3	STRUCTURAL DEVELOPMENT OF THE FOLD-AND-THRUST BELT: DISCUSSION .....	122
CHAPTER 6 MICROFABRICS .....		133
6.1	MICROSTRUCTURAL VARIATIONS IN THE MAP AREA .....	134
6.1.1	MICROFABRICS IN THE BASEMENT ROCKS .....	136
6.1.1.1	Basement rocks deformed at very low metamorphic grade .....	137
6.1.1.2	Basement rocks in the low grade thrust sheets .....	138
6.1.1.3	Basement rocks in the low to medium grade thrust sheets .....	140
6.1.1.4	Basement rocks in the medium grade thrust sheets .....	141
6.1.1.5	Quartz-porphyroclastic mylonites in reactivated normal faults .	141
6.1.2	MICROFABRICS IN THE QUARTZITIC ROCK TYPES .....	142
6.1.2.1	Quartzites in the low grade thrust sheets .....	144
6.1.2.2	Quartzites in the low to medium grade thrust sheets .....	145
6.1.2.3	Quartzites in the medium grade thrust sheets .....	145
6.1.2.4	Quartz C-axis fabrics .....	146
6.1.3	MICROFABRICS IN THE METAPELITIC AND SEMI-PELITIC ROCKS .....	149
6.1.3.1	Metapelites in the low grade thrust sheets .....	149
6.1.3.2	Metapelites in the low to medium grade thrust sheets .....	151
6.1.3.3	Metapelites in the medium grade thrust sheets .....	151
6.1.3.4	Metapelites in the medium to high grade thrust sheets .....	152
6.1.4	MICROSTRUCTURES AND DEFORMATION MECHANISMS .	152
6.2	INDICATIONS FOR NON-COAXIAL FLOW .....	153
6.3	RELATIONSHIPS BETWEEN PORPHYROBLASTS AND MATRIX FOLIATION .....	158
6.3.1	LOW GRADE THRUST SHEETS .....	159
6.3.2	LOW TO MEDIUM GRADE THRUST SHEETS .....	159
6.3.3	MEDIUM GRADE THRUST SHEETS .....	161
6.3.4	MEDIUM TO HIGH GRADE THRUST SHEETS .....	162
6.4	DISCUSSION AND CONCLUSIONS .....	164
CHAPTER 7 METAMORPHIC DEVELOPMENT OF THE THRUST BELT ..		182
7.1	MINERAL ASSEMBLAGES AND METAMORPHIC FIELD GRADIENT .....	184
7.1.1	METAMORPHISM IN DIFFERENT ROCK TYPES OF GAGNON TERRANE .....	186
7.1.1.1	Mineral assemblage zones in metapelitic and quartzo-feldspathic rocks .....	187
7.1.1.2	Petrogenetic grid for the pelitic and quartzo-feldspathic rocks	194
7.1.2	METAMORPHISM OF THE IRON FORMATIONS AND MAFIC ROCK TYPES .....	196
7.1.2.1	Mineral assemblages in the iron formations .....	196

7.1.2.2 Mineral assemblages in the mafic rock types .....	197
7.1.3 INTERPRETATION .....	198
7.2 CHEMICAL ZONING IN GARNETS .....	199
7.2.1 CHEMICAL PROFILES FOR GARNETS IN GAGNON TERRANE .....	201
7.2.1.1 Prograde zoned garnets without retrogression .....	202
7.2.1.2 Prograde zoned garnets with minor retrogression .....	202
7.2.1.3 Prograde zoned garnets with retrograde rims .....	206
7.2.1.4 Garnets with retrograde zoning profiles .....	206
7.2.1.5 Garnet with a compositional break .....	207
7.2.2 INTERPRETATION .....	207
7.3 GEOTHERMOBAROMETRY .....	208
7.3.1 THERMOMETERS AND BAROMETERS USED IN THIS STUDY .....	209
7.3.1.1 Mineral equilibria of the thermometers and barometers .....	210
7.3.2 EQUILIBRIUM CONSIDERATIONS .....	212
7.3.3 P-T PATHS FROM ZONED GARNETS .....	213
7.3.4 METHODS USED FOR CALCULATION OF P-T VECTORS AND P-T PATHS .....	214
7.3.5 RESULTS OF THE GEOTHERMOBAROMETRY .....	216
7.3.5.1 Comparison of thermometers and barometers .....	223
7.3.5.2 Results for the northern sub-area .....	227
7.3.5.3 Results for the western area .....	228
7.3.5.4 Results for the central/eastern area .....	229
7.3.6 INTERPRETATION AND DISCUSSION OF THE GEOTHERMOBAROMETRY RESULTS .....	230
7.3.6.1 Non-systematic variations in P-T determinations .....	233
7.3.6.2 Regional variations in metamorphic grade .....	235
7.4 DISCUSSION AND CONCLUSIONS .....	238
CHAPTER 8 THERMOTECTONIC DEVELOPMENT OF THE FOLD-AND-THRUST BELT: DISCUSSION AND SYNTHESIS ...	247
8.1 MODEL FOR THE DEVELOPMENT OF THE BELT .....	247
8.1.1 VALIDITY OF THE BULLDOZER-WEDGE MODEL FOR A PLASTIC BELT .....	251
8.1.2 STEP ONE: EMPLACEMENT OF MOLSON LAKE TERRANE .	252
8.1.3 STEPS TWO AND THREE: FORMATION AND ACCRETION OF THE THRUST SHEETS .....	255
8.1.4 STEP FOUR: DEVELOPMENT OF THE LOWER THRUST SYSTEM .....	260
8.1.5 IMPLICATIONS OF THE MODEL .....	263
8.1.5.1 Underplating versus accretion at the toe .....	263

8.1.5.2	Inversion of the metamorphic gradient by underplating .....	264
8.1.5.3	Crustal thickening in the basement .....	271
8.1.5.4	Calculations of displacement and shortening .....	272
8.2	THE TRANSPRESSIVE SETTING OF THE BELT .....	273
8.3	IMPLICATIONS FOR THE REGIONAL TECTONICS .....	277
8.4	COMPARISON WITH THE GRENVILLE FRONT AND PARAUTOCHTHONOUS BELT ELSEWHERE IN THE GRENVILLE PROVINCE .....	280
8.5	GAGNON TERRANE AS A CRYSTALLINE FORELAND FOLD-AND-THRUST BELT .....	282
8.6	SUGGESTIONS FOR FUTURE RESEARCH; TESTING OF THE MODEL .....	284
8.7	CONCLUSIONS .....	286
REFERENCES	.....	288
APPENDIX A	SOURCES FOR COMPILATION OF MAPS .....	304
APPENDIX B	ABBREVIATIONS .....	306
APPENDIX C	LITHOLOGICAL DESCRIPTION OF THE ROCKS OF THE KNOB LAKE GROUP .....	308
APPENDIX D	STRUCTURAL ORIENTATION DATA .....	313
APPENDIX E	OBSERVED MINERAL ASSEMBLAGES .....	324
APPENDIX F	GARNET ZONING PROFILES .....	328
APPENDIX G	ELECTRON MICROPROBE ANALYTICAL PROCEDURES .	337
APPENDIX H	THERMODYNAMICS AND CALIBRATIONS OF THE APPLIED THERMOBAROMETERS .....	339
APPENDIX I	MICROPROBE ANALYSES AND MINERAL CHEMISTRY ...	347
Geological maps and cross sections	.....	in pocket

## LIST OF TABLES

Table 7.1	Diagnostic mineral assemblages in metamorphic zones and model reactions that occur at zone boundaries .....	190
Table 7.2.a	Geothermobarometric results from the northern and western sub-areas .....	218
Table 7.2.b	Geothermobarometric results for central/eastern sub-area .....	219
Table C.1	Stratigraphy and lithological characteristics of the Knob Lake Group	310
Table C.2	Mineralogy and depositional environment of the formations .....	312
Table E.1	Mineral assemblages in the meta-pelitic and quartzo-feldspathic rock types .....	325
Table E.2	Mineral assemblages in the mafic rock types .....	327
Table G.1	Statistics of analyses of K GNT .....	338
Table G.2	Statistics of analyses of KK amphibole .....	338
Table H.1	Thermodynamic data .....	345
Table H.2	Activity - composition relations .....	346
Table I.1	Garnet analyses .....	348
Table I.2	Biotite analyses .....	357
Table I.3	Muscovite analyses .....	362
Table I.4	Plagioclase analyses .....	364

## LIST OF FIGURES

Fig. 1.1	Tectonic map of the eastern part of the Grenville Province in Labrador and eastern Québec .....	2
Fig. 1.2	Simplified topographic map of the fieldwork area with the main geographical features .....	7
Fig. 2.1	Tectonic map of the Grenville Province, showing the subdivision into allochthonous and parautochthonous belts .....	12
Fig. 2.2	Tectonic map of western Labrador showing the position of the map area with respect to the Gagnon, Molson Lake and Lac Joseph terranes .....	17
Fig. 3.1	Simplified stratigraphic columns for parts of the map area .....	30
Fig. 3.2	Simplified sections through the schematically restored sedimentary basin on the continental margin of the Superior Craton in the Early Proterozoic .....	33
Fig. 4.1	Lithotectonic map of the Grenville Province in southwestern Labrador .....	36
Fig. 4.2	Metamorphic zonation and subdivision of the map area into thrust sheets .....	42
Fig. 4.3	Variations of the stratigraphy in the thrust sheets in two sections through the area .....	43
Fig. 5.1	Tectonic map of western Labrador indicating the key areas which were mapped in detail .....	57
Fig. 5.2	Schematic example of interference of structures from the upper and lower thrust systems .....	59
Fig. 5.3	Orientations of poles to foliation planes from two parts of the Grenville Front .....	65
Fig. 5.4	Detailed map of the southern Flatrock Lake area .....	71
Fig. 5.5	Schematic cross sections through the southern part of the Flatrock Lake area .....	72

Fig. 5.6	Boudins and pinch and swell structures in the banded Sokoman Formation .....	74
Fig. 5.7	Asymmetric boudins and folds in banded Sokoman Formation near the southern end of Flatrock Lake .....	74
Fig. 5.8	Low-strain lens of basement rock in mylonitic reworked basement in a ductile thrust in the Goethite Bay area .....	76
Fig. 5.9	Sketch of outcrop containing two generations of reverse faults in rocks of the Sokoman Formation at the southern end of the Flatrock Lake thrust sheet .....	76
Fig. 5.10	$F_1$ - $F_2$ fold interference in rocks of the Menihék Formation at the northern end of Flatrock Lake .....	78
Fig. 5.11	$F_{1U}$ - $F_{2U}$ fold interference in rocks of the Sokoman Formation in the Wide Valley area .....	78
Fig. 5.12	$F_1$ sheath fold in the Sokoman Formation in the Sickle Lake shear zone .....	79
Fig. 5.13	Field sketch of a fold nappe in banded rocks of the Sokoman Formation, southwest of Flatrock Lake .....	79
Fig. 5.14	Schematic cross sections through the Bruce Lake area .....	82
Fig. 5.15	Sketch of an $F_2$ fold with a curvilinear fold axis at a high angle to the folded elongation lineation .....	88
Fig. 5.16	Shear bands in basement rocks in the shear zone of the floor thrust of the Lorraine Lake thrust sheet .....	88
Fig. 5.17	Schematic cross section through the Rivière aux Fraises area .....	93
Fig. 5.18	Map of the Emma Lake thrust stack .....	97
Fig. 5.19	Cross sections through the Emma Lake thrust stack .....	98
Fig. 5.20	Sketch of a road section through gneisses of the Wabush Lake thrust sheet .....	107
Fig. 5.21	Summary of stereo plots, west of Wabush and Shabogamo Lakes .....	112
Fig. 5.22	Schematic development of structures around Early Proterozoic growth faults in the South Flatrock Lake and Emma Lake areas .....	119

Fig. 5.23	Schematic summary of the structural development of Gagnon terrane in cross section .....	126
Fig. 6.1	Examples of quartz C-axis fabrics from S-C mylonites in quartzites of the map area .....	147
Fig. 6.2	Schematic summary of kinematic indicators observed in thin sections of rocks from the map area .....	155
Fig. 6.3	Schematic representation of the microstructural relationships between porphyroblasts and foliation in different metamorphic zones in the area	160
Fig. 6.4	Summary of the timing of growth and recrystallization of metamorphic porphyroblasts and deformation in different metamorphic zones .....	166
Fig. 7.1	Map of metamorphic zoning based on mineral assemblages in metapelitic and quartzo-feldspathic rocks .....	185
Fig. 7.2	Schematic A'KF and AFM diagrams of mineral assemblages in metapelitic rocks .....	189
Fig. 7.3	Petrogenetic grid for metapelitic rocks in the map area .....	195
Fig. 7.4	Four examples of chemical profiles through garnets with photomicrographs of the analyzed grains .....	203
Fig. 7.5	Summary of garnet zoning profiles from samples in the map area .....	205
Fig. 7.6	Metamorphic pressures and temperatures in the map area determined from garnet rims and matrix assemblages .....	217
Fig. 7.7	P-T vectors from garnet core and rim analyses, combined with matrix minerals, for several parts of the map area .....	222
Fig. 7.8	P-T paths constructed using chemical profiles through garnets in combination with matrix minerals .....	224
Fig. 7.9	Summary of P-T paths in different parts of the area .....	232
Fig. 7.10	Schematic illustration of the effect of the section plane and resorption on P-T vectors obtained from zoned garnets .....	234
Fig. 7.11	Estimated peak metamorphic pressures and temperatures, determined from thermobarometry on zoned garnets, in the southern part of the map area .....	237

Fig. 8.1	Schematic summary of the thermotectonic development of the fold-and-thrust belt in southwestern Labrador .....	250
Fig. 8.2	Schematic section through a moving thrust wedge showing a section of $D_{1U}$ strain near the base of the wedge and $D_{2U}$ in the remainder of the wedge .....	256
Fig. 8.3	Cartoon of the thermal development at the base of a thrust wedge during underplating, showing inversion of the metamorphic gradient ..	268
Fig. 8.4	Schematic diagram of the dominant overriding thrust wedge and the underlying sediments of the Gagnon terrane, showing the dimensions of the thrust wedge and the calculated original distance between points in the Wabush Lake thrust sheet and in the Rivière aux Fraises area ...	274
Fig. 8.5	Schematic model for the transpressive setting and oblique convergence of Molson Lake and Gagnon terranes and the Superior foreland .....	276
Fig. 8.6	Cartoon showing the relative positions of Gagnon and Molson Lake terranes before and after the Grenvillian thrusting .....	279
Fig. 8.7	Sketch of a thrust belt which involves both basement and cover rocks, with different erosion levels for the different parts of the Grenville Front .....	279
Fig. A.1	Tectonic map of Gagnon terrane in southwestern Labrador showing the sources for the compilation of the map of Figure 1A .....	305
Fig. D.1	Map of distribution of datasets and stereoplots for the different thrust sheets in the map area .....	314
Fig. F.1	Schematic chemical profiles through zoned garnets in metapelite .....	330
Fig. F.2	Chemical profiles through garnets from the map area .....	333
Fig. F.3	Location map for samples used for thermobarometry .....	336
Fig. I.1	Partial triangular diagrams of the compositions of the garnets used for geothermobarometry .....	367
Fig. I.2	Composition diagram of the biotites used for geothermobarometry ....	368
Fig. I.3	Composition diagram of the white micas used for geothermobarometry .....	369
Fig. I.4	Partial triangular diagrams of the composition of plagioclase used for geothermobarometry .....	370

- Fig. 1A Geological map of the Grenville Province in southwestern  
Labrador .....in pocket
- Fig. 1B Cross sections through Gagnon terrane, southwestern Labrador in pocket
- Fig. 2 Geological map of the Bruce Lake area in Gagnon terrane,  
southwestern Labrador .....in pocket

## LIST OF PLATES

Plate 5.1	Archean Basement. Gneissic banding in a rock of granodioritic composition, containing folded xenoliths with a two-pyroxene + feldspar composition .....	128
Plate 5.2	Mylonite in the Bruce Lake shear zone .....	128
Plate 5.3	High-strain quartz-carbonate iron formation .....	129
Plate 5.4	$F_2$ fold in boudinaged banded carbonate-quartzite rocks of the Sokoman Formation, near the southern end of Flatrock Lake .....	129
Plate 5.5	Anastomosing foliations in basement phyllonite .....	130
Plate 5.6	Stretching lineation in a quartzite of the Sokoman Formation near a thrust fault, south of Flatrock Lake .....	130
Plate 5.7	Strongly asymmetric $F_2$ folds in foliated banded carbonate-quartzite rocks of the Sokoman Formation, near the southern end of Flatrock Lake .....	131
Plate 5.8	Fold interference pattern in mylonitic basement rocks .....	131
Plate 5.9	Asymmetric $F_2$ fold in gneiss of the Attikamagen Formation on the Trans Labrador Highway north of Blueberry Hill .....	132
Plate 5.10	Foliation boudinage in gneisses in the shear zone between Molson Lake terrane and Gagnon terrane .....	132
Plate 6.1	Least deformed basement rock at low Grenvillian metamorphic grade .....	168
Plate 6.2	Breakup of large feldspar grains into lozenge-shaped fragments along conjugate shear planes .....	168
Plate 6.3	Contrast between brittle feldspar and plastic quartz in basement proto-mylonite .....	169
Plate 6.4	Pulled apart Archean biotite in basement proto-mylonite .....	169
Plate 6.5	Basement protomylonite with angular and pulled apart fragments of feldspar and a rounded quartz porphyroclast in "hard" orientation with wide recrystallized tails .....	170
Plate 6.6	Basement protomylonite with feldspar porphyroclasts .....	170

Plate 6.7	Quartz porphyroclasts with recrystallized tails in a basement mylonite .....	171
Plate 6.8	Basement mylonite with mica-rich matrix .....	171
Plate 6.9	Basement mylonite at amphibolite facies metamorphic grade with two trails of microcline .....	172
Plate 6.10	Two large plagioclase porphyroclasts in a basement mylonite recrystallized at amphibolite facies metamorphic grade .....	172
Plate 6.11	Quartz porphyroclasts in phyllonitic mylonite .....	173
Plate 6.12	Deformation of strongly sericitized feldspars in basement rocks close to a reactivated normal fault .....	173
Plate 6.13	S-C mylonite in a quartzite of the Sokoman Formation in the Flatrock Lake thrust sheet .....	174
Plate 6.14	S-C mylonite in a quartzite of the Sokoman Formation in an out-of-sequence thrust at the roof of the Flatrock Lake thrust sheet ...	174
Plate 6.15	S-C mylonite in a quartzite of the Sokoman Formation in the Emma Lake thrust stack .....	175
Plate 6.16	S-C mylonite in coarse grained quartzite of the Wishart Formation ...	175
Plate 6.17	S <sub>1</sub> foliation in micaschist of the Menihek Formation in the south Flatrock Lake area .....	176
Plate 6.18	Crenulation cleavage (S <sub>2</sub> ) in a graphitic schist of the Menihek Formation in the North Flatrock Lake area .....	176
Plate 6.19	Polygonal arc (F <sub>2</sub> ) in crenulated schist of the Menihek Formation near O'Brien Lake .....	177
Plate 6.20	Foliation in a high grade gneiss of the Attikamagen Formation near Moose Head Lake .....	177
Plate 6.21	Rotated garnet in the Menihek Formation near Emma Lake .....	178
Plate 6.22	Rotated garnet in the Menihek Formation near Carol Lake .....	178
Plate 6.23	Fractured garnet in Menihek Formation near Rivière aux Fraises .....	179
Plate 6.24	Staurolite and garnet porphyroblasts in the Wishart Formation near Goethite Bay .....	179

Plate 6.25	Poikiloblastic garnet in a gneiss of the Attikamagen Formation, Moose Head Lake .....	180
Plate 6.26	Poikiloblastic kyanite (Ky <sub>1</sub> ) in a gneiss of the Attikamagen Formation, Flora Lake .....	180
Plate 6.27	Detail of garnet with kinked internal foliation .....	181
Plate 7.1	Biotite from a basement rock east of Bruce Lake, probably of Archean age and originally rich in titanium .....	244
Plate 7.2	Amphibolite grade mineral assemblage in metamorphic zone 4 consisting of garnet, staurolite and kyanite in a coarse-grained quartz matrix .....	244
Plate 7.3	Retrograde growth of chloritoid, replacing staurolite .....	245
Plate 7.4	Diagnostic mineral assemblage of metamorphic zone 5, garnet + biotite + kyanite in a matrix of predominantly muscovite + quartz ..	245
Plate 7.5	Antiperthitic exsolution of microcline in a plagioclase grain .....	246
Plate 7.6	Partially resorbed garnet in a rock of the Attikamagen Formation in the Duley Lake thrust sheet at the southern end of Flora Lake .....	246

# CHAPTER 1

## INTRODUCTION

Regional mapping projects carried out in the Grenville Province in Labrador over the last 15 years by the Newfoundland Department of Mines and Energy, have generated important new ideas about the Grenvillian Orogeny in Labrador (summarized by Wardle et al., 1986; Rivers et al., 1989). The recognition of Archean and Early to Middle Proterozoic rocks in the Grenville Province, which form the continuation of the adjoining older structural provinces, and the discovery of the previously unknown Labradorian Orogeny (Thomas et al., 1985, 1986) have led to a new tectonic subdivision of the Grenville Province in Labrador and eastern Québec as shown in Figure 1.1 (Rivers and Nunn, 1985; Rivers and Chown, 1986). This division into first order parautochthonous and allochthonous belts (Chapter 2), each consisting of several second order lithotectonic terranes, was extended to cover the whole Grenville Province in eastern Canada (Rivers et al., 1989).

Besides leading to a better definition of the Grenvillian lithotectonic framework, the recognition of these terranes and belts has also posed many questions. For instance: what are the relationships between the terranes, both before and after their assembly into the Grenville Province? What is their origin and age? How and when were they assembled? What deformation and metamorphic events have affected them? Detailed studies of the terranes and their boundaries are needed to address these problems and form a logical next step towards a better comprehension of the Proterozoic tectonic processes in the Grenville Orogen.

This thesis is a detailed study of the tectono-metamorphic development of the external part of the Grenville Province in an area adjacent to the Grenville Front in southwestern Labrador, outlined in Figure 1.1. It addresses several of the questions

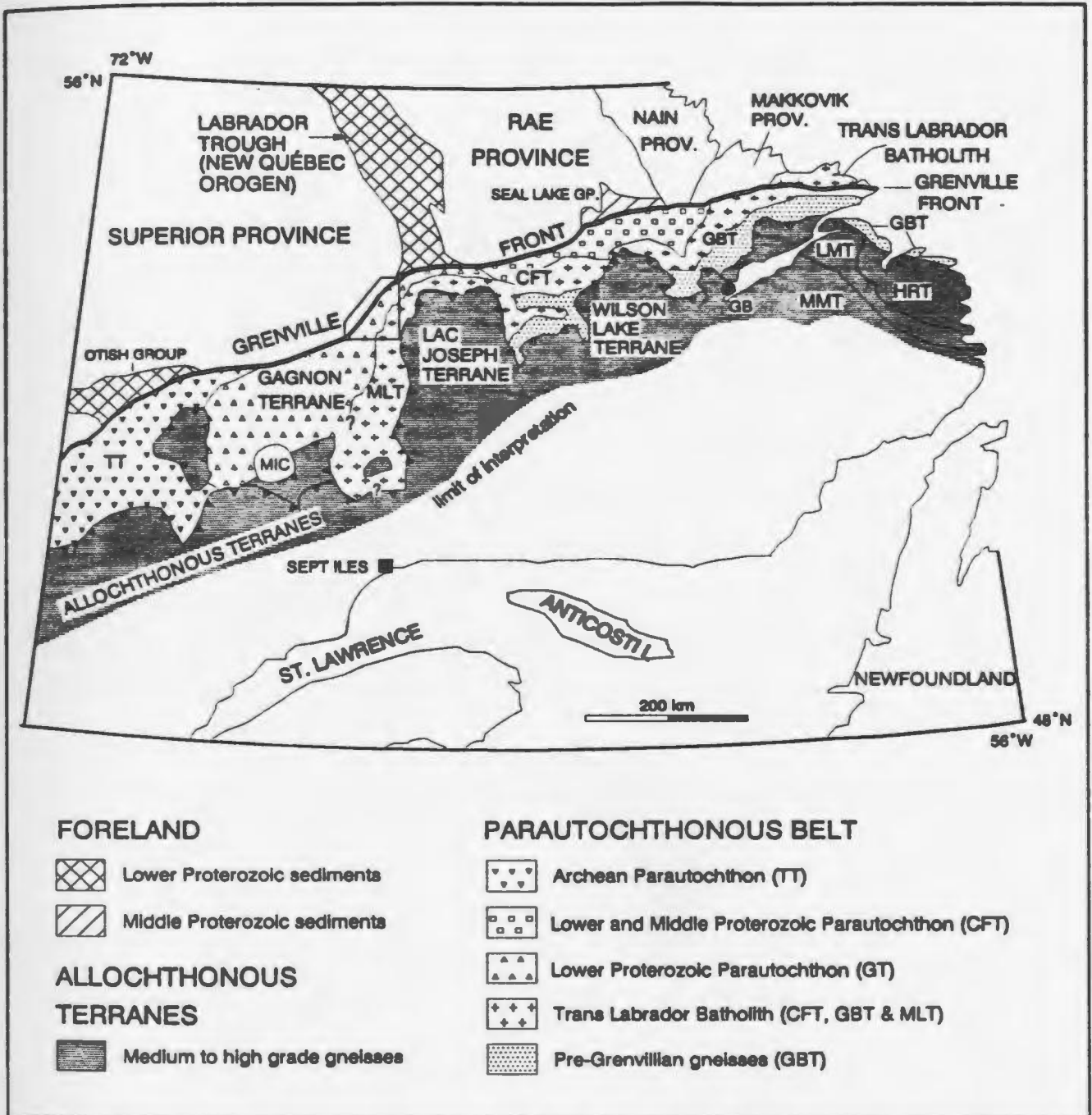


Fig. 1.1 Tectonic map of the eastern part of the Grenville Province in Labrador and eastern Québec. The location of the fieldwork area in southwestern Labrador is outlined. CFT = Churchill Falls terrane, GBT = Groswater Bay terr., HRT = Hawke River terr., LMT = Lake Melville terr., MLT = Molson Lake terr., MMT = Mealy Mountains terr., TT = Timiskaming terr. GB = Goose Bay, MIC = Manicouagan impact crater. Modified from Rivers and Chown (1986).

raised above as they apply to the study area. Also more general aspects of the metamorphic and structural development of metamorphic fold-and-thrust belts will be addressed.

## 1.1 GRENVILLIAN TECTONICS

The Grenville Province has been recognized as a structural entity in the southeast of the Canadian Precambrian shield since the early twentieth century (Wilson, 1918, 1925). It was originally distinguished in southern Québec and Ontario by; 1) the transition from greenstone belts in the neighboring Superior Province to quartzo-feldspathic gneisses in the Grenville Province; 2) the prevailing high grade of metamorphism; 3) the distinctive metasedimentary rocks of the former Grenville Series (now the Grenville Supergroup); and 4) its structural grain (Thomson, 1956; Wynne-Edwards, 1972). The Grenville Province is defined as that part of the Canadian Shield which was affected by the Grenvillian orogeny about 1000 Ma ago (Stockwell, 1961; Wynne-Edwards, 1972; Easton, 1986). It is part of the Grenvillian orogenic belt, characterized by rocks yielding similar K/Ar and Ar/Ar ages, which stretches from Mexico and Texas in the southeast to the Sveco-Norwegian orogen in southern Scandinavia (Gower, 1985).

Until recently, there was little consensus on a tectonic model for the Grenville Province and the role of plate tectonic processes was equivocal. For many years the absence of a clear suture zone or the remains of ancient oceanic crust were cited as evidence for intracontinental tectonic processes (e.g. Wynne-Edwards, 1976; Baer, 1981). However, the interpretation of Brown et al. (1975) that certain mafic and ultramafic rocks in the Central Metasedimentary Belt in Ontario represent remnants of oceanic crust (i.e. an ophiolite complex) was subsequently incorporated into a tectonic model featuring arc-continent and continent-continent collision within a conventional plate-tectonic framework (Windley, 1986). Presently most workers in the Grenville Province assume a continental collision model (Moore, 1986). Several sites for suture zones within the Grenville Province have been suggested (Thomas and Tanner, 1975; Windley, 1981, 1986; Rondot, 1986), but it is possible that the actual locus of collision

is hidden in the present Appalachian orogen to the southeast (Dewey and Burke, 1973). The recent recognition of terranes separated by major ductile shear zones led to the conclusion that the Grenville orogeny is a compressional event characterized by reworking and imbricate stacking of blocks of older crust in northwest directed movement, which resulted in considerable crustal thickening and high grade metamorphism (Davidson, 1984, Moore, 1986, Rivers et al., 1989).

## 1.2 THRUST TECTONICS

The Grenville Front forms the northwestern limit of Grenvillian thrust activity, as has been recognized for several decades (Wynne-Edwards, 1972). However, details of the structural and metamorphic signature of the Grenville Front remain obscure for most of its length. Rivers (1983a) was the first to propose a foreland fold-and-thrust belt nature for the Grenville Front zone in western Labrador. This study was designed to follow up on this preliminary conclusion. Detailed mapping in an area west and north of Labrador City/Wabush in southwestern Labrador during this study has confirmed that the rocks in this part of the Grenville Province are the deeply exhumed remnants of a foreland fold-and-thrust belt (van Gool et al., 1987a, b; 1988a, b; 1989). This warrants an approach from a thrust tectonic perspective.

Since the work of Dahlstrom (1969, 1970) and Boyer and Elliott (1982), there has been a surge of papers on all aspects of fold-and-thrust belts that has significantly improved the understanding of the development of these structures, which form large parts of most orogenic belts. This has not only benefitted the academic world in its knowledge of geology, but has also served as a tool in prospecting for oil reserves and mineral deposits.

Some of the papers on thrust tectonics were concerned with the general geometry, stacking order and kinematics of thrust belts (Elliott and Johnson, 1980; Boyer and Elliott, 1982; Butler, 1982; Mitra, 1986; de Paor, 1988). Other studies concentrated on the mechanics of thrust sheet movement (Elliott, 1976; Chapple, 1978; Davis et al., 1983; Dahlen et al., 1984; Dahlen and Barr, 1989), deviations from the regular geometry (passive roof duplexes, Banks and Warburton, 1986; out-of-sequence thrusts,

Morley, 1988; Lucas, 1989; surge zones, Coward, 1982) or thermal patterns within thrust belts (Oxburg and Turcotte, 1974; England and Richardson, 1977; England and Thompson, 1984; Shi and Wang, 1987; Karabinos and Ketcham, 1988; Barr and Dahlen, 1989).

Thrust belt geometries have been described predominantly for thin-skinned thrust belts at low metamorphic grades in upper-crustal levels. Schmid and Haas (1989) argued that these geometries cannot be traced to deeper levels of the crust where higher pressures and temperatures favor different deformation mechanisms to determine the geometry of structures. In the study area in western Labrador, the thrust belt geometry has been described in rocks which have been exhumed from mid-crustal levels and which have been deformed by ductile processes. These rocks represent a deeper level foreland fold-and-thrust belt than those generally preserved in Paleozoic and Mesozoic orogenic belts. Thus, the map area provides a valuable opportunity to study processes that take place at deeper levels of foreland fold-and-thrust belts. The fact that the stratigraphy of the area is well known (Rivers, 1980 e), although not of a layer-cake type, helps considerably in the reconstruction of the geometry of the belt.

### **1.3 PURPOSE AND SCOPE OF THE THESIS**

In this thesis the results of a field, petrographic and mineral chemistry study on the structural and metamorphic development of part of the Grenvillian foreland fold-and-thrust belt in southwestern Labrador are described. A model is presented for the thermotectonic development of the belt in which the pressure and temperature distribution and evolution are addressed in relation to the kinematic development. The approach taken in the study is to relate all data to a thrust tectonic framework. This approach is well established for younger, high-crustal level fold-and-thrust belts, but has had only limited application to deep-level fold-and-thrust belts and has not previously been applied in the map area or anywhere along the Grenville Front.

The significance of the presented model for the regional geology is discussed together with the implications for the relations with the surrounding terranes of the Grenville Province in Labrador. Finally conclusions are drawn for the structural and

metamorphic development of metamorphic thrust belts in general. The results will be compared with other well known fold and thrust belts, both those developed at low and at high metamorphic grades.

Topics that are addressed specifically include:

- the geometry and kinematics of the thrust belt;
- the stacking order of the thrust sheets and the timing of thrust movement;
- the mode of accretion of material to the thrust wedge;
- the involvement of basement rocks in the belt and basement - cover interaction;
- the ductile nature of the thrusting;
- the variations in structural style, in microstructures and deformation mechanisms through the map area;
- the variation of metamorphic grade in the area;
- the P-T paths of the different thrust sheets;
- the metamorphic development and causal and temporal relation with the thrusting event;
- the inversion of the metamorphic field gradient.

#### **1.4 METHODS OF RESEARCH**

Fieldwork was carried out in three consecutive summers, from 1986 to 1988 and was concentrated in the area west of Labrador City, in the vicinity of the Grenville Front (Figures 1.1 and 1.2). Within the map area, several key areas west of Wabush Lake and Shabogamo Lake were mapped in detail on a 1:10,000 scale (see Chapter 5). These areas were selected on the basis of regional structural and metamorphic relationships, accessibility and abundance of exposure, in order to cover along and across strike geological variations within the belt. Results are presented in a 1:50,000 scale map of the Bruce Lake area (Figure 2 in pocket in the back of the thesis) and in figures in the text of Chapter 5. For correlations between the key areas some reconnaissance traverses were done in the intervening areas. East and south of Wabush

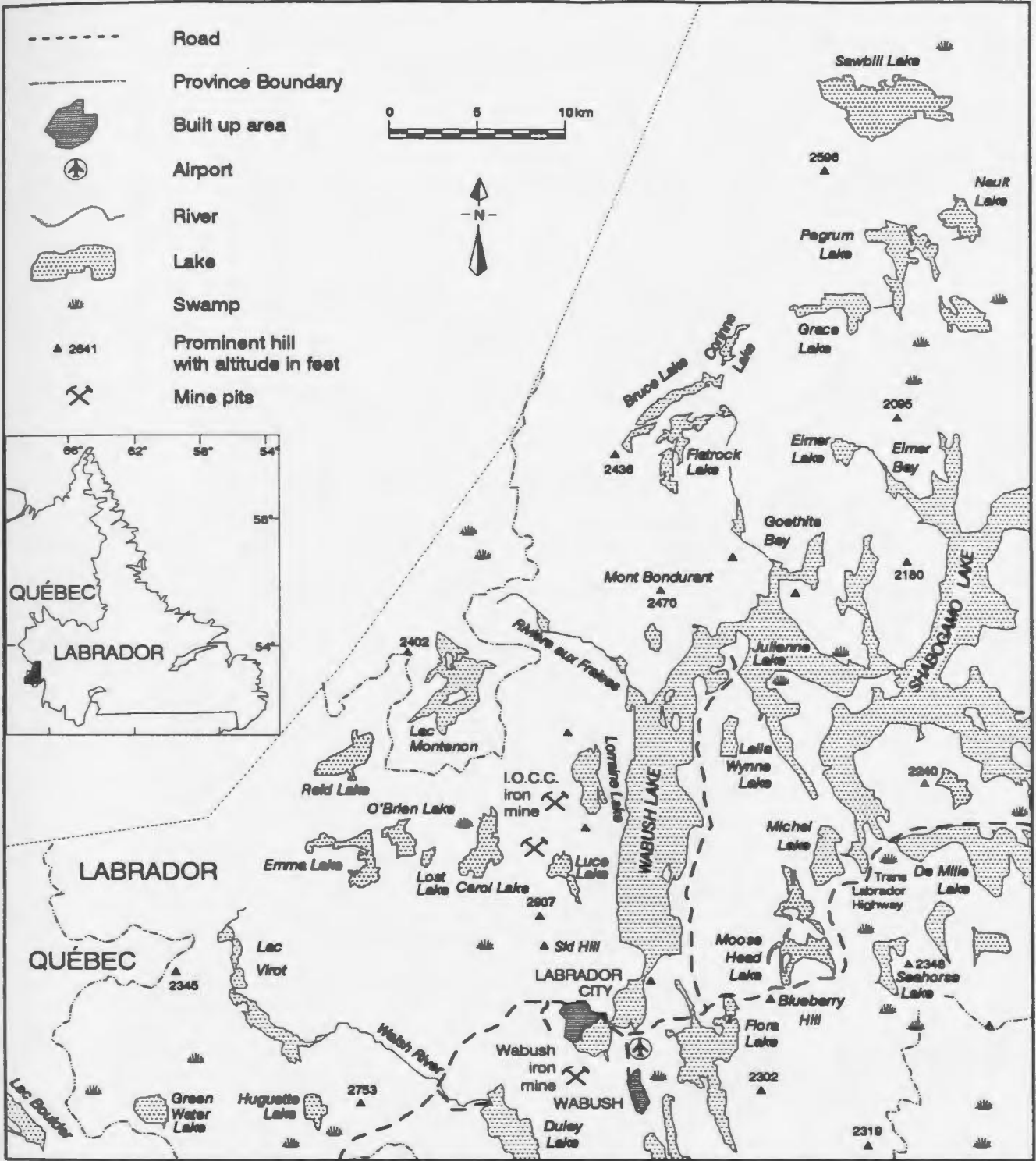


Fig. 1.2 Simplified topographic map of the fieldwork area with the main geographical features.

Lake, mapping was mainly restricted to reconnaissance work and sampling for petrography and thermobarometry. In this part of the map, only the Flora Lake shear zone to the east of Flora Lake and an area around Moose Head Lake (Figure 1.2) were studied in more detail. The mapping was restricted to the rocks of Gagnon terrane and the boundary zone with the overlying Molson Lake terrane, both of which are defined in Chapter 2. The 1:100,000 scale map of the area (Figure 1A in pocket) is a compilation of the small scale maps, reconnaissance mapping and the partly re-interpreted geological maps of Rivers (1980a,b,c; 1985a,b,c). Information obtained from the detailed mapping in the better exposed areas was used to extrapolate structures into adjoining areas and for the re-interpretation of the pre-existing maps. Appendix A lists the sources from which the maps were compiled.

Fieldwork was directed towards the mapping of the mesoscopic and macroscopic structural geometry of the different stratigraphic units, various structural elements and metamorphic mineral assemblages. A geometric reconstruction of the belt, combined with data on the kinematics of the belt resulted in an interpretation of the stacking order and the movement pattern of the thrust sheets.

Rock samples were collected for petrographical and petrological studies and geothermobarometry. Regional variations of metamorphic mineral assemblages, pressure and temperature data from geothermobarometry, P-T paths from zoned garnets and the timing of growth of porphyroblasts with respect to phases of deformation were analyzed in order to reconstruct the metamorphic development of the belt and the causal and temporal relation between movement of the thrust sheets and the metamorphism.

## **1.5 GEOGRAPHICAL DESCRIPTION OF THE MAP AREA**

The area shown in the map of Figure 1.2 is situated in southwestern Labrador, around Wabush/Labrador City and the Iron Ore Company of Canada (I.O.C.C.) iron mine, just east of the Québec border. The area is roughly bounded by the coordinates 66°32'W, 67°23'W, 52°52'N and 53°28'N. Forests, lakes and peat bogs dominate the area, with a topographic relief ranging from the level of Wabush Lake at 1750 feet to almost 3000 feet in the highest hills immediately west of Wabush Lake. The majority

of the hills does not exceed 2500 feet and most of the area ranges in altitude between 1800 and 2200 feet. The areas underlain by metasediments of low metamorphic grade, closest to the Grenville Front, have particularly low relief. Only areas underlain by "pristine" basement rocks (i.e. not reworked during the Grenvillian orogeny), by large gabbro bodies or by medium to high grade metasediments have higher elevations. The part of the map area that is best exposed and has easiest access is the area in which the I.O.C.C. iron mine is located, roughly bounded by Labrador City in the south, Carol Lake in the west, the northern tip of Lorraine Lake in the north and Wabush Lake in the east (Fig. 1.2). This area was avoided in this study because it had been previously mapped in detail by company geologists in order to outline the extent of the iron ore reserves. This is not to say, however, that the findings of this study are in agreement with existing detailed maps for this area.

With the exception of the road network in the vicinity of the two towns, in the mining areas and the Trans Labrador Highway, most of the area is accessible only by boat, float plane, helicopter or on foot. Most of the mapping was carried out from fly camps throughout the map area. Traverses in the eastern part of the map area were restricted to those parts that were easily accessible from the Trans Labrador Highway (Figure 1.2) or by boat from Wabush Lake and Flora Lake.

Abundant lakes, wetlands, heavy forest cover, and glacial debris generally prevent good exposure of the rocks in the area. Only areas underlain by massive quartzites, iron formations, gabbros and the Ashuanipi Complex in the west are well exposed. The latest glaciation left obvious marks in the terrane in the form of boulders, eskers, drumlins, glacial tills and polished glacial pavements.

Any mention in the thesis of "the map area" refers to the area delineated in Figure 1.2 or in the 1:100,000 map in the pocket in the back of the thesis (Figure 1A). This is the same area that appears in maps throughout the thesis. Wherever the map is used to show the distribution of metamorphic facies, stratigraphic variations, P-T data etc., the main features of the geology (the main thrust faults) are shown, generally without reference to them in the legends of these maps.

## 1.6 ORGANIZATION OF THE THESIS

The thesis is organized as follows. First the regional geological (Chapter 2) and stratigraphic (Chapter 3) frameworks are established, into which the study is placed. Next, in Chapter 4, the large-scale features of the map area and the thrust belt geometry are discussed. In the same chapter a subdivision of the area into separate thrust sheets is also presented. This is followed by a detailed description of the key areas and a structural synthesis in Chapter 5. In Chapter 6 the microstructural variations throughout the area are described and the deformation mechanisms and the timing of deformation and metamorphism are discussed. Chapter 7 presents the metamorphic features and a geothermobarometric study. A model for the thermal and structural evolution of the thrust belt is presented in a synthesis of the results of the study in Chapter 8.

The appendices contain detailed descriptions, definitions, research methods, chemical analyses, etc., on which the study is based, but which are not essential to the main body of the text. The sources for the compilation of the two fold-out maps are given in appendix A. Appendix B is a list of abbreviations used in the thesis. Each of the other appendices is specific to a certain chapter and is referred to at the appropriate location.

## **CHAPTER 2**

### **GRENVILLE GEOLOGY AND TECTONIC SETTING OF THE MAP AREA**

The Grenville Province represents the youngest Precambrian orogeny in the Canadian shield. It consists of a collage of terranes of pre-Grenvillian ages that have been assembled in the Grenvillian orogeny (Moore, 1986). Some of these terranes can be correlated to the foreland, others do not obviously have any known correlatives outside the Grenville Province. Stacking of the terranes occurred generally in a northwest-directed movement on major ductile shear zones (Davidson, 1984). The Grenville Front is the northwestern boundary of this tectonic activity.

The map area in southwestern Labrador incorporates the Grenville Front and a 20 to 30 km wide belt to the south, in which the deformation is related to the movement on the Grenville Front. In order to understand the tectonics in this part of the Grenville Province an introduction to Grenvillian geology and a more regional overview of the geology of southwestern Labrador and the adjacent part of eastern Québec is presented.

#### **2.1 THE GRENVILLE FRONT**

On a continental scale the Grenville Front is a rectilinear northeast trending structure, exposed for approximately 2000 km along strike (Figure 2.1), bounding rocks characterized by Grenvillian metamorphism, deformation and K-Ar isotopic ages to the southeast and truncating pre-Grenvillian structures of the older structural provinces to the northwest. Along most of its length it is the site of tectonic emplacement of the rocks of the Grenville orogen on their tectonic foreland (Wynne-Edwards, 1972; Rivers et al., 1989). Recent seismic data from central Ontario indicate that the Grenville Front in that area is a shallow-dipping planar feature that extends to the crust-mantle interface (Green et al., 1988). The Grenville Front is also

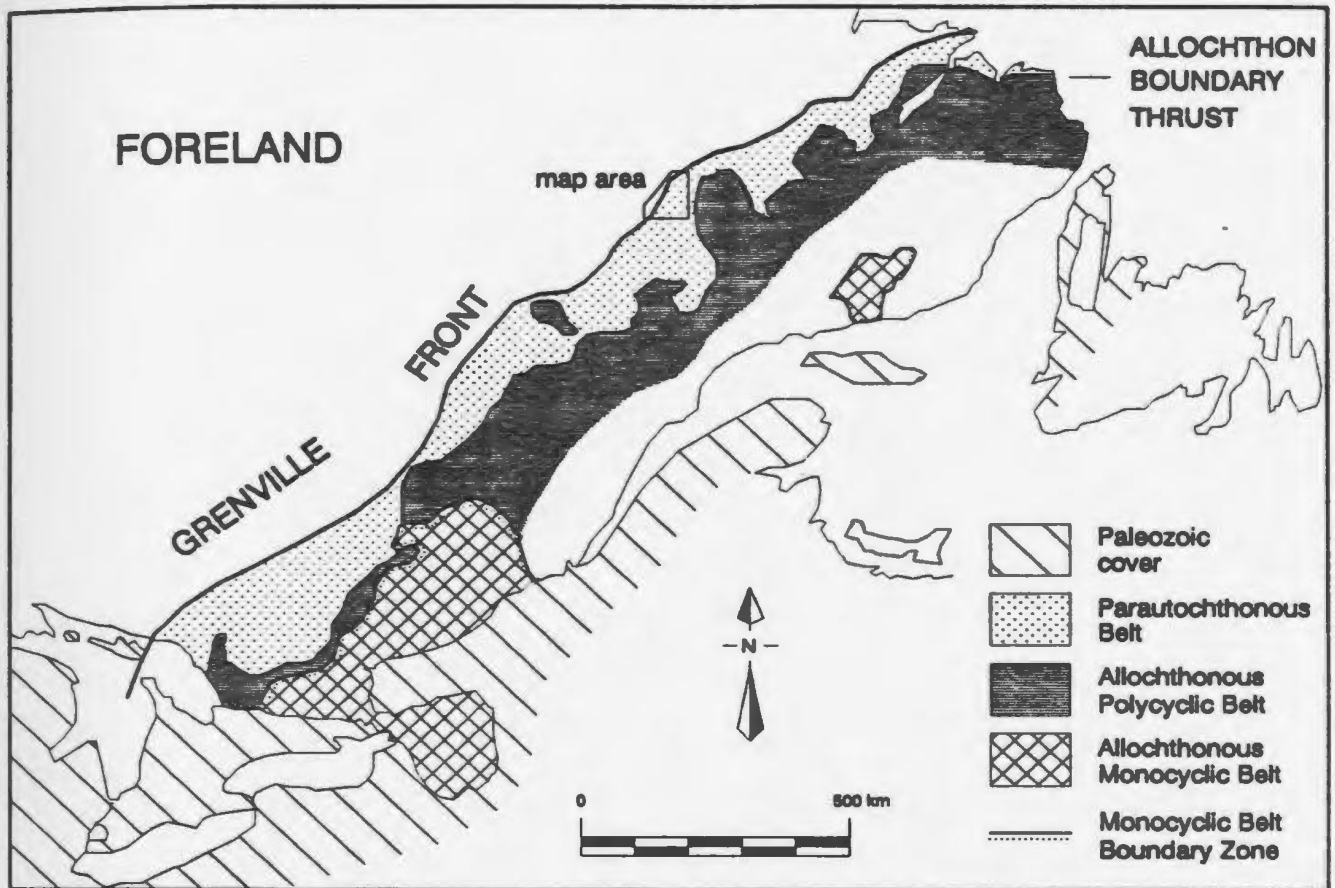


Fig. 2.1 Tectonic map of the Grenville Province, showing the subdivision into allochthonous and parautochthonous belts, after Rivers et al. (1989). The tectonic affinity of the unshaded area is unknown, due to lack of appropriate data.

the northwestern limit of a wide zone of crustal thickening by stacking of imbricate thrust slices. This zone of northeast striking structures, bounded by the Grenville Front in the northwest was defined by Wynne-Edwards (1972) as the Grenville Front Tectonic zone. This definition, or the more informal term Grenville Front Zone, is still in use, but the classification of Wynne-Edwards (1972) is largely superseded by a new subdivision of the Grenville Province by Rivers et al. (1989), which is discussed in section 2.2. Many workers have shown that some lithologies can be traced from within the Grenville Province across the Grenville Front, which implies that the Front is not the site of an orogenic suture (Moore, 1986).

General agreement exists that the Front is mainly characterized by northwest directed contractional faulting on southeast dipping thrust planes, although strike slip movement on the Grenville Front has also been recognized, as, for instance, in the Otish Mountains (Chown, 1979). Phenomena that are now generally associated with Grenville Front tectonics include imbricate stacking of thrust sheets, mylonitization, development of L-S fabrics, relatively high pressure metamorphism and an increase of the metamorphic grade across the Front towards the southeast up to high amphibolite or granulite facies. There exists, however, also considerable variation in the tectonic style along the Grenville Front (Chown, 1979; Davidson, 1986; Owen et al., 1986; Indares and Martignole, 1989; Rivers, 1992). Part of this is due to the fact that different workers have emphasized different aspects of the Front. The main variations are in the width of the zone affected by the thrust related deformation, steepness of the (telescoped) metamorphic gradient and the number of planes among which the displacement is distributed. In spite of the differences, all of these situations can fit in a foreland fold-and-thrust belt model.

On a smaller scale, determining the location and a definition for the Grenville Front is not straightforward, as structural, metamorphic and chronological fronts may not coincide. Problems of this kind have been discussed by Gower et al. (1980) for the Grenville Front in eastern Labrador and by Davidson (1986) for the Killarney area in central Ontario. On the local scale in the map area, and for the purpose of this thesis,

the Grenville Front is defined as the sole thrust of the thrust system. In southwestern Labrador this is the western-most Grenvillian thrust recognized in surface exposure (Fig. 1A and 1B, in pocket), which is not a major thrust, but a narrow shear zone with an offset in the order of hundreds of meters, developed at lower to middle greenschist facies in Archean basement rocks. Since there are no significant Grenvillian metamorphic effects outside the shear zone in the adjacent basement rocks, this definition based on structural characteristics is also the metamorphic front. Because the displacement on a thrust fault can diminish laterally and die out on a lateral tip line, the Grenville Front as defined here does not have to be one continuous feature and it can sidestep along strike.

There is a possibility that a lower thrust exists, either in the sub-surface, forming a blind thrust front (Morley, 1986), or outcropping west of the surveyed area. Recent mapping to the northwest of the study area (James and Stephenson, 1992; James, pers. comm. 1992) has indicated the possibility that a more westerly (i.e. lower) thrust exists in the Grenville Front zone in western Labrador. James and Stephenson (1992) interpreted a lineament with a magnetic signature similar to that of the Front defined here, as a Grenvillian thrust, which would move the locus of the Grenville Front 5 to 10 km farther northwest. This information became available at a late stage during the final preparation of the thesis and has not been incorporated in the text or the maps, but it has no significant effect on the conclusions of the thesis.

## **2.2 TECTONIC SUBDIVISION OF THE GRENVILLE PROVINCE**

After an original subdivision of the province into lithotectonic segments by Wynne-Edwards (1972), Rivers et al. (1989) proposed a new subdivision of the Grenville Province into three first-order tectonic belts, parallel to the northeast trend of the orogen, separated by major shear zones. They are the Parautochthonous Belt, the Allochthonous Polycyclic Belt and the Allochthonous Monocyclic Belt. Each of the belts is subdivided again into lithotectonic terranes (or nappes, James and Connelly, 1992). The following section summarizes the subdivision of the Grenville Province into belts as proposed by Rivers et al. (1989).

Separated from the foreland by the Grenville Front is the Parautochthonous Belt (Fig.2.1). It is underlain by rocks that are the equivalents of those in the adjoining foreland, but have been affected by Grenvillian deformation and metamorphism. The original age of these rocks ranges from Archean to Middle Proterozoic. Many gently southeast dipping shear zones are the result of northwest directed thrust movement, which emplaces rocks of the Parautochthonous Belt on the tectonic foreland and causes thickening of the crust. This is reflected in a negative gravity anomaly southeast of the Grenville Front, which is most pronounced in Labrador and Eastern Québec (Wynne-Edwards, 1972; Thomas and Tanner, 1975; Rivers et al., 1989) and which is estimated to represent a present increased thickness of the crust in the order of 5 to 10 kilometers (Wynne-Edwards, 1972). Medium to high metamorphic pressures are characteristic of the rocks in the Parautochthonous Belt and kyanite is the dominant alumino-silicate. The grade of metamorphism generally increases towards the southeast, away from the Grenville Front. Since lithologies have been correlated across the Grenville Front, displacements of the rocks of the Parautochthonous Belt are interpreted to be minor in the order of tens of kilometers at most.

The Allochthonous Polycyclic Belt (Fig. 2.1), tectonically overlying the Parautochthonous Belt and separated from it by the Allochthon Boundary Thrust, is composed of several far travelled high grade terranes (Rivers et al., 1989). These terranes contain rocks of pre-Grenvillian age which generally cannot be correlated to equivalent terranes in the foreland. Northwest directed transportation has been estimated to exceed 100 km for some of these terranes. Where exposed, the Allochthon Boundary Thrust is characterized by sub-horizontal mylonites with generally southeast plunging extension lineations. Prior to the Grenvillian event, the rocks in the Allochthonous Polycyclic Belt were affected by at least one orogenic cycle, although locally intrusive rocks occur that are younger than the latest pre-Grenvillian event, and thus are monocyclic. During the Grenvillian orogeny, these pre-Grenvillian terranes were assembled into the Grenville Province.

The **Allochthonous Monocyclic Belt** comprises the Wakeham terrane in eastern Québec and several terranes underlain by rocks of the Grenville Supergroup in Ontario and western Québec (Fig. 2.1), previously named the Central Metasedimentary Belt. Rocks in both regions are of Middle Proterozoic age and show imprints of the Grenvillian orogeny only. The Monocyclic Belt Boundary Zone, which forms the contact with the underlying rocks of the Allochthonous Polycyclic Belt, is a tectonic feature and both contractional and extensional movement have been inferred. The amounts of displacement along the contacts are presently unconstrained.

### **2.3 THE PARAUTOCHTHONOUS BELT IN EASTERN QUEBEC AND WESTERN LABRADOR**

The Parautochthonous Belt, in which the map area is located, has been subdivided into several lithotectonic terranes (Figures 1.1 and 2.2), two of which occur in the map area. Gagnon terrane (Rivers et al., 1989) adjoins the Grenville Front and is mainly composed of Lower Proterozoic metasediments of the Knob Lake Group and their Archean crystalline basement. It forms the southern extension of the Labrador Trough into the Grenville Province. Both metasediments and basement rocks were intruded by Middle Proterozoic gabbros of the Shabogamo Intrusive Suite and tonalites whose age is not precisely established.

The metamorphic grade in Gagnon terrane ranges from (sub-)greenschist facies at the Grenville Front in the north of the map area, to upper amphibolite facies near its boundary in the southeast of the map area (Rivers, 1983b). Gagnon terrane is cut by many closely spaced, southeast dipping thrusts which are a result of the telescoping of the belt during the Grenvillian orogeny and form a foreland fold-and-thrust belt (Rivers, 1983a). Lack of significant deformation and metamorphism in Knob Lake group sediments just north of the map area, north of the Grenville Front and west of the front of the New Québec orogen, and the post-Hudsonian age of the Shabogamo gabbros suggest that prior to the Grenville orogeny the rocks in the map area were undeformed (Rivers, 1983a). The front of the Hudsonian deformation in the New Québec orogen is interpreted to bend towards the east where approaching the Grenville Front and does

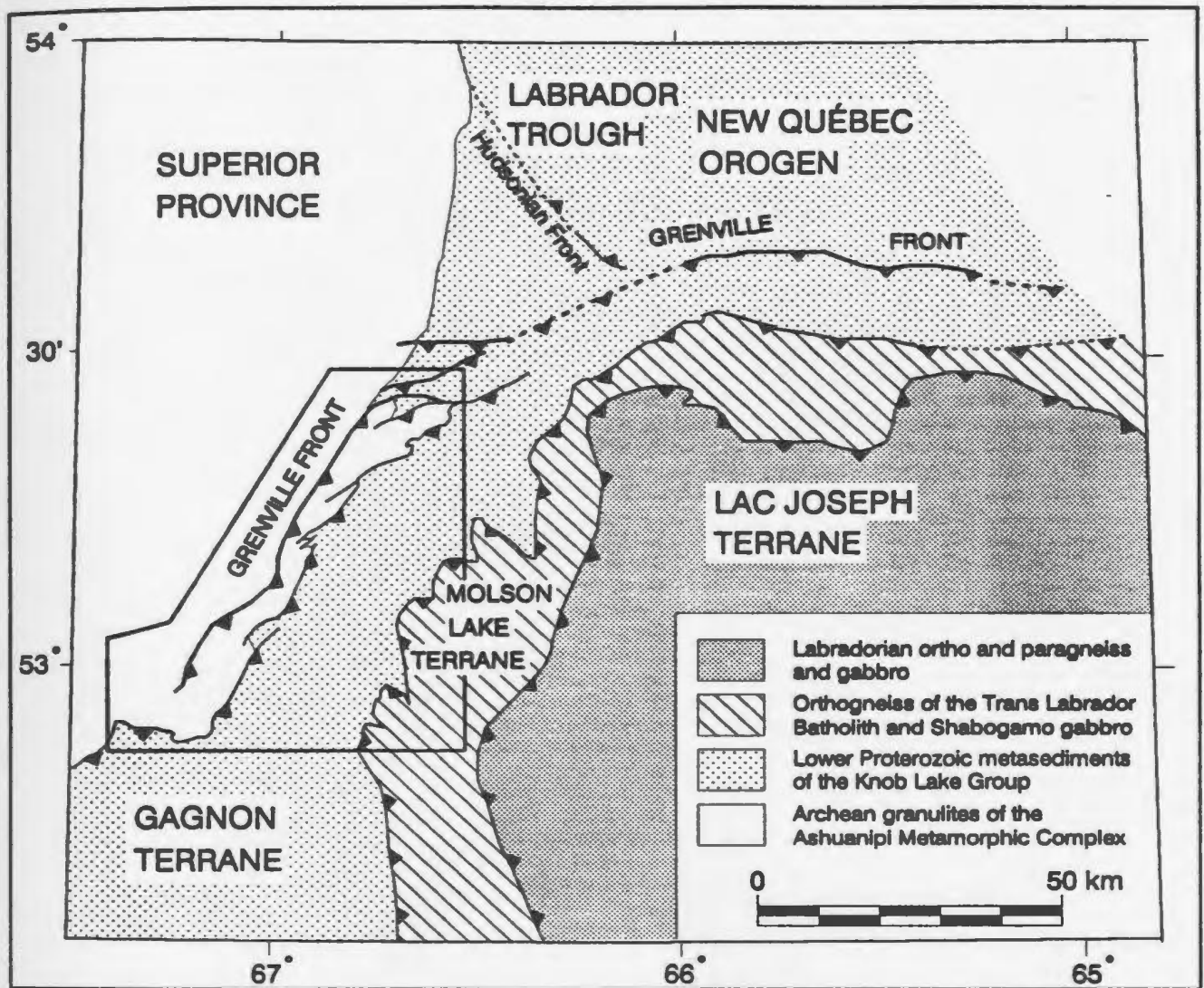


Fig. 2.2 Tectonic map of western Labrador showing the position of the map area with respect to the Gagnon, Molson Lake and Lac Joseph terranes as well as the Grenvillian and Hudsonian orogenic fronts. Modified from Connelly (1991).

not intersect the rocks in the map area (Fig. 2.2). Therefore the rocks in the map area present a good opportunity to study the effects of Grenvillian deformation and metamorphism.

The second terrane in the Parautochthonous Belt in southwestern Labrador is Molson Lake terrane, which was recently defined by Connelly et al. (1989a) and which structurally overlies Gagnon terrane. This dominantly igneous terrane forms the eastern part of the Parautochthonous Belt (Fig. 2.2), separated from Gagnon terrane by a commonly shallowly southeast-dipping ductile shear zone. The rocks in this terrane are granitoids dated at approximately 1635 Ma (U-Pb on zircon, Connelly et al., 1989b) that are interpreted as the southwestern extension of the Trans Labrador Batholith of Labradorian age and are assumed to represent an arc above a subduction zone (Connelly, 1991; Fig. 1.1). These granitoids were intruded by Middle Proterozoic gabbros of the Shabogamo Intrusive Suite. The rocks near the base of Molson Lake terrane were metamorphosed at high pressures and were emplaced on Gagnon terrane on a crustal-scale shear zone. Emplacement, deformation and metamorphism are of Grenvillian age (Connelly, 1991).

Within the Parautochthonous Belt south of the map area, Gagnon terrane is bounded to the southwest by Timiskaming terrane (Fig. 1.1), composed of Archean metasediments that were reworked during the Grenvillian orogeny. The nature of the boundary is interpreted to be a thrust (Rivers and Chown, 1986). The Churchill Falls terrane, composed of Labradorian age orthogneisses and polycyclic paragneisses, adjoins Gagnon terrane to the northeast (Fig. 1.1). The boundary between Gagnon and Churchill Falls terranes is not exposed.

The parautochthonous terranes are bounded to the southeast by the allochthonous, polycyclic Lac Joseph terrane (Figures 1.1 and 2.2), composed mainly of upper amphibolite to granulite grade paragneisses and gabbros of Labradorian age (Nunn et al., 1984, 1986; Rivers and Nunn, 1985; Connelly et al., 1989a, b, 1991). The Grenvillian imprint on these rocks is minor and can only be demonstrated close to the

tectonic boundary with the underlying terranes (Connelly, 1991). Emplacement of the Lac Joseph terrane on the Parautochthonous Belt took place late during the Grenvillian orogeny (Connelly and Nunn, 1988; Connelly, 1991).

The rocks of the foreland form part of the Archean Superior Province to the west and the Labrador Trough of the New Québec orogen to the north (Hoffman, 1989; Rivers et al., 1989). The former is a high grade gneiss terrane that acted as a cratonic basement upon which the sediments of the Labrador Trough, comprising a continental shelf and slope sedimentary sequence, was deposited.

The metasediments in Gagnon terrane form part of the Kaniapiskau Supergroup, which constitutes the supracrustal fill of the Labrador Trough (Dimroth, 1972; Wardle and Bailey, 1981). The platformal portion of these sediments, which comprises the sediments in Gagnon terrane, is known as the Knob Lake Group. The Knob Lake Group sediments were deposited on the eastern margin of an Early Proterozoic continent, which is preserved in the Archean age rocks of the Superior Province (Wardle and Bailey, 1981; Rivers, 1983a). The Labrador Trough rocks in Gagnon terrane were not affected by the Hudsonian orogeny and the basin geometry was presumably preserved until the Grenvillian orogeny. However, the extent of the Knob Lake Group rocks to the east is obscured by the intrusion of the Labradorian age Trans Labrador Batholith and the emplacement of Lac Joseph and Molson Lake terranes. This presents us with an enigma concerning the eastern continuation of the rocks in the map area and the pre-Grenvillian relationship between the rocks in the two terranes of the Parautochthonous Belt.

#### **2.4 PREVIOUS WORK IN THE MAP AREA**

Klein (1966) summarized the history of geological exploration in southwestern Labrador and eastern Québec, which started with the first reconnaissance surveys by Low (1895). Exploration activity in the area has concentrated on the iron ore occurrences west of Wabush Lake and to the southwest of the map area. Extensive mapping and drilling programs were undertaken in the areas of high grade ore, the results of which were reported in internal mining and exploration company reports.

Knowles and Gastil (1959) and Gastil and Knowles (1960) published the first regional maps with a description of the stratigraphy and structure in the map area. A more detailed study of an area which encompassed the northern half of the area described in this thesis was published by Fahrig (1960, 1967) in a map on a 1 inch to 4 miles scale.

A comprehensive evaluation of the tectonic and metamorphic development of the Grenville orogen in western Labrador was published by Rivers (1983a, b), as part of a mapping project of the Newfoundland Department of Mines and Energy (Rivers, 1978, 1980d, e; Rivers and Massey, 1979). This project resulted in a series of maps on 1:50,000 and 1:100,000 scales (Rivers, 1980 a, b and c, 1985 a, b and c). Publications by Rivers and co-workers on the tectonic subdivision of the Grenville Province incorporate this work (Rivers and Chown, 1986; Rivers et al., 1989).

Part of the early work for this thesis has been published in G.S.C. Current Research volumes (van Gool et al., 1987a, 1988a) and in internal reports for the Geological Survey of Canada (van Gool et al., 1987b, 1988b, 1989). A detailed structural analysis of the Emma Lake area has been carried out as part of a study for a B.Sc. honours thesis (Brown, 1988; Brown et al., 1991). Recent detailed studies in adjacent areas have been undertaken by Brown (1990) in the northeastern part of Gagnon terrane north of Lac Joseph terrane, by Connelly (1991) in Molson Lake and Lac Joseph terranes east of the study area, by Indares (in press) south and southwest of the study area in Gagnon and Molson Lake terranes and by James and Stephenson (1992) in the Archean rocks of the Ashuanipi Metamorphic Complex in the Superior Province northwest of Sawbill Lake.

## **CHAPTER 3**

### **STRATIGRAPHY AND LITHOLOGY OF THE MAP AREA**

The map area is underlain by rocks of three distinct lithotectonic terranes: the Superior Province foreland, and the parautochthonous Gagnon and Molson Lake terranes.

Because rocks that originated from the Superior Province are incorporated into Gagnon terrane, locally preserved in their original state, the lithologies of these two terranes are discussed together under the heading of Gagnon terrane. Since rocks of Molson Lake terrane were excluded from the detailed study, they are not described in length.

#### **3.1 GAGNON TERRANE**

Gagnon terrane in southwestern Labrador is underlain by rocks of at least three different ages. Archean gneisses and granites of the Ashuanipi Metamorphic Complex form a crystalline basement which is unconformably overlain by metasediments of the Lower Proterozoic Knob Lake Group and both basement and cover rocks have been intruded by Middle Proterozoic gabbros of the Shabogamo Intrusive Suite. In the high grade part of Gagnon terrane tonalites of probably Middle Proterozoic age occur.

Appendix C is a table of detailed lithological descriptions of rock types of the Knob Lake Group and their Archean basement in the map area. A brief overview of the main characteristics of the stratigraphic units in Gagnon terrane follows.

##### **3.1.1 LITHOLOGICAL DESCRIPTIONS**

The crystalline basement on which the Knob Lake Group sediments were deposited consists of Archean mafic and quartzo-feldspathic gneisses and migmatites, all with granulite facies mineralogies and late granitoids which were virtually undeformed prior to the Grenvillian Orogeny. These rocks form part of the Ashuanipi

undeformed prior to the Grenvillian Orogeny. These rocks form part of the Ashuanipi Metamorphic Complex in the Superior Province and have been affected by Kenoran metamorphism and deformation. They have yielded cooling ages of approximately 2400 Ma (2425 Ma, K/Ar on biotite, Fahrig, 1967; 2386 and 2371  $\pm$  25 Ma, Ar/Ar on biotite, Dallmeyer, 1982). The Ashuanipi Metamorphic Complex consists of a complex of probable supracrustal lithologies that has been injected by orthopyroxene-bearing granitoid, resulting in the formation of migmatites. The majority of the basement rocks consists of two feldspar-biotite gneisses and migmatites  $\pm$  opx. Mafic rocks contain cpx + opx + pla  $\pm$  gnt. These rocks have been affected by at least two phases of deformation. Post-kinematic granites are especially common in the southwestern part of the map. Locally they were affected by pervasive brittle deformation. Within Gagnon terrane these rocks have been variably retrogressed and reworked by Grenvillian metamorphism and deformation. The different original lithologies of the Ashuanipi Metamorphic Complex have not been distinguished in the map. A more detailed description of the rocks of the Ashuanipi Metamorphic Complex north and northwest of the map area is presented by James and Stephenson (1992).

The rocks of the Knob Lake Group in Gagnon terrane form the southern extension of the Labrador Trough. The stratigraphy of the central and northern parts of the Labrador trough has been described in detail by Dimroth (1972) and Wardle and Bailey (1981). The stratigraphy of these miogeoclinal metasediments can be correlated across the Grenville Front without major changes (Rivers, 1980e, 1983a). The Lower Proterozoic Knob Lake Group forms the lower part of the Kaniapiskau Supergroup, which is the complete continental margin sequence in the Labrador Trough (Dimroth, 1972; Wardle and Bailey, 1981). The Knob Lake Group stratigraphy in the map area consists from bottom to top of the following formations.

The Attikamagen Formation consists of quartzo-feldspathic gneisses, interleaved with garnet-biotite or aluminous schists and gneisses. Thin intercalations of dolomitic marble, calc-silicate and metavolcanic amphibolites occur locally, which may be correlatives of the Denault and McKay River Formations respectively (see below). In

the map area the rocks of the Attikamagen Formation do not occur at low metamorphic grade, so their original sedimentary character is only known from occurrences in the New Québec Orogen, where they are shales, siltstones and greywackes (Wardle and Bailey, 1981). In the northern and central parts of the Labrador Trough, this formation has been subdivided into a western sequence, which is interpreted to have been deposited at shallow to moderate depths on a platform, and an eastern sequence, deposited in a deep water turbiditic environment, interpreted as a continental slope facies. The same subdivision applies to the study area. With the observations of intercalations of rocks correlable with the younger Denault and McKay River formations in the eastern facies of the Attikamagen, it is likely that deposition of rocks in the eastern facies continued after sedimentation of the western facies had ceased.

In the study area the Denault Formation generally forms a pure, massive, coarse-crystalline dolomitic marble, which locally contains calc-silicates. It was a dolomitic shallow water deposit, which in areas of low metamorphic grade to the north of the study area contains remains of stromatolites (Wardle and Bailey, 1981; Brown, 1991). It is interpreted to have formed a reef on the edge of the continental shelf and is now preserved in a narrow strip, approximately parallel to the strike of the belt. It separates platformal deposits to the west from deeper water sediments to the east.

The Wishart Formation is a mature quartzite, representing a proximal (littoral) depositional environment. The majority of these rocks are pure, massive, coarse-grained, recrystallized quartzites. In the map area no sedimentary structures were preserved. The base of the formation is occupied by a thin pelitic unit, which occurs as a muscovite rich schist. The Wishart Formation may be a lateral, more proximal, equivalent of the Denault Formation (Gastil and Knowles, 1960).

The Sokoman Formation is a banded iron formation containing a carbonate-quartzite member, a chert-oxide member and a carbonate-silicate member. Its appearance varies with its metamorphic grade. Whereas carbonates (predominantly Fe-rich) dominate the lowest and highest member at low metamorphic grade, silicates (Fe-rich amphiboles and pyroxenes) are more abundant at higher grades. It is banded

on scales varying from millimetres to metres. Sedimentary structures and features such as oolites and stromatolites, which are preserved locally in the central Labrador Trough, indicate that it is a shallow water deposit. Lateral facies changes are common in the Sokoman Formation. The oxide member is mined in the iron mines in the area.

The McKay River Formation forms lenses (generally less than 20 m thick) of amphibolite that are interpreted to be derived from mafic volcanoclastic sediments. It occurs in the Attikamagen Formation in the southeast of the map area as layered sequences of amphibolite which are rich in either garnet, sulphides or plagioclase, and in the western part of the map as thin, well layered intercalations of chlorite-actinolite schist in the Sokoman Formation and near the bottom of the Menihek Formation. In the map area it does not appear in the same stratigraphic position that it occupies farther to the northeast, where it is situated in between the Denault and the Wishart formations.

The Menihek Formation forms the top of the Knob Lake Group sequence in the map area. In the western part of the map area it is a homogeneous pelitic schist, rich in graphite and biotite, with a dark-grey to black appearance. Primary bedding can seldom be recognized due to the lack of compositional variation. In most places rocks of the Menihek Formation lie directly on top of the Sokoman Formation without metatuffs of the McKay River Formation separating the two. The southeastern occurrences of the Menihek Formation are more rich in quartz and feldspar and generally contain garnet and kyanite, which makes these rocks quite similar in appearance to the Attikamagen Formation.

The Knob Lake Group sediments were deposited unconformably and with onlap on the Archean basement. In a few outcrops in the map area the original undisturbed contact between the basement and the overlying Sokoman Formation is preserved, but generally the basement-cover interface is a site of strain localization and the contact is sheared. Within the stratigraphic sequence, the Menihek Formation is deposited conformably on the Sokoman Formation, locally separated by greenschists of the

McKay River Formation. The nature of other contacts within the sequence is uncertain, but it is likely that there was tectonic activity during deposition of the older formations (Wardle and Bailey, 1981).

Gabbros of the Middle Proterozoic **Shabogamo Intrusive Suite** with an intrusive age of  $1375 \pm 60$  Ma (Rb-Sr and Sm-Nd, whole rock, Brooks et al., 1981) intruded both basement and sediments. They commonly consist of medium to coarse-grained olivine gabbro but include minor norite and anorthosite (Gower et al., 1991). The gabbros form elongated bodies which are locally folded on a map scale and are interpreted to be sills where they intruded the supracrustal rocks (Rivers, 1980d). Corona textures in rocks of the Shabogamo Intrusive Suite in Gagnon terrane have been described in detail by Rivers and Mengel (1988). The size and the number of the intrusive bodies increases towards the higher thrust sheets in the southeast, suggesting that the locus of igneous activity lay in that direction.

**Foliated tonalite** occurs in several places within the Attikamagen Formation. These rocks have a gneissic banding and a composition that are similar to the quartzo-feldspathic gneisses of the surrounding Attikamagen Formation, which makes them hard to distinguish from the country rocks. They consist mainly of antiperthitic plagioclase, quartz and biotite ( $\pm$  muscovite,  $\pm$  clinozoisite). The intrusive bodies are generally small, the biggest of them, informally called the Michel Lake pluton, located on the peninsula between Wabush and Shabogamo lakes, south of Julienne Lake (Fig. 1A, in pocket). A second body occurs near Fermont, just south of the map area. Both bodies have been affected by the same deformation events as the surrounding Early Proterozoic sediments. The age of the tonalites is bracketed between that of the Early Proterozoic Knob Lake Group, in which they intruded, and the age of Grenvillian deformation. A whole rock Rb/Sr radiometric age of  $970 \pm 50$  Ma for the tonalite in the map area was interpreted to reflect the age of the metamorphic banding in the rock (Brooks et al., 1981). Foliated tonalite bodies other than the Michel Lake pluton were too small to be represented on the maps.

### 3.1.2 SIMILARITIES IN APPEARANCE OF SOME STRATIGRAPHIC UNITS

In the field it can be hard to distinguish between the three formations that can occur as quartzo-feldspathic rocks. Especially at elevated metamorphic grade and high strain, the reworked rocks of the Archean basement occur as quartzo-feldspathic schists or gneisses which are indistinguishable in the field from schists and gneisses of the Attikamagen Formation or from the eastern quartzo-feldspathic facies of the Menihek Formation. This is specifically a problem in the Elmer Lake thrust sheet in the northern-central part of the map (for thrust sheet locations see Chapter 4) and the gneissic rocks east of Wabush Lake. Also thin, porphyroclastic-mylonitic slices of basement rocks in the western, sediment-dominated part of map can easily be confused with deformed, clastic rocks. At low metamorphic grade in the western part of the map area and very high strain, the basement rocks are transformed into phyllonites, which are very similar to graphite-poor phyllites of the Menihek Formation. Since the unconformable contact between Archean basement and sedimentary cover is often the locus of high strain, the basement has locally at the contact a phyllitic character, much like the phyllites and schists of the Menihek Formation. This has led early workers to place the Menihek Formation, at that time called Nault Formation (see Rivers, 1980e), at the bottom of the sedimentary sequence (e.g. Klein, 1966) instead of at the top. Another source of error is the similar appearance of rocks of the Attikamagen and Menihek formations at amphibolite facies in the southeastern part of the map area. Both can appear as quartzo-feldspathic gneisses or pelitic schists, rich in micas, garnet and alumino-silicates.

Only with careful observations of field relationships and petrographic study is it possible to distinguish between these different formations with similar appearances. The location of the rocks in a stratigraphic sequence helps in many cases to determine the protolith, as in the identification of the Menihek Formation south of Wabush Lake on top of the Sokoman Formation (Figure 1A, in pocket). Unfortunately the Attikamagen Formation, where present, directly overlies the basement, which makes it impossible to distinguish between the two on the basis of stratigraphic relations. In

many cases, especially in the Elmer Lake thrust sheet and around Mont Bondurant, a gradual strain gradient from very low strain basement rocks, which were easily identified, into problematic gneisses and schists was used to help identify the basement rocks. Appendix C contains a list of criteria that were used to distinguish between the protoliths of rock types with similar appearances. Careful chemical analysis could possibly be used in the distinction of protoliths, but this was outside the scope of this study.

As a result of careful re-examination of the schists and gneisses, the map in this thesis diverges considerably from pre-existing maps with respect to the amount of basement rocks that occur within the Parautochthonous Belt. Most of the basement rocks in the Elmer Lake thrust sheet and in the Mont Bondurant area, and to a minor extent in the adjoining thrust sheets, were previously interpreted as part of the Attikamagen Formation in the maps of Rivers (1980 a, b, c, 1985 a, b, c). Also some of the occurrences of the Menihok Formation in the west of the map were re-interpreted as basement rocks. In the Attikamagen Formation east of Wabush Lake and in the south of the map area there may be occurrences of basement rocks which have not been identified as such. Occurrence of basement rocks in this part of the map area would require a re-interpretation of the location of the basal detachment in the area.

### **3.2 MOLSON LAKE TERRANE**

Molson Lake Terrane has been recently defined (Connelly et al., 1989a) as a terrane within the Parautochthonous Belt of western Labrador, composed of intrusive rocks and structurally overlying Gagnon Terrane. Work by Connelly (1991) and preliminary reconnaissance of the boundaries of Molson Lake terrane by the author has resulted in the recognition of at least two lithological units.

- Metagabbros of the Shabogamo Intrusive Suite, which in Molson Lake terrane have distinctive coronitic textures (Rivers and Mengel, 1989). South of the map area eclogitic mineral assemblages have been reported (Indares, in prep.). The gabbros in Molson Lake terrane are the equivalents of those in Gagnon terrane, but are more abundant and form larger plutonic bodies.

- Granitoids with a crystallization age of approximately 1635 Ma (U-Pb analysis on zircon, Connelly et al, 1989b) that have been interpreted as the southwestern extension of the Trans Labrador batholith (Connelly, 1991). Both equigranular pink granites and megacrystic grey granites were observed close to the western boundary, in different states of deformation, but generally homogeneously foliated.

### **3.3 RESTORATION OF THE SEDIMENTARY BASIN**

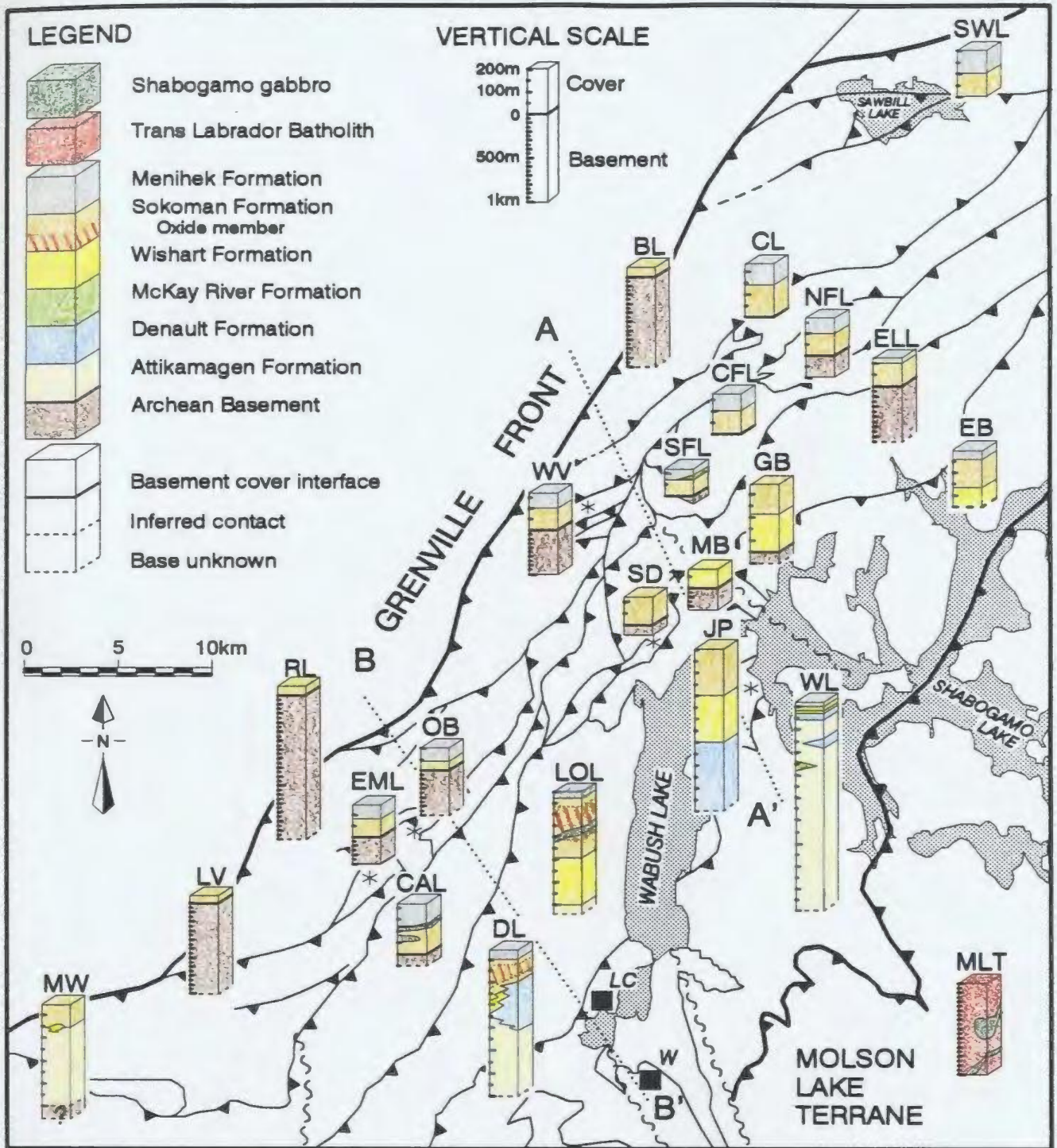
Sedimentation of the Knob Lake Group took place in a marine basin on a subsiding continental shelf, which deepened to the east onto the continental slope (Rivers, 1983a). It formed the eastern margin of an Early Proterozoic continent, represented by the rocks of the Superior Province. Wardle and Bailey (1981) presented a model for the sedimentary basin of the Kaniapiskau Supergroup in the central and northern parts of the Labrador Trough. In their model the rocks were deposited on the western margin of a proto-oceanic rift system. Rivers (1983a) schematically reconstructed the sedimentary basin for the Knob Lake Group within the Gagnon terrane in southwestern Labrador. Below follows a revision of this model, encompassing the new data from the mapping project.

#### **3.3.1 VARIATIONS IN THE STRATIGRAPHIC SEQUENCE**

The distribution of the formations is shown in the 1:100,000 map (Figure 1A in pocket) and in Figure 3.1. Schematic stratigraphic columns are drawn in Figure 3.1 for different parts of the area, showing variations in the stratigraphic sequence and in thickness of the formations. Each column represents one thrust sheet or part of one and is named with an acronym, which is explained in the figure and referred to in the text. Names and locations of the thrust sheets are introduced in Chapter 4.

Rapid lateral changes in thickness of the formations are common in the area. This is caused by both original lateral variations and tectonic changes in thickness. Original thicknesses of the formations are difficult to determine because of the highly deformed state of the rocks. The numbers used for the construction of figure 3.1 are approximations, especially where stratigraphic columns were drawn for areas that were

Fig. 3.1 Simplified stratigraphic columns for parts of the map area, indicating the variations in the stratigraphic sequence and thickness. Note that the vertical scales for the cover and basement are different, except for those areas where the thickness of the basement is only minor. Each column covers the rocks from either the floor thrust or the lowest exposed unit to the highest exposed unit in the area. A-A' and B-B' indicate the locations of the sections in Figure 3.2. Columns that have their base not exactly in the area that they represent have an asterisk marking the right location. BL = Bruce Lake thrust sheet (t.s.), CAL = Carol Lake t.s., CFL = central Flatrock Lake t.s., CL = Corinne Lake t.s., DL = Duley lake thrust sheet, EB = Elmer Bay area, EML = Emma Lake area, ELL = Elmer Lake area, GB = Goethite Bay area, JP = Julienne Peninsula, LOL = Lorraine Lake t.s., LV = Lac Viot area, MB = Mont Bondurant area, MLT = Molson Lake terrane, MW = Mount Wright area, NFL = north Flatrock Lake t.s. OB = O'Brien Lake thrust sheet, RL = Reid Lake t.s., SD = Sokoman Duplex, SFL = south Flatrock Lake t.s., SWL = Sawbill Lake area, WL = Wabush Lake t.s., WV = Wide Valley area. LC = Labrador City, W = Wabush.



not mapped in detail. Furthermore, within small areas the thickness is locally not constant and an average was taken. These rapid changes imply the existence of a significant basement topography at the time of deposition, presumably caused by block faulting of the passive continental margin. Only in the Emma Lake area direct indications of the existence of Early Proterozoic extensional faults in the basement were found, but other structures in the western part of the area suggest that extensional faults may be quite common (Chapter 5). The assumption is made that the block faults join in a lower detachment and form a linked extensional fault system as is proposed for passive continental margins by Wernicke (1981, 1985) and Lister et al. (1986). This proposed geometry of the continental margin in the map area is further discussed in Chapters 5 and 8.

In the occurrences of sediments farthest to the northwest in the map area (Fig. 3.1), the Sokoman Formation unconformably overlies the basement (SWL and BL), although locally the contact is of a tectonic nature as in the Corinne Lake area (CL). In these western thrust sheets, the lower carbonate iron-formation member is missing, as in all thrust sheets in the northern part of the map. Towards the east the lower carbonate/silicate member appears near Carol Lake (CAL) and occurs further only in the Lorraine Lake (LOL) and Duley Lake (DL) thrust sheets. The Sokoman Formation is thickest in the southern part of the map, in the I.O.C.C. mine area (Fig. 1.2).

The Wishart Formation occurs farthest west in the Goethite Bay and Lorraine Lake thrust sheets (EB, GB, MB and LOL) west of Wabush Lake. Its thickness varies greatly within a small area, but also on a larger scale from north to south in the map area. The estimated thickness varies from approximately 50 metres near Mont Bondurant, to up to 200 metres south of Lorraine Lake. In the central part of the area the Wishart Formation directly overlies the basement (MB, GB and EB), as is the case in most of the western part of the Labrador Trough. In the southern part of the Lorraine Lake thrust sheet, however, the Wishart Formation overlies the Attikamagen Formation and the basement is not exposed. The actual thickness of the Attikamagen Formation here is unknown.

The Denault Formation appears as a relatively narrow strip of 2 to 3 km wide, east and south of Wabush Lake, marking the eastern edge of the continental shelf (DL and JP). East of it we find a thick succession of metapelites and psammites of the eastern facies of the Attikamagen Formation (WL and DL), interpreted as turbiditic deposits on the continental slope.

### 3.3.2 PALINSPASTIC RECONSTRUCTION OF THE BASIN

From the data in Figure 3.1, combined with data from Wardle and Bailey (1981) and the model for the continental margin of Rivers (1983a), a schematic reconstruction was made of the restored depositional basin, as is shown in two cross sections in Figure 3.2. The relative original positions of parts of the basin have been preserved in the map pattern since no overstepping of thrust sheets took place within Gagnon terrane (see Chapter 5). The result of the restoration of the depositional basin in the Early Proterozoic is shown in two parallel cross sections through the central and the southern part of the map. This is a schematic restoration, which shows the spatial relationships between the formations, and does not involve balancing of cross sections.

The sedimentary sequences restore to define a continental shelf with a shallow part in the northwest and a deeper part in the southeast, and the rocks east of Wabush Lake representing the margin and slope deposits. The sediments were deposited with an onlap onto the basement and as a result the lower stratigraphic units appear furthest to the southeast, indicating that the depositional basin became deeper towards the southeast. The sequence and thickness of the formations also changes laterally, as can be seen in a comparison of the two sections in Figure 3.2, suggesting the existence of a significant basement topography and non-uniform subsidence at the time of deposition. A basement high seems to have existed in the central-northern part of the map area in section A-A', where most basement is exposed and where the stratigraphic units are thinnest. This part of the area presumably submerged fairly late, and slowly, in the depositional history. The sedimentary basin was considerably deeper and subsidence was interpreted to be faster in the southern part of the map, where the older units are exposed and where the stratigraphic sequence is significantly thicker. A considerable

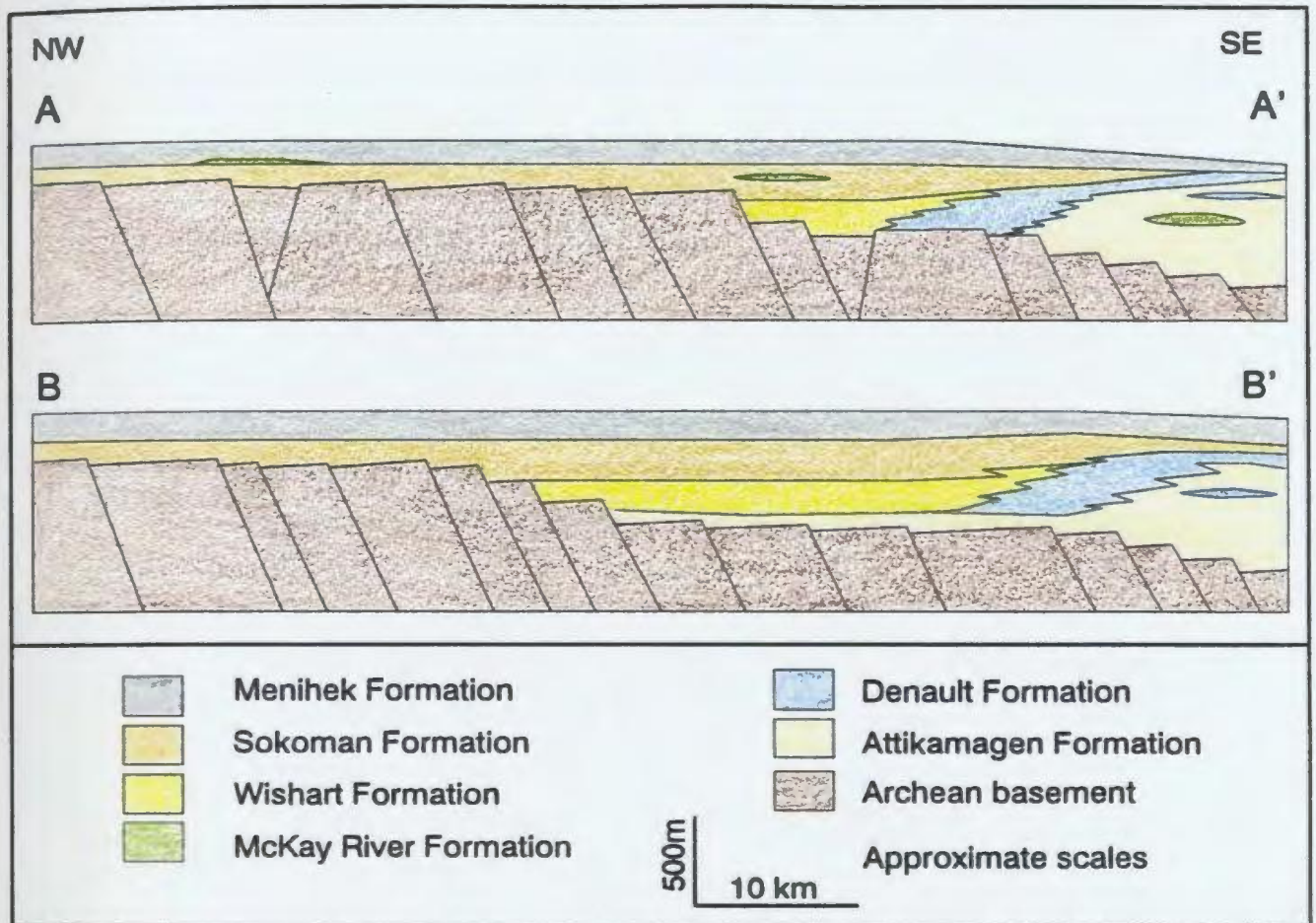


Fig. 3.2 Simplified sections through the schematically restored sedimentary basin on the continental margin of the Superior Craton in the Early Proterozoic, showing the distribution of the formations of the Knob Lake Group. The sections are not balanced and are not accurately scaled. The locations of the sections are indicated in Figure 3.1.

increase in the amount of exposed rocks of the Attikamagen Formation southwest of the map area, suggests an increase of the original depth of the basin towards the south. Northeast of the basement high at Mont Bondurant, north of section A-A', the deeper part of the shelf widens again and contains thick deposits of the Sokoman Formation lithologies.

The site of the Denault Formation marks a break in the stratigraphy, which supports the interpretation that these dolomitic marbles are an ancient reef at the edge of the continental shelf. East of the Denault Formation the basin deepened rapidly to form the continental slope which contains deposits several kilometers thick of the Attikamagen Formation.

The continental shelf and slope were underlain by basement rocks which were broken up in a system of block faults which presumably join at depth in a common shallow-dipping detachment.

It should be noted that the total thickness of the sediments in the map area is extremely thin compared to other orogens and present continental margins. The rocks in the shallow northwestern part of the shelf comprise no more than 200 m in total and are locally less than 100m thick. The sequence on the deeper southeastern part of the shelf is estimated between 500 and 800 m thick.

The depositional basin may have opened to an oceanic basin to the southeast, but since there are no remains of such a basin exposed east of the Wabush Lake thrust sheet, such interpretations are largely speculative in the context of this study.

## **CHAPTER 4**

### **THRUST BELT GEOMETRY OF GAGNON TERRANE IN THE LABRADOR CITY / WABUSH AREA**

Gagnon terrane in southwestern Labrador is a foreland fold-and-thrust belt in which rocks of the Grenvillian Parautochthonous Belt are emplaced on the Superior Province foreland by northwest-directed thrusting. For an evaluation of the tectonic development of the area, knowledge of the geometry of the belt and an understanding of the dynamics of the thrust sheets are prerequisites.

This chapter presents a general description of the main features of the Grenvillian fold-and-thrust belt in the map area. It includes discussions of the overall thrust belt geometry and its main metamorphic and structural features which form the framework to which the detailed descriptions in the following chapters can be related. After a detailed discussion of the variations in structural style and metamorphic grade in chapters 5, 6 and 7, a coherent model for the development of the belt is presented in Chapter 8.

The description below and the subdivision into thrust sheets are based mainly on the 1:100,000 scale map and cross-sections (Fig. 1A and 1B in pocket) and the tectonic map in Figure 4.1. Only a small portion of this map is based on fieldwork done in the course of this thesis. The remainder is taken from partially re-interpreted maps by Rivers (1985a, b, c) and Fahrig (1967) (see Appendix A). Therefore, small parts of the map may not be completely consistent with the presented model. Small scale features are left out of this map and are presented only in the more detailed maps in the text of Chapter 5 and in Figure 2 (in pocket). The cross sections in Figure 1B (in pocket) incorporate more details and interpretations than the 1:100,000 scale map in Figure 1A. As a result, many of the structures shown in the cross-sections do not match similar features in the map.

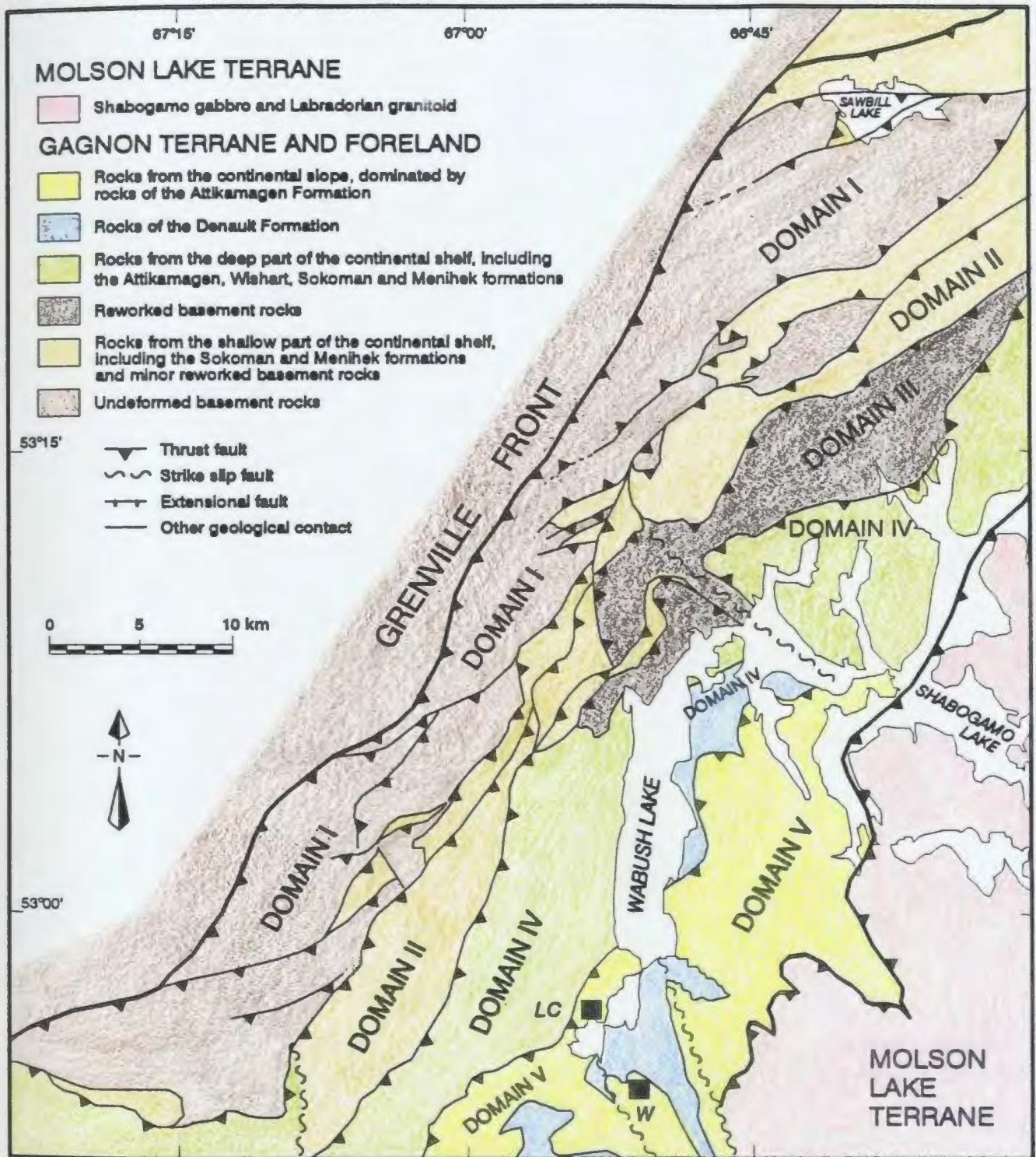


Fig. 4.1 Lithotectonic map of the Grenville Province in southwestern Labrador. The lithotectonic domains I to V in Gagnon terrane are described in the text. LC = Labrador City, W = Wabush.

Most of the small scale and large scale structures are a direct result of the thrust movement. Rivers (1983a) recognized three generations of Grenville age structures, of which the first two were directly attributed to thrusting. The oldest Grenvillian structure that can be recognized in the area is a regionally developed, shallowly southeast-dipping foliation, which is axial planar to isoclinal, locally rootless  $F_1$  folds and which forms the mylonitic foliation in the shear zones. South to southeast-plunging mineral lineations indicate the orientation of maximum elongation in the  $S_1$  foliation plane and together with shear-sense criteria indicate the northwest-directed movement. Northeast-trending folds which overprint this foliation were grouped together by Rivers (1983a) into a second generation of structures,  $F_2$ , which are northwest-vergent and directly related to the same thrusting event. Although the same structures were recognized in this study, their subdivision and tectonic connotation is different from that of Rivers (1983a) as will be documented in the Chapter 5. The  $D_1$  and  $D_2$  structures dominate the map pattern in a zone up to 20 km wide southeast of the Grenville Front and control the NNE-trending structural grain of the belt. The youngest structures are kilometer-scale, ENE-vergent, south-southeast-plunging cross folds ( $F_3$ ), which are restricted to the southeast corner of the map. These folds are dominant in Molson Lake terrane, in the footwall of the floor thrust of Molson Lake terrane and in the rocks of the Denault Formation. In the part of Gagnon terrane directly south to southeast of the map area they give the belt a northwest-trending structural grain.

The thrust faults in the map area form a linked system which accommodates considerable crustal shortening. The most important characteristics of the system are discussed below and the belt is compared with existing models for foreland fold-and-thrust belts. Rivers (1983a) was the first to recognize the importance of thrusting in the Grenville Province in southwestern Labrador and suggested that the area represents a foreland fold-and-thrust belt. In his model a northwest-vergent thrust stack developed in the early Proterozoic shelf sediments during  $D_1$ , with a bedding-parallel sole thrust near the base of the sedimentary cover. Where the thrust front reached a buttress formed by basement rocks at the western end of the

sedimentary basin, thrust propagation was inhibited and the thrust stack started folding ( $D_2$ ). During the last stage of development of the belt a small portion of the basement rocks was plucked off the buttress and incorporated in the thrust stack. These generations of structures were interpreted to be formed during progressive stages of the development of the thrust belt. The Grenville Front was located at the main boundary between basement and cover rocks. Rivers (1983a) suggested a possible presence of more basement rocks in the belt than shown in his model. It has been found in this study that the role of the basement rocks is far more important than previously recognized and this thesis documents the major role of the basement rocks in the development of the belt. However, the actual extent of the basement rocks in the fold-and-thrust belt remains unresolved in this study and they could be more widespread than shown in the maps accompanying the thesis. As noted earlier, in many places penetrative reworking of the basement rocks has prevented their positive identification and discrimination from their metamorphosed sedimentary cover (Section 3.1.2).

A second source for comparison of the fold-and-thrust belt in Gagnon terrane are the models that exist for the geometry of thrust belts and collisional orogens in general (e.g. Boyer and Elliott, 1982; Butler, 1982; Hatcher and Williams, 1986). The features of these models that are emphasized in this study are: 1) thrust sheets are generally stacked in a piggy back sequence; 2) the sole thrust of a thrust system follows a staircase trajectory of flats and ramps, cutting up in the stratigraphy in the direction of movement. In systems containing both basement and cover rocks, the sole thrust cuts up from the basement into the sedimentary cover towards the foreland; 3) the average size of the thrust sheets increases towards the hinterland and crystalline thrust sheets are generally larger than non-crystalline sheets; 4) development of a foreland thrust belt is commonly controlled by the emplacement of a dominant thrust sheet, with dimensions an order of magnitude larger than the sheets in the underlying system. These features will be compared to those of the fold-and-thrust belt in southwestern Labrador.

#### 4.1 LITHOTECTONIC DOMAINS IN THE MAP AREA

In the lithotectonic map in Figure 4.1 the rocks of Gagnon terrane are grouped into one of five lithotectonic domains which form zones parallel to the trend of the whole belt. The arrangement of the domains reflects the outline of the original sedimentary basin and the palinspastically restored positions of the sediments on the continental shelf and margin (Fig. 3.2). In Figure 4.1 the rocks of the Denault Formation are given a separate colour to emphasize their position at the margin of the continental shelf, separating platform and slope sediments (see Section 3.3.2). However, in the description below they are grouped together with the remainder of the stratigraphically higher shelf sediments. Each of the domains consists of a number of thrust sheets which can be set apart from the others on the basis of stratigraphy, metamorphic grade and structural characteristics. From northwest to southeast these domains are:

##### Domain I

Thrust sheets adjacent to the Grenville Front consist predominantly of crystalline basement rocks that are not notably affected by Grenvillian deformation on outcrop scale, but are transected by several Grenvillian shear zones. Only in the northern end of this domain, in the Sawbill Lake thrust sheets, is a significant amount of cover rocks present, consisting of the Sokoman and Menihek formations. If the position of the Grenville Front is chosen 5 to 10 km further west, as proposed by James and Stephenson (1992), domain I will extend up to this new boundary.

##### Domain II

Southeast of domain I is a belt of thrust sheets containing predominantly metasedimentary rocks of the shallow part of the continental shelf, represented by the Sokoman and Menihek formations. Of the Sokoman Formation only the two upper (oxide and carbonate) members are present. Basement rocks in domain II are subordinate and appear as: i) thin, highly deformed slices near the floor of the thrust sheets; ii) as less deformed bodies in the cores of fold nappes; or iii) as

large, virtually undeformed inliers. The thrust sheets in this domain can be extremely thin. They vary in thickness from about 100 m to several hundreds of meters.

#### Domain III

Overlying the northern part of domain II is a belt of rocks dominated by intensely deformed basement rocks, locally with small amounts of metasedimentary cover preserved. Rocks of the Sokoman and Menihek Formations in this domain are similar in appearance and thickness to those in domain II. A few kilometer-sized lenses of less deformed basement rocks are also present.

#### Domain IV

This domain, adjacent to Wabush and Shabogamo Lakes, is dominated by metasedimentary rocks of the deeper part of the continental shelf and contains the complete stratigraphic sequence of the Knob Lake Group in the region. In the southern part of the domain the metasediments are folded in kilometer-scale, north-northeast-trending  $F_2$  folds which are overturned to the northwest. In the central part of domain IV around Mont Bondurant, and farther south, highly sheared basement rocks are present, similar to those in domain III. They are interpreted to represent an ancient basement high (see Section 3.3). At the eastern margin of domain IV a zone of rocks of the Denault Formation marks the edge of the Early Proterozoic continental shelf.

#### Domain V

The easternmost domain, east and south of Wabush Lake, is dominated by rocks of the Attikamagen Formation, that were deposited on the continental slope. South of Wabush Lake the domain also contains significant amounts of marble of the Denault Formation. The sequence of clastic metasediments is interpreted to be up to several kilometers thick and is strongly folded in originally northwest-verging  $F_2$  folds which are overprinted by southeast-plunging  $F_3$  folds of kilometer-scale. No basement rocks have been positively identified in this domain, but they may nevertheless be present.

Lateral boundaries between the lithotectonic domains are not everywhere well defined. The Grenville Front separates the lithotectonic domains in Gagnon terrane from the Superior Province foreland to the northwest. To the southeast they are bounded by the overlying Molson Lake terrane, which is regarded as the dominant thrust sheet, in the sense of Boyer and Elliott (1982). In the southeastern part of the map area, Molson Lake terrane overlies domain V, but further north it oversteps the thrust sheets of domain V and directly overlies rocks of domain IV. With the exception of domain I, the size of the thrust sheets increases slightly towards the interior of the orogen. The fact that basement rocks are most abundant in the structurally lowest sheets near the front of the belt and absent in the highest sheets does not conform to existing models for thrust belt geometry.

#### **4.2 SUBDIVISION OF GAGNON TERRANE INTO THRUST SHEETS**

The northwestern part of Gagnon terrane consists of an imbricate stack of thrust sheets, bounded by thrusts that dip shallowly to moderately to the southeast (Rivers, 1983a; van Gool et al., 1987a, b, 1988a, b; Brown et al., 1991). The highest, furthest travelled thrust sheets are found in the southeast. The bounding thrusts occur as ductile shear zones, in which the shear strain is concentrated. Subsidiary thrusts divide the thrust sheets into separate horses to form imbricate fans or duplexes. The horses, or thrust slices, between the thrusts all reveal a penetrative foliation and folds. The thrust sheets are outlined and named in Figure 4.2 and coded according to the grade of metamorphism. For some of the thrust sheets shown in the map, lack of outcrop or field observations resulted in ill-constrained boundaries. In many cases they are defined by abrupt changes in stratigraphy rather than by recognition of a major thrust fault in the field. Only in well-exposed parts of the area, which were mapped in detail, have thrust sheet boundaries been observed. In much of the remainder of the map the boundaries have been inferred. Differences in stratigraphy that were used for subdivision in thrust sheets are shown along two sections through the area in Figure 4.3. The thrust sheets are described below from the lowest structural level in the northwest to the highest in the southeast.

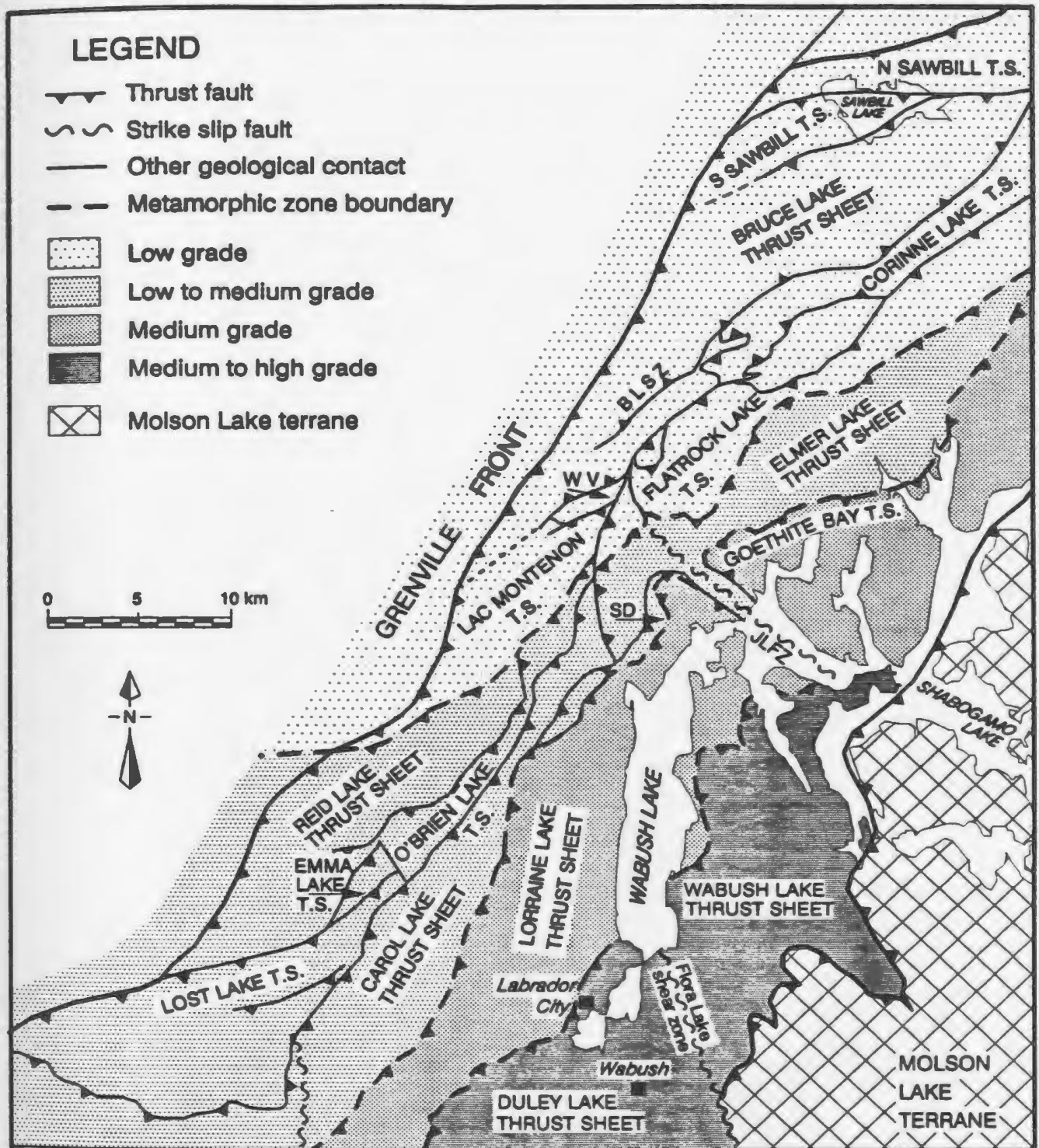


Fig. 4.2 Metamorphic zonation and subdivision of the map area into thrust sheets. Only the structures that form thrust sheet boundaries are indicated. BLSZ = Bruce Lake shear zone; JLFZ = Julienne Lake fault zone; SD = Sokoman Duplex; WV = Wide Valley triangle zone. TS = thrust sheet.

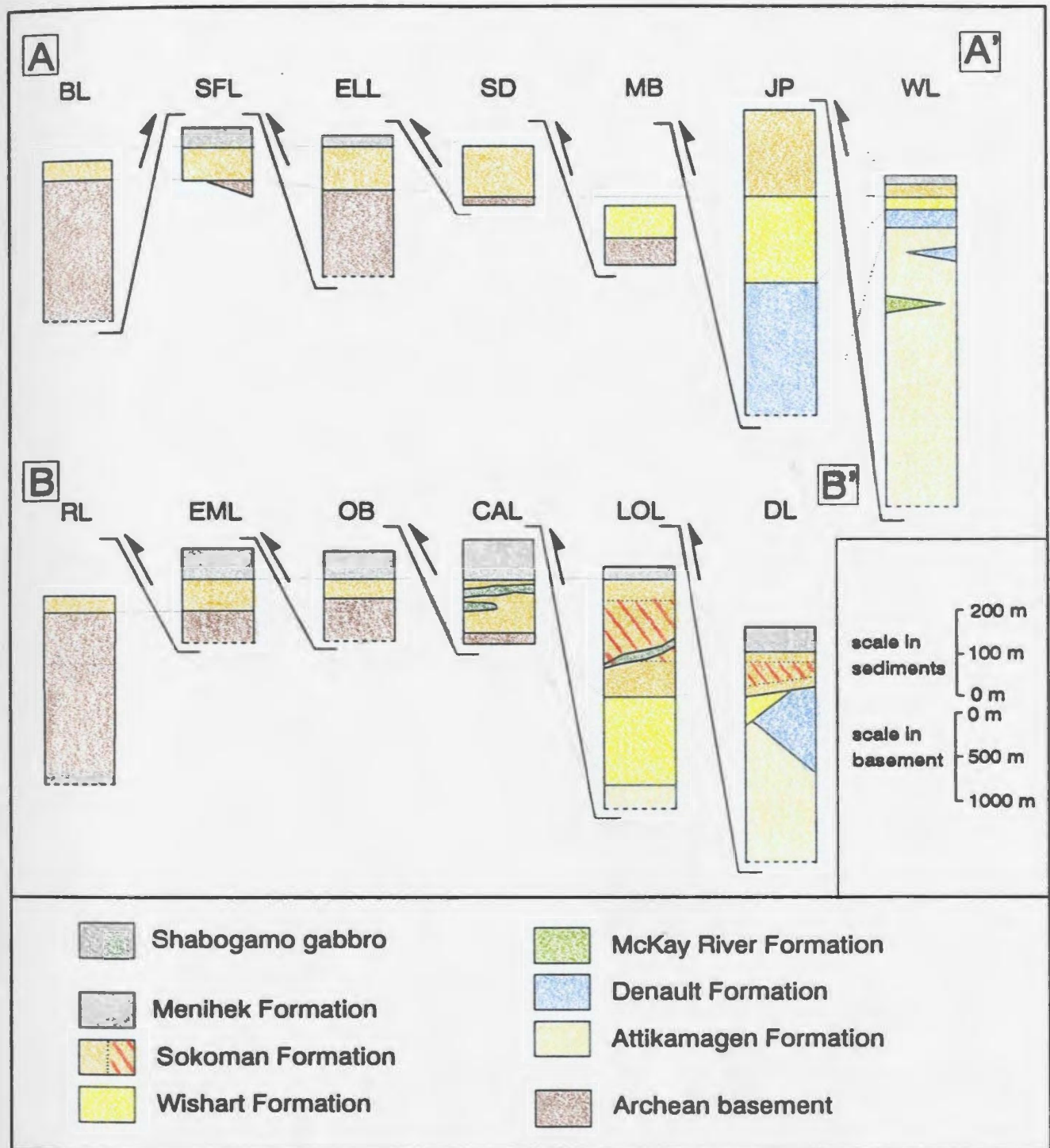


Fig. 4.3 Variations of the stratigraphy in the thrust sheets in two sections through the area. The lines of section from which the stratigraphic columns are taken is shown in Figure 3.1, which are the same as the restored sections in Figure 3.2. For explanation of the acronyms see Figure 3.1.

#### 4.2.1 DOMAIN I

The lowest thrust sheets are the northern and southern Sawbill Lake thrust sheets. They consist of a thin sequence of shallowly dipping cover rocks (Sokoman and Menihek formations) and are underlain by Archean basement rocks, from which the cover rocks are detached.

The Bruce Lake, Lac Montenon and Reid Lake thrust sheets contain several kilometers of basement rocks and up to 50 meters of cover rocks of the Sokoman Formation, which are detached from the basement. The rocks in the Reid Lake and Bruce Lake thrust sheets are cross-cut by several steeply southeast-dipping thrusts (dip angles between 40° and 60°). Away from these thrusts, the Archean basement rocks show virtually no traces of Grenvillian deformation or metamorphism on outcrop scale.

The Lost Lake thrust sheet is a thin, basement-dominated thrust sheet, which in its northeastern part is sandwiched between two sediment-dominated sheets. The southwestern part of the thrust sheet is not well-defined.

#### 4.2.2 DOMAIN II

The Corinne Lake thrust sheet contains rocks of the Sokoman and Menihek formations and two basement inliers. The basement-cover contact is a zone of localized high strain and forms a detachment, but displacement is estimated to be minor. Rocks in the Corinne Lake thrust sheet are folded, but no internal subsidiary thrusts were observed. A large window in the south of the thrust sheet exposes the underlying, almost pristine basement.

In the Flatrock Lake thrust sheet metasediments of the Sokoman and Menihek formations are dominant, but thin sheets of intensely deformed basement rocks are incorporated into the thrust sheet. The floor thrust cuts up in the direction of movement from a shallow level in the basement to the base of the sedimentary cover, but does so non-systematically. Rocks of the sedimentary cover, together with their crystalline basement, are interleaved by thrusting and folding on the scale of tens to hundreds of meters.

The **Wide Valley** area, previously referred to as the **Wide Valley thrust sheet** (van Gool et al., 1987b), forms a triangle zone between southeast and locally northwest-dipping thrust faults. It is also dominated by rocks of the **Sokoman** and **Menihek** formations, which are overlain by thick sheets of basement rocks. The boundary of the triangle zone to the southwest is not well defined.

The southwestern part of the **O'Brien Lake thrust sheet** contains predominantly reworked basement rocks. The remainder of the thrust sheet contains biotite schists, which probably represent imbricated rocks of the **Menihek Formation**, but could, at least in part, be phyllonitic basement mylonites. Rocks of the **Sokoman Formation** are subordinate.

The **Emma Lake thrust stack** contains rocks of the basement as well as the **Sokoman** and **Menihek** formations, which are repeated in a stack of fold nappes, interpreted as a duplex by Brown et al. (1991). The floor thrust lies well in the basement (>200m) and basement rocks are intensely deformed, together with the overlying sediments, by shearing and folding. The thrust stack is truncated in the northeast by a high angle fault.

The floor thrust of the **Carol Lake thrust sheet** in the southwest of the map cuts 100 to 200 m into the basement, which is overlain by rocks of the **Sokoman** and **Menihek** formations. With the exception of one small area, basement rocks had not previously been recognized in the **Carol Lake thrust sheet** and it is likely that a considerable proportion of the rocks depicted as **Menihek Formation** in the map is actually reworked, phyllonitic basement. Basement and cover rocks are interleaved on a fairly small scale by both thrusting and intense folding.

The **Sokoman duplex** is a 150m thick sheet of rocks of the **Sokoman Formation** interleaved with thin slices of basement rocks, and possibly represents a part of the sediments detached from the underlying **Elmer Lake thrust sheet** (Section 4.2.3). The duplex consists of an imbricate stack of subsidiary thrusts which rejoin in the roof. It is the only thrust sheet in the map area which could be mapped as a true duplex. To the northeast the duplex is cut off or ends in a lateral ramp.

### 4.2.3 DOMAIN III

The Elmer Lake thrust sheet overlies the Flatrock Lake thrust sheet and consists mainly of highly deformed basement rocks, containing several large (km-size) lenses of low strain (i.e. with respect to the Grenvillian deformation) Archean basement. Only thin slices (<50m) of cover rocks appear in the thrust sheet. It appears that most of the sedimentary cover has been tectonically removed from the thrust sheet, since the roof thrust, which is best constrained at the foot of Mont Bondurant, is situated in basement rocks.

In previous work the strongly deformed basement rocks in the Elmer Lake thrust sheet were interpreted as metasediments of the Attikamagen Formation (Rivers, 1985b) or their equivalents (Fahrig, 1960, 1967). It is possible that pockets of quartzo-feldspathic basal conglomerate are present near ancient fault escarpments of block faults, which presumably existed in the area. However, these have not been identified as such and are assumed to be at most a minor component of the thrust sheet. Amphibolites are common in the Elmer Lake thrust sheet, most of which were originally mapped as metagabbros (Rivers, 1985b). Some of the amphibolite bodies have been re-interpreted as an original mafic component of the basement complex.

### 4.2.4 DOMAIN IV

The Lorraine Lake thrust sheet, in which the I.O.C.C. iron mine is located, contains the greatest thickness of both the Sokoman and the Wishart formations (together over 400 m). Rocks of the basement as well as all formations of the Knob Lake Group are exposed in the thrust sheet. A significant N-S lateral variation in stratigraphic and structural character is displayed. The northern part of the thrust sheet, previously separated from the southern part as the Mont Bondurant thrust sheet (van Gool et al., 1987a), is dominated by strongly deformed basement with a small amount of quartzite of the Wishart Formation.

The southern part of the Lorraine Lake thrust sheet is dominated by metasediments and basement rocks are not exposed. The exact position of the floor thrust with respect to the contact between basement and the Attikamagen Formation in

the southern part is unknown, but, on account of the lack of exposed basement rocks in this part of the thrust sheet, it is assumed that the floor thrust originated at the basement-cover contact. The position of the Lorraine Lake floor thrust in the southern part of the map is inferred from the abrupt transition in stratigraphy and metamorphic grade along a line east of Carol Lake, which lies along the extension of an observed thrust fault near Rivière aux Fraises (Fig. 1A; see Chapter 5). South of Carol Lake the floor thrust cuts up to the level of the Wishart and Sokoman formations. The floor thrust of the Lorraine Lake thrust sheet is one of the most important in the area. Across the boundary between the Carol Lake and the Lorraine Lake thrust sheets, from east to west, the lower part of the stratigraphy is lost: both Attikamagen and Wishart Formations and the oxide member of the Sokoman Formation do not appear west of the boundary. On the other hand, basement rocks appear in the Carol Lake thrust sheet, which seem to be absent in the southern part of the Lorraine Lake thrust sheet (Fig. 4.3, section B-B').

The transition from the northern to the southern part of the thrust sheet is gradual and lies between the northern end of Lorraine Lake and d'Aigle Bay at the mouth of Rivière aux Fraises. In the transition zone the basement is overlain by a thin cover of rocks of the Attikamagen Formation, which are recognized by the appearance of kyanite and staurolite in the schists and gneisses. Further north, the rocks of the Attikamagen Formation wedge out and rocks of the Wishart Formation lie directly on the basement.

The floor thrust of the Lorraine Lake thrust sheet cuts laterally, from south to north, from the cover into the basement. This is interpreted as an effect of original basement topography, rather than lateral ramping. Near Mont Bondurant in the north of the thrust sheet, the floor thrust cuts into a basement high, rather than riding over it, deforming the basement rocks while incorporating them into the thrust sheet.

The structural style in the northern part of the Lorraine Lake thrust sheet is dominated by shearing and thrusting. Folding becomes more important towards the south. From Lorraine Lake southwards, no thrusts were mapped by previous workers

and large-scale folding is supposed to be the dominant style of deformation (Rivers, 1980a, c, 1983a). It is possible, however, that the continuity of the stratigraphy, as presented in the map and cross section of figures 1A and 1B, has been disrupted by thrusting in this part of the area, as was found to be the case in most of the areas surrounding the Lorraine Lake thrust sheet.

East of Wabush Lake a band of rocks of the Denault Formation is overlain by quartzites of the Wishart Formation and carbonate and oxide members of the Sokoman Formation, the latter two exposed in a syncline in the Julienne Peninsula. In the absence of exposure in critical areas, these metasediments east of Wabush Lake are interpreted as the eastern continuation of the Lorraine Lake thrust sheet, although they may form a separate structural unit.

The **Goethite Bay thrust sheet**, which may be the northern extension of the Lorraine Lake thrust sheet, forms an imbricate stack of thrust slices which are dominated by massive rocks of the Sokoman and Wishart formations in the Goethite Bay area. Rocks of the Menihek Formation are only exposed in the northeastern part of the thrust sheet near Elmer Bay. Thin basement slices (up to 50 m in thickness) are exposed at its western boundary, close to the floor thrust and on the northeastern shore of Julienne Lake. The original floor thrust is interpreted to lie at the base of the Wishart Formation and the basement slices were introduced afterwards by thrusting that originated at a lower level. A transition in the stratigraphic sequence, similar to that between the Carol Lake and Lorraine Lake thrust sheets, is found at the floor thrust of the Goethite Bay thrust sheet (Fig. 3.2, compare columns GB and ELL, representing part of the Goethite Bay thrust sheet and the underlying Elmer Lake thrust sheet).

#### **4.2.5 DOMAIN V**

The **Duley Lake thrust sheet** south of Wabush Lake contains rocks that originated on the continental margin. It stretches beyond the map boundaries to the southwest for several tens of kilometers, where it is dominated by massive dolomitic marbles of the Denault Formation and gneisses of the Attikamagen Formation. It is separated from the Wabush Lake thrust sheet to the north and Molson Lake terrane to

the east by the Flora Lake fault zone, a steeply dipping strike-slip shear zone along Flora Lake. This thrust sheet may not be completely disconnected from the Lorraine Lake thrust sheet. The boundary zone consists of a kilometer-scale, overturned, northwest-vergent antiform of which the lower limb is partially thrust through (Fig. 1B, in pocket). The Duley Lake thrust sheet is characterized by an interference pattern of large-scale, northeast-trending folds ( $F_2$ ) and younger southeast-trending folds ( $F_3$ ) (Rivers, 1983a).

The Wabush Lake thrust sheet is dominated by gneisses and migmatites of the Attikamagen Formation. Thin lenses of dolomitic marble and amphibolite also occur and the thrust sheet incorporates the Michel Lake pluton, as well as smaller orthogneiss occurrences, for example north of Moose Head Lake (not indicated in Figure 1A). Basement rocks may be present in the thrust sheet, but are not recognized as such, because of the similarity of metasediments and deformed basement rocks at high metamorphic grade and high strain.

No internal thrusts were recognized in this thrust sheet. Both  $F_2$  folds that were originally northwest-vergent and kilometer-scale northeast-vergent  $F_3$  folds dominate this area. The nature of the contact with the dolomitic marbles of the Denault Formation to the northwest is not clear due to lack of exposure. The regional southeast dip of the enveloping surface of the bedding in the area suggests that the rocks of the stratigraphically lower Attikamagen Formation to the southeast structurally overlie the marbles. The boundary is drawn as a single continuous but folded thrust, but it may well be that locally the Attikamagen and Denault formations are tectonically interleaved. The Wabush Lake thrust sheet is overlain by rocks of Molson Lake terrane, from which it is separated by a wide ductile shear zone. The enveloping surface of this shear zone dips shallowly to the southeast, but is folded in a train of large-scale cusped and lobate  $F_3$  cross-folds.

#### 4.2.6 LARGE SCALE FAULT ZONES

The Grenville Front is defined as the lowest Grenvillian thrust fault that has been recognized. West of Sawbill and Bruce lakes it has a clear topographic expression as a

valley which can easily be traced on air photos and geomagnetic maps. It was mapped on the ground for approximately 20 km along strike southwest of Sawbill Lake. Further southwest its trace is lost and the Front is tentatively connected with the thrust through Lac Montanon. Possibly the northern-most part of the thrust dies out southwestwards in a tip line and the Grenville Front sidesteps to a higher thrust. It is also possible that a lower, unrecognized or not emergent thrust forms the true sole thrust of the system (cf. James and Stephenson, 1992; see Section 2.1).

West of Bruce Lake an oblique-slip shear zone was mapped with an apparent extensional component of displacement. This steeply southeast-dipping Bruce Lake shear zone is 100 to 200 m wide (Fig. 2, in pocket). It can be traced for over 20 km and is inferred to extend northwards for at least another 15 km. In the northeast it separates basement rocks to the west from metasediments to the east. In its southern extent, where the shear zone cuts into basement rocks, it is decorated with thin slices of rocks of the Sokoman Formation. Fahrig (1960, 1967) mentioned a normal fault separating the metasediments from the Archean basement in the area south of Sawbill Lake, probably referring to this shear zone. The normal faulting was interpreted as a post thrusting relaxation during the last stages of Grenvillian deformation (Fahrig, 1967). In this study, the Bruce Lake shear zone is re-interpreted as an overturned backthrust (see Chapter 5).

A zone extending from Julienne Lake towards the northwest, forms the termination of the Lorraine Lake, Wabush Lake and Goethite Bay thrust sheets as well as the northern limit of the rocks of the Denault and Attikamagen formations in the map area (Fig. 4.1). It also forms the site of the transition of the trend of the belt from 035° in the south to 050° in the north of the map. This tectonic break is named the Julienne Lake fault zone. Its northwestern extension is formed by a wide shear zone (the Sickle Lake shear zone, see Chapter 5) that forms the southern boundary of the Flatrock Lake thrust sheet. These two shear zones are tentatively connected to form a continuous, steeply southwest-dipping, oblique-slip fault zone with a right-lateral component of displacement, causing a clock-wise rotation in plan view of the structures

in the southern end of the Flatrock Lake thrust sheet. However, no evidence of a continuous shear zone is found in the Elmer Lake thrust sheet because of poor exposure. The fault may possibly be linked to a lateral ramp at a lower crustal level or a transfer fault in the basement.

### 4.3 METAMORPHISM IN THE MAP AREA

Gagnon terrane has a telescoped, inverted metamorphic gradient which is typical for thrust belts in general. The peak metamorphic conditions vary from lower greenschist facies in lithotectonic domain I in the northwest, to upper amphibolite facies in domain V in the southeast of Gagnon terrane, with peak metamorphic temperatures varying from approximately 350°C in the north of the map, to approximately 750°C in the southeast (Chapter 7). The presence of kyanite as the stable aluminosilicate in the metapelites indicates an intermediate metamorphic pressure series (Rivers, 1983b; Chapter 7) in the terminology of Miyashiro (1973). Grenvillian metamorphic grade in Molson Lake terrane is of upper amphibolite grade (Rivers, 1983b, Connelly, 1991), with local indications of high pressures (Indares, in prep.).

Figure 4.2 shows the subdivision of the map area into metamorphic zones indicating the peak metamorphic grades for Gagnon terrane. The four zones are: 1) low grade zone (lower greenschist facies), covering the Sawbill Lake, Bruce Lake, Corinne Lake, Flatrock Lake, Wide Valley and Lac Montanon thrust sheets; 2) low to medium grade zone (upper greenschist facies): Read Lake, Emma Lake, Lost Lake, O'Brien Lake, Carol Lake and Elmer Lake thrust sheets; 3) medium grade zone (lower amphibolite facies): Goethite Bay and Lorraine Lake thrust sheets; 4) medium to high grade zone (upper amphibolite facies): Wabush Lake and Duley Lake thrust sheets.

This metamorphic zonation does not coincide exactly with the division into lithotectonic domains. In the western part of Gagnon terrane it is obvious that the two are oblique with respect to each other (Fig. 4.2). In each of the lithotectonic domains the metamorphic grade increases from northeast to southwest. Towards the southwest, rocks have been exhumed from increasingly deeper crustal levels and the present erosion level forms an oblique cut through the fold-and-thrust belt.

#### **4.4 THREE-DIMENSIONAL GEOMETRY OF THE FOLD-AND-THRUST BELT**

The lack of significant topographic relief in the map area prevents a true three-dimensional reconstruction of the structures. The geometry of the belt at depth can only be interpreted from data at the surface, in which the oblique erosional cut through the belt is helpful. The geometry described below is only one possible interpretation, which appears to be the most logical, but others cannot be excluded.

The general geometry of the belt in the third dimension is outlined in Figure 1B (in pocket), which presents three cross sections on a 1:100,000 scale across the strike of the thrust belt. Many of the structures are represented schematically either because their true geometry is unknown, or because their size is too small to be presented on a true scale. The sections are not rigorously balanced, because of: 1) a lack of detailed information along the length of the sections; 2) changes in thickness of the sedimentary cover as a result of original basement topography and ductile deformation; 3) the oblique orientation of the sections with respect to the movement direction. They show that Gagnon terrane in southwestern Labrador consists of an upper system of thin-skinned sediment-dominated thrust sheets intersected and underlain by a stack of basement thrust sheets of several kilometers in thickness. Together they form thrust systems on two different scales and levels.

The upper, sediment-dominated system consists of lithotectonic domains II, IV and V and is intersected by the reworked basement rocks of domain III. In contrast to existing models, this belt appears not to have a sole thrust that cuts progressively up-section in the direction of movement. A geometry that would be expected, according to the rule of an upward cutting sole thrust, would show from southeast to northwest a decreasing amount of basement involved in the thrust belt. Instead the sediment dominated system has a maximum amount of basement incorporated in the center of the belt, in the Carol Lake, Elmer Lake and northern part of Lorraine Lake thrust sheets (Fig. 1B, in pocket, and Fig. 4.3).

The presence of the thin basement slices in the thrust sheets forms a mechanical problem. The detachment fault of the system must have cut at a shallow level in the basement, rather than follow the basement-cover interface, which forms a level of mechanical discontinuity and of strain localization and would be a favourable site for the basal detachment. This will be discussed further in Chapter 5.

The lower thrust system is developed in the basement and contains thrust sheets which are several kilometers thick. Thrusts cut up from this basement thrust belt into the overlying detached sediments, where they cause folding and out-of-sequence thrusting, most notably in domain II (Fig. 1B, sections I and II). The extent of the downward continuation of the sole thrust of this system into the subsurface towards the southeast is not known. Major extensional faulting would be needed during thrusting, to bring the lower detachment from the base of the metasediments in the east, to deep in the basement in the western part of the map. In order to avoid this extensional geometry, which would be mechanically unfavourable and for which there is no evidence, the lower thrust system is interpreted to extend from the west underneath the upper system to the east at progressively deeper crustal levels. The depth to the sole thrust is interpreted to be related to the spacing of the thrusts in the basement at the surface, which is generally in the order of 2 to 5 km and the depth to the sole thrust is expected to be of the same order of magnitude in most of the map area. The basement thrust system is not a leading imbricate fan (Boyer and Elliott, 1982) which would have the largest displacement on the most frontal thrust. The westernmost exposed thrust, the Grenville Front, is a narrow shear zone which does not display indications of a higher strain or larger displacements than other thrusts in domain I. The Grenville Front in the map area is thus not a crustal-scale thrust which reaches to the base of the crust, as is seen in the seismic section across the Grenville Front in Lake Huron and Georgian Bay (Green et al., 1988). However, it is interpreted to join other basement thrusts in a detachment horizon which reaches down into lower crustal levels.

The geometry of the Grenville Front thrust belt in southwestern Labrador is at first approximation not compatible with the thrust belt model presented by Boyer and Elliott (1982), in that its sole thrust does not appear to cut up from basement to cover in the direction of movement. Also the dual character of the lower and upper system is not explained by the Boyer and Elliott (1982) model. However, the development of the foreland fold-and-thrust belt in Gagnon terrane as a result of the emplacement of Molson Lake terrane as the dominant thrust sheet does fit this model. Assuming that the displacement on the floor thrust of Molson Lake terrane is larger than on any thrust in Gagnon terrane (see Chapters 5 and 8), the thrust belt forms a trailing imbricate stack (Boyer and Elliott, 1982)

The present description of the thrust belt also diverges from Rivers' (1983a) thrust belt model for the area. The main difference lies in the increased role of the basement rocks and the absence of a switch of deformation style from dominant thrusting early in the history of the belt to dominant folding later in the development (Rivers, 1983a). A basement buttress at the northwestern end of the belt as proposed by Rivers is not likely to be present there. Two other locations where basement buttresses of a smaller size are present, are the transition from the deeper part of the shelf to the shallower part of the shelf and the transition from the shelf to the continental slope. At these two locations major fault escarpments are expected, as depicted in Figure 3.2, which probably played a role in the folding of the rocks in the Lorraine Lake and Wabush Lake thrust sheets. In Chapter 8 a model will be presented that accommodates the deviations of the geometry of the belt as proposed here, from the existing models. First the details of the geometry, structural relationships, kinematics, metamorphic development and other aspects of the belt are discussed in the ensuing chapters.

## CHAPTER 5

### STRUCTURAL DEVELOPMENT OF THE FOLD-AND-THRUST BELT

The structures on all scales in the map area are related to the northwest-directed thrust movement within the fold-and-thrust belt. The overall structural setting of the rocks in Gagnon terrane is comparable to that in the footwall of a dominant thrust sheet, similar to the model proposed by Boyer and Elliott (1982), but the structures diverge from this model in some important aspects, as discussed in Chapter 4. The main difference is the existence of an upper, sediment-dominated thrust system, in which the thrust sheets range from about 100 m up to about 2 km in thickness, and a lower, basement-dominated thrust system in which the thrust sheets are all several kilometers thick. The emplacement of Molson Lake terrane, which formed the dominant thrust sheet (Boyer and Elliott, 1982), presumably provided the load for the metamorphism and caused the deformation of the rocks in the underlying Gagnon terrane (Connelly, 1991). Thrusts and folds have deformed the rocks in the area and structures of several phases of ductile deformation have been recognized. The subdivision of structures presented below diverges somewhat from that proposed by Rivers (1983a) for Gagnon terrane and a stronger emphasis is placed on the setting of the structures in the thrust belt than on their relative timing.

The first part of this chapter consists of a detailed description of structures in the map area. This is followed, in the second part of the chapter, by an evaluation of the observed geometries. The detailed structural analysis incorporates only the Grenvillian structures. The Archean structures in the basement gneisses and the Early Proterozoic extensional structures of the thinned continental margin are not discussed in detail. Plates in this and the following chapters are grouped together at the end of the chapter.

## 5.1 DETAILED DESCRIPTIONS OF THE STRUCTURES IN GAGNON TERRANE

Several key areas, which are better exposed than most of the map area, were selected to cover different structural and metamorphic settings. These key areas, which are indicated in Figure 5.1, were mapped on a 1:10,000 scale, whereas the remainder of the mapping was done on a 1:20,000 scale (see Chapter 1 and Appendix A). Detailed maps are presented only for the Emma Lake and the South Flatrock Lake areas and a separate map of the Bruce Lake area is included on a 1:50,000 scale (Fig. 2, in pocket), which covers several of the key areas. The locations of the detailed maps and of the Bruce Lake area are also shown in Fig. 5.1. For the remainder of the key areas separate maps were not warranted since they do not reveal more information than the 1:100,000 or 1:50,000 maps (Figures 1A and 2 respectively). Cross sections are presented for all maps. As discussed in Chapter 4, the cross-sections in Figure 1.B show more detail and interpretation than the map of the same scale. As a result there is not a perfect match between the two figures. Variations in the original thicknesses of the formations and the ductile nature and the non-cylindricity of the structures prevented the balancing of the cross sections. Many of the sections were constructed perpendicular to the strike of the structures, which is at an angle to the movement direction. Three cross sections through the whole area (Figure 1B, in pocket) schematically show the relationships between the different thrust sheets and the variations in large-scale structures, both observed and interpreted.

Structural orientation data are presented in Appendix D, plotted in lower hemisphere, equal area projection. The orientation data are generally compiled for fairly large areas, which incorporate many structures, varying from outcrop-scale to hundreds of meters in size. As a result the smaller structures are averaged out into rather nondescript and poorly defined clusters in the stereonet diagrams. A further subdivision of the data into smaller areas would reflect the smaller structures. A summary of the orientation data is presented in Section 5.2. Notations of orientations of planar and linear features used in the thesis are azimuth (dip-direction) / dip (e.g.

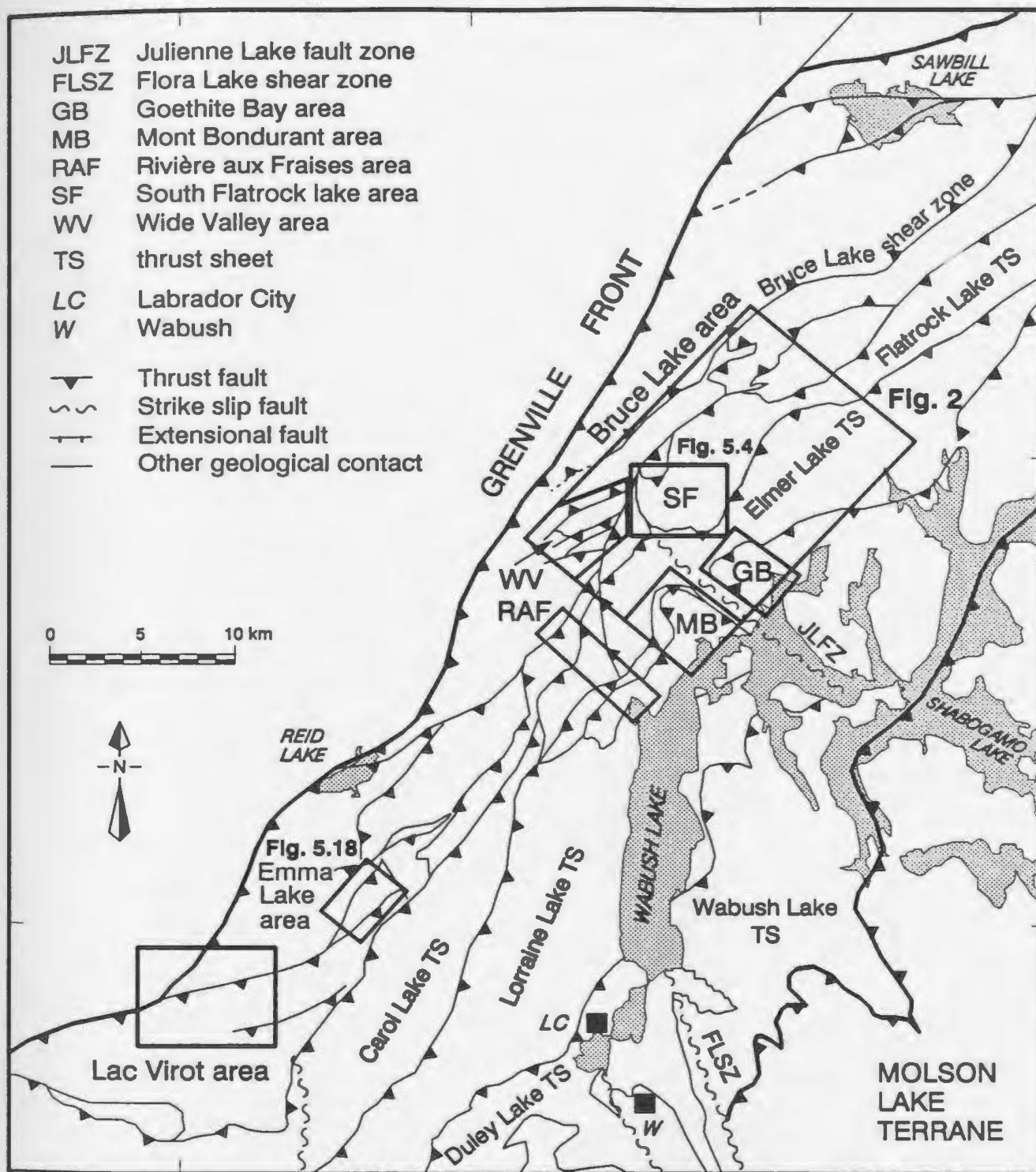
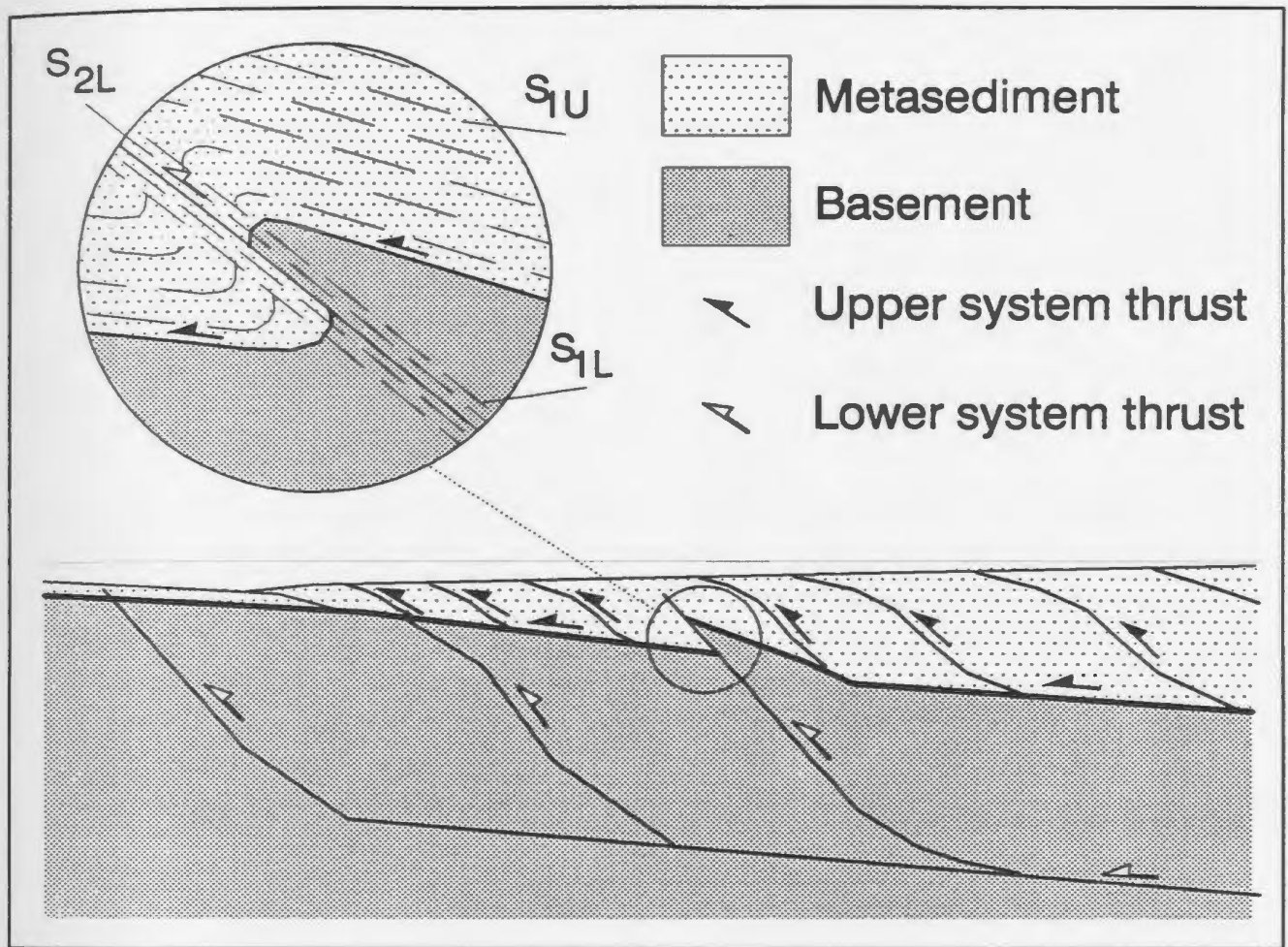


Fig. 5.1 Tectonic map of western Labrador indicating the key areas which were mapped in detail. Names of the major thrust sheets are also shown. The map includes the locations of figures 5.4 and 5.18, as well as the location for Figure 2 (in pocket).

148/78) and plunge -> azimuth (e.g. 34->145) respectively. Locations of all thrust sheets are shown in Figure 4.2, and the larger thrust sheets are also indicated in Figure 5.1. Topographical localities mentioned in the text are indicated in Figure 1.2.

### **5.1.1 NOMENCLATURE AND AGE RELATIONSHIPS OF THE STRUCTURES**

In the map area structures of several different generations were mapped, of which most are genetically closely related. Broadly the structures can be divided into two age groups: 1) those related to the northwest-directed thrusting; 2) those related to the southeast-plunging kilometer-scale cross-folds. Within the thrust-related structures, several generations of overprinting structures were observed, which could not be regionally correlated. The main problem in subdivision of structures in different deformation phases is that the thrust belts are dynamic bodies which constantly change their shapes heterogeneously. Deformation is partitioned into those parts where movement is concentrated or where shape changes are taking place, e.g. as a result of movement of part of a belt over a ramp or localized sticking of the sole thrust, and thrusting, folding and faulting can take place contemporaneously in several parts of a belt, while other parts are passively transported without being deformed. The classical numbering of generations of structures according to their relative age fails in such a case, because it either becomes highly complicated if it is to account for all the localized structures, or if groups of structures are related to processes in a thrust belt, as is done in this thesis, the relative time connotation of the numbering is lost. Coward and Potts (1985) and Holdsworth (1990) reported similar problems of correlating generations of structures in thrust belts. An example of the problems that can arise, is the situation where one generation of early structures affecting the rocks in the upper, sediment-dominated thrust stack in Gagnon terrane ( $D_1$  in a local numbering scheme), is followed by a thrust which cuts up from the basement (where it is a  $D_1$  structure) into the sediments (where it is a  $D_2$  structure). Such a situation is sketched in Fig. 5.2. This type of interference of structures of the lower and higher thrust systems is most common in lithotectonic domain II.



**Fig. 5.2** Schematic example of interference of structures from the upper and lower thrust systems. A thrust from the lower system breaches through its roof and causes out-of-sequence thrusting in the upper sediment-dominated thrust system, which already has a penetrative thrust-related fabric ( $S_{1U}$ ). The deformation related to this thrust that originated in the basement creates first generation structures in the basement ( $S_{1L}$ ) and second generation structures in the overlying metasediments ( $S_{2L}$ ). The subscripts U and L refer to structures that originate in the upper and lower thrust system respectively.

The subdivision of structures used here is based on overprinting relationships on outcrop scale, which means that no regional correlation can be made between equally numbered generations of structures and that the time connotation of the numbers is lost. On the other hand, the common occurrence of similar overprinting patterns throughout the belt suggests that all parts of the belt have gone through similar phases of development. Structures that are grouped together may therefore represent similar processes that took place in different parts of the belt at different times.

The Grenvillian structures are subdivided into: 1) a regionally penetrative foliation  $S_1$ ; 2) structures related to the west-directed thrusting which deform the  $S_1$  foliation ( $D_2$ ); 3) structures related to the large-scale cross folding  $F_3$ . This is a subdivision which is most convenient for use in the field and is based on outcrop-scale overprinting relationships rather than on regional phases of deformation. The  $D_2$  structures in the western part of the area cannot be correlated regionally and they represent a wide variety of ages, types and orientations of structures which formed after the development of the  $S_1$  and during the northwest-directed thrusting event. In lithotectonic domain V the structures are more regionally consistent and can be correlated through the thrust sheets. The  $F_3$  cross-folds postdate all  $D_2$  structures and are related to a different stress field. They dominate the southeastern part of the map, in lithotectonic domain V and Molson Lake terrane, and re-fold the structures in domain IV, but have no obvious effect on the lower domains.

In addition to this subdivision, a separate subscript is used to distinguish between deformation related to either the upper or lower thrust system, in those cases where enough information is available to do so. For structures that originated in the lower level, basement-dominated thrust system, the subscript "L" is added to foliation or fold references (e.g.  $S_{1L}$ ,  $F_{2L}$ ). For those structures that originated in the upper level, sediment-dominated thrust system, the subscript "U" is added (e.g.  $S_{1U}$ ,  $F_{2U}$ ). Wherever no indications existed for linkage of structures to the upper or lower level

system, the extra subscript was omitted. This distinction is mainly used in the detailed descriptions. In the maps and cross sections the distinction between lower and upper system structures was made only in the labelling of the thrust faults.

The majority of the shallow to moderately dipping shear zones in the area repeat parts of the stratigraphy. The near-down-dip elongation lineation, kinematic indicators suggesting northwest-directed movement of the hanging wall, combined with the contractional nature of the shear zones indicate that they are thrust faults. Both regular-sequence and out-of-sequence thrusts were recognized. The definition of these terms is based on local overprinting relationships. A regular-sequence thrust cuts into the footwall of an older thrust. A thrust fault that is younger than a thrust in its footwall is defined as an out-of-sequence thrust, even if the thrust did originate in a regular piggy back sequence. This situation can occur if a regular-sequence thrust breaches the roof thrust of a duplex and cuts into the hanging wall.

### 5.1.2 PRE-GRENVILLIAN STRUCTURES

Basement rocks which have not been affected by a penetrative Grenvillian deformation reveal part of a complex Archean tectonic history. In the high-grade gneisses and migmatites, as well as the amphibolites, structures of at least two generations can be regionally recognized. The older is a penetrative gneissosity, forming a mm to dm-scale irregular banding. This gneissic layering is locally parallel to the axial plane of folds in xenoliths with an even older foliation (Plate 5.1). The gneissosity was folded in generally tight folds which lack an axial planar fabric. The fabrics are coarse and are compatible with the pre-Grenvillian granulite-facies metamorphism. Megacrystic granites of pre-Grenvillian age cross-cut these structures. They are affected by brittle deformation of which the age is unknown.

Another set of pre-Grenvillian structures is poorly documented in the area or elsewhere. These structures are the Early Proterozoic extensional faults which formed during the breakup of the Superior continent. Their geometry presumably controlled the architecture of the continental margin on which the Knob Lake Group sediments were deposited. They appear to exist in the Labrador Trough to the north (Dimroth,

1978; Wardle and Bailey, 1981), but have not been properly documented. In the map area they were recognized near Emma Lake, where they are growth faults, marked by significant differences in thickness of the Sokoman Formation on either side (see section 5.1.7). Rapid changes in stratigraphic thickness and other indirect indications of their existence throughout the map area suggest that such faults are common.

All these structures are overprinted by deformation related to the Grenvillian orogeny. Any further mention in the text of deformation of the basement rocks, or lack thereof, refers to Grenvillian deformation, unless otherwise specified.

### 5.1.3 THE GRENVILLE FRONT

The most westerly observed shear zone in the map area is formed by a several hundred meters wide zone of heterogeneously strained rocks. This shear zone is named Grenville Front in this thesis, but as noted, a lower Grenvillian thrust may exist 5 to 10 km further west (James and Stephenson, 1992); see Section 2.1). The metamorphic grade at the Grenville Front changes from low greenschist facies in the north near Sawbill Lake to upper greenschist facies near Lac Viot in the southwest of the map. At the lowest metamorphic grades in the north of domain I, the basement rocks in the shear zones are almost cataclastic, but in most of the area they form protomylonites, mylonites and ultramylonites (in sequence of increasing strain, containing respectively 10% to 50%, 50% to 90% and 90% to 100% matrix; Sibson, 1977). Generally, the strain increases towards the center of the shear zone. The highest-strain domains in the shear zones form an anastomosing pattern of generally discrete, mm to cm wide strongly foliated zones. They wrap around commonly asymmetric lenses of low-strain rocks on the scale of mm to hundreds of meters. A few ultramylonitic zones of several meters wide were observed. Towards the shear zone boundaries the frequency of these discrete movement zones decreases. The foliation ( $S_{II}$ ) is formed by extremely fine-grained aligned sheet silicates, predominantly chlorite and muscovite. Stretching lineations were observed in only a few locations.

The sense of movement on the Grenville Front is indicated by the asymmetrically anastomosing pattern of foliations and shear bands, often defining S and C planes (Berthé et al., 1979), asymmetric tails or pressure shadows on feldspar porphyroclasts, asymmetric low-strain lenses or asymmetric folds in the shear zones. In combination with the south-southeast plunge of the  $L_3$  (Appendix D, Fig. D.1B, bottom) all kinematic indicators on outcrop-scale suggest oblique, north-northwest-directed thrusting.

The southern part of the Grenville Front in the map area is developed at middle to upper greenschist facies and has a slightly different character. It is well exposed on the northwestern shore of Reid Lake and west of the northern tip of Lac Virot (Fig. 5.1; Fig. 1A, in pocket). At Reid Lake strongly sheared rocks of the basement and Sokoman Formation represent the southwestern extension of the Grenville Front. The higher metamorphic grade is expressed in the fact that biotite is the dominant sheet silicate rather than chlorite (Chapter 7). The shear zone at Reid Lake is between 200 and 500 meters wide and the rocks in it range from protomylonites to ultramylonites. In contrast to the northern part of the Grenville Front, deformation here is more homogeneous throughout the shear zone. Oriented micas, quartz ribbons and pressure shadows around feldspar porphyroclasts define the foliation. All rocks have L-S fabrics in which the lineation is defined by rodded quartz or aligned amphibole needles. S-C planes, shear bands and asymmetric low-strain lenses and pressure shadows indicate an oblique, sinistral-reverse sense of shear, a result of northwesterly directed displacement of the Reid Lake thrust sheet. A large body of high-strain rocks of the Sokoman Formation is incorporated in the shear zone.

Structures in the Grenville Front shear zone have distinct orientations in the two areas. The strike of the Grenville Front, as measured in the map over a length of several kilometers, is  $035^\circ$  north of Bruce Lake, compared to  $050^\circ$  near Reid Lake. A similar difference in orientation is reflected in measurements of foliation planes in and near the shear zone that forms the Grenville Front. Foliation planes were plotted with separate symbols for foliations in high-strain and low-strain domains in and near the

Front (Fig.5.3). High-strain foliations are predominantly penetrative C-planes in mylonites with significant grain size reduction. Low-strain foliations are predominantly S-planes that are formed by preferred orientations of micas and elongated quartz grains or small fractures in rocks that have not been affected by significant grain-size reduction. The numbers of measurements are low so the mean orientations of clusters of data points are approximate. Nevertheless, the patterns are believed to be significant, because they are similar to those in the adjacent areas (see Appendix D)

Near Bruce Lake the foliation planes plot in two clusters which are separated by 35 to 45° (Fig. 5.3a). Orientations of foliations in the high strain domains within the shear zone are different from those in both low strain lenses and outside the main part of the shear zone, where the rocks reveal lower strain levels. These two orientations (125/55 for the high strain foliations and 170/65 for the low strain foliations) are similar to the orientations of two sets of S and C planes in the shear zone (Fig. 5.3a). The strike of the Grenville Front between Bruce and Sawbill lakes coincides with the strike of the high-strain foliations in the shear zone. The mean orientation of the foliations in the high-strain domains (where S and C-planes are virtually parallel) is assumed to represent the bulk flow plane, parallel to the orientation of the Grenville Front shear zone on a large scale.

Foliations measured in the shear zone near Reid Lake show a different distribution pattern (Fig. 5.3b). They are concentrated in a single cluster with two sub-maxima, which show a weak separation of high-strain and low-strain foliations, in orientations similar to those near Bruce Lake, but closer together (separation 20 to 30°). The sub-maximum containing predominantly high-strain foliations is sub-parallel to the map-scale strike of the Grenville Front and is also interpreted to represent the flow-plane and the orientation of the shear zone. The smaller angle between the two clusters may indicate a higher accumulated strain, which resulted in greater progressive rotation of the foliation planes towards the flow plane. The scatter of the foliation planes is thought to be caused by the anastomosing pattern of the foliation in the shear zone.

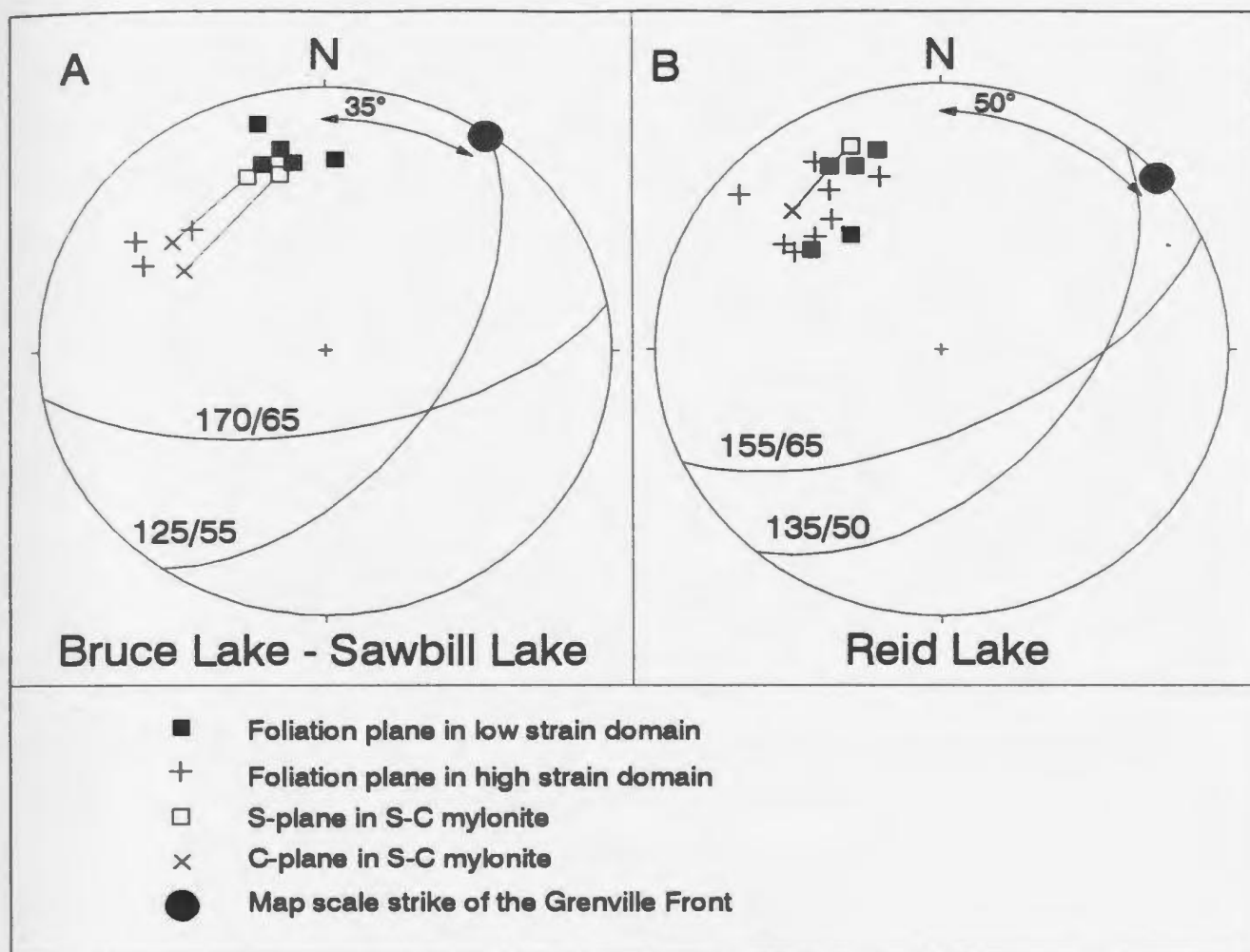


Fig. 5.3 Orientations of poles to foliation planes from two parts of the Grenville Front, northwest of Bruce Lake to Sawbill Lake (A) and west of Reid Lake (B). The foliations are plotted separately as measured in high-strain and low-strain rocks. Definitions of high-strain and low-strain foliations are given in the text. S and C planes measured in one outcrop of an S-C mylonite are connected with lines. The great circles represent the approximate orientations of the two (sub-) clusters. The strike of the high-strain foliation is virtually parallel to the Front in both places and is interpreted to represent the flow plane of non-coaxial shear. Plotted in lower hemisphere, equal area projection. See text for further discussion.

The orientations of S and C planes and high and low strain foliations in both plots in Figure 5.3 suggest an oblique reverse movement with a large component of strike-slip. The general south-southeast plunge of the extension lineations is in agreement with this conclusion. The difference in orientation of the structures in the two parts of the Grenville Front are due to either an heterogeneity of the stress field, or to the fact that the orientations of the shear zones were determined by pre-existing structures, such as pre-Grenvillian extensional faults, which were originally non-parallel. The dip of the Grenville Front, as indicated by the foliation in the high strain domains, is moderately steep (50 to 55°), which is in accord with the oblique-slip nature of the shear zone.

#### 5.1.4 STRUCTURES IN THE LOWER THRUST SHEETS, DOMAINS I, II, III AND IV

The oldest Grenvillian structural element that can be recognized in the field is the  $S_1$  schistosity, which is pervasive in the metasediments, but in the basement rocks in domain I is concentrated in shear zones. The  $S_1$  commonly has a mylonitic character and kinematic indicators combined with a stretching lineation ( $L_3$ ), which is well developed in medium to high-strain rocks, suggest a component of simple shear, moving the upper block to the northwest. Both S and C planes were recognized. Specifically in the high strain zones the observed foliations are predominantly C-planes. Boudins in the iron formations, extreme flattening of grains as well as shear band cleavage in the mica schists indicate a large component of extension during shear movement. The  $S_1$  foliation is sub-parallel to the bedding in the metasediments, both dipping shallowly to moderately to the southeast. In the majority of the locations where an angular relationship between the two could be determined, the foliation was steeper than the bedding, indicative of a northwestern vergence of the structures. The orientations of  $L_3$  lie in the southeast-dipping  $S_1$  plane with a strong maximum in the SSE. The orientation ranges from down-dip in the  $S_1$  plane to oblique with a southerly pitch.  $F_1$  folds have an axial planar foliation defined by  $S_1$  and are generally tight to isoclinal and asymmetric.  $F_1$  folds axes are curvilinear and generally plunge SSE. In

the thrust sheets of the upper level system the  $S_{1U}$  foliation is pervasive, but the strain increases towards the shear zones which form the thrusts. In the lower level thrust system, the  $S_{1L}$  foliation is concentrated in the shear zones and is not penetrative on outcrop scale in the interior of the basement thrust sheets.

All structures deforming the  $S_1$  foliation are grouped together in  $D_2$ , even though they represent a wide range of relative ages of formation.  $D_2$  structures are mainly folds, or fold nappes, which also show a variation in fold-axis orientations, but the maximum orientations are commonly shallowly south- to southwest-plunging. These folds are asymmetric, northwest-vergent and the axial planes dip moderately to steeply to the southeast. In the thrust sheets of lithotectonic domain II the  $F_2$  folds are commonly related to fold nappes which appear on a scale ranging from centimeters to hundreds of meters. In the basement rocks of domain I  $F_2$  folds are found only in shear zones in the southern part of the map area, in the Reid Lake and Lost Lake thrust sheets.

All Grenvillian structures in the area are formed by ductile deformation, with only a few exceptions. The ductile nature of the deformation is discussed in more detail in Chapter 6. All kinematic indicators of both  $D_1$  and  $D_2$ , in the upper and the lower thrust system indicate northwest-directed movement. The kinematic indicators are discussed in more detail in Chapter 6.

### 5.1.5 BRUCE LAKE AREA

Figure 2 (in pocket) shows the geology of the Bruce Lake area. Parts of the area were described previously by van Gool et al. (1987a and b, 1988a and b, 1989). It comprises parts of lithotectonic domains I, II, III and IV and covers the Bruce Lake, Corinne Lake, Flatrock Lake, Wide Valley, Elmer Lake, Goethite Bay thrust sheets and the northern part of the Lorraine Lake thrust sheet. The structures in the different levels of thrust sheets are discussed in sequence, from the lowest in the west to the highest in the east.

### 5.1.5.1 Basement rocks

Most of the basement rocks in domain I are not affected by a penetrative Grenvillian deformation visible on outcrop-scale, except in the shear zones that cut them and in the cores of fold nappes. The basement rocks originally have an Archean coarse gneissic banding (Plate 5.1), which in most areas dips steeply either north or south and is folded over moderately east-southeast-plunging fold axes and subvertical east- to southeast-striking axial planes, which are also of Archean age (Appendix D, Fig. D.1B). In areas of penetrative Grenvillian overprint these orientations change, e.g. in the Emma Lake area (Appendix D, Fig. D.1B).

The shear zones in domain I have identical characteristics to the shear zone that forms the Grenville Front and likewise show slight variations with increase in metamorphic grade from northeast to southwest. Orientations of the  $S_{1L}$  foliation planes are similar to those of the Grenville Front (cf. Fig. D.1B, bottom and Fig. 5.3) and show approximately the same concentrations of data in a steep low strain and a somewhat shallower high strain cluster as in the northern part of the Grenville Front, suggesting the same movement pattern. Elongation lineations are more common and plunge south-southeast, slightly oblique in the high strain foliation plane (Fig. D.1B).

Deformation of the basement rocks inside the thrust sheets in domain I is generally negligible on outcrop scale. However, close inspection shows a poorly defined  $S_{1L}$  fabric consisting of preferentially oriented microfractures. At higher metamorphic grades the fractures change to microshears, which are coated with microscopic micas (see Chapter 6). The density of the microshears increases with strain. East of Bruce Lake, the strain in the basement rocks is higher than in the remainder of Domain I. Minor shear zones are spaced at hundreds of meters and form a small imbricate thrust stack, whereas the rocks in between have a weak but pervasive  $S_{1L}$  fabric.

### 5.1.5.2 Bruce Lake shear zone

A shear zone of several hundreds of meters width, consisting of protomylonites, mylonites and ultramylonites, runs along the west shore of Bruce Lake. The rocks in this shear zone have identical characteristics to those in other shear zones elsewhere in the basement. The Bruce Lake shear zone forms a zone of well-foliated, high-strain rocks and contains several low-strain lenses ranging from tens of meters to hundreds of meters in size. Feldspar porphyroclasts are common in the shear zone and they are quite angular (Plate 5.2). Locally, near the Wide Valley area, quartz porphyroclasts are common. At two bends in the shear zone slices of moderately deformed rocks of the Sokoman Formation occur at the southeastern boundary. The Bruce Lake shear zone can be mapped for at least 20 km along strike, but is inferred to extend at least 15 km further to the northeast (cf. James and Stephenson, 1992).  $S_{1L}$  in the shear zone, predominantly formed by C-planes, is steeply ESE-dipping to vertical with a stretching lineation which plunges steeply SSE (Fig. D.1C). S and C planes, shear bands and tailed porphyroclasts indicate an oblique dextral-normal sense of movement, suggesting that the shear zone has an extensional geometry in its present orientation. However, in section 5.3.2 it is argued that the Bruce Lake shear zone is an overturned backthrust.

### 5.1.5.3 Corinne Lake and Flatrock Lake thrust sheets

Structures in the Corinne Lake and Flatrock Lake areas are similar and are discussed together. The southern part of the Flatrock Lake thrust sheet is the best exposed part of the map area and many of the field examples of structures in the lowest thrust sheets are taken from there. The good exposure warranted making a separate detailed map and cross sections of the South Flatrock Lake area (Figures 5.4 and 5.5). Figure 2 (in pocket) covers the Corinne Lake thrust sheet and the central part of the Flatrock Lake thrust sheet.

These two lowest thrust sheets of domain II consist of rocks from the middle and upper (quartz-oxide and carbonate) members of the Sokoman Formation and graphitic schists of the Menihok Formation, as well as thin sheets of strongly deformed basement rocks in the Flatrock Lake thrust sheet and inliers of less deformed basement rocks in

# LEGEND

## Lower Proterozoic



**Menihek Formation**

*Graphitic and garnetiferous biotite schists*



**Sokoman Formation**

*Banded iron formations*

## Archean



**Ashuanipi Metamorphic Complex**

*Gneisses, migmatites and granites*

## SYMBOLS



**Bedding (inclined, vertical, overturned)**



**S<sub>1</sub> foliation (inclined, vertical)**



**S<sub>2</sub> axial plane**



**F<sub>1</sub> fold axis or intersection lineation**



**F<sub>2</sub> fold axis**



**Stretching lineation**



**Antiform, synform, with direction of plunge**



**Overturned antiform, synform, with direction of plunge**



**Geological contact (defined, approximate)**



**Thrust fault, upper system or unspecified (defined, approximate)**



**Thrust fault, lower system (defined, approximate)**



**Mylonitic foliation**



**High angle fault (defined, approximate)**



**Location of cross section**

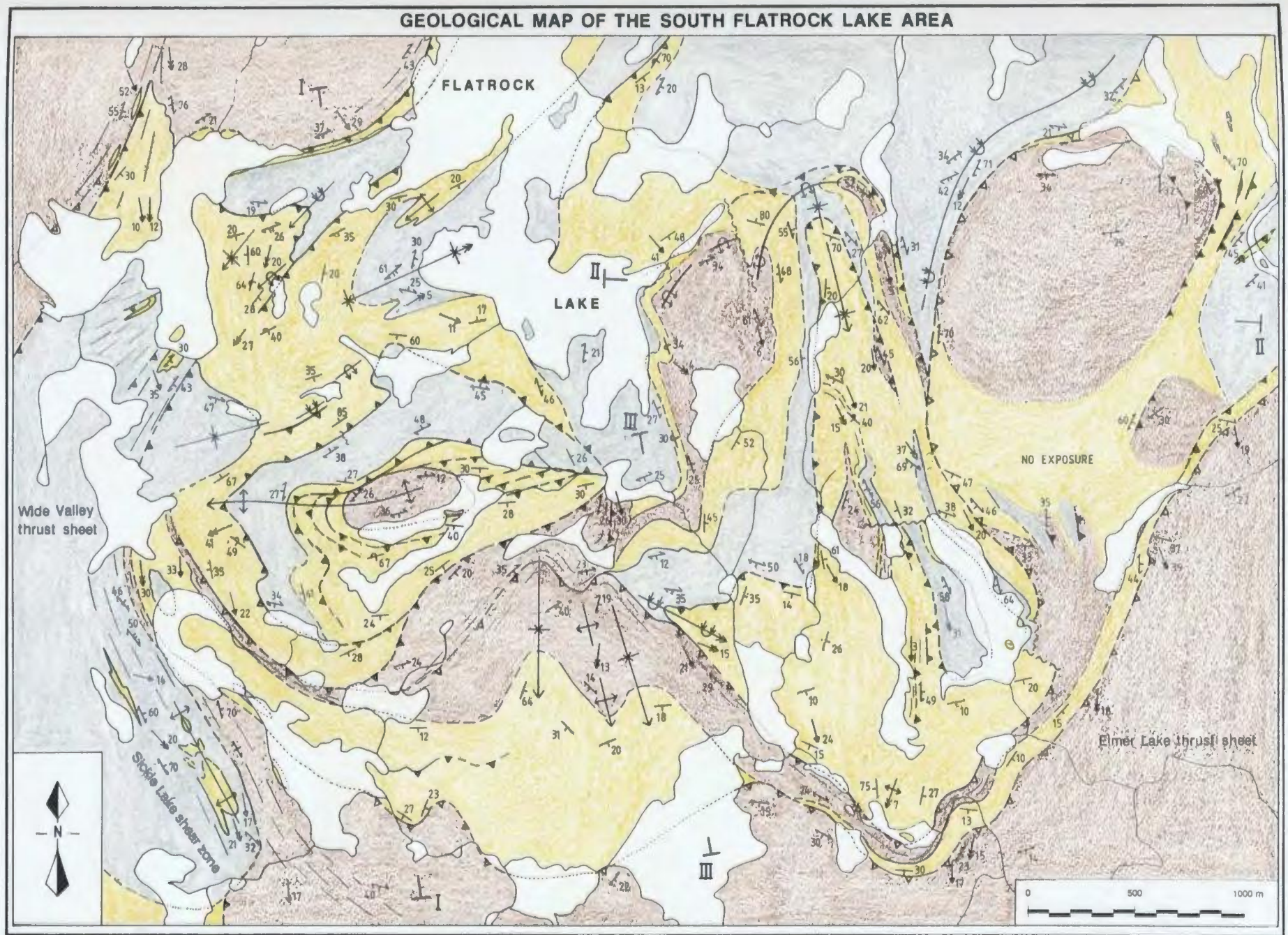


Fig. 5.4 Detailed map of the southern Flatrock Lake area. Cross sections I, II and III are shown in Figure 5.5.

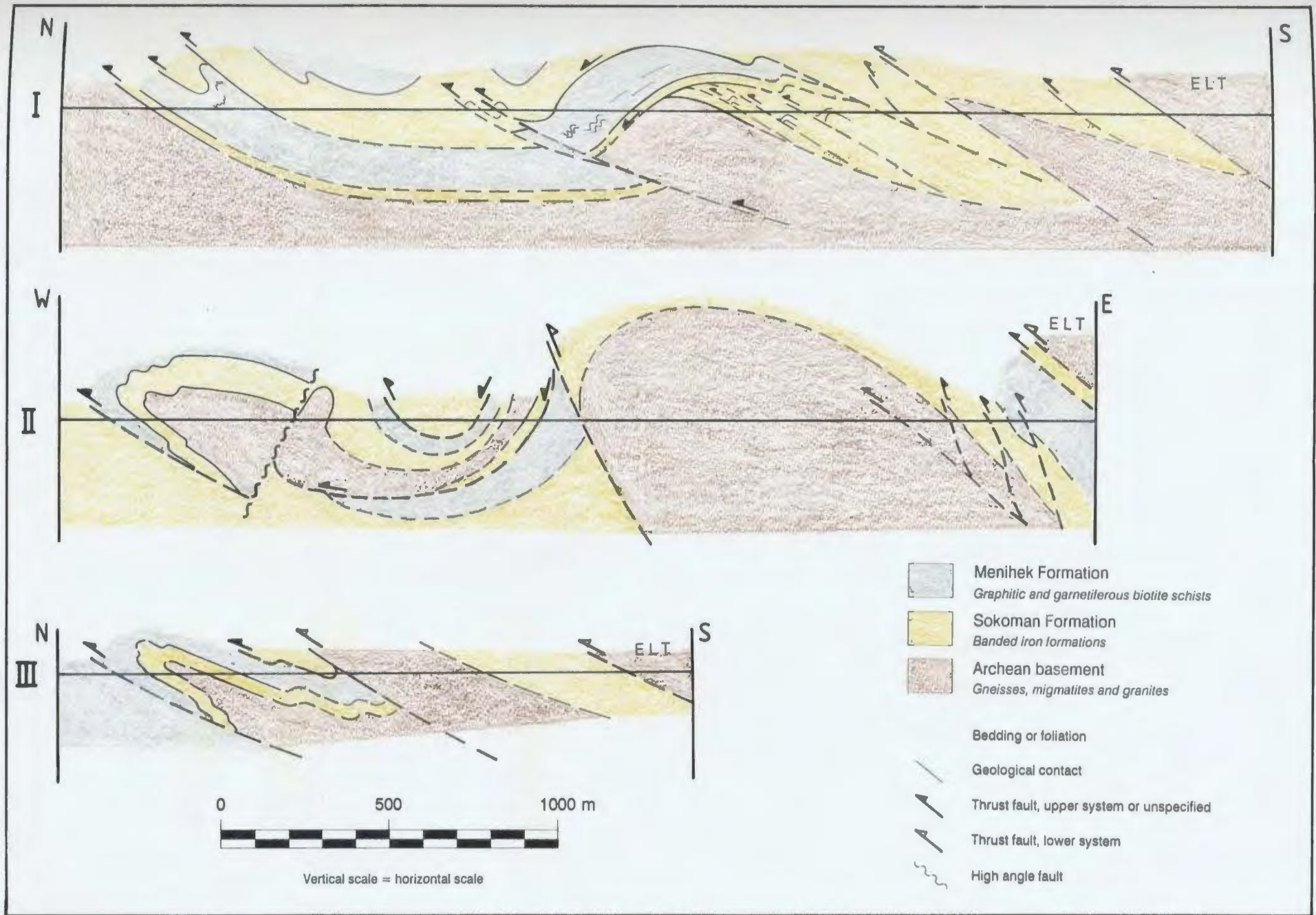


Fig. 5.5 Schematic cross sections through the southern part of the Flatrock Lake area. The sections are not parallel to the movement direction and are not balanced. They incorporate information from both sides of the sections, which was projected along the plunge onto the plane of the sections. Locations of the sections are shown in Figure 5.4. ELT = Elmer Lake thrust sheet.

both thrust sheets. These rocks are deformed by imbricate ductile thrusts and folded in generally northwest-vergent folds. Thrusts are either shallowly southeast-dipping, related to the upper thrust system, or steeply southeast-dipping and related to the lower thrust system. The regionally penetrative  $S_{1U}$  foliation is associated with the shear zones, but not restricted to them. Overall, the strain of the rocks increases from the Corinne Lake thrust sheet in the north towards the southern part of the Flatrock Lake thrust sheet.

### Small-scale structures

The  $S_{1U}$  in the Menihok Formation forms a schistosity of aligned micas and flattened quartz grains, locally resembling a slaty cleavage. Zones of high shear-strain are characterized by an anastomosing shear band cleavage. In the Sokoman Formation the character of the foliation varies with the rock type, but it is generally formed by flattened quartz or carbonate grains, aligned specular hematite or flattened concretions of siderite (commonly replaced by limonite), which are nearly spherical in rocks of very low strain and provide excellent strain indicators. With higher strain the foliation becomes more intense and finer spaced and especially quartz-rich rocks take on a platy fabric (Plate 5.3). In rocks with interlayered carbonate and quartz-rich bands, the carbonate layers are progressively boudinaged with increasing strain (Fig. 5.6, Plate 5.4). Quartz or ankerite/dolomite usually fills the boudin necks. Locally the boudins are rotated, suggesting a component of simple shear during flattening (Fig. 5.7; Goldstein, 1988). In zones of very high strain, the boudins form isolated lenses of carbonate material surrounded by a platy, mylonitic matrix which can form kinematic indicators (Plate 5.3). Rocks in the thin basement slices are virtually all strongly deformed and show a range of strain intensities from protomylonite to ultramylonite. The foliation is defined by fine-grained, aligned micas, quartz-ribbons, pressure shadows around porphyroclasts and by lenses of lower-strain material. S and C planes commonly form an anastomosing network. Feldspar and less commonly quartz form angular to rounded porphyroclasts. Phyllonites are formed in the highest-strain rocks and generally contain shear bands, which together with the phyllonitic foliation define

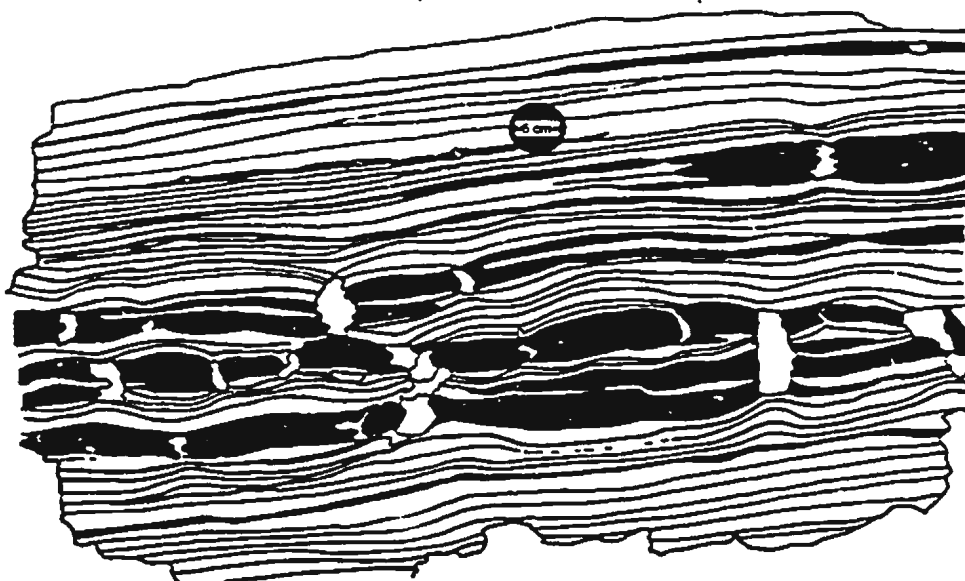


Fig. 5.6 Boudins and pinch and swell structures in the banded Sokoman Formation in the southern part of the Flatrock Lake thrust sheet. The black layers are carbonate lithologies (mainly siderite), the remainder of the rock is thinly banded quartzite with thin carbonate seams. Boudin necks (in white) consist of dolomite and quartz. The diameter of the lens cap near the top of the outcrop is 5 cm. Traced from a photograph.

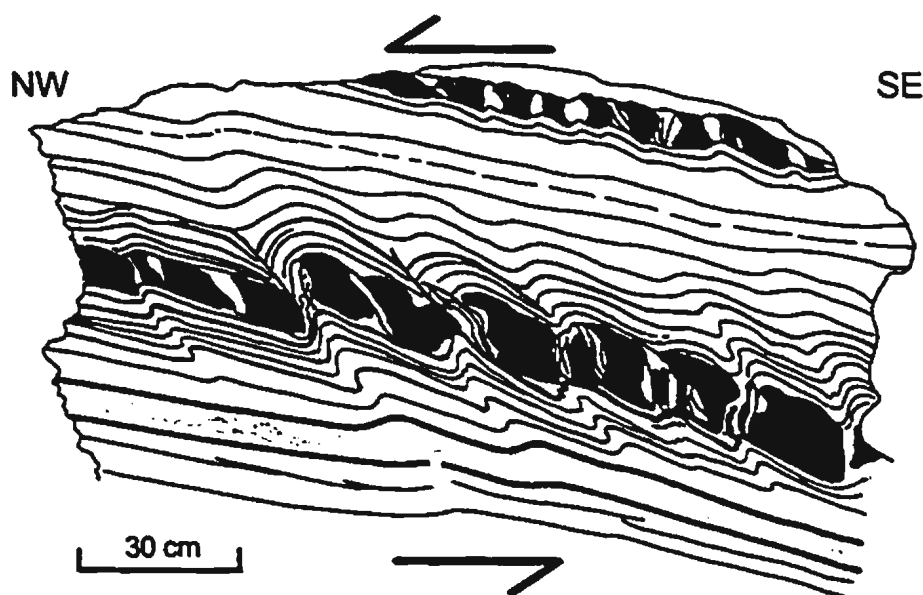


Fig. 5.7 Asymmetric boudins and folds in banded Sokoman Formation near the southern end of Flatrock Lake. The boudins consist of carbonate-rich material (mainly siderite). The boudin necks are filled with dolomite and the surrounding rock consists predominantly of quartzite interbedded with thin carbonate layers. Asymmetry of the folds and boudins indicates northwest-directed movement. Note the decrease of the number of layers from left to right between the main boudinaged carbonate layer and the shaded layer underneath, indicating the presence of a footwall ramp underneath the boudinaged layer. Traced from a photograph.

an anastomosing pattern (Plate 5.5). The basement rocks in these thin slices in lithotectonic Domain II are more homogeneously deformed than in Domain I, where strain localization is more common. The deformation of the rocks in the large basement inliers is more similar to that in Domain I, although they generally contain a weak foliation of oriented micas or micro shears.

The intensity of the  $S_{IV}$  foliation, and thus the strain, increases towards the thrusts, which are formed by ductile shear zones. The subsidiary ductile thrusts, which repeat the stratigraphy within the lower thrust sheets are commonly up to several meters wide and have a well developed mylonitic fabric, which, especially in the basement rocks, is characterized by reduced grain sizes. The displacement on these thrusts is in the order of tens to hundreds of meters. The thrust sheet boundaries are formed by high-strain, ductile shear zones which are tens of meters to more than 100 meters in width and which show multiple repetitions of thinned stratigraphy on the scale of meters to several tens of meters. The repetitions are not always systematic, suggesting that either out-of-sequence thrusting took place or that deformation was strongly heterogeneous. Asymmetric shapes of outcrop-scale low-strain lenses (Fig. 5.8), pressure shadows or tails around porphyroclasts, asymmetric boudins (Fig. 5.7) and shear band cleavage (Plate 5.5) consistently indicate a northwest-directed, reverse sense of shear. Displacement on these thrusts, which form the sole thrusts of the thrust sheets, is estimated to be in the order of kilometers to tens of kilometers.

Most rocks in the lower thrust sheets, except schists of the Menihok Formation, are L-S tectonites. A well developed mineral- or stretching lineation ( $L_2$ ), which is down-dip in the foliation plane, or slightly oblique with a southerly pitch, is common throughout the area, but is more pronounced in the higher-strain zones. The  $L_3$  is oriented quite consistently throughout the area and has a shallow south-southeasterly plunge. In the quartzites the lineation is defined by elongated or rodded quartz grains (Plate 5.6). Alignment of amphiboles (grunerite or cummingtonite in the Sokoman Formation and actinolite in the basement rocks), elongated carbonate minerals or pressure shadows around porphyroclasts form the  $L_3$  in most other rock types. At very

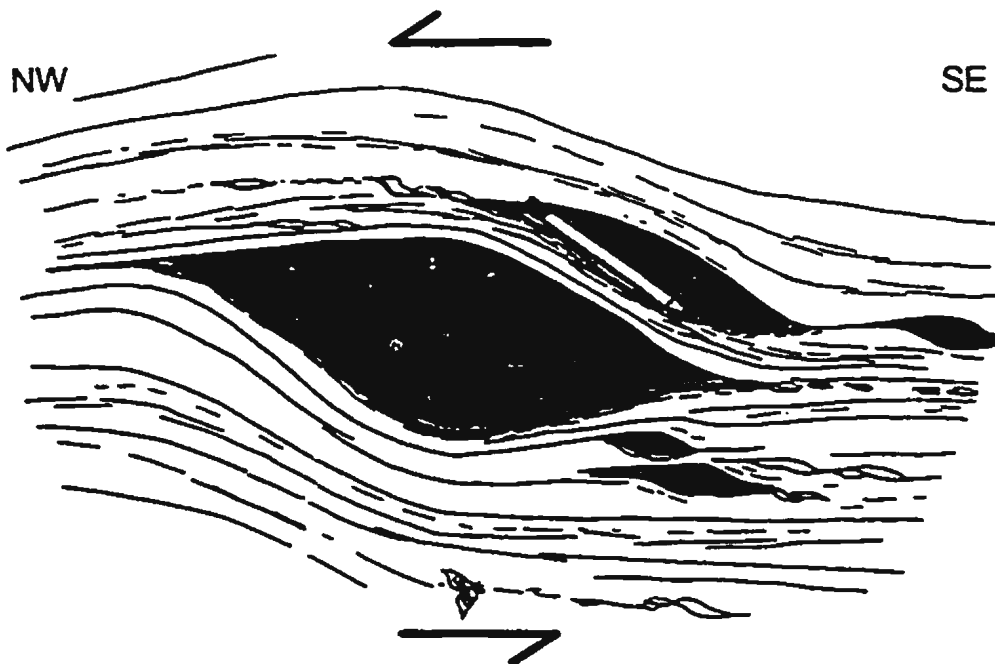


Fig. 5.8 Low strain lens of basement rock in mylonitic reworked basement in a ductile thrust in the Goethite Bay area. The shaded material consists of low-strain granitic basement. The remainder is biotite schist. Most of the low-strain lenses and porphyroclasts are asymmetric in shape and indicate northwest-directed thrust movement. Moth with wingspan of about 4 cm, at bottom of outcrop for scale. Traced from a photograph.

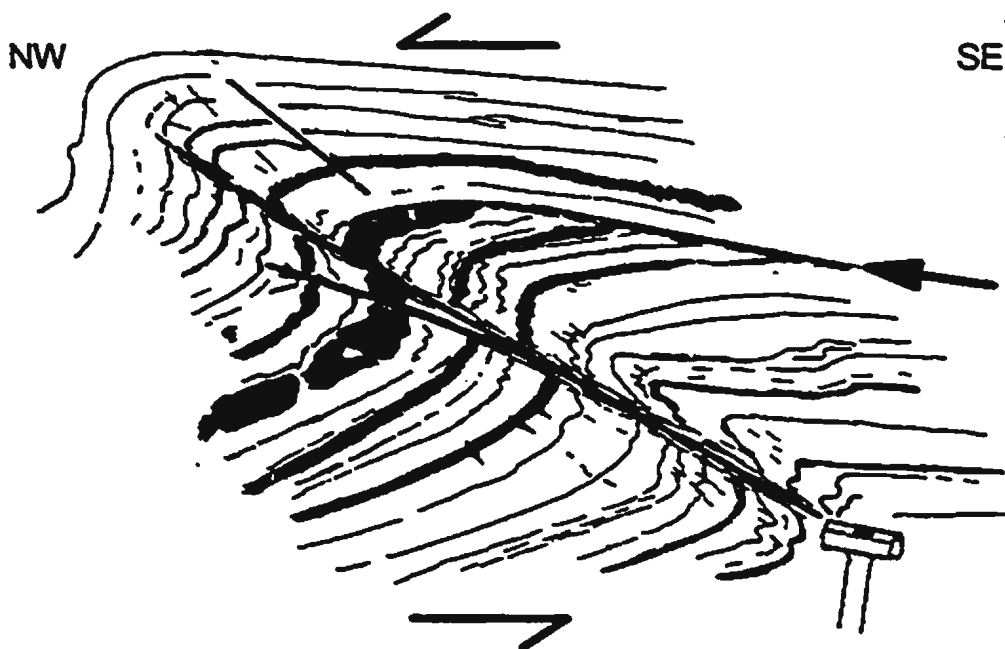


Fig. 5.9 Sketch of outcrop containing two generations of reverse faults in rocks of the Sokoman Formation at the southern end of the Flatrock lake thrust sheet. The older  $D_{1U}$  fault (at arrow) cuts at a small angle through the bedding in a footwall ramp at the right hand side of the outcrop, but is parallel to the bedding in a flat on the left. The younger reverse fault is steeper and is associated with an  $F_2$  fold. Traced from a photograph.

high shear-strains the lineations can become dominant and form  $L > S$  tectonites. Elongation lineations are not well developed in the schists of the Menihek Formation, presumably as a result of insufficient prismatic minerals.

Small intra-formational  $D_{1U}$  thrusts were observed in several outcrops and examples are shown in figures 5.7 and 5.9. In the latter, a fault (at arrow) cuts at a low angle through bedding in a footwall ramp and becomes parallel to bedding in both footwall and hanging wall in the flat at the left part of the outcrop. Both the bedding and the thrust fault were folded by a younger  $D_2$  structure. These early reverse faults can only be recognized where they form ramps, or where they repeat the stratigraphy. In the flats within the Sokoman Formation they cannot be recognized. Presumably such faults are abundant on a wide range of scales. They may be an important factor in the thickening of the formations and hamper estimation of original thicknesses.

The  $S_{1U}$  foliation planes are generally oriented sub-parallel to  $S_0$  (the sedimentary layering), and both dip shallowly to the south-southeast (Figures D.1D, D.1E and D.1F).  $F_{1U}$  folds have an  $S_{1U}$  axial planar cleavage and most are asymmetric, isoclinal, intrafolial folds (Fig. 5.10 and 5.11), which suggests that bedding planes have been transposed towards the  $S_{1U}$ .  $F_{1U}$  folds are not common. In the few outcrops where a distinct angle between  $S_0$  and  $S_{1U}$  exists,  $S_{1U}$  is the steeper of the two.  $F_{1U}$  fold axes and  $S_0$ - $S_{1U}$  intersection lineations are curvilinear and have variable orientations which lie in a shallowly south-dipping plane, with a maximum in the south-southeast, close to that of the  $L_3$  (Figures D.1D, D.1E and D.1F). Sheath folds are common in high-strain zones (Fig. 5.12), where they are interpreted to have formed during progressive simple shear by re-orientation of passive  $F_{1U}$  fold axes, which were originally at a high angle to the direction of shear, towards the axis of elongation (Cobbold and Quinquis, 1980).

The general northwest-vergence of  $F_{1U}$  folds, as proposed by Rivers (1983a), is not in agreement with this orientation of the fold axes. The original vergence was lost by the reorientation of the fold axes, but in rock faces parallel to the elongation lineation, at small angles to the fold axes, northwest-vergent asymmetries are more common than south-vergent ones.



Fig. 5.10  $F_{1U}$ - $F_{2U}$  fold interference in rocks of the Menihok Formation at the northern end of Flatrock Lake. The graphitic biotite schist (dashed) has a strong  $S_{1U}$  schistosity which is axial planar to isoclinal  $F_{1U}$  folds with angular fold hinges. The enveloping surface of  $S_{1U}$  in the sketch is about horizontal. Quartzo-feldspathic layers (in white) do not show a clear foliation. The contact between the two is assumed to represent bedding ( $S_0$ ).  $F_{2U}$  folds, with axial planes dipping to the left, refold the  $F_{1U}$  folds and the  $S_{1U}$  schistosity, resulting in a complex fold interference pattern. Traced from a photograph.

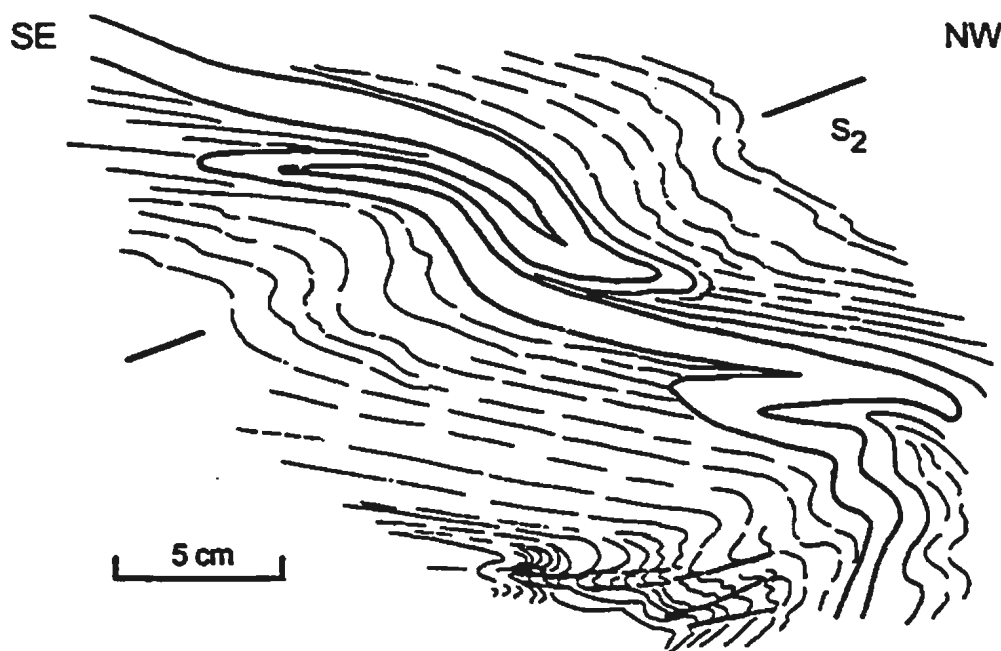


Fig. 5.11  $F_{1U}$ - $F_{2U}$  fold interference in rocks of the Sokoman Formation in the Wide Valley area. A quartz-rich layer in a well foliated quartz-carbonate matrix is folded in isoclinal  $F_{1U}$  folds. The  $S_{1U}$  schistosity forms the dominant foliation in the surrounding rocks and is axial planar to the  $F_{1U}$  folds. Younger  $F_{2U}$  folds, with an axial plane that dips shallowly to the left, caused a fold interference pattern. In the bottom right-hand corner an  $S_{2U}$  crenulation cleavage is developed. Note that both generations of folds are northwest-vergent.

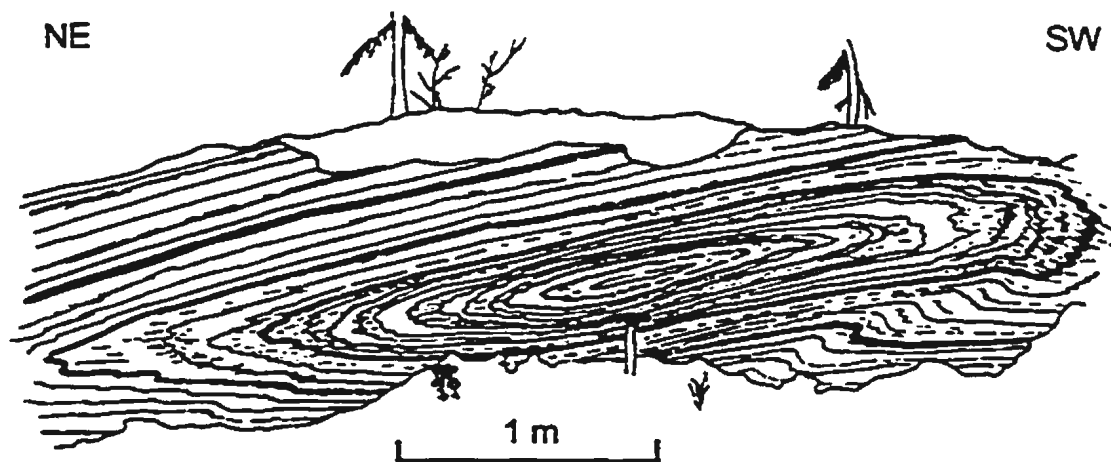


Fig. 5.12  $F_1$  sheath fold in the Sokoman Formation in the Sickle Lake shear zone, south of the Flatrock Lake thrust sheet. The fold axis of this fold, like most other folds in the shear zone, is parallel to the stretching lineation, parallel to the direction of view. Note the  $F_2$  fold in the bottom right-hand corner of the outcrop. Traced from a photograph.

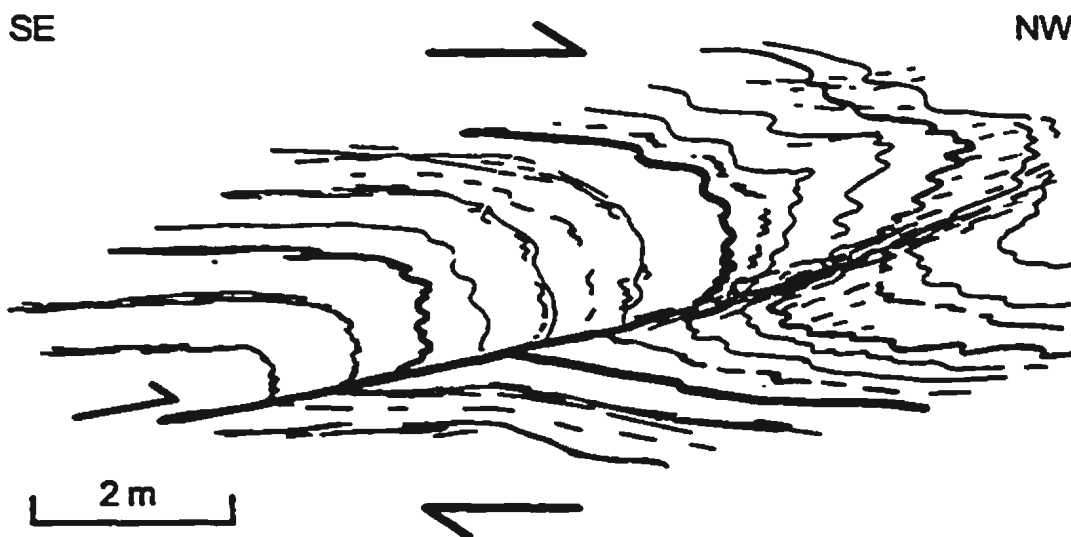


Fig. 5.13 Field sketch of a fold nappe in banded rocks of the Sokoman Formation, southwest of Flatrock Lake. The sketch is composed from several smaller outcrops. The reverse fault in the left part of the diagram changes into an asymmetric fold towards the right. Both a hanging wall anticline and a footwall syncline are developed.

A second generation of structures is characterized by asymmetric  $F_{2U}$  folds, which are predominantly northwest-vergent. They overprinted  $F_{1U}$  folds and folded the  $S_{1U}$  foliation, as well as the  $L_{1U}$  and  $L_3$  lineations (Fig. 5.10 and 5.11). The geometries of  $F_{2U}$  folds vary widely, but the majority of them are similar folds which lack an axial planar cleavage and have interlimb angles between  $60^\circ$  and  $90^\circ$  (Plates 5.4 and 5.7). Most of the  $F_{2U}$  folds have shallowly plunging fold axes, axial planes dipping between  $30$  and  $60^\circ$  and are commonly overturned. The  $S_{2U}$  dip-directions are similar to the  $S_{1U}$ , but they are  $10$  to  $40^\circ$  steeper. Locally in the Sokoman Formation, especially in the Corinne Lake thrust sheet, folds have axial planar foliations consisting of widely spaced parallel quartz veins, indicating extension in the outer part of the fold hinge. In zones of  $D_{2U}$ -strain in schists of the Menihek Formation and in phyllonites in the basement or the Sokoman Formation,  $S_{2U}$  forms a crenulation cleavage which is axial planar to  $F_{2U}$  folds (Fig. 5.10). At high  $D_{2U}$ -strain this crenulation cleavage has become the dominant cleavage in the rocks and locally obliterated the  $S_{1U}$  foliation, forming a transposed schistosity. In a few locations several generations of  $F_{2U}$  folds of similar style formed overprinting patterns. These multiple generations of  $F_{2U}$  folds presumably developed during one progressive deformation event. Locally  $F_{2U}$  folds formed hanging wall anticlines or footwall synclines and are obviously directly related to the thrusting. Figure 5.9 is a line drawing of an  $F_{2U}$  fold which sheared through along the axial plane to form a small fold nappe. An older  $D_{1U}$  thrust fault, indicated by the solid arrow, is affected by the  $F_{2U}$  folding. Similar fold nappes exist on the scale of tens of meters throughout the Flatrock Lake thrust sheet (e.g. section I in Fig. 5.5).

Figure 5.13 is a sketch of such an  $F_2$  fold nappe on a larger-scale in the southern part of the Flatrock Lake thrust sheet. A reverse fault with a hanging wall antiform and a footwall synform changes in the direction of movement into a ductile, asymmetric, northwest-verging  $F_2$  fold. The fault changes from left to right from a brittle fracture to a zone of thin-platey or schistose rocks which increases in width from a centimeter to approximately ten centimeters and changes into a zone of intense crenulation with a well developed axial planar cleavage. Towards the northwest the high-strain zone dies

out in a widening zone of progressively less intense and more open folding. In the high-strain zone a new post- $S_{1U}$  foliation is formed. These fold nappes are either restricted to the sediments and form true  $D_{2U}$  structures, or they form at the tips of thrusts that cut into the sediments from the lower thrust system and are  $D_{2L}$  structures. In only few cases was it possible to establish this link to either the lower or the upper thrust system.

The wide variety of styles and multiple generations of post- $S_1$  folds suggests that they formed under varying conditions during an extended period of thrusting.

$F_{2U}$  fold axes are curvilinear and show a wide spread of orientations within a shallowly south dipping plane (Figures D.1D, D.1E and D.1F). In the lowest-strain rocks they generally plunge shallowly to the southwest, almost orthogonal to the north-northwest movement direction of the thrust belt. With increasing strain the fold axes progressively rotated towards orientations parallel to the elongation axis in the south-southeast. In the shear zones  $F_{2U}$  folds locally form sheath folds. In the Corinne Lake thrust sheet, the  $S_0$  and  $S_{1U}$  were folded over shallow, south-southeast-plunging  $F_{2U}$  and  $F_{2L}$  fold axes, of which the latter are related to thrusting in the basement.

#### Large-scale structures

In the Corinne Lake thrust sheet and the central-western part of the Flatrock Lake thrust sheet the metasediments are detached from the underlying basement (Fig. 5.5, section I; Fig. 5.14 section D), as suggested by the high-strain zone at the contact between the two units. However, locally thin sheets of basement rocks are incorporated into the Flatrock Lake thrust sheet. This is most common towards the trailing edge, where the floor thrust lies within the basement. The basement-cover contacts in this part of the thrust sheet are nonetheless strained, presumably as a result of strain incompatibility, and small shear zones splay off the contact (Fig. 5.5, section I).

In the Corinne Lake area the metasediments are folded in a series of northwest-vergent folds on the scale of tens to hundreds of meters (Fig. 5.14, section I;

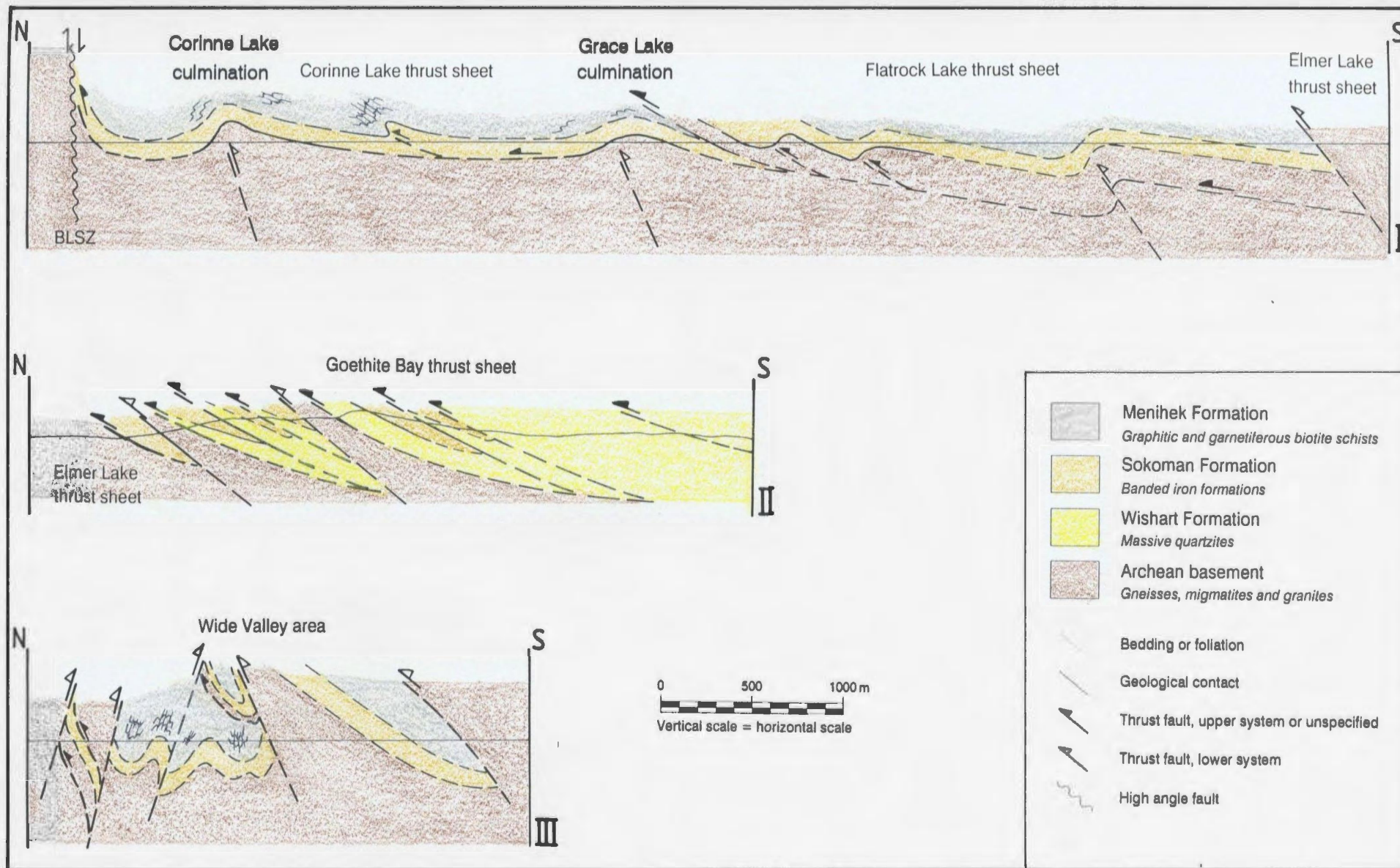


Fig. 5.14 Schematic cross sections through the Bruce Lake area. Topographic relief is negligible, except in the Goethite Bay area (section II). BLSZ = Bruce Lake shear zone. Locations of the sections are shown in Figure 2 (in pocket).

Map 2). There is no thrust repetition within the thrust sheet. The northwest boundary of the thrust sheet is formed by the Bruce Lake shear zone, along which the metasediments are folded in a synform to accommodate the movement on the shear zone. Two basement culminations, consisting of low-strain basement rocks, occur as windows in the area, the smaller, western one is the Corinne Lake culmination, the larger eastern one is the Grace Lake culmination. The asymmetry of the small-scale  $F_{2U}$  folds does not change across the basement culminations, but their axial planes do fold over the dome. It is inferred that the basement culminations were exhumed by thrust faulting in the lower thrust system after development of the  $F_{2U}$  folds. A stack of steeply southeast-dipping, meter-scale, brittle reverse faults, with cm to dm-scale offsets, situated in the metasediments near the western edge of the Corinne Lake culmination, is assumed to be related to this late thrust activity in the basement, but no major continuous thrust fault exists in the metasediments. The fold in the center of the thrust sheet is a true  $F_{2U}$  structure, which caused the development of a second crenulation cleavage in the schists of the Menihek formation.

The Flatrock Lake thrust sheet consists of a stack of thin thrust slices which repeat the stratigraphy (Fig. 5.5). The thrusts themselves are folded. Thin sheets of basement rocks are interleaved with metasediments mainly in the southern part of the thrust sheet, but they appear near the leading edge in the north as well, e.g. at the southwestern end of the Grace Lake culmination, in the floor of the Flatrock Lake thrust sheet. Three kilometer-size culminations of low-strain basement rocks occur in an array near the eastern boundary of the thrust sheet. The southernmost of these was uplifted on a  $D_{1L}$  thrust (Fig. 5.5, section II) and a similar structural setting is assumed for the two others. The rocks of the Flatrock Lake thrust sheet are strongly folded and fold nappes are common and locally overturned (Fig. 5.5 and 5.13). A detailed map of the south Flatrock Lake area (Fig. 5.4) shows the structures in the southern part of the thrust sheet. One large overturned basement-cored fold east of the southern end of Flatrock Lake forms a kilometer size fold nappe with an overturned limb and strongly curvilinear fold axis. This fold nappe is presumed to be continuous with the

basement-cored fold just west of the large basement inlier in the southeast, as is shown in section II in Figure 5.5. This section was constructed perpendicular to the movement direction, and the fold nose is intersected twice in the western part of the section. The southeastern part of the thrust sheet is dominated by west-dipping structures related to backthrusts. All structures in the southern part of the thrust-sheet are rotated into an east-west orientation, presumably due to movement on the Sickie Lake/ Julienne Lake shear zone. Note that in spite of this rotation, the elongation lineations in the rotated part of the thrust sheet are still consistent with those in the remainder of the area, suggesting that the lineations were constantly regenerated during the development of the belt.

An oval shaped exposure of basement rocks in the southwest of the Flatrock Lake thrust sheet (Fig. 5.4) forms the core of an eyelid-window (Boyer and Elliott, 1982). Several thrusts were folded over this core and joined in a roof thrust. This situation is seen in the map in the west side of the window and is sketched in cross section I in Figure 5.5. The Flatrock Lake thrust sheet is overlain by the Elmer Lake thrust sheet which is emplaced by an  $D_{1L}$  thrust cutting up from the lower thrust system and forming an out-of-sequence thrust in the upper thrust system. This situation is shown in the southern parts of sections I and III in Figure 5.5. In section III a  $D_{1L}$  thrust carrying basement rocks cross-cuts and folds an older  $D_{1U}$  thrust which emplaced rocks of the Sokoman Formation on top of schists of the Menihék Formation.

#### 5.1.5.4 Sickie Lake shear zone

The southern boundary of the Flatrock Lake area is partially formed by the Sickie Lake shear zone (Fig. 5.4). It is a several hundred meters wide strike-slip fault zone, consisting predominantly of mylonitic and ultramylonitic rocks. Although the protoliths of many of these mylonitic rocks cannot be clearly determined, the shear zone appears to be dominated by sheared basement rocks in the southeast and by rocks of the Menihék Formation in the remainder of the zone. Low-strain lenses consist of all three rock types that are found in the surrounding areas (basement, Menihék and Sokoman

formations). Generally the rocks are very fine-grained and have an  $L > S$  fabric. Lower-strain rocks are intensely folded into isoclinal folds with fold axes at low angles to the  $L_3$  and sheath folds are common (Fig. 5.12).

The shear zone is outlined by a string of lakes at the southwestern boundary of the Flatrock Lake thrust sheet. It is steeply dipping at the southeastern end in the map of Figure 5.4, but farther northwest the shear zone swings around to more northerly and northeasterly trends and shallows out to form the floor thrust of the basement sheet west of the southern part of Flatrock Lake. The Sickle Lake shear zone appears to affect the orientation of the floor thrust of the Elmer Lake thrust sheet and is inferred to postdate movement on this basement-rooted floor thrust. The structure is most likely a tear fault related to the lower level thrust system. It is tentatively linked with the Julienne Lake fault to the southeast (see Chapter 4).

The great circle distribution of  $S_1$  planes in the stereoplot of Figure D.1G (Appendix D) is mainly caused by folding on a small scale. The calculated fold axis, the orientations of the maximum concentration of  $F_2$  fold axes and the maximum of the  $L_3$  all have virtually the same SSE-plunging orientation, parallel to the regional orientation of  $L_3$ . The  $F_2$  fold axes, however, have a wide spread of orientations, predominantly in the southeastern quadrant, suggesting that folding occurred around fold axes that progressively rotated towards the axis of elongation of the strain ellipsoid.

#### 5.1.5.5 Wide Valley area

In the Wide Valley area in the southwestern part of the map of Figure 2 (Fig. 4.2), metasediments and basement rocks are cross-cut by steep thrust faults of the lower thrust system. The rocks in the area form the southern extension of the Flatrock Lake thrust sheet, but are separated from it by the Sickle Lake shear zone and a tip of the Elmer Lake thrust sheet. The cross section in Figure 5.14 (section III) shows that the area forms a triangle zone between northwest- and southeast-dipping thrusts rather than a thrust sheet as previously proposed by van Gool et al. (1987b). The area is poorly exposed and the map and cross-section are based on a minimum of information.

Small-scale structures are similar to those in the high-strain zones of the Flatrock Lake thrust sheet. Two generations of post- $S_{1U}$  folding are common in the banded iron formations. All rocks, with the exception of schists of the Menihek Formation, are strongly lineated. Foliations, axial planes, fold axes and stretching lineations are generally steep (Fig. D.1H), as a result of the thrusting in the basement.

The northwestern boundary of the Wide Valley triangle zone is a steeply dipping backthrust, which emplaced basement rocks against the metasediments in the area. Actual changes in dip direction from northwest to southeast along strike are found in the bounding shear zone in the west. This is probably a result of folding and overturning of the ductile backthrust during progressive simple shear of the belt. The sheets of basement rocks were emplaced on  $D_{1L}$  thrusts which rooted in the basement, and formed out-of-sequence thrusts with respect to those in the metasediments. The axial planes of the  $F_2$  folds fan through the area (Fig. 5.14), which is a result of the late thrusting and back-thrusting of the basement. The southwestern extensions of the main basement thrusts are not known. The area is overlain to the east by a triangular area dominated by metasediments, from which it is separated by a N-W trending oblique thrust that runs towards Rivière aux Fraises in the southeast.

#### **5.1.5.6 Elmer Lake thrust sheet**

The Elmer Lake thrust sheet stretches from north of Elmer Bay to Rivière aux Fraises and consists predominantly of sheared basement rocks. Small pockets or lenses of folded metasediments are found locally, consisting predominantly of rocks of the Sokoman Formation.

A progressive strain gradient was observed from kilometer-sized lenses of low-strain basement rocks to protomylonitic and mylonitic quartzo-feldspathic rocks. On outcrop-scale the structures are quite similar to those in the thin basement slices in the Flatrock Lake thrust sheet. The rocks have a penetrative monoclinic  $S_1$  fabric, implying a simple shear component of deformation, and contain small asymmetric lenses of low-strain rocks and well-rounded or eye-shaped porphyroclasts. The  $S_1$  schistosity is defined by aligned biotite, muscovite and locally chlorite as well as quartz

ribbons and elongated feldspar porphyroclasts. The orientations of the  $S_1$  planes plotted in figures D.11 and D.1J (Appendix D) are predominantly south-dipping, but this is presumed to be an effect of the distribution of the sampling points, which are concentrated in areas where the foliation locally has a more southerly dip-azimuth.  $F_1$  folds were not observed in the basement rocks.  $F_2$  folds are asymmetric, northwest-vergent and lack an axial planar cleavage.  $S_2$  axial planes are steep, southeast-dipping and the folds are commonly overturned. Fold axes are curvilinear, but are not re-oriented completely towards the  $L_3$ . No sheath folds were observed. Structures in the scarce metasediments are similar to those in the highest-strain zones of the Flatrock Lake thrust sheet. These rocks are generally intensely folded mylonites with curvilinear fold axes with a wide range of orientations (Fig. 5.15).

The highest-strain rocks were observed near the floor thrust, near the boundaries with the undeformed basement inliers and around the gabbro bodies. Besides these, no internal shear zones were identified, but it is likely that they are present. The metasediments in the thrust sheet occur both in thrust slices and infolded pockets, but contacts which could be used to determine their structural position were rarely exposed. Gabbro bodies of the Shabogamo Intrusive Suite, which are quite common in the northern part of the thrust sheet, are strongly deformed at the boundaries, but the cores of the larger bodies appear to be undeformed.

The age of the structures in the Elmer Lake thrust sheet relative to the deformation in the upper or lower thrust system is not clear. The floor thrust south of Flatrock Lake cuts up from the lower basement thrust system and forms an out-of-sequence thrust with respect to thrust planes within the underlying metasediments of the Flatrock Lake thrust sheet (Fig. 5.5). Other structures, specifically those in the sediments away from the floor thrust, are most likely related to thrusting in the upper level thrust system. The floor thrust of the Elmer Lake thrust sheet is a  $D_{1L}$  thrust cutting up from the lower system. A splay from this thrust cuts into the Flatrock Lake

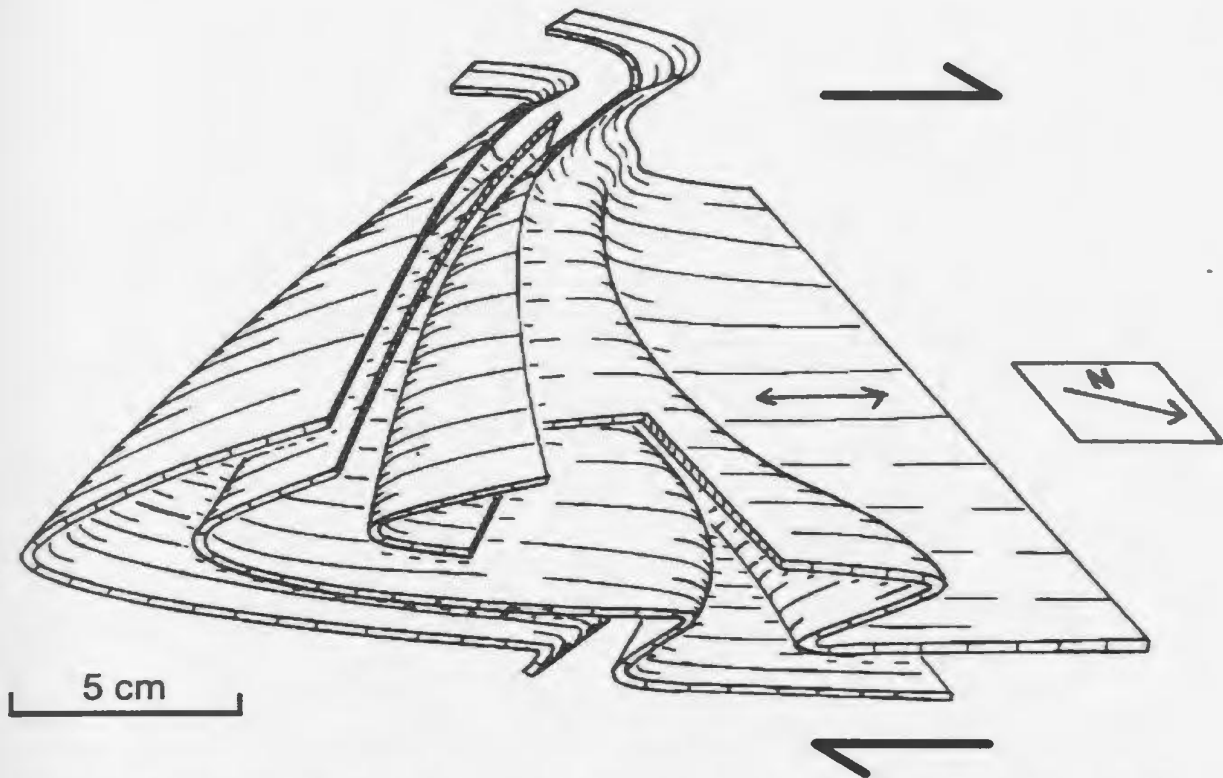


Fig. 5.15 Sketch of an  $F_2$  fold with a curvilinear fold axis at a high angle to the folded elongation lineation. Asymmetry of the fold is consistent with a northwest-directed thrust movement. The folded plane is the bedding, which is parallel to the  $S_{1U}$  and the lineation in the planes is the elongation lineation  $L_S$ . The overall orientation of the fold axis is perpendicular to the  $L_S$ , but its orientation fluctuates over  $90^\circ$ . Reconstructed from serial sections through a sample from an outcrop northeast of Elmer Lake.

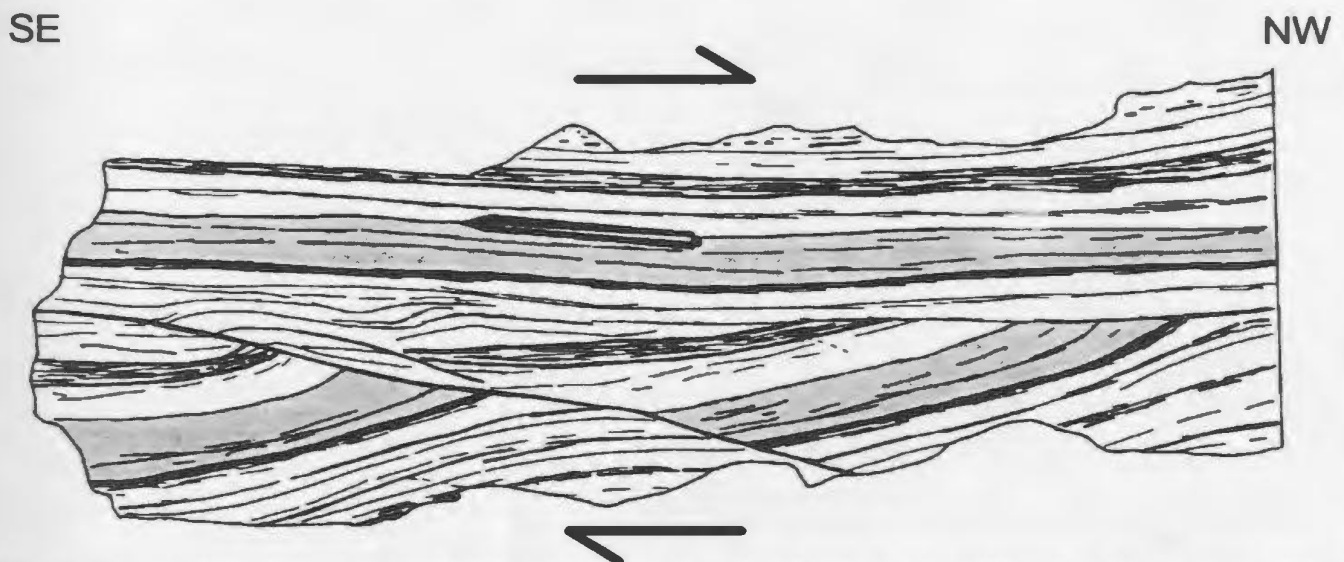


Fig. 5.16 Shear bands in basement rocks in the shear zone of the floor thrust of the Lorraine Lake thrust sheet, 2 km east of Mont Bondurant. Note that the foliation in the blocks between the shear bands has undergone an antithetic rotation. Displacement on the shear band at the bottom left is about 20 cm. The shaded layers in the bottom and the top of the outcrop, which are more quartz- and feldspar-rich than the surrounding schists, are possibly parts of the same layer, which would suggest much larger displacement on the shear band through the centre of the outcrop. The pen is about 15 cm long. Traced from a photograph.

thrust sheet and causes out-of-sequence thrusting there (Fig. 5.5, section III). However, for most of the structures in the basement rocks it is not possible to determine the timing of deformation.

#### 5.1.5.7 Goethite Bay area

The Goethite Bay area (Fig. 5.1) forms the southwestern end of the Goethite Bay thrust sheet (Map 2, in pocket). The area is dominated by interleaved massive quartzites of the Wishart and Sokoman formations, the latter mainly Fe oxide-bearing. Lithological layering is generally absent in the Wishart Formation and occurs mainly on a meter-scale in the Sokoman Formation. Several thin slices of basement rocks are incorporated into the Goethite Bay thrust sheet (Fig. 5.14, section II).

The dominant structures on outcrop-scale are the  $S_{1U}$  foliation and a well-developed elongation lineation. The foliation is mainly defined by stretched and flattened quartz grains, which are generally quite coarse (up to several mm long). In the mica-rich member of the Wishart Formation aligned muscovites form a schistosity. This  $S_{1U}$  is draped around garnet porphyroblasts and postdates the peak of metamorphism. Small aligned kyanite crystals together with elongated quartz grains locally define a mineral lineation in these rocks. In the oxide- and silicate-bearing quartzites of the Sokoman Formation, specular hematite and grunerite are aligned along the foliation and lineation respectively. Folds are not commonly observed in the area.  $S_0$ - $S_1$  intersection lineations ( $L_{1U}$ ) are at a very small angle to the  $L_3$ . The absence of abundant folds is an effect of the massive, homogeneous character of the rocks in the area. The basement rocks show a strong foliation consisting of a schistosity in rocks with abundant micas and a gneissic layering in the quartzo-feldspathic rocks, indicative of deformation at elevated metamorphic grades. Low-strain lenses and porphyroclasts are less common than in the basement rocks that were deformed at a lower metamorphic grade.

Shear zones are not clearly recognizable in small-scale structures in the quartzites. The grain-size of the rocks is slightly reduced near the thrust surfaces, but strain is either not clearly concentrated in the thrust zones, or post-kinematic recrystallization

has obliterated the mylonitic structures and textures. In Chapter 6 it is demonstrated that post-kinematic recrystallization did indeed take place. Mylonitic textures were only observed in the reworked basement rocks near the floor thrust, especially in the higher of the two basement slices in the lateral ramp that forms the southwestern boundary of the thrust sheet. Homogeneous shearing, rather than folding, seems to have been the predominant deformation mechanism. Most of the thrust planes are defined by outcrop patterns where units are cut off. These patterns are not consistent with a single phase of thrusting, since not all thrusts emplace older rocks on top of younger. The floor of the thrust sheet was formed originally by the basement-cover detachment, but later thrusting, originating in the lower system, introduced the two basement slices into the Goethite Bay thrust sheet.

The stereo plots (Fig. D.1K, Appendix D) show the same orientation patterns as the surrounding areas with  $S_0$  and  $S_{1U}$  dipping slightly shallower than elsewhere. Folding at the lateral ramp in the southwest caused the poles to the foliation planes to be distributed in a great circle.  $L_3$  and  $L_{1U}$  are parallel and virtually down-dip in the  $S_{1U}$  plane.  $F_{2U}$  fold axes show a wide spread in a shallowly southeast-dipping plane.

#### 5.1.5.8 Mont Bondurant area

The Mont Bondurant area (Fig. 5.1; Figure 2 in pocket) is underlain by two thrust sheets overlying the Elmer Lake thrust sheet. The lower of the two is the Sokoman Duplex, the only thrust sheet that was actually mapped as a duplex, and the higher one is the northern extension of the Lorraine Lake thrust sheet (previously set apart as the Mont Bondurant thrust sheet, van Gool et al., 1987). This part of the map area is poorly exposed and many of the boundaries between rock types are inferred, rather than observed.

The Sokoman duplex consists of banded iron formations, both oxide and carbonate members, interleaved with slices of basement rocks, which are up to tens of meters wide. Ductile thrusts splay off the floor thrust and rejoin in the roof. Small-scale structures are similar to those in the Flatrock Lake thrust sheet, with mylonitic structures in the ductile thrusts. The  $S_0$  and the  $S_{1U}$  are sub-parallel and few

isoclinal  $F_{1U}$  folds were observed, with mainly southeast-plunging fold axes. Boudinage of the carbonate layers is common in the layered carbonate-quartzite rock types. The rocks are strongly folded in northwest-verging, overturned  $F_{2U}$  folds, which locally have a weak axial planar fabric, consisting of a fracture cleavage. Open southeast-plunging  $F_3$  folds also have affected the duplex and the overlying thrust sheet. This is reflected in the stereo plots in Figure D.1L in Appendix D.  $S_{1U}$  foliations show a wide spread in orientations. The maximum in the southwestern orientations is caused mainly by the  $F_3$  folding and the ill-defined great circle distribution over a southwest-plunging axis is a result of the  $F_{2U}$  folding, illustrated by the maximum of  $F_{2U}$  fold axes in an equivalent orientation. The maximum concentrations of the  $F_{1U}$  fold axes and the  $L_3$  have similar orientations.

The Lorraine Lake thrust sheet in the Mont Bondurant area consists predominantly of basement rocks. Near the floor thrust, just north of the top of the hill, a thin slice of rocks of the Sokoman Formation occurs, presumably sheared off the iron formation rocks in the footwall (footwall plucking; Platt and Legett, 1986). Near the shore of Wabush Lake, the presence of two bands of quartzites of the Wishart Formation suggests that the thrust sheet consists of a stack of thrust slices, similar to the other thrust sheets in the area. However, this could only be recognized where rocks other than those of the basement are involved.

The basement rocks are penetratively sheared and a strong protomylonitic to mylonitic foliation is developed, similar to that in Plate 5.8. Porphyroclasts, as well as their pressure shadows, and lenses of lower-strain rocks are asymmetric. Together with shear bands (Fig. 5.16), and combined with the south-southeast-plunging  $L_3$ , these observations suggest north-northwest directed thrusting. The orientation of the  $L_3$  in both the Sokoman duplex and the Lorraine Lake thrust sheet is more southerly than in the lower thrust sheets and the Goethite Bay thrust sheet, suggesting a slightly different movement direction for these rocks (Appendix D, Figures D.1L and D.1M). The rocks in the thrust sheet are folded in a similar style to the underlying duplex.  $F_1$  folds are not common and are generally isoclinal, with fold axes at a low angle to  $L_3$ .  $F_2$  fold

axes have a range of orientations but are predominantly northwest-vergent. The rocks in the Mont Bondurant area are folded into a kilometer-size  $F_3$  synform which plunges to the southeast and has a fairly steep axial plane. Outcrop-scale  $F_3$  folds are rare and occur as very gentle, meter-scale folds. The floor thrust, which is well exposed in the slopes east of Mont Bondurant, consists mainly of straight gneisses containing asymmetric low-strain lenses, asymmetric shear folds and shear bands (Fig. 5.16).

The relative age of the structures in this part of the Lorraine Lake thrust sheet is not obvious. Noting the continuity of the structures with the sediment-dominated part of the thrust sheet in the south and the thin nature of the basement sheet, most of the deformation can presumably be related to the upper, sediment-dominated thrust system.

#### 5.1.6 RIVIERE AUX FRAISES AREA

A section across the strike of the thrust belt was mapped near Rivière aux Fraises, just north of the I.O.C.C. mine area, west of Wabush Lake (Fig. 5.17 and Figure 1A). This area forms the transition between the thrust-dominated part of the belt to the north, and the fold-dominated area to the south. The section incorporates several thrust sheets and the structures show a wide variation on outcrop scale. The exposure in the area is poor and distances between outcrops are generally larger than the amplitude of the stratigraphic repetitions and the size of the structures, which inhibited construction of a detailed map. For this area, only the large-scale structures can be indicated, based mainly on stratigraphic repetitions. Figure 5.17 is a cross section through the area which shows the stack of thrust sheets.

The lowest unit in the Rivière aux Fraises area is a thick package of rocks of the Menihék Formation, consisting mainly of fine-grained graphitic biotite schists, with some intercalations of phyllonitic basement rocks, which are too small to show in the section. This unit lies directly on top of the virtually undeformed basement to the west and no rocks of the Sokoman Formation are exposed in between. The nature of this basement - Menihék contact is not well understood. It may be an effect of extensional faulting, or it may indicate that the Sokoman Formation was locally not deposited, eg.

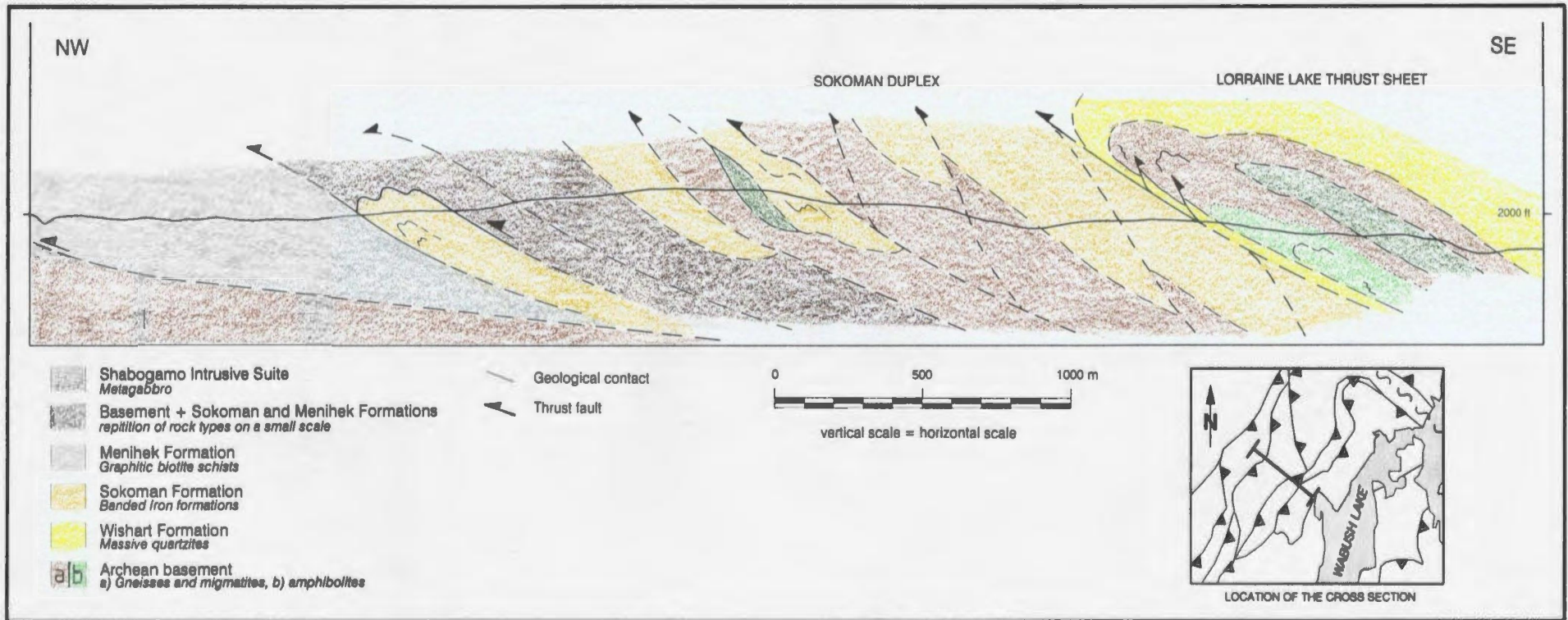


Fig. 5.17 Schematic cross section through the Rivière aux Fraises area. The inset map is a detail of the tectonic map showing the location of the cross section.

on basement highs, and the Menihek Formation immediately overlies basement. To the south of the Rivière aux Fraises area the Sokoman Formation re-appears between the basement and the rocks of the Menihek Formation.

The fabric in the Menihek Formation is a schistosity defined by oriented micas and flattened quartz grains, locally resembling a slaty cleavage. Locally a shear band cleavage was recognized which probably represents a high-strain zone.

Northwest-verging  $F_{2U}$  folds occur locally and are commonly associated with an  $S_{2U}$  crenulation cleavage. The high-strain zones, the presence of the thin basement slices and the  $F_{2U}$  folds indicate that this unit was thickened significantly by folding and thrusting.

Overlying the package of rocks of the Menihek Formation are two thrust slices which show, where exposed, a repetition of rocks of the basement and the Sokoman and Menihek formations on a scale of 10 to 20 meters. The rocks are reworked gneisses with a fine-spaced schistosity, fine-grained and well foliated banded oxide and carbonate iron formations and fine-grained biotite schists for the three lithological units respectively. The structures on outcrop-scale are very similar to those in the Flatrock Lake and Emma Lake thrust sheets. A mylonitic character is preserved in some outcrops. Rocks of the basement and Sokoman Formation are L-S tectonites and are folded in northwest-verging overturned  $F_{2U}$  folds that have curvilinear fold axes at high angles to the  $L_S$ . One fold nappe in rocks of the Sokoman Formation (possibly a large-scale sheath fold) occurs at the floor of these thrust slices. Strain concentration in thrust faults is not obvious in the field, which may be an effect of the poor exposure.

The next thrust slice in the cross-section of Figure 5.17, which is only exposed south of the river, contains basement and Sokoman Formation rocks, with minor gabbro. The structures are similar to those in the two thrust slices underneath, but appear to have formed at somewhat higher metamorphic grade. The foliation is shallowly dipping near the valley floor, but gets steeper uphill to the south, suggesting that the floor thrust is close to the level of the river. This thrust slice lacks the small-scale repetition of the stratigraphy of the lower sheets.

North of the river, the southern end of the basement-dominated Elmer Lake thrust sheet is bounded to the southwest by an oblique ramp. This boundary, delineated mainly from air photo interpretation, plunges beneath the units to the east and offsets the rocks in the overlying Sokoman duplex.

The Sokoman duplex in the Rivière aux Fraises area contains considerably more basement rocks than further north. Poor exposure prevents reconstruction of the internal large-scale structures, but several horses containing basement and Sokoman Formation rocks are presumed to be present.

The upper thrust sheet in the east, the Lorraine Lake thrust sheet, consists of well foliated biotite schists and gneisses which have been interpreted as reworked basement, because locally low-strain augen of basement rocks were recognized. Small-scale structures are similar to those in the Mont Bondurant area. Overturned and extremely thinned sequences of basement, Wishart and Sokoman Formation rocks at the floor thrust suggest that this part of the Lorraine Lake thrust sheet forms a fold nappe with a thinned lower fold limb. Fold asymmetries in the basement rocks one kilometer southwest of the river indicate a southeast vergence in accordance with an overturned fold limb. The rocks here are strongly folded on outcrop-scale and at least two generations of folds overprint the  $S_1$  schistosity (Plate 5.8). The sequence of these lithologies is repeated, indicating that at least this lower fold limb is cross-cut by thrust faults. Since the thrust planes themselves are not exposed, it is not clear whether these faults are an effect of the thrust movement of the Lorraine Lake thrust sheet over the underlying Sokoman Formation, or whether they formed at a later stage of deformation, during thrusting in the footwall.

The stereo plots of structural elements in the Rivière aux Fraises area in Figure D.1N (Appendix D) represent many small and large-scale structures in four different thrust sheets. Planar structures show a wide spread of orientations, but the overall pattern of southeast-dipping planes is still present.  $F_{1U}$  fold axes and lineations are

completely re-oriented towards the  $L_3$ ,  $F_{2U}$  axes are rotated away from their original sub-horizontal southwest-northeast trend and now lie in a shallow southeast-dipping plane.

### 5.1.7 EMMA LAKE AREA

Figures 5.18 and 5.19 are a map and cross-sections of the Emma Lake area. This part of the thrust belt consists of an imbricate stack of basement cored fold nappes which repeat the local stratigraphy of basement, Sokoman and Menihek Formations several times. The thrust stack was described previously by van Gool et al. (1988a, b) and by Brown et al. (1991). The structures in the area have a northeasterly plunge and from southwest to northeast progressively higher structural levels of the stack are exposed. This oblique plan view of the structures enables the construction of a down-plunge projection cross-section, but the non-cylindricity of the structures prevents the construction of one section for the whole area. Four separate cross-sections were constructed by down-plunge projection of small parts of the map. The projection planes are steeply dipping to the west perpendicular to the plunge of structures in the parts of the map they represent. Section III in Figure 5.19 has been modified from the true projection to accommodate the strongly non-cylindrical basement dome in this part of the area.

On outcrop-scale the structures are similar to those in the Flatrock Lake area, but in the metasediments of the Emma Lake area a concentration of strain in ductile thrusts is less obvious and basement rocks play a more important role.  $F_{1U}$  folds are tight to isoclinal and angular relationships between  $S_0$  and  $S_{1U}$  are obvious in many places. The vergence and style of  $D_{1U}$  structures changes across the hinges of the fold nappes. In the back limb  $F_{1U}$  folds are west- to northwest-verging with moderate interlimb angles (up to about  $60^\circ$ ) and varying orientations of the fold axes. In the overturned forelimbs most  $F_{1U}$  folds are isoclinal, west-verging and fold axes plunge predominantly at low angles to the  $L_3$ . All  $F_{1U}$  axes lie in a southeast-dipping plane, with fold axes in the highest strain rocks furthest rotated towards the orientation of  $L_3$ .  $F_{2U}$  folds are more open, generally asymmetric and northwest-verging; they are non-cylindrical and fold

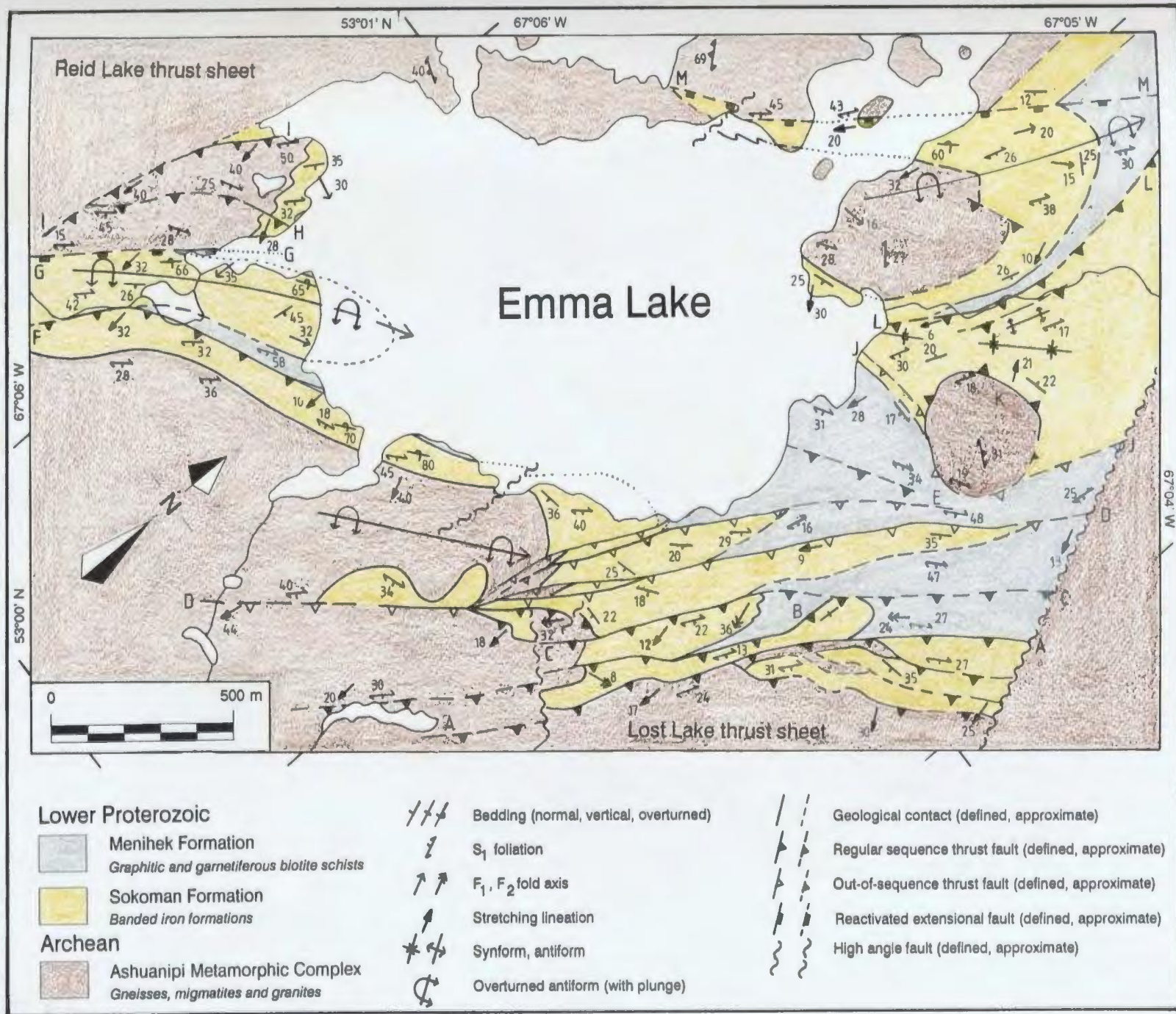


Fig. 5.18 Map of the Emma Lake thrust stack. Cross sections are shown in Figure 5.19.

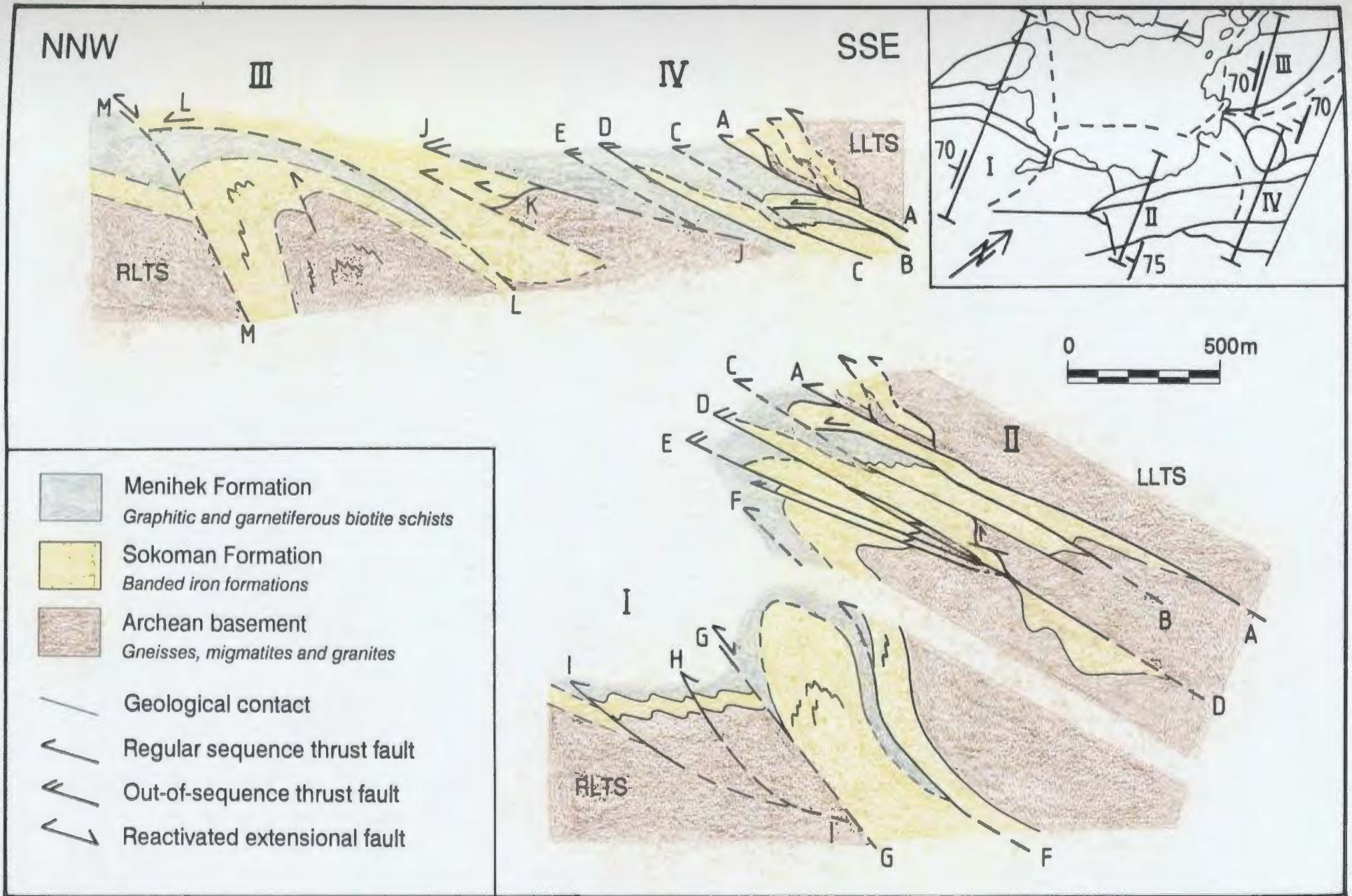


Fig. 5.19 Cross sections through the Emma Lake thrust stack. The sections are constructed by down plunge projection on true profile planes. The orientations of the profile planes and the areas used for each of the profiles are shown in the inset. LLTS = Lost Lake thrust sheet; RLTS = Reid Lake thrust sheet.

axes are distributed in a southeast-dipping plane, with maxima in the northeast and southwest (Fig. D.10 in Appendix D). The stereo plots show the southeastern dip of  $S_0$ ,  $S_{1U}$  and  $S_{2U}$  planes, with the increase of the dip angle from the oldest to the youngest structures. The  $L_s$  lies obliquely in the foliation plane, which may be a result of either the tilt of the area or an oblique convergence of the belt. Several late, north to northwest-trending, brittle faults of different scales cut the area. They are presumed to be steep, with sinistral to oblique displacement that commonly varies from several meters to tens of meters, relatively raising the western block. The most significant of these faults truncates the Emma Lake thrust stack to the east.

Original basement-cover contacts are preserved locally, but in many places these contacts are strained, especially in the overturned limbs of the fold nappes. These contacts are interpreted as original unconformable contacts which were sheared as a result of strain incompatibility. Deformation in the basement rocks in the cores of the fold nappes is not everywhere obvious on outcrop-scale, but significant deformation must have taken place to form the nappes. Only in the antiform in the northern corner of the Emma Lake map area the basement rocks are intensely folded.

Two structures in the area are of special interest, as they show an inversion of the stress regime from extensional to compressional. The two fold nappes furthest to the northwest, one southwest of the lake, the other northeast of the lake, both formed against a basement buttress (Figure 5.19, sections I and III). In both structures the thickness of the Sokoman Formation changes drastically across a steep fault (faults G and M), from several hundreds of meters east to less than one hundred meters west of the fault. In the overturned limbs of the fold nappes, the rocks of the Sokoman Formation are intensely folded, whereas west of the faults rocks are significantly less deformed. Both faults G and M are interpreted as original growth faults, active during the deposition of the Sokoman Formation. During Grenvillian thrusting, the fault escarpments acted as buttresses against which the fold nappes formed, causing intense localized shortening east of them, whereas the rocks on top of the escarpment were relatively protected. In the northeastern structure (fault M), the growth fault was

reactivated in a reverse movement. Reactivation of fault G is not obvious, but here two shortcut faults (Hayward and Graham, 1989; faults H and I) cut into the footwall. These are the only documented examples of Early Proterozoic extensional faulting in the whole map area, but the assumption is made that similar structures exist throughout that part of the thrust belt in which basement is involved in the thrusting.

Another feature that is well-documented in the Emma Lake area is out-of-sequence thrusting. In the cross-sections several thrusts emplace younger rocks on top of older, which is incompatible with the contractional nature of thrust faults, which emplace deeper level (older) rocks on top of higher level (younger) rocks. This is documented in faults D, E and J and several smaller thrusts in the map. This phenomenon can be explained by out-of-sequence thrusting in an established thrust stack, where the stratigraphic sequence is disturbed. Most of the out-of-sequence thrusts are found in the southeastern part of the map, where they cut through the back limb of the upper fold nappe at a lower angle than the dip of the bedding. For instance, fault J places schists of the Menihek Formation directly on top of basement rocks. This fault is expected to cut off the lower parts of several of the overlying thrust slices as is schematically drawn in cross section III in Figure 5.19. These out-of-sequence thrusts do not seem to be linked to deformation in the lower thrust system and are interpreted to be a result of deformation within the upper thrust system. This is in contrast with the out-of-sequence thrusts in the Flatrock Lake thrust sheet which are a result of regular sequence thrusting in the lower thrust system (section 5.1.5.3).

The roof thrust of the system emplaced a massive basement sheet, the Lost Lake thrust sheet, on top of the Emma Lake thrust stack. The thickness of this thrust sheet suggests that its floor thrust may form part of the lower level thrust system and therefore could be an out-of-sequence thrust with respect to the thrusts in the underlying thrust stack. The small thrust stack in between the basement sheet and thrust A could equally have been emplaced later (Fig. 5.19, sections II and IV).

### 5.1.8 LAC VIROT AREA

The Lac Virot area (Fig. 5.1 and Figure 1A, in pocket) in lithotectonic domain I is characterized by kilometer-size basement sheets and thin outliers of metasediments of the Sokoman Formation more than 7 kilometers northwest of the main metasedimentary thrust sheets. The area covers parts of the Reid lake and Lost Lake thrust sheets, which are dominated by basement rocks with the iron formation rocks forming thin, highly deformed slices along ductile thrusts in the basement. All structures in the Lac Virot area are assumed to be related to thrusting in the lower, basement-dominated thrust system. Only the quartz-rich part of the oxide member and the upper carbonate member of the Sokoman Formation are present.

The majority of the basement rocks show minor Grenvillian deformation on outcrop-scale, consisting of a weak schistosity ( $S_{1L}$ ) defined by isolated oriented micas, elongated or flattened quartz grains and cracked feldspars. In the shear zones, which form ductile thrusts, the basement rocks are strongly reworked to biotite schists which have a mylonitic fabric ( $S_{1D}$ ), which was partially obliterated by post-kinematic recrystallization. Type I S-C mylonites (Lister and Snoke, 1984) with predominantly quartz porphyroclasts were found locally in the shear zone furthest to the northwest (see Chapter 6). Most shear zones contain asymmetrically tailed feldspar and quartz porphyroclasts; they have a well-developed mineral lineation and multiple generations of approximately west-verging  $F_{2L}$  folds. The metasediments, which occur only along the shear zones, have a strong L-S fabric and northwest verging asymmetric  $F_{2L}$  folds of several generations and early  $F_{1L}$  folds, which have fold axes at low angles to the stretching lineations, are common.

The main shear zone in this area, north and west of Lac Virot, is a steeply southeast-dipping fault zone that splays off the Grenville Front at Reid Lake. Another possible interpretation is that this fault zone is the lowest in the basement thrust stack and forms the Grenville Front. Kinematic indicators suggest that the movement direction of the hanging wall is to the northwest. This makes the shear zone an oblique-slip fault (reverse - sinistral), forming an oblique ramp. Towards the southwest

the orientation of the fault changes from a north-northeast strike to a northeast strike, and the displacement pattern becomes dominantly dip-slip reverse. Rocks of the Sokoman Formation at the junction of the Read Lake shear zone and the Lost Lake floor thrust, and in the slices of iron formation about one kilometer to the east, have a platy fabric with a well-developed stretching lineation, defined by extremely elongated quartz grains and oriented amphiboles. These rocks are intensely folded into highly non-cylindrical folds.  $F_{1L}$  fold axes plunge steeply sub-parallel to the stretching lineation and sheath folds are common. The remainder of the thrusts in the Lac Viroit area have a lower dip angle and their strike is approximately parallel with the orientation of the whole belt, but they are still steeper than most of the thrust faults in the thrust belt, which occur mainly in the metasediments. Orientation data (Fig. D.1P, Appendix D) show a wide spread of orientations of all structural elements, mainly because they represent both steeply and shallowly dipping shear zones.

#### 5.1.9 CAROL LAKE THRUST SHEET

Only a small part of the Carol Lake thrust sheet (Fig. 1A, in pocket), approximately between Emma Lake and Carol Lake, was mapped for this study and poor exposure prevented the construction of a detailed map. The rocks in the area form thin (< 100m) slices of strongly sheared and metamorphosed basement, with a thin cover of the silicate member of the Sokoman Formation (between 30 and 100m) and a larger thickness of schists of the Menihek Formation (> 70m). The rocks in the thrust sheet are strongly foliated and the usual indicators of intensive, northwest-directed shearing during  $D_{1U}$  were found. The rocks are all L-S tectonites with a well-developed stretching lineation. The thrust sheet consists of an imbricate stack of thrust slices which repeats the stratigraphy on the scale of 100 to 150 meters.  $F_{2U}$  folding was regionally quite intensive and in the Menihek Formation an  $S_{2U}$  crenulation cleavage is the dominant foliation. Northwest-verging  $F_{2U}$  folds of a size range similar to the fold nappes in the Flatrock Lake area were observed, but no clear fault activity could be connected with them. It should be noted that as a result of the similarity in appearance between sheared basement rocks and the schists of the Menihek formation, some of the

rocks interpreted as Menihék schists could actually be part of the basement. In this part of the map area the contact between highly sheared basement rocks within the upper sediment-dominated thrust system and the low-strain, basement-dominated system is preserved in a few places.

In the stereo plots of Figure D.1P (Appendix D) all foliations were taken together, and they incorporate both  $S_{1U}$  and  $S_{2U}$  planes, on average dipping moderately to the south-southeast. Insufficient lineations and fold axis data were measured to form a pattern, but their orientations are similar to those in adjacent areas.

#### 5.1.10 LORRAINE LAKE THRUST SHEET

This description only concerns the southwestern part of the thrust sheet, south of Rivière aux Fraises (Fig. 5.1, Fig. 1A). It is based on the re-interpretation of pre-existing maps (Rivers, 1985a, b and c), a study of field notes of Rivers (unpublished data) and two reconnaissance traverses in the central and northern part of this part of the thrust sheet. The Lorraine Lake thrust sheet contains iron ore deposits which are presently mined by the Iron Ore Company of Canada. The area of the iron deposits has been intensively drilled and excavated and the geometry of the structures is fairly well known, but has only been reported in confidential mine reports. The maps published by Rivers (1985a, b and c) are partially based on these confidential reports.

The  $S_{1U}$  foliation in this part of the map area is sub-parallel to the bedding. No  $F_{1U}$  folds were observed but they may well be present. In an outcrop about one kilometer north of Lorraine Lake, reworked basement rocks have a monoclinic fabric, indicating a simple shear component in the deformation. Shear bands, asymmetric pressure shadows around porphyroclasts and rare S-C planes suggest northwest-directed shear. In the central part of the thrust sheet no indications of simple shear deformation were found. The foliation in the schists is defined by aligned micas and flattened quartz and feldspar grains. Rocks of high quartz-feldspar content have a gneissic character. In the iron formations, aligned specular hematite, amphiboles, micas and flattened quartz formed a fairly coarse schistosity. In the massive quartzite member of the Wishart Formation the coarse grain size (> 1 cm), the homogeneous composition and

the strong post-tectonic recrystallization resulted in a rock with no obvious foliation. With the exception of one localized fault west of Lorraine Lake, no internal thrusts have been recorded in this part of the Lorraine Lake thrust sheet. It is not clear if other thrust faults are present, or whether they were not recognized due to strong recrystallization after deformation combined with poor exposure.

The rocks in this area are folded in a series of  $F_{2U}$  folds on the scale of hundreds of meters to kilometers. These folds have a trend parallel to that of the strike of the thrust belt. The folds are overturned to the northwest and the fold axes are curvilinear, presumably as an effect of later ( $D_3$ ) folding over southeast-plunging fold axes (Rivers, 1983a). In outcrops of the basement north of Lorraine Lake, a fold interference pattern of two generations of  $F_{2U}$  folds was observed in the overturned limb of a large-scale  $F_{2U}$  fold (Plate 5.8). The outcrop pattern in the map is complicated by the topographic relief, because the hills in this area are of a similar size to the amplitude of the folds. The large-scale  $F_2$  folds in this thrust sheet may form fold nappes, similar to those in lithotectonic domain II, but they have not been recognized as such.

The orientation data in Figure D.1R show a moderate easterly dip for the maximum concentrations of  $S_0$  and  $S_1$  planes. Both the pole to the  $S_1$   $\pi$ -girdle and the measured fold axes have a southerly plunge, at a small angle to the  $L_3$ .

The absence of exposed basement rocks and the presence of rocks of the Attikamagen Formation in the southern part of the Lorraine Lake thrust sheet suggest that this part of the thrust sheet represents a basin. The northern part of the thrust sheet contains an original basement high, on which the rocks of the Wishart formation directly overlie the basement.

#### **5.1.11 STRUCTURES IN THE HIGHEST THRUST SHEETS, DOMAIN V**

Structures in the Wabush Lake and the Duley Lake thrust sheets are more consistent than in the western part of the map area, presumably as a result of the more homogeneous lithology and the higher metamorphic grade. The three main generations of structures that can be recognized in the field can be correlated reasonably well

through this lithotectonic domain. These structures are best developed in the gneisses of the Attikamagen and Menihék formations and in the iron formations of the Sokoman Formation. The homogeneous marbles of the Denault Formation reveal on outcrop-scale a penetrative foliation formed by slightly flattened and elongated dolomite crystals, which is not easily recognizable. The structural descriptions below are for the gneisses of the Attikamagen Formation, which form the major part of the upper lithotectonic domain, and which are the only rock type studied in detail. No basement rocks were positively identified in the highest lithotectonic domain of Gagnon terrane. It is assumed that all structures are related to deformation in the upper, sediment-dominated thrust system.

#### 5.1.11.1 Wabush Lake thrust sheet

Rocks of the Attikamagen Formation dominate the Wabush Lake thrust sheet (Fig. 5.1 and Fig. 1A, in pocket). They form a several kilometers thick package and exhibit a more homogeneous deformation than in the lower thrust sheets which are strongly layered on outcrop-scale and on the scale of tens of meters in the different stratigraphic units. The small-scale structures in the Wabush Lake thrust sheet are quite consistent in appearance. The oldest structure that can be recognized in outcrop is the  $S_1$  foliation, defined by a preferred orientation of flattened quartz and feldspar, micas and kyanite. Muscovite has overgrown the  $S_1$  in a random orientation. A gneissic banding or differentiated layering is common and consists of a repetition of quartz-feldspar-rich and mica-rich layers (Plate 5.9). Migmatitic layering occurs in rocks which have been partially melted. No indications of simple shear were found related to the  $S_1$ .  $F_1$  folds are uncommon and insufficient data are available for the determination of preferred orientations of  $F_1$  fold axes or  $L_1$  intersection lineations. Stretching lineations have only been observed in the vicinity of the floor thrust of the overlying Molson Lake terrane.

$F_2$  folds in the Wabush Lake thrust sheet are commonly asymmetric open to tight folds with a similar fold geometry (Plate 5.9). In a few examples a weakly developed axial plane foliation is present in the form of isolated aligned biotite flakes. Most  $F_2$  folds lack an axial planar fabric. The fold axes have a wide range of orientations due to

both their original curvilinear nature and the re-folding during later  $D_3$ . The  $S_2$  axial planes dip moderately to steeply to the southeast in their original orientation, but they are folded in  $F_3$  folds. The  $F_2$  folds are approximately northwest-vergent.

$F_2$  folds were recognized in outcrops throughout the thrust sheet and have been mapped out on a larger scale. Figure 5.20 is a sketch of a road section along the Trans Labrador Highway just north of Blueberry Hill, showing a large-scale  $F_2$  fold and  $F_1$ - $F_2$  overprinting, which are characteristic for the Wabush Lake thrust sheet. The syncline west of Moose Head Lake (Figure 1A), containing rocks of the Denault, Sokoman and Menihék formations, is also an  $F_2$  structure, and similar  $F_2$  structures are present throughout the thrust sheet, but are not as clearly outlined by contrasting rock types.

$F_3$  folds are predominantly kilometer-scale, open folds with consistently oriented, moderately southeast-plunging fold axes. The short, steeply northeast-dipping limbs and longer, shallowly southwest-dipping limbs make them northeast-vergent. Outcrop-scale  $F_3$  folds are uncommon and no axial planar foliation is developed.

In the map  $F_3$  structures are most obvious in the boundary between Molson Lake terrane and lithotectonic domain V and in the contact between the Attikamagen and Denault formations. They are well outlined by the latter contact just south of the map area (Rivers, 1985c). Near these boundaries these structures form a large-scale cusped-lobate fold train. At the boundary between Gagnon and Molson Lake terranes the less competent gneisses of the Attikamagen Formation occupy the cores of the tight, angular antiforms, whereas the more competent granitoids of Molson Lake terrane occupy the open, well-rounded synforms. The  $F_3$  folds determine the foliation patterns in the stereo plots in Figures D.1S, D.1T and D.1U in Appendix D. Foliations define great circles and  $F_3$  fold axes that plunge shallowly to the southeast. Overall, the  $F_3$  fold axes plunge between  $20^\circ$  and  $30^\circ$  to  $150$ - $160^\circ$ . The plots for the foliations have a maximum in a steeply northwest-dipping orientation. Fold axes ( $F_1$  and  $F_2$  combined) show a wide spread of orientations as a result of multiple fold overprinting and possible reorientation by shearing.

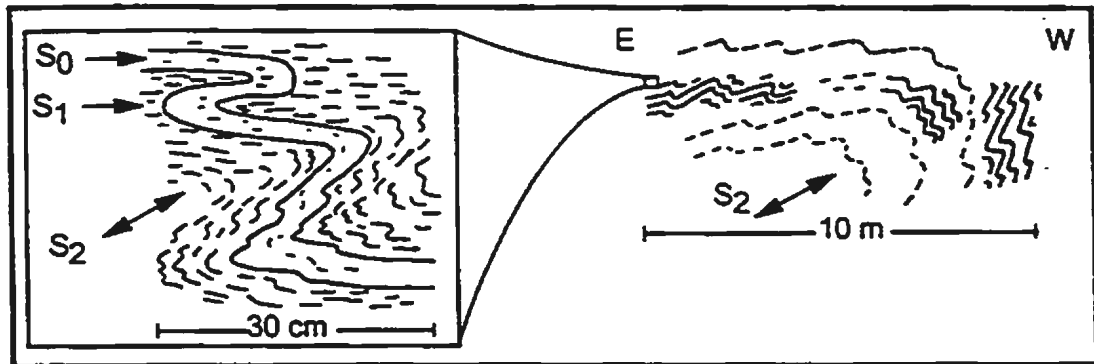


Fig. 5.20 Sketch of a road section through gneisses of the Wabush Lake thrust sheet along the Trans Labrador Highway north of Blueberry Hill. The bedding is folded in isoclinal  $F_1$  folds with a penetrative  $S_1$  axial planar cleavage.  $S_1$  is folded in  $F_2$  folds which lack an axial plane fabric.  $S_2$  in the figure indicates the orientation of the axial plane. The main  $F_2$  fold is northwest vergent.

The boundaries of the Wabush Lake thrust sheet are poorly exposed. The boundary with the Duley Lake thrust sheet is formed by the Flora Lake shear zone (section 5.1.11.2). The boundary with the marbles of the Denault Formation to the northwest is interpreted to be a thrust fault, folded by  $F_3$ . The enveloping surface of the  $S_1$  foliations in the marbles and in the gneisses of the Wabush Lake thrust sheet dip southeast and suggest that the marbles dip underneath the gneisses. However, the possibility exists that the enveloping surface of the bedding, which on a small-scale is transposed towards the  $S_1$ , dips the opposite way, which would possibly make this boundary a normal sedimentary contact, similar to the interpreted contact between the Atikamagen and Denault Formations in the Duley Lake thrust sheet.

The roof of the Wabush Lake thrust sheet is formed by a wide ductile shear zone which separates the thrust sheet from the overlying Molson Lake terrane. Bands of dolomitic marble of the Denault Formation have been mapped in many locations near the roof of the thrust sheet and are commonly overlain by pelitic schists, which are rich in garnet, kyanite and locally graphite, and which are interpreted as rocks of the Menihek Formation. The inferred layer of Menihek Formation may indicate that the roof thrust of the Wabush Lake thrust sheet lies in the top of the stratigraphic sequence in this part of Gagnon terrane, suggesting that the floor thrust of Molson Lake terrane moved over the metasediments on a flat and that the ramp on which it cut up through the sediments lies further to the southeast. The shallow dips of the structures in this part of the area are also in accord with the interpretation of this part of the Gagnon terrane roof as a flat.

#### **5.1.11.2 Flora Lake shear zone**

The Flora Lake shear zone, exposed on the eastern shore of Flora Lake (Fig. 5.1 and Fig. 1A, in pocket), is a kilometer wide zone of straight gneisses which are interpreted to represent a zone of very high ductile strain. Intense recrystallization after and possibly during the movement in the shear zone has obliterated virtually all indications of high strain or sense of displacement. The straight character of the gneisses, the virtual lack of folds which are abundantly present in the wall rocks, the

presence of extremely elongated lenses (several kilometers in length and less than 100 meters wide) of marble and amphibolite (presumed to represent recrystallized gabbros), together with the mixing of lithologies in the shear zone and the left-lateral offset of rocks of the Denault and Attikamagen formations (Fig. 1A) suggest high strain. In only one outcrop, two-thirds down Flora Lake from the trans-Labrador Highway, were kinematic indicators observed. In this outcrop asymmetric quartz ribbons in a deformed pegmatite confirmed the left lateral offset of the zone. Mineral lineations are rare. The shear zone offsets both thrust sheet boundaries in Gagnon Terrane, and also the floor thrust of Molson Lake Terrane, into which it can be traced further south (Indares, pers. comm. 1991).

The  $S_1$  foliation of the Wabush Lake thrust sheet curves into the steep orientation of the shear zone in a sense that is consistent with the left lateral offset of the shear zone. This and the fact that the shear zone offsets the floor thrust of the Molson Lake terrane suggests that movement postdated the  $D_1$  in the Wabush Lake thrust sheet. Figure D.1W shows the orientations of foliations and lineations in the shear zone. The main orientation of the foliation is parallel to the shear zone boundary, but the foliation planes fan through the shear zone and define a great circle distribution which has a pole in a similar southeast plunging orientation to the  $F_3$  fold axes from the Wabush Lake thrust sheet and Molson Lake terrane. Therefore this orientation pattern is interpreted to be a result of the  $F_3$  folding which mainly postdated the shearing.

#### 5.1.11.3 Duley Lake thrust sheet

Work in the Duley Lake thrust sheet (Fig. 5.1 and Fig. 1A, in pocket) was restricted to a reconnaissance traverse and a partial re-interpretation of the existing map patterns. The small-scale structures are similar to those in the Wabush Lake thrust sheet. The outcrop pattern shows fold interference on kilometer-scale, which is more obvious in a map that extends further south (Rivers, 1985c). The older of two fold sets ( $F_1$  or  $F_2$ ) forms a syncline that strikes northeast, between Duley Lake and Wabush Lake. Part of this structure is interpreted as a monocline above a hanging wall ramp in which the rocks of the Attikamagen Formation are cut out of the Duley Lake thrust

sheet (Fig. 1B, in pocket, cross-section III). This structure is overprinted by south-plunging  $F_3$  folds which have axial planes perpendicular to those of the older folds. Near the contact between marbles of the Denault Formation and the gneisses of the Atikamagen Formation, the  $F_3$  folds have the same cusped-lobate geometry as in the Wabush Lake thrust sheet, but here the marbles are the least competent and occupy the cores of angular synforms. These structures are more pronounced just south of the map area (Rivers, 1985c).

The foliation planes are folded in a dome and basin type of structures by the interference of the two fold generations, which is reflected in a fairly large spread of foliation orientations (Appendix D, Fig. D.IV) with a maximum of 132/41. The data do not define a great circle distribution.

The northwestern boundary of the Duley Lake thrust sheet is not well defined and the Lorraine Lake and Duley Lake thrust sheets may be semi-continuous, since the mismatch of the stratigraphy across the boundary just south of Wabush Lake appears to be minor. The thrust sheet is separated from Molson Lake terrane and the Wabush Lake thrust sheet by the steeply dipping kilometer-wide Flora Lake shear zone. The Duley Lake thrust sheet is the southwestern extension of the Wabush Lake thrust sheet.

#### 5.1.12 THE FLOOR THRUST OF MOLSON LAKE TERRANE

The boundary between Gagnon and Molson Lake terranes can be divided into parts that are steeply-dipping with a north-northwest strike, and those that are folded in  $F_3$  folds and have an enveloping surface that dips shallowly southeast. The folded and shallow-dipping parts are interpreted as the original floor thrust of Molson Lake terrane, which are offset by the steep, sinistral strike-slip shear zones, of which the Flora Lake shear zone is one. The strike-slip zones are several times wider than the shallow shear zones (one kilometer versus hundreds of meters) and can be traced into Gagnon terrane. Presumably they also cut into Molson Lake terrane (Indares, in press, pers. comm. 1991). The shear zone at the boundary between the two terranes near Seahorse Lake may be interpreted as either a strike-slip zone or a part of the floor

thrust folded into a steep orientation. The width of the zone (slightly over a kilometer), as well its orientation and straight character, which are all similar to the Flora Lake shear zone, suggest that these two shear zones are strike-slip zones of the same set.

In the ductile shear zone that forms the floor thrust of Molson Lake terrane straight gneisses were formed in which evidence for shear-strain is scarce. In the shear zone north of Seahorse Lake (Fig. 2.1, Fig. 1A) a strain gradient was observed from a low-strain lens into the high-strain shear zone. Within a megacrystic granite, the rocks change over several meters from a slightly deformed granite to a gneiss in which the K-feldspar megacrysts are progressively sheared into long streaks (flaser) consisting of quartz and feldspar. This structure may, however, be related to the strike-slip shear zones. Foliation boudinage (Plate 5.10; Platt and Vissers, 1980) in gneisses of the shallow-dipping floor thrust, just south of Blueberry Hill, suggests significant extension in these rocks. The nature and orientation of the  $S_1$  foliation in the shear zone are identical to the Wabush Lake and Duley Lake thrust sheets and the emplacement of Molson Lake terrane is inferred to have been contemporaneous with and presumably the cause of the  $D_1$  deformation in these two thrust sheets.

Deformation in Molson Lake terrane is expressed as a schistosity, which is defined by oriented biotite and flattened quartz. The fabric becomes more penetrative towards the floor thrust, where it is mylonitic. The fabric in Molson Lake terrane is folded in kilometer-scale southeast-plunging cross-folds (Fig. D.1X) which correlate with the  $F_3$  folds in Gagnon terrane.

## 5.2 SUMMARY OF THE STRUCTURAL ORIENTATION DATA

The plotted orientation data in Appendix D show certain patterns and trends that confirm observations made in outcrops and maps. Some of these trends are summarized in Figure 5.21.

1) The overall south-southeastern dip of the structures in the western part of the map area is obvious from the plots of the poles to planar elements. Figure 5.21.A shows the maximum contour values of  $S_1$  as great circles for most of the data sets in

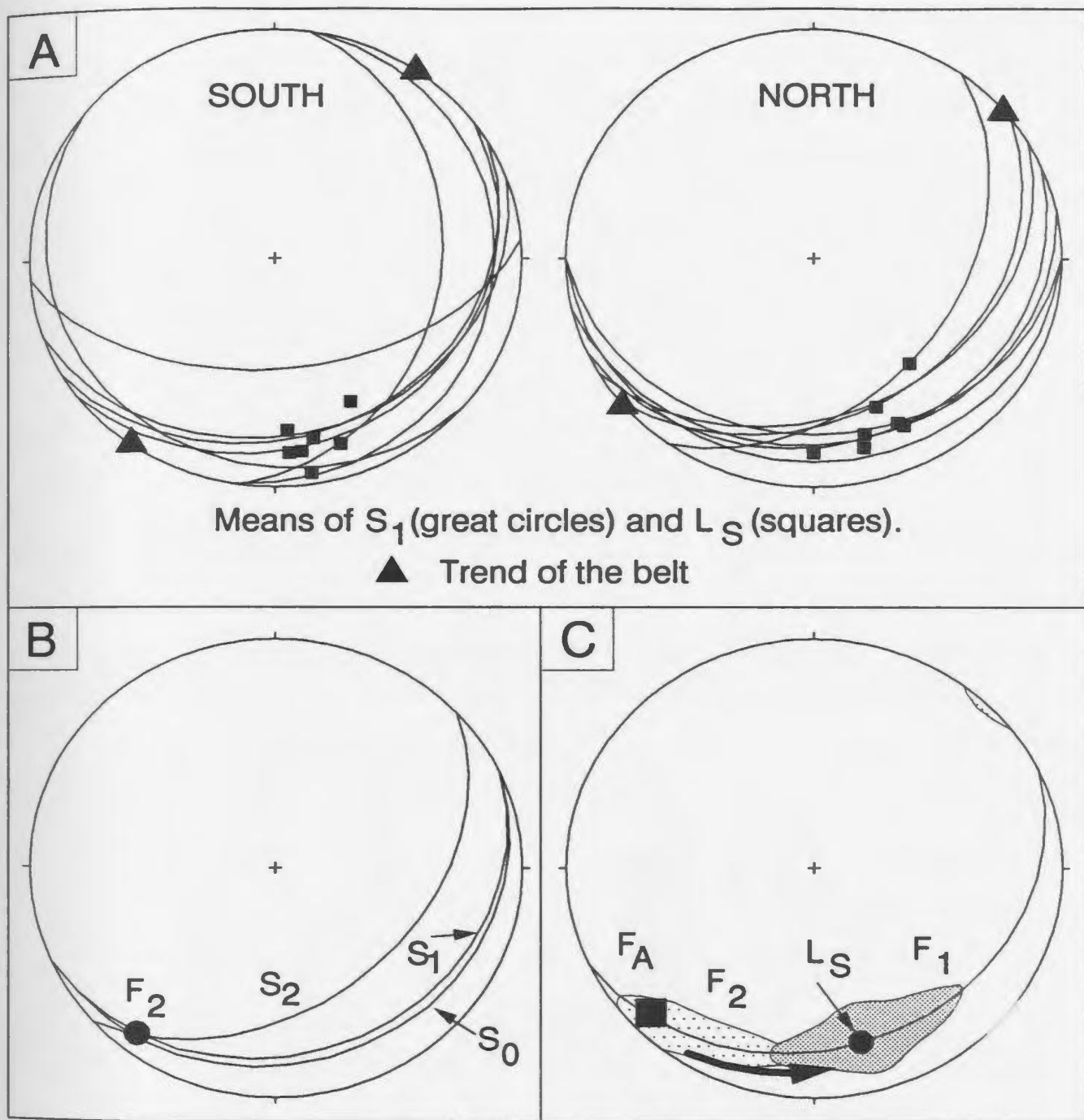


Fig. 5.21 Summary of stereo plots, west of Wabush and Shabogamo Lakes. A) shows the orientations of the maximum orientations of the  $S_1$  planes and elongation lineations ( $L_S$ ) for each of the areas in Figure D.1A in Appendix D, separated for the areas north and south of the Sickle Lake shear zone/Julienne Lake fault. B) is an idealized example of the angular relationships between  $S_0$ ,  $S_1$  and  $S_2$ , suggesting a northwest vergence of both  $D_1$  and  $D_2$  structures. C) shows the orientations of  $F_1$  (dark shaded area) and  $F_2$  (light shaded area) fold axes with respect to the elongation lineation ( $L_S$ , black dot) and the original orientation of most fold axes ( $F_A$ , black square), which is at a high angle to the  $L_S$ . The bold arrow indicates the direction of re-orientation with increasing strain.

Appendix D. It also shows that in spite of a significant spread in orientations of the foliation planes, the elongation lineations are quite constant in orientation throughout the area. This suggests that movement was rather homogeneously towards the north-northwest in the whole belt, in spite of variation in the orientations of flow planes.

2) In the southeastern part of the map, in lithotectonic domain V and Molson Lake terrane, the large-scale  $F_3$  folding dominates both the map pattern and the distribution of data in the stereo plots. Poles to foliation planes have a great circle distribution which defines the large-scale  $F_3$  fold axis, which plunges approximately  $30^\circ$  to  $155^\circ$ . This orientation does not coincide with any group of small-scale fold axes, as a result of the generally rare occurrence of small-scale  $F_3$  folds.

3) In those areas where sufficient measurements of  $S_0$ ,  $S_1$  and  $S_2$  were recorded, the angular relationships between the planes reflect the northwestern vergence of both  $D_1$  and  $D_2$  structures. The maximum orientations of  $S_0$  and  $S_1$  have approximately the same azimuth,  $S_2$  has generally a slightly more easterly dip. In most areas  $S_1$  is slightly steeper than  $S_0$  and  $S_2$  is significantly steeper than  $S_1$  (Fig. 5.21.B). The angle between  $S_0$  and  $S_1$  is generally very small as a result of the transposition of the  $S_0$  towards the  $S_1$ .

4) The orientations of the fold axes with respect to the elongation lineations ( $L_3$ ) are summarized in Figure 5.21.C. The majority of all fold axes is distributed in a southeast-dipping plane. Most plots of  $F_1$  fold axes and intersection lineations have a maximum in a shallowly SSE-plunging orientation, close to that of  $L_3$ . In plots of the  $F_2$  fold axes the maximum is not as well defined. The maximum contour level in most  $F_2$  plots is considerably lower than in those for  $F_1$ . The orientations of the fold axes are strongly dependent on strain in the rocks. For example, in the Corinne Lake thrust sheet, where strain levels are low, fold axes have a wide distribution in a south-dipping plane, there is no strong alignment of  $F_1$  with  $L_3$  and the majority of the  $F_2$  axes lie in the southwestern quadrant, although the maximum  $F_2$  orientation plunges to the south (Fig. D.1D in Appendix D). In high-strain zones, e.g. the Sickle Lake shear zone (Fig. D.1G), both  $F_1$  and  $F_2$  are oriented at low angles to the  $L_3$ .

These observations of progressive re-alignment of fold axes with increasing strain are consistent with field observations of increasing non-cylindricity of folds with increasing strain and the presence of sheath folds in the shear zones. With increasing strain, fold axes rotated progressively away from their originally shallow southwest plunge at a high angle to the  $L_3$  towards the direction of elongation (Cobbold and Quinquis, 1980).

5) The last important observation to be made from the orientation data, is the oblique nature of the structures in the belt. In the Figure 5.21.A the trend of the belt and the foliations and lineations are plotted for parts of the area south and north of the Julienne Lake fault zone/Sickle Lake shear zone. The lineations indicate movement towards  $340-350^\circ$ , which is at a  $45-55^\circ$  angle to the trend of the belt in the south and at a  $60-70^\circ$  angle to the belt in the north. Furthermore, the strikes of the  $S_1$  planes are oblique with respect to the belt and the  $L_3$  lies slightly obliquely in the  $S_1$  planes. These orientations are not likely to be a result of a regional tilting of the area, because lineations and foliations cannot be rotated back over one sub-horizontal axis to restore a possible original situation of  $L_3$  and  $S_1$  perpendicular and parallel respectively to the strike of the fold-and-thrust belt.

The orientations of the  $F_2$  and  $S_2$  structures also attest to the oblique setting.  $F_2$  fold axes are interpreted to be related to the NNW thrusting of the belt and are expected to be perpendicular to the  $L_3$ , with a WNW-ESE trend. However, the fold axes plunge shallowly between SW and SSE and only few  $F_2$  axes rotated from a NE plunge towards the  $L_3$ . This is in agreement with the orientation of the  $S_2$  being slightly oblique with respect to the  $S_1$ , resulting in a shallow SW plunge at the intersection of the two planes, as shown in Figure 5.21.B. This suggests that the  $F_2$  fold system is oblique with respect to the direction of thrusting, but more orthogonal with respect to the belt.

### 5.3 EVALUATION OF THE STRUCTURES

In this second part of the chapter the relations and variations of the structures are discussed and a model for the structural development of the fold-and-thrust belt is

proposed. In this discussion the fold-and-thrust belt, formed by both Gagnon and Molson Lake terranes, is assumed to constitute a thrust wedge with some of the characteristics that were presented by Chapple (1978) and Davis et al. (1983). Chapter 8 includes a more detailed discussion of how the observed structures relate to this model and some justification for the use of this model is presented. First the most important points of the previous descriptions will be highlighted.

### 5.3.1 VARIATIONS OF THE STRUCTURES THROUGH THE BELT

1) Because of the lack of topographic relief the field data do not place constraints on the geometry of the tip lines of the thrusts. Almost all thrust stacks have been drawn as imbricate fans, rather than duplexes (Boyer and Elliott, 1982), leaving the nature of the geometry of the thrust system unresolved. The Sokoman duplex at the foot of Mont Bondurant is the only thrust sheet that has been mapped as a duplex, because this hill provided enough relief for exposure of both floor and roof thrusts. Most of the structures in the map area are of a ductile nature, which implies that they were formed at many kilometers depth (see also Chapters 6 and 7). Since the thin sedimentary pile present in Gagnon terrane is insufficient to build up such an overburden, the terrane must have been deformed underneath an overriding thrust sheet, presumably Molson Lake terrane. Therefore the assumption is made that most of the thrust stacks described here form duplexes, of which the subsidiary thrusts rejoin the floor thrust of the overriding sheet. This interpretation is used in the construction of the cross sections in Figure 1B (in pocket).

2) Most of the Grenvillian structures in the map area were formed by plastic deformation, with only a few exceptions. Thrusts occur generally as shear zones, most of the rocks have a fabric that is formed by preferentially oriented metamorphic minerals and folds were formed by shear folding or flexural flow. The only observed brittle structures are minor extensional faults in the iron formations above the Corinne Lake culmination, and scarce strike-slip faults throughout the area with offsets on the scale of meters. Although all thrust-related structures are ductile, thrusting itself causes discontinuity of strata, which by definition is a brittle phenomenon. Possibly the thrusts

originally formed as brittle faults, but most of the subsequent movement took place later by ductile shearing on the established zones of weakness, if such zones were present. No indications of such an early brittle strain history were found, but they may have been obliterated by later ductile deformation and recrystallization.

3) The cumulative strain of the rocks increases from the lowest to the highest thrust sheets. Although local perturbations of the regional trend exist, e.g. in the thrusts themselves or around low-strain lenses, several indications suggest that the rocks in the highest thrust sheets have the highest strain. The strain gradient is best documented in the northern part of the area, especially in the rocks of the Sokoman Formation. In the northern Sawbill Lake thrust sheet, the bedding is shallowly dipping ( $\pm 10^\circ$ ) and is deformed into broad gentle folds. The strain in these rocks is very low. Strain in the Corinne Lake thrust sheet is higher, the foliation is more penetrative and boudins are developed in the banded iron formations. The average aspect ratio of the strain ellipse in the X-Z plane in siderite concretions in the Sokoman Formation is about  $X:Z = 2:1$ . The strain in the Flatrock Lake thrust sheet is considerably higher. Boudins are more elongated and further separated and siderite concretions have been measured with aspect ratios up to  $X:Z = 7:1$ . In the Sokoman Duplex and the base of the Goethite Bay thrust sheet streaks of siderite with aspect ratios in the order of 20:1 may represent elongated and recrystallized siderite concretions. In the higher thrust sheets strong post-kinematic recrystallization prevents a good evaluation of the strain. Nonetheless, the penetrative schistosity and gneissosity and the elongate shape of low-strain lenses suggest that overall the rocks have a high strain. This strain gradient is confirmed by the increase of estimated displacement on the thrust faults, which ranges from tens up to hundreds of meters in the lowest thrust sheets, to kilometers in the higher thrust sheets. Results of quartz fabric analyses, described in Chapter 6, also support an increase in strain from the lowest to the highest thrust sheets.

4) The increase of accumulated strain is interpreted to be an indication of a longer strain history for the highest thrust sheets. This interpretation is supported by observations which are described in more detail in Chapter 6, which suggest the

existence of a pre-S<sub>1</sub> fabric in rocks of lithotectonic domain V, preserved in garnet porphyroblasts. The main D<sub>1</sub> deformation in the Wabush Lake thrust sheet took place after the peak of metamorphism, while in the lower thrust sheets little D<sub>1</sub> deformation took place after the peak of metamorphism (see Chapter 6). This may suggest that the deformation front swept through the area from southeast to northwest. Deformation started first in the highest thrust sheets and continued while the deformation incorporated progressively lower thrust sheets. This is in agreement with thrust belt models that predict that higher thrust sheets have travelled progressively larger distances (Boyer and Elliott, 1982).

5) A trend of decreasing strain localization, from the lower to the higher thrust sheets, also exists in the fold-and-thrust belt. In the northern part of domain I the deformation took place mainly by shearing on discrete movement planes, whereas the basement blocks have a low strain internally. In domain II virtually all rocks are highly strained, but there are strong strain gradients into the shear zones that form the thrust planes. Similar partitioning of the strain is not obvious in the remainder of the lithotectonic domains. Presumably most of the strain of thrust movement was accommodated in the thrust faults, but post-kinematic recrystallization erased most of the evidence of the higher strain in these zones. The thrusts in the higher thrust sheets are much more widely spaced than in domain II, where they locally occur within tens of meters of each other.

This variation in strain partitioning through the belt is assumed to be caused mainly by the increasing metamorphic grade towards the southeast. Strain localization decreases with increasing ductility of the rocks. Also the increase of accumulated strain towards the southeast and the actual position in the thrust wedge will have an effect on the overall strain partitioning in the rocks, as is discussed later.

### 5.3.2 INFLUENCE OF EARLY PROTEROZOIC EXTENSIONAL FAULTS ON THE DEVELOPMENT OF THE THRUST BELT

Normal faults, which were part of the extensional fault system that presumably formed during the collapse of the continental margin on which sediments of the Knob Lake group were deposited during the Early Proterozoic (Chapter 3), caused rapid changes in stratigraphic thicknesses and had an important impact on the structural development. They acted as buttresses which prevented easy propagation of thrust faults. Figure 5.22 schematically shows two different modes of development of structures around these pre-Grenvillian extensional faults as interpreted from geometries in the South Flatrock Lake and Emma Lake areas (Fig. 5.5, section I; Fig. 5.19, section I and III, faults G and M). The main difference between the two situations in Figure 5.22 is the level of the floor thrust, which in the south Flatrock Lake area (A) is located at or near the basement-cover contact and in the Emma Lake area (B) at a shallow level in the basement. In the first case a stack of small fold nappes formed in front of the buttress and moved onto the basement horst, whereas in the latter case a single, large, basement-cored nappe formed. In both areas footwall shortcut faults (Hayward and Graham, 1989) cut into the basement horst and incorporated it as a thin basement slice into the thrust stack. The extent of reactivation of the extensional fault in A is not known, because the fault is not exposed. In the Emma Lake area the reactivation (inversion) was minor, in the order of tens of meters. The footwall shortcut faults may well have been an important mechanism of introducing thin slices of basement rocks throughout the map area. Gillcrist et al. (1987) proposed a similar mechanism for the introduction of thin basement slices into a thrust stack in the western Alps (c.f. Hatcher and Williams, 1986)

A similar basement configuration, but on a larger scale, is interpreted to exist at the boundary between the Lorraine Lake and the Carol Lake thrust sheets. Across the boundary from east to west at least three hundred meters of the stratigraphic sequence are lost (see Figure 4.3). Two of the most likely explanations for this dramatic change in stratigraphy are:

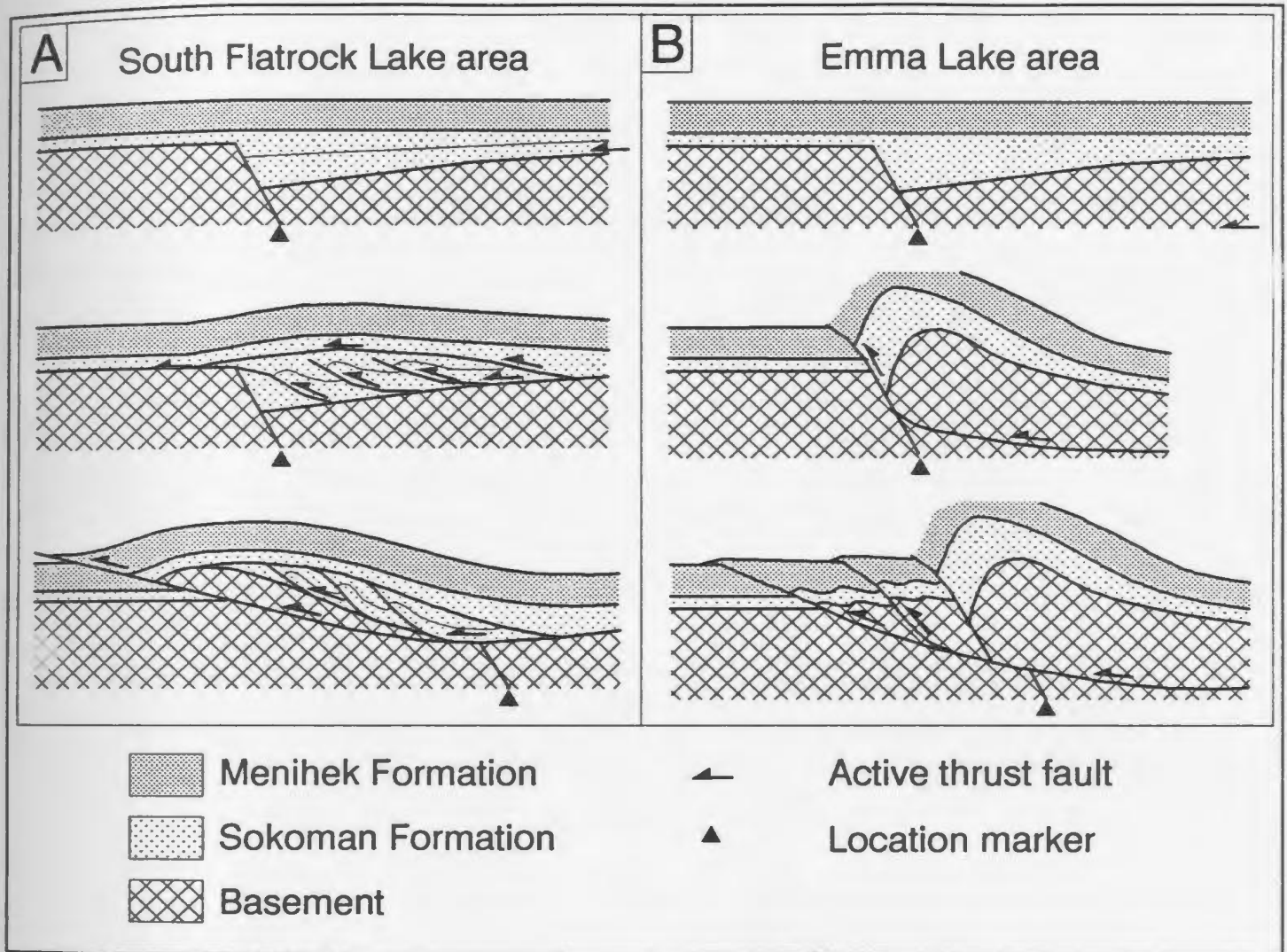


Fig. 5.22 Schematic development of structures around Early Proterozoic growth faults in the South Flatrock Lake and Emma Lake areas. In the Flatrock Lake area (A) a stack of small fold nappes was formed in front of the buttress, after which a thin slice of basement rocks was incorporated into the thrust stack by a shortcut fault and subsequently intensely deformed. This structure is illustrated in Figure 5.5, section I. In the Emma Lake area (B) the floor thrust is located in the basement. Here a single, large, basement cored fold nappe was formed, with slight reactivation (inversion) of the extensional fault. Shortcut faults again cut off thin basement slices. This structure is shown in Figure 5.19, sections I and III. Note that in both A and B the top of the Menihek Formation is formed by an overlying thrust sheet, not by a free surface. The triangle indicates the position of the extensional fault, which is regarded as a point of no displacement in the footwall.

- 1) the transition of the stratigraphic sequence between the two thrust sheets was originally gradational, formed by an onlap of the sediments onto a shallow basement slope, as proposed by Rivers (1983a). Subsequent thrusting on the floor thrust of the Lorraine Lake thrust sheet either placed this transitional area on top of the Carol Lake thrust sheet, from where it has been exhumed and eroded, or it was overthrust by the Lorraine Lake thrust sheet and is presently buried underneath it. This solution requires a displacement of many kilometers on the Lorraine Lake floor thrust;
- 2) the transition could have been localized at a major step in the basement, formed by one or more extensional faults with a total throw of hundreds of meters. This explanation does not require major displacement, but a more complex configuration would arise at the boundary.

A significant break in the metamorphic gradient across the Lorraine Lake floor thrust (see Chapter 7), supports the theory of major displacement. On the other hand, the existence of a major basement buttress at this location would be in accord with two observed phenomena in this part of the belt, which are similar to those sketched in Figure 5.22. Firstly, the series of large overturned  $F_2$  folds in the Lorraine Lake thrust sheet may have formed as a result of the obstruction of propagation of the detachment fault at such a basement buttress. Secondly, a step in the basement could explain the presence of basement rocks in the Carol Lake thrust sheet by footwall shortcut faulting, whereas they are presumed to be absent in the southern part of the Lorraine Lake thrust sheet. Not enough information is available to rule out either possibility.

The assumed presence of pre-Grenvillian extensional faults in the basement controlled the deformation in the western part of the thrust belt. In Section 5.1.3 it was suggested that the orientation of the Grenville Front was determined by pre-existing structures. The steep attitude of the basement thrusts and their oblique orientation with respect to the movement direction suggest that they could be inverted extensional faults. The results of a microstructural study of some of these faults are in accord with that

assumption (see Chapter 6). The overall trend of the belt is interpreted to have been controlled by the orientation of the continental margin and the extensional fault system, rather than being perpendicular to the direction of thrusting.

During the later stages of development of the thrust belt, when the detachment level stepped down from the upper to the lower thrust system, existing zones of weakness, formed by the extensional fault system, were used for the thrust movement, rather than new faults being formed. The existing linked system of extensional faults was reactivated to accomplish crustal shortening. The oblique orientation of the existing faults with respect to the direction of thrusting facilitated their reactivation (Etheridge, 1986). In the case of orthogonal convergence, the steep dip of the extensional faults would make reactivation as reverse faults mechanically unfavourable.

Most of the shear zones in the basement dip steeply to the southeast, but northwest dipping shear zones were observed as well. In the Wide Valley area the shear zones show a variation along strike between steeply northwest-dipping and steeply southeast-dipping. In the latter orientation, they have a normal fault geometry. It is assumed that these shear zones formed by the reactivation of northwest-dipping extensional faults and formed back thrusts. They were re-oriented during a late stage of deformation in the thrust belt. Locally they were steepened, elsewhere they were overturned to give an apparent extensional geometry. The Bruce Lake shear zone is also interpreted to be an overturned backthrust, rather than being a true extensional structure. Along most of its length the Bruce Lake shear zone is steeply southeast dipping, but the dip angle varies and locally the zone dips steeply northwest. This suggests that the shear zone has been folded, and presumably it has been folded from a northwest-dipping orientation into its present orientation. Folding is interpreted to be a result of simple shear in the basement rocks. This interpretation is supported by the relatively strong deformation of the basement rocks east of Bruce Lake. This interpretation of the Bruce Lake shear zone is shown in cross section I in Figure 1B.

### 5.3.3 STRUCTURAL DEVELOPMENT OF THE FOLD-AND-THRUST BELT: DISCUSSION

The Grenvillian foreland fold-and-thrust belt in western Labrador consists of two thrust systems on two different scales and levels and with different geometries. The relations between the two systems and the interpretation of the structures within them, with respect to the development of the thrust belt as a whole, is the subject of this section.

The upper and lower thrust systems, or at least the exposed parts of them, are significantly distinct, as is documented in the first part of this chapter and in Chapter 4. These dissimilarities are caused by differences in rock type, metamorphic grade, structural level, the presence of pre-existing faults in the basement rocks and possibly other, less obvious factors. In lithotectonic domain II, interference structures between the two systems indicate that the thrusting in the lower system postdated deformation in the upper system. This order of development is in accord with the regular sequence of thrusting in which thrusts in the footwall are younger than those in the hanging wall. It should be noted, however, that the in-sequence basement thrusts that breach the floor thrust of the upper system, cause out-of-sequence thrusting in the metasediments (cf. Fig. 5.2).

The length of the time gap between thrusting in the upper and lower systems is uncertain. Axial planes of  $F_{2U}$  folds change dip across a basement uplift in the Corinne Lake thrust sheet (Fig. 5.14, section I), which indicates that the thrusting in the basement there postdated  $D_{2U}$ . In the Goethite Bay thrust sheet the out-of-sequence thrusts introducing the basement rocks into the thrust sheet were not affected by as strong a recrystallization as the original  $D_{1U}$  sole thrust, which means that metamorphic temperatures had declined by the time that thrusting in the basement took place and that a significant time gap exists between the two events. On the other hand, in Chapter 6 will be shown that  $D_1$  deformation in the Emma Lake area (= thrusting at the upper detachment level) did not significantly outlast the peak of metamorphism there, which is interpreted as a stepping down of the thrust activity to the lower system shortly after the

metamorphic peak in the upper system. The fact that movement directions in the two systems are identical (compare Appendix D, Figure D.1B and Figure 5.21.A) and that the metamorphic zoning in the west of the map area is virtually continuous from one system to the other, indicates that the two systems represent progressive stages of development of a single orogenic cycle.

Throughout the upper, sediment-dominated thrust system at least two generations of structures have been observed, in most locations represented by  $S_1$  foliation and  $F_2$  folds. These two generations of structures do not represent two different deformation events on the scale of the thrust belt. They are interpreted to represent progressive phases of a continuous orogenic event for several reasons. i) Both  $D_1$  and  $D_2$  structures correspond to a north-northwest directed kinematic framework. Elongation lineations in rare  $S_2$  foliation planes have the same azimuth as those that are folded by  $F_2$  folds. ii) A wide range of styles of  $F_2$  folds exists, with a wide range of orientations, which suggests that they were affected by a variety of strain paths, rather than all having been formed at one specific time during the development of the belt. iii)  $F_1$  folds in low strain rocks in the Corinne Lake thrust sheet have similar geometries and orientations as  $F_2$  folds.

The fact that  $D_2$  structures cannot be correlated through the area may indicate that they form locally to accommodate shape changes in parts of the thrust wedge as a result of movement over ramps, obstruction of propagation of thrusts, e.g. by ancient fault escarpments in the basement, or thrust activity at a lower level (cf. Coward and Potts, 1985). This means that there is no time connotation to the numbering of structures other than on a very local scale.  $F_2$  folds in one level of the thrust belt could have been forming at the same time as  $S_1$  was developing in a lower structural level closer to the front of the thrust wedge. Figure 5.2 shows that even on a local scale the timing of structures can get complicated where interference between the upper and lower thrust belts occurs.

Although structural styles vary through Gagnon terrane, in virtually every part of the belt a similar structural relationship is found, consisting of the early development of a penetrative mylonitic foliation and thrusts, followed by folding, which is locally also related to (out-of-sequence) thrusting. This implies that every part of the belt went through a similar sequence of development.  $D_1$  and  $D_2$  structures represent sequential stages of a progressive strain path, common to most of the rocks in the belt. These two stages are: 1) deformation in the footwall of the overriding dominant thrust sheet and incorporation into the thrust wedge; and 2) deformation within the thrust wedge as a result of the movement of the wedge. Each stage is characterized by a particular stress regime and deformation style.

Deformation in the sediments started in stage 1 by emplacement of the overriding dominant thrust sheet. This provided a load and a shear strain regime. The dominant thrust sheet originally consisted of Molson Lake terrane and progressively incorporated parts of the metasediments, and subsequently also basement rocks, of Gagnon terrane. Movement of the thrust wedge occurred predominantly by deformation of the metasediments, which acted as a major shear zone. During this first stage the sediments were buried, which induced the metamorphism, and the rocks were deformed by plastic non-coaxial shear strain, causing development of the mylonitic foliation and lineation. Since the sedimentary cover was quite thin, all of these rocks were affected by simple shear deformation. One by one, thrust sheets were accreted to the sole of the thrust wedge, each going through a similar development. This leads to the conclusion that the deformation front swept through the area from southeast to northwest and that the earliest structures in the upper thrust sheets are older than the earliest structures in the lower thrust sheet.

Stage 2 started for each volume of rock after its incorporation in the thrust wedge. The transition between the two stages is assumed to have been gradual rather than abrupt, since the local stress regimes in footwall and hanging wall in the vicinity of the sole thrust are not considered to have been significantly different in an overall plastic deformation environment. Only after a volume of rocks was removed from the high

shear strain regime near the basal thrust, either by movement on a subsidiary thrust onto a lower thrust slice and into a higher level of the thrust sheet, or by cutting down of the basal thrust, could the processes of stage two become dominant. Deformation in stage two was related to the deformation within the thrust wedge during its north-northwest directed movement, while the rocks were uplifted as a result of erosion at the top of the wedge. This deformation included simple shear of the wedge as a whole to enable movement up a sloping sole thrust (Chapple, 1978) and also localized strain to adjust the shape of the wedge to maintain its critical taper, due to changes in friction at the sole, movement over ramps, incorporation of new thrust sheets into the wedge at the toe or the sole and changes in erosion rates at the surface (Platt, 1986). Structures developed during this stage were mainly folds, out-of-sequence thrusts and fold nappes, while the rocks were still in a simple shear regime.

Because the rocks continued to deform after they were incorporated in the thrust wedge, the highest thrust sheets in the southeast, which were the first to be accreted to the thrust wedge, have the longest strain histories, and the highest accumulated strains. This is in agreement with the observed strain gradient and deformation history in the map area.

Figure 5.23 is a schematic diagram of the structural development of Gagnon terrane as seen in cross section. In diagram A the continental margin is sketched, consisting of a shallow and a deeper part of the shelf and the continental slope, with sediments overlying a block-faulted crystalline basement. The Grenvillian deformation in Gagnon terrane starts with the emplacement of Molson Lake terrane which formed the overriding dominant thrust sheet (or thrust wedge). For reasons explained in Chapter 8, Molson Lake terrane was transported quite far over the shelf before thrusting in the metasediments took place. Transportation of the thrust wedge is assumed to have taken place mainly by shearing in rocks of the Menihek Formation, which formed an easy glide horizon. Possibly a large part of the rocks of the Menihek Formation formed duplexes that were accreted to the toe of the overriding thrust sheet and transported out of the area. The underlying metasediments also deformed due to

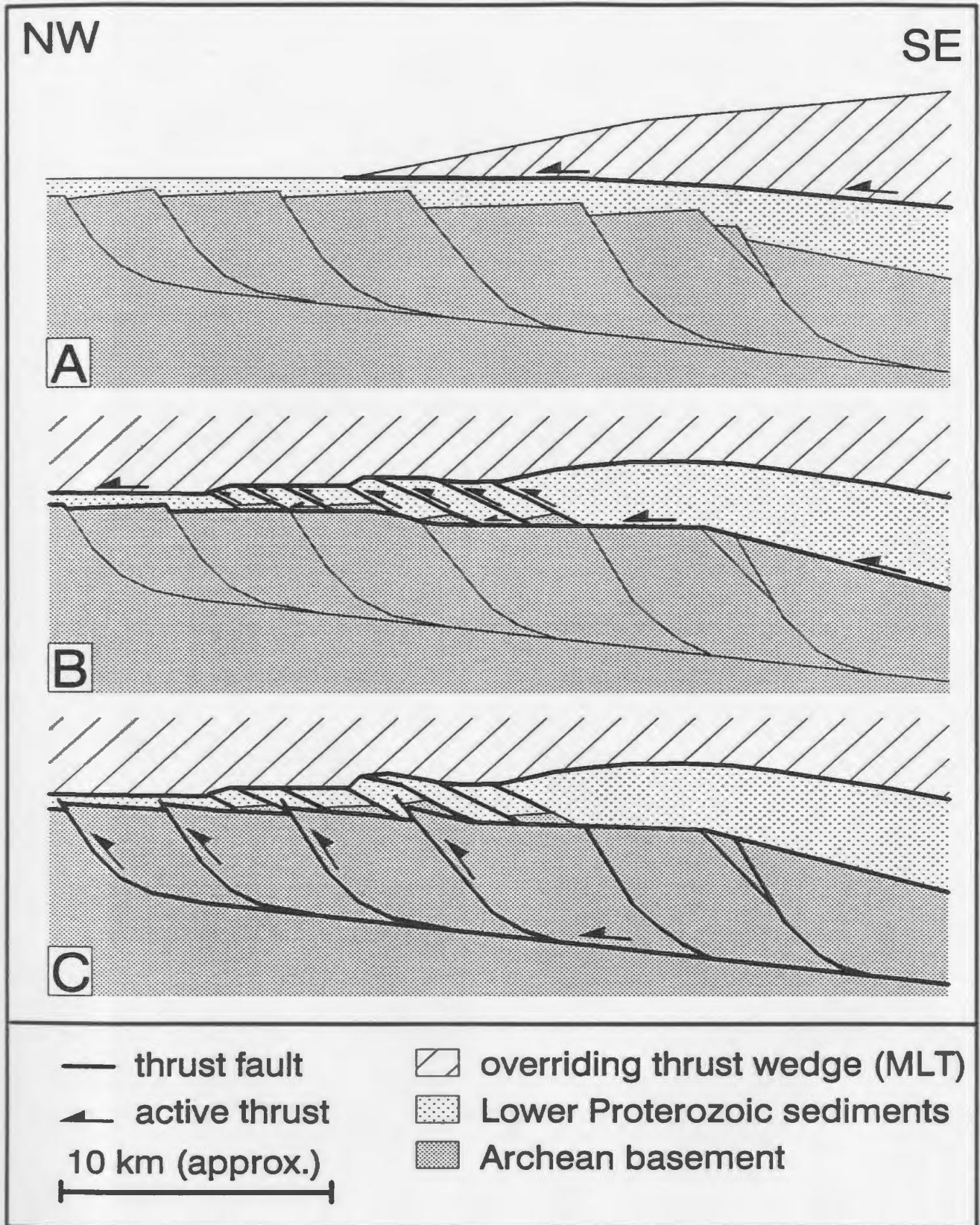


Fig. 5.23 Schematic summary of the structural development of Gagnon terrane in cross section. The vertical scale is substantially exaggerated. MLT = Molson Lake terrane. For explanation see text.

the load of the thrust wedge. In the next step (B) the basal detachment has stepped down to the basement-cover contact and the upper, sediment-dominated thrust system developed. Thrust sheets were stacked in piggy back sequence, while incorporating thin slices of basement rocks by footwall shortcut faulting. In the last diagram (C), the basal detachment stepped down once more and the lower thrust system formed in the basement, reactivating pre-existing extensional faults. The lower detachment is possibly located at the extensional detachment horizon formed during Early Proterozoic rifting, which had an orientation that was favourable for reactivation as a thrust fault.

This model for the development of the foreland fold-and-thrust belt has many similarities to models of foreland fold-and-thrust belts at high crustal levels. But the mid-crustal level metamorphic grade and the dual thrust systems of an upper thin-skinned belt and a lower basement dominated belt are assumed to be uncharacteristic for foreland belts. These points and others are discussed in Chapter 8, where a model is proposed for the development of the Gagnon terrane in western Labrador that explains the interaction of the deformation and the thermal evolution of the belt.



Plate 5.1

**Archean Basement. Gneissic banding in a rock of granodioritic composition, containing folded xenoliths with a two-pyroxene + feldspar composition. The banding in the gneiss is axial planar to folds in the xenoliths in the center of the photo. These two rock types form the predominant basement lithologies before Grenvillian deformation and metamorphism.**

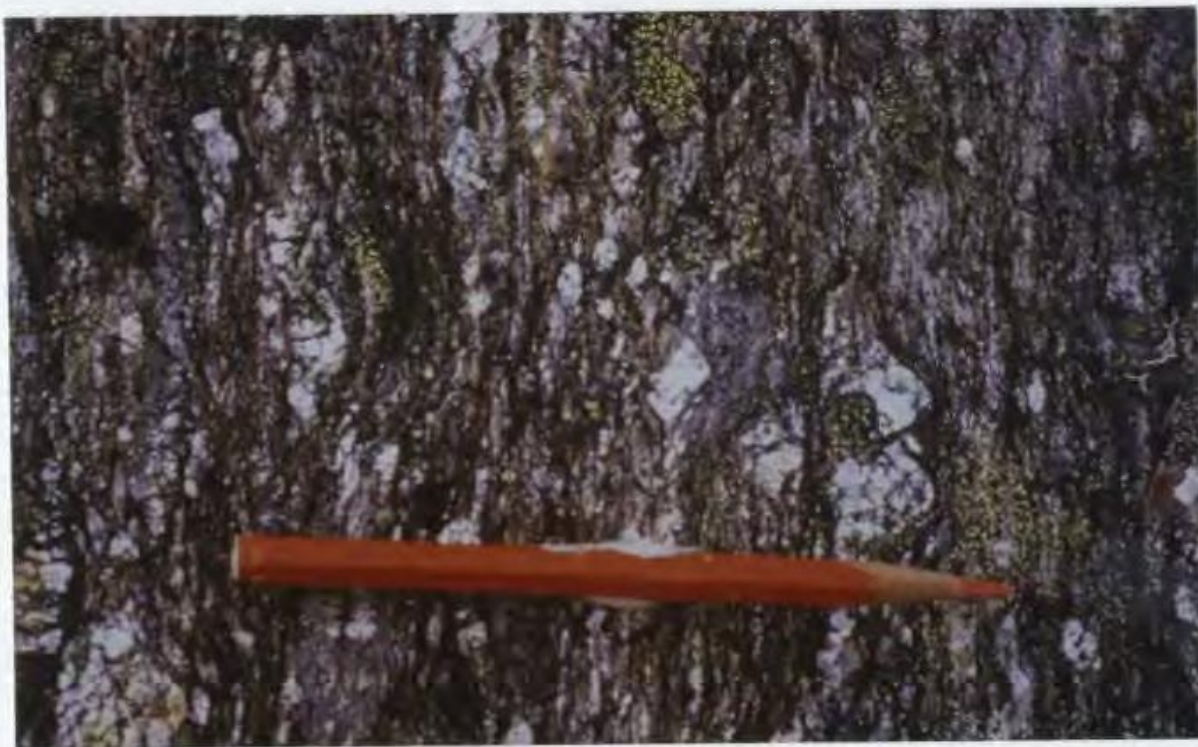


Plate 5.2

**Mylonite in the Bruce Lake shear zone. The photo is taken of a vertical wall looking northeast, just south of Bruce Lake. The porphyroclasts are feldspars or locally (above pencil tip) have a granitic composition. The sense of movement is dextral.**



Plate 5.3

High-strain quartz-carbonate iron formation. A matrix of platy, predominantly quartz-rich rocks surrounds a carbonate lens, formed by an isolated and flattened boudin, and quartz veins, interpreted to be the original fill of the boudin neck. The asymmetric shape of the carbonate lens and the foliation wrapping around it indicates sinistral shear. Outcrop 4 km west of Lac Virot.



Plate 5.4

$F_2$  fold in boudinaged banded carbonate-quartzite rocks of the Sokoman Formation, near the southern end of Flatrock Lake. The  $S_{1U}$  foliation is parallel to the bedding and both are folded in a northwest-verging fold. Note that the boudin necks are rotated in opposite senses in the two limbs.



Plate 5.5

Anastomosing foliations in basement phyllonite. The fine-grained mylonitic foliation combined with shear bands define an anastomosing pattern, creating fish-shaped domains. The sense of shear is dextral.



Plate 5.6

Stretching lineation in a quartzite of the Sokoman Formation near a thrust fault south of Flatrock Lake. The lineation is formed by rod-like quartz. The photo was taken looking down on a foliation plane.



Plate 5.7

Strongly asymmetric  $F_2$  folds in banded and foliated carbonate-quartzite rocks of the Sokoman Formation, near the southern end of Flatrock Lake. The overturned limb of the fold on the left is partially sheared. The  $S_{10}$  foliation is parallel to the bedding. The folds are northwest-vergent.



Plate 5.8

Fold interference pattern in mylonitic basement rocks. The mylonitic  $S_1$  foliation is folded by two generations of  $F_2$  folds. The younger folds have an axial plane which dips shallowly to the right, the axial plane of the older, tight folds is itself folded. Outcrop 2 km NNE of Lorraine Lake.



**Plate 5.9** Asymmetric  $F_2$  fold in gneiss of the Attikamagen Formation on the Trans Labrador Highway north of Blueberry Hill. The fold is northwest-vergent. The banded gneiss with granitic (S.L.) leucosomes is characteristic of the rocks of the Attikamagen Formation in the Wabush Lake thrust sheet.



**Plate 5.10** Foliation boudinage in gneisses in the shear zone between Molson Lake terrane and Gagnon terrane. The boudin necks are filled with pegmatitic quartzo-feldspathic veins. Outcrop 400m southwest of the top of Blueberry Hill.

## CHAPTER 6

### MICROFABRICS

In the previous chapter the geometry of the Grenville Front fold-and-thrust belt in western Labrador was described and one of the conclusions was that it comprises structures found in thrust belts at high crustal levels, but that the deformation was of a ductile nature, typical of mid-crustal levels. However, since modes of deformation are scale dependent (e.g. some ductile shear zones deform by brittle processes on a microscopic scale; Sibson, 1977; Hadizadeh and Rutter, 1983), microstructural analysis is required for an assessment of the mechanisms that controlled the flow of the rocks in the map area. A combination of field and petrographic observations can provide more information than either one alone. This is specifically true for the evaluation of kinematic indicators and deformation-metamorphism relationships. Furthermore, some of the textural features described here are essential for the interpretation of the metamorphic data in Chapter 7.

This chapter has a threefold purpose. In the first place, the ductile-plastic nature of the deformation is illustrated. Secondly, the non-coaxial nature of the deformation is demonstrated and the direction of flow is determined from kinematic indicators. Finally the variations in the temporal relationship between deformation and metamorphism are determined from microstructural relationships between metamorphic minerals and the deformed matrix. It should be stated that data and results presented in this chapter are based on a preliminary petrographic study and electron microscope imaging has not been utilized for an evaluation of microstructures and deformation mechanisms. Although on the basis of the data presented here some general conclusions can be drawn about the mechanical behaviour of the fold-and-thrust belt, a more detailed study is needed for the construction of a quantitative mechanical model for the structural development of the belt.

All microstructural descriptions and photomicrographs in this chapter are from thin sections cut parallel to the elongation lineation and perpendicular to the foliation plane. The grain sizes reported below for approximately equidimensional grains (quartz, feldspars, garnet) represent their diameters, and for elongated minerals (micas, kyanite) they are the sizes of the longest axes. Wherever the term recrystallization is used without further specification, it indicates dynamic crystallization induced by strain, incorporating both recrystallization by progressive rotation of subgrains and grain boundary migration, neither of which involve effective transport of material (c.f. Urai et al., 1986).

The photomicrographs that accompany this chapter (Plates 6.1 to 6.27) are presented in a sequence that shows the progressive development of the structures with increasing metamorphic grade for each of the rock types discussed in the chapter. Some plates contain features that are referred to in different sections. These plates are placed in a position where their main features form a logical sequence with respect to the following and previous plates. As a result the references to the plates in the text are not strictly sequential. Furthermore, some of the plates used in Chapter 7 are referred to in this chapter as well. All plates are at the end of the chapter.

## **6.1 MICROSTRUCTURAL VARIATIONS IN THE MAP AREA**

Ductile deformation is a process in which three mechanisms are active on the grain scale (White, 1976; Lister and Snoke, 1984; Urai et al., 1986): deformation by crystal plastic processes, recovery and dynamic recrystallization. These three processes compete for control of the rheological behaviour of the rocks and any of them is more or less effective, depending on the conditions at which the deformation takes place (temperature, lithostatic pressure, deviatoric stress, finite strain, strain rate,  $P_{fluid}$ ) and the material properties. Microstructures in the rocks can give reliable indications of what mechanisms have been active during the deformation process and therefore give insight into the mechanical behaviour of the rocks (White, 1976).

During crystal plastic deformation grains develop undulose extinction, kink bands, deformation lamellae and tangles of dislocations which may lead to microfracturing. This is accomplished by the creation and movement of dislocations (line defects) within the crystal structure. Recovery is the process by which dislocations are removed from the grains or organized in low energy configurations such as subgrain walls. This process can be recognized by the formation of subgrains, tilt walls and twist walls across which minor ( $< 10^\circ$ ) differences in lattice orientation exist within single grains. Polygonization is another product of recovery. It is the formation of a mosaic pattern inside a grain consisting of fairly large ( $> 100\mu\text{m}$ ) polygonal areas with slight mismatches in lattice orientation ( $< 3^\circ$ ), generally bounded by kink bands and deformation lamellae, or with ill-defined boundaries (Marjoribanks, 1976). Dynamic recrystallization occurs syn-tectonically as an annealing process and is driven by intragranular lattice-defect energy, grain boundary energy and/or external load-supporting elastic strain energy (Urai et al., 1986). It can be accomplished by progressive rotation of subgrains to increase the lattice mismatch with adjoining subgrains, or by grain boundary migration, as a result of which strained grains are replaced by strain-free grains. The former can be recognized where, within a single grain from core to rim, subgrains show an increasing deviation from the orientation of the host grain (core and mantle structure; White, 1976). The latter can be recognized in lobate or serrate grain boundaries, separating deformed from undeformed crystals. A multitude of publications exists which describe microstructures, textures and deformation mechanisms in rocks that are similar to the ones in the map area. For the terminology used here the reader is referred to Bell and Etheridge (1973), Hobbs et al. (1976), White (1976) and Bouchez (1977).

The variations of microfabrics in the map area have been studied in three different rock types: the quartzo-feldspathic rocks of the Archean basement and their reworked equivalents, metapelites of the Attikamagen, Wishart and Menihok formations, and quartzites of the Wishart and Sokoman formations. In each of these rock types the strain gradient and metamorphic gradient through the area are well reflected in the

microfabric and together these rock types constitute the bulk of the thrust belt. The deformation in these rocks can be regarded as the controlling factor of the mechanical behaviour of the belt as a whole.

For the description of the microstructures the subdivision of the area into four metamorphic zones, which was introduced in section 4.4, is used (Figure 4.2). The microfabrics are fairly consistent within each of these metamorphic zones and local variations are caused mainly by finite strain heterogeneities. The microstructural variations through the metamorphic zones is presented for the three rock types separately.

### **6.1.1 MICROFABRICS IN THE BASEMENT ROCKS**

For the reworked basement rocks used in the following descriptions, the undeformed host rock is in most cases a coarse-grained (several mm) granoblastic gneiss or migmatite consisting of Qtz + Kfs + Pl + Bt ± Pyx (Plate 6.1). Quartz commonly has a xenoblastic crystal shape, filling the spaces between feldspar and pyroxene porphyroblasts. Locally the precursor of the reworked basement rocks is a megacrystic granite with minor biotite.

The descriptions given here present microstructural variations which are similar to those of a single mylonitic shear zone in a gneissic rock deformed at amphibolite grade metamorphism presented by Bell and Etheridge (1973). Simpson (1985) studied microstructures in granites ranging from lower greenschist to amphibolite grade and found a similar range of microstructures. The strain level of the rocks described below ranges from virtually undeformed to ultramylonitic. The protomylonites, mylonites and ultramylonites appear in the thrusts within the basement, in the detachment zone between lower and upper thrust systems, in the thin sheets of basement rocks incorporated in the sediment-dominated thrust sheets, throughout the Elmer Lake thrust sheet and in the northern part of the Corinne Lake thrust sheet. Because of the small grain-size and the high concentration of sheet silicates in the ultramylonites, they are referred to as phyllonites. Plates 6.1 to 6.8 show the range of microstructures with increasing strain and the effects of increasing temperature are shown in Plates 6.9 and

6.10. The different mineral species behave differently under stress at identical conditions, e.g. brittle deformation of feldspar versus ductile deformation of quartz at low temperatures (Plate 6.3), and are described separately in each of the rock types.

#### 6.1.1.1 Basement rocks deformed at very low metamorphic grade

Some of the shear zones in the basement rocks show microstructures which are typical of deformation at very low temperatures (sub-greenschist to low greenschist facies) or high strain rates. Some of these, e.g. in the south Flatrock Lake area, are related to late-metamorphic out-of-sequence thrusts, others are found in regular sequence thrusts, which also show higher temperature microstructures. The latter are assumed to be caused by late movements on pre-existing thrusts.

In outcrop these rocks are fine-grained mylonites and ultra-mylonites with angular porphyroclasts (Plate 5.2). Quartz appears as long (> 1cm) ribbons, with aspect ratios up to 30:1, which wrap around undeformed or fractured feldspar porphyroclasts. Some quartz host grains developed into several ribbons with large lattice mismatches between ribbons (up to 90°), separated by kink boundaries (< 2µm wide) or narrow deformation bands (< 10 µm wide). Zones of "cloudy quartz" are mostly parallel to the ribbons, but can appear in other orientations as well. They contain extremely small (< 2µm), ill-defined subgrains with irregular shapes and small mismatches in lattice orientation. The ribbons show undulose extinction, deformation lamellae, kink bands, and polygons. All these microstructures suggest that deformation occurred by crystal plastic strain with minor recovery. In samples where feldspars did not break down to sericite or zoisite, the rocks have less than 5% matrix, feldspars are intensely fractured (Plate 6.2) and most of the ductile strain was partitioned into the quartz. In cases where replacement of feldspar did take place, the matrix is very fine-grained and consists mainly of quartz, chlorite, white mica and zoisite. Quartz grains in the matrix are also strongly elongated (aspect ratios up to 5:1) and show the same type of cloudy subgrain textures as the large ribbons. Biotite is commonly strongly kinked and pulled apart, or at higher strains both mechanically and chemically broken down to long trails of chlorite.

### 6.1.1.2 Basement rocks in the low grade thrust sheets

Basement rocks in lithotectonic domain I that appear undeformed on outcrop scale generally show signs of low strain in thin section. The first signs of deformation are visible in quartz grains as undulose extinction, subgrains, deformation lamellae and kink bands at the grain boundaries and in deformation bands. With increasing strain the lattice mismatch of the subgrains increases, resulting ultimately in the formation of new grains, and the mantle of subgrains widens, consuming progressively more of the core of the host grain (Plate 6.3). The subgrains are approximately  $20\mu\text{m}$  in size. The quartz cores show polygonization, often with the long axes of the polygons parallel to the projection of the crystallographic C-axis (Plates 6.3 and 6.7). In many cases the mantles of subgrains or newly formed grains are sheared off the host grains and form quartz tails (Plate 6.5 and 6.7). Quartz porphyroclasts can only survive high strain in orientations which are unfavourable for activation of the dislocation slip systems ("hard grains"). In the mylonites the crystallographic C-axes in most of the equidimensional quartz porphyroclasts are orientated at  $30-60^\circ$  to the foliation plane (Plate 6.7) at a low angle to either the X or Z axis of the instantaneous strain ellipsoid, which is assumed to be at  $45^\circ$  to the flow plane. Grains with orientations that are favourable for activation of the slip systems deform to ribbon grains. The majority of the quartz porphyroclasts recrystallize to elongate aggregates of small ( $50-200\mu\text{m}$ ) (sub-)grains, locally with remnants of the host grain in the core (core and mantle structure; plates 6.3 and 6.5, bottom).

Feldspars deformed by both brittle and plastic processes (c.f. Hanmer, 1982; Simpson, 1985). At the lowest strain the large grains are cut by conjugate sets of fractures or shear bands, breaking the grains into lozenge shaped porphyroclasts (Plates 6.2 and 6.3). Feldspar recrystallized along grain boundaries and deformation bands to quartz-white mica mixtures and dilating fractures were filled with quartz, white mica and calcite. The degree of sericitization of feldspars is approximately proportional to the strain in the rock and white mica and zoisite in the feldspars are commonly aligned with the foliation in the matrix. With increasing strain feldspars are progressively

broken down, segregation bands form (Hanmer, 1982), parts of porphyroclasts become further separated and pressure shadows start to form (Plate 6.5). Porphyroclasts are progressively rounded as a result of a combination of rotation and removal of asperities by strain induced chemical breakdown (Plate 6.6). In relatively incompetent (mica-rich) matrices or where grains do not rotate, feldspars can retain their original asymmetric lozenge shape (Plate 6.8).

Biotite grains that are oriented with their (001) planes parallel with the shortest axis of the strain ellipsoid are pulled apart in a direction perpendicular to their cleavage planes (Plate 6.2, left side of photo, and Plate 6.4). The dilation sites are filled in with newly grown (green) biotite, quartz and rarely white mica. Biotites do not commonly form kinks, which is possibly a result of the network of rutile needles in the grains (Plate 6.4, see also Plate 7.1). At higher strains the biotites with (001) planes at low angles to the foliation are pulled apart as well, but they tend to separate parallel to the cleavage planes, forming mica fish and mica trails (Plate 6.7).

The volume of matrix versus porphyroclasts increases with strain as a result of recrystallization of quartz and breakdown of feldspar to quartz-mica ( $\pm$  zoisite) aggregates or small ( $< 100\mu\text{m}$ ) porphyroclasts and of pyroxenes to fine-grained actinolite and/or chlorite. At low strain the matrix originates as a thin network surrounding porphyroclasts or filling fractures and deformation bands (Plate 6.2). With increasing strain it forms a foliation anastomosing around the porphyroclasts and delineating S and C planes (Plate 6.6; c.f. Berthé et al., 1979). In the mylonites (matrix constitutes over 50% of the rock) the matrix forms a fine-grained, well foliated mass which wraps asymmetrically around the porphyroclasts. Preferentially oriented micas and elongated quartz grains ( $\pm$  zoisite,  $\pm$  actinolite) define the foliation. Quartz in the matrix is deformed, which is suggested by undulose extinction, subgrains and serrated grain boundaries. Grain sizes are 20-50 $\mu\text{m}$  for quartz and around 20 $\mu\text{m}$  for the micas. Shear bands, which generally originate on porphyroclasts, are common in

the mylonites and ultramylonites, and they locally form Type I S-C mylonites (Lister and Snoke, 1984). Rigid crystals such as epidote, apatite, tourmaline, actinolite are locally boudinaged and form trails of fragments.

### 6.1.1.3 Basement rocks in the low to medium grade thrust sheets

On mesoscopic scale the same variation in strain from mesoscopically undeformed rocks to ultramylonites is observed. However, the variations in microstructures are less distinct as a result of stronger syn- and post-kinematic recrystallization.

The most obvious difference between these rocks and those in the lower grade thrust sheets is the increased grain size in the matrix. Quartz and micas are in the order of  $100\mu\text{m}$ . The matrix is well-foliated, mainly as a result of the preferred orientation of the micas, whereas in high strain areas the quartz grains are elongated as well. The grain shapes and boundaries of the quartz in the matrix are more sharply defined than in the lower grade rocks, but grain boundaries are curved or serrated. The matrix quartz grains are internally kinked or show undulose extinction. In many samples a differentiation has taken place, separating mica-rich bands from quartz-rich bands (Plate 6.8).

All porphyroclasts show signs of static and/or dynamic recrystallization. Quartz porphyroclasts are aggregates of new, strain-free grains ( $>200\mu\text{m}$ ), commonly with one or several larger grains in the centre as relics of the host grain. Quartz grain boundaries tend to be lobate, suggesting recrystallization by grain boundary migration. The aspect ratios of the aggregates increase with strain and individual new grains may have elongate grain shapes as well.

Mica and zoisite inclusions in feldspar porphyroclasts are larger and less abundant than at lower grades, and tend to be oriented parallel to crystallographic orientations of the hosts, rather than parallel to the foliation in the matrix. New growth of feldspar occurs as inclusion-free rims in pressure shadows and in originally dilated brittle cracks

in the porphyroclasts. Feldspar recrystallizes along narrow deformation bands within grains. Lobate grain boundaries, suggesting grain boundary migration between feldspar grains, and recrystallized trails were observed in a few samples.

Biotite porphyroclasts are progressively stretched out with increasing strain and are completely recrystallized. In the least deformed samples the biotites form decussate aggregates of randomly oriented, completely recrystallized grains, replacing larger biotites or pyroxenes. In rocks with larger strains biotite forms mica-rich bands with individual grains oriented approximately parallel to the foliation.

#### **6.1.1.4 Basement rocks in the medium grade thrust sheets**

Strong post- or late-kinematic recrystallization has erased much of the original microstructures and the rocks show generally equilibrium textures. The rocks are coarse-grained (average grain size  $>500\mu\text{m}$ ) schists and gneisses with preferentially oriented micas defining the foliation. In some samples thin layers of predominantly quartzitic, feldspathic or micaceous composition may represent completely recrystallized and stretched out porphyroclasts (Plate 6.9). All phases have slightly curved or straight grain boundaries. In lower strain rocks feldspar porphyroclasts are still recognizable and locally the foliation wraps asymmetrically around them (Plate 6.10). Recrystallized tails on K-feldspar porphyroclasts are common. Plagioclase porphyroclasts commonly have wide inclusion-free overgrowth rims in the pressure shadows (Plate 6.10). Pre-existing cracks in porphyroclasts are healed by recrystallization or new growth. Quartz porphyroclasts were not observed and are assumed to have completely recrystallized to aggregates of smaller grains.

#### **6.1.1.5 Quartz-porphyroclastic mylonites in reactivated normal faults**

Some of the relatively steep thrusts in the basement in the western part of the area (lithotectonic Domain I), which are assumed to be reactivated extensional faults (Chapter 5), are formed by mylonites in which the porphyroclasts are predominantly quartz grains and the matrix is mica-rich (Plate 6.11). This phenomenon was observed specifically in the Grenville Front thrust north of Bruce Lake, in the back thrust west of

the Wide Valley triangle zone and a few other thrusts in Domain I. The host rocks in which these fault zones developed are similar to the basement rocks of all other shear zones. The fact that only quartz, and locally biotite, survived the mylonitization is in contrast to the fact that in most other shear zones strain was accommodated mainly by plastic deformation of quartz and feldspar porphyroclasts survived longest (Plate 6.3).

The reason for this phenomenon is assumed to be a weakening of the feldspars by hydrous alteration (c.f. Janecke and Evans, 1988). During pre-Grenvillian extensional faulting and subsequent sedimentation, the fault zones were presumably saturated with fluids, which later caused intense sericitization of the feldspars, but had no major weakening effect on the quartz grains. This is observed in the less deformed wall rocks, in which the feldspars are replaced to a large extent by a very fine-grained white mica and quartz aggregate, preferentially along fractures and grain boundaries (Plate 6.12). The large original quartz grains commonly have preserved their irregular xenoblastic grain shapes and are not strongly deformed. Most of the strain was partitioned into the fine-grained quartz-mica mixture. In virtually undeformed wall rocks near the shear zones, the feldspars are also replaced by sericite, suggesting that the sericitization of the feldspars happened statically before Grenvillian deformation and was not induced by the strain. When the extensional faults in the basement were reactivated during the Grenvillian thrust event, the fine-grained quartz-sericite-feldspar mixture formed a weak matrix which accommodated most of the strain and the competent quartz grains were less deformed. Together with the oblique orientation of these faults with respect to the direction of thrusting (Chapter 5), the hydrous alteration enabled the reactivation of these pre-existing fault zones during compression, which was favoured over development of new low-angle reverse faults in undeformed basement rocks.

### 6.1.2 MICROFABRICS IN THE QUARTZITIC ROCK TYPES

Rocks of both the Sokoman and the Wishart formations contain virtually pure quartzites and provide the opportunity to study the microstructural behaviour of quartz in the map area.

The quartzites in the Sokoman Formation were derived from cherts (Wardle and Bailey, 1981). The purest quartzites are found in the oxide member of the formation, but in most of the samples small amounts of magnetite, hematite, carbonate, amphibole or mica are still present. Rocks that contained up to 30% of other minerals were used for this study. Carbonate grains or layers were more competent than the quartz matrix. Single grains form porphyroclasts, locally with  $\sigma$  or  $\delta$  shaped tails (Passchier and Simpson, 1986) and the foliation wrapping around them, and carbonate layers are commonly boudinaged on microscopic scale. Oxide grains are generally too small to analyze their rheological behaviour with respect to quartz. Micas are aligned in the foliation planes in the rocks. Because of the fine-grained nature of the precursor, no quartz porphyroclasts were formed and the rocks deformed homogeneously.

The quartzites of the Wishart Formation were derived from generally pure ortho-quartzites (Wardle and Bailey, 1981). These rocks occur only in the amphibolite facies thrust sheets and their original sedimentary character has completely been erased. They are now predominantly well foliated, pure, coarse-grained quartzites, locally containing muscovite and, less frequently, garnet, staurolite or kyanite.

Four examples of quartzites are shown in Plates 6.13 to 6.16 with increasing metamorphic grade. The majority of the studied quartzite samples consisted of Type II S-C mylonites (Lister and Snoke, 1984) with a mylonitic foliation plane defined by platy minerals or trails of fractured grains, which represents the flow plane (or C-plane) on the scale of observation. The S-planes are oblique to the flow plane and are defined by elongated quartz grains, preferred orientations of grain boundaries or alignment of grains with similar crystallographic orientation. The S-planes originated along the X-Y plane of the instantaneous strain ellipsoid, but rotated towards the flow plane with progressive non-coaxial shear. Continuous recrystallization may reset the "strain clock" which results in a cyclic creation, rotation and destruction of the S-planes, which therefore can show a range of angles with respect to the C-Plane between  $0^\circ$  and  $45^\circ$  (usually between  $10^\circ$  and  $40^\circ$ ; Lister and Snoke, 1984). This type of structure, in which the angle between S and C planes is independent of the finite strain, has been

referred to as steady-state foliation (Means, 1981). Alignment of platy minerals with the flow plane suggests that the X-axis of the finite strain ellipsoid has rotated into an orientation virtually parallel to the flow plane.

In the majority of the samples the flow plane is approximately parallel to the bedding on the scale of the thin section. Only in folds in which quartz is elongated along the axial plane, are bedding and mylonitic foliation obviously at an angle to each other. In few other samples a small angle ( $< 10^\circ$ ) exists between the two. The mesoscopically visible  $S_1$  foliation plane corresponds in all cases to the C-plane in the thin section.

In virtually all analyzed rocks the quartz displays a crystallographic preferred orientation, as determined in most thin sections by inserting the gypsum plate in the microscope. The interference colors of the quartz grains changed from dominantly blue to dominantly orange during rotation of the thin section. C-axis fabrics were determined of fourteen samples from different parts of the area, and are discussed together in section 6.1.2.4.

#### 6.1.2.1 Quartzites in the low grade thrust sheets

In virtually all samples the quartz grains define both a crystallographic and grain shape fabric. The lowest strain rocks have a polygonal (foam) texture with slightly elongated grains in some domains. The equilibrium grain size is  $\pm 50-100\mu\text{m}$ . In rocks with higher strain the quartz grains become more elongated and they show undulose extinction, kink bands and small subgrains (10 to  $20\mu\text{m}$ ). The quartz foliation (S-plane) is oblique to the flow plane (C-plane), the latter being defined by trails of magnetite or hematite, or locally grunerite or chlorite (Plate 6.13). With increasing strain the following changes are observed (Plate 6.14): the aspect ratio of the grains increases; the grain boundaries become serrated and less sharply defined; the long axes of the grains progressively rotate towards the flow plane; the crystallographic C-axes progressively align (more homogeneous orange or blue colour with gypsum plate inserted). The angle between S and C-planes varies from  $30^\circ$  to  $40^\circ$  in the lowest strain rocks, to

between  $10^\circ$  and  $20^\circ$  in the rocks with the highest strain. In the most extreme cases in the ductile thrusts, the grains have aspect ratios of up to 1:20 and they consist of clouds of ill-defined subgrains with similar crystallographic orientations (Plate 6.14).

#### **6.1.2.2 Quartzites in the low to medium grade thrust sheets**

At higher temperatures of deformation dynamic recrystallization is a more important mechanism. In most of the samples the grain boundaries are serrated or lobate, suggesting grain boundary migration (Plate 6.15). Grain sizes range from 150 to  $400\mu\text{m}$ , which is a significant increase from the lower grade rocks and suggests grain growth. All rocks have a grain-shape and a crystallographic fabric, which varies from weak to moderately strong. Flow planes are indicated by grunerite needles, trails of magnetite or carbonate, or by trails of fine-grained quartz, commonly strongly elongated along the flow plane. The S-planes are not well developed because of irregular grain shapes and larger variation in orientations of the long axes of the grains. No relation was found between the qualitatively estimated strain intensity and the angle between the S and C-planes, which varied in most samples between  $25^\circ$  and  $50^\circ$ . Angles between S and C-planes larger than the theoretical maximum of  $45^\circ$  reflect an alignment of grain boundaries parallel to subgrain structures during recrystallization, rather than extension at a high angle to the flow plane (Lister and Snoke, 1984). Intra-crystalline deformation was restricted to undulose extinction and kink bands and few subgrains were observed. All these observations are consistent with significant dynamic recrystallization in a steady-state foliation.

#### **6.1.2.3 Quartzites in the medium grade thrust sheets**

The following microstructures were observed in both the quartzite member and the quartz-rich part of the pelitic member of the Wishart Formation and in the quartzitic oxide member of the Sokoman Formation in the Goethite Bay area and the southeastern part of the Rivière aux Fraises area. Plate 6.16 is an example of a quartzite of the Wishart Formation in the Goethite Bay area.

The grain size in these rocks is variable within samples and ranges from 200 $\mu$ m to several mm, with the majority being between 0.5 and 1mm. The S-C mylonite microstructures are not always readily recognizable. All studied samples have a strong crystallographic preferred orientation of the quartz grains. The shapes of most grains are extremely irregular, especially the larger ones. The grain boundaries are formed by straight or slightly curved segments at angles to each other, which together define a strongly curvilinear trace. In many cases parts of the grain boundaries and small elongated grains are still aligned along the S-plane at a 20–45° angle to the flow plane, or parallel to it. In the larger grains, larger angles between grain boundaries and C-planes have been observed (Plate 6.16). These observations suggest a partial static recrystallization after the formation of the S-C mylonite. Much of the original S-C fabric was presumably destroyed by exaggerated grain growth of some of the grains at the cost of others, but some of the original grain boundaries were preserved (c.f. Lister and Snoke, 1984). The flow plane is in some cases indicated by recrystallized "fish" and trails of muscovite, carbonate or apatite. In other cases strings of fine-grained quartz, commonly decorated with small opaque particles, outline the flow plane. The large irregular grains tend to extend across the flow planes, suggesting that the growth occurred post-kinematically.

A few of the quartzites occurring near the out-of-sequence thrusts in the area are S-C mylonites similar to the ones described in the previous section of the low- to medium-grade thrust sheets. This indicates that no static recrystallization followed the out-of-sequence thrusting and that probably the thrust movement took place at lower temperatures than the regular sequence thrusting.

#### 6.1.2.4 Quartz C-axis fabrics

Figure 6.1a shows six examples of C-axis fabrics from quartzites which were deformed at different metamorphic grades. All diagrams are plotted in the same orientation with respect to the microstructures and approximately with respect to geographic coordinates (looking NE). The trace of the foliation is horizontal and the extension lineation is horizontal E-W (Fig. 6.1b). The bulk flow plane, parallel with

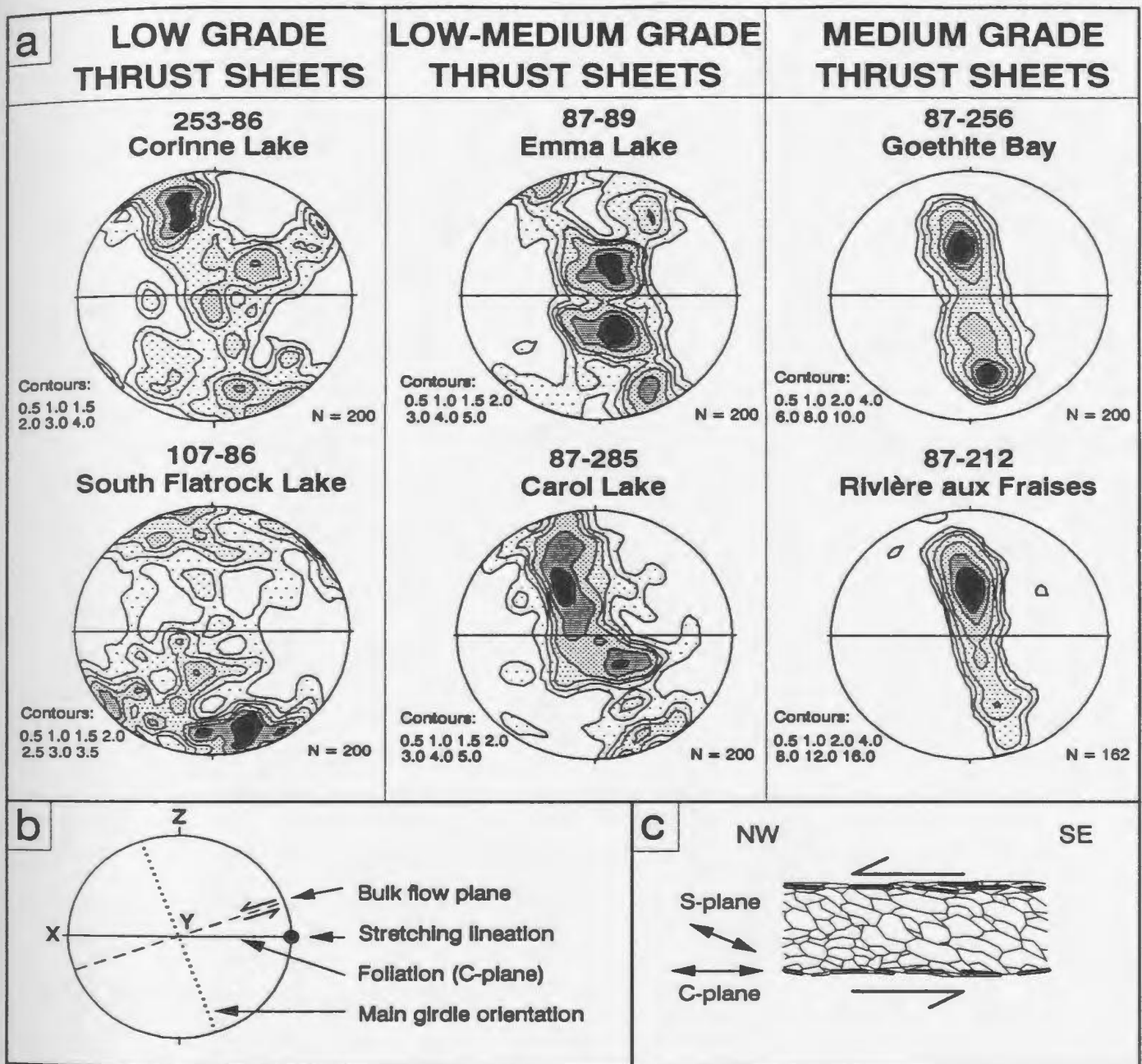


Fig. 6.1 Examples of quartz C-axis fabrics from S-C mylonites in quartzites of the map area. a) Typical crystallographic fabrics for different metamorphic zones. The definition of the fabric skeleton and the concentration in maxima increases with metamorphic grade. All fabrics have the same asymmetry with respect to the mylonitic foliation. The fabrics are plotted in lower hemisphere equal area projection. N = number of measurements. The data-points are contoured using a Gauss-like counting function. Contour levels are expressed as multiples of uniform distribution. b) shows the orientations of the different fabric elements in the plots. X, Y and Z are the principal axes of the finite strain ellipsoid, with the X-Y plane assumed parallel with the mylonitic foliation plane and the stretching lineation parallel with the X axis. The orientation of the plots with respect to the microstructures is schematically shown in c).

the shear zone boundaries, is indicated perpendicular to the main girdle, as suggested by Lister and Williams (1979). Many studies of quartz petrofabrics have shown that the interpretation of crystallographic preferred orientations is not simple and the patterns are not always consistent in predicting the direction of non-coaxial flow (Lister and Williams, 1979; Simpson and Schmid, 1983; Bouchez et al., 1983). The diagrams have to be studied in relation to the microstructures. The quartzites from which these diagrams were taken are all Type II S-C mylonites, which in themselves provide reliable kinematic indicators (Lister and Snoke, 1984).

The most obvious trends from the lowest to the highest thrust sheets are the better definition of the girdles, the change of crossed girdles to single girdles and the increase of maximum concentrations. All diagrams show the same asymmetry and have maxima on the same central girdle which is inclined with respect to the Y-Z plane of the finite strain ellipsoid (Fig. 6.1b). This configuration suggests northwest directed non-coaxial flow, which is consistent with the observed microstructures of the S-C mylonites (Fig. 6.1c). The crossed and single girdle patterns are indicative of near plane strain deformation (Law, 1990). The fabric diagrams from the low grade thrust sheets approach Type II crossed girdles (Lister and Williams, 1979) and have maxima at high angles to the foliation plane, which is consistent with slip on the basal plane (Lister, 1981). In the low- to medium-grade thrust sheets the fabrics change to Type I crossed girdles (Lister and Williams, 1979), consisting of one dominant girdle and two less developed "legs", which sometimes are absent, as in sample 87-285 (Fig. 6.1a). The maxima are oriented at small angles to the Y-axis of the finite strain ellipsoid, which is consistent with slip on the prism plane at higher temperatures (Lister, 1981; Law et al., 1990). In the medium-grade thrust sheets dynamic recrystallization is an important mechanism in the development of the fabric. The axes define an incomplete single girdle with maxima at approximately 40° from the Y-axis. This is a pattern similar to that from a shear zone in a quartzite in the Torridon area in NW Scotland, which was interpreted to have deformed by glide on the rhomb  $\langle a \rangle$  slip system (Law et al.,

1990). The stronger development of one of the two maxima may be an effect of post-kinematic, static recrystallization (Hobbs et al., 1976, p.135), or of the existence of an older, pre-shearing crystallographic fabric.

The main observations to be made from Figure 6.1 are that: 1) the rocks deformed by non-coaxial, northwest-directed flow; 2) towards the higher thrust sheets progressively higher temperature slip systems and deformation mechanisms were active, resulting in different orientations of the maxima in the fabric diagrams; 3) increasingly higher strains are inferred to be responsible for the progressively better definition of the patterns and higher maximum concentrations towards the higher thrust sheets. Similar changes in slip systems with increasing temperature have been described by Lister (1981) and Law et al. (1990). The increase of the finite strain from the lower to the higher thrust sheets is consistent the observed strain gradient on mesoscopic scale (Chapter 5). In the map area it is not clear to what extent variations in factors other than temperature and finite strain have played a role in the variation of observed crystallographic fabrics.

### **6.1.3 MICROFABRICS IN THE METAPELITIC AND SEMI-PELITIC ROCKS**

The metapelitic rocks of the Attikamagen and Menihek formations differ from the remainder of the rock types in the primary abundance of phyllosilicates, which can define a primary fabric that forms a pervasive sub-horizontal anisotropy on a grain-scale before the start of the deformation. Mylonites in the basement rocks commonly develop a foliation which is similar to that of the metapelites, but this does not happen until a certain level of accumulated strain. In areas where true metapelites are absent, the mica-rich mylonitic basement rocks can be used to demonstrate microstructures of mica-rich rocks (e.g. in the Elmer Lake thrust sheet).

#### **6.1.3.1 Metapelites in the low grade thrust sheets**

At greenschist metamorphic grade these rocks are graphitic phyllites or schists, containing very fine-grained micas, graphite, quartz and minor K-feldspar and plagioclase. The graphite is either evenly distributed throughout the rock as fine dusty

particles or it is concentrated along cleavage planes in mica stacks and along shear bands. The rocks have a lithological layering defined by different quartz/mica ratios. On average, quartz and feldspar grains are smaller than  $50\mu\text{m}$  and micas are up to  $100\mu\text{m}$  long. The grain sizes decrease with progressive strain. Many of the samples contain structural elements of three generations: an early foliation, a shear band cleavage and a younger crenulation cleavage, of which the first two are  $S_1$  structures and the crenulation cleavage is an  $S_2$ . The early foliation consists of oriented micas (Plate 6.17) and is commonly parallel to bedding. In a few samples it forms an axial planar fabric of isoclinal folds. At low strains quartz shows an equilibrium texture with sharply defined, straight grain boundaries and has undulose extinction. Single grains are slightly elongated, commonly as a result of the definition of their boundaries by parallel micas. At higher strains the quartz grains are more elongated and show kink bands and subgrains. In the rocks with the highest strain quartz and feldspar generally form elongate lenses with micas wrapping around in an anastomosing pattern, forming a micro-scale shear band cleavage (Plate 6.17). In these rocks, mica-rich bands in a quartz-rich matrix are locally boudinaged, form mica fish, or show pinch-and-swell structures. The necks of the mica fish are formed by microscopic shear zones.

Mesoscopically visible shear bands in the metapelites occur only in high strain zones. These shear bands originate from the microscopic ones at the boudin necks. They consist of extremely fine-grained material ( $< 1\mu\text{m}$ ), of which only the aligned micas can be recognized. The early foliation curves into the shear bands and the two are assumed to be genetically related (c.f. Platt and Vissers, 1980; Platt, 1984).

$F_2$  folding resulted in a crenulation cleavage in the mica-rich bands (Plate 6.18). In folds with relatively large interlimb angles (up to  $120^\circ$ ) the micas are kinked or bent. In tighter folds the kink band boundaries migrated or the micas recrystallized to form polygonal arcs, in which the individual micas outline an almost continuous range of orientations, forming a complete arc (Plate 6.18). Micas in the fold limbs aligned to

form a crenulation cleavage, or locally a differentiated layering, which became the dominant structure and in a few outcrops it is the only foliation that can be recognized on mesoscopic scale.

#### **6.1.3.2 Metapelites in the low to medium grade thrust sheets**

Recrystallization of quartz and mica was more intense in these rocks. The average grain size increases for quartz to 100-200 $\mu$ m and for micas up to 400 $\mu$ m. In layers or lenses where no graphite is present, the average grain size is significantly larger (quartz: 0.5mm, mica: 1mm), suggesting that the graphite in the rocks inhibited grain growth by pinning of migrating grain boundaries (Urai et al., 1986). Quartz grains have an equilibrium texture with minor kinking or undulose extinction. In high-strain rocks plagioclase has fine-grained subgrain textures (Plate 6.21). The  $S_1$  foliation consists of preferentially oriented micas. Lens-shaped mica-fish are absent and where mica layers terminate abruptly, the ends appear frayed instead of pinched off. This is a result of growth of some of the micas across the rim of the mica band after deformation. Shear bands are only recognizable in thin section by the alignment of micas along them at a low angle to the foliation.

Compared with the crenulations in the lower grade thrust sheets, the polygonal arcs contain a smaller number of larger crystals that outline the fold hinge, which are not or only slightly bent and which have larger mismatches in orientations (Plate 6.19). Where a crenulation cleavage is formed in relatively quartz-rich rocks, the fold hinges are represented by isolated cross-micas and the crenulations themselves are often not recognizable anymore. This commonly resulted in the formation of a differentiated layering.

#### **6.1.3.3 Metapelites in the medium grade thrust sheets**

The only metapelites observed in this part of the area are from the lower pelitic member of the Wishart Formation. These rocks differ from the ones described above in their high quartz content. Even in the layers with the highest content of mica, the quartz forms the load-bearing framework. These rocks deformed by homogeneous

shear rather than by folding. The foliation is generally defined by isolated, aligned micas. Quartz grains in the pelitic layers have a fairly homogeneous size with an average of  $300\mu\text{m}$ . They have equilibrium grain shapes and boundaries and reveal virtually no internal deformation.

#### **6.1.3.4 Metapelites in the medium to high grade thrust sheets**

At the highest metamorphic grades, the metapelites appear as schists and gneisses. Grain sizes are in the order of millimeters and some of the porphyroblasts are up to several centimeters in diameter. Preferentially oriented micas, kyanite and locally elongated quartz and feldspar grains define a foliation (Plates 6.20, 6.25 and 6.26). In many cases the rocks have a gneissic or differentiated layering. Cross-micas commonly occur in the differentiated layering and in a few samples graphite flakes outline isoclinal folds with an axial plane parallel to the foliation. This suggests that the main foliation ( $S_1$ ) in the rocks is a second generation structure, possibly a recrystallized crenulation cleavage, and that a pre-existing foliation, which cannot be recognized mesoscopically, was completely transposed towards the  $S_1$ . The boundaries between quartz grains tend to be straight, but quartz-plagioclase boundaries are strongly curved, suggesting migration of these boundaries. However, this is interpreted as a recrystallization driven by a metamorphic reaction rather than by deformation. The foliation in the rock is draped around the porphyroblasts, locally in an asymmetric pattern.

#### **6.1.4 MICROSTRUCTURES AND DEFORMATION MECHANISMS**

The microstructures described in the previous sections indicate that the rocks in the map area deformed predominantly by ductile-plastic processes. In the lowest grade thrust sheets the quartz grains generally formed the load-bearing framework, specifically in the quartz-rich rocks, and deformed by crystal plastic processes. Feldspars deformed by brittle processes at the lowest temperatures, but subgrain formation and recrystallization occurred in the low to medium grade, and higher grade, thrust sheets. In the higher grade thrust sheets the organization of dislocations in feldspars into subgrains, the progressive rotation of subgrains in core-mantle structures and the presence of lobate grain boundaries indicate that recovery and recrystallization

were dominant. Crystal plastic deformation of feldspar took place as well as recovery and recrystallization and new crystallization in pressure shadows.

The grain growth of different mineral species in the matrix could only take place if their constituent components could diffuse through the rock and concentrate in growing grains. It is therefore likely that diffusion also played an important role in the deformation of the matrix (White, 1976).

The variation in deformation mechanisms in the map area is a result of a variation in temperature, finite strain, strain rate, deviatoric stress, lithostatic pressure, fluid pressure and composition and material properties. The variations in finite strain (Chapter 5) and the lithostatic pressure and temperature (Chapter 7) are fairly well established, but the remainder of the controlling factors are poorly constrained. The changes in microstructures seem to occur at the same places as the changes in metamorphic grade (floor thrusts of the Elmer Lake, Goethite Bay and Corinne Lake thrust sheets). It seems likely that the metamorphic pressure and temperature were important factors in the regional variation of deformation mechanisms. The other factors are expected to have caused changes on a smaller scale, for example, within thrust sheets or single shear zones.

## **6.2 INDICATIONS FOR NON-COAXIAL FLOW**

The ductile nature of the deformation has been established in the previous sections, but no specific attention was paid to the type of flow. All naturally occurring deformation falls between the end members of pure shear and simple shear and is heterogeneous on most scales (Ramsay and Huber, 1983; Platt and Behrmann, 1986; Law et al., 1986). Lister and Williams (1983) indicated that a more useful distinction is that between coaxial and non-coaxial flow, which refers to the strain path rather than to the finite state of strain. Any component of progressive simple shear will result in non-coaxial flow and the latter term covers the whole range of strain paths between progressive pure shear and progressive simple shear (not including the pure shear end member).

The microstructures described above contain many indications of a component of pure shear. A bedding parallel extension is indicated by the development of foliation parallel to bedding, by alignment of micas, elongation of quartz grains, pressure shadows around porphyroclasts, pulled apart biotites, feldspar and other porphyroclasts and boudinage of mica and carbonate layers in a quartz-rich matrix. However, a strong component of non-coaxial flow in the deformation is suggested by the following kinematic indicators observed in the rocks of the map area (letters in square brackets refer to sketches of the structures in Figure 6.2):

[a] asymmetric pressure shadows and foliation wrapping asymmetrically around porphyroblasts (Simpson and Schmid, 1983; c.f. asymmetric matrix stream lines around type  $\theta$  porphyroclasts, Hooper and Hatcher, 1988); [b] crystallographic orientations of different types of quartz porphyroclasts (Bouchez, 1977; Marjoribanks, 1978); [c and d] snowball garnets or other rotated porphyroblasts (see next section, Rosenfeld, 1970); [e and f]  $\sigma$  and  $\delta$  shaped recrystallized tails on porphyroclasts (Passchier and Simpson, 1986); [g and h] synthetic and antithetic shear between fragments of fractured porphyroclasts (Simpson and Schmid, 1983); [i] asymmetric shape of porphyroclasts; [j] mica-fish and trails and steps in the foliation trails on porphyroclasts (Lister and Snoke, 1984); [k] rotation of parts of pulled apart biotites; [l and n] S-C mylonites (Berthé et al, 1979; Lister and Snoke, 1984); [m] asymmetric crystallographic fabrics of quartz (Lister and Williams, 1979; Bouchez et al, 1983); [o] shear bands (Platt and Vissers, 1980); [p] asymmetric shear folds. Microstructures in the S-C mylonites indicate that the flow plane was parallel to the bedding planes. The strong elongation parallel to bedding indicates that the finite strain ellipsoid and the bedding plane, which probably originated at an angle to each other, rotated towards each other with increasing strain.

Several studies indicated that care must be taken with the interpretation of different kinematic indicators, which can show shear senses that are opposite to the actual orientation of the flow (e.g. antithetic shear bands, Behrmann, 1987; quartz C-axis fabrics, Lister and Williams, 1979; Passchier, 1983; rotated tailed

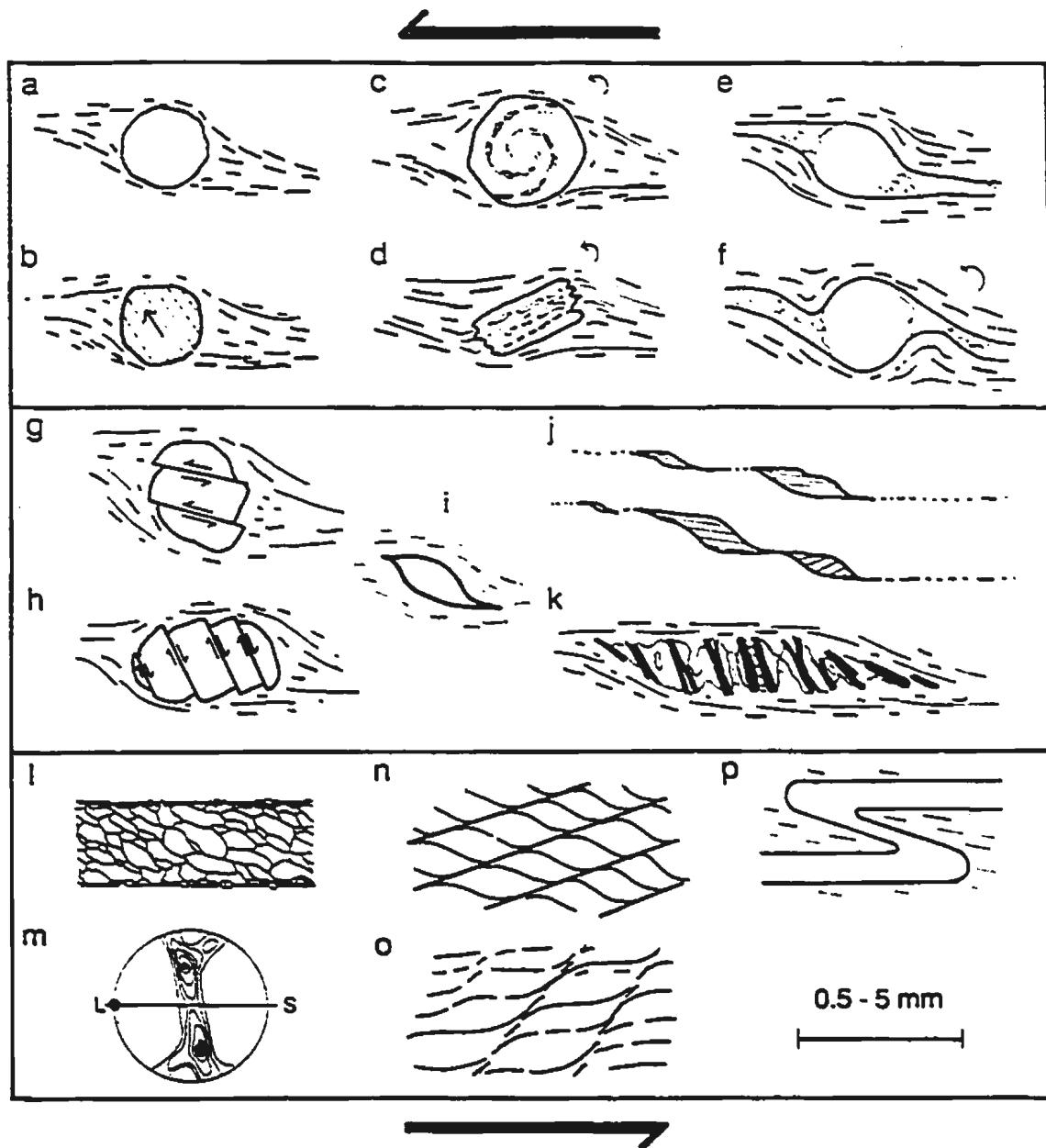


Fig. 6.2 Schematic summary of kinematic indicators observed in thin sections of rocks from the map area. All indicate a sinistral, northwest-directed sense of shear. The bulk foliation plane is horizontal. a) asymmetric pressure shadow and foliation wrapping asymmetrically around porphyroclast; b) oblique orientation of the slip systems in globular quartz porphyroclast. The arrow indicates the projection of the C-axis, dashed lines are kink band boundaries; c) spiral inclusion trails in rotated garnet; d) rotated porphyroclast with straight  $S_1$ ; e)  $\sigma$  tailed porphyroclast; f)  $\delta$  tailed porphyroclast; g) synthetic slip between fragments of fractured porphyroclasts; h) antithetic slip between fragments of fractured porphyroclast (card deck model); i) asymmetric shape of porphyroclast; j) mica fish and trails; k) pulled apart biotite porphyroclast; l) Type II S-C mylonite; m) asymmetric quartz C-axis fabric; n) Type I S-C mylonite; o) shear bands; p) asymmetric shear fold. The scale is variable, approximately between 0.5 and 5 mm.

porphyroclasts, Passchier and Simpson, 1986; Hanmer, 1990). It is therefore useful to collect data from as many sources as possible to avoid misinterpretation. In the map area virtually all kinematic indicators consistently reflect northwest-directed movement. The few cases which are not consistent with this direction of flow can be explained as local heterogeneities in the flow pattern.

With respect to the flow pattern the map area can be subdivided in three parts: 1) The basement dominated thrust sheets of the lower thrust system (lithotectonic domain I); 2) the shelf sediment dominated thrust sheets, including the Elmer Lake thrust sheet, in the central part of the map area (domains II to IV); 3) the Wabush Lake and Long Lake thrust sheets (domain V).

1) In the lower thrust system the deformation is partitioned mainly into the shear zones, in which asymmetric tailed porphyroclasts, asymmetric pressure shadows, microshears in feldspars, crystallographic orientations in quartz porphyroclasts, S-C planes and shear bands indicate non-coaxial flow towards the northwest. The intervening basement rocks are only weakly deformed and no distinction could be made between coaxial and non-coaxial deformation.

2) In lithotectonic domains II, III and IV of the upper thrust system, non-coaxial flow was determined in virtually every sample and outcrop in which indicators for the type of flow were present, both in the thrusts related to fold nappe formation or thrust sheet emplacement and in the less deformed rocks in between. The reworked basement rocks contained the same kinematic indicators as the basement rocks in the shear zones in lithotectonic domain I. S-C mylonites, asymmetric quartz C-axis fabrics and steps in the foliation planes were used in the quartzites, and shear bands, mica fish, asymmetric folds or crenulations and rotated garnets and kyanites indicated the type and direction of flow in the metapelitic rocks.

3) In the eastern part of Gagnon terrane (lithotectonic domain V) very few indicators of non-coaxial flow were found. Only a few of the garnets in the area showed minor rotation (see next section) and in a minority of the samples the foliation curved asymmetrically around the porphyroblasts, stepping up in the assumed direction

of transport. The intense recrystallization in these medium to high grade metamorphic rocks may have erased some of the information about the type of flow, but the scarcity of remaining indicators and the dominantly straight inclusion trails in the garnets suggests that the simple shear component of the deformation was minor.

In summary, the area consists of a wide upper belt east and south of Wabush Lake in which  $D_1$  deformation is pervasive and appears dominantly coaxial with a minor non-coaxial component; a central sediment-dominated belt consisting of thin thrust sheets which show pervasive non-coaxial deformation; and a lower belt in the basement rocks in which non-coaxial deformation is partitioned into narrow shear zones.

This type of deformation partitioning, or vorticity gradient, is somewhat similar to that observed by Platt and Behrmann (1986) in a major shear zone in the Betic Cordillera and by Law et al. (1986) in the Moine thrust belt in the Northern Highlands of Scotland. Both studies found that in the vicinity of a shear zone the deformation had a dominant non-coaxial component, but in the less deformed areas in between the shear zones, deformation had a dominantly coaxial character.

The difference in behaviour between the two sediment-dominated parts of the area can be explained by the difference in thickness of the sedimentary sequence. During emplacement of Molson Lake terrane on the thick sequence of continental slope sediments of domain V, the shear deformation was presumably partitioned into the highest sediments, closest to the thrust plane, which evolved into the wide shear zone separating the two terranes. The deformation in the remainder of the underlying sediments was caused mainly by the tectonic loading and had only a minor non-coaxial component. When the thrust wedge was emplaced on the continental shelf, the incompetent rocks of the Menihek probably took up most of the strain (see Chapters 5 and 8), but the total thickness of the sedimentary cover was so small that all metasediments were effectively in the vicinity of the shear zone and were all affected by both the load and the shear strain. The complete cover sequence of the shelf rocks acted as a shear zone over which the overriding thrust wedge moved.

When the basement was involved in the thrusting at a later stage, the different rheology and the existence of weakened zones (the pre-existing extensional fault zones) caused the partitioning of the shear strain into narrow zones. The deformation in the intervening basement rocks was dominated by tectonic loading and adjustment of the shape as a result of movement on the thrusts.

### **6.3 RELATIONSHIPS BETWEEN PORPHYROBLASTS AND MATRIX FOLIATION**

A microstructural study of the relationship between the development of foliations and the growth of metamorphic minerals is invaluable for the evaluation of the timing as well as the causal relationship between deformation and metamorphism. Zwart (1962) introduced the use of inclusion trails in porphyroblasts in the interpretation of tectonic developments in orogens and this technique has been applied in many studies (e.g. Rosenfeld, 1970; Powell and McQueen, 1976; Jamieson and Vernon, 1987; Reinhardt and Rubenach, 1989).

Garnet, kyanite and staurolite porphyroblasts from metapelites in the map area were studied for this purpose. These minerals are generally poikiloblastic, are rigid during deformation and tend to preserve the internal structure during retrograde metamorphism and thus they are good indicators of the strain path during growth. The angle between the inclusion trail ( $S_i$ ) and the foliation in the matrix ( $S_m$ ), the curvature of  $S_m$ , the transition of the foliation from porphyroblast to matrix (straight, curved or discontinuous) and the curvature (or lack of it) of  $S_m$  around the porphyroblast provide information about the development of the foliation before, during or after the growth of the porphyroblast. The chemical zoning in garnets in the map area has been used to estimate P-T paths and the results suggest that the garnets grew during prograde metamorphism with increasing pressure and temperature (Chapter 7). After evaluating the geometrical relation between deformation and garnet growth, the timing of the deformation relative to the changes in P and T can be determined.

This study was carried out on thin sections which were preferentially cut perpendicular to the foliation and parallel to the stretching lineation where one existed, such that in case of rotation of porphyroblasts the rotation axis is perpendicular to the plane of the section. The foliation to which the microstructures of the porphyroblasts are compared, is the regional  $S_1$  foliation which developed during emplacement of the thrust sheets. The microstructures are described separately for thrust sheets of different metamorphic grades. The relationships are sketched in Figure 6.3 and examples are shown in Plates 6.21 to 6.27, ordered from the lowest to the highest grade thrust sheets.

### 6.3.1 LOW GRADE THRUST SHEETS

The lack of poikiloblastic porphyroblasts in the lower greenschist facies thrust sheets prevents a precise analysis of the relationship between deformation and metamorphism. The metamorphic minerals in this area, predominantly micas, define the  $S_1$  foliation and the deformation and metamorphism were broadly synchronous (Fig. 6.3a). During deformation the temperature was high enough to activate ductile deformation mechanisms and recrystallization of micas in  $F_2$  crenulations to polygonal arcs, even in the late stages of deformation (Fig. 6.3b).

Microfabrics in out-of-sequence thrusts in the area include kinks in micas, fine-grained subgrains in quartz and other features typical of deformation at low metamorphic grade (see section 6.1.1.1). This suggests that deformation in the out-of-sequence thrusts took place during retrograde metamorphism.

### 6.3.2 LOW TO MEDIUM GRADE THRUST SHEETS

The majority of the garnets in the Emma Lake and Carol Lake thrust sheets have curved or double spiral-shaped inclusion trails, indicating syn-kinematic garnet growth (i.e. snowball-garnets, Spry, 1969) in a non-coaxial kinematic regime (Plates 6.21 and 6.22). The cores of these garnets have overgrown a foliation, suggesting that garnet growth started after the onset of deformation and metamorphism was late-syntectonic (Fig. 6.3c and d).  $S_2$  curves slightly around these garnets, suggesting that flattening

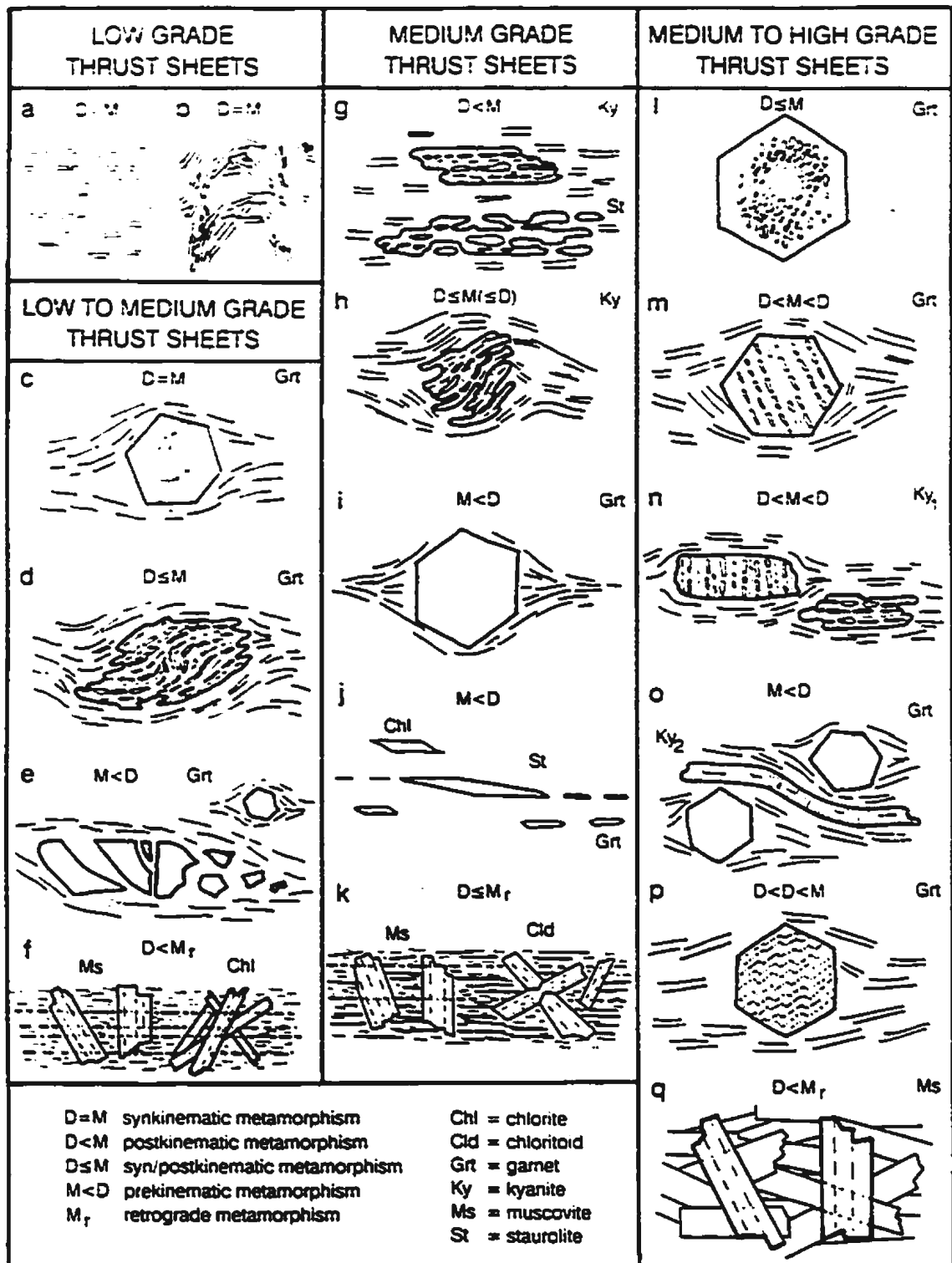


Fig. 6.3 Schematic representation of the microstructural relationships between porphyroblasts and foliation in different metamorphic zones in the area. D and M represent deformation and metamorphism respectively. The mineral names refer to the large porphyroblasts. For explanation see text, section 6.3.

took place during or after garnet growth.  $S_1$  and  $S_2$  are connected through the rims of the garnets, but in the garnet shown in Plate 6.21 the foliation is strongly curved just outside the grain in the left lower corner, suggesting minor deformation after growth of the porphyroblast. This late deformation took place after the development of the regional  $S_1$  foliation. In some of the shear zones continuity between  $S_1$  and  $S_2$  was lost. Flattening around the garnets was stronger and fractured garnets indicate strong deformation after garnet growth (Plate 6.25 and Fig. 6.3e). These shear zones were active after the peak of metamorphism ( $D_2$ ).

In several samples chlorite and muscovite overgrow the foliation randomly or in orientations preferentially perpendicular to the pre-existing micas (Fig. 6.3f). Trails of opaque dust parallel to  $S_2$  continue straight through the superposed micas. This is evidence of a late, retrograde and post-kinematic growth.

### 6.3.3 MEDIUM GRADE THRUST SHEETS

Observations are from the pelitic member in the Wishart Formation in the Goethite Bay and Rivière aux Fraises areas. Kyanite and staurolite are generally oriented parallel with the foliation and have inclusion trails formed by coarse-grained quartz and opaque phases which in most cases are parallel with  $S_0$  (Plate 6.24 and Fig. 6.3g). Inclusions in garnets do not always form internal foliations (cf. Plate 6.24 with Plates 6.16 and 7.2). A few nearly equidimensional kyanites with a curved  $S_1$  were observed, indicating growth during rotation (late-synkinematic, Fig. 6.3h). At the margins of the grains  $S_1$  is parallel with the overall orientation of the foliation, but the micas in the matrix in the pressure shadows next to the kyanite porphyroblasts are oriented at a high angle to the  $S_1$ . Thus the  $S_1$  in the rim is parallel with  $S_0$ , but discontinuous with the immediately adjacent micas. The foliation wraps asymmetrically around these grains. In all rocks where a mica foliation is present, this foliation wraps around the garnets, in some samples indicating considerable flattening after growth (Fig. 6.3i). Plate 6.16 shows a staurolite with a lozenge shape and asymmetric tails, which is interpreted to have been deformed during non-coaxial flow (cf. mica fish and trails, Lister and Snoke, 1984; Fig. 6.3j). Rotation of garnets and kyanites also

indicates a shear component in the deformation. These relationships indicate deformation before, during and after growth of the porphyroblasts.  $S_i$  and  $S_e$  are inferred to be the result of the same progressive non-coaxial deformation which formed the  $S_i$  foliation.

In this part of the area chloritoid locally replaced staurolite during retrograde metamorphism and grew post-kinematically in random orientations (Plate 7.3). Muscovite also shows microstructures related to post-kinematic, retrograde growth (Fig. 6.3k).

#### 6.3.4 MEDIUM TO HIGH GRADE THRUST SHEETS

In this part of the map area garnet and kyanite form large porphyroblasts which show consistent  $S_i$  -  $S_e$  relationships. The garnets are zoned with respect to both inclusion patterns and chemical composition (see section 7.2; Fig. 6.31). The most common inclusion pattern shows a core with dusty inclusion trails. Towards the rim the inclusions progressively increase in size, probably as a result of the increase of metamorphic grade during growth. In this part of the grains the trails are mainly formed by elongated quartz inclusions and in very few samples this part of the inclusion trail is slightly curved. The rims of the majority of the garnets are virtually free of inclusions. The asymmetry of the curved inclusion trails is consistent on the scale of a thin section and the angle of the curvature is always less than  $90^\circ$ . Bell (1985) suggested that this type of curved inclusion trails is not necessarily indicative of syn-kinematic growth during non-coaxial flow. It can also originate from growth during the development of asymmetric crenulation cleavage which results in the rotation of the foliation plane with respect to static garnets. The consistency of the asymmetry is in agreement with both northwest-directed shear and dominantly northwest verging folds and the garnets could have grown under either circumstance.

$S_e$  wraps around the larger garnet porphyroblasts (Fig. 6.3m). In many of the samples  $S_i$  and  $S_e$  are at high angles to each other and the two are not connected at the grain boundaries (Plate 6.25; Fig. 6.3m). Commonly the orientation of the  $S_i$  is consistent within all the garnets in a thin section, which makes rotation of the garnets

unlikely. The deformation that caused the development of the regional  $S_1$  foliation occurred broadly after the growth of the garnets. The high angles between  $S_i$  and  $S_e$  and the discontinuity of the foliations at the grain boundaries may suggest that they represent two separate generations of structures, respectively older and younger than the garnet. This is in agreement with the observation that at least locally the  $S_1$  foliation in the matrix is a crenulation cleavage, interpreted to be a second generation structure (section 6.1.3.4). The two foliations are referred to as  $S_{1-}$  and  $S_1$  respectively.

Two different types of kyanite porphyroblasts were observed, which are interpreted to represent two different stages of kyanite growth. The older kyanite porphyroblasts ( $Ky_1$ ) show  $S_i - S_e$  relationships similar to the garnets. They are very coarse grained, often several cm long, have subidioblastic crystal shapes, poikiloblastic textures and a coarse internal foliation. These kyanites are all aligned with the foliation plane. Although generally  $S_i$  is parallel with the long dimension of the crystals, and therefore parallel with  $S_e$ , in some grains  $S_i$  and  $S_e$  are at high angles to each other and discontinuous (Plate 6.26, Fig. 6.3n). Like the garnets, these kyanites grew before the development of the regional  $S_1$ .

The second type of kyanite porphyroblasts ( $Ky_2$ ) is not poikiloblastic, is much smaller ( $< 2$  mm), idioblastic to subidioblastic, grows preferentially in the mica-rich layers and is statistically aligned with the foliation (Plate 7.4).  $Ky_2$  porphyroblasts grew later than  $Ky_1$  when the metamorphic grade was higher and the foliation was too coarse to be incorporated in the small porphyroblasts. They possibly grew as a result of the breakdown of staurolite, whereas the older kyanite formed earlier in the prograde metamorphic sequence (Chapter 7, section 7.1). One observation of a  $Ky_2$  porphyroblast that was curved along with the foliation in between two garnets is an indication of deformation after growth (Fig. 6.3o).

Two samples suggest that multiple deformation events occurred before garnet growth. In these samples garnet has overgrown kink bands in fine-grained inclusion trails (Plate 6.27, Fig. 6.3p). Elongated opaque minerals, probably graphite, are aligned along the inclusion trails and suggest that these trails are structural features

rather than sedimentary, and represent a first deformation event. The kinking of this foliation before garnet overgrowth would be a second deformation. It suggests a complicated deformation history before the attainment of moderate metamorphic grade.

In many samples muscovite has overgrown the  $S_1$  foliation in random orientations, commonly replacing either biotite or kyanite (Fig. 6.3q). This indicates a late, post- $D_1$  growth of muscovite.

#### 6.4 DISCUSSION AND CONCLUSIONS

The microstructures described in this chapter all indicate that the deformation in the map area occurred by predominantly crystal-plastic processes. In the lowest thrust sheets the feldspar crystals, as well as other rigid minerals like apatite and epidote, deformed by brittle fracturing, but the load bearing matrix deformed in a ductile fashion. The area shows a variation of deformation mechanisms from the lowest thrust sheets to the highest. At the lowest metamorphic grades grain deformation processes dominated, mainly by movement of dislocations, resulting in formation of kinks, subgrains, deformation lamellae and quartz ribbons. Towards higher metamorphic grades recovery processes and dynamic recrystallization became more important in the deformation of the rocks. These are mechanisms which are not expected in high crustal level foreland fold-and-thrust belts and they are not likely to enhance the localization of strain in narrow zones to form thrusts. Strain localization in these rocks was more likely a result of high strain rates, competence contrast between basement and cover rocks, and pre-existing zones of weakness, which are inferred to have played an important role in the deformation of the basement.

Another important conclusion of the microstructural study is that the majority of the rocks deformed by non-coaxial flow with a large component of simple shear. All kinematic indicators support the field observations that the thrusting was directed to the north-northwest. The component of simple shear in the flow decreased from the lowest thrust sheets to the highest. The movement of the overriding Molson Lake terrane was accommodated by shearing of the metasediments in Gagnon terrane, most of which is inferred to have been accommodated by the rocks in the immediate vicinity of the

thrust, which for most of the area are the rocks of the Menihek Formation. The deformation affected the stratigraphically lower sedimentary units as well. Since from northwest to southeast the thickness of the sedimentary package increased, the shear strain was distributed over a wider zone, resulting in a progressively lower component of simple shear in the total strain.

Figure 6.4 summarizes the conclusions that can be drawn from the study of the relations between porphyroblasts and foliations. It shows the variations in timing between growth of metamorphic minerals and deformation through the area. Only the diagnostic minerals (micas, garnet, kyanite, staurolite and chloritoid) are used in the diagram. It is assumed that the end of the new growth of the metamorphic minerals approximately coincided with the temperature peak of metamorphism (which is proven for the garnets in Chapter 7) and that the porphyroblasts (with the exception of chloritoid) did not grow significantly during retrograde metamorphism, although recrystallization of micas was still possible after the P-T peak.

In the low grade part of the area, the Wide Valley, Flatrock Lake and Corinne Lake thrust sheets and the underlying basement, metamorphism and  $D_1$  deformation are assumed to be broadly synchronous. In the low to medium grade thrust sheets metamorphism was late-synkinematic, with deformation ( $D_2$ ) continuing in some shear zones after the peak of metamorphism. Recrystallization of micas and quartz during retrograde metamorphism continued at least until the end of  $D_1$  deformation. The history of the medium grade part of the area is similar, with more intense post-metamorphic peak deformation. In the eastern, highest grade part of the area the large angle between the inclusion trails in the porphyroblasts and the  $S_1$  foliation in the matrix suggests that the two are the results of two different events, the first being a pre- to syn-metamorphic deformation event, the second a post-metamorphic event. There are no indications of a time lag between the two and the possibility exists that the two structural elements are part of the same progressive deformation event.

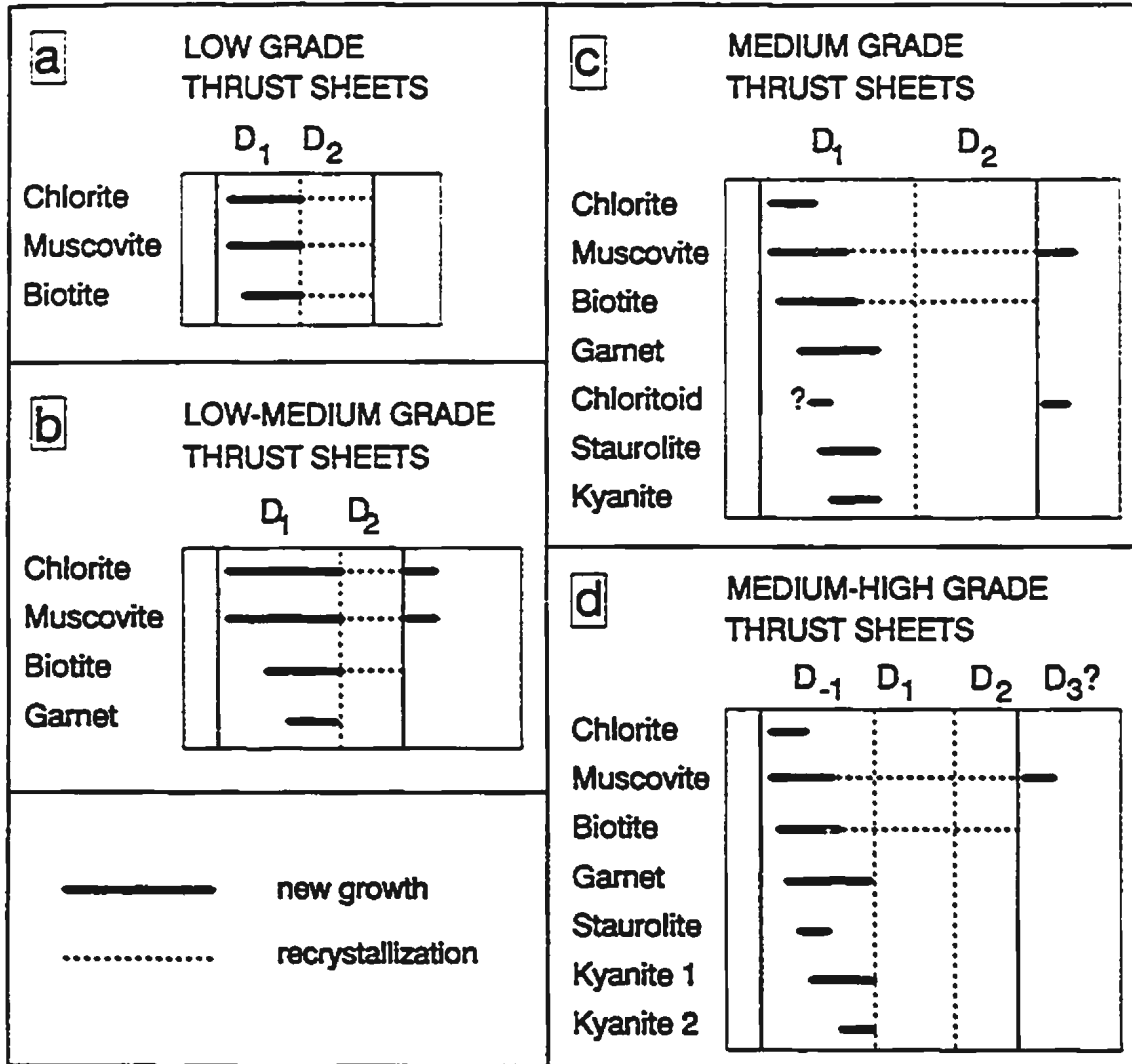
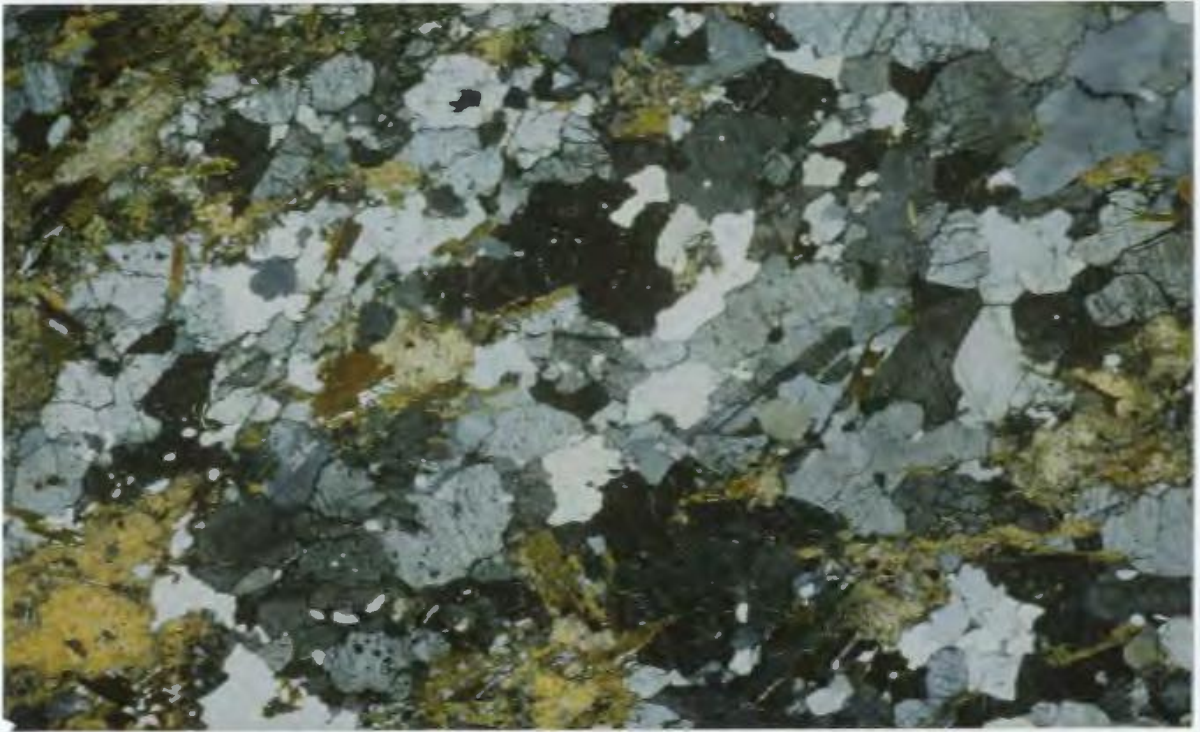


Fig. 6.4 Summary of the timing of growth and recrystallization of metamorphic porphyroblasts and deformation in different metamorphic zones. The horizontal time scale is relative and the time between deformation events is uncertain.

These observations show a trend in the variation in the timing of metamorphism and deformation. In all thrust sheets garnet growth started some time after the onset of deformation as indicated by the presence of internal fabrics in the garnet cores. The main variation through the area lies in the deformation after the peak of metamorphism, which is insignificant in the lowest thrust sheets but becomes more important towards the higher thrust sheets. All rocks went through the same initial state of burial underneath an overriding thrust sheet which caused deformation and metamorphism. The peak of metamorphism was reached when the thrust wedge stopped progressing with respect to the underlying sediments, i.e. when the sediments were incorporated into the thrust wedge. This means that the metamorphic peak in the upper thrust system moved towards the northwest in the metasediments with the thrust front. The deformation following the metamorphic peak took place in the thrust wedge itself during movement. The tectonic history of the highest thrust sheets after incorporation in the thrust wedge (and thus after peak metamorphism) is longer than in the lower thrust sheets. This is consistent with the fact that in a thrust wedge the rocks towards the trailing edge have the longest strain history, because they have accumulated a certain strain at the time that the lowest sheets are being incorporated in the wedge (Chapple, 1978; Platt, 1986). During progressive movement of the thrust wedge, the higher thrust sheets will keep deforming and accumulating strain under retrograde metamorphic conditions, while the lowest sheets are at the first stages of deformation and metamorphism. Each thrust sheet will go through the same process when overridden by and subsequently incorporated in the thrust wedge, but the earliest incorporated sheets will have a longer history and higher accumulated strain than those near the toe of the wedge.



1.8 mm

Plate 6.1

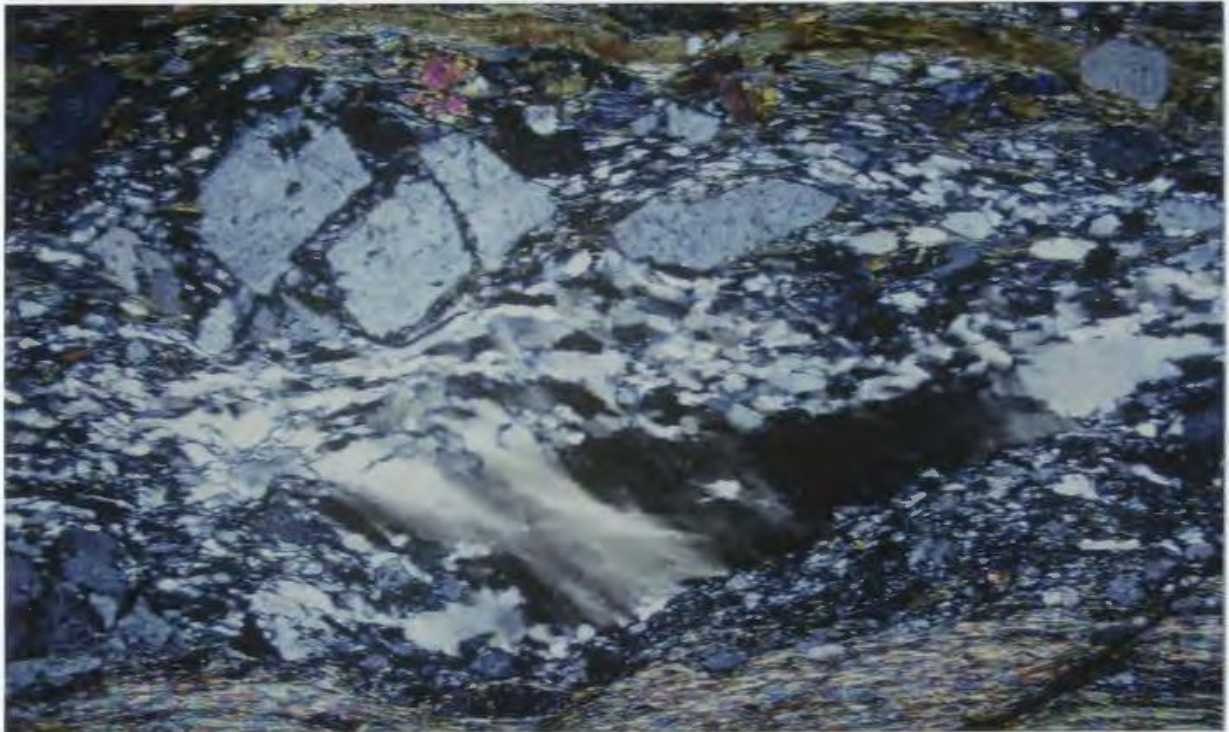
Least deformed basement rock at low Grenvillian metamorphic grade. The rock has retained its pre-Grenvillian coarse grained texture consisting of Qtz (white and light grey), Fsp (darker grey), Bt (brown) and fine-grained masses of Act (yellow/orange) replacing Cpx. (crossed nicols)



1.9 mm

Plate 6.2

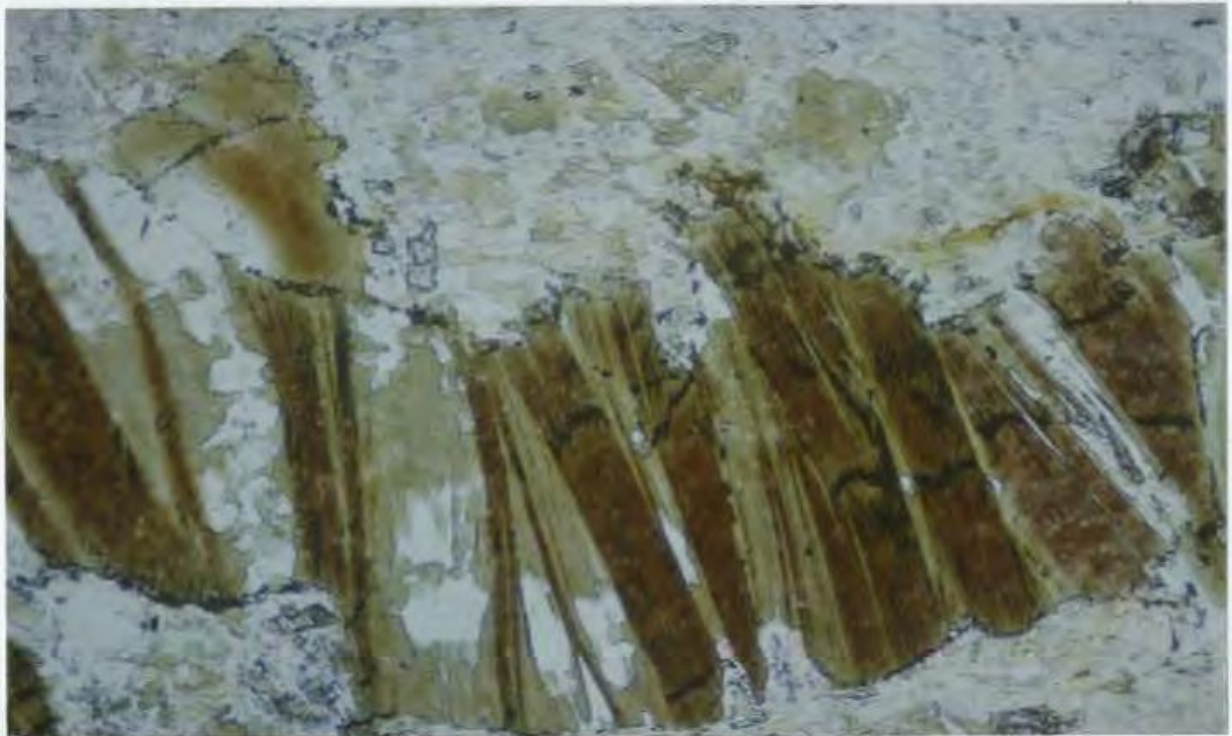
Breakup of large feldspar grains (grey colors) into lozenge-shaped fragments, in the top of the photo along conjugate shear planes, which approximately align along S and C-planes (dipping to the left and right resp.). Extensional fractures dominate the lower part of the photo. Along the shear planes Fsp recrystallized to Qtz + Ms. Note the pulled apart biotite in the left. (crossed nicols)



0.6 mm

Plate 6.3

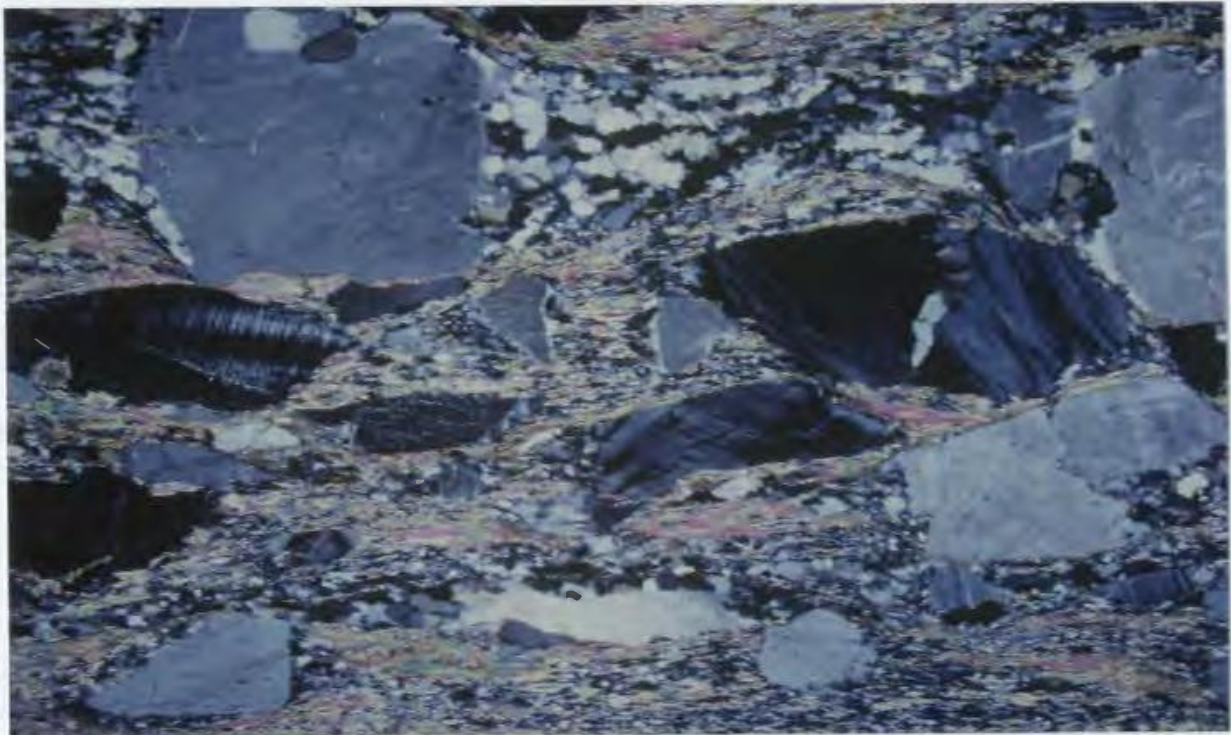
Contrast between brittle feldspar (top of photo) and plastic quartz (centre) in basement proto-mylonite. The quartz porphyroblast shows polygonization in the lower part of the grain and subgrains which are progressively rotated to form new grains along horizontal deformation bands in the top and along the grain boundaries. The feldspar fragments are pulled apart. (crossed nicols)



150  $\mu$ m

Plate 6.4

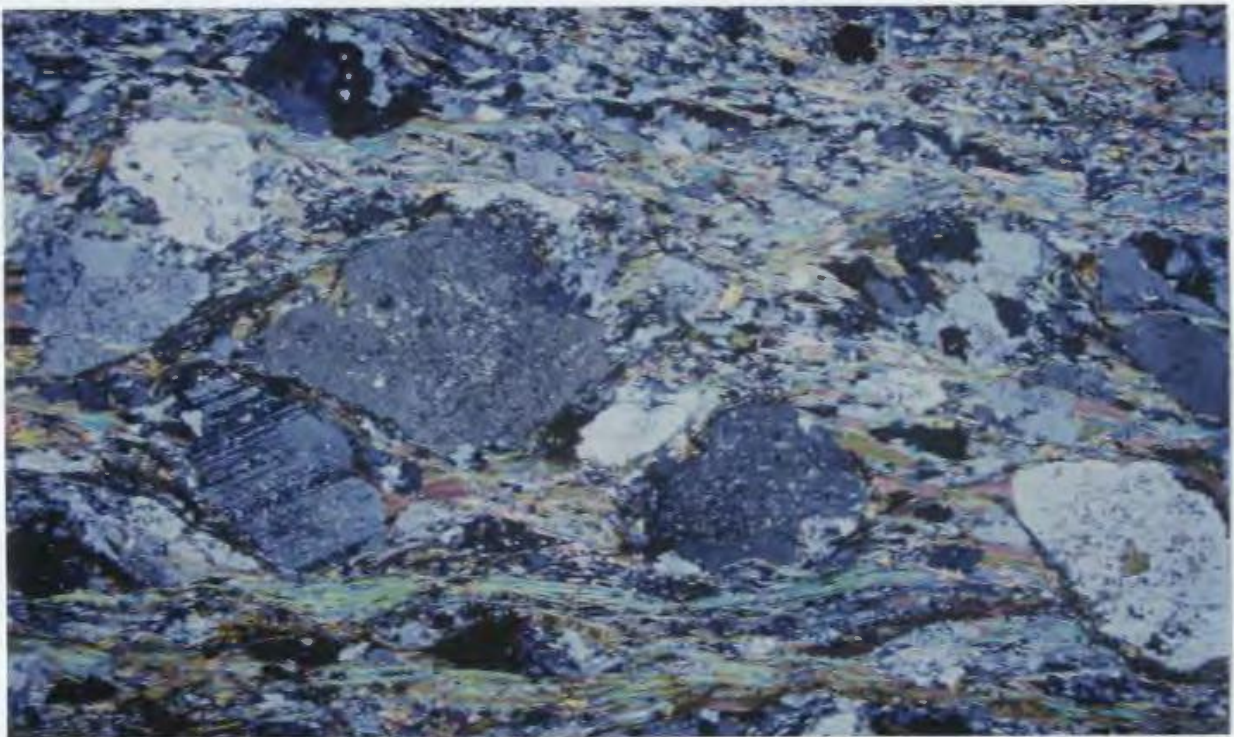
Pulled apart Archean biotite in basement proto-mylonite. The original biotite (brown) contains a network of rutile needles aligned along the cleavage plane (cf. Plate 7.1) and streaks of sphene (fine-grained, dark bands). The dilation sites between the fragments of the "old" biotite are filled in with newly grown, greenish biotite and quartz.



0.6 mm

Plate 6.5

Basement protomylonite with angular and pulled apart fragments of feldspar and a rounded quartz porphyroblast in "hard" orientation (see text) with wide recrystallized tails (top left). The gap in the fractured feldspar (centre-right) is filled with quartz fibres. Note the elongated and partially recrystallized quartz grain (white) near the bottom of the photo. (crossed nicols)



0.6 mm

Plate 6.6

Basement protomylonite with feldspar porphyroclasts. The foliation anastomozes around the porphyroclasts. The porphyroclasts have been rounded slightly by chemical breakdown (strain induced) of asperities. The C-plane is horizontal, S-planes dip to the right, but are not well developed. (crossed nicols)



0.6 mm

Plate 6.7

Quartz porphyroclasts with recrystallized tails in a basement mylonite. The core of the central quartz grain is polygonized, with kink bands bounding the polygons parallel to the projection of the C-axis, dipping to the left. Note the mica fish formed by biotite (dark brown). (crossed nicols)



0.8 mm

Plate 6.8

Basement mylonite with mica-rich matrix. Asymmetric pressure shadows on the elongated porphyroclast in the top of the photo indicate a dextral sense of shear. Note the recrystallized margins around the small elongated quartz grain (clear grey) beneath. The blue and green bands consist of white mica and have thin biotite rims (brown). (crossed nicols)

1.4 mm



Plate 6.9

**Basement mylonite at amphibolite facies metamorphic grade with two trails of microcline, one above and one below the central biotite-rich band (brown colour). They represent completely recrystallized K-feldspar porphyroclasts, elongated parallel with the foliation, which is defined by biotite and muscovite. (crossed nicols)**

0.6 mm



Plate 6.10

**Two large plagioclase porphyroclasts in a basement mylonite recrystallized at amphibolite facies metamorphic grade. The foliation, which is horizontal in the thin section, wraps asymmetrically around the porphyroclasts, indicating dextral shear. (crossed nicols)**

0.6 mm

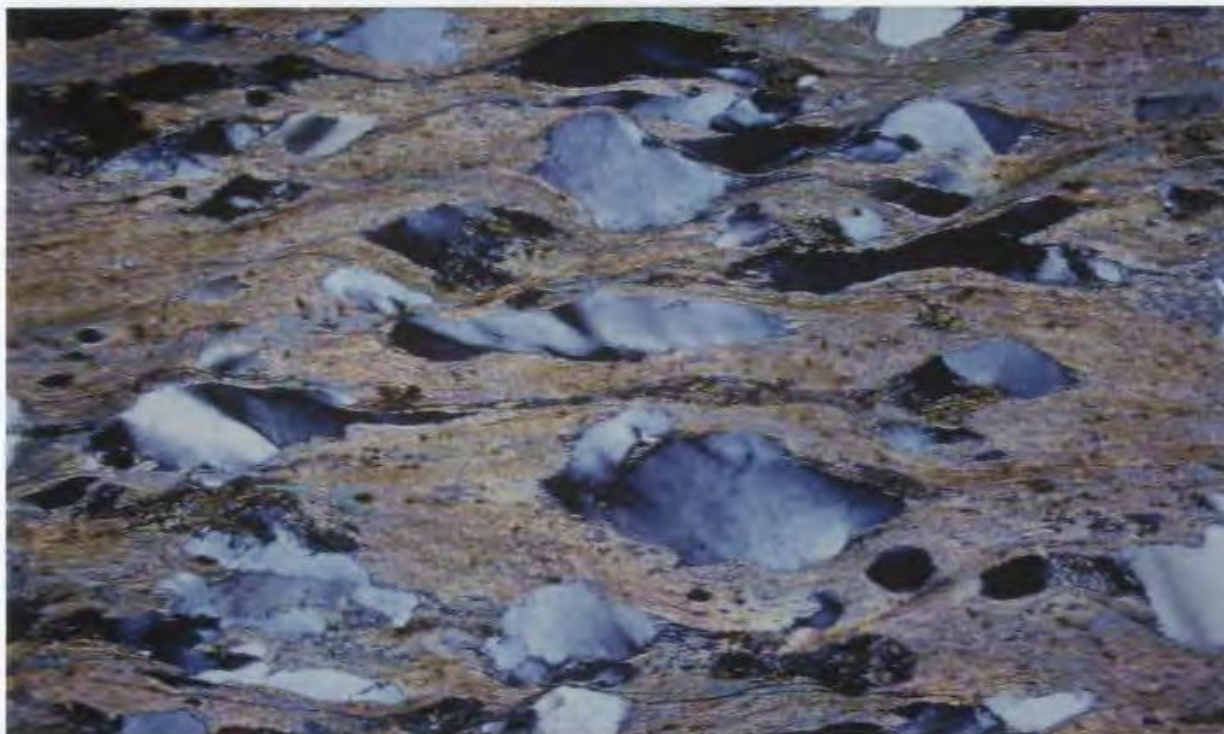


Plate 6.11

Quartz porphyroclasts in phyllonitic mylonite. The quartz grains were deformed but remained intact, without forming subgrains or recrystallizing. Most of the strain in the rock is accommodated by the fine-grained quartz-mica matrix. Note the shear bands which indicate a sinistral sense of shear. (crossed nicols)

1.0 mm



Plate 6.12

Deformation of strongly sericitized feldspars in basement rocks close to a reactivated normal fault. The deformation in the quartz (clear grey) is weak relative to the feldspars. Sericitization of feldspar is concentrated along cracks and old grain boundaries. Note the fine-grained subgrains at the quartz boundaries and the pulled apart biotite grains. (crossed nicols)



150  $\mu\text{m}$

Plate 6.13

S-C mylonite in a quartzite of the Sokoman Formation in the Flatrock Lake thrust sheet. The C-plane is horizontal, outlined by iron oxides. The S-plane, defined by elongated quartz grains, dips to the left. The quartz grains are undulose, have polygons and few ill-defined subgrains. Dextral sense of shear. (crossed nicols)



150  $\mu\text{m}$

Plate 6.14

S-C mylonite in a quartzite of the Sokoman Formation in an out-of-sequence thrust at the roof of the Flatrock Lake thrust sheet. The old quartz grains are strongly elongated at low angles to the C-plane (horizontal). The grains contain many ill-defined subgrains which are also elongated but are oriented at higher angles to the C-plane. Sinistral sense of shear. (crossed nicols)

0.6 mm



Plate 6.15

S-C mylonite in a quartzite of the Sokoman Formation in the Emma Lake thrust stack. The C-Plane is horizontal, the S-plane dips to the right at about  $40^\circ$  and is defined by irregularly shaped, elongated grains. The irregular grain boundaries indicate grain boundary migration. Sinistral sense of shear. (crossed nicols)

0.6 mm



Plate 6.16

S-C mylonite in coarse grained quartzite of the Wishart Formation. The C-plane is subhorizontal, defined by staurolite (yellow) and chlorite (greenish grey). The S-plane is dipping to the right at  $\pm 50^\circ$ , vaguely defined by preferred grain boundary orientations. Note the asymmetric tails on the staurolite. Garnets contain fine-grained quartz inclusions. Sinistral sense of shear. (crossed nicols)

150  $\mu\text{m}$

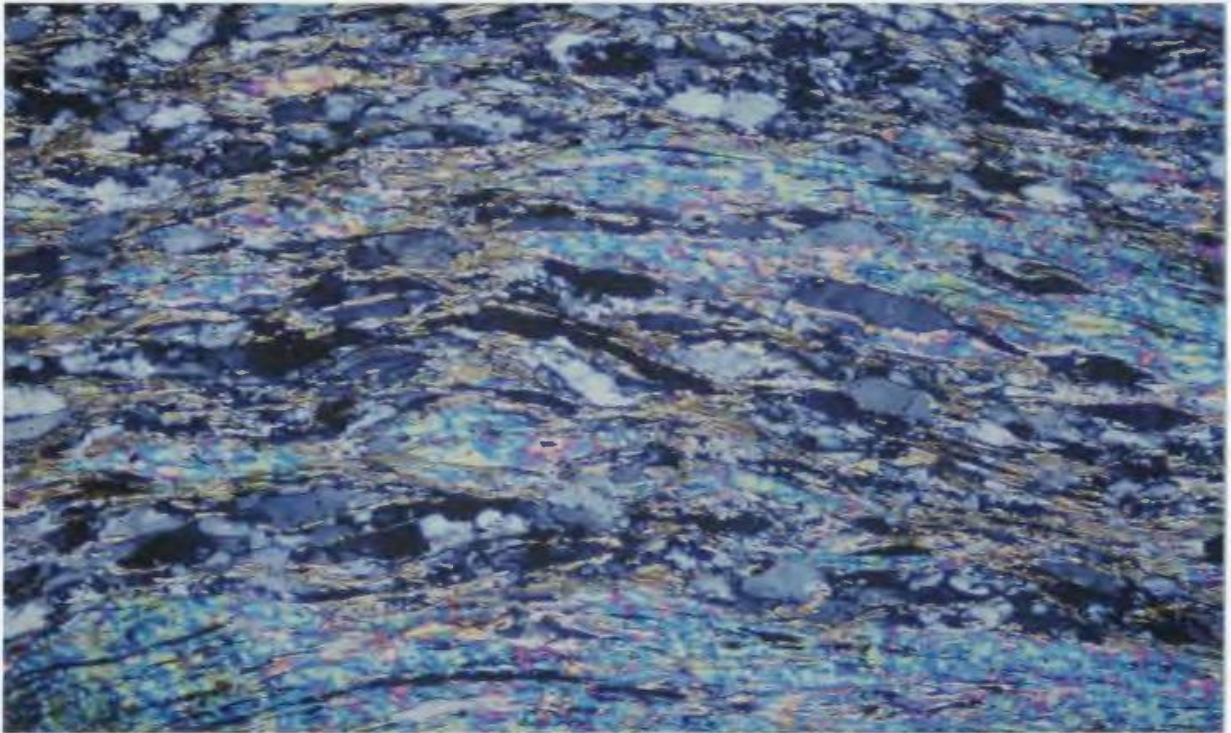


Plate 6.17

$S_1$  foliation in micaschist of the Menihek Formation in the south Flatrock Lake area. A foliation of fine-grained micas anastomoses around elongated grains of feldspar, deformed quartz and mica fish consisting of white mica. Note the fine-grained rims of biotite (green-brown) on the white mica grains (blue-green). Microscopic shear bands drape around porphyroclasts and mica-fish. (crossed nicols)

0.6 mm

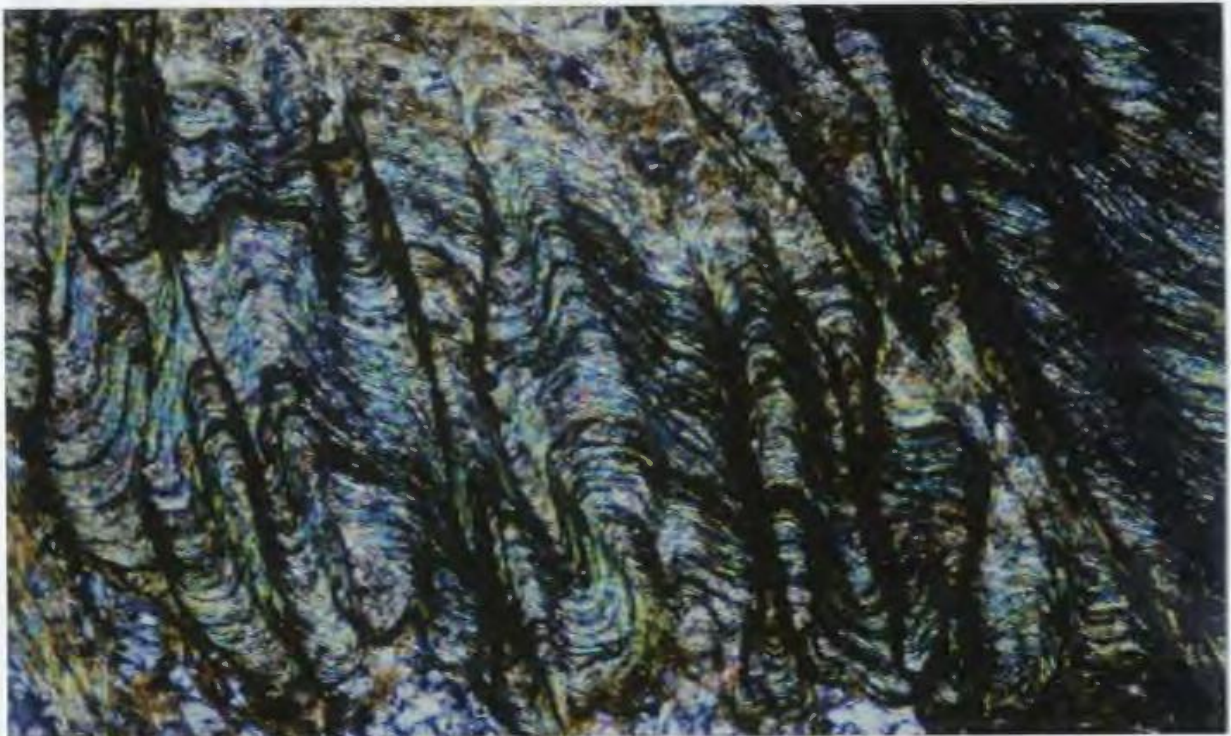


Plate 6.18

Crenulation cleavage ( $S_2$ ) in a graphitic schist of the Menihek Formation in the North Flatrock Lake area. The very fine-grained micas form polygonal arcs. Some of the micas are slightly curved. Graphite is black, white mica is blue/green, biotite is brown. (crossed nicols)

150  $\mu\text{m}$



Plate 6.19

Polygonal arc ( $F_2$ ) in crenulated schist of the Menihék Formation near O'Brien Lake. Biotite is dark green/brown, white mica is all other bright colours. Compare this polygonal arc with the continuous arcs of the finer grained crenulations in Plate 6.18. The micas in this crenulation are straight and are at larger angles to each other than in the previous plate. (crossed nicols)

0.6 mm

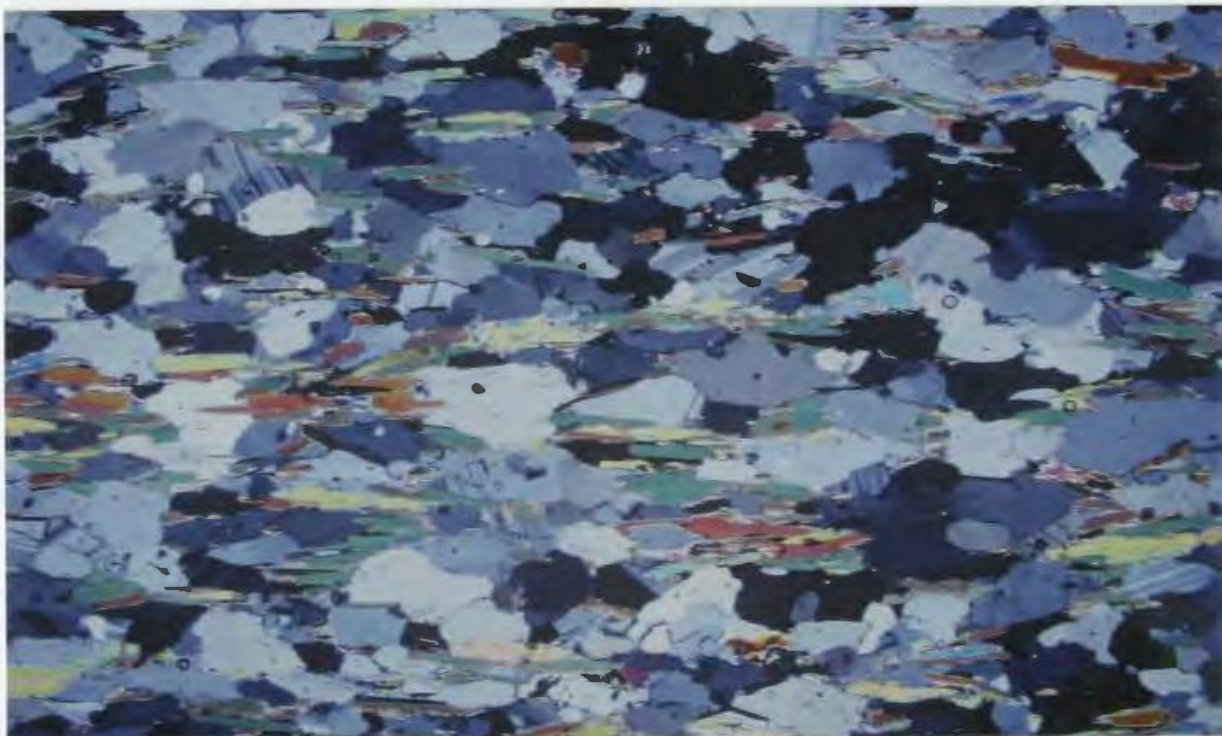


Plate 6.20

Foliation in a high grade gneiss of the Attikamagen Formation near Moose Head Lake. The foliation ( $S_1$ ) is determined by isolated biotite (dark green and red/brown) and muscovite (bright green/yellow and blue) crystals. The quartz and plagioclase grains are slightly elongated. (crossed nicols)

1.5 mm



Plate 6.21

Rotated garnet in the Menihek Formation near Emma Lake. Sinistral rotation of  $90^\circ$ . Post-metamorphic deformation has bent the micas at the lower left margin of the grain. Note that the quartz grain size of the inclusions in most of the garnet is similar to that in the matrix. The extremely fine-grained material in the matrix (grey to white) is feldspar, containing subgrains. (crossed nicols)

350  $\mu\text{m}$

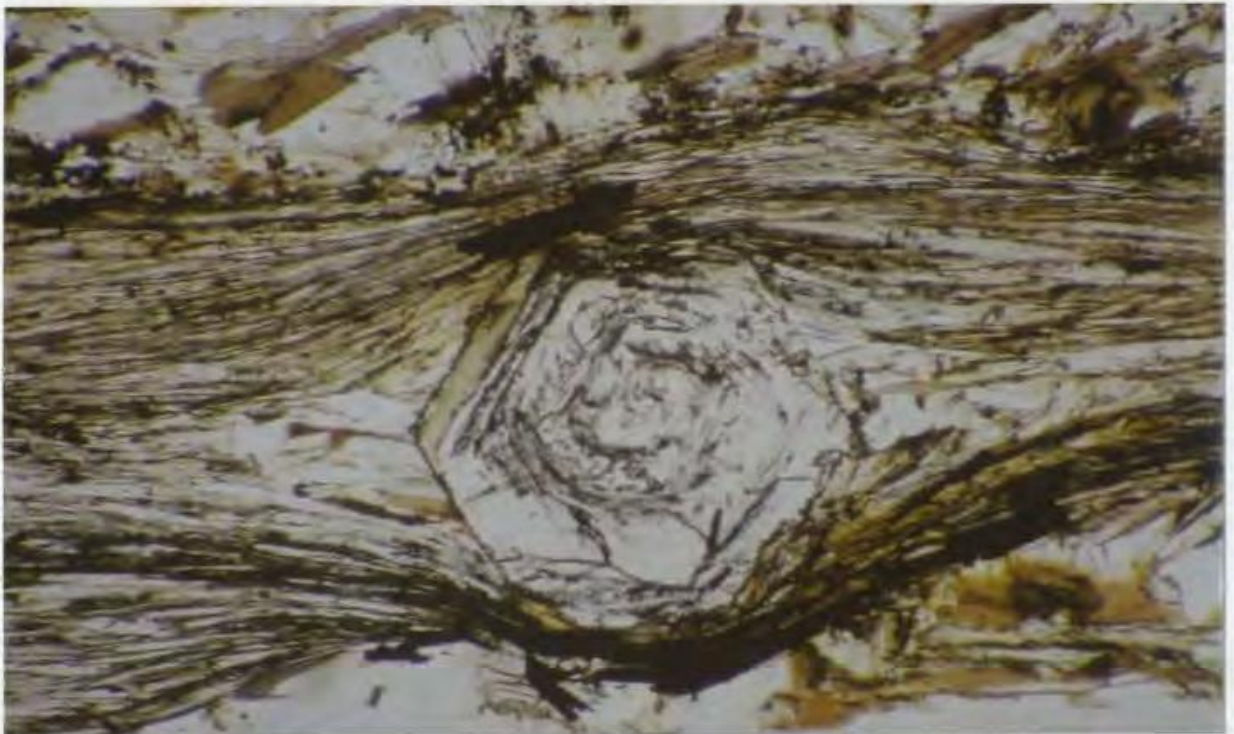
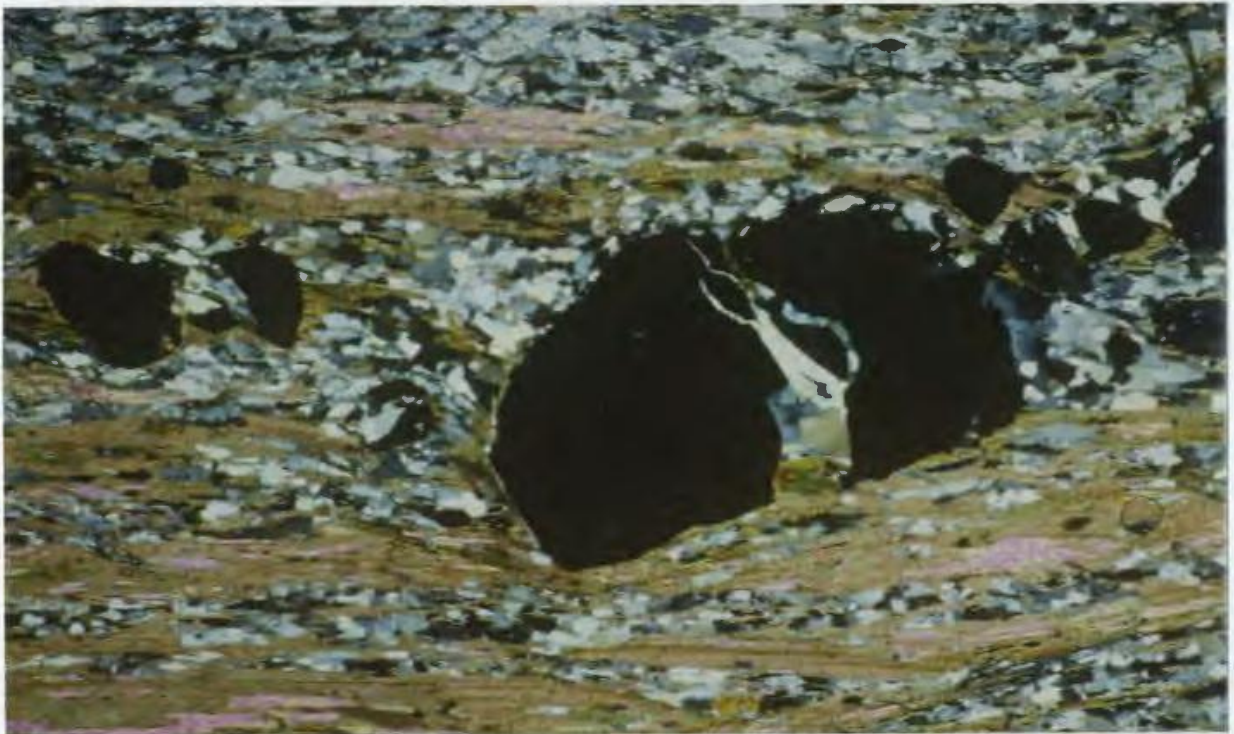


Plate 6.22

Rotated garnet in the Menihek Formation near Carol Lake. Sinistral rotation is approximately  $520^\circ$ . The internal foliation, indicated by a trail of dusty inclusions, continues without a break or change in orientation from the garnet into the matrix foliation ( $S_1$ ).



1.1 mm

Plate 6.23

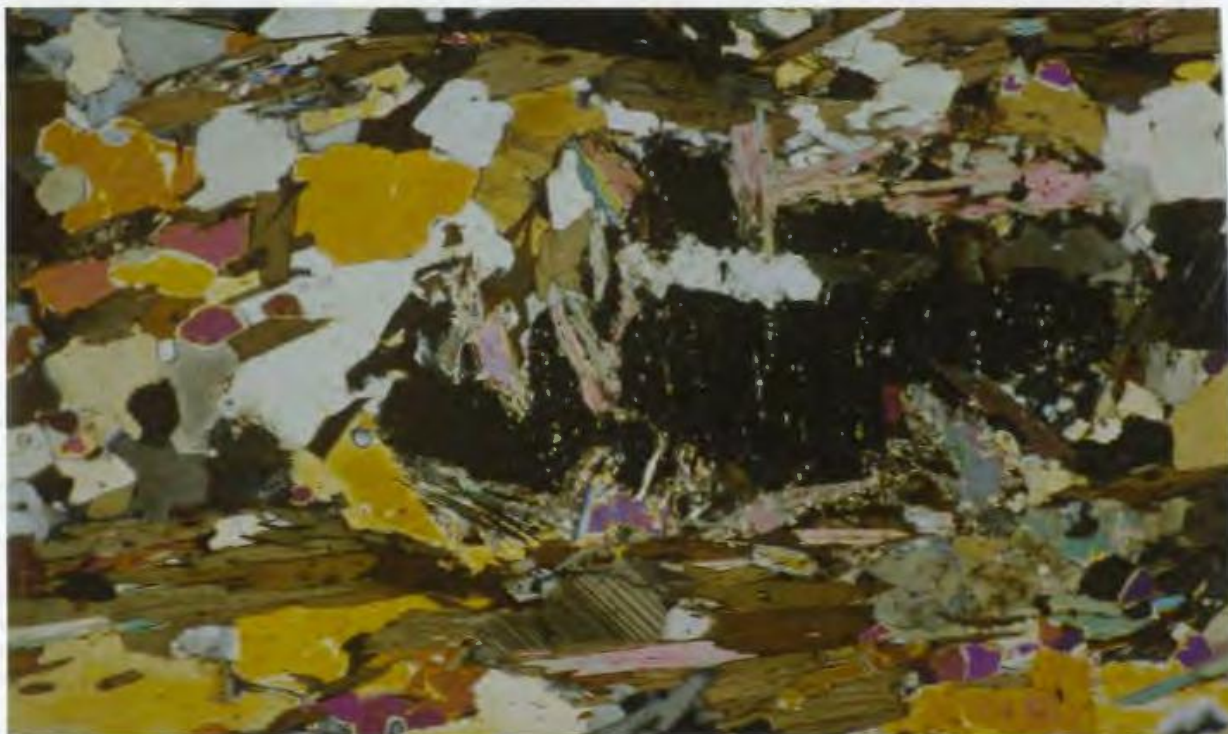
Fractured garnet in Menihék Formation near Rivière aux Fraises. A trail of angular garnet fragments extends to both left and right of the photomicrograph. The  $S_1$  foliation is outlined by biotite (greenish brown) and muscovite (red to pink). (crossed nicols)



1.0 mm

Plate 6.24

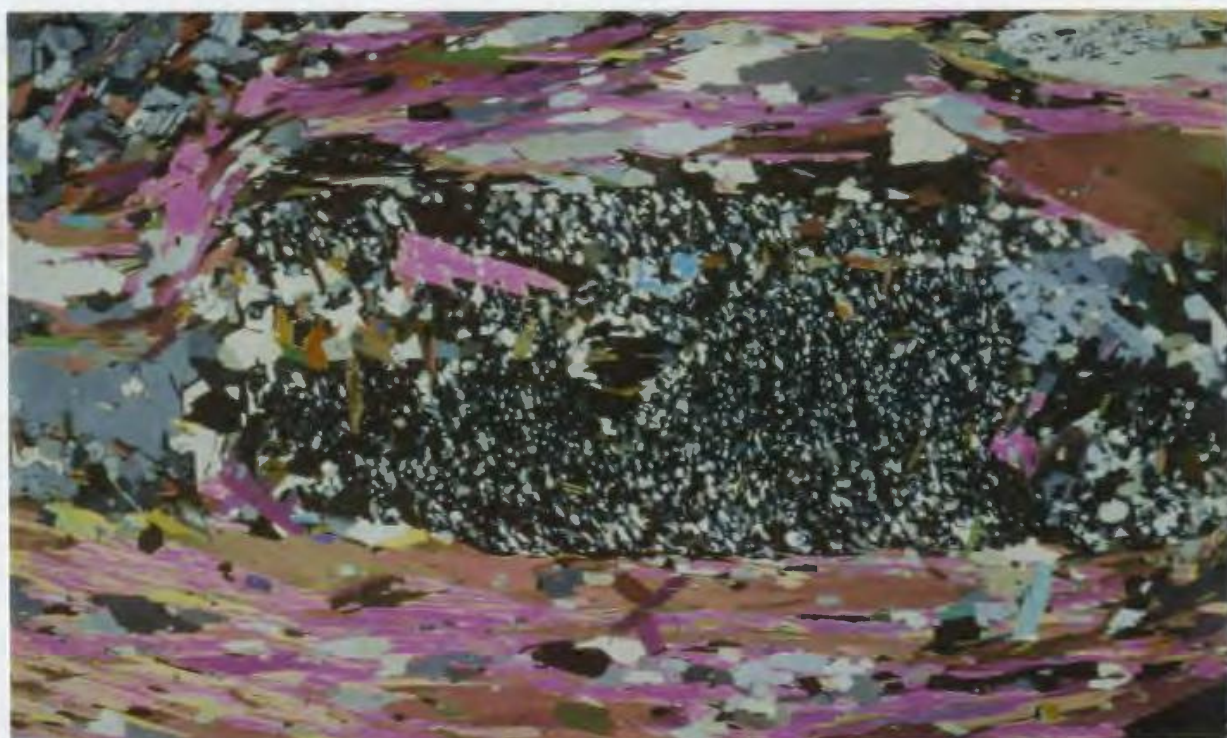
Staurolite (yellow) and garnet (black, skeletal, replaced by hematite) porphyroblasts in the Wishart Formation near Goethite Bay. Both minerals have overgrown a foliation and post-metamorphic sinistral shear has caused the external foliation ( $S_1$ ) to wrap asymmetrically around the central garnet and has rotated the garnet in the top left corner. Sinistral sense of shear.



1.0 mm

Plate 6.25

Poikiloblastic garnet in a gneiss of the Attikamagen Formation, Moose Head Lake.  $S_1$  (indicated by fine-grained quartz inclusions) and  $S_2$  are perpendicular, vertical and horizontal respectively, and are discontinuous at the grain boundary. The garnet (in extinction) is partially resorbed. The thin section is too thick, resulting in yellow to red interference colours for quartz. (crossed nicols)



1.8 mm

Plate 6.26

Poikiloblastic kyanite ( $Ky_1$ , in extinction) in a gneiss of the Attikamagen Formation, Flora Lake.  $S_1$  and  $S_2$  are at a high angle (steeply dipping to the right and horizontal respectively) and not continuous, but the inclusion trails bend slightly towards  $S_2$  at the edges of the grain. The  $S_2$  foliation (=  $S_1$ ) bends slightly around the kyanite. (crossed nicols)



0.8 mm

---

**Plate 6.27** Detail of garnet with kinked internal foliation. The garnet (cream colour) extends beyond the boundaries of the photomicrograph to a total size of several cm. It has overgrown a kinked foliation, outlined by dusty inclusion trails and graphite flakes. Coarse quartz inclusions (white) cross-cut the foliation.

## CHAPTER 7

### METAMORPHIC DEVELOPMENT OF THE THRUST BELT

Recent developments in geothermobarometry (overviews by Essene, 1982, 1989) and numerical modelling of both the thermodynamics of chemical zoning in minerals (Spear and Selverstone, 1983; Spear et al., 1984) and of the thermal development of orogenic belts (Oxburgh and Turcotte, 1974; Barr and Dahlen, 1989) have dramatically improved the understanding of the metamorphic development of orogenic belts. A dynamic view of metamorphism, with variations in pressure and temperature viewed as a result of tectonic movement, replaced a view of early metamorphic workers of metamorphism as a static process occurring at some fixed depth in the crust. Presently a principal aim of metamorphic studies is to reconstruct the variations in pressure and temperature (P-T paths) that affected small volumes of rock, rather than to estimate peak metamorphic pressures and temperatures across a metamorphic belt. The latter, referred to as metamorphic field gradient (Spear et al., 1984) or metamorphic geotherm (England and Richardson, 1977), reveals aspects of the spatial variation of the metamorphism, but does not give information about evolving metamorphic conditions that single rock volumes have experienced.

The P-T path of any rock is controlled by a combination of tectonic movements within the crust, which disturb the regional pattern of isobars and isotherms, and heat flow, which will tend to restore a thermal equilibrium state. Numerical modelling of these processes has provided a better understanding of the relation between the tectonic and thermal evolution of orogenic belts (e.g. Oxburgh and Turcotte, 1974; England and Richardson, 1977; England and Thompson, 1984; Davy and Gillet, 1986; Shi and Wang, 1987; Thompson and Ridley, 1987; Karabinos and Ketcham, 1988; Barr and Dahlen, 1989). These studies have provided a background for a meaningful interpretation of the P-T paths estimated from zoned minerals or mineral assemblages

and reactions, and many authors have shown that important deductions concerning orogenic processes can be made (e.g. Royden and Hodges, 1984; Rubie, 1984; Spear et al., 1984, 1990; St. Onge, 1987; Chamberlain and Karabinos, 1987; Anovitz and Essene, 1990). Thus an analysis of the metamorphic development of an area and its relation with the structural evolution is a prerequisite for a comprehensive regional tectonic study.

In the last decade, the reconstruction of P-T paths has become more sophisticated with the widespread application of geothermobarometry (overviews by Essene, 1982, 1989) and thermodynamic modelling of the growth of zoned minerals, especially garnets (Spear and Selverstone, 1983; Spear et al., 1984). Using these methods a more realistic, quantitative reconstruction can be made of the variations of pressure and temperature in time and space.

The metamorphic development of the Grenvillian fold and thrust belt in western Labrador is closely linked to and caused by the imbricate stacking of thrust sheets. The purpose of this chapter is to document and interpret the variations in thermal and baric evolution through the map area and link them to structural development of the belt. This will be achieved through a reconstruction of the metamorphic field gradient, P-T paths for different parts of the area and the relation between deformation and metamorphism.

For the determination of the metamorphic field gradient the variations in mineral assemblages and the interpretation of mineral reactions were used to provide qualitative information about the metamorphic history of the area. Variations in pressure and temperature in both space and time were determined quantitatively using geothermobarometry. Information about parts of the P-T paths was obtained from chemical analyses of cores and rims of minerals, together with chemical profiles of zoned garnets.

For a reconstruction of the temporal and causal relationships between metamorphism and deformation, the microstructural and microtextural relations described in Chapter 6 provide essential information. In this chapter the distribution of

mineral assemblages and P-T paths through the area, specifically across thrust sheet boundaries, are used in the analysis of the thermotectonic development of the fold-and-thrust belt.

In this chapter frequent reference is made to the peak of metamorphism. Generally the shape of P-T loops in metamorphic belts are such that the maximum pressure and maximum temperature are reached at different times. In Section 7.3 it is shown that in the study area peak pressures and temperatures were attained simultaneously. As a result, reference to the "peak of metamorphism", without specifying peak temperature or pressure, is warranted.

This chapter discusses only the Grenvillian metamorphism in Gagnon terrane. The pre-Grenvillian metamorphic development of the Archean basement and the metamorphism of Molson Lake terrane are beyond the scope of this thesis.

## **7.1 MINERAL ASSEMBLAGES AND METAMORPHIC FIELD GRADIENT**

The increase in metamorphic grade in the map area towards the southeast was first reported by Gastill and Knowles (1960) and Fahrig (1960, 1967). The metamorphic zonation in the area, based on mineral assemblages in metapelitic and quartzo-feldspathic rocks, was documented in detail by Rivers (1983b). The metamorphic zones and reaction isograds trend north-northeast and the increase in metamorphic grade is from lower greenschist facies in the northwest to upper amphibolite facies in the southeast (Fig. 7.1). Since the work for this thesis did not encompass a detailed petrological study, it has not resulted in significant new contributions to the metamorphic zoning. This section contains a summary of Rivers' (1983b) work with only minor new additions. Rivers' (1983b) work dates from before the subdivision of the area into different terranes and thus had to be adapted to this new situation. Because of the denser sample coverage in a few parts of the area, adjustments could be made to some of the zone boundaries.

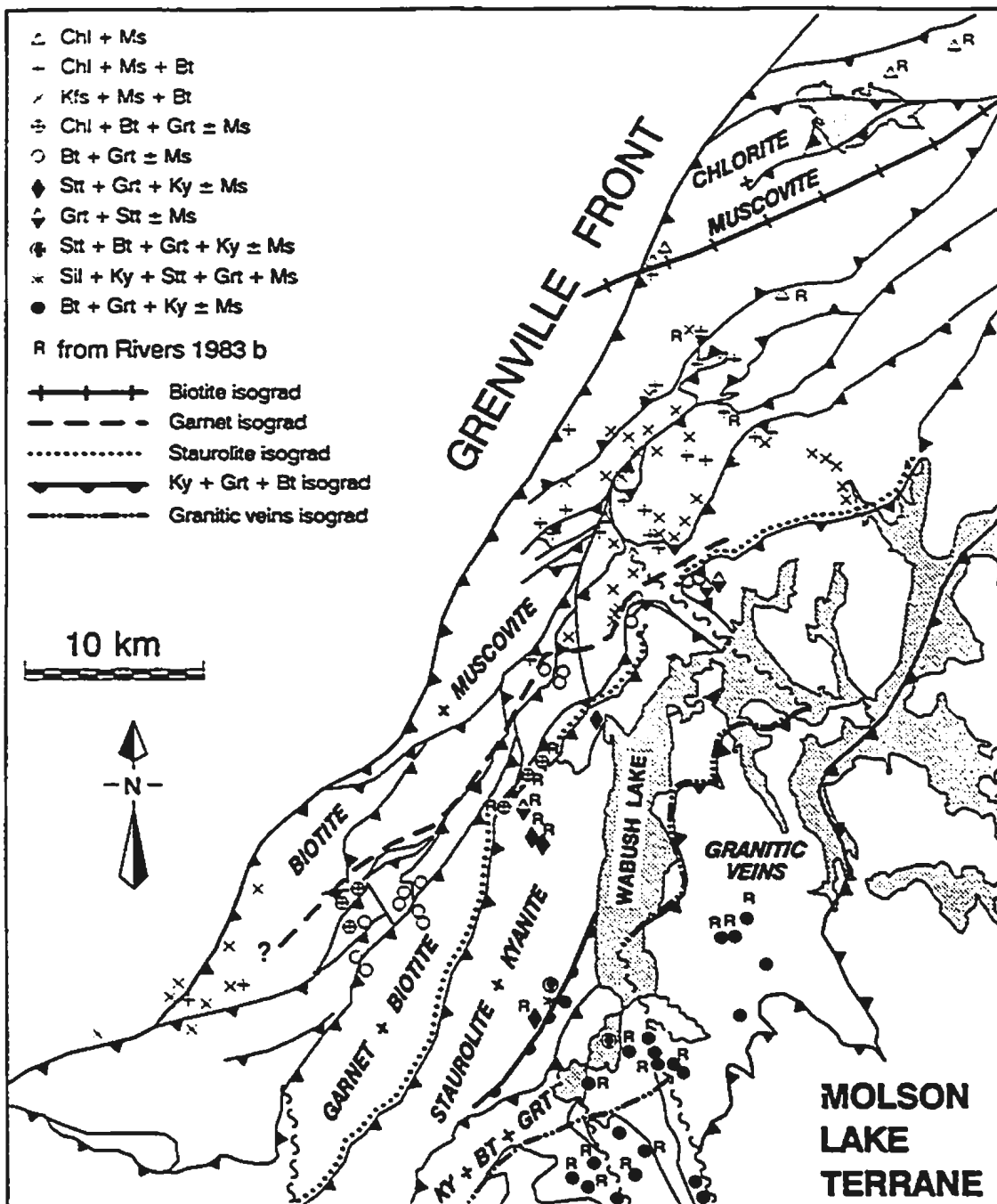


Fig. 7.1 Map of metamorphic zoning based on mineral assemblages in metapelitic and quartzo-feldspathic rocks. Locations of diagnostic mineral assemblages are shown. Assemblages with granitic veins are widespread east of the granitic veins isograd, and individual locations are not indicated on the map. The map includes new data as well as data from Rivers (1983b).

### 7.1.1 METAMORPHISM IN DIFFERENT ROCK TYPES OF GAGNON TERRANE

Rivers' (1983b) metamorphic zonation in the Gagnon terrane is based on mineral assemblages in the widespread metapelitic and quartzo-feldspathic rocks of the Early Proterozoic Attikamagen, Wishart and Menihek formations and of the reworked parts of the Archean basement. In rocks of the basement, the Grenvillian metamorphism is a retrograde event, whereas in the metasediments of the Knob Lake Group, which were not affected by metamorphism prior to the Grenvillian orogeny, the metamorphism is prograde.

The Archean basement rocks were originally of granulite grade, as attested by the occurrence of assemblages containing two pyroxenes in mafic rock types. Only those parts of the basement which were affected by penetrative Grenvillian deformation are significantly retrogressed. Far into the Grenville Province, up to Mont Bondurant, lenses of basement rocks occur which are virtually undeformed on outcrop scale and have most of their original granulite facies mineral assemblages preserved. Metamorphic reworking varies with the strain in the rocks. At low metamorphic grades retrogression at the lowest strains is characterized by incipient sericitization of plagioclase and breakdown of pyroxenes to actinolite or chlorite. At highest strain levels and elevated metamorphic grades the rocks are completely recrystallized and are indistinguishable from the quartzo-feldspathic metasediments. Two important facts have to be kept in mind when studying these retrograde rocks: 1) only the recrystallized matrix is considered for the mineral assemblage indicating the Grenvillian metamorphic grade, and the relict (possibly unstable or metastable) porphyroclasts are disregarded; 2) the mineral assemblage is often only an indicator of the grade of metamorphism at the time of deformation, which was not necessarily coeval with the peak of metamorphism.

In the rocks of the Knob Lake Group the Grenvillian metamorphic event is prograde and the prograde mineral reactions can be studied. For this purpose the pelitic and semi-pelitic rocks of the Attikamagen and Menihek formations and the

pelitic member at the base of the Wishart Formation are best suited because of their widespread occurrence throughout the area. Mineral reactions in the carbonate and silicate members of the Sokoman Formation could be used as metamorphic indicators as well, but most of these reactions are very much dependent on the mobility and the activities of  $H_2O$  and  $CO_2$  and require knowledge of these parameters for a true evaluation of metamorphic grade (Klein, 1966; Butler, 1969; Rice and Ferry, 1982). The rocks of the Denault Formation are found in a very small part of the map area and cover only a narrow range of metamorphic grades. In the Menihek Formation the high graphite content and the resulting low  $a_{H_2O}$  in the rocks probably enhanced dehydration reactions, shifting the stability fields of mineral assemblages and possibly resulting in buffering processes (Ohmoto and Kerrick, 1977; Rice and Ferry, 1982; Ferry and Burt, 1982; Pattison, 1989).

In general, mafic rock types are also suitable as indicators of metamorphic grade. In the map area the metavolcanic rocks of the McKay River Formation and those at the base of the Menihek Formation, the gabbros of the Shabogamo Intrusive suite and mafic rocks in the basement could be used. However, none of these rock types, with the exception of the gabbros, are sufficiently abundant for the construction of a regional metamorphic zoning pattern. The original compositional layering in some of the volcanic rocks makes them less suitable for comparative purposes. The gabbros of the Shabogamo Intrusive suite in Gagnon terrane have the disadvantage of having preserved their original pre-Grenvillian mineral assemblages (Rivers and Mengel, 1988), with the exception of zones of high strain at their margins.

#### 7.1.1.1 Mineral assemblage zones in metapelitic and quartzo-feldspathic rocks

In the map area six metamorphic zones were recognized, each with its own diagnostic mineral assemblage (Rivers, 1983b). With metamorphic grade increasing from lower greenschist to upper amphibolite facies these zones are:

- Zone 1 chlorite - muscovite
- Zone 2 biotite - muscovite
- Zone 3 garnet - biotite

- Zone 4    staurolite - kyanite  
 Zone 5    biotite - kyanite - garnet  
 Zone 6    biotite - kyanite - garnet - granitic veins

The areal distribution of the zones and the locations of samples with diagnostic mineral assemblages are shown in Figure 7.1. The diagnostic assemblages for each zone and the reactions that separate the different zones are given in Table 7.1. and in schematic A'KF and AFM diagrams in Figure 7.2. Besides the reactions shown in Table 7.1 many more continuous reactions are expected to have taken place, but only the reaction isograds that separate the mineral assemblage zones are reported here. The majority of the metapelitic and quartzo-feldspathic rocks east of the biotite isograd contain quartz, plagioclase, biotite, muscovite, epidote and retrograde chlorite, with variable modal compositions (Appendix E). Graphite is common in rocks of the Menihek Formation. Sphene, pyrite, magnetite, apatite, rutile, zircon and carbonate appear as accessory minerals. At intermediate and high metamorphic grades garnet is common and in the metapelites staurolite and kyanite appear at few locations (Fig. 7.1). Appendix E gives all observed mineral assemblages for each of the zones. A detailed discussion of the assemblages and reactions was given by Rivers (1983b), of which the following is a summary with minor modifications.

**Zone 1** is defined by prograde mineral assemblages in the Menihek Formation north of Sawbill Lake in the northern part of the map area and on retrograde assemblages in the shear zones in the basement. It is characterized by co-existing Chl + Ms  $\pm$  Mc (Fig. 7.2a). Pyrophyllite has not been identified. In reworked basement rocks, pre-existing feldspar breaks down to form muscovite (phengite), zoisite and quartz. Pyroxenes and biotite are replaced by chlorite.

**Zone 2**, characterized by the occurrence of biotite, is strongly depleted in chlorite, suggesting that the rocks (especially the reworked basement rocks) are rich in potassium and [R2] (Table 7.1) was the main biotite forming reaction (Fig. 7.2a and b). Rocks of the Menihek Formation contain the sub-assemblage muscovite-biotite with chlorite. In plate 6.17 biotite forms fine-grained rims on coarser grained lenses of

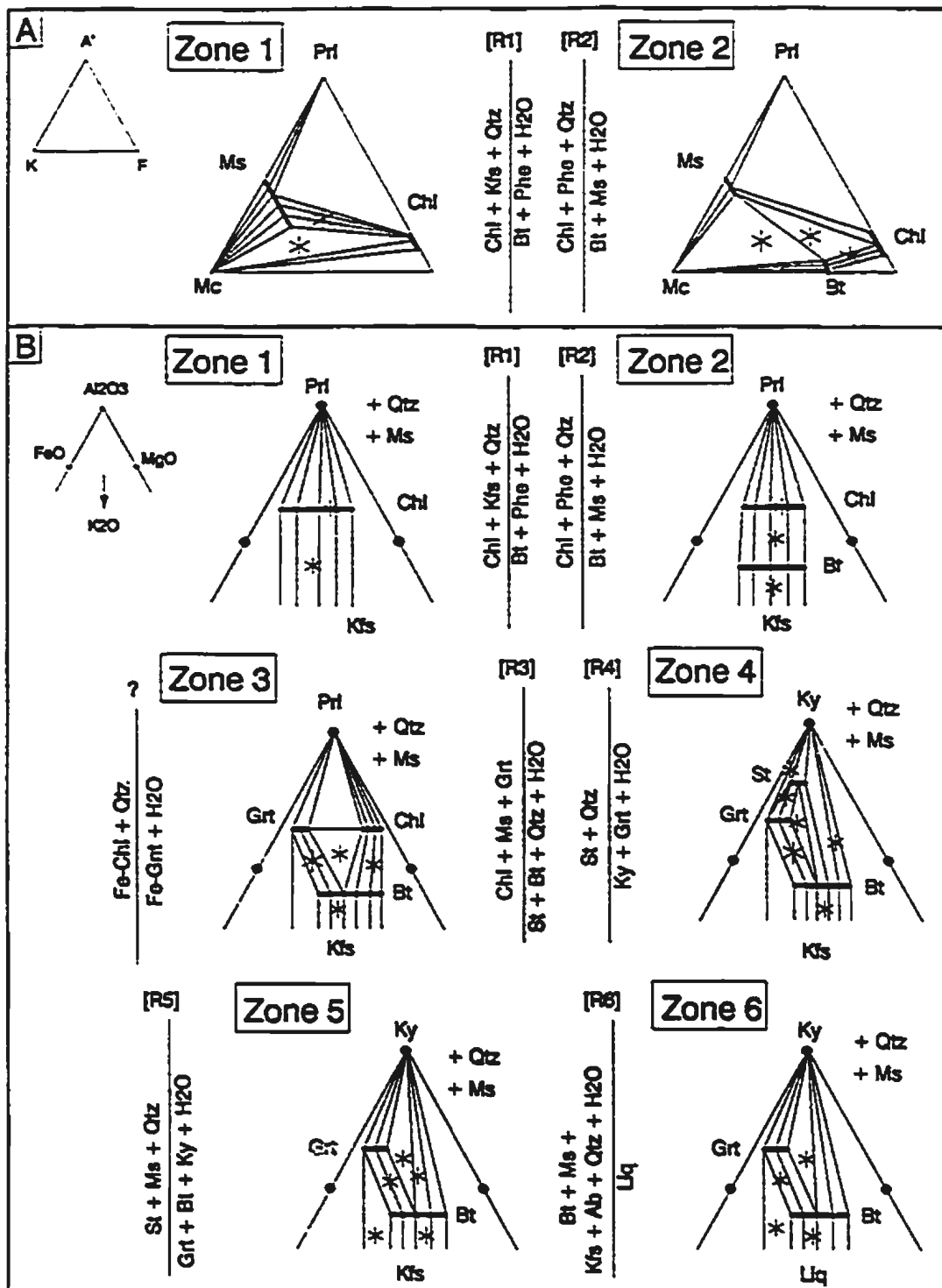


Fig. 7.2 Schematic A'KF and AFM diagrams of mineral assemblages in metapelitic rocks. The zone and reaction numbers correspond with mineral assemblage zones and reactions introduced in Table 7.1 and Fig. 7.1. A'KF and AFM diagrams after Rivers (1983b). The AFM diagrams are projected through muscovite. Stars indicate observed mineral assemblages, including observations by Rivers (1983b).

Table 7.1 Diagnostic mineral assemblages<sup>1</sup> in metamorphic zones and model reactions that occur at zone boundaries (after Rivers, 1983b).

Zone	Mineral assemblages	Reactions at zone boundaries
1	Qtz + Ms + Chl	
	Qtz + Ms + Chl + Mc	
		[R1] Chl + Kfs + Qtz = Bt + Phe + H <sub>2</sub> O
		[R2] Chl + Phe + Qtz = Bt + Ms + H <sub>2</sub> O
2	Qtz + Bt + Kfs ± Ms	
	Qtz + Chl + Bt ± Ms	
		not specified (see Section 7.1.1.1)
3	Qtz + Chl + Bt + Grt ± Ms	
	Qtz + Bt + Grt ± Kfs ± Ms	
		[R3] Chl + Ms + Grt = St + Bt + Qtz + H <sub>2</sub> O
		[R4] St + Qtz = Grt + Ky + H <sub>2</sub> O
4	Qtz + St + Grt + Ky ± Ms	
	Qtz + St + Grt ± Bt ± Ms	
		[R5] St + Ms + Qtz = Grt + Bt + Ky + H <sub>2</sub> O
5	Qtz + Ky + Bt + Grt ± Ms	
		[R6] Bt + Ms + Kfs + Ab + Qtz + H <sub>2</sub> O = Liq
6	Qtz + Ky + Bt + Grt + Liq ± Ms	
		[R7] Bt + Ms + Ab + Qtz + H <sub>2</sub> O = Ky + Liq
		[R8] Bt + Ms + Ab + Qtz = Kfs + Ky + Liq

<sup>1</sup> The assemblages shown are those that separate them from the lower grade zones. Some also appear in higher grade zones.

white mica, and are interpreted as late overgrowths. In reworked basement rocks, pre-Grenvillian Ti-rich biotites show exsolution of rutile needles in sagenitic intergrowths and sphene occurs along cracks and grain boundaries (Plate 7.1). Newly grown biotite, which is light green in color and lacks inclusions, grew along the rims of the Archean biotite grains, which are reddish brown in color (Plates 7.1 and 6.4). Pyroxenes are replaced by actinolite, which locally also forms coronas around relics of orthopyroxene.

Within zone 2 a possible jump in metamorphic grade exists across the thrust

between the Flatrock Lake and Elmer Lake thrust sheets. This jump is not indicated by a change in mineral assemblages, but by a marked increase in grain size and change in microstructures from footwall to hanging wall (Chapter 6).

The western boundary of zone 2, the first occurrence of biotite stable with muscovite, lies approximately 5 km northwest of the boundary drawn by Rivers (1983b) and intersects the Grenville Front north of Bruce Lake (Fig. 7.1).

Zone 3 is characterized by the presence of garnet in addition to the phases in zone 2. The boundaries of this zone are poorly defined, which is partly the result of the bulk composition of the rocks in the zone and partly because of poor coverage in the field of the southwestern and northeastern parts of the zone. Most of the reworked basement rocks in the Elmer Lake thrust sheet and elsewhere are too rich in potassium to form garnet and contain the non-diagnostic assemblage  $Qtz + Bt + Kfs \pm Ms$  (Fig. 7.2, Plates 6.5 and 6.6). The Lac Viot area probably lies within the garnet isograd, but no garnet has been observed in the quartzo-feldspathic or semi-pelitic rocks in this area. Only rocks of the Attikamagen, Wishart and Menihék formations and more Al-, Mg- and Fe-rich parts of the basement contain garnet-bearing assemblages.

The "garnet-in" isograd cuts across several major thrust sheets, but seems to be offset by the thrust faults. Several garnet producing reactions have been published (see e.g. Winkler, 1979), all for different bulk rock and mineral compositions. The topology of Figure 7.2b suggests that part of the garnet was formed by the reaction  $Fe-Chl + Qtz = Fe-Gnt + H_2O$ , but this does not account for the other components of the garnet, which were formed by other reactions. No single reaction can represent the garnet isograd in the map area (see Rivers, 1983b).

Zone 4 is characterized by the appearance of staurolite + kyanite (Plate 7.2) and is considered to mark the onset of amphibolite-facies or medium-grade metamorphism (Winkler, 1979). The transition from zone 3 to zone 4 coincides with the floor thrusts of the Lorraine Lake and Goethite Bay thrust sheets (Fig. 7.1), suggesting a metamorphic jump across these thrusts. This explains why staurolite and kyanite seem to appear at the same isograd, even though they are interpreted to have formed by

different reactions, [R3] and [R4] respectively. Other reactions for the formation of kyanite and staurolite are possible (see e.g. Winkler, 1979, Rivers, 1983b), but evidence for them was not found in this study, possibly because part of the metamorphic gradient was removed by the Lorraine Lake floor thrust. Possibly for the same reason there is no zone in which primary chloritoid is stable, which elsewhere has commonly been reported as a precursor of staurolite in pelitic rocks. In the pelitic member of the Wishart Formation staurolite is locally replaced by chloritoid in a retrograde reaction (Plate 7.3). In these rocks staurolite is still present as inclusions in garnet or as metastable relics.

In zone 4 the only occurrence of sillimanite in the area was found. It appears in both the Attikamagen and Sokoman formations in the core of the anticline at the Ski Hill north of Labrador City (Fig. 1.2) at the eastern boundary of zone 4 (Fig. 7.1). In the Attikamagen Formation it overgrows all other minerals, including those that delineate the  $S_1$ , and is locally associated with quartz veins. It is a retrograde replacement of kyanite in the area and is not relevant for the construction of the metamorphic field gradient in the area, which concerns only peak metamorphic conditions. It suggests that locally the P-T conditions evolved from the kyanite to the sillimanite field in the retrograde part of the P-T path.

In zone 5 the breakdown products of staurolite,  $Grt + Bt + Ky$ , form the diagnostic assemblage (Fig. 7.2, Plate 7.4). Many samples from zone 5 contain two morphologically different species of kyanite, which are an early coarse-grained  $Ky_1$  and a younger finer grained  $Ky_2$  (see Chapter 6).  $Ky_1$  appears to be similar to the kyanite occurring in zone 4, which suggests that  $Ky_2$ , which only appears in zone 5, is formed by the staurolite breakdown reaction [R5]. Two occurrences of rocks containing both reactants and products of this reaction are found near Labrador City (Fig. 7.1), the western one, at the Ski Hill, defining the location of the isograd. The staurolite in the sample from the southern end of Wabush Lake is metastable. Lack of observations makes the zone ill defined. Rocks in many locations east and south of Wabush Lake in zones 5 and 6 contain the staurolite breakdown assemblage.

The melt isograd defines the western boundary of zone 6. This zone is characterized by appearance of *in situ* granitic veins. The veins give the rocks a gneissic banding, parallel to the regional foliation (Plate 5.9). Melting is restricted to certain bulk rock compositions and occurs first in the quartzo-feldspathic rocks, in which reaction [R6] is responsible for the formation of granitic melt. At this elevated metamorphic grade most of the pelitic rocks lack K-feldspar and many are devoid of plagioclase and/or muscovite and show no signs of partial melting. Reaction [R7] in Table 7.1 was proposed by Rivers (1983b) to be responsible for partial melting of K-feldspar free assemblages, but the assemblage  $Bt + Ms + Ab + Qtz$  has been recorded in samples from close to the boundary with Molson Lake terrane without signs of melt production. Low  $a_{H_2O}$  may locally have prevented this reaction taking place. The upper limit of the metamorphic grade in the upper thrust sheets is the vapour absent reaction [R8], since in zone 6 the assemblage  $Ms + Bt + Ab + Qtz$  is still stable and the assemblage  $Ky + Kfs$  has not been observed within Gagnon terrane. This indicates that either the temperature did not attain the level of the reaction curve or the reaction is not consistent with the compositions of the phases involved.

Antiperthitic exsolution in plagioclase (Plate 7.5), indicative of the attainment of high temperatures during metamorphism, occurs only in the Wabush Lake thrust sheet and was not observed in the adjacent Duley Lake thrust sheet west of the Flora Lake shear zone. This may indicate that there was a slight difference in maximum temperature in the two thrust sheets, or that the present erosion surface cuts through a deeper level of the Wabush Lake thrust sheet than through the Duley Lake thrust sheet. Alternatively, the contrast in exsolution patterns may have been caused by different cooling histories.

East of Wabush Lake the melt isograd coincides with the Wabush Lake floor thrust. Towards the southwest the location of the isograd is less well defined due to the lack of rocks with suitable mineral assemblages. The isograd seems to be offset by the Flora Lake fault zone, an observation which is in accordance with the shear zone being the western limit of antiperthitic plagioclase.

Chlorite occurs as a late retrograde phase in most zones, overgrowing or replacing pre-existing minerals. Breakdown of garnet, commonly to form biotite and plagioclase (Plate 7.6), and late growth of muscovite, locally replacing kyanite or biotite, are also retrograde features. Late muscovite and chlorite generally lack a preferred orientation and overgrow the  $S_1$  foliation.

The metamorphic grade in Molson Lake terrane is higher than in Gagnon terrane, as indicated by preliminary geothermobarometry by the author and by data from Connelly (1991) and Indares (in press). Recently eclogitic mineral assemblages have been reported from Molson Lake terrane south of the map area (Indares, in prep). The metamorphism of Molson Lake terrane has been discussed in detail by Connelly (1991).

#### 7.1.1.2 Petrogenetic grid for the pelitic and quartzo-feldspathic rocks

The petrogenetic grid shown in Figure 7.3 is from Rivers (1983b). Two metamorphic field gradients are plotted, one from Rivers (1983b), based on metamorphic peak mineral assemblages only, and one from this study, incorporating information from both mineral assemblages and geothermobarometry (section 7.3). The former is positioned 1 to 2 kbar lower than the gradient obtained in this study, but shows the same trend, except for the swing into the sillimanite stability field at the high temperature end. Rivers' (1983b) metamorphic field gradient was constructed before the subdivision of the area into the different tectonic terranes and the K feldspar-kyanite and K feldspar-sillimanite assemblages were obtained from Lac Joseph terrane. These assemblages are now known to be of Labradorian rather than Grenvillian age (Connelly, 1991). The higher pressures for the metamorphic field gradient determined in the present study is not apparent from observed mineral assemblages, but is a result of the use of geothermobarometric estimates.

The positions of the reaction curves are not firmly fixed in P-T space, but are dependent on the compositions of the participating phases and the activity of water. All curves are drawn assuming  $a_{H_2O} = 1$ . Lower water activities will move the dehydration reactions to lower temperatures and the water consuming melt reactions to higher temperatures, shifting the invariant point of the system of melting reactions

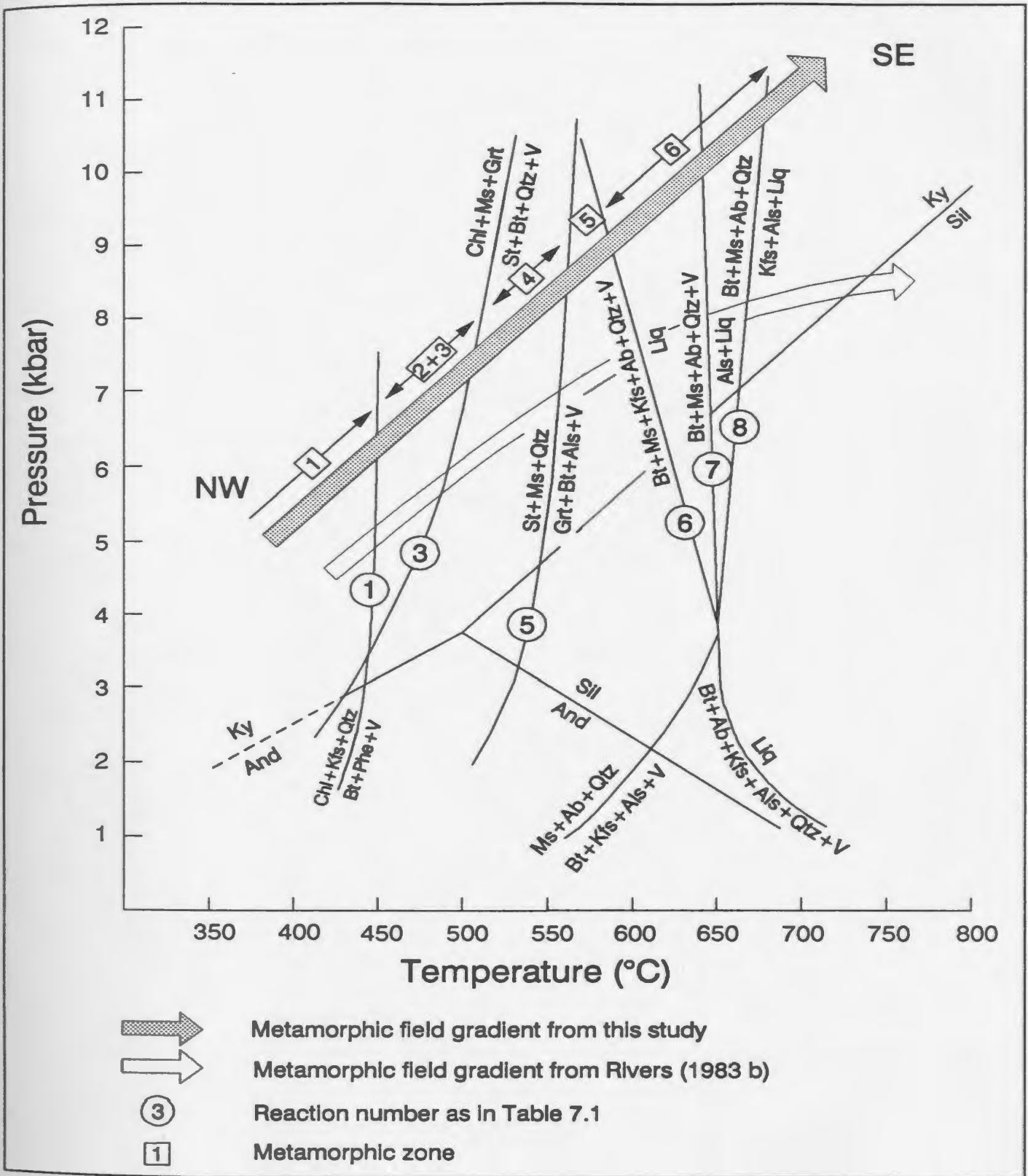


Fig. 7.3 Petrogenetic grid for metapelitic rocks in the map area. Reaction curves are from Rivers (1983b) and are drawn assuming that  $P_{H_2O} = P_{lithostatic}$ . The zone and reaction numbers correspond with mineral assemblages zones and reactions introduced in Table 7.1 and Fig. 7.1.

along curve [R8]. Rivers (1983b) assumed  $a_{\text{H}_2\text{O}} = 1$  for zones 1 to 5, but the water activity may have dropped in zone 6 at the onset of melting by extraction of water from the rocks by the melt producing reaction. The activity of albite in plagioclase is also likely to be smaller than 1 (Section 7.3), which will also move the melting reactions to higher temperatures. Changes in Fe/Mg ratios in micas will shift the positions of curves involving these minerals. Although the absolute positions of the reaction curves may not be correct, their relative positions are and they reflect the sequence of isograds observed in the field. Initial observation suggests that the width of zones 2 and 3 in the P-T grid is too narrow compared to their width in the map relative to the other assemblage zones. This suggests that reaction curve [R1] should be shifted to lower temperatures to widen the field of zones 2 and 3.

### **7.1.2 METAMORPHISM OF THE IRON FORMATIONS AND MAFIC ROCK TYPES**

The increase in metamorphic grade is also reflected in the mineral assemblages in the iron formations and the mafic rock types, but the changes in mineral assemblages with metamorphic grade of these rocks have not been studied systematically for this thesis. No separate metamorphic zones have been outlined for the mafic rock types and iron formations, but the observed changes in assemblages agree with the metamorphic zones inferred from the assemblages in the metapelites.

#### **7.1.2.1 Mineral assemblages in the iron formations**

The metamorphism of banded iron formations has been the subject of many petrological and petrographical studies. Several of these were performed on the rocks of the Sokoman Formation of the Labrador Trough, including the iron formations of southwestern Labrador and eastern Québec (Mueller, 1960; Chakraborti, 1966; Klein, 1966, 1973, 1978; Butler, 1969; Dimroth and Chauvel, 1973). Mineral compositions and equilibria in the banded iron formations of Wabush Lake and Mount Wright (just south of the map area) were described in great detail by Klein (1966) and Butler (1969). The main change with metamorphic grade is the transition of the carbonate rocks, which contain Fe-Mg-Ca carbonates and quartz, to silicate rocks as a result of

decarbonization reactions. The oxide members of the Sokoman Formation consist predominantly of quartz, hematite and magnetite and undergo no mineralogical change with metamorphic grade. Only the grain size increases towards the higher grade areas, hematite changes its crystal habit to specularite and the minor amounts of carbonates present in these rocks react to produce silicates (mainly grunerite).

In the Flatrock Lake / Corinne Lake area (muscovite-biotite zone) the oxide member of the Sokoman Formation consists of quartz with either one or both Fe-oxides and negligible amounts of grunerite and/or carbonate. The carbonate member contains  $Sd + Ank + Fe-Dol + Qtz \pm Gru \pm Hem \pm Mag$ . Intermediate compositions between these two members are observed as well. In the garnet zone (zone 3) grunerite schists are common, consisting of  $Gru + Qtz + Sd \pm Mag \pm Hem \pm Fe-Dol \pm Tr \pm Bt \pm Stp \pm Chl$ .

In the staurolite-kyanite zone (zone 4) a variety of silicate rocks occurs in the iron formations. They contain quartz, carbonates, Ca-Fe amphiboles, Ca-Fe pyroxenes, garnet (Alm), Fe-oxides and sporadically biotite and retrograde chlorite. The most common amphiboles are cummingtonite-grunerite and actinolite, with subordinate riebeckite-tremolite and magnesioriebeckite. Beside orthopyroxenes the following clinopyroxenes are found: diopside, aegirine-augite, rhodonite, ferrosilite (Klein, 1966). In the study area pyroxenes become more abundant with increasing metamorphic grade to the southeast.

Klein (1966, 1973, 1978) and Butler (1969) showed that the mineral assemblages depend not only on bulk rock composition and metamorphic grade, but also strongly on the mobility and partial pressures of  $H_2O$  and  $CO_2$ . For a complete list of observed mineral assemblages in the iron formations of the area and a discussion on mineral reactions and fluid compositions the reader is referred to the works of Klein (1966) and Butler (1969).

### 7.1.2.2 Mineral assemblages in the mafic rock types

Mineral assemblages in these rock types have not previously been studied in detail, apart from the igneous assemblages and textures in the gabbros of the Shabogamo Intrusive suite (Rivers and Mengel, 1988). The data presented here result from a cursory petrographic study. A complete table of all observed metamorphic mineral assemblages in the mafic rock types in the map area is presented in Appendix E.

At greenschist grade (zone 2) the mafic rocks contain the metamorphic mineral assemblage  $Pl + Chl + Act + Zo + Ilm \pm Qtz \pm Bt \pm Kfs \pm Ap$ . Olivine, orthopyroxene and clinopyroxene are locally preserved as metastable relics and commonly show reaction rims. With increasing metamorphic grade the chlorite content decreases and that of biotite and actinolite increases. In the upper greenschist/lower amphibolite facies (eastern part of zone 2 and zone 3) the assemblages contain  $Pl + Hbl + Act + Bt + Grt + Ep + Zo + Ilm + Spn \pm Qtz \pm Ap \pm Chl$ . In the highest grade amphibolites of the Wabush Lake thrust sheet (zone 6)  $Hbl + Bt + Grt + Pl + Spn + Ilm \pm Ep \pm Cpx \pm Dol \pm Qtz \pm Rt \pm Ap$  commonly occur together. No direct comparison has been made between the metamorphic zonation in the metapelites and the changes in mineral assemblages in the mafic rock types, but the variations in mafic mineral assemblages are consistent with the reported metamorphic zonation.

### 7.1.3 INTERPRETATION

The Grenville Front fold-and-thrust belt in southwestern Labrador shows a telescoped Grenvillian metamorphic gradient with an increase in metamorphic grade from lower greenschist to upper amphibolite facies across a distance of 30 km. On the scale of the map the metamorphic gradient is inverted with the highest metamorphic grades occurring in the structurally highest units.

On a small scale an inverted metamorphic gradient exists across the floor thrust of the Lorraine and Goethite Bay thrust sheets, with a decrease in metamorphic grade from the hanging wall to the footwall of the thrust fault. Furthermore a part of the

metamorphic field gradient may have been omitted at this thrust boundary. The retrograde metamorphism in the hanging wall (chloritoid replacing staurolite) may be of a higher grade than the prograde metamorphism in the footwall (garnet grade). A similar situation may exist at the floor thrust of the Wabush Lake thrust sheet. Inverted metamorphic gradients, either on the scale of an orogen or on the scale of single thrust faults, are a common feature of thrust belts (e.g. Rice, 1985; Jamieson, 1986; Boyle, 1987; Crowley, 1988; Treloar et al., 1989).

Besides an increase in metamorphic grade from the lowest to the highest thrust sheets, the metamorphic grade also increases slightly along the strike of the belt towards the southwest. This is indicated by the trend of the isograds in the western part of the map, which are oriented at an angle to the trend of the belt and cut through several thrust sheets. This is a result of the oblique nature of the convergence of the terranes (Chapter 5) and is further discussed in Chapter 8.

The metamorphic field gradient in the map area characterizes the thrust belt as a medium to high pressure facies metamorphic belt with increasing P and T towards the southeast. These conditions are typical for the Parautochthonous Belt in most of the Grenville Province (Wynne-Edwards, 1972; Rivers et al., 1989). Although very few detailed studies of mineral assemblages and thermobarometric studies have been performed in the Parautochthonous Belt (Indares and Martignole, 1989, 1990a; Indares, in press; Bethune and Davidson, 1988) which hampers a direct comparison, the results of this section are consistent with the overall relatively high-pressure character of the metamorphism in the Parautochthonous belt.

## **7.2 CHEMICAL ZONING IN GARNETS**

Chemical zoning in garnets and other minerals has been studied quantitatively since the introduction of the electron microprobe in the early 1960's (see review by Tracy, 1982). Zoning patterns reflect mineral reactions that took place during growth or later diffusion. Such patterns have been used qualitatively and quantitatively for the reconstruction of the metamorphic evolution of tectonic events. Lately the use of numerical computer models has become more common since the introduction of the

Gibbs method for thermodynamical modelling of garnet zoning, which enabled the quantitative reconstruction of P-T paths (Spear and Selverstone, 1983; Spear et al., 1984; Spear, 1989). Such quantitative P-T paths, in combination with numerical thermal models, have led to major improvements of the understanding of tectonic processes in orogenic belts.

Garnets are particularly useful for the purpose of reconstructing P-T paths because: 1) garnets are common in metamorphic rocks and occur in a large variety of rock types over a wide range of metamorphic conditions; 2) exchange reactions between garnets and other minerals are accurate indicators of metamorphic pressures and temperatures; 3) slow intracrystalline diffusion rates in garnet at low to medium temperatures enable the preservation of the chemical composition of the garnet over a range of P-T conditions in both prograde and retrograde paths; 4) garnets are commonly poikiloblastic and can record development of the foliation in the matrix during growth, which creates the opportunity to relate the P-T path to the deformation history.

The slow diffusion in garnet is an important factor, not only in the preservation of a chemical zoning pattern once it exists, but also in the actual creation of the zoning. Material in the interior of a garnet is excluded from the reacting chemical system and minerals in the matrix react with, or are in equilibrium with, the outer rim of the garnet only. Chemical zoning patterns in garnets can be attributed to either one of two processes (Tracy, 1982), 1) fractionation and/or reaction partitioning during prograde growth, producing growth zoning patterns, or 2) diffusional processes during retrograde metamorphism, which give diffusional or retrograde zoning patterns. Appendix F contains a detailed discussion of the different zoning patterns in garnets.

A typical growth zoning pattern for garnets in metapelites, at metamorphic grades ranging from greenschist to lower amphibolite grade, shows for spessartine and grossular bell-shaped profiles (Fig. F.1.a, Appendix F). Pyrope and almandine concentrations, as well as the ratio  $Mg/(Mg + Fe)$ , usually increase from the core towards the rim. Both spessartine and pyrope profiles commonly show reversal of the

slopes near the rims, which is interpreted to be a retrograde (diffusion controlled) effect. In composition maps of the garnet grains, the zoning patterns are generally concentric.

In retrograde chemical profiles the trends for spessartine and pyrope are the reverse of those observed in lower grade growth zoning patterns (Fig. F.1.b, Appendix F). Fe and Ca patterns are less straightforward and vary, mainly with bulk rock compositions and reactant phases present in the matrix (Crowford, 1977; Woodsworth, 1977). Zoning patterns in composition maps are concentric, but localized patterns at the rim near contacts with Fe-Mg phases (mainly biotite) may occur in high grade rocks.

The chemical profiles through garnets analyzed for this study are discussed in the ensuing section. The P-T paths determined from the garnet profiles are presented in Section 7.3.

#### **7.2.1 CHEMICAL PROFILES FOR GARNETS IN GAGNON TERRANE**

A total of 16 garnets was selected from several parts of the study area for detailed analysis of chemical zoning patterns. The sample locations were selected to cover most of the area where garnets occurred. In most of the samples garnet occurred as part of a thermobarometric mineral assemblage so that P-T paths could be determined. The results of the analyses are presented in Appendix F (Figure F.2), together with a sample location map (Figure F.3), and they are summarized below. Analytical procedures and operating conditions of the electron microprobe are described in Appendix G.

In the map area the compositional profiles of the garnets varied with metamorphic grade, similar to the variation described by Dempster (1985). Three different types of prograde zoning profiles were recognized, which show increasing effects of retrogression with higher metamorphic grade. In the part of the map area with the highest metamorphic grade several garnets revealed a diffusion zoning pattern. In the

following section a description is given for each of the four profile types and an example of each type is shown in Figure 7.4. The general character of the profiles for each of the types is summarized in Figure 7.5.

#### 7.2.1.1 Prograde zoned garnets without retrogression

*Samples 158-86 (Mont Bondurant area), 87-75 and 87-81 (O'Brien Lake area), Figures 7.4a and 7.5a.* All these garnets have a typical growth zoning profile with a bell-shaped curve for spessartine, and 'V' shaped curves for almandine and pyrope, which in the case of the latter is hardly perceptible because of the vertical scale of the diagram. The variations in concentrations in sample 87-75 are minor, which may be an effect of a tangential cut through the grain. The garnets are unzoned with respect to grossular, with the exception of a sawtooth perturbation in the profile close to the rim. This sawtooth coincides with a break in the curves of almandine and spessartine indicating a change in conditions for growth, or the presence of inclusions just below or above the plane of the thin section. In sample 87-81 this break coincides with the transition from an inclusion-free core to a rim with fine-grained graphite inclusions which define an internal foliation parallel to, and continuous with, the external foliation. No significant retrograde effects are noted. Plots of the variation of  $Mg/(Fe + Mg)$  through the garnets show that during growth this ratio increased, levelling off near the rim.

#### 7.2.1.2 Prograde zoned garnets with minor retrogression

*Samples 87-283 and 88-32 (Carol Lake thrust sheet), figures 7.4b and 7.5b.* The profiles for these two garnets are similar to the ones described above, with the exception of minor variations near the rims. Grossular shows a sharp increase close to the right hand rim in both profiles. A similar effect is noted for the other elements at about  $100\mu$  from the right hand rim, reversing the general increasing or decreasing trend. The  $Mg/(Mg + Fe)$  ratio is virtually unzoned with a slight decrease towards the rims in sample 87-283. Variations in the composition of sample 88-32 are minor, which is possibly a result of a tangential cut through the external part of the garnet.

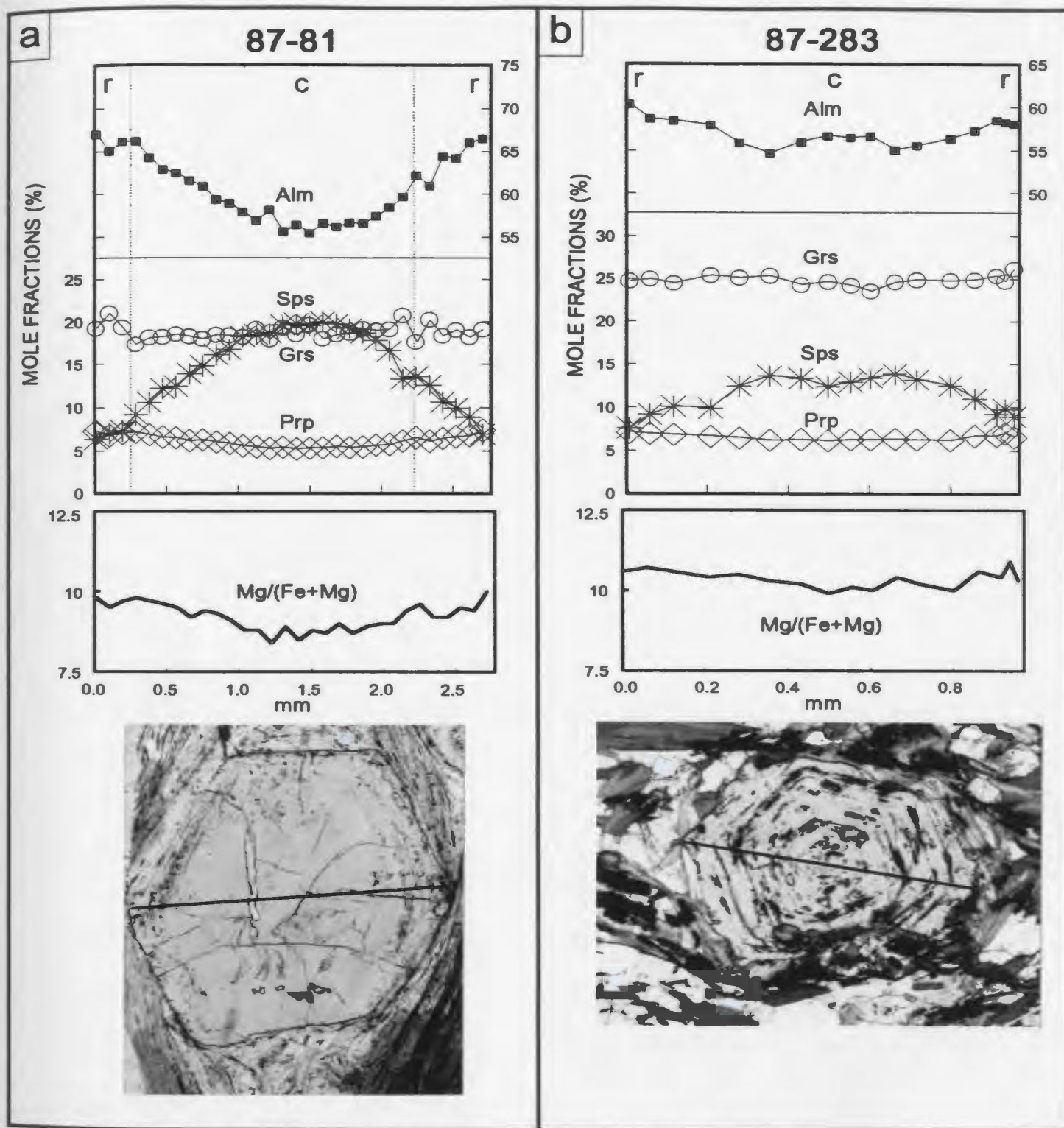


Fig. 7.4 Four examples of chemical profiles through garnets from the map area and photomicrographs of the analyzed garnets. Sample locations are shown in Fig. F.3 in Appendix F. The sizes of the garnets in the photomicrographs are shown in the profiles. r = rim, c = core.

a) Growth zoning profile from the O'Brien Lake thrust sheet. b) Growth zoning profile from the Carol Lake thrust sheet.

Continued on the next page.

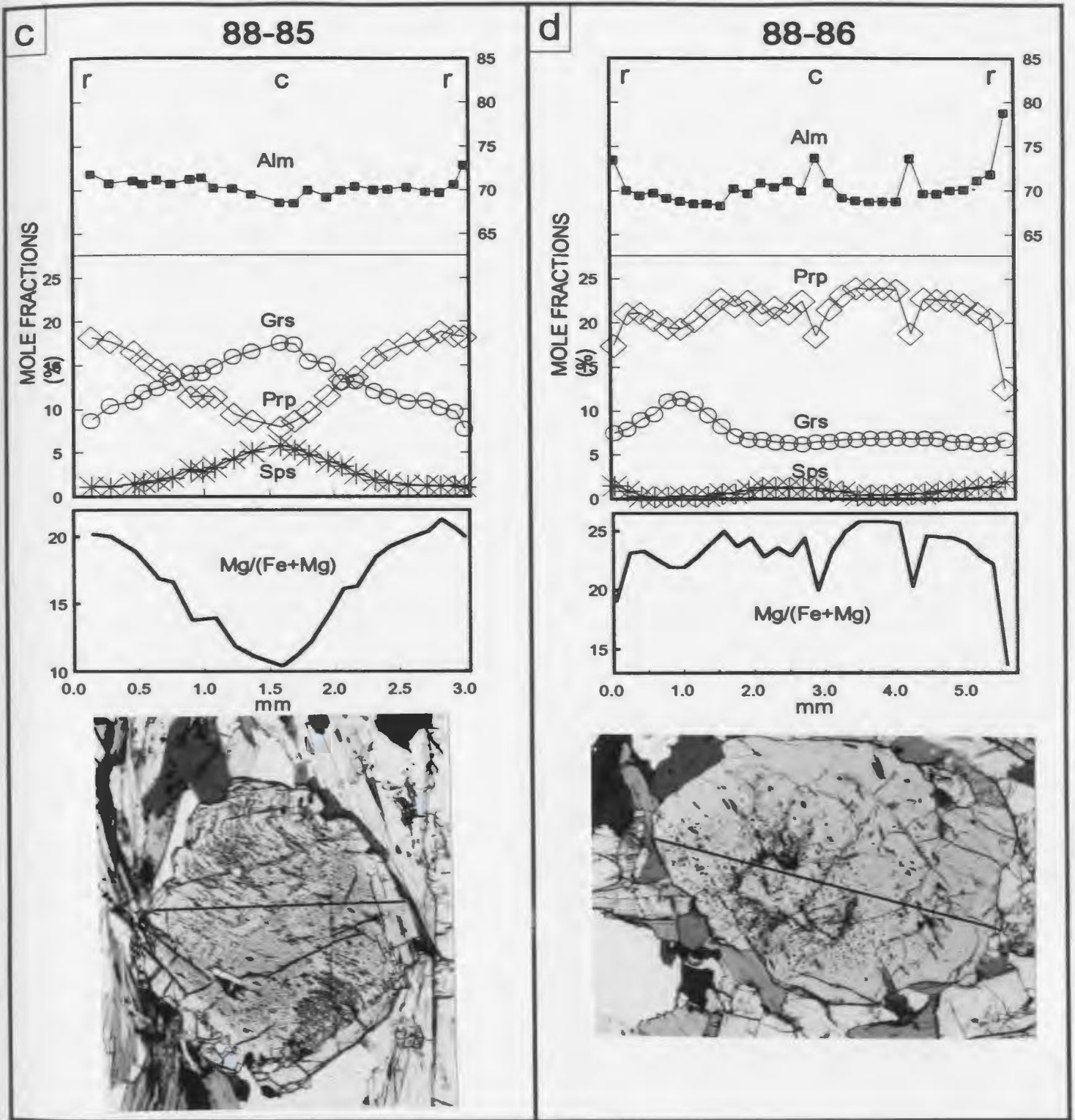


Fig. 7.4 continued.

c) Growth zoning profile with retrogression at the rims from the northern end of Flora Lake. d) Mainly homogenized and retrograde profile from the southern end of Flora Lake.

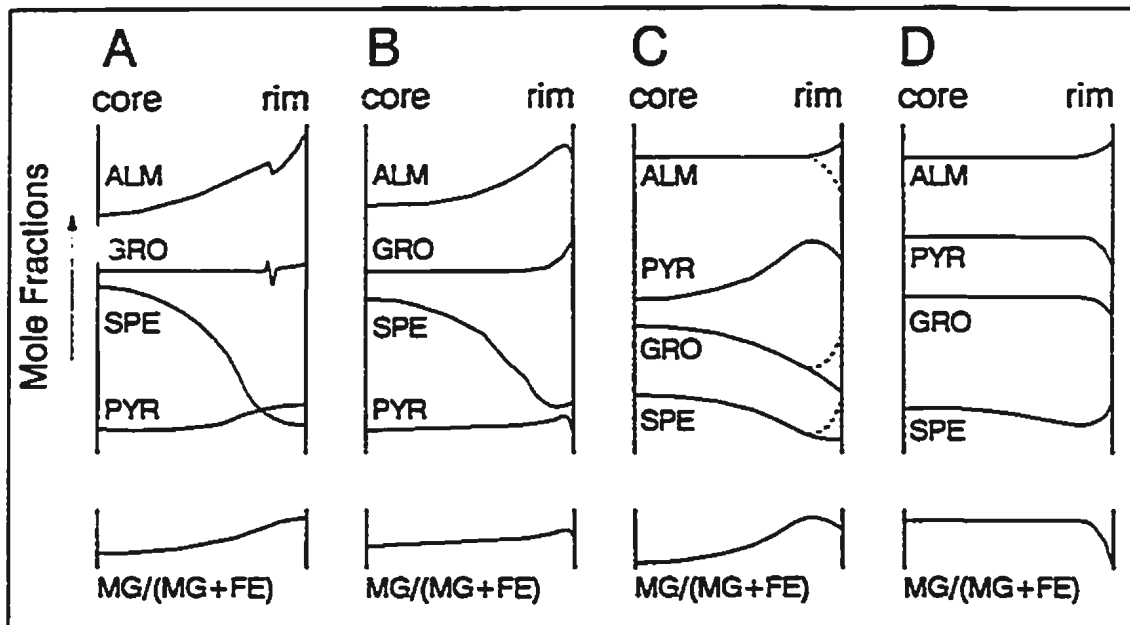


Fig. 7.5 Summary of garnet zoning profiles from samples in the map area. A) western and northern area; B) Carol Lake and Lost Lake thrust sheets; C) central/eastern area pro-grade zoned garnets; D) central/eastern area diffusion zoned garnets. Relative concentrations of components and slopes of curves vary between samples.

### 7.2.1.3 Prograde zoned garnets with retrograde rims

*Samples 88-48 (Lorraine Lake thrust sheet), 88-55, 88-80, 88-85, 88-98, 88-123 (all Wabush Lake thrust sheet), Figures 7.4c and 7.5c.* These samples have growth zoning profiles with in most cases a narrow retrograde rim. Spessartine displays bell-shaped profiles in all samples, although in some cases it is hardly perceptible, with commonly an upward curve near the rims. Grossular profiles can be divided into two sets. One set has virtually flat profiles with a sharp drop near the rims (88-55 and 88-123), the other has bell-shaped profiles. The latter only occurs in assemblages that lack plagioclase or in which the anorthite component in plagioclase is very low. In these cases presumably the fractionation of calcium, rather than changing partitioning coefficients, controlled the shape of the curve. The pyrope profiles display V-shaped curves typical for growth zoning, with a downward trend close to the rim. Almandine profiles do not have a consistent trend, except for an increase near the rims in most of the samples.  $Mg/(Mg + Fe)$  ratios in all cases increase from core to rim with small retrograde decreases near the rim.

The profiles of samples 88-80 and 88-98 have symmetry planes which lie off the center of the profiles, with part of the right hand side of the profiles being cut off. Both garnets are partially resorbed in a manner which corresponds to an off center location of the symmetry planes. The asymmetry of the profile of sample 88-55 may be caused either by the same resorption effect or by coalescence of several small nuclei.

### 7.2.1.4 Garnets with retrograde zoning profiles

*Samples 88-58 (Wabush Lake thrust sheet), 88-50, 88-86 and 88-87 (Duley Lake thrust sheet), figures 7.4d and 7.5d.* All these garnets are characterized by a lack of compositional zoning in the interiors, with exception of spessartine, which shows a slight decrease towards the rim. The lack of zoning is interpreted to be a result of homogenization by intracrystalline diffusion. Mn, which has the lowest diffusion coefficient (Tracy, 1982; Tucillo et al., 1990), preserved its original bell-shaped growth profile to some extent. The rims show effects of retrograde diffusion zoning. At the garnet rims the concentrations of Fe and Mn increase and Mg decreases. The Ca

profiles do not show a consistent trend in the samples, but decrease slightly near the rims in two of them. Peaks in Mg and Fe in samples 88-86 and 88-87 seem to be related to inclusions in the garnet. The Mg/(Mg + Fe) ratio is constant in the interiors of all these garnets, with a decrease at the rims. The width of the retrograde rims varies between 50 and 200  $\mu$ . The observed width is dependent on the angle at which the rim is cut. It must be noted that the lack of zoning in these garnets may be caused by a tangential section through the outer part of the grain. This may apply specifically to the garnet of sample 88-58, which has a rather small diameter and is the only one from the Wabush Lake thrust sheet.

#### **7.2.1.5 Garnet with a compositional break**

Garnets from sample 87-120 from Rivière aux Fraises show evidence of two phases of growth, separated by a phase of deformation. Profile 120(3) (Appendix F, Fig. F.3) shows a break in composition which coincides with a band of inclusions in the grain. At the break grossular decreases and pyrope increases, each by approximately one order of magnitude. This grain, as well as others in the section, is strongly fractured and displays a new rim overgrown on the fractured grain. This feature is interpreted as a result of a Grenvillian overgrowth on a possibly pre-Grenvillian (Archean) core.

#### **7.2.2 INTERPRETATION**

The chemical profile data, summarized in Figure 7.5 show that:

- The garnets in the area grew under prograde metamorphic conditions as shown by the growth zoning profiles. In most of the area the growth zoning profiles in the garnets were preserved, indicating that the temperature for homogenization was not reached or was not passed for long enough to destroy the prograde zoning pattern;
- Towards the area of higher peak metamorphic grades the rims of the garnets are progressively re-equilibrated by retrograde diffusion. With increase of the peak temperature the P-T loop became longer and there was more time available during cooling for retrograde diffusion to distort the original growth zoning pattern;

- The garnets in the Duley Lake thrust sheet were homogenized, implying that they reached temperatures higher than approximately 650°C. The relict growth zoning profiles for spessartine in these garnets may indicate that the temperature was not far, or not long, above the threshold for homogenization and only the elements with higher diffusion rates (Fe and Mg) homogenized;
- The absence of a major break in composition of the garnets, with the exception of sample 87-120, suggests that the garnets grew in a single prograde metamorphic event with minor re-equilibration of the garnet rims during the retrograde part of the P-T path.

### 7.3 GEOTHERMOBAROMETRY

For a quantitative evaluation of the range of pressures and temperatures that affected the map area, some of the suitable mineral assemblages were chemically analyzed for geothermobarometry. This was done with two purposes: 1) to quantitatively record the variation of "peak" metamorphic pressures and temperatures through the area; 2) to establish parts of the P-T path recorded in the rocks during burial and exhumation, using both core-rim analyses and chemical profiles through garnets.

Geothermobarometry is based on mineral equilibria which are either strongly pressure dependent (large  $\Delta V$ ) or temperature dependent (large  $\Delta H$ ). Determination of pressures and temperatures requires the calculation of the positions of equilibrium curves in a P-T grid from compositional and thermodynamic data of the participating phases. Simultaneous solution of a barometer-thermometer pair gives a P-T point for the equilibration of a certain assemblage, assuming that both the barometer and the thermometer closed at the same time. Many mineral equilibria have been calibrated for the purpose of calculating metamorphic pressures and temperatures (see reviews by Essene, 1982, 1989; Newton 1983).

A method for accurate reconstruction of variations in P-T conditions during mineral growth involves analyses of assemblages containing minerals with chemical

zoning. In this respect garnet is useful for the reasons that were mentioned in the previous section. The abundance of garnets in the metapelites of the map area makes them a useful object for study in this thesis. Two methods can be used to reconstruct evolving P-T conditions: 1) analyses of cores and rims of garnets; 2) compositional profiles through chemically zoned crystals. Pairs of core-rim analyses provide less complete information in that they only provide two points of a P-T path (a P-T vector, Mengel and Rivers, 1989) without indications of the P-T path in between, whereas a chemical profile provides virtually continuous information about the period of growth or retrograde diffusion of a grain, with which a more complete P-T path can be reconstructed. Spear and Selverstone (1983) and Spear et al. (1984) successfully applied the Gibbs method to chemically zoned garnets for the quantitative reconstruction of P-T paths. This method involves thermodynamic modelling of changes in composition during garnet growth with progression of P and T.

### **7.3.1 THERMOMETERS AND BAROMETERS USED IN THIS STUDY**

In the map area the rocks best suited for thermobarometry are the metapelitic rocks of the Attikamagen and Menihek formations and locally the reworked and re-metamorphosed Archean basement rocks (see discussion in section 7.1). Several reasonably accurate thermometers and barometers have been calibrated for pelitic rocks, that can be used in the reworked basement rocks as well. The Attikamagen and Menihek formations are sufficiently widespread to permit an estimation of P and T for a large part of the area. Garnet is a common mineral in these formations in which it co-exists with quartz plus one or more of the following: Bt, Ms, Pl and Ky (for full mineral assemblages see Appendix E). Because only equilibria that contain garnet were used, the part of the area northwest of the garnet-in isograd is not covered by geothermobarometry.

The set of thermometers and barometers used in this study was mainly taken from the paper by Hodges and Crowley (1985), who empirically calibrated several mineral equilibria for the pelitic assemblage Grt+Bt+Ms+Pl+Als+Qtz from a large number of published pressure and temperature data of natural assemblages. They used linear

regression to calibrate the thermodynamic equilibrium expression by comparison with the Grt-Bt thermometer of Ferry and Spear (1978, with corrections of Hodges and Spear, 1982) and the Grt-Als-Qtz-Pl barometer of Newton and Haselton (1981). This provides a set of thermobarometers which yield consistent results in different assemblages (all sub-sets of the one mentioned above) in different parts of the study area. Based on the initial results of this study, the decision was made to use the original Grt-Bt thermometer of Ferry and Spear (1978) rather than the calibration used by Hodges and Crowley (1985), which gave unrealistically high temperatures (see discussion in Section 7.3.5). The barometers that were used are Grt-Ms-Pl-Bt (Hodges and Crowley, 1985) and Grt-Ky-Qtz-Pl (Hodges and Royden, 1984).

#### 7.3.1.1 Mineral equilibria of the thermometers and barometers

Fe-Mg exchange between garnet and biotite is a widely used thermometer and a multitude of calibrations exists, both experimentally and empirically determined. Many of these are based on the experiments and calibrations of Ferry and Spear (1978), with adaptations for non-ideality of garnet solid solutions using different activity models, whereas others are based on separate experimental data (Hodges and Spear, 1982; Pigage and Greenwood, 1982; Perchuk and Lavrent'eva, 1983; Perchuk et al., 1985; Indares and Martignole, 1985a and b; Ganguly and Saxena, 1984; Hoinkes, 1986). The thermometer is based on the exchange reaction:

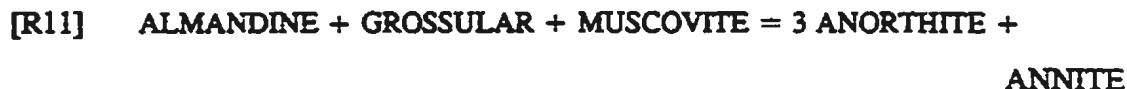


which requires garnet and biotite co-existing in equilibrium. This occurs quite commonly in the metapelitic and quartzo-feldspathic rocks of the study area. Appendix H gives details of the calibrations used in this study.

For pressure estimates in pelitic rocks the reactions involving net transfer of Ca between plagioclase and garnet can be used. The Grt+Als+Qtz+Pl (GASP) and Grt-Ms-Pl-Bt (GMPB) barometers are most appropriate for the rocks in the map area and both were calibrated in the study by Hodges and Crowley (1985). For pelitic mineral assemblages that contain kyanite the equilibrium



was used for pressure estimates. It was originally proposed as a barometer by Ghent (1976), but the calibration used here was published by Hodges and Royden (1984). For assemblages which lack aluminum silicates the following equilibrium was used:



Barometer [R11] was originally calibrated by Ghent and Stout (1981). It is the one used for most samples in this study. Plate 7.6 shows an example of a garnet which was partially resorbed by this reaction. It shows a xenoblastic garnet within a cluster of biotite and plagioclase grains. Muscovite occurs only at the rim of this cluster. The foliation which folds around this cluster suggests that it outlines the original shape of the garnet before breakdown.

A third geobarometer [R12] was used for a few samples which lacked plagioclase, but contained kyanite, as well as biotite and muscovite:



Hodges and Crowley (1985) and Essene (1989) argued that the uncertainties in the thermodynamic values for this equilibrium are too high to make it a reliable barometer.

A short introduction to the thermodynamics of thermobarometry is presented in Appendix H, as well as the separate temperature and pressure expressions of the thermometers and barometers used in this study.

Five assemblages were used for analysis, all of which contain at least Grt + Bt + Qtz.

- Qtz - Grt - Bt - Ky - Pl  $\pm$  Ms
- Qtz - Grt - Bt - Ky  $\pm$  Ms
- Qtz - Grt - Bt - Pl  $\pm$  Ms
- Qtz - Grt - Bt  $\pm$  Ms
- Qtz - Grt - Bt - Ky - Sil - St

### 7.3.2 EQUILIBRIUM CONSIDERATIONS

For results of geothermobarometry to have any geological significance, the minerals from which pressures and temperatures were calculated must have been in equilibrium. Careful petrography and mineral chemistry analyses are required for an evaluation of the state of equilibrium of a rock. Microtextures and overprinting relationships give indications about the equilibrium of mineral assemblages. For example, idioblastic crystal shapes and straight grain contacts (e.g. Plate 7.4) can be signs of equilibrium of co-existing minerals. Mineral zoning, coronas and symplectites generally indicate disequilibrium on a certain scale, but some of the minerals involved in these textures can still be stable together.

When studying equilibrium conditions in rocks we have to keep in mind that the samples are at a complete disequilibrium under the conditions at which we observe them (approximately 1 bar and 298°K). The observed mineral compositions represent the state of the rock frozen in at the time that diffusion rates slowed down to such an extent that they could not maintain effective chemical communication between reactive phases during decrease of P and T. In the case of net transfer reactions an equilibrium can also be frozen in when one of the reactants in the system is depleted or unavailable (low activity of H<sub>2</sub>O generally prevents retrograde hydration reactions to occur). Such a situation is only preserved if the composition of the participating minerals are not changed by any other reaction. Another problem is that textural equilibrium may have been achieved without chemical equilibrium (Duebendorfer and Frost, 1988), if grain boundary migration ceased at a different temperature than the diffusion driven by exchange reactions. Lasaga (1983) discussed in detail the kinetics of exchange reactions and the influence of diffusion rates on thermobarometry, addressing some of the above mentioned problems (see also Tracy et al., 1976; Jiang and Lasaga, 1990).

With all these considerations in mind, finding evidence for chemical equilibrium between groups of minerals would be a major study in itself. Most thermobarometric studies only superficially assess these problems and assumptions are made about the equilibrium state. For the purpose of this study minerals were interpreted to be in

equilibrium if, on the scale of a thin section, mutual grain contacts were sharp and straight, or for those cases where they were separated up to a few tens of microns, if the crystal shape was idioblastic or subidioblastic and the minerals were not separated by a reaction product. Minerals affected by low grade retrograde reactions (e.g. plagioclase replaced by sericite, biotite or garnet partially broken down to form chlorite) were not used for thermobarometry. If calculated pressures and temperatures were consistent and in accordance with the observed mineral assemblage the results were interpreted to be geologically significant.

In the case of zoned minerals, as for example the garnets in this study, the interpretation of equilibrium is more complicated. As a result of the slow diffusion rates within garnets, the (unzoned) matrix minerals are in equilibrium with the garnet rims only and the garnet is internally in disequilibrium, resulting in zoning patterns as discussed in Appendix F.

### 7.3.3 P-T PATHS FROM ZONED GARNETS

Numerous studies have shown that P-T paths can be reconstructed using chemical zoning profiles of metamorphic minerals, most of which are based on zoning patterns in garnet (e.g. Tracy, 1982; Lasaga, 1983; Spear et al., 1984, 1990; Indares and Martignole, 1985a, 1989, 1990a, b; St. Onge, 1987; Burton et al., 1989; Jiang and Lasaga, 1990). A requirement for the reconstruction of the prograde part of the history is that the existing growth zoning pattern is preserved during the post-growth thermal evolution. For construction of the retrograde part of the history, ion exchange and diffusion at the garnet rim is required, such that the changing rim composition reflects the equilibrium at decreasing P and T.

Preservation of growth zoning or core compositions of retrograde zoned garnets depends on many factors, including the peak metamorphic temperature, the size of the garnet, the difference in composition between core and rim, the post growth thermal history (time available for diffusion, uplift rate) and the strain path. Using a numerical model for binary (Mg-Fe) diffusion in garnets Lasaga (1983) and Jiang and Lasaga (1990) calculated that up to middle/upper amphibolite facies conditions ( $\pm 650^{\circ}\text{C}$ )

garnets of over 1 mm in diameter can preserve their growth zoning pattern or core composition during retrograde metamorphism. In a similar study Muncill and Chamberlain (1988) estimated the influence of uplift rates on the rate of homogenization and found that differences are to be expected from garnets found in different structural settings (e.g. antiforms versus synforms) as a result of differences in uplift rates and time available for diffusion/homogenization. Homogenization will affect the core and rim compositions first, which will result in an over-estimate of the core temperature and an under-estimate of the rim temperature in the case of a prograde zoned garnet (Jiang and Lasaga, 1990; Muncill and Chamberlain, 1988).

#### **7.3.4 METHODS USED FOR CALCULATION OF P-T VECTORS AND P-T PATHS**

From all samples from the map area containing at least the mineral pair Grt-Bt, microprobe analyses were taken from a garnet rim in stable equilibrium with biotite and, where available, muscovite and plagioclase, providing at least a temperature estimate (Grt-Bt), and in most cases also a pressure estimate (Grt-Bt-Ms-Pl, Grt-Pl-Ky-Qtz or Grt-Bt-Ms-Ky), which can be combined to give a P-T point. Analyses of garnet cores were combined with matrix minerals or with compositions of micas and plagioclase in equilibrium with the garnet rim to obtain a P-T point for the garnet core.

P-T paths for garnet growth and retrograde diffusion were constructed using the chemical profiles presented in Section 7.2 and Appendix F. Only ten of those garnets occurred in an assemblage which was suitable for thermobarometry. For every analyzed point in a garnet a pressure and temperature was calculated, assuming equilibrium with rim biotite, muscovite and plagioclase, and using the intersection point of the barometer and the thermometer. P-T points obtained in this manner were connected to form a P-T path. This provides more continuous information about the evolving P-T history during growth and retrogression of the garnet, rather than two end points of this path connected by a vector.

For calculations of P-T points from the interiors of the garnets two assumptions were made: 1) during the growth of a garnet its composition was controlled by the same set of reactions as those frozen in at the garnet rim; 2) a sufficiently large reservoir of Bt+Ms+Pl was present during garnet growth and re-equilibration, such that their compositions did not change significantly as a result of the reactions with the garnets (Tracy et al., 1976). Samples that were chosen for analysis, appeared to meet these requirements. With the exception of sample 87-120 (Appendix F), garnets in the analyzed samples do not have major jumps in their compositional profiles, suggesting that no change in the growth controlling reaction occurred. Justification for the second assumption lies in the observation that in all samples the matrix minerals used for thermobarometric calculations have high modal abundances relative to garnet. Analyses of biotites, muscovites and plagioclases in the matrix at distances of over a centimeter from the nearest garnet in the plane of the section, are not significantly different from the same minerals in contact with garnet, suggesting that at peak metamorphic temperatures garnets were in equilibrium with a large volume of rock and matrix compositions did not change significantly as a result of reaction with the garnets during retrograde metamorphism, when the garnets remained in equilibrium with a progressively smaller volume of the surrounding matrix. In six samples plagioclase was significantly zoned, with increasing anorthite content from core to rim. In these cases the garnet core was presumed to have been in equilibrium with the plagioclase core.

The garnets analyzed for thermobarometry had a very low abundance of inclusions other than quartz, chlorite, ilmenite and graphite. This prevented the use of inclusions for the quantitative calculation of parts of the P-T path. Only a few of the garnets had inclusions of Bt, Ms or Pl (87-81, 87-117, 88-50, 88-85 and 88-87). P-T calculations using these inclusions were not significantly different from those calculated using matrix Bt, Ms and Pl. Calculated values diverged up to 30°C and 200 bar, suggesting that the assumptions made above are valid in a first approximation. As an example, the pressure calculated near the core of a garnet next to a plagioclase

inclusion in sample 88-87 (Grt 2) at 545°C was 6.8 kbar using the composition of the plagioclase inclusion, compared to 6.6 kbar using the composition of a matrix plagioclase near the rim of the garnet (GASP barometer).

It must be kept in mind that, with the exception of the garnet rims, the P-T values obtained with this method are only estimates. Because of the many uncertainties and assumptions made for P-T calculations of the interiors of the garnets, the constructed P-T paths are assumed to be only semi-quantitative indicators of changes of P and T in time, anchored in P-T space by their end points. The trends of increasing or decreasing P and T, not their absolute magnitudes, are interpreted to be real and are used to draw conclusions about the thermotectonic development of the area.

### **7.3.5 RESULTS OF THE GEOTHERMOBAROMETRY**

Chemical analyses used for the thermodynamic calculations are presented in Appendix I, together with a short description of the mineral chemistry. Figure F.3 (Appendix F) is a sample location map of the samples used for mineral chemistry analyses. For the presentation of the geothermobarometry results the map area was divided into three sub-areas, a northern (N), a western (W) and a central/eastern (C/E) sub-area, which is shown in figures 7.6 and F.3. Table 7.2 shows the results of the garnet core-rim analyses for each of the three areas. Within each sub-area the data are presented separately for each thrust sheet or tectonic unit. For those samples which lack a barometer assemblage a pressure was substituted for the calculation of the temperature. In most cases analyses of different garnet grains from a single sample resulted in overlapping P-T ranges. With a few exceptions, only the vector with the largest P-T range is reported in Table 7.2.

Temperatures and pressures obtained from garnet rims are presented in a map in Figure 7.6. For those samples which yielded both a temperature and a pressure, a P-T vector is plotted in a P-T diagram in Figure 7.7 using a core and a rim P-T point. Ten of the samples for which a chemical profile of garnet is available (Section 7.2)



Table 7.2.a Geothermobarometric results from the northern and western sub-areas

SAMPLE	GRAIN (1)	$P_{\text{GMPB}}$ (kbar) (2)	$T_{\text{FC}}$ (°C) (3)	$P_{\text{GMPB}}$ (kbar) (2)	$T_{\text{MC}}$ (°C) (3)	P-T VECTOR (5)	ASSEM- BLAGE (4)	LOCA- TION (6)
<b>NORTHERN SUB-AREA (7)</b>								
142-86	GA3 r	(6)	618	(6)	686	C<R	GBMP	MB
	GA3 c	(6)	553	(6)	626			
158-86	GA2 r	6.4	489	8	567	C≤R	GBMP	MB
	GA2 c	5.7	477	7.7	543			
87-117	GA2 r	6.4	472	8.1	546	?	GBMPC	RAF
	GA2 c1	7.8	549	8.8	617			
	GA2 c2	4.8	411	6.1	472			
87-198A	GA1 r	(6)	427	(6)	485	C=R	GBMP(C)	GB
	GA1 c	(6)	415	(6)	475			
87-255B	GA2 r	(6)	694	(6)	700	C<R	GBMToC	GB
	GA2 c	(6)	638	(6)	648			
87-271	GA1 r	(6)	418	(6)	487	C>R	GB(M)P	GB
	GA1 c	(6)	482	(6)	533			
<b>WESTERN SUBAREA</b>								
<b>O'Brien Lake area</b>					$T_m = 445 \pm 11^\circ\text{C}$ $P_m = 5.7 \pm 0.4\text{kbar}^{(8)}$			
87-51	GA2 r	5.3	441	6.9	517	C<R	GBMPC	OB
	GA2 c	4.2	406	5.8	480			
87-81	GA2 r	6.5	467	8.2	545	C<R	GBMP	OB
	GA2 i	5.9	455	7.6	530			
	GA2 c	4.9	425	6.3	494			
87-83	GA2 r	5.9	435	7.5	506	C<R	GBMP	OB
	GA2 c	5.7	433	7.3	503			
87-86	GA2 r	5.5	442	7.1	512	C=R	GBMP	OB
	GA2 c	5.1	433	6.5	499			
	GA4 r	5.5	441	6.9	506	C<R	GBMP	
	GA4 c	3.8	392	5.0	448			
<b>Emma Lake area</b>					$T_m = 454 \pm 16^\circ\text{C}^{(9)}$			
87-65	GA1 r	(6)	458	(6)	536	C=R	GBA	EL
	GA1 c	(6)	466	(6)	548			
87-75	GA2 r	(6)	438	(6)	503	C≤R	GMC(B)	EL
	GA2 c	(6)	425	(6)	484			
87-93	GA1 r	(6)	450	(6)	507	C<R	GBMP	EL
	GA1 c	(6)	365	(6)	415			
87-94	GA1 r1	(6)	486	(6)	539	C>R	GBMP	EL
	GA1 r3	(6)	443	(6)	496			
	GA1 c	(6)	505	(6)	563			
88-32	GA1 r	(6)	450	(6)	506	C≤R	GBM(PC)	EL
	GA1 c	(6)	431	(6)	493			
<b>Carol Lake thrust sheet</b>					$T_m = 519 \pm 51^\circ\text{C}^{(10)}$			
87-279	GA1 r	(6)	570	(6)	643	C<R	GBM(P)C	CAL
	GA1 c	(6)	517	(6)	604		gcc	
87-283	GA1 r	7.1	469	9.2	563	C<R	GB(M)PC	CAL
	GA1 c	6.5	450	8.6	543			

Table 7.2.b Geothermobarometric results for central/eastern sub-area

SAMPLE	GRAIN	P <sub>OMP</sub> (kbar) (1)	T <sub>FB</sub> (°C) (2)	P <sub>OMP</sub> (kbar) (3)	T <sub>HC</sub> (°C) (4)	P <sub>OASP</sub> (kbar) (5)	T <sub>FB</sub> (°C) (6)	P <sub>OASP</sub> (kbar) (7)	T <sub>HC</sub> (°C) (8)	P <sub>MABK</sub> (kbar) (9)	T <sub>FB</sub> (°C) (10)	P <sub>MABK</sub> (kbar) (11)	T <sub>HC</sub> (°C) (12)	P-T VECTOR (13)	ASSEM- BLAGE (14)	LOCA- TION (15)
Lorraine Lake thrust sheet																
88-48	GA3 r	(8)	566	(8)	584					9.3	571	10.3	592	C<R	GBMKSJ	SKI
	GA3 c	(8)	460	(8)	495					3.6	445	5.6	488		(C)	
Duley Lake thrust sheet																
													$T_m = 595 \pm 48^\circ\text{C}^{(1)}$		$P_m = 7.7 \pm 1.2\text{kbar}$	
88-45A	GA4 r	8.1	592	8.9	632	8.3	592	9.2	633	6.2	585	8.1	629	C>R	GBMPK	WL
	GA4 c	8.5	612	9.3	652	8.8	613	9.6	654	6.7	605	8.6	650		(St)	
88-50	GA1 r	6.8	563	7.4	597	6.7	563	7.4	596	5.7	559	7.3	596	C>R	GBMPK	WAB
	GA1 c	7.0	572	7.7	607	7.0	573	7.7	607	5.9	568	7.5	606			
	GA2 r					5.7	518	6.4	553					C>R	GB(M)PK	
	GA2 l					6.5	532	7.2	568							
	GA2 c					8.9	625	9.8	666							
88-52B	GA2 r									7.4	621	7.9	632	C<R	GBMK	WAB
	GA2 c									3.3	544	4.8	581			
88-85	GA2 r									4.8	525	6.6	567	C<R	GBM(P)K	NFL
	GA2 l									5.9	592	7.8	640			
	GA2 c									-4.3	337	-1.5	405			
88-86	GA1 r	9.0	659	9.6	689	9.0	660	9.5	689					C>R	GBMPK	SFL
	GA1 c	10.0	735	10.8	763	10.2	735	10.8	764							
88-87	GA1 r	9.0	645	9.7	676	9.2	646	9.9	678	6.9	636	8.3	671	C≤R	GBMPK	SFL
	GA1 c	8.3	632	8.7	657	8.1	631	8.6	657	6.8	624	8.0	653			
	GA2 r	7.6	596	8.2	624	7.5	595	8.1	624	6.0	590	7.3	620	C<R	GBMPK	
	GA2 c	6.6	537	7.1	565	6.7	544	7.1	565	4.1	528	5.4	559			

Table 7.2.b (Continued)

SAMPLE	GRAIN	P <sub>OMP</sub> (kbar)	T <sub>FS</sub> (°C)	P <sub>OMP</sub> (kbar)	T <sub>HC</sub> (°C)	P <sub>OASP</sub> (kbar)	T <sub>FS</sub> (°C)	P <sub>OASP</sub> (kbar)	T <sub>HC</sub> (°C)	P <sub>WABK</sub> (kbar)	T <sub>FS</sub> (°C)	P <sub>WABK</sub> (kbar)	T <sub>HC</sub> (°C)	P-T VECTOR	ASSEM- BLAGE	LOCA- TION
	(1)	(2)	(3)	(2)	(3)	(2)	(3)	(2)	(3)	(2)	(3)	(2)	(3)	(2)	(4)	(5)
Wabush Lake thrust sheet														P <sub>m</sub> = 9.0 ± 1.7kbar T <sub>m</sub> = 624 ± 52°C <sup>(6)</sup>		
87-287	GA1 r	10.0	665	11.8	749									C>R	GBMPE	JP
B	GA1 c	11.7	755	13.4	836										(C)	
88-55	GA1 r	8.7	609	10.0	673									C<R	GBMPMc	BH
	GA1 c	7.0	490	8.9	579											
88-57	GA1 r	(8)	694	(8)	780									C>R	BP(GMC)	BH
	GA1 c	(8)	780	(8)	846											
88-58	GA1 r	(8)	634	(8)	652									C>R	GBM	BH
	GA1 c	(8)	661	(8)	679											
88-61	GA1 r	(8)	653	(8)	728									C>R	GM(B)E	BH
	GA1 c	(8)	686	(8)	792											
88-72	GA1 r	(8)	620	(8)	744									C≤R	GBAP	EFL
	GA1 c	(8)	595	(8)	716											
88-74A	GA1 r	7.1	601	7.4	618	6.9	600	7.2	617	4.6	591	5.3	610	C>R	GBMPK	NFL
	GA1 c	9.5	659	9.9	679	9.5	659	9.9	680	5.8	644	6.7	666			
88-76A	GA1 r	11.8	674	14.6	799									C<R	GBMP	DOL
	GA1 c	10.1	615	12.4	714											
88-80	GA2 r	11.0	650	12.1	702	10.8	658	12.3	705	9.1	642	11.5	699	C<R	GBMPK	BH
	GA2 c	9.8	593	11.0	646	10.8	601	10.6	649	6.2	579	8.7	638			
88-89	GA1 r	(8)	618	(8)	690									C>R	GBP	SFL
	GA1 c	(8)	726	(8)	792											
88-90	GA2 r	(8)	587	(8)	629									C>R	GBP(M)	SFL
	GA2 c	(8)	689	(8)	728											
88-98	GA2 r	(8)	715	(8)	735									C<R	GBM	SL
	GA2 c	(8)	655	(8)	697											
88-104	GA1 r	(8)	580	(8)	631									C>R	GBPA	SFL
	GA1 c	(8)	610	(8)	683											
88-122	GA1 r	8.4	576	10.3	664									C<R	GBMP	MHL
	GA1 c	6.1	465	8.0	553											
	GA2 r	6.4	504	7.9	574									C>R	GBMP	
	GA2 c	8.9	591	10.9	685											
88-123	GA1 r	8.7	579	10.6	667									C<R	GBMP	MHL
	GA1 c	6.6	467	8.7	562											
88-129	GA1 r	(8)	676	(8)	711					11.1	689	12.8	730	C<R	GBMPK	MHL
	GA1 c	(8)	516	(8)	567					1.8	443	4.4	501			

Table 7.2 (continued)

- $P_{GMPB}$  = pressure from gnt-mus-bio-pla barometer  
 $P_{GASP}$  = pressure from gnt-kya-qtz-pla barometer  
 $P_{MABK}$  = pressure from mus-gnt-bio-kya barometer  
 all barometer calibrations from Hodges and Crowley (1985)
- $T_{FS}$  = temperature from gnt-bio thermometer, Ferry and Spear (1978)  
 $T_{HC}$  = temperature from gnt-bio thermometer, Hodges and Crowley (1985)
- 1 GA# indicates a garnet in a thin section  
 r = rim analysis, c = core analysis, i = inclusion in garnet
- 2 Pressures and temperatures were obtained by simultaneous solution of the GMPB barometer + FS thermometer (third and fourth column) and the GMPB barometer + HC thermometer (fifth and sixth column) respectively. Pressures and temperatures in b are calculated the same way using the GASP and MABK barometers.  
 Pressures in brackets are assumed for temperature calculation in those samples for which no pressure could be determined.
- 3 The P-T vector indicates whether P and T increase or decrease from core to rim:  
 C=R no significant change  
 C<R increase in P & T  
 C<R small/insignificant increase in P & T  
 C>R decrease in P & T  
 C>R small/insignificant decrease in P & T
- 4 A = amphibole, B = biotite, C = chlorite, cc = calcite, E = epidote, g = graphite, G = garnet, K = kyanite, M = muscovite, Mc = microcline, P = plagioclase, Si = Sillimanite, St = staurolite, To = tourmaline  
 All assemblages include quartz. Minerals in brackets are not in equilibrium.
- 5 abbreviations indicate approximate locations of sample outcrops as in the following list:
- |                               |  |
|-------------------------------|--|
| BH = Blueberry Hill           | NFL = North end of Flora Lake            |
| CAL = Carol Lake thrust sheet | OB = O'Brien Lake                        |
| DOL = Dolomite quarry         | RAF = Riviere aux Fraises                |
| EFL = east of Flora Lake      | SFL = South end of Flora Lake            |
| EL = Emma Lake                | SKI = Ski hill, Labrador City            |
| GB = Goethite Bay area        | SL = Seahorse Lake                       |
| JP = Julienne Peninsula       | WAB = Wabush town and surroundings       |
| MB = Mont Bondurant           | WL = islands in south end of Wabush Lake |
| MHL = Moose Head Lake         |  |
- These locations are indicated in Fig. 1.1.
- 6  $P_m$  = Mean rim pressure using GMPB and GASP barometer  
 $T_m$  = Mean rim temperature using FS thermometer  
 $\pm$  one standard deviation
- 7 no average P and T calculated for the northern sub-area, see text.

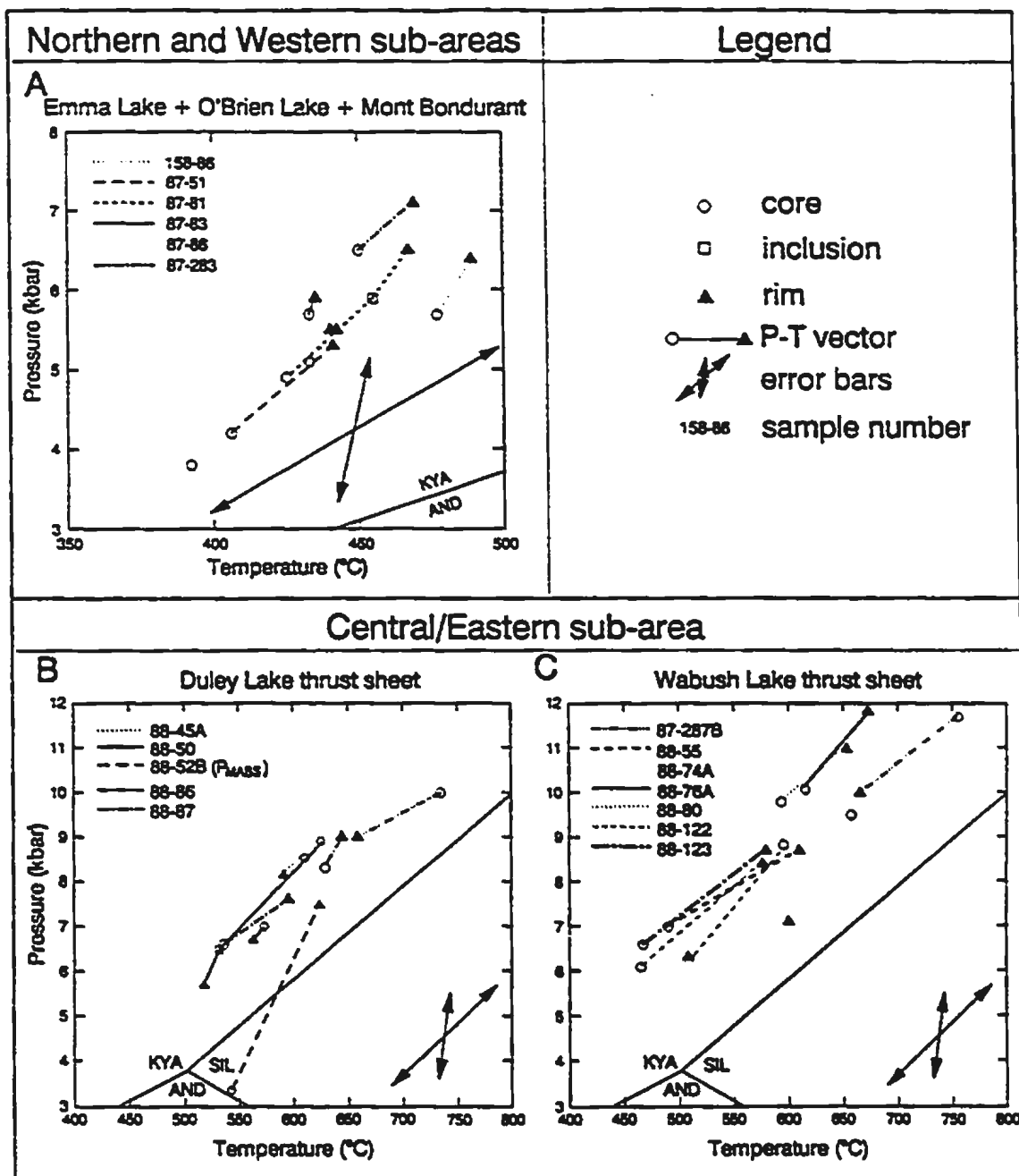


Fig. 7.7 P-T vectors from garnet core and rim analyses, combined with matrix minerals, for several parts of the map area. a) Northern and Western sub-areas, Elmer Lake thrust sheet near Mont Bondurant, O'Brien Lake thrust sheet and Carol Lake thrust sheet; b) Duley Lake thrust sheet in the central/eastern sub-area; c) Wabush Lake thrust sheet in the central/eastern sub-area. Note the difference in scale between a) and the other diagrams. Aluminum silicate stability fields from Holdaway (1971).

contained the right mineral assemblage for both thermometry and barometry. From these profiles a P-T path was determined using the method described in the previous section. The results are plotted in P-T diagrams in Figure 7.8.

### 7.3.5.1 Comparison of thermometers and barometers

For the western and northern sub-areas (Table 7.2.a) temperatures were estimated using the Grt-Bt thermometers from Ferry and Spear (1978) ( $T_{FS}$ ) and Hodges and Crowley (1985) ( $T_{HC}$ ) combined with pressure estimates from the Grt-Ms-Pl-Bt barometer from Hodges and Crowley (1985) ( $P_{GMPB}$ ). In some samples plagioclase was not present or was too sodic to be used for pressure calculation (plagioclase compositions of  $X_{Ca} \leq 0.2$  result in over-estimation of the pressure, Hodges and Crowley, 1985). In these cases a pressure of 6 kbar was used in the temperature calculation, which is approximately the average maximum pressure calculated for the area.

Results from the central/eastern sub-area are shown in Table 7.2.b, separated for each thrust sheet. Since in this part of the map area the pelitic mineral assemblages in some outcrops include alumino-silicates, two additional barometers could be used: the Grt-Ky-Pl-Qtz barometer ( $P_{GASP}$ ) and the Ms-Grt-Bt-Ky barometer ( $P_{MABK}$ ), both calibrated by Hodges and Crowley (1985). All barometers were again combined with both thermometers ( $T_{FS}$  and  $T_{HC}$ ) for comparison. In assemblages which lacked a barometer a pressure of 8 kbar was substituted, which is approximately the average pressure for the area, calculated using garnet rim compositions.

A comparison of the temperatures from the two thermometers shows that  $T_{HC}$  is systematically higher than  $T_{FS}$ . The difference ( $\Delta T = T_{HC} - T_{FS}$ ) ranges for individual samples from 6°C to 125°C. Calculated for the separate sub-areas the average  $\Delta T$  is  $57 \pm 22^\circ\text{C}$  for the northern area,  $69 \pm 12^\circ\text{C}$  for the western area and  $57 \pm 30^\circ\text{C}$  for the central/eastern area. Besides the differences in temperature, the pressures calculated in simultaneous solution with  $T_{HC}$  are 1 to 2 kbar higher than the ones calculated using  $T_{FS}$ , due to the positive slope of the barometer curves in P-T space. The slope of both barometers is in the order of 1 kbar/50°C.

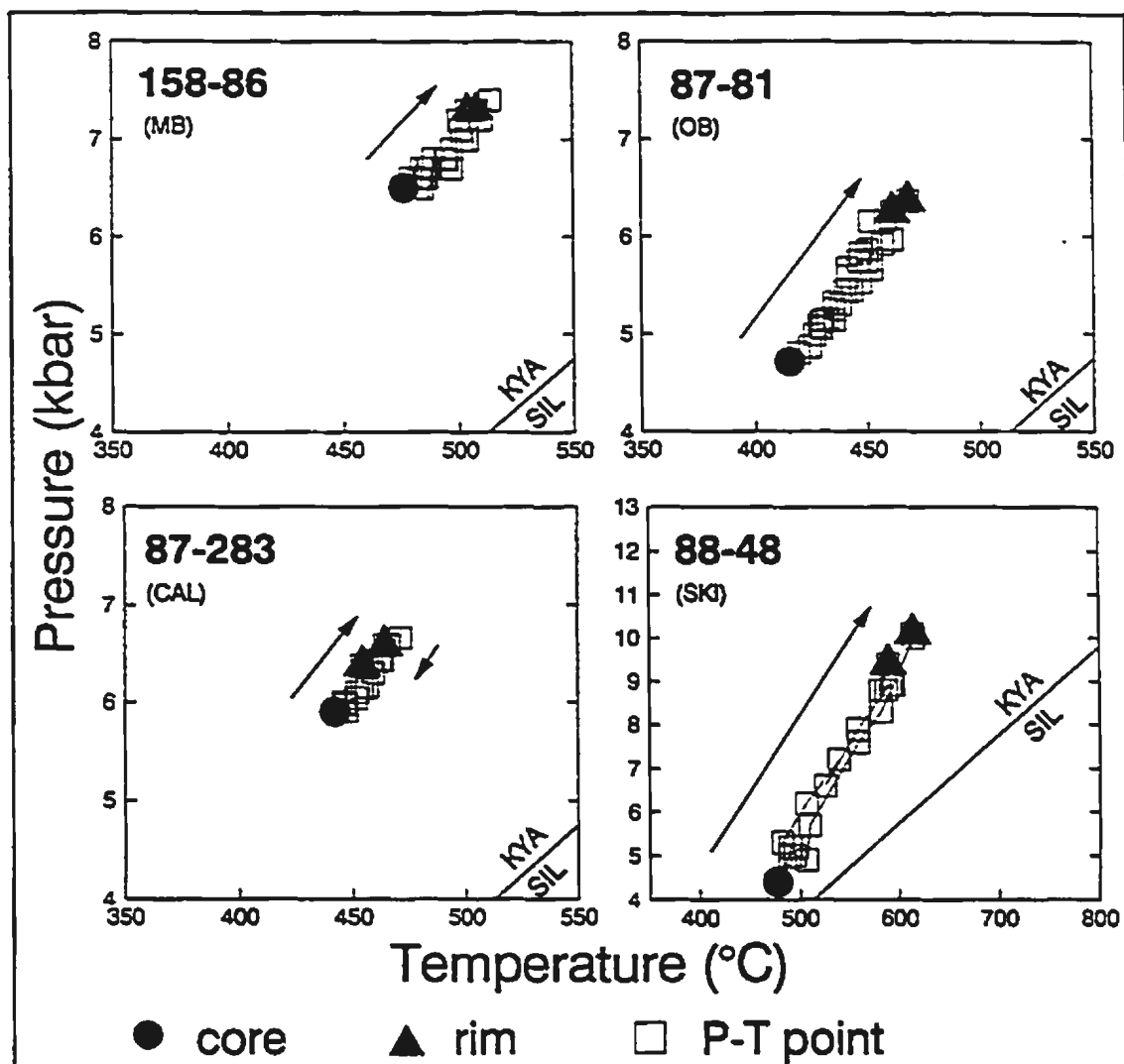


Fig. 7.8 P-T paths constructed using chemical profiles through garnets in combination with matrix minerals. Each diagram consists of a double path: from the core of a garnet to the two rims. The sizes of the squares or the presence of a connecting line have no significance and variations are for clarity of the diagrams. Note that the scale and extent of the axes in the first three diagrams are different from the remainder. P and T are calculated using  $P_{\text{OMPb}}$  and  $T_{\text{FS}}$  with the exception of sample 88-48 for which  $P_{\text{MABX}}$  was used. The arrows emphasize the prograde and retrograde paths. The acronyms underneath the sample numbers indicate the sample locations and are explained in Table 7.2. Sample locations are indicated in Fig. F.3 (Appendix F). Aluminum silicate stability fields from Holdaway (1971). continued on the next page.

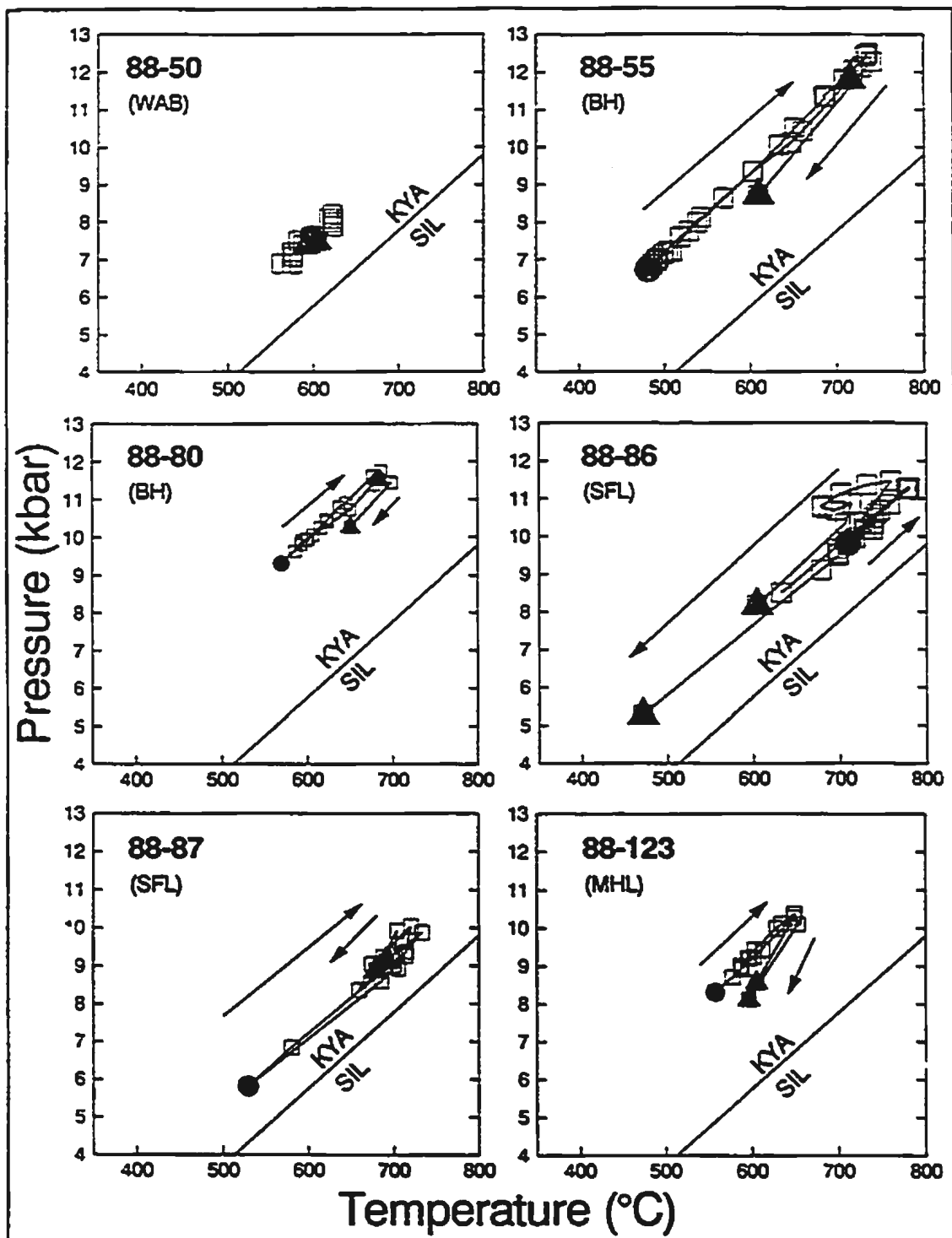


Fig. 7.8 Continued

Both temperatures and pressures calculated using  $T_{HC}$  are unrealistically high. For instance, in some samples from the Emma Lake/O'Brien Lake area, estimates of  $T_{HC}$  would imply metamorphic temperatures that are usually found in the amphibolite facies, which is inconsistent with the observed greenschist facies mineral assemblages. The same inconsistency between P-T estimates using  $T_{HC}$  and mineral assemblages were also found in the higher thrust sheets. For this reason only the Ferry and Spear (1978) Grt-Bt thermometer was used for data presentation in figures 7.6 to 7.8 and their interpretation.

Pressures calculated with the GMPB and GASP barometers are nearly identical and the difference is in most samples less than 0.2 kbar. Many of the samples in the central/eastern area contain the Grt-Ms-Pl-Bt assemblage for which the GMPB barometer could be used and the GASP barometer was only required for sample 88-50, in which one of the garnets was not accompanied by stable muscovite. The low precision of the MABK barometer, as indicated by Hodges and Crowley (1985), is demonstrated in a comparison with the two other barometers. It considerably underestimates the pressure, in most cases up to 2 or 3 kbar for rim pressures. Core pressures are even further removed from the values of the other two barometers, which results for sample 88-85 even in negative pressures (Table 7.2.b). In terms of the orientations of the P-T vectors, however, the results are consistent with the GMPB and GASP barometers, so it can be used for this purpose (Fig. 7.7, sample 88-52B; Fig. 7.8, sample 88-48).

For data presentation and interpretation the results from the GMPB barometer were used, combined with  $T_{FS}$ , except for those samples in which this assemblage was not present. The accuracy assumed for  $P_{GMPB}$  and  $P_{GASP}$  is within 1 kbar, for the thermometer within 50°C. Considering the accuracy of approximately 1% of the mineral analyses (Appendix G), these error estimates are reasonable, as was shown by Hodges and Crowley (1985). P-T vectors and paths plotted in figures 7.7 and 7.8 show that the differences in P and T between cores and rims often fall within the error bars. This does not mean that the vector is not significant. The size of the error bars depends

to a large extent on the uncertainties in the thermodynamic data used for calibration of the thermometers and barometers. The error in the chemical analysis contributes only a small part of the error for the pressure and temperature calculations (McKenna and Hodges, 1988). Since the same calibration is used for both end points in the P-T vectors and the variations in chemical composition within single garnets are minor, their relative positions are correct within the error of the microprobe analysis and the errors in the assumptions mentioned in Section 7.3.4. Although the absolute positions of the vectors in P-T space can change up to the amount shown by the error bars, their end points will tend to change in the same manner, thus the orientation of the P-T vector will remain valid with respect to increases and decreases of P and T.

### 7.3.5.2 Results for the northern sub-area

The results from the northern area (Table 7.2.a) are from widely separated sample locations (Fig. 7.6), covering several thrust sheets. Calculation of an average P and T is not meaningful because it would combine information from different metamorphic and structural levels.

The samples from around Mont Bondurant and Goethite Bay are from near the roof thrust of the Elmer Lake thrust sheet. The Julienne Lake fault zone separates two areas of slightly different temperatures, with the one to the north showing the lower temperatures (with exception of sample 87-255, which seems to give an unrealistically high temperature). Sample 87-198 is located in a slice of basement rocks which moved from the footwall of the Goethite Bay floor thrust into the level of the overlying thrust sheet by out of sequence thrusting. This temperature represents the lower grade Elmer Lake thrust sheet rather than the overlying Goethite Bay thrust sheet, of which mineral assemblages indicate a significantly higher metamorphic grade ( $T > 500^{\circ}\text{C}$ ).

The P-T vector and P-T path from sample 158-86 (Fig. 7.7a and 7.8) shows growth of the garnet with increasing P and T, which is consistent with the growth zoning profile (Fig. F.2, Appendix F). Garnet 2 in sample 87-117 is a large aggregate of grains which are fragments of one larger disintegrated grain, some with new overgrowths. The core (c1) and rim of one fragment show a retrograde vector, but

analyses from the core (c2) of another fragment show a significantly lower P and T than the previous two (Table 7.2). This inconsistency could be an effect of a complicated history of different ages of garnet, for which the chemical profile from sample 87-120 (from a nearby outcrop) provides indications (Section 7.2.1.5). In general, the P-T paths for garnets from the northern part of the area are interpreted to be prograde (increasing P and T), with retrogression mainly in the high strain rocks.

### 7.3.5.3 Results for the western area

The average P and T calculated from garnet rim compositions from the western sub-area are (Table 7.2.a): for the Emma Lake and O'Brien Lake areas  $T = 450 \pm 14^\circ\text{C}$ ,  $P = 5.7 \pm 0.4$  kbar; for the two samples from the Carol Lake thrust sheet  $T = 519 \pm 51^\circ\text{C}$  and only one pressure estimate of 7.1 kbar. This is in good agreement with results from the Emma Lake area presented by Brown (1988; see also Brown et al., 1991). All samples suggest garnet growth under increasing P and T, with the exception of sample 87-94, which is a strongly poikiloblastic grain which either may not have grown radially or has grown late in the evolution during the retrograde part of the metamorphic event (cf. microstructure of similar garnet 88-93 in Plate 6.21).

The P-T vectors and P-T paths for the western sub-area are plotted in figures 7.7.a and 7.8 respectively. Figure 7.7.a shows that the P-T vectors consistently show a prograde P-T path for the area, with both P and T increasing, which is in agreement with the prograde zoning profiles in the garnets of the area (Fig. 7.5.a, Section 7.2.1). The P-T path derived from the garnet profile of sample 87-81 from the O'Brien Lake area (Fig. 7.8) is consistent with the P-T vectors. This observation combined with the lack of retrograde zoning in all but one of the garnets of the Emma Lake and O'Brien Lake areas suggests that the P-T conditions obtained from garnet rims represent a metamorphic peak. The data from the Carol Lake thrust sheet (Fig. 7.7.a and Fig. 7.8, sample 87-283) indicate a mainly prograde P-T path with slight retrograde diffusion at the garnet rim. The peak metamorphic grade is somewhat higher than in the structurally lower Emma Lake thrust stack, although the difference is not statistically significant because of the small number of data.

#### 7.3.5.4 Results for the central/eastern area

In Table 7.2.b the results from the central/eastern sub-area have been subdivided for the three major thrust sheets: the Lorraine Lake, Duley Lake and Wabush Lake thrust sheets. For the Lorraine Lake thrust sheet only one data point is available (566°C). The average garnet rim temperature and pressure for the Duley Lake thrust sheet (samples from near Labrador city and Wabush) is  $595 \pm 48^\circ\text{C}$  and  $7.7 \pm 1.2$  kbar; for the Wabush Lake thrust sheet:  $624 \pm 52^\circ\text{C}$  and  $9.0 \pm 1.7$  kbar. These results show a minor increase in pressure and temperature from west to east. Garnet rim pressures and temperatures plotted in a map (Fig. 7.6) do not show a consistent trend.

P-T vectors have been plotted for the two thrust sheets in lithotectonic domain V in Figure 7.7.b and c. The vectors in these plots are not as consistent as in the lower grade western area. In the case of sample 88-122 two garnets in one thin section give two opposite vectors (Fig. 7.7.c). Two vectors for sample 88-87 (Fig. 7.7.b) cover two different parts of P-T space, but both show an increase in P and T. The P-T vector for sample 88-52B (Fig. 7.7.b) has steeper slope than the remainder of the vectors, starting in the sillimanite field. However, no evidence for sillimanite growth has been found in the sample. The pressures for the sample were calculated using the MABK barometer and are probably too low, especially for the core, resulting in a vector that is too steep. The prograde orientation of the vector is still valid.

In spite of inconsistency and opposite orientations of the P-T vectors in the area, they occupy a narrow zone in P-T space. The vectors from the Wabush Lake thrust sheet indicate slightly higher pressures and define a zone that is slightly further removed from the kyanite-sillimanite reaction boundary than the vectors from the Duley Lake thrust sheet. Assuming that opposite vectors represent prograde and retrograde parts of a P-T path, the P-T loop for the metamorphic development must be very tight.

The P-T paths plotted in Figure 7.8 give a better impression of the P-T evolution of the rocks in the area. Of these P-T paths the one for sample 88-48 from the Lorraine Lake thrust sheet has been calculated using the MABK barometer and is too steep. All others have been calculated using the GMPB barometer and can be

subdivided in two groups, which (maybe coincidentally) represent the two thrust sheets in the southeast of the area: garnets with a retrograde chemical profile in the Duley Lake thrust sheets (88-50, 88-86 and 88-87) and garnets with a growth zoning profile and retrograde rims in the Wabush Lake thrust sheet (88-55, 88-80 and 88-123). The first group has been homogenized at peak metamorphic conditions at around 10 to 11 kbar and 700 to 800°C with retrogression of the garnet rims. Only sample 88-87 of the first group shows a partial prograde path, which may be related to biotite inclusions close to the analysis points in the center of the grain. The chemical profile (Appendix F, Fig. F.2) shows a constant (homogenized) composition for most of the interior of the garnet. The second group shows both the prograde and retrograde parts of the P-T path, confirming the observation made from the P-T vectors that the P-T loop is, indeed, very tight. Unfortunately the retrograde part of the path is not well constrained. The retrograde rims are between 50 and 200 microns wide and with the spacing of analysis points used in this study they are undersampled. The metamorphic peak recorded by this second group of garnets is approximately 10.5 to 12.5 kbar and 650 to 750°C.

Both the P-T vectors and the P-T paths show that the prograde and retrograde paths from the Wabush Lake thrust sheet lie at slightly higher pressures than the paths from the Duley Lake thrust sheet. This may be an indication of slightly different thermal and tectonic histories of the two thrust sheets. This confirms the interpretation of Chapters 4 and 5 that the Flora Lake shear zone, which separates the two thrust sheets, and which also separates Gagnon terrane from Molson Lake terrane in the southeastern part of the map, is a significant tectonic break.

### **7.3.6 INTERPRETATION AND DISCUSSION OF THE GEOTHERMOBAROMETRY RESULTS**

In the northern sub-area the density of sample points is too low and the variation in results too large for a detailed interpretation of the results. In the Mont Bondurant-Goethite Bay area mineral assemblages from the Goethite Bay thrust sheet suggest that the peak metamorphic grade was well into the amphibolite facies after

which the rocks were affected by a retrograde metamorphism, which is indicated by the replacement of staurolite by chloritoid. In the Elmer Lake thrust sheet results from thermometric analyses on rocks from the footwall of the Sokoman Duplex floor thrust indicate a peak temperature of approximately 500°C, which is the lower limit of the amphibolite facies. The estimated temperature for a garnet-biotite pair from the Sokoman Duplex is significantly higher (618°C), confirming the conclusion based on mineral assemblages that the thrust fault between Elmer Lake and Carol Lake thrust sheets in the footwall and Goethite Bay and Lorraine Lake thrust sheets in the hanging wall forms a significant metamorphic break (Section 7.1.3).

In the western sub-area, the results for the Emma Lake/O'Brien Lake area consistently indicate growth of the garnets under increasing pressure and temperature conditions as summarized in Figure 7.9. The peak metamorphic conditions recorded by the garnet rims are approximately 6 kbar and 450°C. The P-T path is fairly steep, which is in agreement with the thermal model for thrust belts of Davy and Gillet (1986), which suggests a low geothermal gradient with relatively high pressures for a stack of thin thrust sheets. No information is available about the retrograde part of the P-T path. For the Carol Lake thrust sheet only a small number of data is available, but the tectonic and thermal development is interpreted to be similar to that of the Emma Lake thrust sheet, with only slightly higher metamorphic grade.

The variation of the P-T vectors and the wide range of calculated rim temperatures in the central/eastern area may have several causes. In the first place the area from which these samples are taken is quite large and incorporates a range of metamorphic conditions and structural settings. On the other hand, apparently conflicting results from within a single thin section (e.g. sample 88-122) indicate that other factors play a role as well. The small scale, non-systematic variations are caused by the method of analysis, local disequilibrium, domainal equilibrium and diffusion processes, and do not reflect real differences in metamorphic history of the rocks. Both aspects are discussed below.

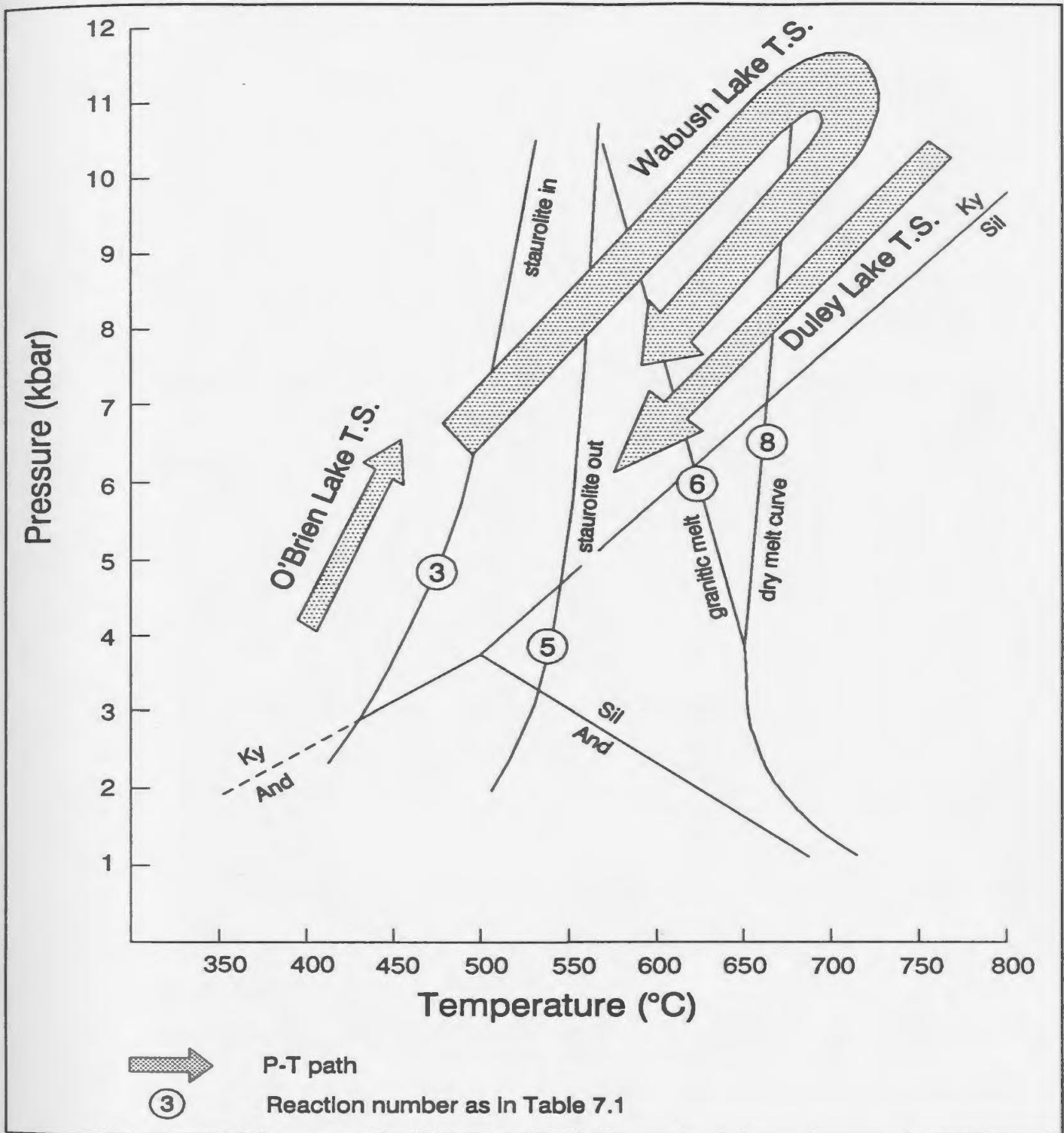


Fig. 7.9 Summary of P-T paths in different parts of the area. In the western sub-area, represented by the P-T path from the O'Brien Lake thrust sheet, only the prograde path is preserved. In the Wabush Lake thrust sheet in the central/eastern sub-area both the prograde and retrograde path are preserved. In the Duley Lake thrust sheet retrograde P-T paths and vectors are dominant. Reaction curves are from Rivers (1983b).

### 7.3.6.1 Non-systematic variations in P-T determinations

Non-systematic variations in estimated metamorphic conditions have been recorded in many geothermobarometric studies. Hodges and Royden (1984) indicated that a suite of samples that was affected by the same conditions, showed a wide range of rim pressures and temperatures. This was interpreted as a result of equilibria frozen in at different times during retrogression, which together defined a retrograde P-T trajectory (cf. Tracy et al., 1976; Indares and Martignole, 1985a; Mengel and Rivers, 1989). The effect of incomplete re-equilibration of a garnet rim with respect to matrix biotites was shown by Duebendorfer and Frost (1988) to be the cause of a wide range of temperatures calculated from one single garnet. Garnets in contact with biotite grains show local halos of chemical zoning around the biotite, in which areas diffusion continued longer and to lower temperatures than in other parts of the rim (Tracy et al, 1976). This can also lead to differences in calculated rim temperatures from one sample.

Another factor which has a significant effect on the observed zoning patterns and the calculated P-T vectors is the location of the cut through the garnet (the "sphere effect", Indares and Martignole, 1985a). Figure 7.10.a shows how P-T vectors obtained from a hypothetical garnet, which has a growth zoned core and a retrograde zoned rim defining a P-T loop, can have a range of orientations. A tangential cut through the garnet rim will reveal only the last part of the P-T loop and only a cut through the core will incorporate the whole P-T history of the garnet. The effect of resorption on the P-T path determined from a radial cut through a garnet is shown in Figure 7.10.b. The P-T paths derived from the different cuts do not contain the complete retrograde history. The figure also shows a compositional halo around a biotite in contact with the garnet, where retrogression continued longer than in the remainder of the garnet. A cut through this halo will result in a P-T vector with an end point at lower P and T. If the two effects are combined, P-T vectors calculated from a garnet can link any two points on the P-T loop, resulting in a wide range of orientations of P-T vectors (Fig. 7.10.c). Since the P-T path for the Wabush Lake thrust sheet

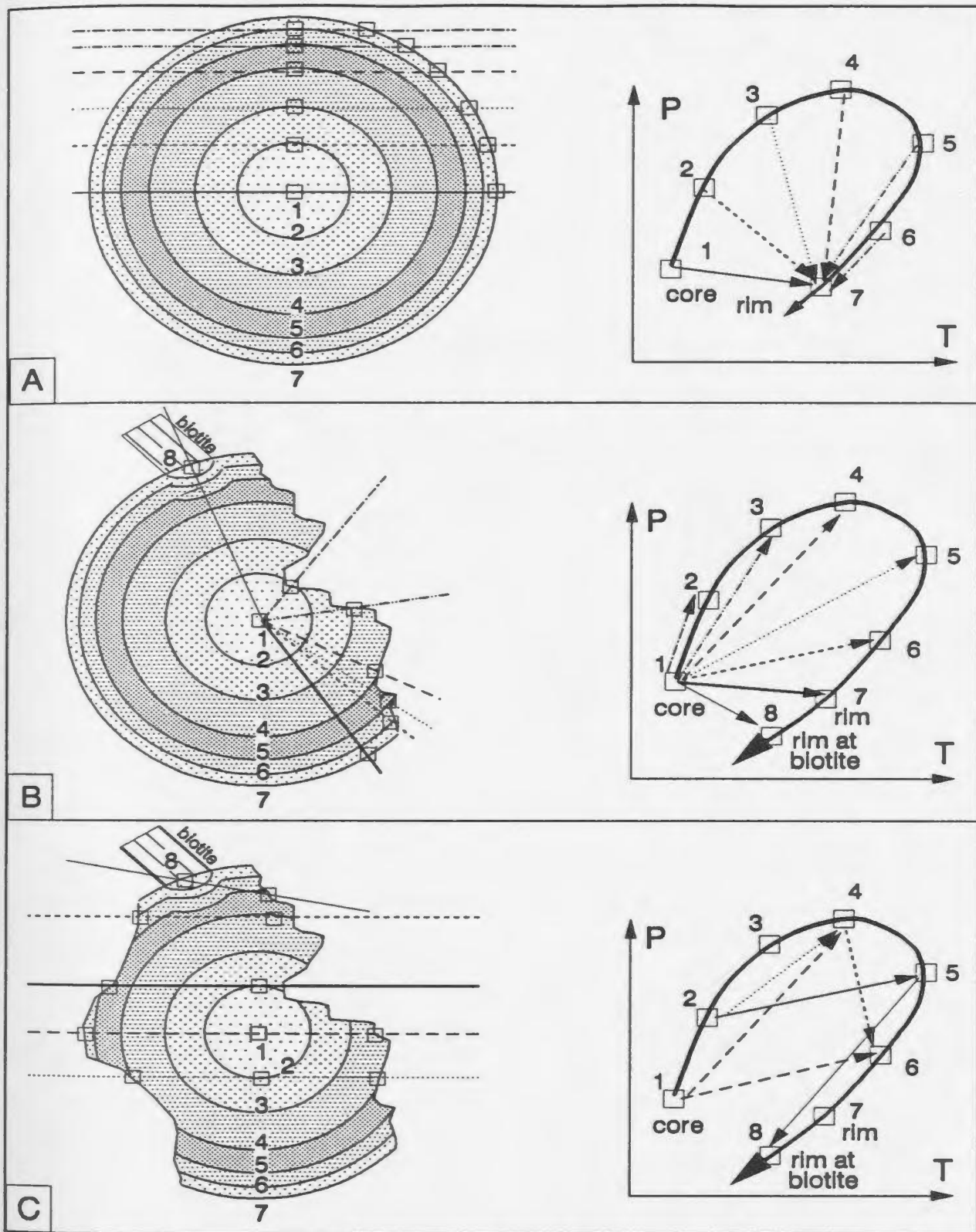


Fig. 7.10 Schematic illustration of the effect of the section plane and resorption on P-T vectors obtained from zoned garnets. Lines represent thin section cuts through a hypothetical, originally circular garnet with growth zoning in the central part and retrograde zoning near the rim. Higher densities of dot patterns indicate higher metamorphic grades. Numbers are P-T points in the P-T diagrams which coincide with circles (spheres) in the garnet. Squares indicate analysis points in the garnet. P-T vectors are constructed from core and rim analyses. A) effect of different (tangential) sections. B) effect of partial resorption on P-T vectors from different radial sections. C) combined effects of A and B.

forms a "hairpin" loop, cut and resorption effects in these garnets resulted in P-T vectors that are all virtually parallel, connecting two points on one line from lowest to highest P and T recorded by the garnets, but they can point either in a prograde or a retrograde orientation, depending on the locations of the cut and the profile through the garnet.

It is expected that all these factors influenced the calculation of P-T vectors and rim P-T points in the central/eastern area. Many of the analyzed garnets have subidioblastic crystal shapes as a result of partial resorption. In sample 88-98 (Fig. F.2, Appendix F) the asymmetry of the garnet chemical profile and the difference in composition of the opposite rims, a result of resorption, is obvious. Note also the difference in P-T points derived from two opposite rims in the P-T paths of samples 88-55, 88-80 and 88-86 (Fig. 7.8). The opposite orientations of the P-T vectors derived from sample 88-122 (Fig. 7.7) are probably caused by a combination of a tangential cut and resorption. These closely spaced, parallel prograde and retrograde vectors in this sample support the conclusion that the P-T loop was indeed very tight.

#### 7.3.6.2 Regional variations in metamorphic grade

In order to evaluate the regional variations in metamorphic development, these non-systematic variations in P-T estimates must be removed. A comparison of either peak metamorphic conditions or P-T paths in the area will give the most significant information. In growth-zoned garnets the peak metamorphic conditions were recorded in the rims which, during retrograde metamorphism, were destroyed by intergranular diffusion at the rims or by homogenization of the garnets as a result of increased intragranular diffusion rates. For the reconstruction of the P-T loops that represent the different thrust sheets, the assumption was made that those P-T paths that show the largest variations have been least affected by diffusional effects and give the closest approximation to the real variations in pressure and temperature (Muncill and Chamberlain, 1988; Jiang and Lasaga, 1990). The P-T paths estimated for different

parts of the area are shown in Figure 7.9. Figure 7.11 is a map of the variation of the peak metamorphic conditions through the southern part of the area.

The P-T path for the Wabush Lake thrust sheet is best documented in samples 88-55, 88-80 and 88-123 (Fig. 7.8), which show both prograde and retrograde paths. They indicate that close to the eastern boundary of Gagnon terrane the prograde part of the P-T path shows a fairly steep increase in pressure and temperature up to a maximum of approximately 700 to 750°C and 11 to 12 kbar (Fig. 7.9). The retrograde path closely follows the prograde path at slightly lower pressures. All P-T vectors from core-rim analyses outline parts of this loop and are consistent with these conclusions. The estimated P-T loop is also in agreement with the occurrence of kyanite as the stable aluminosilicate in the eastern part of the area.

In the Flora Lake shear zone, P-T vectors tend to be retrograde. High strain will tend to break down the larger garnet grains and some strain induced recrystallization may take place. The garnets in the shear zone are significantly smaller than those in the remainder of the area and therefore will be homogenized more easily (Lasaga, 1983). In the Flora Lake shear zone deformation continued after the peak of metamorphism and may have enhanced retrograde reactions at the garnet rims, thus promoting the retrograde diffusional zoning.

In the Duley Lake thrust sheet retrograde P-T paths and vectors seem to be dominant, but prograde vectors also occur. The maximum P and T, which are recorded at the southern end of Flora Lake, are similar to those of the Wabush Lake thrust sheet, but at somewhat lower pressures: 700 to 800°C and 10 to 11 kbar. Towards the northwest pressures and temperatures decrease somewhat (Fig. 7.11). Around Wabush and Labrador City the metamorphic peak is estimated at 600 to 650°C and 8 to 9 kbar indicating a fairly steep metamorphic field gradient.

Data from the Lorraine Lake thrust sheet farther west are from just one outcrop at the Ski Hill north of Labrador City, which indicates a peak temperature of slightly below 600°C. The pressure from this outcrop, 9.3 kbar, was estimated using  $P_{\text{MAX}}$  and is assumed to be too high. The mineral assemblage in this outcrop contains kyanite

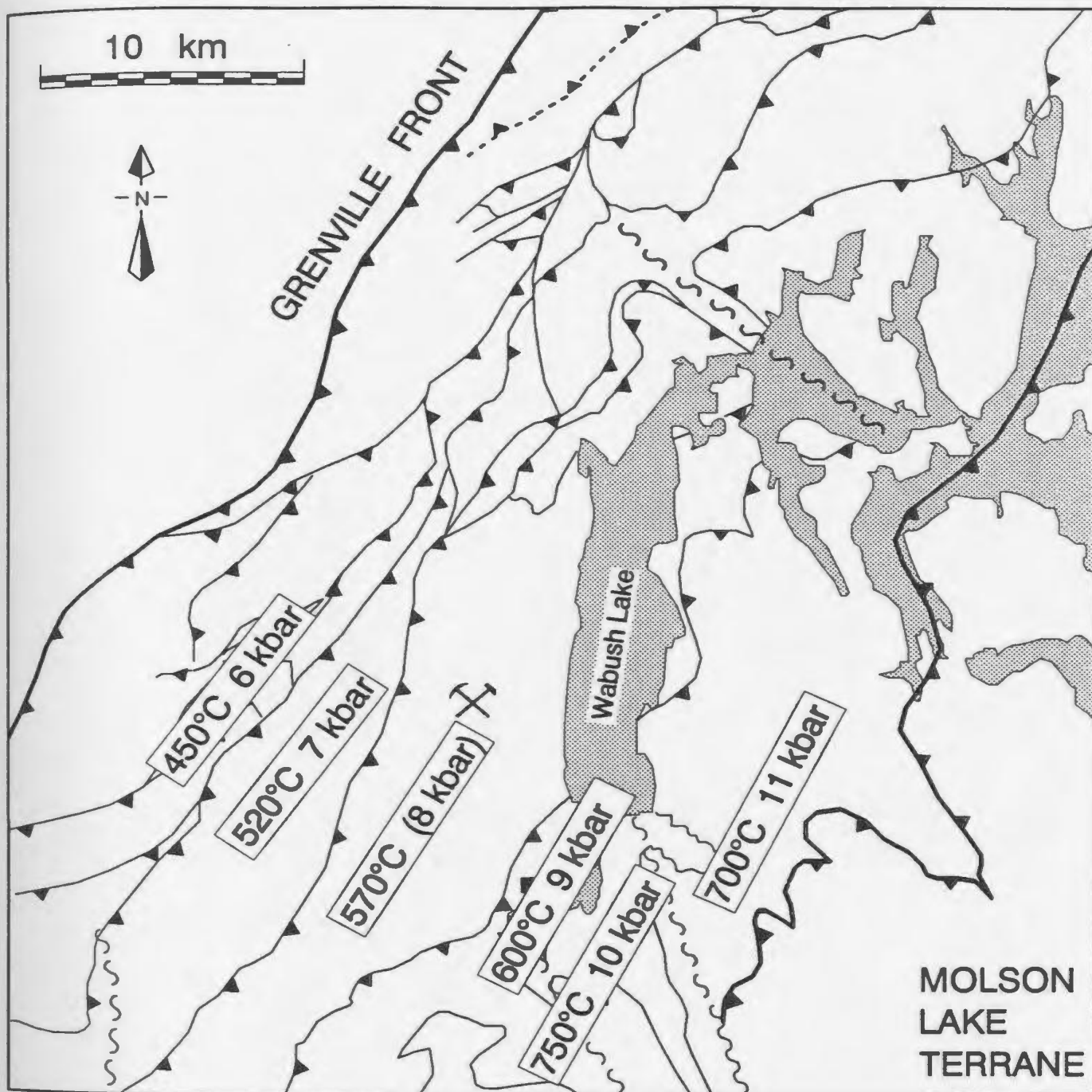


Fig. 7.11 Estimated peak metamorphic pressures and temperatures, determined from thermobarometry on zoned garnets, in the southern part of the map area. The presented pressures and temperatures are conservative averages of the peak conditions shown in Fig. 8.

overgrown and replaced by sillimanite, indicating that the P-T path for the anticline in this part of the area must have reached into the sillimanite stability field as a result of rapid uplift with minor cooling. This is, however, the only recorded occurrence of sillimanite in the map area and the results for this one outcrop are not expected to be representative for the whole thrust sheet.

The trend of decreasing peak metamorphic grade continues towards the northwest to the Emma Lake/O'Brien Lake area where the peak P-T estimates are 450°C and 6 kbar. The prograde P-T path in this western part of the area is somewhat steeper than in the east. This may either indicate faster burial with less time for the isotherms to relax, or it may be an effect of the stacking of thin thrust sheets, which results in lower temperatures for a given amount of thickening than is the case for a smaller number of thicker thrust sheets representing the same increase in thickness (Davy and Gillet, 1986). It should be noted that the difference in peak metamorphic grade between the Carol Lake thrust sheet and the Emma Lake thrust stack is larger, over a shorter distance, than the difference in the peak P and T between the Carol Lake and Lorraine Lake thrust sheets. This may suggest that the floor thrust of the Carol Lake thrust sheet forms a break in the metamorphic field gradient in the same manner as the floor thrust of the Lorraine Lake thrust sheet.

#### 7.4 DISCUSSION AND CONCLUSIONS

Although all the data are consistent with the thermal history described above, there is an unresolved problem. Chemical profiles through garnets from the eastern part of the area show that some seem to have been homogenized, whereas others have preserved the growth zoning pattern to some extent. Most of the prograde-zoned garnets are found in the Wabush Lake thrust sheet and the majority of the garnets with retrograde zoning are from the Duley Lake thrust sheet, but both types of garnet appear in both thrust sheets, often in close proximity.

Preservation of growth zoning profiles in garnets which have been heated up to approximately 750°C indicates that, in spite of the increased diffusion rates at these temperatures, the garnets have not had enough time to homogenize. This is likely a

result of fast cooling rates after the metamorphic peak, induced by rapid uplift and erosion. In contrast, in some parts of the upper thrust sheets the rocks seem to have cooled more slowly and increased diffusion rates prevailed long enough to homogenize the garnets.

Tectonic movements also have an influence on the cooling rates of the rocks, and therefore on the homogenization of the garnets. Rocks in hanging walls of thrusts or in cores of antiforms are uplifted faster than in footwalls of thrusts and in synforms and relaxation of the distorted isotherms in the former structures will result in increased cooling rates (Chamberlain and Karabinos, 1987; Muncill and Chamberlain, 1988). This phenomenon could have played a role in the faster cooling of the rocks in the Wabush Lake thrust sheet. Geometric analysis of the thrust sheets in Chapter 5 suggested that the displacement on the Wabush Lake floor thrust is significantly larger than on the Duley Lake floor thrust (see cross sections in Figure 1B, in pocket), which may have given the Wabush Lake thrust sheet an increased cooling rate in comparison to the Duley Lake thrust sheet. No other relationships between homogenization of garnets and structural setting have been observed.

Another factor may also contribute to the variations in garnet zoning patterns on a small scale. The presence of small intrusive bodies, like those found north of Moose Head Lake, could cause significant disturbances in the thermal pattern of the rocks. Unexposed plutons could have locally retarded the cooling in the rocks of both thrust sheets and in this way increased the homogenization effects locally. However, these plutons may not be of Grenvillian age and their role in the variations of the garnet profiles is uncertain.

Possibly the absence of a prograde zoning pattern does not reflect homogenization of the garnets. The garnets that lack prograde zoning may have been cut through their rims, incorporating only the retrograde part of a complete zoning pattern (Fig. 7.10.a). However, the analyzed garnets were carefully selected to avoid this problem and it is not expected that many of the analyzed garnets show such dramatic cut effects. Another plausible explanation is related to the bulk composition of the rocks. Garnets

that grew rapidly, late in the prograde path would not have a prograde zoning pattern. The fact that most of the garnets with retrograde P-T vectors are found in rocks containing kyanite (assemblage Qtz-Bt-Ms-Grt-Pl-Ky) may suggest that these garnets were produced by the staurolite-breakdown reaction



which occurs at temperatures far above the first occurrence of garnet, close to the peak pressures and temperatures. In this way, the early prograde part of the P-T path may have been omitted in these garnets. The partial prograde paths in the cores of garnets 88-86 and 88-87, which have an otherwise flat profile, favours this explanation, rather than an incomplete homogenization of the garnets.

A comparison of the P-T data from geothermobarometry and the mineral assemblage zoning as presented in section 7.1 shows that the calculated pressures and temperatures diverge somewhat from those indicated in the petrogenetic grid (Fig. 7.3), but the two are not incompatible. Calculated pressure and temperature near the garnet isograd at O'Brien Lake are approximately 6 kbar and 450°C, which is only slightly above reaction curve [R1] in the petrogenetic grid. In the field this isograd is remote from the Emma Lake area (Fig. 7.1). It seems likely that the estimated temperatures for [R1] are too high. The calculated temperature in the Carol Lake thrust sheet seems slightly too high with respect to the staurolite-in isograd [R3]. The location of the staurolite breakdown reaction [R5] in the P-T grid fits well with the estimated temperature of 570°C at the Ski Hill. The temperatures of the rocks near the melt isograd are 600-650°C, whereas the P-T grid indicates that melting could take place at  $\pm 580^\circ\text{C}$  in a water saturated system. The highest calculated temperatures, from near Molson Lake terrane, range up to 750°C, but melt reaction [R8] has not taken place in these rocks. The melt curves [R6], [R7] and [R8] should be moved up at least 50°C, if the thermobarometry results are correct. This suggests that the  $a_{\text{H}_2\text{O}}$  in the fluid and the  $a_{\text{Ab}}$  in plagioclase in the high grade metamorphic zones were significantly lower than 1.

The estimated peak metamorphic conditions in the eastern part of the map area attest to a medium to high pressure metamorphic event, which is best explained by a rapid loading of the crust. The metamorphic grades lie in between the classical Barrovian type facies series and the eclogite facies conditions. These conditions are rather uncommon in most orogens, but seem to be characteristic of the Grenvillian Parautochthonous Belt (Wynne-Edwards, 1972; Indares and Martignole, 1985a, 1990a; Rivers et al., 1989).

The metamorphic grade increases from the structurally lowest to the highest thrust sheets, resulting in a regionally inverted metamorphic gradient, which is characteristic for thrust belts. A jump in metamorphic grade is inferred across the floor thrusts of the Goethite Bay and Lorraine Lake thrust sheets, and possibly across some of the higher thrust faults as well. Inverted metamorphic gradients are generally explained by the emplacement of thrust sheets of a relatively high metamorphic grade on top of lower grade rocks (e.g. Jamieson, 1986; Crowley, 1988; Karabinos and Ketcham, 1988; Rice et al., 1989; Chamberlain et al., 1989; Treloar et al., 1989). This is consistent with the rule that thrust faults place rocks from a deeper level on top of rocks from a higher level. If thrusting is of the same age as the metamorphism, this would create an unstable thermal situation which is not likely to be preserved (e.g. Crowley, 1988). In Chapter 8 the creation and preservation of inverted metamorphic gradients is discussed in detail.

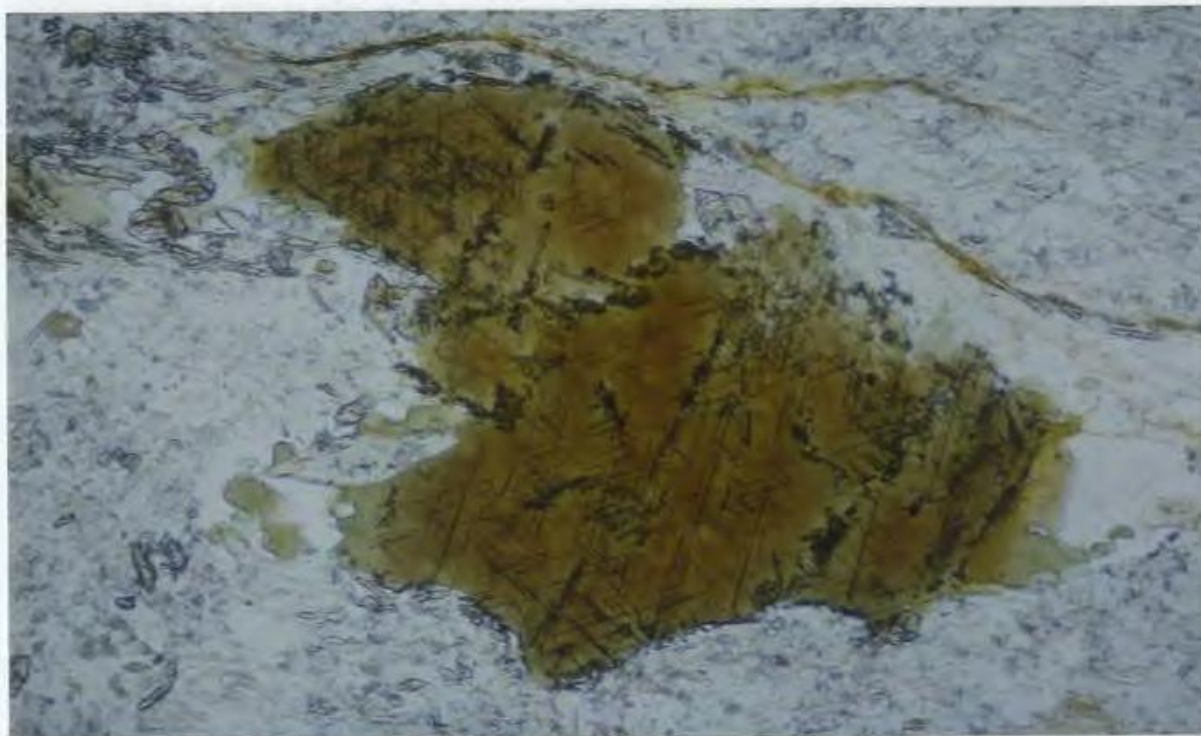
The hairpin shape of the P-T path indicates that when the peak of metamorphism was reached, cooling and decompression followed immediately, without any time for thermal relaxation between the prograde and retrograde part of the paths. This suggests that at some time after a period of prograde metamorphism, the system switched rapidly to retrograde metamorphism. Prograde metamorphism at any location is inferred to take place when the volume of rock in question is in the footwall of a moving thrust wedge, before its incorporation into the wedge. It achieves its maximum pressure and temperature as a result of tectonic burial underneath the overthrusting wedge. After incorporation into the advancing thrust wedge, the rock volume is progressively

exhumed. Thus, the onset of thrust activity in the floor of the Wabush Lake and Duley Lake thrust sheets is interpreted to terminate progressive metamorphism and the thrust activity caused cooling and uplift of the rocks during retrograde metamorphism. Stacking of thrust sheets caused thickening of the crust resulting in an increase in erosion above the locus of the thickening, indicated by the decompressive nature of the retrograde P-T paths. Numerical models of the thermal evolution of thrust belts have shown that increased cooling is expected in the hanging wall of major thrust faults (Davy and Gillet, 1986; Chamberlain and Karabinos, 1987; Shi and Wang, 1987; Karabinos and Ketcham, 1988). As mentioned above, the relaxation of distorted isotherms in the hanging wall of a thrust fault will enhance cooling rates. Emplacement of the rocks of the Wabush Lake thrust sheet on top of cooler metasediments in the lower thrust sheets possibly provided an extra cooling mechanism. The sediments in the footwall experienced prograde metamorphism as a result of the emplacement of warmer rocks on top.

This geothermobarometry study has shown that the use of P-T vectors obtained from garnet core and rim analyses can lead to spurious results when used for growth zoned garnet with retrograde rims. For these garnets only chemical profiles should be used for the reconstruction of the P-T path, which give a more complete history of variations of pressure and temperature during garnet growth and retrogression. Ideally a compositional map of the garnet should be used for the determination of the best profile line through the garnet (e.g. Duebendorfer and Frost, 1988; Tucillo et al., 1990; Spear et al., 1990). Similarly, plotting of P-T conditions obtained from retrograde garnet rims and matrix minerals on a map (Fig. 7.6) does not give significant information. It will lead to the comparison of different points on the P-T paths for different parts of the area. On a map only the use of peak metamorphic conditions can be meaningful (Fig. 7.11).

An interpretation of the P-T data obtained by thermobarometry results in the following picture for the metamorphic development of Gagnon terrane in southeastern Labrador. P-T paths from zoned garnets in the central/eastern part of the map area

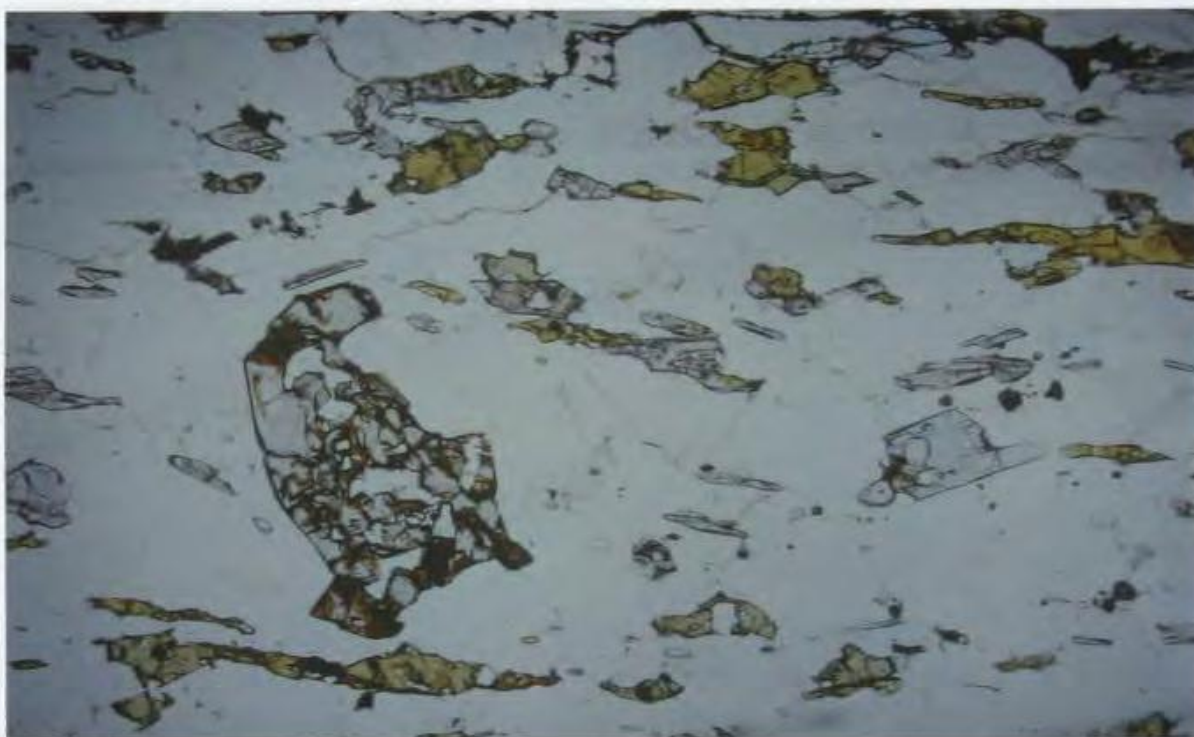
indicate a fairly steep, "hairpin" P-T loop which has a peak at 700 to 750°C and 11 to 12 kbar near the eastern boundary of Gagnon terrane. Peak metamorphic pressures and temperatures decrease rapidly westwards to the syncline at the southern end of Wabush Lake (600 to 650°C, 9 to 10 kbar). From there westwards, the peak pressures and temperatures drop more gradually to 450°C and 6 kbar at Emma Lake and O'Brien Lake. This variation of peak metamorphic pressures and temperatures indicates a telescoped and inverted metamorphic gradient through the thrust belt.



150  $\mu\text{m}$

Plate 7.1

**Biotite from a basement rock east of Bruce Lake, probably of Archean age and originally rich in titanium. The brown core contains a sagenitic intergrowth of rutile needles and trails of sphenic inclusions, and is overgrown by a rim of green Grenville-age biotite. The matrix consists of fine-grained chlorite, muscovite, quartz feldspar and epidote. (plane polarized light)**



0.6 mm

Plate 7.2

**Amphibolite grade mineral assemblage in metamorphic zone 4 consisting of garnet (large porphyroblast on the left with hematite staining), staurolite (yellow) and kyanite (colorless, high relief) in a coarse-grained quartz matrix. Sample of the pelitic member of the Wishart Formation in the Goethite Bay thrust sheet. (plane polarized light)**



0.6 mm

Plate 7.3

Retrograde growth of chloritoid (gray-blue and pale yellow-green twins), replacing staurolite (yellow), of which an unstable remnant is located in the lower right-hand corner. The garnet (large porphyroblast in the top) contains inclusions of staurolite outside the field of view. The matrix contains quartz and muscovite. Wishart Formation near Goethite Bay. (plane polarized light)



0.6 mm

Plate 7.4

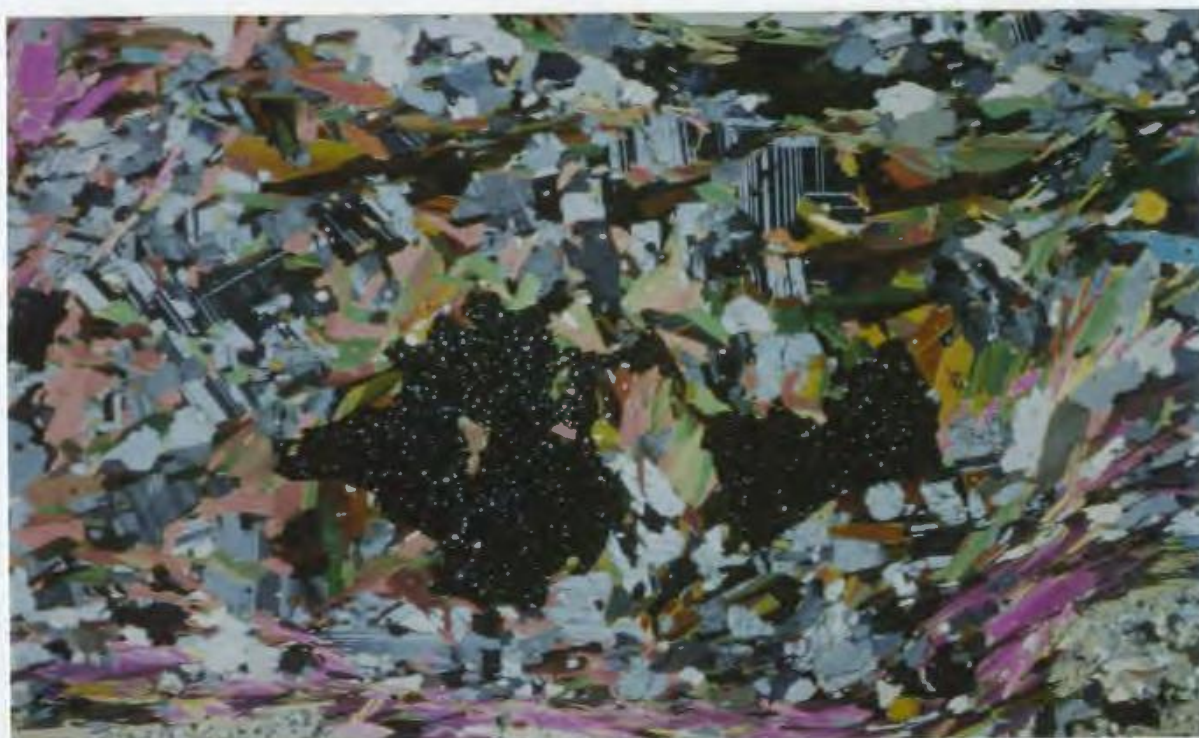
Diagnostic mineral assemblage of metamorphic zone 5, garnet (black) + biotite (dark green to brown) + kyanite (pale yellow and white), in a matrix of predominantly muscovite + quartz. Sample from Wabush town in the Duley Lake thrust sheet. (crossed nicols)



0.6 mm

Plate 7.5

Antiperthitic exsolution of microcline in a plagioclase grain. In a rock of the Attikamagen Formation in the Wabush Lake thrust sheet near the Michel Lake tonalite. The micas at the top and the bottom are muscovite. (crossed nicols)



1.2 mm

Plate 7.6

Partially resorbed garnet in a rock of the Attikamagen Formation in the Duley Lake thrust sheet at the southern end of Flora Lake. The area surrounding the garnet is depleted in muscovite, which is abundant in the remainder of the matrix, and enriched in biotite and plagioclase. This suggests that garnet was broken down by the reaction  $Gnt + Ms = Pl + Bt$ . (crossed nicols)

## CHAPTER 8

### **THERMOTECTONIC DEVELOPMENT OF THE FOLD-AND-THRUST BELT: DISCUSSION AND SYNTHESIS**

In this final chapter a model is presented for the development of the Grenvillian fold-and-thrust belt in southwestern Labrador, which accommodates the structural as well as the metamorphic characteristics of the belt. The tectonic development is interpreted in the light of the bulldozer-wedge model for thrust belts and aspects of the mechanics of the development are discussed qualitatively. Subsequently the significance of the model is discussed with respect to thrust belt models in general, to the regional tectonics of western Labrador, to other parts of the Parautochthonous Belt in the Grenville Province and to other fold-and-thrust belts worldwide.

#### **8.1 MODEL FOR THE DEVELOPMENT OF THE BELT**

In the previous chapters many characteristics of the map area were presented and discussed. Here, these characteristics are placed in the context of the developing fold-and-thrust belt and their interaction is integrated in a tectonometamorphic model. Listed below are the main aspects of Gagnon terrane in the map area which must be incorporated in the model for the development of the belt:

- Gagnon terrane consists of an upper, sediment-dominated thrust system and a lower, basement-dominated system;
- all structures indicate that the rocks were affected by ductile deformation. Thrusts occur as ductile shear zones;
- the rocks in the upper thrust system were affected by an early phase of predominantly simple shear during which a regionally penetrative  $S_{1U}$  foliation developed. Kinematic indicators, in combination with the elongation lineation, indicate

north-northwest-directed thrust movement. In a subsequent progressive stage of development the foliation was folded in northwest-vergent  $F_{2U}$  folds and north-northwest-directed out-of-sequence thrusts developed. Kilometer-scale south-southeast-plunging  $F_3$  cross-folds are dominant in the southeastern part of the map, where they overprint all other structures;

- deformation in the lower, basement-dominated thrust system was predominantly localized in narrow ductile shear zones. These shear zones are rather steep and indicate oblique, sinistral-reverse, north-northwest-directed movement on them. They are interpreted as reactivated extensional faults;
- the overall strain increases towards the higher thrust sheets in the upper thrust system and is progressively less concentrated in shear zones. The simple shear component of the non-coaxial flow decreases towards the structurally highest thrust sheets;
- foliations and elongation lineations in both systems are oblique with respect to each other and with respect to the trend of the belt;
- Gagnon terrane exhibits a telescoped, inverted metamorphic gradient, with the highest pressures and temperatures in the highest thrust sheets, decreasing towards the structurally lower parts of the belt. The floor thrusts of the Lorraine Lake and Goethite Bay thrust sheets, and probably also others, form a break in the metamorphic gradient;
- the thrust sheets in lithotectonic domain V went through a hairpin-shaped P-T path. Cooling and decompression started immediately following the metamorphic peak;
- the peak metamorphic pressures in the eastern part of Gagnon terrane in the map area indicate an overburden of up to 30 km, which cannot realistically be constituted by the structural thickness of the stacked sedimentary thrust sheets;
- the metamorphic gradient is oblique with respect to the trend of the fold-and-thrust belt. As a result the metamorphic grade increases from north to south within each of the lithotectonic domains;

- microstructural relations between porphyroblasts and metamorphism indicate that in the highest thrust sheets in lithotectonic domain V the  $D_1$  deformation postdated or outlasted the peak of metamorphism, whereas in domain II  $S_1$  developed syn-metamorphically.  $D_2$  and younger deformation occurred throughout the belt during retrograde metamorphism.

Most of these observations and their significance have been discussed individually in the previous chapters. In this chapter these points are discussed in relation to each other and a model for the thermotectonic development of Gagnon terrane is presented, which incorporates all of these aspects. Figure 8.1 is a synopsis of the model, showing the large-scale features of the development of the belt in cross section, together with P-T paths and microstructures in two monitor points, which reflect data from the Wabush Lake thrust sheet and the Emma Lake thrust stack. It should be noted that the sections in the figure are not to scale. On a true scale the metasedimentary rocks in the belt form a layer of almost negligible thickness compared to the whole thrust wedge. The package of platformal sediments can virtually be regarded as a single datum plane. Below the main aspects of the different steps are summarized and in sections 8.2.2 to 8.2.4 they are discussed in detail.

Diagram A of Figure 8.1 is a sketch of the continental margin before onset of the Grenvillian orogeny. It shows the extended continental crust overlain by the shallow and deeper parts of the platform and the thicker sedimentary pile on the continental slope. In diagram B the overriding thrust wedge, consisting of Molson Lake terrane, has moved on top of and over the sediments at the continental margin, causing an increase of the lithostatic pressure and the temperature (due to thermal relaxation) in the underlying sediments. In the next step (C) the basal detachment has stepped down to the basement-cover contact and the thrust sheets in the southeast are incorporated in the thrust wedge. Thrust sheets move with the thrust wedge under decreasing pressure and temperature as a result of uplift and erosion. In diagram D the northwestern thrust sheets, comprising the shallow platform sediments, have also been incorporated in the thrust wedge. In the final diagram (E) the basal detachment has stepped down and the

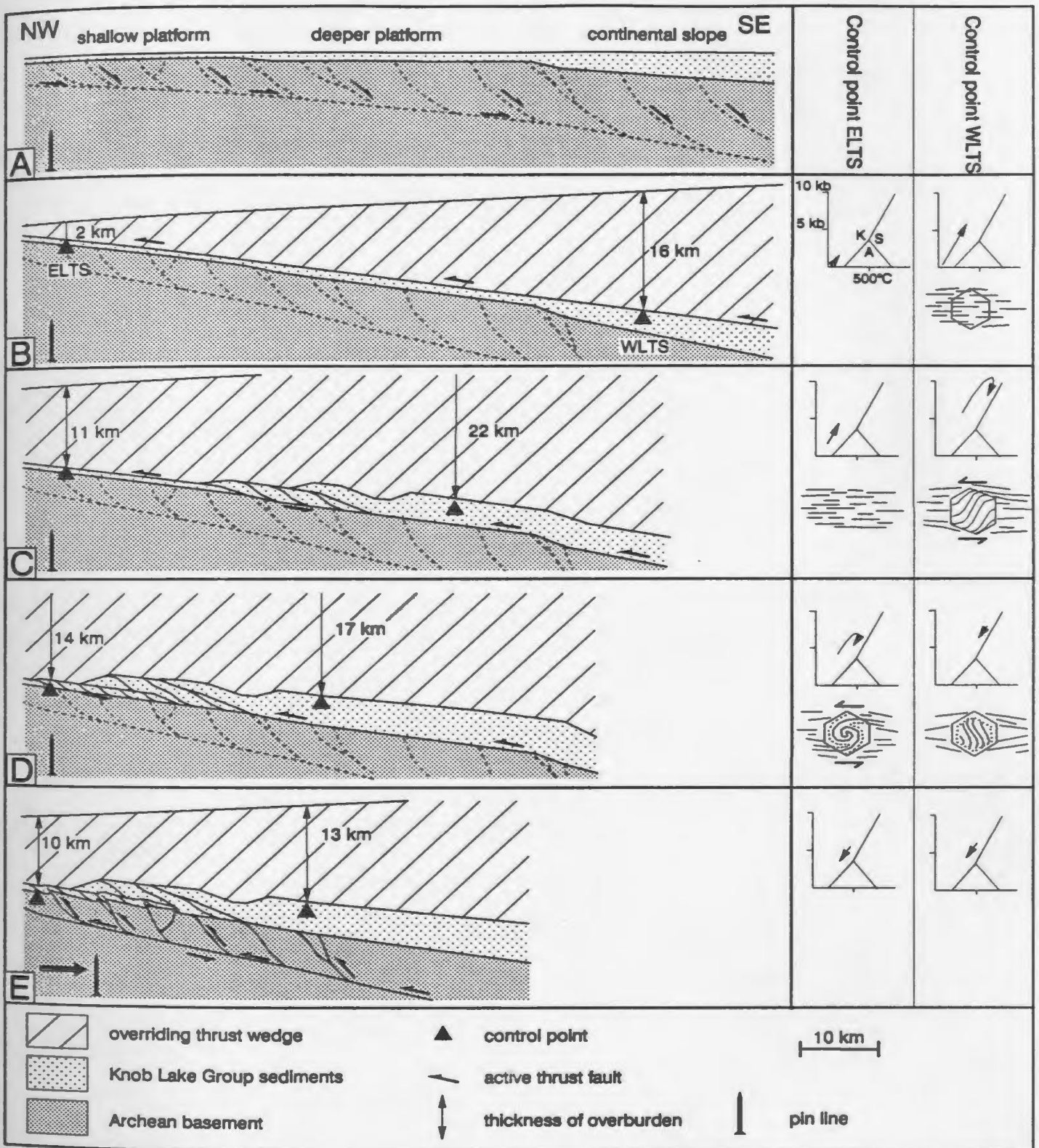


Fig. 8.1 Schematic summary of the thermotectonic development of the fold-and-thrust belt in southwestern Labrador. For two control points P-T paths and garnet microstructures are shown. Note that the pin line, which lies in undeformed basement rocks, is moved in figure E. The top of the overriding wedge is cut off in figures C to E. The diagram is approximately scaled, with exception of the thickness of the metasediments, which is three to four times exaggerated. A = andalusite, K = kyanite, S = sillimanite, ELTS = Emma Lake thrust stack, WLTS = Wabush Lake thrust sheet.

lower thrust system formed in the basement. The four steps between these five diagrams are discussed in detail below. The development as presented here hinges on the bulldozer wedge model, which is applicable to high-level thrust belts and accretionary wedges that deform by brittle processes (Davis et al., 1983). In the following section the use of the bulldozer wedge model for the mid-crustal thrust belt in southwestern Labrador is justified.

### **8.1.1 VALIDITY OF THE BULLDOZER-WEDGE MODEL FOR A PLASTIC BELT**

The imbricate thrust stack geometry of the fold-and-thrust belt in western Labrador suggests that the belt has at least some of the characteristics of a critical thrust wedge of upper crustal thrust belts (Chapple, 1978; Davis et al., 1983), but also exhibits signs of plastic behaviour of mid-crustal orogenic belts. Most mechanical models for fold-and-thrust belts, or accretionary wedges, apply to Coulomb-type materials, in which cohesive strength is equal to shear stress at the base, moving over a basal detachment by frictional sliding (Davis et al., 1983; Dahlen and Barr, 1989). These models, called critical-wedge or bulldozer-wedge models, regard a thrust belt as an orogenic wedge, tapered in the direction of movement and on the verge of Coulomb failure. The critical taper of a stable, gliding wedge, is determined by the strength of the rocks and friction at the base. Interaction of several processes maintains this critical angle. Increased friction at the base, shortening of the wedge, or accretion of material at the sole by underplating will result in an increase of the taper and are counteracted by a decrease of the friction at the base, extensional deformation within the wedge or accretion at the toe of the wedge. Erosion at the surface will affect the taper as well (Koons, 1989; Beaumont et al., 1992).

Strictly, these models cannot be applied to the mid-crustal level thrust belt in southwestern Labrador, which deformed by crystal-plastic processes, as demonstrated in Chapter 6. However, Chapple (1978) and Platt (1986) presented models for plastic thrust wedges which have the same general characteristics as described above. Chapple (1978) discussed a plastic thrust wedge, moving over a weak layer at the base (e.g.

shale or salt) which forms a ductile movement zone. The wedge is constantly yielding internally due to (sub-)horizontal compressive stress and internal deformation creates and maintains the surface slope that forms the critical taper. Because the whole wedge is continually deforming, the higher thrust sheets that are incorporated earlier have a higher accumulated strain than the lower thrust sheets that become part of the wedge at a later stage. Platt (1986) argued that the general features of a plastically deforming orogenic wedge are similar to those of the bulldozer wedge used for upper crustal thrust belts. Mylonitization and grain-size reduction at the base of a moving thrust wedge create the weak layer on which the thrust wedge moves by viscous flow (Platt, 1986).

A detailed study of the mechanical behaviour of the thrust belt in southwestern Labrador is beyond the scope of this thesis. The thrust wedge model is used here in a qualitative sense. No attempt was made to quantify any of the factors that control the deformation in the belt. Many of the structural relationships in the map area agree with the general features of the bulldozer wedge model described above and following Chapple (1978) and Platt (1986) the model can be used to explain the tectonic development of Gagnon terrane.

### **8.1.2 STEP ONE: EMPLACEMENT OF MOLSON LAKE TERRANE**

The early part of the tectonic development is dominated by the movement of Molson Lake terrane over the metasediments of the continental shelf and margin. During this stage of emplacement of the overriding thrust wedge the metamorphic grade of the rocks in Gagnon terrane increased. The sediments acted as a glide horizon for the movement of the thrust wedge and were deformed.

The emplacement of an overriding thrust wedge is required because maximum metamorphic pressures in the map area indicate an overburden of approximately 30 km in the upper thrust sheets and 15 km around Emma Lake. These thicknesses could only have been reached by stacking of sediments within Gagnon terrane if the thin stratigraphic sequence was repeated many tens of times. The actual structural thickness of the cover sequence is estimated to be less than one kilometer for the thrust sheets in lithotectonic domains II to IV and in the order of 5 km for the highest thrust sheets.

Therefore, an external load is required. The decrease of the maximum metamorphic pressures from southeast to northwest suggests that the overriding thrust sheets formed a wedge tapering to the northwest.

The thrust wedge is assumed to be formed by the Molson Lake terrane. The high strain rocks at the contact between the two terranes, which were deformed at high temperatures, and the continuity of the structures across the contact suggest that the overlying terrane was emplaced early during the tectonic history. The estimated peak metamorphic conditions of Molson Lake terrane (Connelly, 1991; Indares, in press) indicate a total thickness in the order of 40 km, which is sufficient to form the required load on the rocks of Gagnon terrane. Connelly (1991) proposed that Molson Lake terrane was emplaced on the foreland, causing the creation of a fold-and-thrust belt in its footwall.

The interpretation that the prograde metamorphism in Gagnon terrane was caused by the emplacement of Molson Lake terrane is in accord with the numerical models for the thermal development of the crust during thickening by the emplacement of a large thrust wedge (England and Thompson, 1984; Karabinos and Ketcham, 1988). The load of the overriding thrust sheet provided the pressure increase, while the increase in temperature was caused by the relaxation of isotherms, and possibly by the conduction of heat from the relatively hot overriding Molson Lake terrane. The rocks in Gagnon terrane experienced prograde metamorphism as long as they remained in the footwall of the advancing thrust wedge.

In this first stage of development, the rocks of Gagnon terrane were underthrust beneath Molson Lake terrane down to about 30 km maximum. No direct evidence exists as to whether they moved down in the footwall of the overriding thrust sheet, or whether the rocks followed a downward-directed particle path inside the thrust wedge, as proposed by Dahlen and Barr (1989) for Coulomb-type (brittle) thrust wedges. In the first case the thrust sheets would have formed after the rocks were tectonically buried, with accretion into the thrust wedge taking place by underplating (cf. Platt, 1986). In the second case, the thrust sheets would have formed at high crustal levels by

accretion at the toe and subsequently moved down within the thrust wedge. In Section 8.1.2 it is argued that the first scenario is more likely and that the thrust sheets were incorporated at the base of the thrust wedge, after emplacement of Molson Lake terrane. In this first stage of development, the floor thrust of Molson Lake terrane remained the main site of translation. If any rocks were accreted to the overriding thrust wedge during this phase, they were most likely accreted at the toe and subsequently transported out of the map area with the northwest moving thrust wedge.

This large translation of the thrust wedge without incorporating parts of the underlying sediments can be explained by the presence of the rocks of the Menihek Formation at the top of the Knob Lake Group in the area (as exposed presently). These rocks formed mudstones and graphitic shales at the time of incipient emplacement of the overriding thrust sheet and are interpreted to have formed an easy glide horizon which accommodated most of the strain of the emplacement of Molson Lake terrane. Because of the low friction there was a tendency to extend the thrust wedge, which would have been accomplished by accretion of rocks of the Menihek Formation at the toe, but counteracted by accretion at the base, which would have over-thickened the wedge.

The load of Molson Lake terrane induced an increase of the lithostatic pressure in the underlying sediments. However, it is not clear to what extent the rocks were deformed at this stage. As proposed above, the rocks of the Menihek Formation may have taken up most of the strain of the movement of the thrust wedge, but probably the rocks in the lower part of the stratigraphic sequence were deformed at this time as well. In the field it is impossible to distinguish between structures related to this early period of underthrusting and those related to the later formation of the thrust sheets and their accretion to the thrust wedge. However, inclusion patterns in metamorphic porphyroblasts from all parts of the map area show that a foliation developed during prograde metamorphism, i.e. during the underthrusting beneath Molson Lake terrane. Presumably, all metasediments deformed originally fairly homogeneously by non-coaxial flow to accommodate the movement of the overriding thrust wedge (with a

concentration of the strain in the Menihok Formation) and developed a mylonitic foliation  $S_{1U}$ , an elongation lineation  $L_3$  and  $F_{1U}$  shear folds. During progressive deformation the strain concentrated in narrow zones, which formed the  $S_{1U}$  ductile thrusts, the sedimentary thrust sheets were formed and the rocks were accreted to the thrust wedge, switching from footwall to hanging wall. Probably the difference in strain between the hanging wall and the footwall of the sole of the thrust wedge was minimal in a ductile environment and development of the  $S_{1U}$  foliation was continuous during underthrusting and development of the thrust sheets. Figure 8.2 is a schematic section through the thrust wedge, including the footwall, and shows a zone of  $D_{1U}$  deformation covering part of both the footwall and the hanging wall near the base of the thrust wedge. The dashed lines in both the section and the P-T diagram represent the particle path and its P-T path in this first phase of development of the thrust belt.

### 8.1.3 STEPS TWO AND THREE: FORMATION AND ACCRETION OF THE THRUST SHEETS

In this second phase of the development, separated in two steps in Figure 8.1 (C and D), the sediments are accreted to the thrust wedge by piggy-back stacking of thrust sheets, starting with the highest thrust sheets in the southeast in Figure 8.1.C, progressing towards the northwest in D. The sole of the thrust wedge stepped down from the top of the sediments to their base, the contact with the basement gneisses. During this phase the penetrative  $S_{1U}$  mylonitic foliation in the area continued to develop, as a continuous progression of the underthrusting stage, but the deformation was concentrated in the shear zones by strain localization, especially in the lower grade parts of the belt. The main displacement on the  $D_{1U}$  shear zones is interpreted to have taken place during this phase. Once a thrust sheet was incorporated in the wedge and the main thrust activity moved to a lower level,  $D_{2U}$  deformation became dominant.

The assumption is made that the creation and stacking of the thrust sheets marked the moment of accretion of the rocks to the thrust wedge, because at that time the sole of the thrust wedge, or the main site of translation, cut from a level above the sediments, down to the basement-cover contact. Several features of the rocks indicate

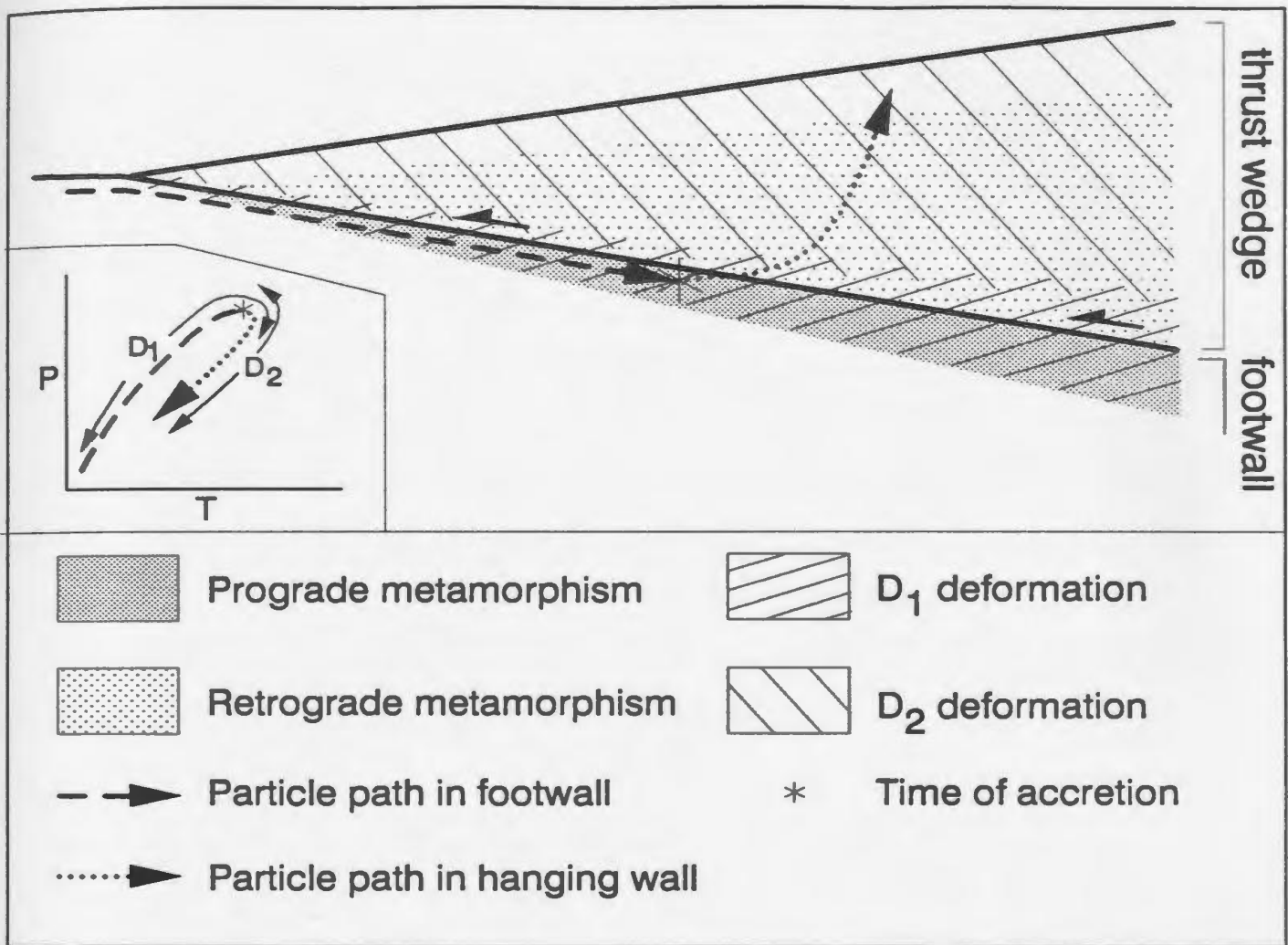


Fig. 8.2 Schematic section through a moving thrust wedge showing a section of  $D_{1U}$  strain near the base of the wedge and  $D_{2U}$  in the remainder of the wedge. Note that  $D_{1U}$  deformation takes place both in the footwall and the hanging wall, and that the zone of  $D_{1U}$  strain widens towards the rear of the wedge as a result of decreasing strain localization. Assuming there is no downward directed particle path within the thrust wedge, the sole thrust approximately separates the rocks in prograde metamorphism in the footwall from those in retrograde metamorphism in the hanging wall.

that the accretion took place at depth at the base of the thrust wedge, rather than at the toe.

1) No penetrative early brittle structures have been recorded in the rocks of Gagnon terrane which could be related to thrust stacking at upper crustal levels in the toe of the thrust wedge. Possibly such structures were originally present but were erased by penetrative ductile overprinting. However, the thrusts in the belt form ductile shear zones, indicating that a significant part of the thrusting took place after the rocks were underthrust to a level below the brittle-ductile transition.

2) The breaks in the metamorphic field gradient at the floor thrusts of the Lorraine Lake and Goethite Bay thrust sheets, and probably also at other thrust sheet boundaries, indicate that the main movement on these thrusts took place at or after the peak of metamorphism, i.e. when the rocks had reached their deepest level, or later. Had the thrust sheets been stacked at higher crustal levels and subsequently transported to lower crustal levels, they would have an uninterrupted metamorphic gradient and the thrust sheets would not each have their own metamorphic and structural characteristics. In accordance with the assumption that the time of thrust stacking coincided with accretion of a thrust sheet to the wedge, this means that the thrust sheets were accreted at the sole of the thrust wedge by underplating (Platt, 1986) after Molson Lake terrane was overthrust.

During the first phase of the development, the metasediments were affected by prograde metamorphism in the footwall of the thrust wedge, but once a thrust sheet was incorporated in the thrust wedge the metamorphic grade decreased. Accretion to the thrust wedge was the cause of, and approximately coincident with, the switch from prograde to retrograde metamorphism. Progression of the thrust wedge with respect to the recently accreted rocks stopped and uplift started as a result of erosion at the top of the thrust wedge, reducing the load. The thrust sheets in the wedge moved on top of cooler rocks in the footwall, which would have contributed to the lowering of their temperature. Numerical thermal models for thrust belts show that a time lag, in the order of a million years, exists between the end of the movement of the thrust wedge

and the actual start of the decrease of the temperature (e.g. Karabinos and Ketcham, 1988). During this period the rocks experience predominantly decompression as a result of erosion, which has an instantaneous effect. The actual length of this time lag in the thrust sheets of the map area is not known, but the hairpin-shaped P-T path suggests that the period of predominant decompression was short and cooling started shortly after the pressure peak was reached. Figure 8.2 is a schematic section through the moving thrust wedge and a P-T path for a volume of rock that was underthrust, incorporated in the thrust wedge and uplifted as part of the wedge. It shows that prograde processes take place in the footwall and retrograde processes in the hanging wall (c.f. Karabinos and Ketcham, 1988). In Section 8.1.5.2 the metamorphic aspects of the underplating are considered in detail.

Figure 8.2 also illustrates that  $D_{1U}$  deformation took place predominantly in the prograde part of the P-T path, whereas  $D_{2U}$  occurred under retrograde conditions. The diagram shows an overlap of  $D_{1U}$  and  $D_{2U}$ , which exists for a thrust sheet as a whole, of which different parts can show different styles of deformation occurring simultaneously. The dotted lines in the section and the P-T diagram represent the particle path and the P-T path, respectively, of a volume of rock after incorporation into the thrust wedge. The figure assumes that there is no downward-directed particle path within the thrust wedge, bringing the thrust sheets down to a lower level after accretion. This is in accordance with the calculated particle paths in the theoretical thrust wedge model of Dahlen and Barr (1989) in situations where a significant part of the rocks are accreted by underplating.

As long as a thrust sheet remained near the base of the thrust wedge, the finite  $D_{1U}$  shear strain increased, but a transition to  $D_{2U}$  occurred when a thrust sheet was thrust over a ramp and the sole thrust activity was transferred to a lower thrust in the footwall. However, Figure 8.2 shows that the width of the zone of  $D_{1U}$  deformation increases towards the rear of the wedge, which is a result of the decrease of the strain localization with increasing metamorphic grades. As a result, the rocks in the Wabush Lake and Duley Lake thrust sheets proceeded to deform homogeneously after they were

accreted, after the metamorphic peak, whereas in the rocks of the Emma Lake thrust stack prograde metamorphism and  $D_{1U}$  deformation stopped virtually simultaneously. These differences in timing of  $D_{1U}$  deformation and metamorphism are shown in the microstructures for the two control points in Figure 8.1.

The observation that the thrust sheets were stacked in piggy-back sequence, means that while the highest thrust sheets were moving with the thrust wedge and in the retrograde part of the P-T path, the metasediments to the northwest were still part of the footwall, being underthrust, and in the prograde part of their P-T path, as is shown in monitor points 1 and 2 in diagram C. The metamorphic peak swept in time through the area from southeast to northwest. This is an important observation with respect to the inversion of metamorphic gradients, discussed in Section 8.1.5.2. Rice (1987) described a similar order of events in the Kalak Nappe Complex in the Norwegian Caledonides, where rocks were progressively buried underneath a wedge moving towards the foreland, resulting in increasing P and T, until they were incorporated into the allochthon by thrust stacking, after which time the pressure, followed with some time lag by the temperature, decreased as a result of erosion. Similar results were reported by Karabinos and Ketcham (1988) from numerical modelling of the thermal development of thrust belts.

The stepping down of the basal detachment from the sole of Molson Lake terrane to the sole of the upper thrust system in Gagnon terrane, may have been related to incipient partial melting in the Wabush Lake thrust sheet, which is assumed to have been the first thrust sheet to be accreted to the thrust wedge. The melt that was produced presumably weakened the rocks to such an extent that shearing on a melt-lubricated shear zone in these rocks became mechanically more favourable than thrusting over the top of the sediments. Possibly the location of the Wabush Lake floor thrust was close to the melt isograd (see Chapter 7). Hollister and Crawford (1986) suggested that anatexis and melt production could be an important cause for weakening of rocks at deep crustal levels and that melt injection in shear zones could induce rapid thrusting and uplift. This may explain the rapid uplift of the rocks of the Wabush Lake

and Duley Lake thrust sheets, which was suggested by the preservation of the prograde zoning in garnets in spite of estimated peak metamorphic temperatures in the realm of garnet homogenization, and also agrees with rapid uplift rates for Molson Lake terrane calculated by Connelly (1991) from U-Pb and Ar-Ar geochronology data.

Unfortunately, the floor thrusts of the two highest thrust sheets are not exposed and the theory cannot be checked in the field.

Another possible factor in the switch of the main thrust activity from the top to the bottom of the sediments could be related to a change in friction at the base of the thrust wedge. Once the tip line of the sole thrust reached an area where the Menihek Formation was not present, or where it was disturbed either by Early Proterozoic extensional faults or deformation in the New Quebec orogen, easy movement along the base would have been hampered, resulting in an increase of the taper by thickening of the thrust wedge. Thickening could have been accomplished by either internal shortening, or by accretion of material at the base. Possibly the presence of melt in the Wabush Lake thrust sheet made the latter option more favourable.

#### **8.1.4 STEP FOUR: DEVELOPMENT OF THE LOWER THRUST SYSTEM**

In Figure 8.1.E the sole thrust of the thrust wedge has stepped down a second time and the basement-dominated, lower thrust system has developed. The basement thrust stack is interpreted to have formed by the reactivation of a pre-existing extensional linked fault system. This lower thrust system is only observed in lithotectonic domains I and II, but in the model in Figure 8.1 and in the cross sections in Figure 1.B (in pocket) it is interpreted to extend down underneath the structurally higher thrust sheets, as was suggested in Chapter 4. Since very little information is available on the structures in the basement southeast of lithotectonic domain III, the geometry of the southeastern extension of the basement thrust stack is not clear. The lower thrust system could either form a crustal scale duplex or imbricate fan, or progressively change at higher metamorphic grades in the southeast into a wide zone of more homogeneous deformation.

Structures in the basement rocks exposed in lithotectonic domain III could be related to either the lower or the upper thrust system, and interpretations of these structures may not apply to the lower thrust system. Thrusts that originated in the basement breached into the upper thrust system in lithotectonic domain II and caused out-of-sequence thrusting and folding. This geometry suggests that the thrusts did not rejoin in a roof thrust and formed an imbricate fan rather than a duplex (Boyer and Elliott, 1982). However, in the remainder of the map area breaching lower-system thrusts were not observed, with the exception of the Goethite Bay area (Fig. 5.14), and no interference of upper and lower system thrusts seems to have occurred, which could be an indication that a duplex geometry predominates. A similar crustal scale duplex was inferred by Butler and Coward (1984) underneath the Moine thrust belt in northern Scotland and was interpreted to accommodate significant crustal shortening at mid-crustal levels.

The thrust stack geometry of the lower thrust system, either duplex or imbricate fan, does not necessarily continue unchanged underneath the higher thrust sheets where it is not exposed. Towards higher metamorphic grades in the southeast, strain localization in ductile thrust zones was presumably less important and the rocks may have deformed by more homogeneous strain. This would be in agreement with observations of Schmid and Haas (1989), who described the progressive change of the Schlinig overthrust in the northeastern Italian Alps, which carried the crystalline, upper Austro-Alpine Ötztal nappe. This thrust changes from a single narrow shear zone at sub-greenschist facies, to a many kilometer-wide zone of more homogeneous strain, dominated by folding, at amphibolite facies. Deformation of basement rocks in the Elmer Lake thrust sheet, which is at upper greenschist facies, was pervasively ductile and more homogeneous than in the lower thrust sheets at lower greenschist facies, but it is not certain whether this deformation was linked to the lower or upper thrust system. If the former was the case then this would suggest that the mode of deformation and possibly the thrust stack geometry of the lower system changed towards the southeast. However, in the floor of the Goethite Bay thrust sheet intensely deformed basement

slices were thrust into the upper system, suggesting that the thrust geometry does exist in this part of the map area. Probably the thrust geometry still prevails in the deeper part of the lower thrust system, but the thrust slices become progressively more internally deformed as a result of diminishing strain localization, similar to the trend observed in the upper thrust system.

Several of the observations on the thrusts in the basement indicate that the lower thrust system could be formed by reactivation of a pre-existing extensional fault system, as proposed in Chapter 5. The geometry of a linked system of listric normal faults is actually quite similar to that of an imbricate stack of thrusts. The oblique convergence of the belt enabled the reactivation of the extensional faults as oblique-slip reverse-sinistral faults. In case of orthogonal convergence, the steep dip of the normal faults would have made them unfavourable for reactivation as reverse faults. New, low angle thrusts were also formed, e.g. the floor thrust of the Elmer Lake thrust sheet at the southern end of the Flatrock lake thrust sheet (Fig. 1B, in pocket). It is likely that the lower detachment of the thrust system traced the existing extensional detachment horizon, which presumably extends down to lower crustal levels as shown in models for extensional continental margins by Wernicke (1981) and Lister et al. (1986).

Several factors could have caused the basal detachment to step down from the base of the metasediments to the detachment in the basement. 1) As proposed in step two (Section 8.1.3), an obstruction, e.g. formed by a fault escarpment, or a lateral change in rheology could have restrained the forward movement of the thrust wedge, requiring thickening of the wedge and inducing underplating of the basement rocks. 2) Towards the foreland the cover sequence is assumed to become progressively thinner. Near the tip of the thrust wedge this sequence could have been too thin to accommodate the crustal thickening required to preserve the equilibrium shape of the thrust wedge, which resulted in incorporation of the basement rocks at a deeper level. 3) Movement of the thickest part of the thrust wedge over the ramp formed by the continental margin may have hampered propagation of the thrust wedge, which caused collapse of this ramp, resulting in the development of the basement thrust stack (cf. Jamieson and

Beaumont, 1988). 4) Stacking of cover rocks in thrust sheets in the upper thrust system stripped the cover from a large extent of basement rocks. This led to a large discrepancy between shortening in the cover and the basement. Possibly the lower thrust system formed to accommodate the shortening that was accomplished at higher crustal levels.

It should be kept in mind that this last phase of development in the model does not have to be separated in time from the previous phases. Although in the lower thrust sheets thrusting in the basement postdated thrusting in the upper system, the lower system may have started to develop in the rear of the belt before the thrusting near the front of the upper system ceased.

### **8.1.5 IMPLICATIONS OF THE MODEL**

The way the development of the fold-and-thrust belt is presented in this thesis is an over-simplification. It is unlikely that at any one time just one thrust is active, but one trajectory is expected to accommodate most of the movement at any one time. Heterogeneities in lithology, e.g. formed by the gabbros, or strain heterogeneities likely disturbed the pattern that is presented here on a local scale. Furthermore, the processes described in separate steps are assumed to evolve into each other rather than to be separate phases in time. Regarding the similarity between the model presented here and those presented by Rice (1987), based on field- and petrographic studies, and Karabinos and Ketcham (1988), based on numerical modeling, the interpretation of the development of Gagnon terrane seems valid. The main consequences of the model are discussed below.

#### **8.1.5.1 Underplating versus accretion at the toe**

A moving thrust wedge is a dynamic body which constantly accumulates material by accretion and loses it by erosion. Accretion can take place either at the toe of the wedge (Davis, Suppe and Dahlen, 1983) or at the sole of the wedge by underplating (Platt, 1986). It was argued above that the rocks in Gagnon terrane were accreted by underplating. This explains best the ductile nature of the thrusts, the breaks in the

metamorphic gradient and the distinct structural and metamorphic character of each of the thrust sheets. If the thrust sheets were stacked before being buried underneath Molson Lake terrane, they would not display the telescoped and inverted metamorphic gradient. Burying the thrust sheets underneath 30 km of rocks after having been stacked, would mean that they followed downward directed particle paths within the thrust wedge along its base (Dahlen and Barr, 1989), which could only be accomplished by major simple shear or out-of-sequence thrusting within the thrust wedge.

In models for thrust belts and accretionary wedges in the upper crust, accretion of material takes place mainly at the toe of the thrust wedge. There could be several reasons for the different mechanism of accretion in the thrust belt of Gagnon terrane. The presence of the low competency rocks of the Menihek Formation may have played an important role by providing an easy glide horizon which kept underlying rocks in the early part of the development of the belt from being accreted. The underplating could also be a compensation for simultaneous accretion at the toe of the wedge or for high erosion rates at the top of the wedge. If the former is an important factor, underplating may be a common feature of deeper parts of thrust belts. Platt (1986) suggested that underplating provides a mechanism for rapid uplift of high-pressure rocks before they can be overprinted by high temperature metamorphism. P-T paths from the Wabush Lake thrust sheet (Chapter 7) exhibit no significant heating after burial ceased, which is in accord with the interpretation of rapid uplift induced by underplating. As discussed below underplating also provides a mechanism for inversion of metamorphic gradients, which is common in metamorphic belts.

#### **8.1.5.2 Inversion of the metamorphic gradient by underplating**

The map area exhibits a regionally inverted metamorphic gradient, which is characteristic for metamorphic fold-and-thrust belts (e.g. Rice et al., 1989). The metamorphic grade increases from the structurally lowest to the highest thrust sheets (Figure 4.2). A jump in metamorphic grade is inferred across the floor thrusts of the Goethite Bay and Lorraine Lake thrust sheets, and possibly across some of the other thrusts as well. Inverted metamorphic gradients are generally explained by the

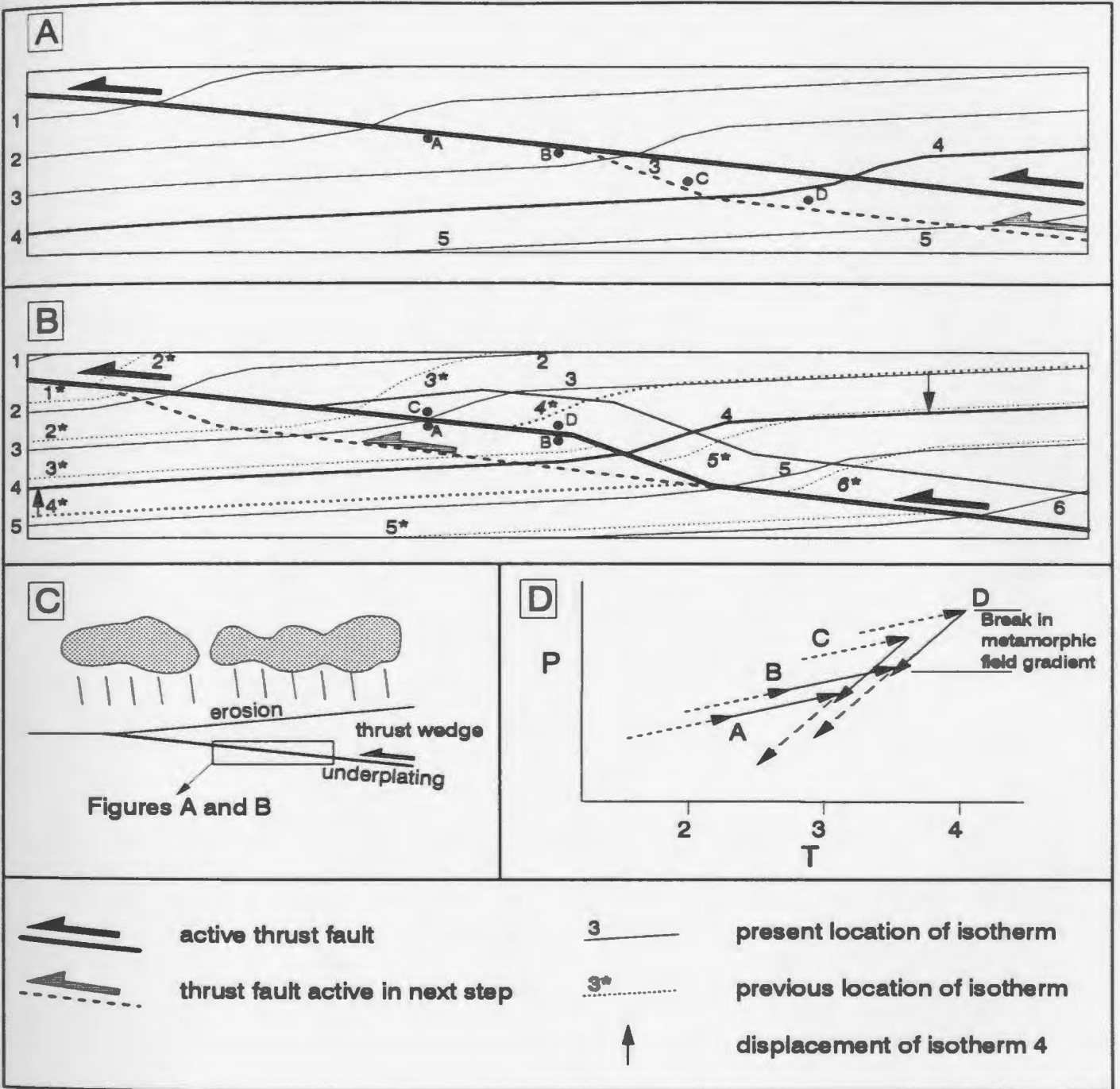
emplacement of thrust sheets of a relatively high metamorphic grade on top of lower grade rocks (e.g. Johnson et al., 1985; Jamieson, 1986; Crowley, 1988; Karabinos and Ketcham, 1988), or recumbent folding of isograds (e.g. Boyle, 1987). The former is consistent with the rule that thrust faults emplace rocks from a deeper level on top of rocks from a higher level. This appears to require that the thrusting takes place after the metamorphic event. In the following discussion it is argued that inversion of a metamorphic gradient and formation of discontinuities in the field gradient occur commonly in thrust belts during thrust stacking at the peak of metamorphism.

Regional metamorphism, other than that caused by heat released from intrusive bodies, is generally a result of thickening of the crust, which causes disturbances in both isotherms and isobars, the movement of which will induce a change in the metamorphic grade in a rock. The isobars will adapt immediately to a changed load and always reflect the thickness of the overburden. Isotherms disturbed by structural movements are restored by transfer of heat, usually modelled as conductive transfer, which is a slower process and re-equilibration of isotherms lags behind that of isobars. A thrust cutting through an originally horizontal isotherm will distort the isotherm and can cause it to overturn if the rate of displacement is faster than re-equilibration of the isotherm by conduction (e.g. Shi and Wang, 1987). Most numerical models for the thermal evolution of thrust belts show that inversion of isotherms is a short-lived phenomenon, which is not easily preserved in an orogenic belt because it forms an unstable thermal configuration (Oxburgh and Turcotte, 1974; England and Thompson, 1984; Crowley, 1988, Barr and Dahlen, 1989). Overturning of isotherms is often mentioned as the cause for inversion of the metamorphic gradient, but it is shown below that preservation of an inverted metamorphic gradient does not require overturning of isotherms at any time. A qualitative model will be presented which is based on observations from the map area and interpretation of the numerical model of Karabinos and Ketcham (1988).

When discussing inversion of metamorphic gradients it is important to note that the gradient observed by a geologist in the field reflects the variation of the peak metamorphic conditions across an area (the metamorphic field gradient, Spear et al, 1984), not a thermal and baric configuration that existed at one time and was frozen in. In Section 8.1.3 it was stressed that from southeast to northwest in the map area the rocks attained their peak metamorphic grade progressively later in the development of the thrust belt. Figure 8.3 shows how stacking of thrust sheets at the base of the thrust wedge at the time they reach their metamorphic peak, is likely to preserve an inverted metamorphic gradient across the thrusts without inversion of isotherms at any point in time. In the figure a configuration of the isotherms is assumed, similar to that presented by Karabinos and Ketcham (1988) and comparable to certain configurations in thermal models by Shi and Wang (1987) and Barr and Dahlen (1989). Distortion of the isotherms due to the thrust activity is continuously counteracted by thermal relaxation, which results in a stable configuration of the isotherms across the thrust surface during thrusting. The geometry of the isotherms is interpreted to be dependent on thrust velocity (strain rate), erosion rate, internal heat production and conduction, but is independent of the displacement on the thrust (finite strain).

The isobars are parallel to the surface of the thrust wedge, dipping shallowly to the left. They are omitted in the figure, but have the same trends of displacement through the rocks as the isotherms, directly reflecting the thickness of the overburden. Isotherms and isobars together define a pattern of isograds. From A to B in Figure 8.3 the basal thrust cuts into the footwall, thus incorporating a new thrust sheet into the wedge. Diagram A shows the future position of the thrust. In diagram B the sole thrust of the wedge is on the verge of cutting down again to incorporate another thrust sheet. Subsequent stacking of thrust sheets in this fashion not only causes inverted metamorphic gradients and metamorphic breaks at the thrusts, but also a regionally inverted gradient through the thrust stack.

**Fig. 8.3** Cartoon of the thermal development at the base of a thrust wedge during underplating, showing inversion of the metamorphic gradient. A and B show in cross section the configuration of isotherms (labelled 1 through 5, from coldest to hottest) near the floor thrust of the thrust wedge at two different times, before and after the incorporation of a thrust sheet. The location of the section is shown in Figure C. The hanging wall moves to the left, the footwall is stationary. The hanging wall cools and decompresses as a result of erosion and the isotherms sink with respect to the moving material points. In the footwall P and T increase as a result of the movement of the thrust wedge, placing a progressively thicker and warmer overburden on top, and the isotherms rise with respect to the material points. It is assumed that the isotherms retain a stable configuration. Isotherms 4 and 4' are emphasized and marked with arrows to highlight the displacement. D shows schematic P-T paths of four points near the base of the thrust wedge, which are marked in Figures A and B. The solid parts of the paths represent the step from stage A to stage B. The arrows with the short and long dashes indicate the P-T paths before stage A and after stage B respectively. A scale and actual temperatures are omitted to make the figure more generally applicable.



The footwall of the basal thrust experiences prograde metamorphism due to the movement of the thrust wedge, progressively increasing the thickness of the overburden and moving progressively warmer rocks on top. As a result, the isotherms in the footwall rise with respect to the material points. This is shown in Figure 8.3 B, where both the present and previous locations of the isotherms are shown. Since the metamorphic grade is rising, the rocks in the footwall will not record the old locations of the isograds (combined isotherms and isobars), except in certain situations in zoned garnets. The metamorphic grade in the hanging wall decreases as a result of unroofing of the wedge and emplacement of the wedge on progressively cooler rocks in the footwall, resulting in a configuration similar to that of a heat exchanger. The isotherms (and isobars) in the hanging wall fall with respect to the material points above the floor thrust, but they rise with respect to the stationary rocks in the footwall, to preserve their stable shape (Karabinos and Ketcham, 1988). The material points in the hanging wall move faster upwards than the isotherms. For a thrust sheet that is incorporated into the thrust wedge this means that it reaches its metamorphic peak at the moment that it is incorporated. With regard to the pressure, the switch from footwall to hanging wall is reflected instantaneously. Both Rice (1987) and Karabinos and Ketcham (1988) suggest there is a time lag before the temperature starts decreasing after incorporation of the thrust sheet, causing the P-T paths to form a loop, resulting in separate pressure and temperature peaks. The hairpin shaped P-T paths obtained from Gagnon terrane exhibit one common pressure and temperature peak, suggesting that the time lag was very short.

In contrast to the rocks in the footwall, the recently incorporated thrust sheet preserves the configuration of the isograds as its peak metamorphic conditions, because after accretion the pressure and temperature decrease. The rocks in the footwall will attain their metamorphic peak later, when they are subsequently incorporated into the thrust wedge. Consequently, the metamorphic field gradient observed in the rocks presently does not represent the thermal configuration at one point in time, but the peak

conditions of the thrust sheets as they were successively accreted to the evolving thrust wedge. The metamorphic peak swept through the thrust stack from the back to the front of the wedge in the same sequence as the thrust sheets were stacked.

In Figure 8.3 a simplified P-T path, consisting of vectors, is shown for four material points (A to D) in the section. The solid arrows in the P-T paths represent the step from diagram A to B. In the development following the situation in diagram B, juxtaposed points have a common retrograde P-T path. Points A and B are located in the footwall and show prograde metamorphism, but in diagram B they are on the verge of becoming part of the hanging wall and have thus reached their metamorphic peak. Points C and D were incorporated in the thrust wedge in diagram A and their metamorphic P and T declined from there on. The points closest to the front of the wedge (A and C) have a slightly lower metamorphic peak than their counterparts further back (B and D). Of more importance is the significant difference in metamorphic peak between points in the hanging wall and the footwall. Although at no point in the development a discontinuity of the pressure or temperature gradient is inferred across the basal thrust, the final metamorphic gradient recorded in the rocks, as observed in the field, will show a break in peak metamorphic pressure and temperature across the floor thrust of the thrust sheets. The metamorphic field gradient is inverted although at any time of the development both pressure and temperature increased downwards.

As a consequence of the model presented, a point in the footwall near the basal thrust cannot attain as high maximum temperatures and pressures as a point in the hanging wall immediately overlying it. The maximum metamorphic grade of the footwall is determined by the thickness of the hanging wall directly overhead at the time that thrust movement between the two stopped. As a result of erosion the thickness of a rock column in the hanging wall decreased from the moment that it became part of the hanging wall. That constantly decreasing column of rock cannot cause as high a metamorphic grade in an adjacent point in the footwall as the maximum P and T

recorded at its base, resulting in inversion of the metamorphic gradient. Within individual thrust sheets, the P and T increase downwards. Inversion occurs only at the thrusts, in steps.

Inversion of the metamorphic gradient and the break in the gradient at a thrust are inherent to piggy-back sequence thrust stacking at the base of a thrust wedge. Only if boundary conditions of the model shown here are changed in such a way that the metamorphic grade in the rocks increases significantly after being accreted to the hanging wall, will inversion not be recorded. This would happen if the rocks were buried deeper after accretion, in a downward-directed particle path within the thrust wedge (Barr and Dahlen, 1989). Since inversion of the metamorphic gradient is a phenomenon recorded in many collisional orogenic belts the qualitative model presented here seems valid.

Most numerical models have failed to explain inversion of the metamorphic gradient in this way. Oversimplifications in the assumptions of the boundary conditions, e.g. instantaneous thrust emplacement (England and Thompson, 1984; Davy and Gillet, 1986), lack of erosion during thrust emplacement (Shi and Wang, 1987), have prevented the occurrence of inversion in these models. Barr and Dahlen (1989) have shown that beneath the basal thrust of their model a temperature inversion occurs when shear heating is introduced in the model, but in no part of the overlying thrust wedge is overturning of the metamorphic gradient recorded in their model. The model presented by Karabinos and Ketcham (1988) does account for the metamorphic inversion, but this aspect of their model was not discussed.

#### **8.1.5.3 Crustal thickening in the basement**

The Parautochthonous Belt in the eastern part of the Grenville Province is characterized by a negative gravity anomaly, which trends parallel to the Grenville Front (Wynne-Edwards, 1972; Rivers et al., 1989). This gravity low is a remnant of Grenvillian crustal thickening. In Gagnon terrane of southwestern Labrador the stacking of Molson Lake terrane on top of rocks of lithotectonic domain V can provide a few kilometers extra thickness of the crust. However, the gravity low is more

widespread than the possible overlap of the two terranes and occurs also farther west. Stacking of thrust sheets of the shelf sediments gives only an increase of thickness in the order of hundreds of meters. Stacking of basement thrust sheets in the lower thrust system is also not expected to result in a significant increase of crustal thickness, as can be seen in the cross sections in Figure 1B (in pocket). The interpretation that the basement thrust stack changes at depth into a zone of ductile deformation which accomplishes significant shortening, could explain the increase of crustal thickness. At depth, the basement system could look very much like the Parautochthon as it is exposed near Georgian Bay in central Ontario, where the Grenville Front marks the northwestern boundary of a 15 to 30 km wide shear zone in medium to high grade metamorphic granitoids of the Parautochthonous Belt, which are juxtaposed against virtually pristine equivalent intrusive rocks (Davidson, 1986; see also Section 8.4).

#### **8.1.5.4 Calculations of displacement and shortening**

In a simple line-balancing exercise, van Gool et al. (1987b) calculated for the central part of the map area in lithotectonic domains II, III and IV a shortening of 50 to 66%. If these numbers are assumed for the whole belt, this would restore the width of the upper thrust system, which is presently about 20 km wide as exposed, to a width of about 40 to 60 km. Similar simple calculations can be done using geobarometric data and an assumed shape of the thrust wedge. Since the thickness of the sediments is minimal compared to the size of the thrust wedge, locations in the sediments can be assumed to be at the bottom of the thrust wedge. The taper of the thrust wedge is taken as  $11^\circ$ , which is the maximum angle for critical thrust wedges at upper crustal levels (Woodward, 1987). Tapers for crystalline thrust sheets are assumed to be smaller (Hatcher and Hooper, 1992), thus the  $11^\circ$  is an over estimation, which will give a minimum for the actual displacements and shortening. The pressures used for the calculations are the peak pressure in the Wabush Lake thrust sheet at Blueberry Hill of 11 kbar and in the Rivière aux Fraises area of 6.4 kbar, which give crustal depths of about 30 and 17 km respectively, using an average density of the crust of  $2.7 \text{ g/cm}^3$ . These two points (samples 88-80 and 87-120, see Figure F.3, Appendix F) were chosen

because they lie approximately along the line of displacement. Figure 8.4 schematically shows the configuration used for the calculations. For the calculations the basal thrust is assumed to be horizontal and the taper is caused by surface topography. These simplifications introduce only a negligible error.

A thrust wedge with a taper of  $11^\circ$  that is 30 km thick above the eastern part of Gagnon terrane had a length of 154 km between the control point in the Wabush Lake thrust sheet to its tip in the northwest. The actual displacement of the wedge over the rocks of the Gagnon terrane must have been larger than this number, since the root of the wedge lies further to the southeast. The horizontal distance between a point buried under 30 km and a point under 16 km is 67 km. This calculation assumes that the peak metamorphic pressure was attained in both points at the same time. In previous sections it was shown that the peak of the metamorphism propagated from southeast to northwest, which means that considerable shortening took place between the time that the two control points reached their respective metamorphic peaks. The 67 km is therefore a minimum and the real original distance between the two points is assumed to be significantly larger. The present horizontal distance between the two points is 23 km, indicating a shortening of about 66%.

This amount of shortening fits with estimates derived from line balancing in the lower thrust sheets, but recalling that 67 km is only a minimum for the restored distance between the two points, the actual shortening for the higher lithotectonic domains may be significantly larger than in the lower domains. This is in accord with the strain increase towards the higher thrust sheets reported in Chapter 5 and with the increase in strain towards the rear of a thrust wedge as suggested by Chapple (1978).

## 8.2 THE TRANSPRESSIVE SETTING OF THE BELT

The structural trend of the Grenville Front on the scale of the whole orogen is approximately ENE ( $065^\circ$ , Fig. 1.1). This is at a high angle to the inferred direction of thrusting in many places in the orogen, which is fairly consistently towards the NNW (several references in Moore et al., 1986). In the map area the trend of the belt varies from NNE ( $035^\circ$ ) in the south to NE ( $050^\circ$ ) in the northern part of the map.

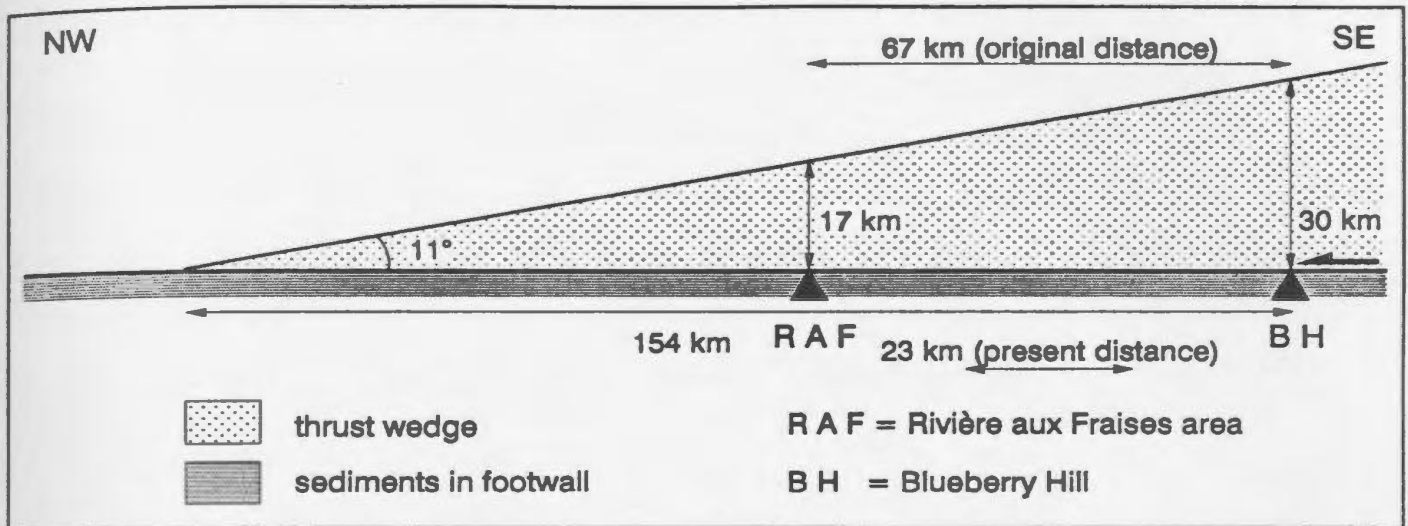


Fig. 8.4 Schematic diagram of the dominant overriding thrust wedge and the underlying sediments of the Gagnon terrane, showing the dimensions of the thrust wedge and the calculated original distance between points in the Wabush Lake thrust sheet at Blueberry Hill and in the Rivière aux Fraises area. The calculations are based on maximum estimated metamorphic pressures. For explanation see text.

Figure 1.1 shows that the map area is situated at the transition between a re-entrant to the northeast and a promontory to the southwest. This places the fold-and-thrust belt in a locally transpressional setting, with the movement direction oblique to the trend of the belt. This is reflected in the oblique nature of the structures as well as the metamorphic zonation in the belt.

In Chapter 5 the oblique nature of the  $S_1$  foliation planes and the  $F_2$  folds with respect to the trend of the belt was discussed. The orientations of the elongation lineations at a relatively small angle to the trend of the belt reflect the oblique convergence of the orogenic front and the craton. The orientation of the continental margin was mainly determined by the block fault system, forming a combination of extensional and transfer faults. The orientation of the block fault system is reflected in the thrust faults in the basement, which are interpreted as reactivated extensional faults.

The oblique collision of the belt is also reflected in several kilometer-scale strike-slip fault zones in the thrust wedge, of which the Flora Lake shear zone is an example. Several other fault zones of the same sinistral displacement and the same magnitude exist south of the map area (Indares, in press; pers. comm., 1991) and the shear zone through Seahorse Lake, separating Molson Lake terrane from the Wabush Lake thrust sheet, is possibly another fault zone of this set. Figure 8.5 shows schematically how these faults accommodated the oblique convergence. The structural front of the thrust wedge approaching from the south-southeast is assumed to have been originally orthogonal with respect to the movement direction as shown in diagram A. When moving onto, and partially incorporating, the continental margin, the western-most parts of the thrust wedge moved furthest up the continental slope and were left behind with respect to the remainder of the thrust belt (B and C). In diagram D the sole thrust of the system has stepped down into the basement and the north-northwest-directed thrust movement progresses by oblique-reverse reactivation of the extensional faults in the basement of the Superior craton.

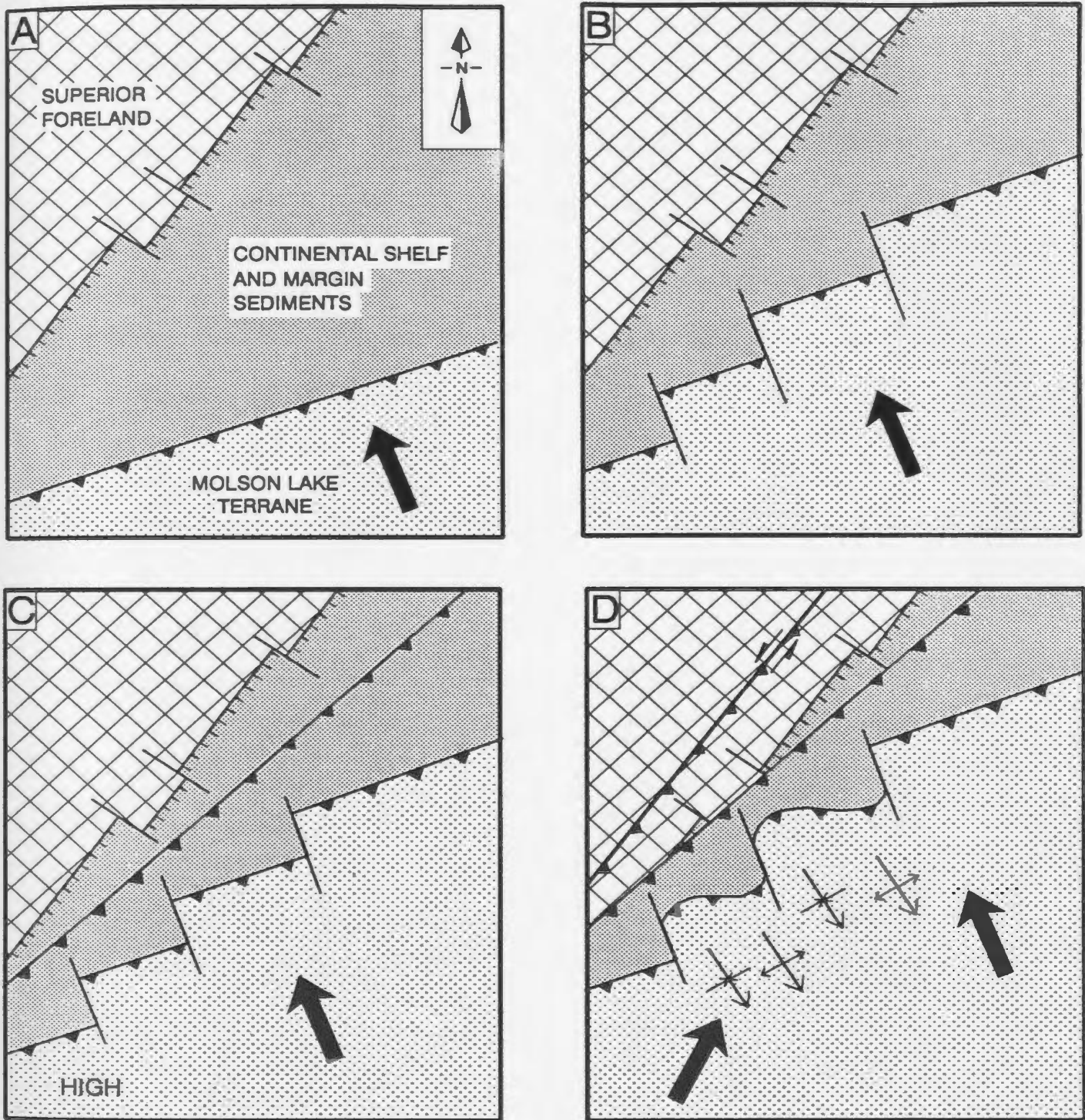


Fig. 8.5 Schematic model for the transpressive setting and oblique convergence of Molson Lake and Gagnon terranes and the Superior foreland. Figures A and B show the foreland-directed thrusting of the Molson Lake terrane. Figures C and D represent the incorporation of the metasediments and the basement rocks, respectively, into the thrust wedge. The oblique convergence caused the formation of a set of strike-slip faults in B. The buildup of a topographic high in the southwest (C) resulted in gravitational spreading towards the northeast, causing  $F_3$  folding (D). Note that the structures are drawn at the present erosion level. The actual tip line of the Molson Lake terrane is expected to have been located tens of kilometers further NW at the end of the orogeny.

In the last two diagrams in Figure 8.5 the inferred origin of the  $F_3$  folds is also indicated (cf. Rivers, 1983a). In the southwest of the approaching thrust wedge, a topographic high formed as a result of: 1) this part of the thrust wedge having moved furthest up the continental slope and consequently having the highest elevation; 2) thrust movement being impeded in this part of the belt and shortening presumably being accommodated by internal thickening of the thrust wedge. The presence of this high changed the topographic slope of the thrust wedge in the southwest of the diagram from its original north-northwest dip to an east-northeast dip. This slope is interpreted to have caused a component of movement in this direction, probably by gravitational spreading (Ramberg, 1981) in an orientation at a high angle to the direction of movement of the thrust wedge, causing the  $F_3$  folding in the area to the east of the high, in the central part of the diagram, which corresponds with the southeastern part of the map area.

Another effect of the transpressional setting of the belt is the oblique nature of the metamorphic zonation (Figure 4.2). Along the strike of the continental margin, which presently also defines the strike of the thrust belt in the map area, from northeast to southwest the thrust wedge had overridden the margin progressively longer distances, and as a result the thickness of the overburden increased in this direction. This effect was enhanced by the thickening of the wedge in the southwest as argued in the previous paragraph. As a result the peak metamorphic grade of the rocks not only increased from the lowest thrust sheets to the highest, but also along strike of the belt from north-northeast to south-southwest. Thus, the present erosional level of the belt provides an apparent oblique erosional cut through the belt, giving indirect information about the development of the belt in the third dimension.

### 8.3 IMPLICATIONS FOR THE REGIONAL TECTONICS

Gagnon terrane contains metasediments that were deposited on the eastern margin of the Superior craton during the Early Proterozoic. The sediments were deposited in a rift-basin, but no evidence for a true oceanic basin has been found. Wardle and Bailey (1981) proposed that a proto-oceanic basin may have existed. The occurrence of rocks

of the Shabogamo Intrusive Suite, dated at 1429 Ma. (Brooks et al., 1981; Connelly et al., 1990) in both Gagnon and Molson Lake terranes, links these two terranes before the Grenvillian orogeny. Moreover, rock types from both terranes can be traced into the foreland, which means that they did not constitute two separate continental plates at the onset of the Grenvillian orogeny. The Grenvillian orogeny caused the two crustal blocks that were laterally juxtaposed to be superimposed (Fig. 8.6). The nature of the transition between the two terranes before thrusting is unknown. Possibly the granitoids that dominate Molson Lake terrane intruded the continental margin sediments east of those that presently make up Gagnon terrane.

The problem arises that Molson Lake terrane in its present form, does not form a crustal wedge up to 30 km thick, required to cause the peak metamorphic pressures in the Wabush Lake thrust sheet. However, Connelly (1991) and Indares (in press) have shown that the peak metamorphic pressures in Molson Lake terrane range up to 12 and 16 kbar (increasing towards the south) which indicates that during the Grenvillian orogeny Molson Lake terrane was at the bottom of a thrust stack up to about 45 km thick, which is sufficient to form a 30 km thick thrust wedge above the eastern part of Gagnon terrane.

These observations make the Grenvillian orogeny in southwestern Labrador an event of superposition and telescoping of terranes, resulting in significant crustal shortening. Peak metamorphic pressures determined in this work and by Connelly (1991) and Indares (in prep), as well as the interpreted reactivation of the extensional fault system in the basement indicate that tectonic activity took place on a crustal scale. The actual driving force for the tectonic movements is still an enigma, to which this thesis can provide little input. A possible collision zone will have to be sought to the southeast of the Parautochthonous terrane.

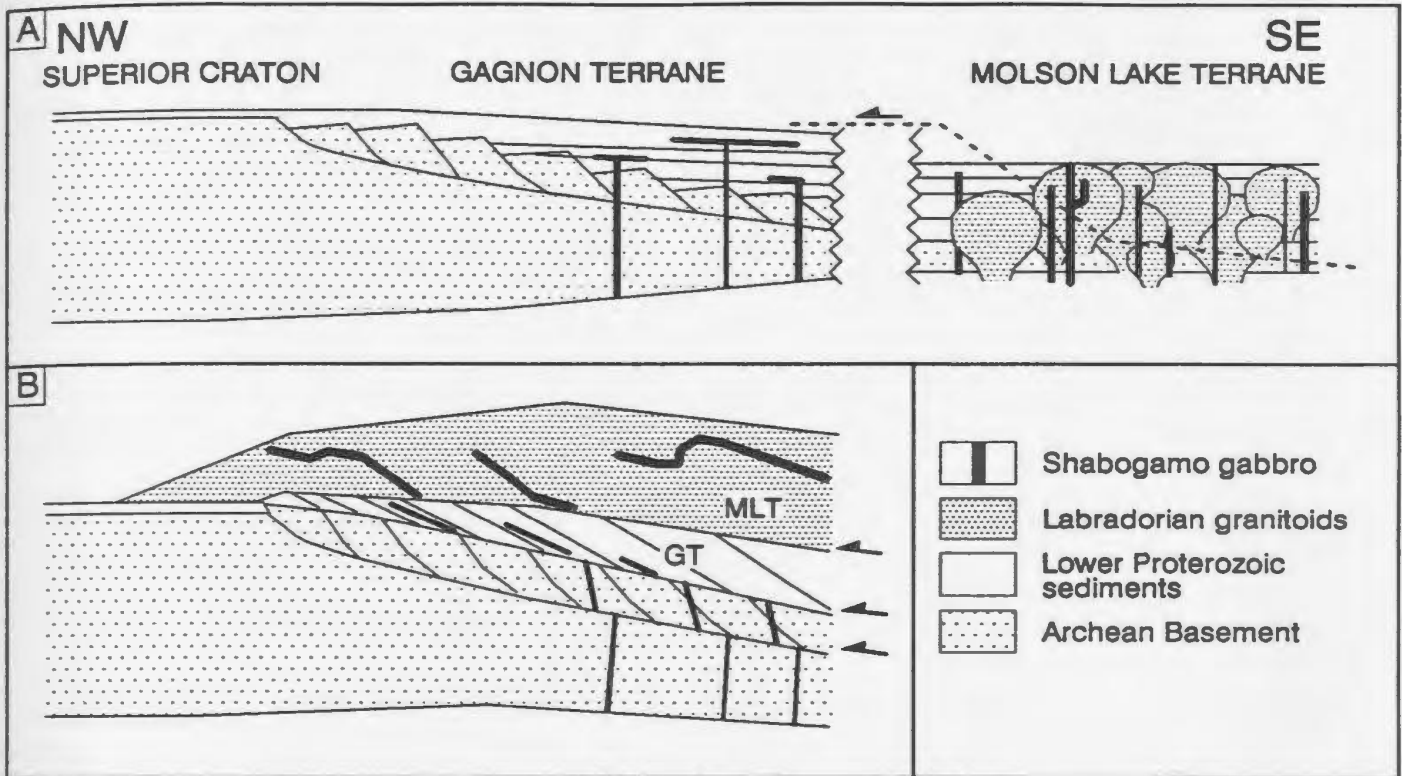


Fig. 8.6 Cartoon showing the relative positions of Gagnon and Molson Lake terranes before (A) and after (B) the Grenvillian thrusting. The rocks of Gagnon terrane originated on the continental shelf and slope. The intrusive rocks in Molson Lake terrane are inferred to have intruded the eastern continuation of the slope sediments.

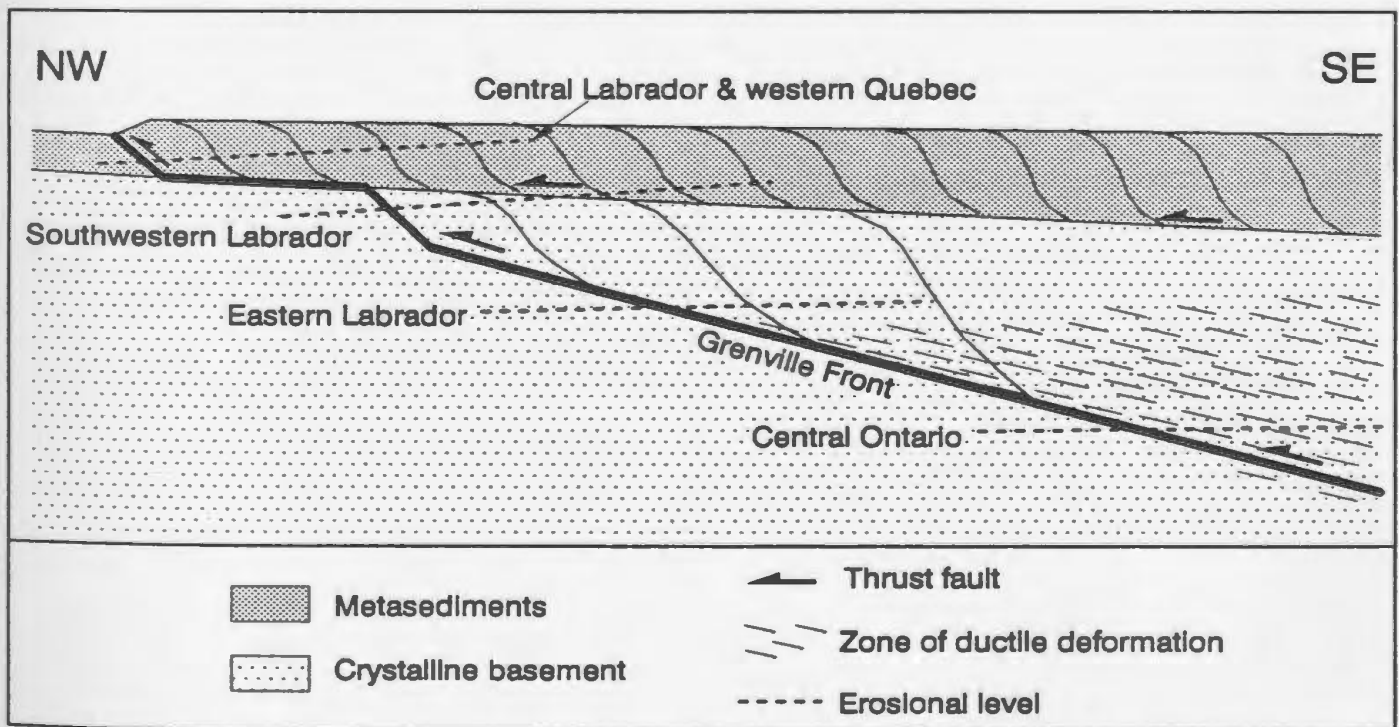


Fig. 8.7 Sketch of a thrust belt which involves both basement and cover rocks, with different erosion levels for the different parts of the Grenville Front.

#### **8.4 COMPARISON WITH THE GRENVILLE FRONT AND PARAUTOCHTHONOUS BELT ELSEWHERE IN THE GRENVILLE PROVINCE**

Rivers et al. (1989) defined the Parautochthonous Belt in the Grenville Province as a tectonic belt that truncates structures in the foreland at the Grenville Front, containing rock types that can be correlated across the Front. The rocks of the Parautochthonous Belt were emplaced onto the foreland by northwest directed thrust movement on the southeast-dipping Grenville Front, but the lithological continuity with the foreland precludes major thrust displacements. Strike slip movement on the Grenville Front has also been recognized, as e.g. in the Otish Mountains (Chown, 1979). Stacking of thrust sheets, mylonitization, development of L-S tectonites and an increase of the metamorphic grade towards the southeast up to upper amphibolite facies, are phenomena that have been described for most parts of the Grenville Front and the adjacent Parautochthonous Belt. Apart from these general characteristics the structural and metamorphic style varies considerably along the trend of the orogen, as is revealed below in examples of the geology of the Parautochthonous Belt in several parts of the Grenville Province. A thorough comparison of the tectonics of the Grenville Front and the Parautochthonous Belt in southwestern Labrador and the remainder of the Grenville Province is hampered somewhat by the fact that this is the first study of Grenville Front tectonics that comprehensively combines structural and metamorphic data in great detail and similar detailed information is not available from elsewhere in the Parautochthonous Belt.

At the coast in eastern Labrador, the northern boundary zone of the Grenville Province is marked by two major thrust fault zones, the Benedict fault and the Cut Throat Island fault, which accommodate most of the thrust displacement (Owen et al. 1986). The Grenvillian metamorphic and structural imprint increase gradually from just north of the Grenville Front towards the south, but are telescoped by the two faults. The rocks in the Parautochthonous Belt in eastern Labrador are granulites of the Makkovik Province and intrusive rocks of the Trans Labrador Batholith.

The geometries of the structures described by Brown (1991) in the northeastern part of Gagnon terrane and by Calon and Hibbs (1980) in central Labrador in rocks of the Seal Lake group are similar to those of the upper thrust system in southwestern Labrador, but no basement was involved in the deformation. Folding post-dated the thrusting and occurred on a large scale. In the northeastern part of Gagnon terrane the Grenvillian thrust stacks and fold nappes overprint older Hudsonian structures in rocks of the Knob Lake Group and out-of-sequence thrusts play an important role in the thrust emplacement (Brown, 1991).

In western Québec, south of Val-d'Or, a wide zone with an increasing metamorphic grade towards the southeast is cut by a number of thrust faults, which form thrust slices that are many kilometers thick and which create an inverted metamorphic gradient (Indares and Martignole, 1989). The thrusting in this area affected rocks of the Abitibi Greenstone Belt.

In central Ontario near Killarney, the Grenville Front is characterized by a break in Grenvillian metamorphic grade from unmetamorphosed foreland to upper amphibolite facies (Davidson, 1986). The Grenville Front is formed by one major structural discontinuity, which in seismic sections can be traced into the lower crust (Green et al., 1988). Southeast of the discontinuity lies a 15 to 30 km wide zone of mylonitic rocks, principally granitoids, at amphibolite facies (Davidson, 1986).

None of these examples mentioned above shows the same configuration of a dual thrust system as seen in southwestern Labrador, which means that either this is a unique situation, or it is a result of the fact that in none of the examples the erosion level cuts through both cover and basement rocks. In spite of the variety of tectonic styles, all situations qualify as foreland thrust belts, but fall into one of two groups: 1) metasedimentary belts (Central and western Labrador and western Quebec) and 2) high grade gneissic and granitoid belts (eastern Labrador and central Ontario). The upper and lower system in southwestern Labrador fall into the first and second group respectively. Thrust belts of the first group exhibit thin-skinned thrust sheets with multiple stacking of thrust sheets or fold nappes, and a gradual transition in

metamorphic grade. Folding was an important style of deformation in the metasediments. In the second group crustal shortening was concentrated in few major shear zones with reverse displacement and significant breaks in the metamorphic grade. Obviously the rheology of the rocks played an important role on the geometry of the belt and the rock type and possibly pre-existing structures in the foreland determined the style of deformation during development of the belt.

The main difference between the separate parts of the Grenville Front and the Parautochthonous Belt is interpreted to be the level of the erosional cut (see also Rivers, 1992). The examples in group 1 comprise rocks exhumed from deep crustal levels, representing the parts of thrust belts in which crystalline basement rocks predominate, whereas the examples from group 2 involve cover rocks found in the higher levels of developing thrust belts. This is schematically shown in Figure 8.7. In the map area in southwestern Labrador both levels are exposed. Of course, other factors besides erosional level, e.g. lithology, stratigraphy, strain rate and total displacement, determine the differences between the different parts of the Grenville Front. As is suggested in Figure 8.7, the basement thrust system in the map area may represent a high level equivalent of the structures at both extremities of the Grenville Province as was suggested in Section 8.1.5.3.

## **8.5 GAGNON TERRANE AS A CRYSTALLINE FORELAND FOLD-AND-THRUST BELT**

Gagnon terrane contains rocks that can be traced into the foreland across the Grenville Front. In this respect the term *foreland* fold-and-thrust belt is applicable. In most other aspects the thrust system resembles crystalline belts in the interiors of other orogenies. The fold nappe geometry of some thrust sheets and the ductile nature of the deformation classifies the sheets as "type F" in the classification of Hatcher and Hooper (1992). In this aspect Gagnon terrane is quite unique as a foreland fold-and-thrust belt. The thrust stack and duplex geometry is on the one hand similar to that in foreland belts such as the Moine thrust belt (Elliott and Johnson, 1980) and the Helvetic nappes in the external parts of the Swiss Alps (Milnes and Pfiffner, 1980), but on the other hand, the

ductile nature of the deformation and the high metamorphic grade are more similar to internal belts in orogens, e.g. the Moine nappe in Sutherland, northern Scotland (e.g. Barr et al., 1986), the Caledonides in Scandinavia (e.g. Burton et al., 1989) or the Variscan nappes in southern Brittany, France (Vauchez et al., 1987).

St. Onge and Lucas (1990) described thrusting in the Early Proterozoic Cape Smith belt in the northeastern Canadian Shield, which shows a similar situation of imbricate thrust stacks in rocks that deformed by ductile processes at greenschist to amphibolite facies. They suggested that the ductile deformation postdated early brittle formation of the thrusts. The thrusts formed zones of weakness along which the ductile shear zones developed during prograde metamorphism. No significant amount of basement rocks was involved in the thrusting. The Kaavi area in the Svecokareliides in eastern Finland (Park and Doody, 1990) is a deep level foreland thrust belt that has many similarities with Gagnon terrane. The belt has thrust geometries similar to high level thrust belts, with sediment-dominated duplexes underlain by larger scale basement duplexes, both formed at metamorphic grades up to high amphibolite facies. Post-thrusting folding on a large scale is more widespread in the Kaavi area. Park and Doody (1990) argued that thrusting occurred at peak metamorphic conditions by ductile shearing, but did not justify the brittle geometry of the ductile structures.

Localization of strain in narrow zones is less common in rocks that deform at medium to high metamorphic conditions, than in rocks at sub-metamorphic grades in higher levels of the crust. Several explanations could be given for the dual character of ductile rheology and brittle morphology of the thrust belt in southwestern Labrador, of which the most important are discussed here. The simplest explanation is that the duplex and thrust stack geometry is not restricted to deformation at high levels of the crust (Park and Doody, 1990; Hatcher and Hooper, 1992) and extremely thin shear zones (tectonic slides, Fleuty, 1964) constitute the actual discontinuities that form the thrust planes. The thrusts can form on mechanical discontinuities that cause strain

localization, for example a basement-cover contact or the brittle-ductile transition (Hatcher and Hooper, 1992) or on pre-existing zones of weakness (St. Onge and Lucas, 1990).

The basal detachment of the upper thrust system in Gagnon terrane lies at or close to the basement-cover contact. Strain incompatibility between the crystalline basement rocks and the overlying metasediments localized the strain on this surface. In the lowest thrust sheets subsidiary thrusts splay off the floor thrusts, whereas in the higher thrust sheets at amphibolite facies folding becomes the mechanism for shortening within the thrust sheets. The subsidiary thrusts in the northwestern part of the map area may have originated at an early stage of the development, when metamorphic grades were lower, but no signs of early brittle deformation were observed, as noted before. High strain rates, which were implied in Section 8.3, could have played a major role in the localization of the strain in thrust planes and the formation of imbricate thrust stacks and duplexes. In the lower thrust system, the pre-existing extensional fault system provided a linked system of zones of weakness with a geometry that was similar to that of an imbricate thrust stack and during the late stages of the development of the thrust belt these faults were reactivated as ductile shear zones.

## **8.6 SUGGESTIONS FOR FUTURE RESEARCH; TESTING OF THE MODEL**

This study presents a comprehensive model of the tectonic and metamorphic development of the thrust belt in southwestern Labrador. However, several questions remain unanswered, assumptions remain to be tested and details of the model are not addressed. This is partly due to the nature of the study, in which only parts of the area under discussion were mapped in detail, and partly due to lack of outcrop in some critical areas, especially the thrust sheet boundaries. Addressing any of the following items could refine the proposed model.

The existence of an extensive pre-Grenvillian extensional fault system has not been proven. Two well-exposed extensional faults in the map area and many structures

that can be interpreted to be related to pre-existing extensional faults suggest the existence of such a fault system. Grenvillian overprinting of possible Early Proterozoic faults will hamper verification of the interpretation in the map area. However, towards the northwest of the Grenville Front these structures may be preserved without Grenvillian overprint, as documented in one example in the northern part of the Labrador Trough (Dimroth, 1978).

The effects of tectonic events between the Early Proterozoic and the Grenvillian orogeny have not been addressed in this study. The Labradorian orogeny, which has been well documented in the overlying Molson Lake and Lac Joseph terranes, has not been reported from Gagnon terrane. In the western part of the map area no more than one phase of deformation is revealed in the rocks. Foliations overgrown by garnets in the Wabush Lake thrust sheet indicate a deformation event before the Grenvillian metamorphic event, which may be either pre- or early Grenvillian. Since this foliation is obliterated outside the garnets, it is impossible to determine its age. Likewise, no observations have been made of a middle Proterozoic tectonic event linked to the intrusion of the Shabogamo Gabbros.

The geometry of the belt has only been observed in two dimensions. The continuation of structures in the subsurface can locally be reconstructed, but in the greater part of the map area it is interpreted. Modelling the structures using aeromagnetic or gravity data could provide additional information. Seismic data would be valuable in a reconstruction of the structures in the thrust belt in the subsurface. A proposed transect through western Labrador and Eastern Quebec in the Lithoprobe program could provide extremely important information about the geometry of the thrust belt in the third dimension.

Besides geophysical research, other means could be used to test the validity of the proposed model. Numerical modelling of the thermal development of the thrust belt could indicate whether the determined P-T paths are consistent with the geometrical development. A more detailed study of the variations of P-T paths through the belt would better constrain the metamorphic history, especially if attention were paid at

transitions across major shear zones. A detailed geochronological study could quantify the progression of metamorphism and uplift and would create a better link of the evolution of Gagnon terrane with that of the overlying terranes as described by Connelly (1991).

## 8.7 CONCLUSIONS

Gagnon terrane in southwestern Labrador constitutes a Grenvillian-age, foreland fold-and-thrust belt which consists of two separate thrust systems. The upper system is an extremely thin stack of thrust sheets which acted as a large scale ductile shear zone on which the overriding Molson Lake terrane moved towards the north-northwest. The lower system consists of an imbricate stack of kilometer-size basement sheets, which is assumed to change downwards, underneath the upper system where it is not exposed, into a wide zone of plastically deformed rocks.

All deformation and metamorphism in the Gagnon terrane in the map area was a result of the emplacement and northwest-directed thrust movement of a thrust wedge, consisting of Molson Lake terrane. A first phase of deformation ( $D_1$ ), the development of an L-S shear fabric, occurred in the footwall and near the base of the thrust wedge, mainly under prograde metamorphic conditions. Accretion of thrust sheets occurred at the peak of metamorphism. The deformation of the rocks after incorporation into the thrust wedge ( $D_2$ ), predominantly folding and out-of-sequence thrusting, was a result of adjustments of the shape of the thrust wedge to maintain its critical taper and took place under retrograde metamorphic conditions.

This study has shown that basement rocks in Gagnon terrane are much more widespread than realized by previous workers. These rocks and the pre-Grenvillian extensional fault system that cuts them were an important factor in the development of the thrust belt and its final geometry. The discovery that a many-kilometer wide belt of basement rocks west of the metasediments was part of the thrust belt resulted in a new location of the Grenville Front locally in the map area, about 5 to 8 kilometers west of

its previous location near the basement-cover boundary. Shortening of basement rocks underneath the exposed level of Gagnon terrane is presumed to have resulted in thickening of the crust.

The location of the map area between a salient and a promontory resulted in a transpressive regime and structures as well as the metamorphic gradient are oblique with respect to the trend of the belt. It also resulted in the formation of large strike-slip shear zones and kilometer scale cross-folds.

Detailed geothermobarometry applied to zoned porphyroblasts, combined with detailed microstructural analysis, can provide a powerful tool to reconstruct the thermotectonic development of orogenic belts. It was shown that in garnets that preserved both prograde and retrograde zoning, chemical profiles can be used to reconstruct P-T paths and that P-T vectors from core and rim analyses can give spurious results. Variations in the relations between deformation and P-T paths through the map area were used to show that emplacement of Molson Lake terrane on top of Gagnon terrane caused prograde metamorphism in the latter and incorporation of thrust sheets in the thrust wedge initiated retrograde metamorphism.

The importance of underplating as a mechanism of accretion of material to a thrust wedge was emphasized. The underplating is interpreted to counteract accretion of material at the toe of the thrust wedge and erosion at the top. Underplating is presumed to be a mechanism for the creation of an inverted metamorphic gradient in this and other metamorphic fold-and-thrust belts.

This thesis has documented that geometries that were introduced for upper-crustal level thrust belts are to a large extent also applicable to fold-and-thrust belts of mid-crustal levels which deform in a ductile fashion. The processes and geometries described here could be expected to be found in thrust belts of which the higher levels are exposed today, but which have a sole thrust that reaches mid-to-lower crustal levels. This has major ramifications on the use of mechanical models for such thrust belts, since they should incorporate both brittle processes at the upper levels and ductile processes at the lower levels of the belt.

## REFERENCES

- Anovitz, L.M. and Essene, E.J., 1990: Thermobarometry and pressure-temperature paths in the Grenville Province of Ontario. *Jrnl. Petrol.*, 31, p.197-241.
- Armstrong, R.L. and Dick, H.J.B., 1974: A model for the development of thin overthrust sheets of crystalline rocks. *Geology*, 2, p.35-40.
- Baer, A.J., 1971: Reappraisal of the Grenville "Orogeny". *Geol. Assoc. Can. Ann. Mtg.*, Sudbury, 1971, Program and abstracts, p.3.
- Baer, A.J., 1981: A Grenvillian model of Proterozoic plate tectonics. In: *Precambrian Plate Tectonics*, A. Kröner (Ed.), *Developments in Precambrian Geology*, 4, Elsevier, p.353-385.
- Banks, C.J. and Warburton, J., 1986: 'passive-roof' duplex geometry in the frontal structure of the Kirthar and Sulaiman Mountain belts, Pakistan. *Jrnl. Struct. Geol.*, 8, p.229-237.
- Barr, D., Holdsworth, R.E. and Roberts, A.M., 1986: Caledonian ductile thrusting in a Precambrian metamorphic complex: The Moine of northwestern Scotland. *Geol. Soc. Am. Bull.*, 97, p.754-764.
- Barr, T.D. and Dahlen, F.A., 1989: Brittle frictional mountain building 2. Thermal structure and heat budget. *Jrnl. Geoph. Res.*, 94 (B), p.3923-3947.
- Beaumont, C., Fullsack, P. and Hamilton, J., 1992: Erosional control of active compressional orogens. In: *Thrust Tectonics*, K.R. McClay (Ed.), Chapman and Hall, London, p.1-18.
- Behrmann, J.H., 1987: A precautionary note on shear bands as kinematic indicators. *J. Struct. Geol.*, 9, p.659-666.
- Bell, T.H., 1985: Deformation partitioning and porphyroblast rotation in metamorphic rocks: a radical reinterpretation. *J. Metam. Geol.*, 3, p.109-118.
- Bell, T.H. and Etheridge, M.A., 1973: Microstructure of mylonites and their descriptive terminology. *Lithos*, 6, p.337-348.
- Bence, A. E. and Albee, A.L., 1968: Empirical correction factors for the electron microanalysis of silicates and oxides. *J. Geol.*, 76, p.382-403.
- Berman, R.G., 1988: Internally consistent thermodynamic data for minerals in the system  $K_2O-Na_2O-CaO-MgO-FeO-Fe_2O_3-Al_2O_3-TiO_2-H_2O-CO_2$ . *J. Petrol.*, 29, p.445-522.
- Berthé, D., Choukroune, P. and Jegouzo, P., 1979: Orthogneiss, mylonite and non-coaxial deformation of granites: the example of the South Armorican shear zone. *J. Struct. Geol.*, 1, p.31-42.
- Bethune, K.M. and Davidson, A., 1988: Diabase dykes and the Grenville Front southwest of Sudbury, Ontario. *Current Research, part C, Geol. Survey Can.*, paper 88-1c, p.151-159.
- Bouchez, J.L., 1977: Plastic deformation of quartzites at low temperature in an area of natural strain gradient. *Tectonophysics*, 39, p.25-50.
- Bouchez, J.L., Lister, G.S., and Nicolas, A., 1983: Fabric asymmetry and shear sense in movement zones. *Geol. Rundschau*, 72, p.401-419.
- Boyer, S.E. and Elliott, D., 1982: Thrust systems. *A.A.P.G. Bull.*, 66, p.1196-1230.

- Boyle, A.P., 1987: A model for stratigraphic and metamorphic inversion at Sulitjelma, central Scandes. *Geol. Mag.*, 124, p.451-466.
- Brooks, C., Wardle, R.J. and Rivers, T., 1981: Geology and geochronology of Helikian magmatism, western Labrador. *Can. J. Earth Sci.*, 18, p.1121-1227.
- Brown, D.L., 1988: Thin-skinned, basement-involved thrust tectonics in the Emma Lake area, Grenville Front Zone, western Labrador. Unpublished B.Sc. thesis, Memorial University of Newfoundland.
- Brown, D.L., 1990: A Structural Analysis of the Grenville Front Zone, Northwest Gagnon Terrane, Labrador. Unpublished M.Sc. thesis, Memorial University of Newfoundland.
- Brown, D.L., van Gool, J.A.M., Calon, T.J. and Rivers, T., 1991: The geometric and kinematic development of the Emma Lake thrust stack, Grenville Front, southwestern Labrador. *Can. J. Earth Sci.*, 28, p.136-144.
- Brown, R.L., Chapple, J.F., Moore, J.M. and Thompson, P.H., 1975: An ensimatic island arc and ocean closure in the Grenville Province of southeastern Ontario, Canada. *Geoscience Canada*, 2, p.141-144.
- Burton, K.W., Boyle, A.P., Kirk, W.L. and Mason, R., 1989: Pressure, temperature and structural evolution of the Sulitjelma fold-nappe, central Scandinavian Caledonides. In: *Evolution of Metamorphic Belts*, J.S. Daly, R.A. Cliff and B.W.D. Yardley (Eds.), *Geol. Soc. Spec. Pub.*, 43, p.391-411.
- Butler, P.Jr., 1969: Mineral compositions and equilibria in the metamorphosed iron formation of the Gagnon region, Quebec, Canada. *J. Petrol.*, 10, p.56-101.
- Butler, R.W.H., 1982: The terminology of structures in thrust belts. *J. Struct. Geol.*, 4, p.239-245.
- Butler, R.W.H. and Coward, M.P., 1984: Geological constraints, structural evolution and deep geology of the Northwest Scottish Caledonides. *Tectonics*, 3, p.347-365.
- Calon, T.J. and Hibbs, D.C., 1980: Structure of an area along the boundary of the Letitia Lake Group and Seal Lake group, central Labrador. IN: *current research, Newfoundland department of Mines and Energy, Report 80-1*, p.177-181.
- Chakraborty, K.L., 1966: Ferromagnesian silicate minerals in the metamorphosed iron-formation of Wabush Lake and adjacent areas, Newfoundland and Quebec. *G.S.C. Bulletin*, 143, 34 p.
- Chamberlain, C.P., 1986: Evidence for repeated folding of isotherms during regional metamorphism. *J. Petrol.*, 27, p.63-90.
- Chamberlain, C.P., and Karabinos, P., 1987: Influence of deformation on pressure-temperature paths of metamorphism. *Geology*, 15, p.42-44.
- Chamberlain, C.P., Zeitler, P.K. and Jan, M.Q., 1989: The dynamics of the suture between the Kihistan island arc and the Indian Plate in the Himalaya of Pakistan. In: *Himalayan Metamorphism*, A.C. Barnicoat and P.J. Treloar (Eds.), *J. Metam. Geol.*, 7, p.135-149.
- Chapple, W.M., 1978: Mechanics of thin-skinned fold-and-thrust belts. *Geol. Soc. Am. Bull.*, 89, p.1189-1198.
- Chown, E.H., 1979: Structure and metamorphism of the Otish Mountains area of the Grenvillian foreland zone, Quebec. *Geol. Soc. Am. Bull.*, 90, p.178-196.
- Cobbold, P.R. and Quinquis, H., 1980: Development of sheath folds in shear regimes. *J. Struct. Geol.*, 2, p.119-126.

- Connelly, J.N. 1990: U-Pb geochronology and the evolution of the Grenville Province of western Labrador. GAC-MAC joint annual meeting, May 1990, program with abstracts, 15, p.A26.
- Connelly, J.N., 1991: Thermotectonic history of the Grenville Province, southwestern Labrador. Unpubl. Ph.D. thesis, Memorial University of Newfoundland.
- Connelly, J.N. and Nunn, G.A.G., 1988: Relationships between the Lac Joseph Allochthon and underlying terranes, southwestern Labrador. GAC-MAC joint annual meeting, May 1988, program with abstracts, 13, p.A24.
- Connelly, J.N., van Gool, J.A.M. and Rivers, T., 1989a: Molson Lake terrane, a new terrane in the Parautochthonous Belt of the Grenville Province in southwestern Labrador. GAC-MAC joint annual meeting, May 1989, program with abstracts, 14, p.A23.
- Connelly, J.N., Heaman, L., Krogh, T. and Rivers, T., 1989b: U-Pb geochronology within the Molson Lake and Lac Joseph terranes, Grenville Province, southwestern Labrador. GAC-MAC joint annual meeting, May 1989, program with abstracts, 14, p.A84.
- Coward, M.P., 1982: Surge zones in the Moine thrust zone of NW Scotland. *J. Struct. Geol.*, 4, p.247-256.
- Coward, M.P. and Potts, G.J., 1985: Fold Nappes: examples from the Moine thrust zone. In: *The Caledonian orogen - Scandinavia and related areas*, D.G.Gee and B.A. Sturt (Eds.). Wiley and Sons, p.1147-1158.
- Crawford, M.L., 1977: Calcium zoning in almandine garnet, Wissahickon Formation, Philadelphia, Pennsylvania. *Can. Mineral.*, 15, p.243-249.
- Crowley, P.D., 1988: Metamorphic break across postmetamorphic thrust faults: An unreliable indicator of structural throw. *Geology*, 16, p.46-49.
- Cygan, R.T. and Lasaga, A.C., 1982: Crystal growth and the formation of chemical zoning in garnets. *Contr. Min. Pet.*, 79, p.187-200.
- Dahlen, F.A. and Barr, T.D., 1989: Brittle frictional mountain building 1. Deformation and mechanical energy budget. *Jrnl. Geoph. Res.*, 94 (B), p.3906-3922.
- Dahlen, F.A., Suppe, J. and Davis, D., 1984: Mechanics of fold and thrust belts and accretionary wedges: Cohesive Coulomb theory. *J. Geoph. Res.*, 89 (B), p.10,087-10,101.
- Dahlstrom, C.D.A., 1969: Balanced cross sections. *Can. J. Earth Sci.*, 6, p.743-757.
- Dahlstrom, C.D.A., 1970: Structural geology in the eastern margin of the Canadian Rocky Mountains. *Can. Petrol. Geol. Bull.*, 18, p.332-406.
- Dallmeyer, R.D., 1982:  $^{40}\text{Ar}/^{39}\text{Ar}$  incremental-release ages of biotite from a progressively remetamorphosed Archean basement terrane in southwestern Labrador. *Earth. Plan. Sci. Lett.*, 61, p.85-96.
- Dallmeyer, R.D. and Rivers, T., 1983: Recognition of extraneous argon components through incremental release.  $^{40}\text{Ar}/^{39}\text{Ar}$  analysis of biotite and hornblende across the Grenvillian metamorphic gradient in southwestern Labrador. *Geochim. Cosmochim. Acta*, 47, p.413-428.
- Davidson, A., 1984: Identification of ductile shear zones in the southwestern Grenville Province of the Canadian Shield. In: *Precambrian Tectonics Illustrated*, A. Kröner and R. Greiling (Eds.). Schweizerbart'sche Verlagsbuchhandlung, Stuttgart, p.263-279.

- Davidson, A., 1986: Grenville Front relationships near Killarney, Ontario. In: The Grenville Province, J.M. Moore, A. Davidson and A.J. Baer (Eds.), G.A.C. spec. pap. 31, p.107-117.
- Davis, D., Suppe, J. and Dahlen, F.A., 1983: Mechanics of fold-and-thrust belts and accretionary wedges. *J. Geoph. Res.*, 88 (B2), p.1153-1172.
- Davy, P. and Gillet, P. 1986: The stacking of thrust slices in collision zones and its thermal consequences. *Tectonics*, 5, p.913-929.
- De Paor, D.G., 1983: Balanced section in thrust belts. Part 1: construction. *Am. Ass. Petrol. Geol. Bull.*, 72, p.73-90.
- Dempster, T.J., 1985: Garnet zoning and metamorphism of the Barrovian type area, Scotland. *Contr. Min. Pet.*, 89, p.30-38.
- Dewey, J.F., 1969: Evolution of the Appalachian/Caledonian Orogen. *Nature*, 222, p.124-129.
- Dewey, J.F. and Burke, K.C.A., 1973: Tibetan, Variscan and Precambrian Basement reactivation: Products of Continental Collision. *Journal of Geology*, 81, p.683-692.
- Diggle, P.J. and Fisher, N.I., 1985: Sphere: a contouring program for spherical data. *Comp. and Geosc.*, 15, p.275-293.
- Dimroth, E., 1972: The Labrador geosyncline revisited. *Am. J. Sci.* v. 272, p.487-506.
- Dimroth, E., 1978: Labrador Trough Area. Ministère des Richesses Naturelles, Québec, Rapport Géologique 193, 396 p.
- Dimroth, E. and Chauvel, J.-J., 1973: Petrography of the Sokoman Iron Formation in part of the central Labrador Trough, Quebec, Canada. *G.S.A. Bull.*, 84, p.111-134.
- Duebendorfer, E.M. and Frost, B.R., 1988: Retrogressive dissolution of garnet: Effect on garnet-biotite geothermometry. *Geology*, 16, p.875-877.
- Easton, R.M., 1986: Geochronology of the Grenville Province. In: The Grenville Province, J.M. Moore, A. Davidson and A.J. Baer (Eds.), G.A.C. spec. pap. 31, p.127-173.
- Elliott, D., 1976: The motion of thrust sheets. *J. Geoph. Res.*, 81, p.949-963.
- Elliott, D. and Johnson, M.R.W., 1980: Structural evolution in the northern part of the Moine thrust belt, NW Scotland. *Trans. R. Soc. Edinburgh: Earth Sciences*, 71, p.69-96.
- England, P.C. and Richardson, S.W., 1977: The influence of erosion upon the mineral facies of rocks from different metamorphic environments. *J. Geol. Soc. London*, 134, p.201-213.
- England, P.C. and Thompson, A.B., 1984: Pressure-temperature-time paths of regional metamorphism I. Heat transfer during the evolution of regions of thickened continental crust. *J. Petrology*, 25, p.894-928.
- Essene, E.J., 1982: Geologic thermometry and barometry. In: Characterization of metamorphism through mineral equilibria, J.M. Ferry (Ed.). *Reviews in mineralogy*, 10, p.153-206.
- Essene, E.J., 1989: The current status of thermobarometry in metamorphic rocks. In: Evolution of Metamorphic Belts, J.S. Daly, R.A. Cliff and B.W. D. Yardley (Eds.), *Geol. Soc. Spec. Pub.*, 43, p.1-44.
- Etheridge, M.A., 1986: On the reactivation of extensional fault systems. *Phil. Trans. R. Soc. London*, A 137, p.179-194.

- Fahrig, W.F., 1960: Shabogamo Lake, Newfoundland and Quebec: 23G, E½. Geological Survey of Canada, Paper 60-9.
- Fahrig, W.F., 1967: Shabogamo Lake map area, Newfoundland-Labrador and Quebec: 23G (east half); Geological Survey of Canada, Memoir 354.
- Ferry, J.M. and Burt, D.M., 1982: Characterization of metamorphic fluid composition through mineral equilibria. In: Characterization of Metamorphism through Mineral Equilibria, J.M. Ferry (Ed.), *Reviews in Mineralogy*, 10, p.207-262.
- Ferry, J.M. and Spear, F.S., 1978: Experimental calibration of the partitioning of Fe and Mg between biotite and garnet. *Cont. Min. Pet.*, 66, p.113-117.
- Fleuty, M.J., 1964: Tectonic slides. *Geol. Mag.*, 101, p.452-456.
- Franceschelli, M., Memmi, I., Pannuti, F. and Ricci, C.A., 1989: Diachronous metamorphic equilibria in the Hercynian basement of northern Sardinia, Italy. In: Evolution of Metamorphic Belts, J.S. Daly, R.A. Cliff and B.W.D. Yardley (Eds.), *Geol. Soc. Spec. Pub.*, 43, p. 371-375.
- Ganguly, J. and Kennedy, G.C., 1974: The energetics of natural garnet solid solution I. Mixing of the aluminosilicate end-members. *Cont. min. pet.*, 48, p.137-148.
- Ganguly, J. and Saxena, S., 1984: Mixing properties of aluminosilicate garnets: constraints from natural and experimental data, and applications to geothermo-barometry. *Am. Mineralogist*, 69, p.88-97.
- Gastil, G. and Knowles, D.M., 1960: Geology of the Wabush Lake area, southwestern Labrador and eastern Quebec, Canada. *Geol. Soc. Am. Bull.*, 71, p.1243-1254.
- Ghent, E.D., 1976: Plagioclase-garnet-Al<sub>2</sub>SiO<sub>5</sub>-quartz: a potential geobarometer-geothermometer. *Am. Mineralogist.*, 61, p.710-714.
- Ghent, E.D., Robbins, D.B. and Stout, M.Z., 1979: Geothermometry, geobarometry, and fluid compositions of metamorphosed calc-silicates and pelites, Mica Creek, British Columbia. *Am. Mineralogist.*, 64, p.874-885.
- Ghent, E.D. and Stout, M.Z., 1981: Geobarometry and geothermometry of plagioclase-biotite-garnet-muscovite assemblages. *Contr. Min. Pet.*, 76, p.92-97.
- Gillcrist, R., Coward, M.P. and Mugnier, J.L., 1987: Structural inversion and its controls: examples from the Alpine foreland and the French Alps. *Geodinamica Acta*, 1, p.5-34.
- Goldman, D.S. and Albee, A.L., 1977: Correlation of Mg/Fe partitioning between garnet and biotite with <sup>18</sup>O/<sup>16</sup>O partitioning between quartz and magnetite. *Am. J. Sci.*, 277, p.750-767.
- Goldstein, A.G., 1988: Factors affecting the kinematic interpretation of asymmetric boudinage in shear zones. *Jrnl. Struct. Geol.*, 10, p.707-715.
- Gower, C.F., 1985: Correlations between the Grenville Province and Sveconorwegian Orogenic Belt - Implications for Proterozoic Evolution of the Southern Margins of the Canadian and Baltic Shields. In: The Deep Proterozoic Crust in the North Atlantic Provinces, A.C. Tobi and J.L.R. Touret (Eds.), Reidel, p.247-257.
- Gower, C.F., Rivers, T. and Brewer, T.S. 1991: Middle Proterozoic mafic magmatism in Labrador, eastern Canada. In: Mid-Proterozoic Laurentia-Baltica, C.F. Gower, T. Rivers and B. Ryan (Eds.). *Geol. Assoc. Canada, special paper 38*, p.385-506.
- Gower, C.F., Ryan, A.B., Bailly, D.G. and Thomas, A., 1980: The position of the Grenville Front in eastern and central Labrador. *Can. Jrnl. of Earth Sciences*, 17, p.784-788.

- Green, A.G., Milkereit, B., Davidson, A., Spencer, C., Hutchinson, D.R., Cannon, W.F., Lee, M.W., Ager, W.F., Behrendt, J.C. and Hinze, W.J., 1988: Crustal structure of the Grenville Front and adjacent terranes, *geology*, 16, p.788-792.
- Grocot, J., 1979: Controls of metamorphic grade in shear belts. *Rapp. Grønlands geol. Unders.*, 89, p.47-62.
- Guidotti, C. V., 1984: Micas in metamorphic rocks. In: Micas. S.W. Bailey (Ed.), *Reviews in Mineralogy*, 13, p.357-467.
- Hadizadeh, J. and Rutter, E. H., 1983: The low temperature brittle-ductile transition in a quartzite and the occurrence of cataclastic flow in nature. *Geol. Rundschau*, 72, p.493-509.
- Hanmer, S.K., 1982: Microstructure and geochemistry of plagioclase and microcline in naturally deformed granite. *J. Struct. Geol.*, 4, p.197-213.
- Hanmer, S.K., 1990: Natural rotated inclusions in non-ideal shear. *Tectonophysics*, 176, p.245-255.
- Hargraves, R.B., 1981: Precambrian tectonic style: a liberal uniformitarian interpretation. In: *Precambrian Plate Tectonics*, A. Kröner (Ed.), Elsevier, p.21-56.
- Hatcher, R.D. Jr. and Hooper, R.J., 1992: Evolution of crystalline thrust sheets in the internal parts of mountain chains. In: *Thrust Tectonics*, K.R. McClay (Ed.). Chapman and Hall, London, p.217-233.
- Hatcher, R.D. Jr. and Williams, R.T., 1986: Mechanical model for single thrust sheets, part I: taxonomy of crystalline thrust sheets and their relationships to the mechanical behaviour of orogenic belts. *Geol. Soc. Am. Bull.*, 97, p.975-985.
- Hayward, A.B. and Graham, R.H., 1989: Some geometrical characteristics of inversion. In: *Inversion Tectonics*, M.A. Cooper and G.D. Williams (Eds.). *Geol. Soc. London, Spec. Publ.* 44, p.17-39.
- Hobbs, B.E., Means, W.D. and Williams, P.F., 1976: *An Outline of Structural Geology*. Wiley and Sons, New York, 571 p.
- Hodges, K.V. and Crowley, P.D., 1985: Error estimation and empirical geothermobarometry for pelitic systems. *Am. Mineralogist*, 70, p.702-709.
- Hodges, K.V. and Royden, L., 1984: Geological thermobarometry of retrograded metamorphic rocks: An indication of the uplift trajectory of a portion of the Northern Scandinavian Caledonides. *J. Geoph. Res.*, 89, p.7077-7090.
- Hodges, K.V. and Spear, F.S., 1982: Geothermometry, geobarometry and the Al<sub>2</sub>SiO<sub>5</sub> triple point at Mt. Moosilauke, New Hampshire. *Am. Mineralogist*, 67, p.1118-1134.
- Hoffman, P.F., 1989: Precambrian geology and tectonic history of North America. In: *The Geology of North America - An Overview*, A.W. Balley and A.R. Palmer (Eds.). G.S.A., *The Geology of North America*, Vol. A, p.447-512.
- Hoinkes, G., 1986: Effect of grossular-content in garnet on the partitioning of Fe and Mg between garnet and biotite. *Contr. Min. Pet.*, 92, p.393-399.
- Hoisch, T.D., 1990: Empirical calibration of six geobarometers for the mineral assemblage quartz + muscovite + biotite + plagioclase + garnet. *Contr. Min. Pet.*, 104, p.225-234.
- Holdaway, M.J., 1971: Stability of andalusite and the aluminum silicate phase diagram. *Am. J. Sci.*, 271, p.97-131.

- Holdaway, M.J., Duthrow, B.L. and Hinton, R.W., 1988: Devonian and Carboniferous metamorphism in west-central Maine: The muscovite-almandine geobarometer and the staurolite problem revisited. *Am. Mineralogist*, 73, p.20-47.
- Holdsworth, R.E., 1990: Progressive deformation structures associated with ductile thrusts in the Moine Nappe, Sutherland, N. Scotland. *Jrnl. Struct. Geol.*, 12, p.443-452.
- Holland, T.J. B. and Powell, R., 1985: An internally consistent thermodynamic dataset with uncertainties and correlations: 2. Data and results. *J. Metam. Geol.*, 3, p.343-370.
- Hollister, L.S., 1966: Garnet zoning: An interpretation based on the Rayleigh fractionation model. *Science*, 154, p.1647-1651.
- Hollister, L.S. and Crawford, M.L., 1986: Melt-enhanced deformation: A major tectonic process. *Geology*, 14, p.558-561.
- Hooper, R.J. and Hatcher, R.D.Jr., 1988: Mylonites from the Towaliga fault zone, central Georgia: products of heterogeneous non-coaxial deformation. *Tectonophysics*, 152, p.1-17.
- Hutton, D.H.W., 1979: Tectonic slides: a review and reappraisal. *Earth-Science Reviews.*, 15, p.151-172.
- Indares, A., in prep: Eclogitized gabbros from the eastern Grenville Province: textural evidence, metamorphic context and implications. Submitted to *Can. J. Earth Sci.*
- Indares, A., in press: Reconnaissance Géologique et Métallogénique des Roches Mafiques et Ultramafiques dans la Région du Lac Opocopa, au Sud de Fermont (Province de Grenville). Unpublished report, Ministère de l'Énergie et des Ressources du Québec.
- Indares, A. and Martignole, J., 1985a: Biotite-garnet geothermometry in granulite-facies rocks: evaluation of equilibrium criteria. *Can. Mineral.*, 23, p.187-193.
- Indares, A. and Martignole, J., 1985b: Biotite-garnet geothermometry in the granulite facies: the influence of Ti and Al in biotite. *Amer. Mineral.*, 70, p.272-278.
- Indares, A. and Martignole, J., 1989: The Grenville Front south of Val-d'Or, Quebec. *Tectonophysics*, 157, p.221-239.
- Indares, A. and Martignole, J., 1990a: Metamorphic constraints on the evolution of the gneisses from the parautochthonous and allochthonous polycyclic belts, Grenville Province, western Quebec. *Can. J. Earth Sci.*, 27, p.357-370.
- Indares, A. and Martignole, J., 1990b: Metamorphic constraints on the tectonic evolution of the allochthonous monocyclic belt of the Grenville Province, western Quebec. *Can. J. Earth Sci.*, 27, p.371-386.
- Irving, E., Emslie, R.F. and Ueno, H., 1974: Upper Proterozoic paleomagnetic poles from Laurentia and the history of the Grenville Structural Province. *J. Geoph. Res.*, 79, p.5491-5502.
- James, D.T. and Connelly, J.N., 1992: Assembly of the Grenville orogen, western Labrador. *Friends of the Grenville Workshop, 1992, program and abstracts.*
- James, D.T. and Stephenson, D.M., 1992: Geology of the southern part of the Archean Ashuanipi Complex, Shabogamo Lake map sheet (NTS 23G), western Labrador. *Current Research, Newfoundland Department of Mines and Energy, Report 92-1, p.367-379.*
- Jamieson, R.A., 1986: P-T paths from high temperature shear zones beneath ophiolites. *J. Metam. Geol.*, 4, p.3-22.

- Jamieson, R.A. and Beaumont, C., 1988: Orogeny and metamorphism: a model for deformation and pressure-temperature-time paths with applications to the central and southern Appalachians. *Tectonics*, 7, p.417-445.
- Jamieson, R.A. and Vernon, R.H., 1987: Timing of porphyroblast growth in the Fleur de Lys Supergroup, Newfoundland. *J. Metam. Geol.*, 5, p.273-288.
- Janecke, S.U. and Evans, J.P., 1988: Feldspar-influenced rock rheologies. *Geology*, 16, p.1064-1067.
- Jiang, J. and Lasaga, A.C., 1990: The effect of post-growth thermal events on growth-zoned garnet: implications for metamorphic P-T history calculations. *Contr. Min. Pet.*, 105, p.454-459.
- Johnson, M.R.W., Kelley, S.P., Oliver, G.J.H. and Winter, D.A., 1985: Thermal effects and timing of thrusting in the Moine Thrust Zone. *J. Geol. Soc. London*, 142, p.863-873.
- Karabinos, P. and Ketcham, R., 1988: Thermal structure of active thrust belts. *J. Metam. Geol.*, 6, p.559-570.
- Klein, C. Jr., 1966: Mineralogy and petrology of the metamorphosed Wabush Iron Formation, southwestern Labrador. *J. Petrol.*, 7, p.246-305.
- Klein, C. Jr., 1973: Changes in mineral assemblages with metamorphism of some banded precambrian iron-formations. *Econ. Geol.*, 68, p.1075-1088.
- Klein, C. Jr., 1978: Regional metamorphism of Proterozoic iron-formation, Labrador Trough, Canada. *Am. Mineral.*, 63, p.898-912.
- Knowles, D.M. and Gastil, G.R., 1959: Metamorphosed iron formation in southwestern Labrador, *Bull. Trans. Can. Inst. Min. Met.*, 62, p.265-272.
- Koons, P.O., 1989: The topographic evolution of collisional mountain belts: a numerical look at the Southern Alps, New Zealand. *Am. Jnl. Science*, 289, p. 1041-1069.
- Koziol, A.M. and Newton, R.C., 1988: Redetermination of the anorthite breakdown reaction and improvement of the plagioclase-garnet-Al<sub>2</sub>SiO<sub>5</sub>-quartz geobarometer. *Am. Mineralogist*, 73, p.216-223.
- Kranck, S.H., 1961: Study of phase equilibria in a metamorphic iron formation. *J. Petrol.*, 2, p.137-184.
- Kretz, R., 1983: Symbols for rock-forming minerals. *Am. Mineralogist.*, 68, p.277-279.
- Kröner, A., 1981: Precambrian plate tectonics. In: *Precambrian Plate Tectonics*, A. Kröner (Ed.), Elsevier, p.57-90.
- Lasaga, A. C., 1983: Geospeedometry: An extension of geothermometry. In: *Kinetics and Equilibrium in Mineral Reactions*, S.K. Saxena (Ed.), *Advances in Physical Geochemistry*, 3, p.81-114.
- La Tour, T.E., 1981: Metamorphism and geothermometry near Coniston, Ontario: a clue to the tectonic evolution of the Grenville Front. *Can. J. Earth Sci.*, 18, p.884-898.
- Law, R. D., 1990: Crystallographic fabrics: a selective review of their applications to research in structural geology. In: *Deformation Mechanisms, Rheology and Tectonics*, p.335-352.
- Law, R.D., Casey, M. and Knipe, R.J., 1986: Kinematic and tectonic significance of microstructures and crystallographic fabrics within quartz mylonites from the Assynt and Eriboll regions of the Moine thrust zone, NW Scotland. *Trans. Royal Soc. Edinburgh: Earth Sciences*, 77, p.9-125.

- Law, R.D., Schmid, S.M. and Wheeler, J., 1990: Simple shear deformation and quartz crystallographic fabrics: a possible natural example from the Torridon area of NW Scotland. *J. Struct. Geol.*, 12, p.29-45.
- Lister, G.S., 1981: The effect of the basal-prism mechanism switch on fabric development during plastic deformation of quartzite. *J. Struct. Geol.*, 3, p.67-75.
- Lister, G.S., Etheridge, M.A. and Symonds, P.A., 1986: Detachment faulting and the evolution of passive continental margins. *Geology*, 14, p.246-250.
- Lister, G.S. and Snoke, A.W., 1984: S-C mylonites. *J. Struct. Geol.*, 6, p.617-638.
- Lister, G.S. and Williams, P.F., 1979: Fabric development in shearzones: theoretical controls and observed phenomena. *J. Struct. Geol.*, 1, p.283-297.
- Lister, G.S. and Williams, P.F., 1983: The partitioning of deformation in flowing rock masses. *Tectonophysics*, 92, p.1-33.
- Loomis, T.P., 1982: Numerical simulation of the disequilibrium growth of garnet in chlorite-bearing aluminous pelitic rocks. *Can. Mineral.*, 20, p.411-423.
- Loomis, T.P., 1983: Compositional zoning of crystals: A record of growth and reaction history. In: *Kinetics and Equilibrium in Mineral Reactions*, S.K. Saxena (Ed.), *Advances in Physical Geochemistry*, 3, p.1-60.
- Loomis, T.P., 1986: Metamorphism of metapelites: calculations of equilibrium assemblages and numerical simulations of the crystallization of garnet. *J. Metam. Geol.*, 4, p.201-229.
- Loomis, T.P. and Nimick, F.B., 1982: Equilibrium in Mn-Fe-Mg aluminous pelitic compositions and the equilibrium growth of garnet. *Can. Mineral.*, 20, p.393-410.
- Low, A.P., 1895: Report of explorations in the Labrador Peninsula along East Main, Koksoak, Hamilton, Manicouagan, and portions of other rivers in 1892, 1893, 1894, 1895. *Geol. Surv. Can. Ann. Rep.* 1895.
- Lucas, S.B., 1989: Structural evolution of the Cape Smith thrust belt and the role of out-of-sequence faulting in the thickening of mountain belts. *Tectonics*, 8, p.655-676.
- Lucas, S.B., 1990: Relations between thrust belt evolution, grain-scale deformation, and metamorphic processes: Cape Smith Belt, northern Canada. *Tectonophysics*, 178, p.151-182.
- Marjoribanks, R.W., 1976: The relation between microfabric and strain in a progressively deformed quartzite sequence from central Australia. *Tectonophysics*, 32, p.269-293.
- McKenna, L.W. and Hodges, K.V., 1988: Accuracy versus precision in locating reaction boundaries: Implications for the garnet-plagioclase-aluminum silicate-quartz geobarometer. *Am. Mineralogist.*, 73, p.1205-1208.
- Means, W.D., 1981: The concept of steady state foliation. *Tectonophysics*, 78, p.179-199.
- Mengel, F., Rivers, T., 1989: Thermotectonic evolution of Proterozoic and reworked Archean terranes along the Nain-Churchill boundary in the Saglek area, northern Labrador. In: *Evolution of Metamorphic Belts*, J.S. Daly, R.A. Cliff and B.W.D. Yardley (Eds.), *Geol. Soc. Spec. Pub.*, 43, p.319-324.
- Mereu, R.F., Wang, D., Kuhn, O. and Forsyth, D.A., 1986: Summary of the results of the 1982 COCRUST long-range seismic experiment across the Ottawa-Bonnechere graben and western Grenville Front. In: *The Grenville Province*, J.M. Moore, A. Davidson and A.J. Baer (Eds.), *Spec.Pap. Geol. Assoc. Canada*, 31, p.235-240.

- Mereu, R.F. and Jobidon, G., 1971: A seismic interpretation of the crust and Moho on a line perpendicular to the Grenville Front. *Can. J. Earth Sci.* vol 8, p.1553-1583.
- Milnes, A.G. and Pfiffner, O.A., 1980: Tectonic evolution of the Central Alps in the cross section St. Gallen-Como. *Ecl. Geol. Helv.*, 73, p.619-633.
- Mitra, G. and Boyer, S.E., 1986: Energy balance and deformation mechanisms of duplexes. *J. Struct. Geol.*, 8, p.291-304.
- Miyashiro, A., 1973: *Metamorphism and Metamorphic Belts*. Allen and Unwin, London, 492 p.
- Moore, J.M., 1986: Introduction: The 'Grenville Problem' then and now. In: *The Grenville Province*, J.M. Moore, A. Davidson and A.J. Bear (Eds.). G.A.C. Special Paper 31, p.1-11.
- Moore, J.M., Davidson, A. and Bear, A.J., 1986: *The Grenville Province*, G.A.C. Special Paper 31, 358 p.
- Morley, C.K., 1986: A classification of thrust fronts. *Am. Ass. Petrol. Geol. Bull.*, 70, p.12-25.
- Morley, C.K., 1989: Out-of-sequence thrusts. *Tectonics*, 7, p.539-561.
- Mueller, R.F., 1960: Compositional characteristics and equilibrium relations in mineral assemblages of a metamorphosed iron formation. *Am. J. Sci.*, 258, p.449-497.
- Muncill, G.E. and Chamberlain, C.P., 1988: Crustal cooling rates inferred from homogenization of metamorphic garnets. *Earth Plan. Sci. Letters*, 87, p.390-396.
- Newton, R.C., 1983: Geobarometry of high-grade metamorphic rocks. *Am. J. Sci.*, 283-A, p.1-28.
- Newton, R.C. and Haselton, H.T., 1981: Thermodynamics of the garnet-plagioclase-Al<sub>2</sub>SiO<sub>5</sub>-quartz geobarometer. In: *Thermodynamics of Minerals and Melts*, R.C. Newton, A. Navrotsky and B.J. Wood (Eds.), p.129-145.
- Nunn, G.A.G., Noel, N. and Culshaw, N.G., 1984: Geology of the Atikonak Lake area, Grenville Province, southwestern Labrador. Current research, Mineral Development Division, Newfoundland Department of Mines and Energy, Report 84-1, p.30-41.
- Nunn, G.A.G., Emslie, R.F., Lefebvre, C.E., Noel, N. and Wells, S., 1986: The Atikonak River massif and surrounding area, western Labrador and Québec. Current research, Mineral Development Division, Newfoundland Department of Mines and Energy, Report 86-1, p.125-145.
- Ohmoto, H. and Kerrick, D.M., 1977: Devolatilization equilibria in graphitic systems, *Am. J. Sci.*, 277, p.1013-1044.
- Owen, J.V., Rivers, T. and Gower, C.F., 1986: The Grenville Front on the Labrador coast. In: *The Grenville Province*, J.M. Moore, A. Davidson and A.J. Baer (Eds.). Geological Association of Canada, Special paper 31, p.95-106.
- Oxburg, E.R. and Turcotte, D.L., 1974: Thermal gradients and regional metamorphism in overthrust terranes with special reference to the Eastern Alps. *Schweiz. Min. Pet. Mitt.*, 54, p.641-662
- Park, A.F. and Doody, J.J., 1990: Structural styles in the deep levels of an Early Proterozoic foreland thrust belt. In: *The Early Proterozoic Trans-Hudson Orogen of North America*, J.F. Lewry and M.R. Stauffer (Eds.). *Geol. Assoc. Can.*, special paper 37, p.313-351.

- Passchier, C.W., 1983: The reliability of asymmetric c-axis fabrics of quartz to determine sense of vorticity. *Tectonophysics*, 99, p.T9-T18.
- Passchier, C.W. and Simpson, C., 1986: Porphyroblast systems as kinematic indicators. *J. Struct. Geol.*, 8, p.831-843.
- Pattison, D.R.M., 1989: F-T conditions and the influence of Graphite on pelitic phase relations in the Ballachulish Aureole, Scotland. *Jrnl. Petrol.* 30, p.1219-1244.
- Perchuk, L.L., Aranovich, L.Ya, Podlesskii, K.K., Lavrent'eva, I.V., Gerasimov, V.Yu, Fed'kin, V.V., Kitsul, V.I., Karsakov, L.P. and Berdnikov, N.V., 1985: Precambrian granulites of the Aldan shield, Eastern Siberia, USSR. *J. Metam. Geol.*, 3, p.265-310.
- Perchuk, L.L. and Lavrent'eva, I.V., 1983: Experimental investigation of exchange equilibria in the system cordierite-garnet-biotite. In: *Kinetics and Equilibrium in Mineral Reactions*, S.K. Saxena (Ed.), Springer-Verlag, p.173-198.
- Pigage, L.C. and Greenwood, H.J., 1982: Internally consistent estimates of pressure and temperature: the staurolite problem. *Am. J. Sci.*, 282, p.943-969.
- Platt, J.P., 1984: Secondary cleavages in ductile shear zones. *J. Struct. Geol.*, 6, p.439-442.
- Platt, J.P., 1986: Dynamics of orogenic wedges and the uplift of high-pressure metamorphic rocks. *G.S.A. Bulletin*, 97, p.1037-1053.
- Platt, J.P. and Behrmann, J.H., 1986: Structures and fabrics in a crustal-scale shear zone, Betic Cordillera, SE Spain. *J. Struct. Geol.*, 8, p.15-33.
- Platt, J.P. and Legett, J.K., 1986: Stratal extension in thrust footwalls, Makian accretionary prism: Implication for thrust tectonics. *Am. Ass. Petrol. Geol. Bull.*, 70, p.191-203.
- Platt, J.P. and Vissers, R.L.M. 1980: Extensional structures in anisotropic rocks. *J. Struct. Geol.*, 2, p.397-410.
- Powell, D. and MacQueen, J.A., 1976: Relationships between garnet shape, rotational inclusion fabrics and strain in some Moine metamorphic rocks of Skye, Scotland. *Tectonophysics*, 35, p.391-402.
- Powell, R. and Holland, T.J. B., 1985: An internally consistent thermodynamic dataset with uncertainties and correlations: 1. methods and a worked example. *J. Metam. Geol.*, 3, p.327-342.
- Powell, R. and Holland, T.J. B., 1988: An internally consistent dataset with uncertainties and correlations: 3. Applications to geobarometry, worked examples and a computer program. *J. Metam. Geol.*, 6, p.173-204.
- Ramberg, H., 1981: The role of gravity in orogenic belts. In: *Thrust and Nappe Tectonics*, K.R. McClay and N.J. Price (Eds.). *Geol. Soc. London, Spec. Publ.* 9, p.125-140.
- Ramsey, J.G. and Huber, M.I., 1983: *The techniques of Modern Structural Geology. Volume 1: Strain Analysis*. Academic Press, London, 307 p.
- Reinhardt, J., Rubenach, M. J., 1989: Temperature - time relationships across metamorphic zones: evidence from porphyroblast - matrix relationships in progressively deformed metapelites. In: *Deformation of Crustal Rocks*, A. Ord (Ed.), p.141-161.
- Rice, A.H.N., 1985: Staurolite growth and metamorphic zones in the Kalak Nappe Complex of northeastern Porsangerhalvøya, north Norway. *Lithos*, 18, p.281-294.
- Rice, A.H.N., 1987: Continuous out-of-sequence ductile thrusting in the Norwegian Caledonides. *Geol. Mag.*, 124, p.249-260.

- Rice, A.H.N., Bevins, R.E., Robinson, D. and Roberts, D., 1989: Thrust-related metamorphic inversion in the Caledonides of Finnmark, north Norway. In: J.S. Daly, R.A. Cliff and B.W.D. Yardley (Eds.), *Evolution of Metamorphic Belts*, Geol. Soc., spec. publ., 43, p. 413-421.
- Rice, J.M. and Ferry, J.M., 1982: Buffering, infiltration and the control of intensive variables during metamorphism. In: *Characterization of metamorphism through mineral equilibria*, J.M. Ferry (Ed.), *Reviews in mineralogy*, 10, p.262-326.
- Rivers, T., 1978: Geological mapping of the Wabush-Labrador City area, southwestern Labrador. In: *Report of activities for 1977*, Mineral Development Division, Newfoundland Department of Mines and Energy, Report 78-1, p.44-50.
- Rivers, T., 1980a: Wabush Lake, NTS23G/2; Mineral development Division, Newfoundland Department of Mines and Energy, Map 80-1, 1:50,000 scale with marginal notes.
- Rivers, T., 1980b: Sawbill Lake, NTS23G/7; Mineral development Division, Newfoundland Department of Mines and Energy, Map 80-2, 1:50,000 scale with marginal notes.
- Rivers, T., 1980c: Flora Lake, NTS23B/15; Mineral development Division, Newfoundland Department of Mines and Energy, Map 80-282, 1:50,000 scale with marginal notes.
- Rivers, T., 1980d: Geological mapping in the Wabush Lake area, southwestern Labrador. In: *Current research*, Mineral Development Division, Newfoundland Department of Mines and Energy, Report 80-1, p.206-212.
- Rivers, T., 1980e: Revised stratigraphic nomenclature for Aphebian and other rock units, southern Labrador Trough, Grenville Province. *Can. J. Earth Sci.*, 17, p.668-670.
- Rivers, T., 1983a: The northern margin of the Grenville Province in western Labrador - Anatomy of an ancient orogenic front. *Precambrian Research*, 22, p.41-73.
- Rivers, T., 1983b: Progressive metamorphism of pelitic and quartzo-feldspathic rocks in the Grenville Province of western Labrador - tectonic implications of bathozone 6 assemblages. *Can J. Earth. Sci.*, 20, p.1791-1804.
- Rivers, T., 1985a: Geology of the Lac Virot area, Labrador-Quebec, parts of 23G and 23B; Mineral Development Division, Newfoundland Department of Mines and Energy, Map 85-25, 1:100,000 scale.
- Rivers, T., 1985b: Geology of the Wightman Lake area, Labrador-Quebec, 23G(SE); Mineral Development Division, Newfoundland Department of Mines and Energy, Map 85-28, 1:100,000 scale.
- Rivers, T., 1985c: Geology of the Opocopa Lake area, Labrador-Quebec, 23B(NE); Mineral Development Division, Newfoundland Department of Mines and Energy, Map 85-29, 1:100,000 scale.
- Rivers, T., 1992: Contrasting styles of crustal shortening in the northern Grenville Province. *Friends of the Grenville workshop, 1992, program and abstracts*.
- Rivers, T. and Chown, E.H., 1986: The Grenville orogen in eastern Quebec and western Labrador - definition, identification and tectonometamorphic relationships of autochthonous, parautochthonous and allochthonous terranes. In: *The Grenville Province*, J.M. Moore, A. Davidson and A.J. Bear (Eds.), G.A.C. special paper 31, p.31-50.
- Rivers, T., Martignole, J., Gower, C.F. and Davidson, A., 1989: A new tectonic division of the Grenville Province, southeast Canadian Shield. *Tectonics*, 8, p.63-84.

- Rivers, T. and Massey, N., 1979: Wabush Lake - Sawbill Lake map area, western Labrador. In: Report of activities for 1978, Mineral Development Division, Newfoundland Department of Mines and Energy, Report 79-1, p.142-147.
- Rivers, T. and Mengel, F.C., 1988: Contrasting assemblages and petrogenetic evolution of corona and noncorona gabbros in the Grenville Province of western Labrador. *Can. J. Earth Sci.*, 25, p.1629-1648.
- Rivers, T. and Nunn, G.A.G., 1985: A Reassessment of the Grenvillian Orogeny in Western Labrador. In: *The Deep Proterozoic Crust in the North Atlantic Provinces*, A.C. Tobi and J.L.R. Touret (Eds.), Reidel, Dordrecht, p.163-174.
- Roach, R.A. and Duffel, S., 1974: Structural analysis of the Mount Wright map area, southernmost Labrador Trough, Quebec, Canada. *Geol. Soc. Am. Bull.*, 85, p.947-962.
- Robin, P.-Y. F. and Jowett, E.C., 1986: Computerized density contouring and statistical evaluation of orientation data using counting circles and continuous weighting functions. *Tectonophysics*, 121, p.207-223.
- Robinson, G.R.Jr., 1983: Calibration of the muscovite-biotite-quartz-garnet-aluminosilicate geothermobarometer (abs.) *EOS*, 64, p.351.
- Robinson, W.G., 1956: The Grenville of New Quebec. In: *The Grenville problem*, J.E. Thomson (Ed.), Royal Soc. Canada, Spec. Publ., 1, p.14-19.
- Rondot, J., 1986: Géosuture dans le Grenville. In: *The Grenville Province*, J.M. Moore, A. Davidson and A.J. Bear (Eds.), G.A.C. special paper 31, p.313-325.
- Rosenfeld, J.L., 1970: Rotated garnets in metamorphic rocks. *G.S.A. special paper*, 129, 105p.
- Royden, L. and Hodges, K.V., 1984: A technique for analyzing the thermal and uplift histories of eroding orogenic belts: A Scandinavian example. *J. Geoph. Res.*, 89, p.7091-7106.
- Rubie, D.C., 1983: A thermal-tectonic model for high-pressure metamorphism and deformation in the Sesia zone, Western Alps. *J. Geol.*, 92, p.21-63.
- Schmid, S.M. and Haas, R., 1989: Transition from near-surface thrusting to intrabasement decollement, Schlinig thrust, eastern Alps. *Tectonics*, 8, p.697-718.
- Schreurs, J., 1985: Prograde metamorphism of metapelites, garnet-biotite thermometry and prograde change of biotite chemistry in high-grade rocks of West Uusimaa, southwest Finland. *Lithos*, 18, p.69-80.
- Seyfert, C.K., 1980: Paleomagnetic evidence in support of a Middle Proterozoic (Helikian) collision between North America and Gondwanaland as a cause of the metamorphism and deformation in the Adirondacks: Summary. *Geol. Soc. Am. Bull.*, 91, p.118-120.
- Shi, Y. and Wang, C.Y., 1987: Two dimensional modeling of the P-T-t paths of regional metamorphism in simple overthrust terrains. *Geology*, 15, p.1048-1051.
- Sibson, R.H., 1977: Fault Rocks and fault mechanisms. *J. Geol. Soc. London*, 133, p.191-213.
- Simpson, C., 1985: Deformation of granitic rocks across the brittle-ductile transition. *J. Struct. Geol.*, 7, p.503-511.
- Simpson, C. and Schmid, S.M., 1983: An evaluation of criteria to deduce the sense of movement in sheared rocks. *G.S.A. Bull.*, 94, p.1281-1288.

- Spear, F. S., 1989: Relative thermobarometry and metamorphic P-T paths. In: Evolution of Metamorphic Belts, J.S. Daly, R.A. Cliff and B.W. D. Yardley (Ed.), p.63-81.
- Spear, F.S. and Selverstone, J., 1983: Quantitative P-T paths from zoned minerals: Theory and tectonic applications. *Contr. Min. Pet.*, 83, p.348-357.
- Spear, F.S., Selverstone, J., Hickmott, D., Crowley, P. and Hodges, K.V., 1984: P-T paths from garnet zoning: A new technique for deciphering tectonic processes in crystalline terranes. *Geology*, 12, p.87-90.
- Spear, F.S., Kixkmott, D.D. and Selverstone, J., 1990: Metamorphic consequences of thrust emplacement, Fall Mountain, New Hampshire. *G.S.A. Bulletin*, 102, p.1344-1360.
- Spry, A., 1969: *Metamorphic textures*. Pergamon Press, Oxford, 350 p.
- St-Onge, M.R., 1987: Zoned poikiloblastic garnets: P-T paths and syn-metamorphic uplift through 30 km of structural depth, Wopmay Orogen, Canada. *J. Petrology*, 28, p.1-21.
- St. Onge, M.R. and Lucas, S.B., 1990: Evolution of the Cape Smith Belt: Early Proterozoic continental underthrusting, ophiolite obduction and thick-skinned folding. In: *The Early Proterozoic Trans-Hudson Orogen of North America*, J.F. Lewry and M.R. Stauffer (Eds.). *Geol. Assoc. Can., special paper 37*, p.313-351.
- Stockwell, C.H., 1961: Structural provinces, orogenies and time classification of rocks of the Canadian Precambrian Shield. In: *Age determinations by the Geological Survey of Canada; Report 2, isotopic ages*. *Geol. Surv. Can. Paper 61-17*, p.108-118.
- Stowell, H.H., 1989: Silicate and sulphide thermobarometry of low- to medium-grade metamorphic rocks from Holkham Bay, south-east Alaska. *J. Metam. Geol.*, 7, p.343-358.
- Thomas, A., Nunn, G.A.G. and Wardle, R.J., 1985: A 1650 Ma Orogenic Belt within the Grenville Province of Northeastern Canada. In: *The Deep Proterozoic Crust in the North Atlantic Provinces*, A.C. Tobi & J.L.R. Touret (Eds.), Reidel, Dordrecht. p.151-161.
- Thomas, A., Nunn, G.A.G. and Krogh, T.E., 1986: The Labradorian orogeny: evidence for a newly identified 1600 to 1700 Ma orogenic event in Grenville Province crystalline rocks from central Labrador. In: *The Grenville Province*, J.M. Moore, A. Davidson and A.J. Bear (Eds.), G.A.C. special paper 31, p.176-189.
- Thomas, M.D. and Tanner, J.G., 1975: Cryptic suture in the eastern Grenville Province. *Nature*, 256, p.392-394.
- Thompson, A.B., 1976: Mineral reactions in pelitic rocks: 1. prediction of P-T-X (Fe-Mg) phase relations. *Am. J. Sci.*, 276, p.401-424.
- Thompson, A.B. and England, P.C., 1984: Pressure - temperature - time paths of regional metamorphism II. Their inference and interpretation using mineral assemblages in metamorphic rocks. *J. Petrology*, 25, p.929-955.
- Thompson, A.B. and Ridley, J.R., 1987: Pressure - temperature - time (P-T-t) histories of orogenic belts. *Phil. Trans. R. Soc. London*, A321, p.27-45.
- Thomson, J.E. (Ed.), 1956: *The Grenville problem*. The Royal Society of Canada, Special Publication, no. 1.
- Tracy, R. J., 1982: Compositional zoning and inclusions in metamorphic minerals. In: *Characterization of metamorphism through mineral equilibria*, J.M. Ferry (Ed.), *Reviews in Mineralogy*, p.355-397.

- Tracy, R.J., Robinson, P. and Thompson, A.B., 1976: Garnet composition and zoning in the determination of temperature and pressure on metamorphism, central Massachusetts. *Am. Mineralogist.*, 61, p.762-775.
- Treloar, P.J., Broughton, R.D., Williams, M.P., Coward, M.P. and Windley, B.F., 1989: Deformation, metamorphism and imbrication of the Indian plate south of the Main Mantle Thrust, north Pakistan. In: *Himalayan Metamorphism*, A.C. Barnicoat and P.J. Treloar (Eds.), *J. Metam Geol.*, 7, p.111-125.
- Trzcieski, W.E. Jr., 1977: Garnet zoning - product of a continuous reaction. *Can. Mineral.*, 15, p.250-256.
- Tuccillo, M.E., Essene, E.J. and van der Pluijm, B.A., 1990: Growth and retrograde zoning in garnets from high-grade metapelites: Implications for pressure-temperature paths. *Geology*, 18, p.839-842.
- Urai, J.L., Means, W.D. and Lister, G.S., 1986: Dynamic recrystallization of minerals. In: *Mineral and Rock Deformation: Laboratory Studies. The Paterson Volume*. B.E. Hobbs and H.C. Heard (Ed.), *Geophysics Monograph*, 36, A.G.U., p.161-199.
- van Everdingen, D.A., van Gool, J.A.M. and Vissers, R.L.M., in press: Quickplot: a microcomputer-based program for processing of orientation data. *Comp. and Geosc.*
- van Gool, J.A.M., Brown, D., Calon, T.J. and Rivers, T., 1988a: The Grenville Front Thrust Belt in Western Labrador. *Current Research, Part C: The Canadian Shield*. Geological Survey of Canada, Paper 88-1C, p.245-253.
- van Gool, J.A.M., Brown, D., Calon, T.J. and Rivers, T., 1988b: The Grenville Front Thrust Belt in Western Labrador. Internal report G.S.C.
- van Gool, J.A.M., Calon, T.J. and Rivers, T., 1987a: Preliminary report on the Grenville Front Tectonic Zone, Bruce Lake area, western Labrador. *Current Research, Part A*, Geological Survey of Canada, Paper 87-1A, p.435-442.
- van Gool, J.A.M., Calon, T.J. and Rivers, T., 1987b: Grenvillian Geology of the Bruce Lake Area in Western Labrador. Internal report G.S.C.
- van Gool, J.A.M., Rivers, T. and Calon, T.J., 1989: Out-of-sequence thrusting in the Grenville Front thrust belt and a new terrane in the Parautochthonous Belt of western Labrador. Internal report, G.S.C.
- Vauchez, A., Maillet, D. and Sougy, J., 1987: Strain and deformation mechanisms in the Variscan nappes of Vendée, South Brittany, France. *Jrnl. Struct. Geol.*, 9, p.31-40.
- Wardle, R.J. and Bailey, D.G., 1981: Early Proterozoic sequences in Labrador. In: *Proterozoic Basins of Canada*, F.H.A. Campbell (Ed.). Geological Survey of Canada, Paper 81-10, p.331-359.
- Wardle, R.J., Rivers, T., Gower, C.F., Nunn, G.A.G. and Thomas, A., 1986: The northeastern Grenville Province: new insights. In: *The Grenville Province*, J.M. Moore, A. Davidson and A.J. Baer (Eds.), G.A.C. spec. pap. 31, p.13-29.
- Wernicke, B., 1981: Low-angle normal faults in the Basin and Range Province: nappe tectonics in an extending orogen. *Nature*, 291, p.645-648.
- Wernicke, B., 1985: Uniform-sense normal simple shear of the continental lithosphere. *Can. J. Earth Sci.*, 22, p.108-125.
- White, S.H., 1976: The effects of strain on the microstructures, fabrics, and deformation mechanisms in quartzites. *Phil. Trans. R. Soc. London (A)*, 283, p.69-86.

- White, S.H., Burrows, S.E., Carreras, J., Shaw, N.D. and Humphreys, F.J., 1980: On mylonites in ductile shear zones. *J. Struct. Geol.*, 2, p.175-187.
- Wilson, M.E., 1918: The subprovincial limitations of pre-Cambrian nomenclature in the St. Lawrence basin: *J. Geol.*, 26, p.325-333.
- Windley, B.F., 1981: Precambrian Rocks in the Light of The Plate Tectonic Concept. In: *Precambrian Plate Tectonics*, A. Kroner (Ed.), Elsevier. p.1-20.
- Windley, B.F., 1986: Comparative tectonics of the western Grenville and the western Himalaya. In: *The Grenville Province*, J.M. Moore, A. Davidson and A.J. Baer (Eds.), G.A.C. spec. pap. 31, p.341-348.
- Winkler, H.G.F., 1979: *Petrogenesis of metamorphic rocks*. 5<sup>th</sup> ed. Springer Verlag, New York, 348 p.
- Wood, B.J. and Fraser, D.G., 1977: *Elementary Thermodynamics for Geologists*. Oxford University Press, Oxford, 303 p.
- Woodsworth, G.J., 1977: Homogenization of zoned garnet from pelitic schists. *Can. Mineral.*, 15, p.230-242.
- Woodward, N.B., 1987: Geological applicability of critical-wedge thrust-belt models. *Geol. Soc. Am. Bull.*, 99, p.827-832.
- Wynne-Edwards, H.R., 1972: The Grenville Province. In: *Variations in Tectonic Styles in Canada*, R.A. Price and R.J.W. Douglas (Eds.). Geological Association of Canada, special paper 11. p.263-334.
- Wynne-Edwards, H.R., 1976: Proterozoic ensialic orogenesis: The millipede model of ductile plate tectonics. *Am. J. Science*, 276, p.927-953.
- Zwart, H.J., 1962: On the determination of polymetamorphic mineral associations, and its application to the Bosost area (Central Pyrenees). *Geol. Rundschau*, 52, p.38-65.

## APPENDIX A

### SOURCES FOR COMPILATION OF MAPS

The map in Figure A.1 shows the sources from which the maps in the thesis were compiled. Some well-exposed parts of the map area were completely re-mapped in detail (1:10,000 scale), but these form only a minor part of the total map area. Other areas were re-interpreted, based on reconnaissance traverses, air photo interpretation, re-interpretation of original data of Rivers (pers. comm. and outcrop data on 1:50,000 scale maps, Rivers, 1980a,b and c) and extrapolation from adjoining areas which were mapped in detail. A few localities in the southeastern part of the map were visited for sample collection only (see Fig. F.3).

In several parts of the map outside the areas mapped in detail, new thrust boundaries were drawn, based either on reconnaissance traverses or on re-interpretation of pre-existing maps. In most cases this involved the re-interpretation of geological contacts in maps by Rivers (1985a, b and c) as thrust faults. This was done only if it was geometrically feasible and possible to do so with a high level of certainty. The trace of the Grenville Front was interpreted from air photos and backed up by reconnaissance in the field through helicopter traversing. The trace of the Bruce Lake shear zone north of Grace Lake was taken from Fahrig. The remainder of the information was taken from maps of Rivers (1985a, b and c).

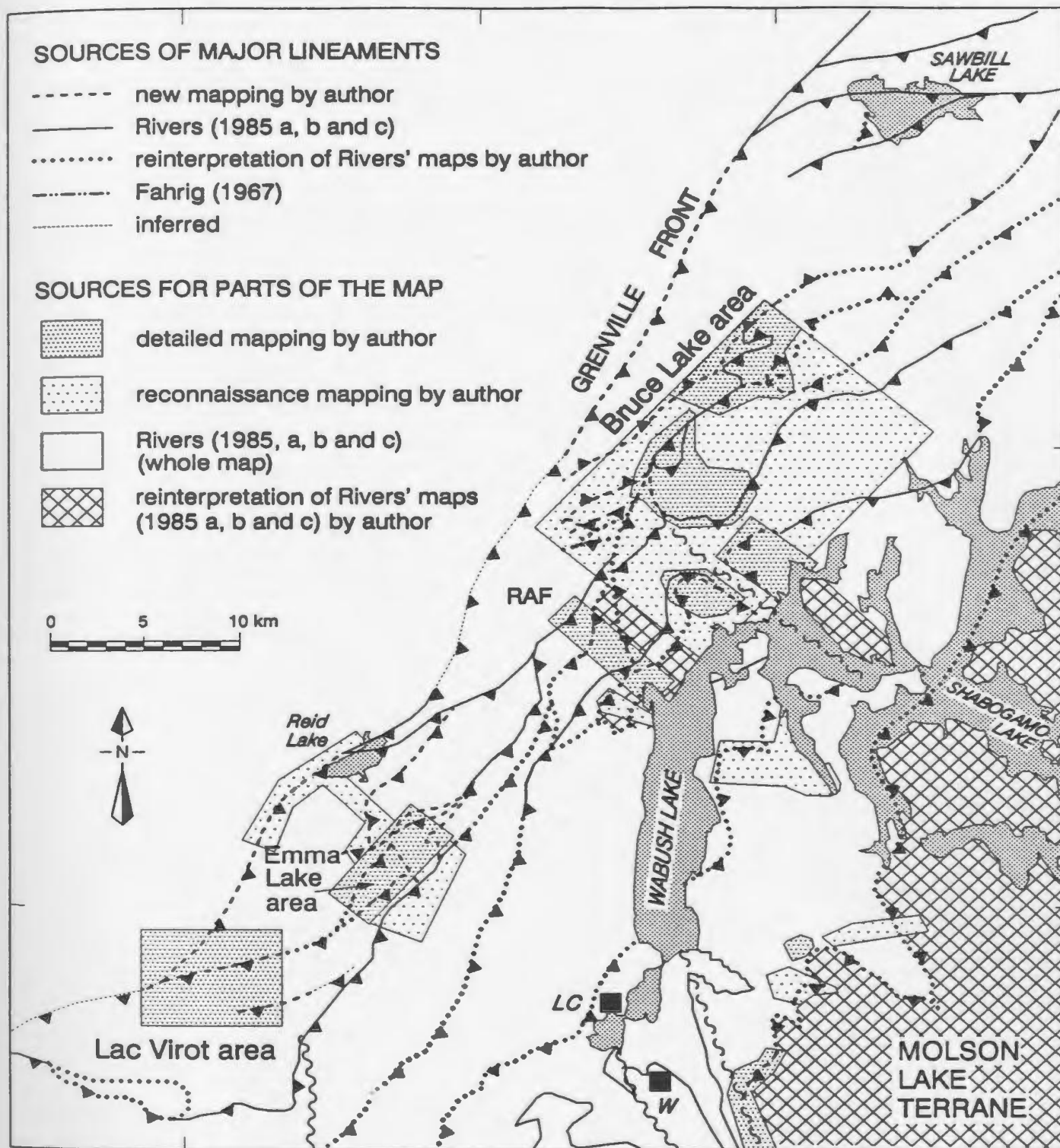


Fig. A.1 Tectonic map of Gagnon terrane in southwestern Labrador showing the sources for the compilation of the map of Figure 1A (in pocket). RAF = Rivière aux Fraïses area. LC = Labrador City, W = Wabush.

## APPENDIX B

### ABBREVIATIONS

The following are two lists of abbreviations used in the text. The first is a list of mineral names. The second list explains abbreviations used in thermodynamics in Chapter 7.

#### MINERAL NAMES

Abbreviations for mineral names according to Kretz (1983), capitalizing the first character for mineral phases and using all lower case characters for components. Abbreviations marked \* are not from Kretz (1983)

Ab	albite	Cpx	Ca clinopyroxene
Act	actinolite	Cum	cummingtonite
Alm	almandine	Czo	clinozoisite
Aln	allanite	Di	diopside
Als*	aluminum silicate (and, ky or sil)	Dol	dolomite
Amp*	amphibole	Ep	epidote
An	anorthite	Fe-Dol*	ferrodolomite
And	andalusite	Gr	graphite
Ank	ankerite	Grs	grossularite
Ann	annite	Grt	garnet
Ap	apatite	Gru	grunerite
Bt	biotite	Gt	goethite
Cal	calcite	Hbl	hornblende
Cel*	cecladonite	Hem	hematite
Chl	chlorite	Hyp	hypersthene
Cld	chloritoid	Ilm	ilmenite
		Kfs	K-feldspar

Ky	kyanite	Rdn	rhodonite
Liq*	granitic melt	Rt	rutile
Lm	limonite	Scp	scapolite
Mag	magnetite	Sd	siderite
Mc	microcline	Sil	sillimanite
Mgs	magnesite	Spn	sphene
Mrg	margerite	Sps	spessartine
Ms	muscovite	St	staurolite
Opx	orthopyroxene	Stp	stilpnomelane
Or	orthoclase	Tr	tremolite
Pg	paragonite	Tur	tourmaline
Phe*	phengite	V*	H <sub>2</sub> O
Phl	phlogopite	Wo	wollastonite
Pl	plagioclase	Zrn	zircon
Prp	pyrope	Zo	zoisite
Qtz	quartz		

### **THERMODYNAMICS ABBREVIATIONS**

**G = Gibbs energy**

**H = enthalpy**

**K = equilibrium constant**

**P = pressure**

**R = gas constant**

**S = entropy**

**T = temperature**

**V = volume**

**Δ = change of a quantity (G, H, S or V) in a reaction**

## **APPENDIX C**

### **LITHOLOGICAL DESCRIPTION OF THE ROCKS OF THE KNOB LAKE GROUP**

The tables on the following pages contain a short description in point form of the most important lithological and mineralogical characteristics of the formations in the Lower Proterozoic Knob Lake Group and of the Archean basement in the map area. The descriptions are given for greenschist and amphibolite metamorphic grade separately. Not all formations are represented at both metamorphic grades. The descriptions in the paragraph below emphasize the differences between the lithological units which in the field can have similar appearances.

#### **DISTINCTIVE CHARACTERISTICS OF SIMILAR ROCK TYPES**

As stated in Section 3.1.2, rocks of the Archenan basement, the Attikamagen Formation and the Menihék Formation can have similar field appearances in certain states of strain and at certain metamorphic grades. Rocks in several parts of the area have been re-assigned to different stratigraphic units from pre-existing maps. The re-interpretations were based on careful examination in the field and on detailed petrographic studies. The following characteristics of the stratigraphic units were used as criteria.

##### **Archean basement**

- Stratigraphic position below the Sokoman Formation.
- The presence of low strain lenses of granulite-grade rocks or granitoids in the reworked basement rocks.
- Felsic and mafic rocks locally occur interlayered.
- Exsolution of rutile needles in biotite (see Chapter 7).
- Amphibole is more common in parts of the basement than in the Attikamagen and Menihék formations.

- K-Feldspar and epidote are common in the basement rocks, especially at lower Grenvillian metamorphic grades.
- Garnet is uncommon in basement rocks and alumino-silicates are absent.
- Mica-rich rocks are uncommon and contain predominantly biotite.

#### **Attikamagen Formation**

- Stratigraphic position below the Sokoman and Denault formations.
- Kyanite is locally present in the higher thrust sheets.
- Pelitic schists contain both biotite and muscovite and commonly contain garnet.
- K-feldspar and amphiboles do not commonly occur.
- Graphite occurs locally.

#### **Menibek Formation**

- Stratigraphic position above the Sokoman and Denault formations.
- Graphite is commonly present.
- Sedimentary layering is preserved at low metamorphic grade.
- Pelitic schists are common and contain both biotite and muscovite.
- Kyanite and garnet are common in rocks of appropriate metamorphic grade.
- K-feldspar and amphiboles are uncommon.

**Table C.1 Stratigraphy and lithological characteristics of the Knob Lake Group**

Formation name	rock type		field appearance	
	greenschist facies	amphibolite facies	greenschist facies	amphibolite facies
<b>MENIHEK FM</b>	Graphitic schist or slate	pelitic schist or gneiss	<ul style="list-style-type: none"> <li>* fine grained,</li> <li>* dark grey to black,</li> <li>* homogeneous, minor compositional variations, locally interlayered with quartz-rich layers</li> <li>* well foliated, commonly crenulated</li> </ul>	<ul style="list-style-type: none"> <li>* medium grained</li> <li>* porphyroblastic</li> <li>* brown weathering colour</li> <li>* foliated</li> </ul>
<b>SOKOMAN FM</b> Upper member	banded carbonate - quartzite iron formations	banded silicate-carbonate iron formation	<ul style="list-style-type: none"> <li>absent or thin in west of the area</li> <li>* fine grained</li> <li>* red-brown, ochre, rarely white</li> <li>* banded with carbonate-rich and quartz-rich layers</li> <li>* siderite concretions</li> </ul>	<ul style="list-style-type: none"> <li>* fine to medium grained</li> <li>* porphyroblastic</li> <li>* dark red-brown or ochre to dirty white colours</li> <li>* layered</li> <li>* foliated and lineated</li> </ul>
Middle member	banded cherty oxide iron formation	quartzitic oxide iron formation	<ul style="list-style-type: none"> <li>* very fine to fine-grained</li> <li>* dark bluish grey</li> <li>* thinly banded to massive</li> </ul>	<ul style="list-style-type: none"> <li>* fine to medium-grained</li> <li>* dark bluish grey, with high quartz content light grey</li> <li>* banded to massive</li> </ul>
Lower member	banded carbonate - silicate iron formation	banded silicate iron formation	<ul style="list-style-type: none"> <li>* fine grained</li> <li>* red brown or ochre</li> <li>* banded to massive</li> <li>* siderite concretions</li> </ul>	<ul style="list-style-type: none"> <li>* medium to coarse grained</li> <li>* porphyroblastic</li> <li>* dark red brown to ochre</li> </ul>
<b>WISHART FM</b> Upper member		orthoquartzite		<ul style="list-style-type: none"> <li>* medium to coarse grained</li> <li>* white</li> <li>* massive</li> </ul>
Lower member		pelitic schist		<ul style="list-style-type: none"> <li>* fine-medium grained</li> <li>* brown-red weathering colour</li> </ul>

Table C.1 continued

Formation name	rock type		field appearance	
	greenschist facies	amphibolite facies	greenschist facies	amphibolite facies
MCKAY RIVER FM	chloritic schist	amphibolite	<ul style="list-style-type: none"> <li>• fine-grained</li> <li>• light grey-green</li> <li>• well foliated, schistose</li> <li>• mm to cm scale layering</li> </ul>	<ul style="list-style-type: none"> <li>• medium to coarse grained</li> <li>• porphyroblastic</li> <li>• dark green</li> <li>• foliated</li> <li>• compositional layering</li> </ul>
DENAULT FM		dolomitic marble		<ul style="list-style-type: none"> <li>• medium to coarse-grained</li> <li>• white, with a yellow weathering colour</li> <li>• massive</li> </ul>
ATTIKAMAGEN FM western and eastern facies		biotite schist/gneiss or pelitic schist		<ul style="list-style-type: none"> <li>• medium to coarse-grained</li> <li>• porphyroblastic</li> <li>• white, yellow or light brown</li> <li>• well foliated</li> <li>• gneissic or differentiated layering</li> <li>• abundant granitic veins</li> </ul>

**Table C.2 Mineralogy and depositional environment of the formations**

Formation name	mineralogy		depositional environment/ sedimentary facies
	greenschist grade	amphibolite grade	
<b>MENIHEK FM</b>	Qtz + Ms + Bt + Chi + Gr ± Ab	Qtz + Bt + Ms ± Pl ± Grt ± Ky ± St	deep marine platform sequence
<b>SOKOMAN FM</b> Upper member	Qtz + Dol + Sd ± Gru ± Mag ± Hem ± Mgs ± Rdn	Qtz + Dol + Sd + Gru ± Grt ± Cpx ± Opx ± Chl ± Mag ± Hem	platformal chemical sediment
Middle member	Qtz (chert) + Mag or Hem	Qtz + Mag or Hem (rarely Mag + Hem)	
Lower member	Qtz + Dol + Sd ± Gru ± Mag ± Hem ± Mgs ± Rdn	Qtz + Dol + Sd + Gru ± Grt ± Cpx ± Opx ± Chl ± Mag ± Hem	
<b>WISHART FM</b> Upper member		Qtz	littoral deposit
Lower member		Qtz + Ms ± Grt ± Ky ± St	
<b>MCKAY RIVER FM</b>	Qtz + Pl + Chl + Zo	Hbl + Bt + Pl + Grt ± Qtz ± Ep ± Chl	metavolcanics/tuffs
<b>DENAULT FM</b>		Dol ± Di ± Tr ± Qtz	stromatolitic reef
<b>ATTIKAMAGEN FM</b> western and eastern facies		Qtz + Ms + Bt + Grt ± Pl ± Ky ± Sil ± St ± Chl	western facies: shallow platform sequence and basal conglomerate eastern facies: turbiditic deposits

## APPENDIX D

### STRUCTURAL ORIENTATION DATA

All structural orientation data and a map showing the subdivision of the data sets are presented in Figure D.1. The data are plotted in lower hemisphere equal area nets and contoured using a computer program for manipulation of orientation data, QUICKPLOT, by van Everdingen et al. (in press). Bedding and foliations are plotted as poles to planes. For the contouring, the program uses a Gauss-like counting curve which produces contour lines in multiples of uniform distribution (Robin and Jowett, 1985). No distinction was made between structural elements related to the upper or the lower thrust system. The data are discussed in Chapter 5.

The orientation data sets contain measurements from the field for the areas that were mapped in detail and data collected in the field combined with data taken from the maps by Rivers (1980a,b,c) for the areas that were not sufficiently covered by field observations. The data sets that are predominantly taken from the maps do not distinguish between different ages of folds and all fold axes are grouped together and presented as  $F_2$  folds. The dip angles of the orientation data in the published maps were originally rounded to multiples of 5 (Rivers, 1980a, b, c). For the contouring of these data a random number between -2 and +2 was added to each of the dips or plunges, to avoid artificial maxima introduced by the rounding. Presumably, this does not significantly change the accuracy of the data set. A rounding of the directions of the dip or the plunge was not detected in the maps.

Eigenvalues of the orientation data sets were calculated to fit great circles through planar data that represent at least a partial great circle distribution. Most of the data sets cover large areas and reflect distribution patterns caused by both small scale and large scale structures. The data sets of foliation measurements that are large enough will show point maxima for the dominant orientation, possibly defining partial great circles. Very small data sets generally lack well defined patterns.



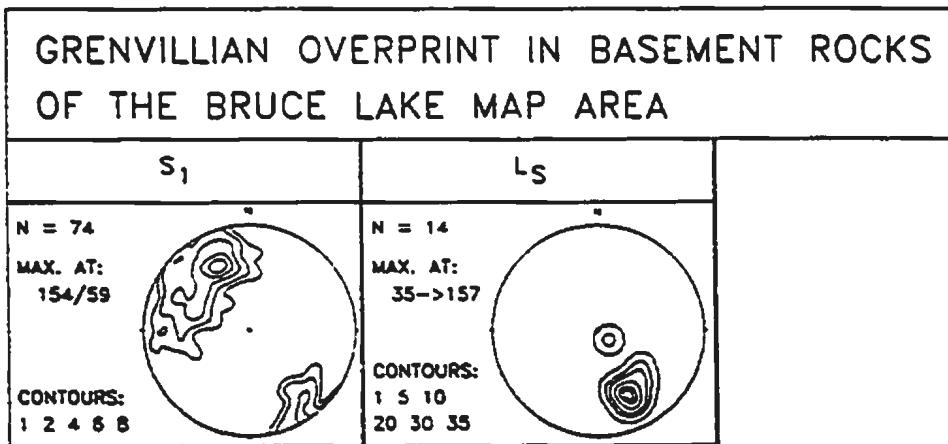
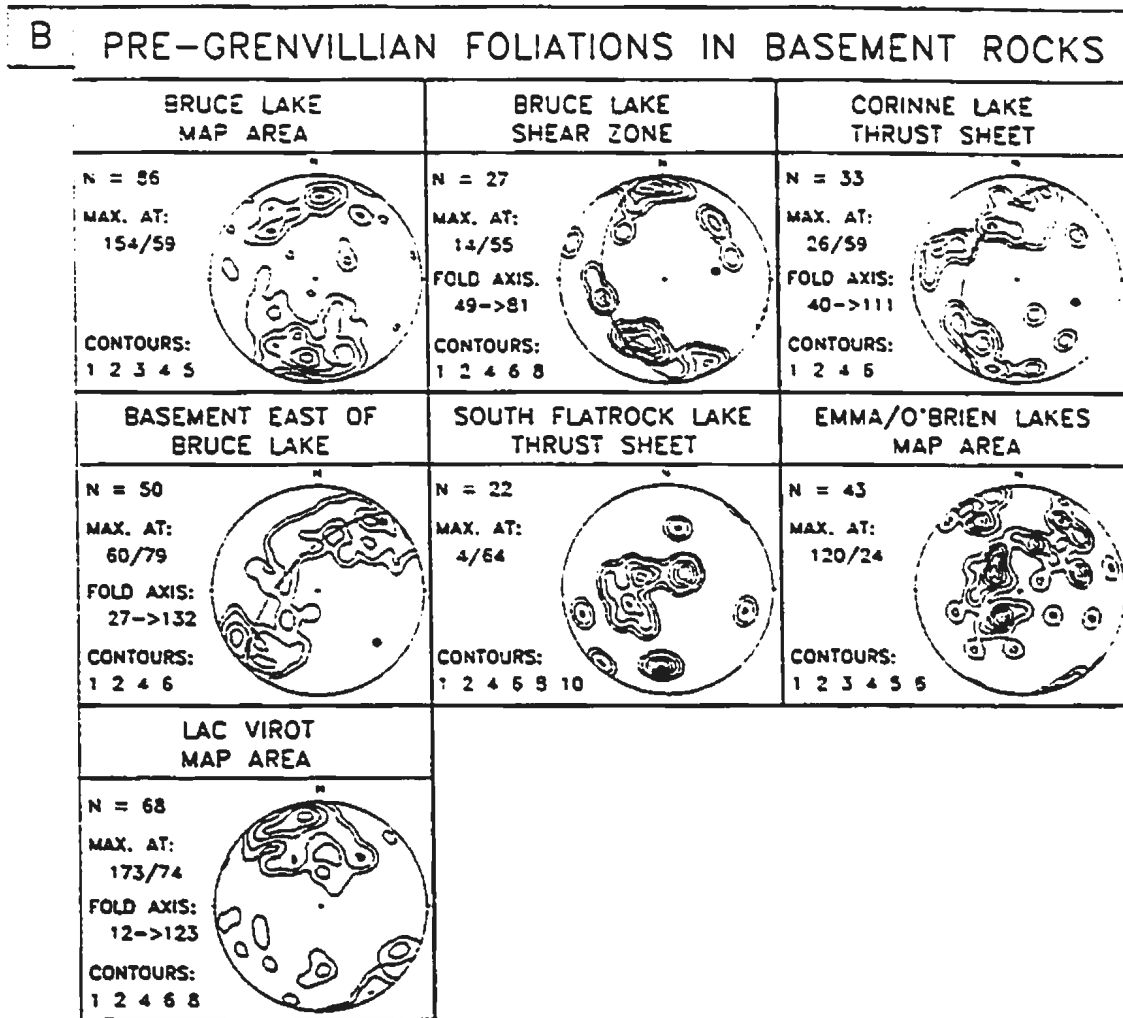


Fig. D.1 continued

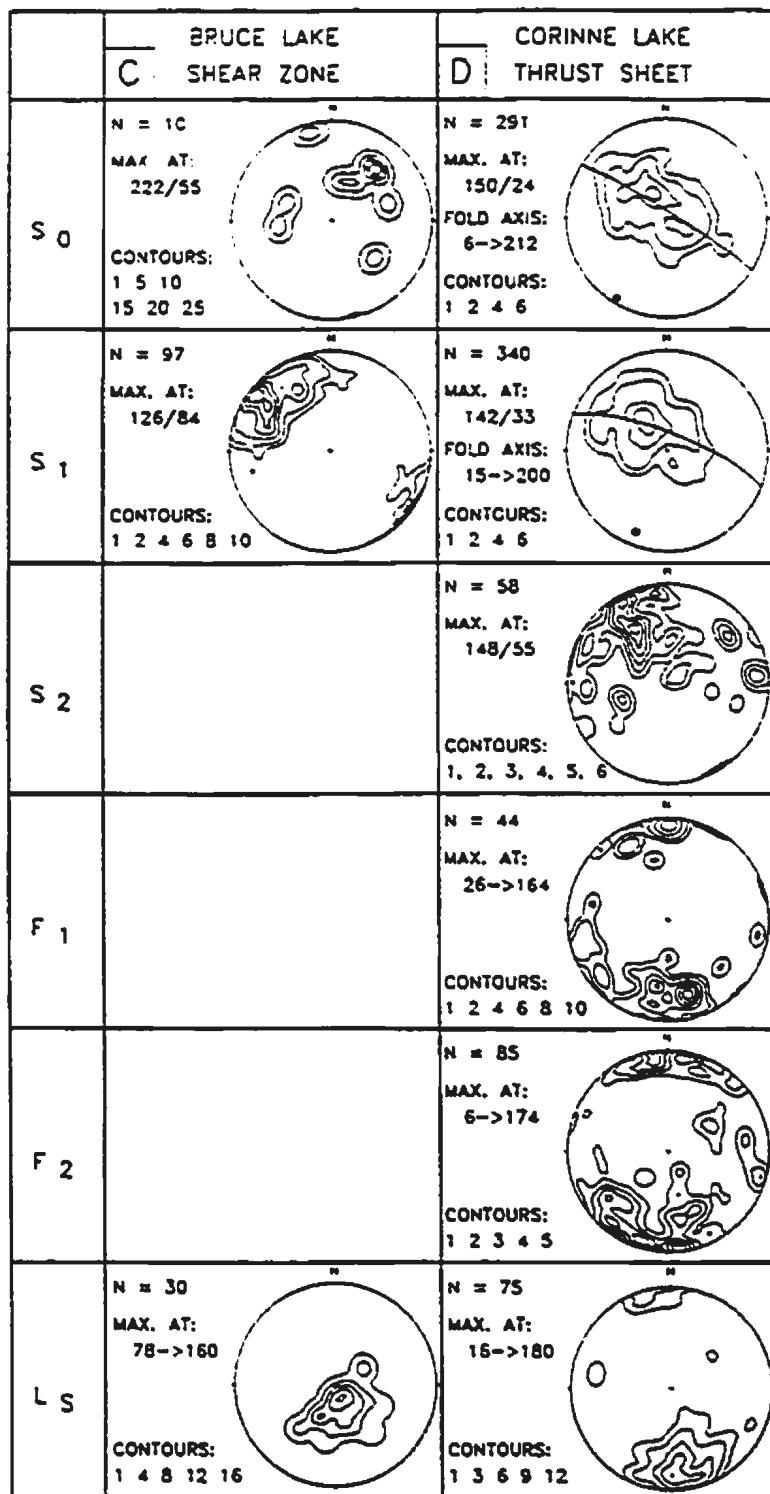


Fig. D.1 continued

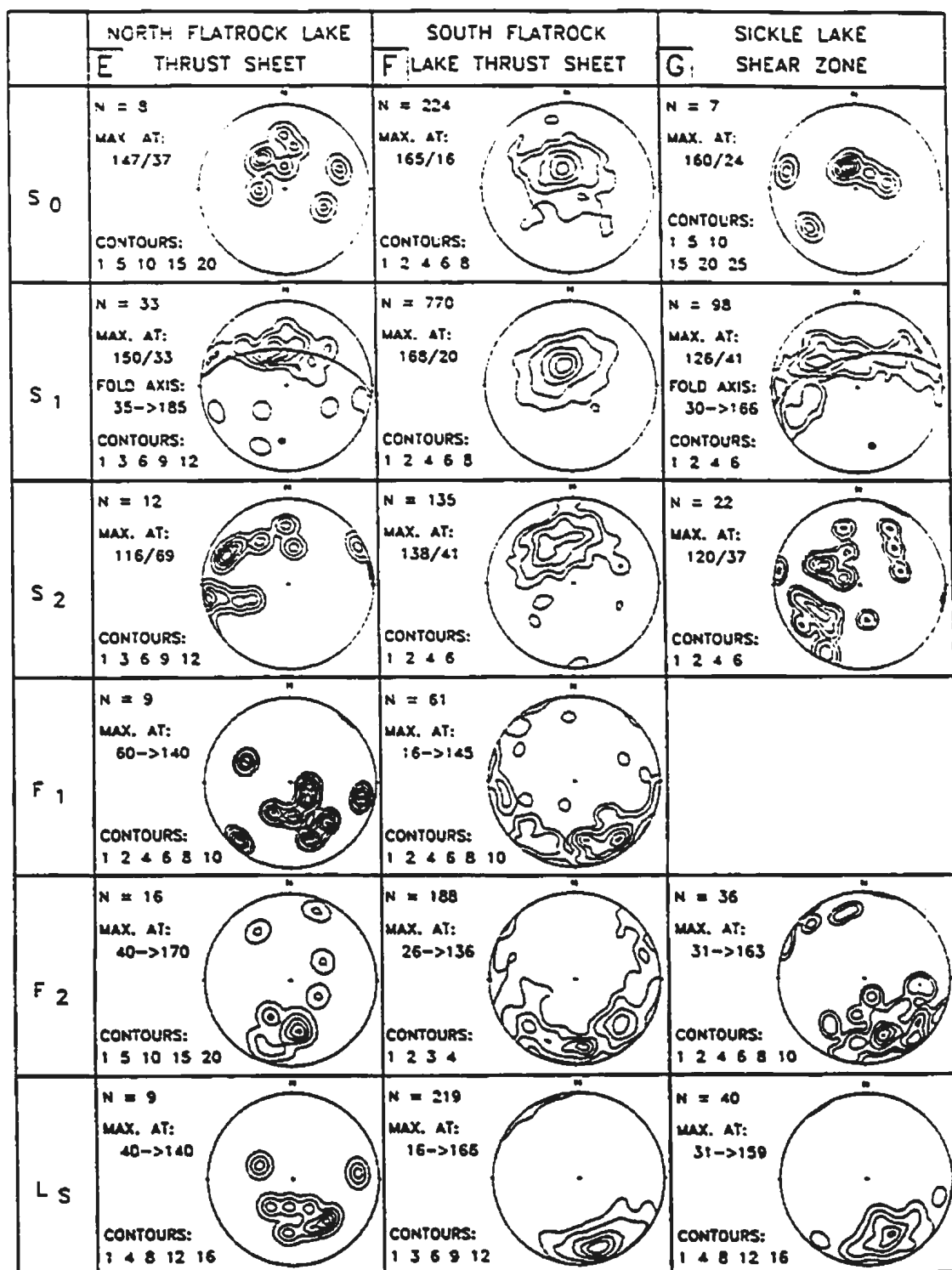


Fig. D.1 continued

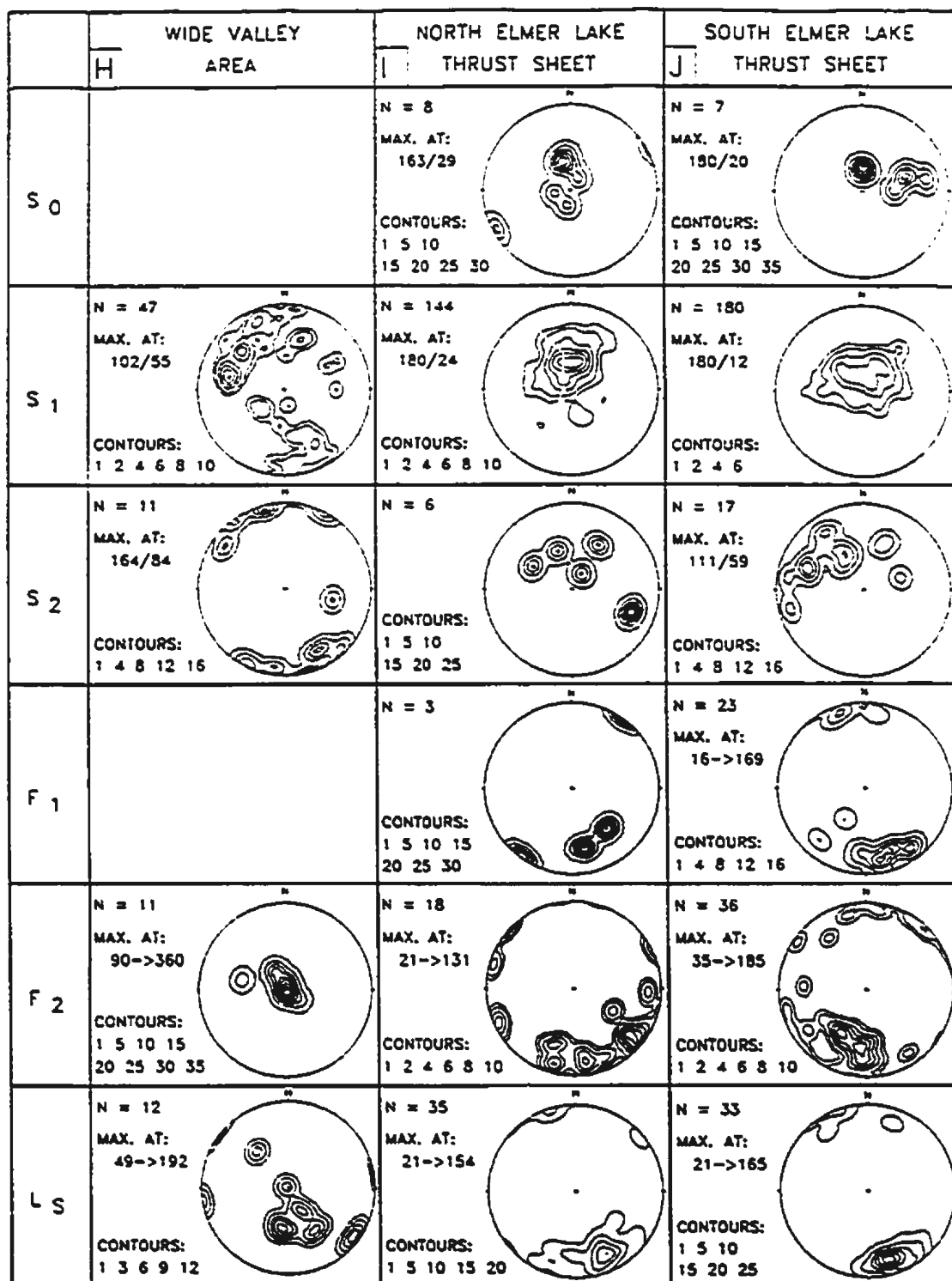


Fig. D.1 continued

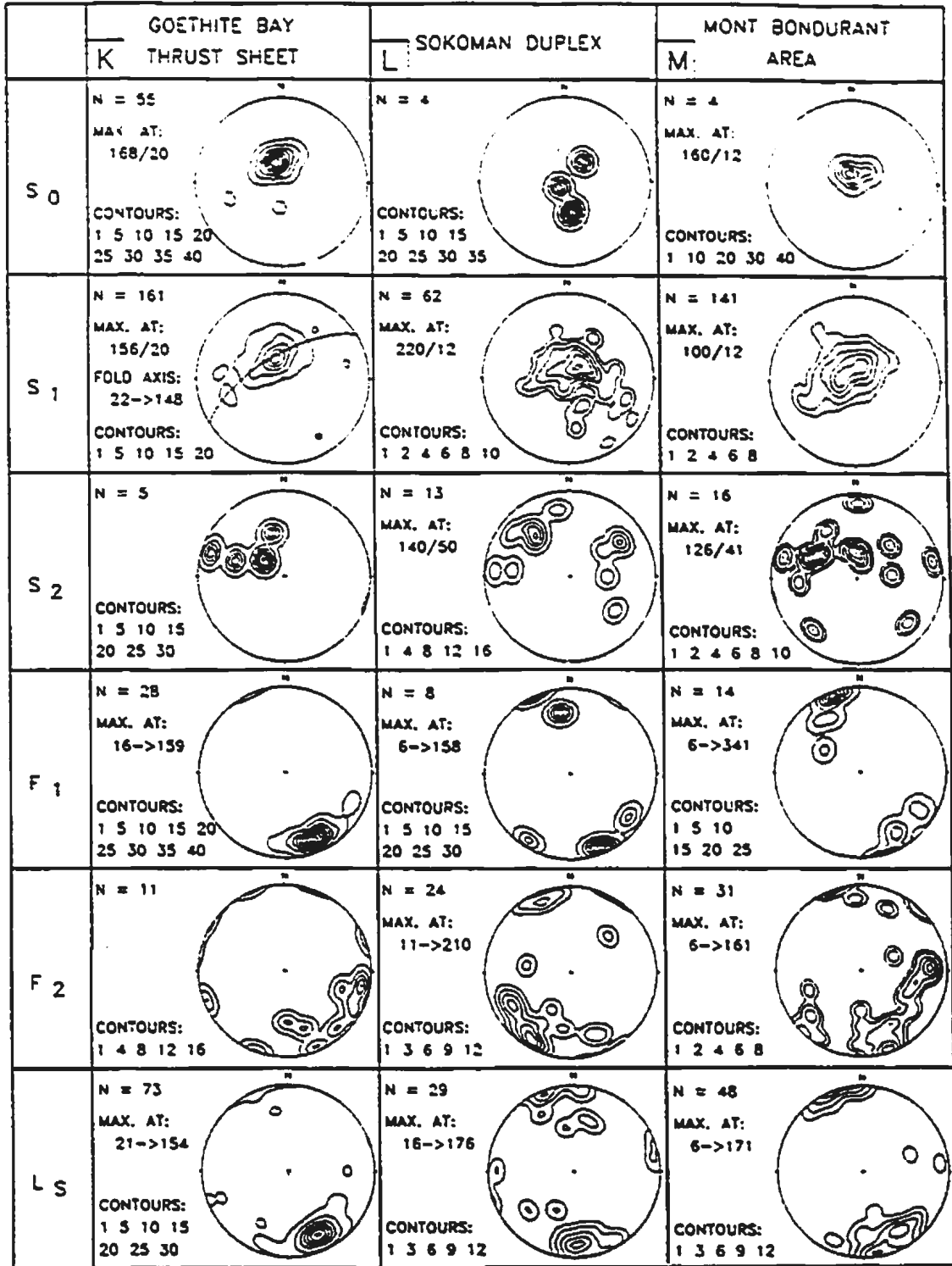


Fig. D.1 continued

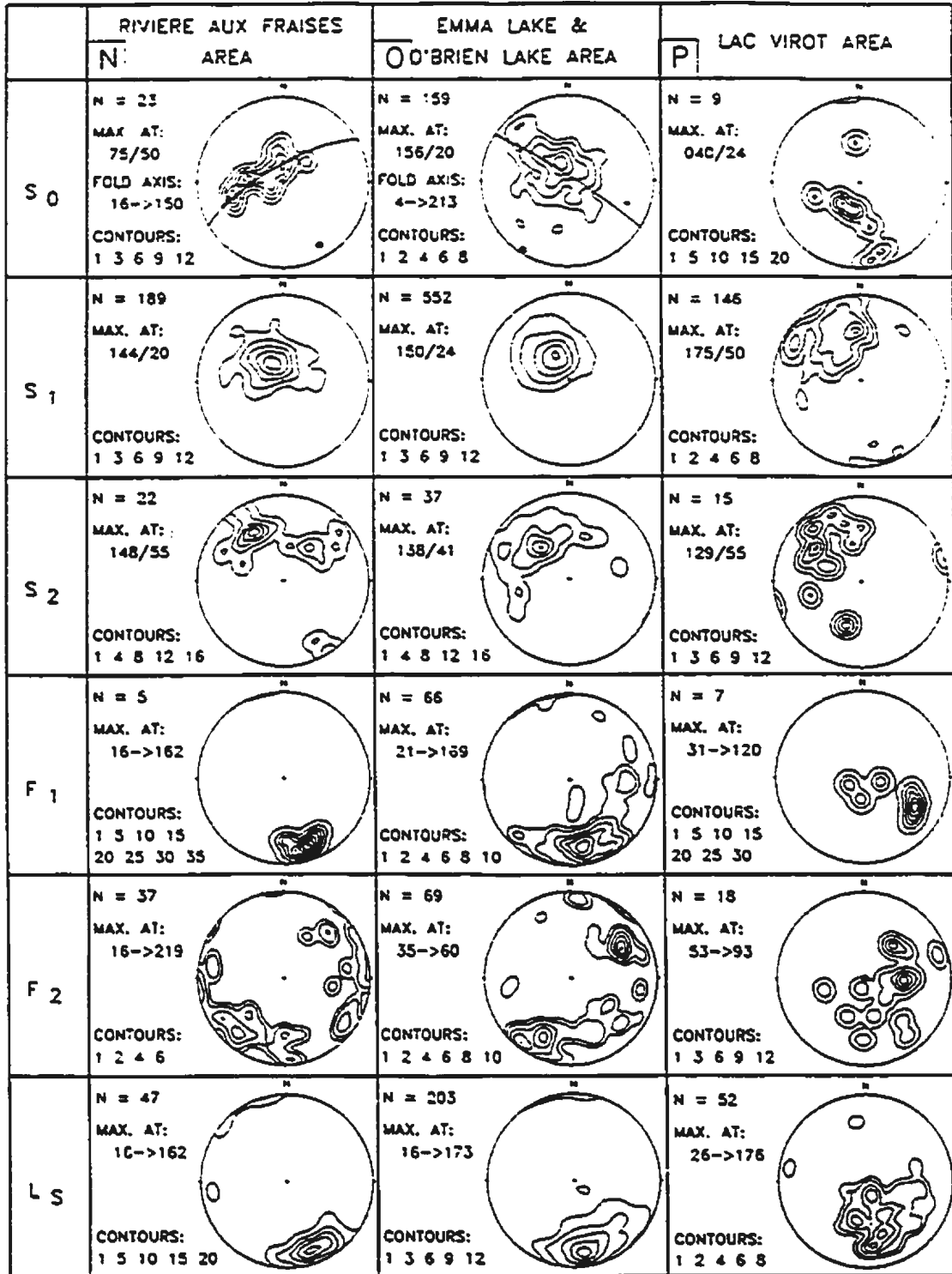


Fig. D.1 continued

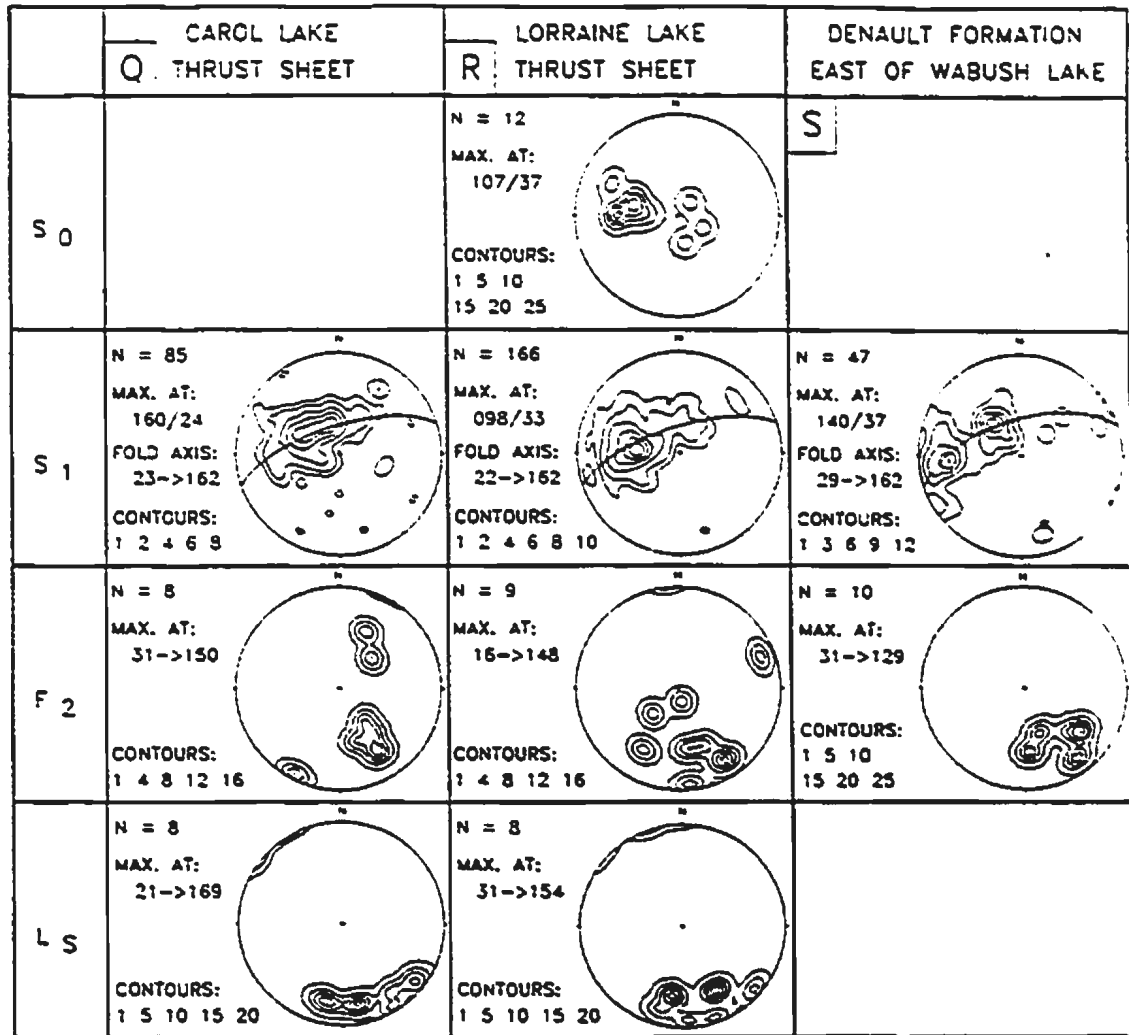


Fig. D.1 continued

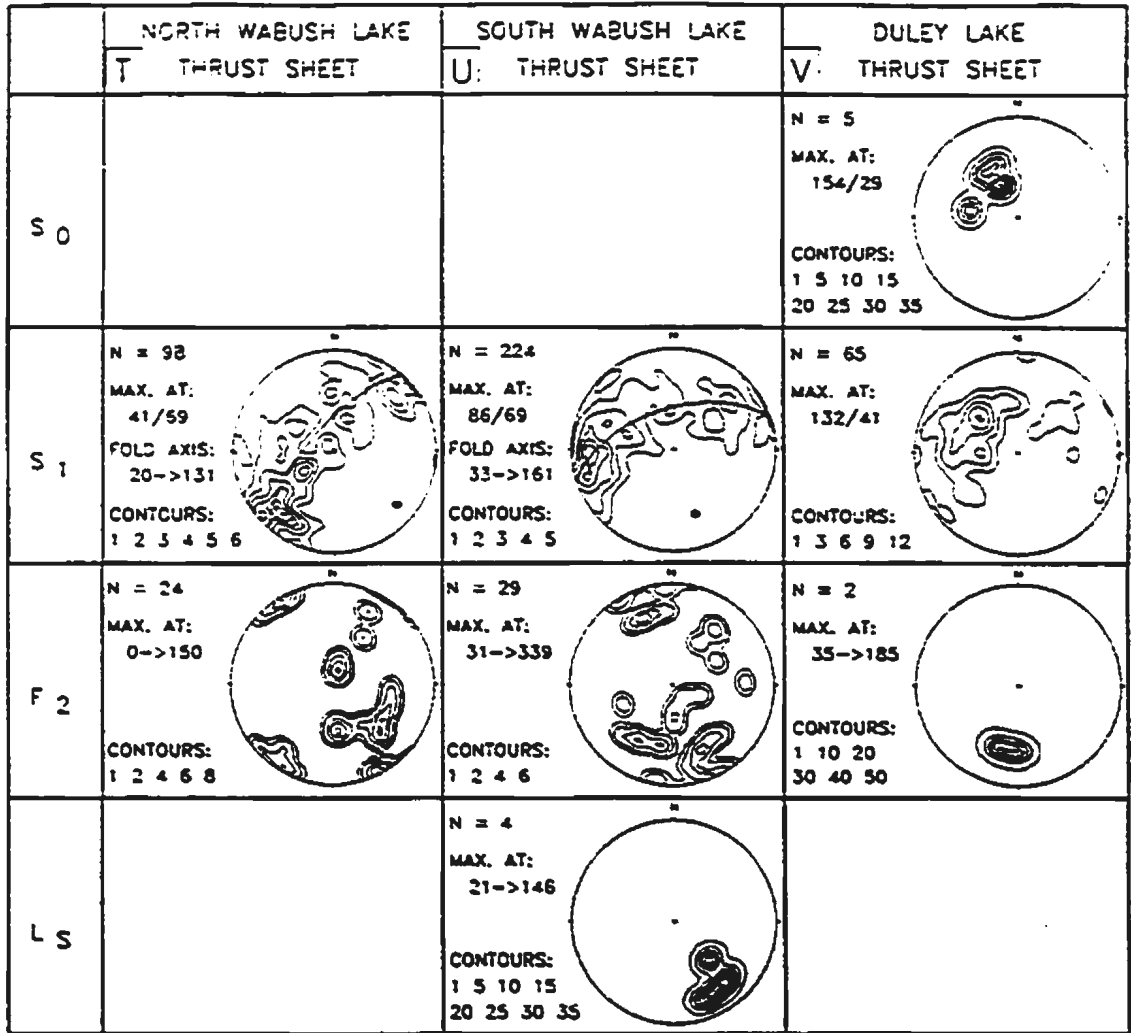


Fig. D.1 continued

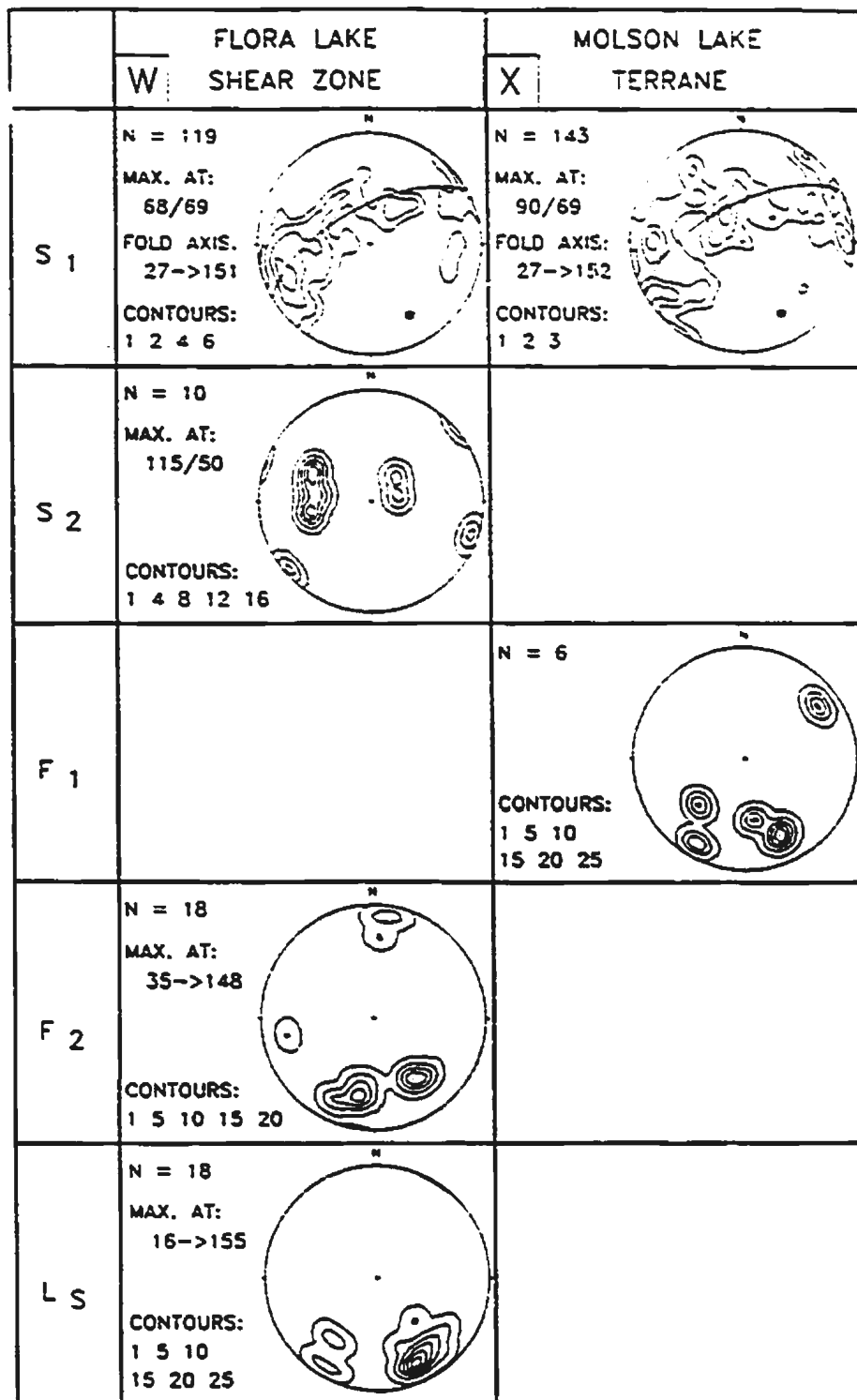


Fig. D.1 continued

## APPENDIX E

### OBSERVED MINERAL ASSEMBLAGES

The two tables in this appendix are lists of the mineral assemblages that were observed in samples from the map area. Table E.1 gives the assemblages in the meta-pelitic and quartzo-feldspathic rock types for each of the metamorphic zones, together with the name of the formation in which it was observed. Table E.2 contains the observed mineral assemblages in the mafic rocks.

Table E.1 Mineral assemblages in the meta-pelitic and quartzo-feldspathic rock types<sup>1</sup>

Formation <sup>2</sup>	Qtz	Pl	Kfs	Bt	Ms	Chl	Ep	Gr	Ap	Spn	Others	
<b>Zone 1</b>												
B	X	X	X		X	X				A	Carb, Zrn, Opq	
<b>Zone 2</b>												
B	X	X	X	X	X		X		±	±	± Act, ± Carb, ± Aln	
B	X	X	X	X	X	R	X		±		± Carb, ± Zr	
B	X	X	U	X	X	X	X		±	±	± Zr, ± Act, ± Carb	
B	X	X		X	X	X	X		±		± Act, ± Aln	
B	X	X	U	X	X					A		
B	X	X		X	X		X		A		Act, Opq	
M	X	X	X	X	X			X		±	± Carb, ± Act	
M	X			X	X	X		X	A		Hem	
M	X	X		X	X			X				
Formation <sup>2</sup>	Qtz	Pl	Kfs	Bt	Ms	Chl	Grt	Ep	Gr	Ap	Spn	Others
<b>Zone 3</b>												
B	X	X	X	X	X	R	X	X				± Tur, ± Py, ± Carb
B	X	X	X	X	X	±R		X		±	±	± Carb, ± Aln, ± Zrn, ± Mag
B	X	X	X	X	R	R						
B	X	X	X	X				X				
B	X	X	X	X	X							Zn
B	X	±		X	X	X	X	±				± Act, ± Ilm
B	X	X		X	X	±		X		±	±	± Tur
B	X	X		X	X	±		X		±	±	± Carb, ± Aln
M	X	X		X	X	±R	X		±	±	±	± Tur
M	X			X	X	±R			X			
M	X		X	X					X			

Table E.1 continued

Formation <sup>2</sup>	Qtz	Pl	Kfs	Bt	Ms	Chl	Grt	St	Ky	Ep	Ap	Spn	Others
Zone 4													
B	X	X	X	X	X					±	±		± Carb
B	X	X	X	X	R					X			Py
B	X	X	X		X					X			
B	X	X		X	X	±	±			X	A		± Zr, ± Aln
B	X	X		X	± R					X	A		± Py
B	X	X			X								
A	X			X	X	X	X				A		Tur
A	X	X		X	X								Aln
W	X				X		X	X	X				
W	X				X								
W	X				X	R	X	U	X				Tur, Cld(R)
W	X				X	R	X				X		Cld(R), Hem
W	X				X		X	X					Hem
W	X				X				X				Tur
W	X				X		X		X				
W	X			X	X	R				X			Cld(R), Hem
W	X			X	X		X						

Formation <sup>2</sup>	Qtz	Pl	Kfs	Bt	Ms	Chl	Grt	Ky	Ep	Ap	Spn	Others	
Zone 5													
A	X	X		X	X		X	X					
A	X			X	X	R	X	X	±	±			± Gra, ± Tur
A	X	X	X	X	X		X				A		Rt
A	X			X	X	R	X	X			±		St(U), Sil, Rt, Zrn
M	X	X		X	X		X	X			A		St(U), Rt, Gra

Zone 6													
A	X	X	X	X	X				X	A	A		
A	X	X		X	X		X	X					Gra, ± Rt, ± Tur
A	X	X		X	R	R	X	±					± Zrn
A	X	X		X	X	R	X		X				
A	X	X		X			X			±			± Carb
A	X	X		X					X	A			
A	X			X	X	±	X		±	±			± Tur

<sup>1</sup> A = accessory mineral, R = retrograde growth, U = unstable relic, X = major or minor component, ± = appears in some samples

The zone numbers refer to the mineral assemblages zones in the meta-pelitic and quartzofeldspathic rock types (section 7.2)

Abbreviations for mineral names as in appendix 1. Carb = unspecified carbonate.

<sup>2</sup> A = Attikamagen Formation, B = basement, M = Menihek Formation, W = Wishart Formation

Table E.2 Mineral assemblages in the mafic rock types<sup>1</sup>

Formation <sup>2</sup>	Qtz	Pl	Bt	Chl	Grt	Ep	Act	Hbl	Spn	Ilm	Others
<b>Zones 1 and 2</b>											
B	X	X	X			X	X		A	A	
B		X		X		X	X		X	X	Kfs, Ap
MC	X	X	X	X		X	X		A	X	Ap
MC		X	X	X					A	A	Zo, Carb
<b>zones 2 and 3</b>											
B	X	X	X				X				Zo
B	X	X	X		X	±	X		±	X	Zo, ±Arf, ±Opx(U)
B	X	X	X		X			X	X	A	
B	X	X	X		X	X	X		X	A	Zo
B	X	X	X				X	X		X	Cpx(U), Ap
B	X	X	X				X			X	Carb
G		X	X	R		X	X			X	
MC		X	X			X	X	X		X	
<b>Zone 4</b>											
B	X	X	X			X	X	X	A		Carb
B	X	X	X			X		X			
B		X	X				X				Carb
<b>Zone 5 no observations</b>											
<b>Zone 6</b>											
G		X	X		X			X	X		Cpx
MC		X			X			X	X		Scp
MC	X	X	X		X	±		X	X	±	±Rt, ±Ap
MC	X				X						Cpx
MC		X	X		X			X		X	Carb

<sup>1</sup> A = accessory mineral, R = retrograde growth, U = unstable relic, X = major or minor component, ± = appears in some samples

The zone numbers refer to the mineral assemblages zones as defined in the meta-pelitic and quartzo-feldspathic rock types (section 7.2)

Abbreviations for mineral names as in appendix 1. Carb = unspecified carbonate.

<sup>2</sup> B = mafic basement rocks, G = reworked gabbro of the Shabogamo Intrusive Suite,  
MC = McKay River Formation (or mafic lenses in the Attikamagen Formation)

## **APPENDIX F**

### **GARNET ZONING PROFILES**

This appendix presents chemical profiles through 16 garnets of the map area, together with a location map for the samples used for geothermobarometry. The presentation of the data is preceded by an introduction to zoning patterns in garnets.

#### **CHEMICAL ZONING PATTERNS IN GARNET**

Slow diffusion rates in garnet are the cause of both the creation of a chemical zoning pattern and its preservation. Material in the interior of a garnet is not part of the chemical system in the matrix and minerals in the matrix react with, or are in equilibrium with, the outer rim of the garnet only. Chemical zoning patterns in garnets can be attributed to either one of two processes (Tracy, 1982), 1) fractionation and/or reaction partitioning during prograde growth, producing growth zoning patterns, or 2) diffusional processes during retrograde metamorphism, which give diffusional or retrograde zoning patterns.

#### **GROWTH ZONING**

Two processes control the distribution of elements in a growing garnet. Bulk rock composition determines which process prevails. One of the processes is reaction partitioning (Trzcieski, 1977; Loomis, 1986). With changing P and T, the partitioning of some elements between the garnet and minerals in the matrix changes, causing progressively decreasing or increasing concentrations of these elements in the garnet. If an abundant supply of Fe-Mg minerals (Bt, Chl, St) and Ca minerals (Pl, Ep, Amp) is available for garnet-forming reactions, zoning in the garnet will reflect changes of the partitioning coefficients with changing P-T conditions.

In the second process, during growth of a garnet at greenschist to middle amphibolite facies the slow intracrystalline diffusion causes concentration of some of the elements in the garnet by fractionation, thereby effectively taking them out of the system. The matrix is progressively depleted of these elements during growth, which is

reflected in bell-shaped curves for the concentration profiles of these elements through the garnet (Hollister, 1966). This is especially obvious for Mn, derived mainly from chlorite, which is strongly partitioned into the garnet, but is not a major constituent of the matrix in pelitic rocks (Loomis, 1982, 1983; Loomis and Nimick, 1982; Tracy, 1982). Elements which are abundant in the matrix, specifically Fe and Mg, will not be significantly depleted by this process and fractionation will have little influence on the zoning patterns for these elements. Loomis (1982, 1983, 1986) and Loomis and Nimick (1982) numerically modelled garnet growth in a pelitic matrix and reproduced growth zoning profiles for Mn, Mg and Fe similar to those found in natural garnets.

Figure F.1.A shows the schematic growth zoning patterns (from the literature) for garnets from metapelites at metamorphic grades ranging from greenschist to lower amphibolite grade. Both spessartine and grossular show bell-shaped profiles, whereas pyrope and almandine concentrations, as well as the ratio  $Mg/(Mg + Fe)$ , usually increase towards the rim. Both spessartine and pyrope profiles commonly show reversals of slope near the rims, which is interpreted to be a retrograde (diffusion controlled) effect. In a composition map of the garnet grains, the zoning patterns are concentric.

#### **DIFFUSION (RETROGRADE) ZONING**

At approximately 650°C diffusion rates within garnet increase significantly, to such an extent that homogenization of garnets can take place in a geologically reasonable time and existing zoning patterns are commonly destroyed (Woodsworth, 1977; Tracy, 1982, Trzcieski, 1977; Lasaga, 1983; Dempster, 1985; Muncill and Chamberlain, 1988; Jiang and Lasaga, 1990). Zoning patterns of garnets affected by medium to high temperature metamorphism are restricted to the rims, with flat chemical profiles in the interiors of the grains (Fig. F.1.B). The zoning in the rims is caused by inter- and intracrystalline diffusion during the retrograde part of the metamorphic event or during a younger lower grade metamorphic event. Lasaga (1983) described the kinetics of these retrograde reactions and the effect of diffusion rates on the zoning pattern (see also Muncill and Chamberlain, 1988; Jiang and Lasaga, 1990). Generally the trends for Mn and Mg are the reverse of those observed in lower grade growth zoning patterns (Fig. F.1.b). Fe and Ca patterns are less straightforward

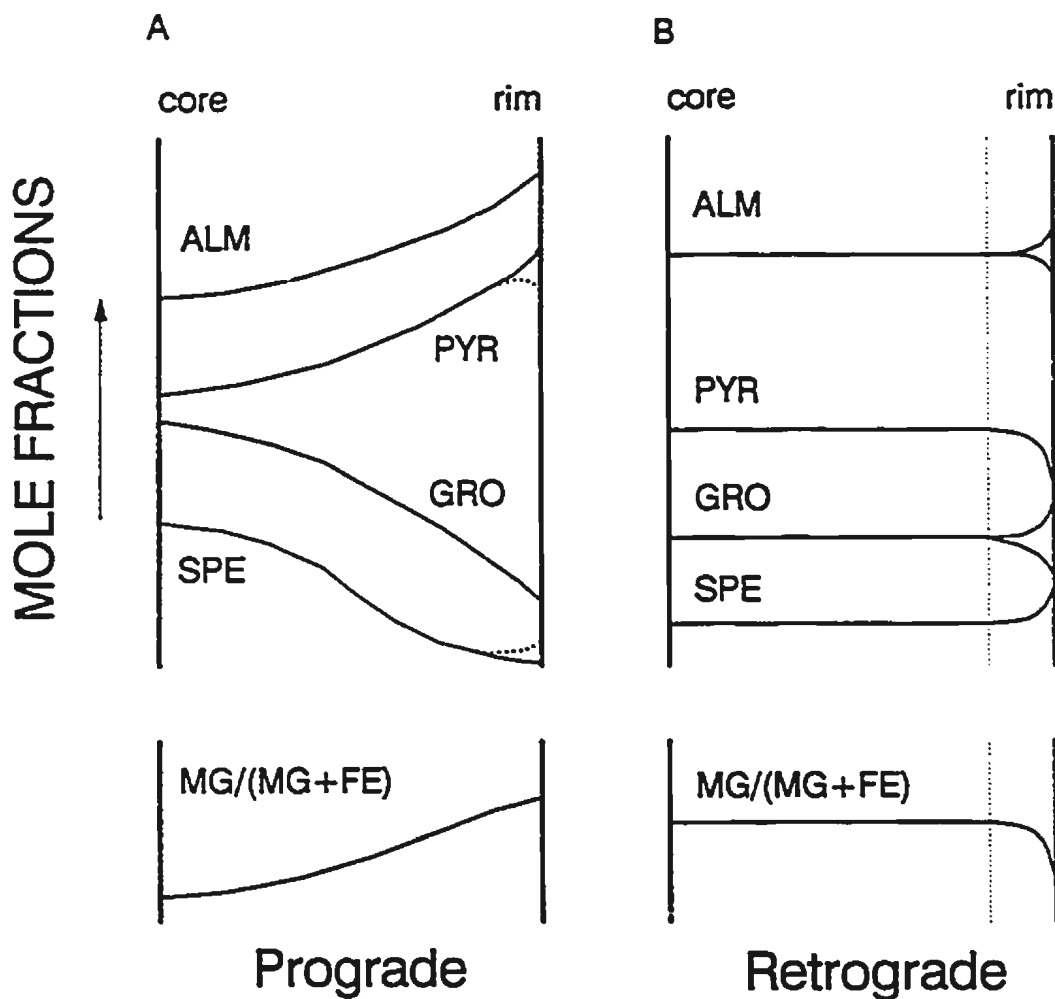


**Fig. F.1** Schematic chemical profiles through zoned garnets in metapelite. A) is a prograde zoning profile for garnets at greenschist to amphibolite facies and B) is a retrograde zoning profile for garnets at upper amphibolite to granulite facies. The relative concentrations of the four components and the slopes of the curves depend on bulk rock composition, growth/diffusion rates and P-T conditions during growth. The dotted curves near the rim in A) represent retrograde diffusion at the rims.

and vary, mainly with bulk rock compositions and reactant phases present in the matrix (Crawford, 1977; Woodsworth, 1977). Zoning patterns in composition maps are commonly concentric, but localized patterns at the rim near contacts with Fe-Mg phases (mainly biotite) may occur in high grade rocks. This is because in these sites the diffusion paths are shorter than for elements in minerals separated from the garnet and diffusion can proceed to lower temperatures (Tracy et al., 1976; Lasaga, 1983). Tucillo et al. (1990) showed that zoning patterns in compositional maps of garnets in high grade rocks are not necessarily concentric and do not have to coincide for different elements. Different diffusion rates may cause variations in homogenization between elements (see also Tracy, 1982). Specifically calcium has a lower diffusion rate and is slower to homogenize than the other elements in garnet (Tucillo et al., 1990).

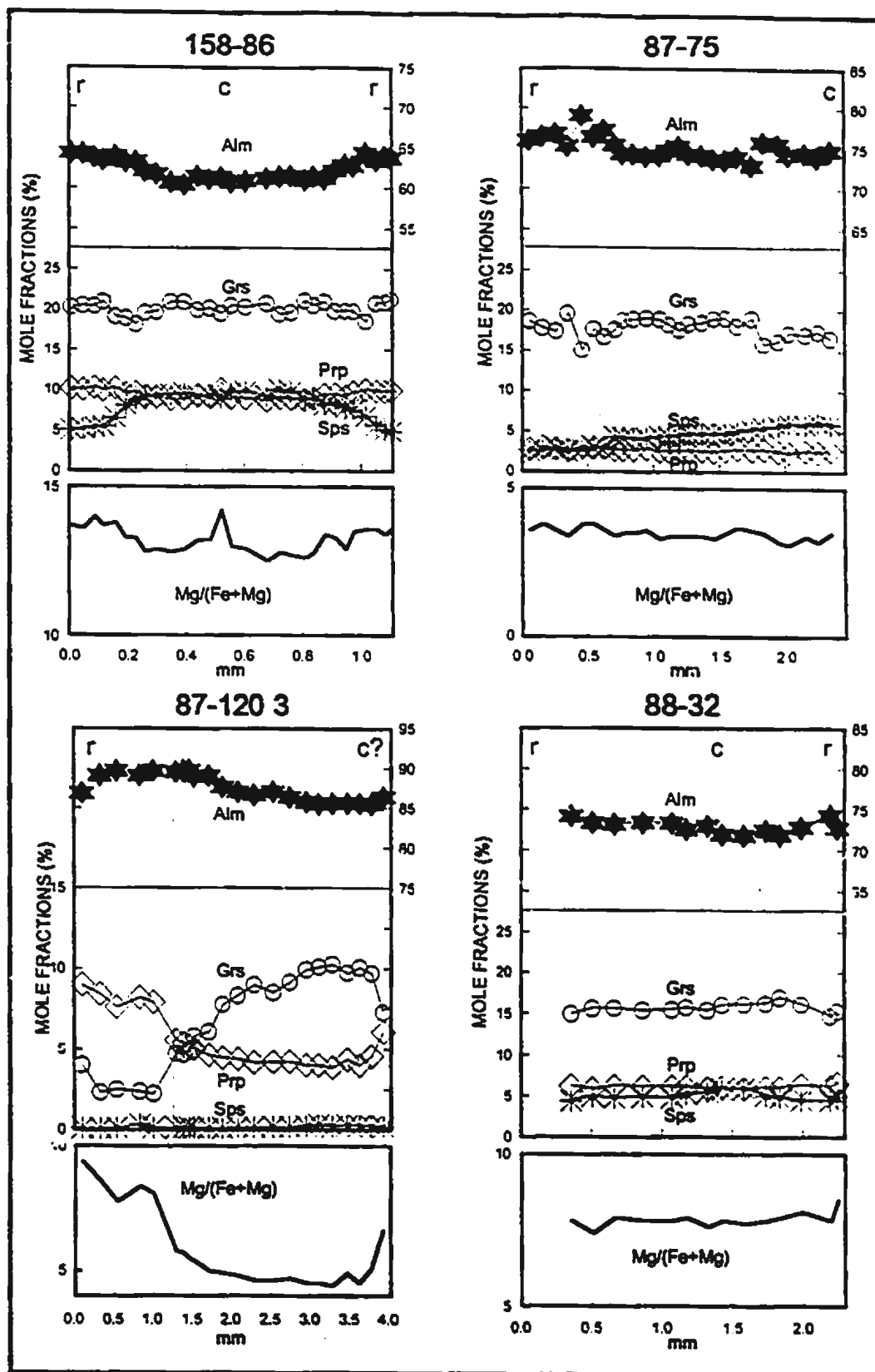
### **CHEMICAL PROFILES OF GARNETS IN GAGNON TERRANE**

A total of 16 garnets was selected from several parts of the study area for detailed analysis of chemical zoning patterns. Each grain was analyzed in approximately 20 to 30 spots along a profile from rim to core to rim, with the exception of the garnet of sample 87-75, which was only analyzed from core to rim. Analytical procedures are presented in Appendix G. For each sample the largest garnet in the thin section was selected, to minimize the cut effect that occurs when a grain is cut tangentially through the margin rather than radially through the core. A second selection criterion was the crystal shape. The most idioblastic grains in a section were preferred for analyses, in order to avoid loss of information by resorption of the garnets (Duebendorfer and Frost, 1988). In some samples all garnets were strongly resorbed and idioblastic or even subidioblastic crystals could not be found. In these cases an effort was made to find a profile line through the garnet which would encompass both the original rim and the original core (with respect to the grain shape before resorption). Spacing of the analysis spots was dependent on the grain size and ranged from 40 to 170 $\mu$ , the majority being around 100 $\mu$ . Grain sizes of the garnets analyzed for chemical profiles varied from approximately 1 mm to 5.5mm.

12 of the 16 profiles are shown in Figure F.2, the remainder are presented in the text of Section 7.2. Figure F.3 is a location map of the samples for the garnet profiles and the samples for thermobarometry.

**Fig. F.2** Chemical profiles through garnets from the map area. The vertical scales are concentrations of components in mole fractions  $\times 100$ , and the ratio  $Mg/(Fe + Mg) \times 100$ . Note that the vertical scales for the  $Mg/(Fe + Mg)$  ratios vary. In the diagram for sample 87-120 3, the vertical scale for grossular, pyrope and spessartine is different from that for almandine. Furthermore, the range of the scale for the almandine component is not constant. c = core, r = rim. Sample locations are indicated in Figure F.3. (continued on following pages)





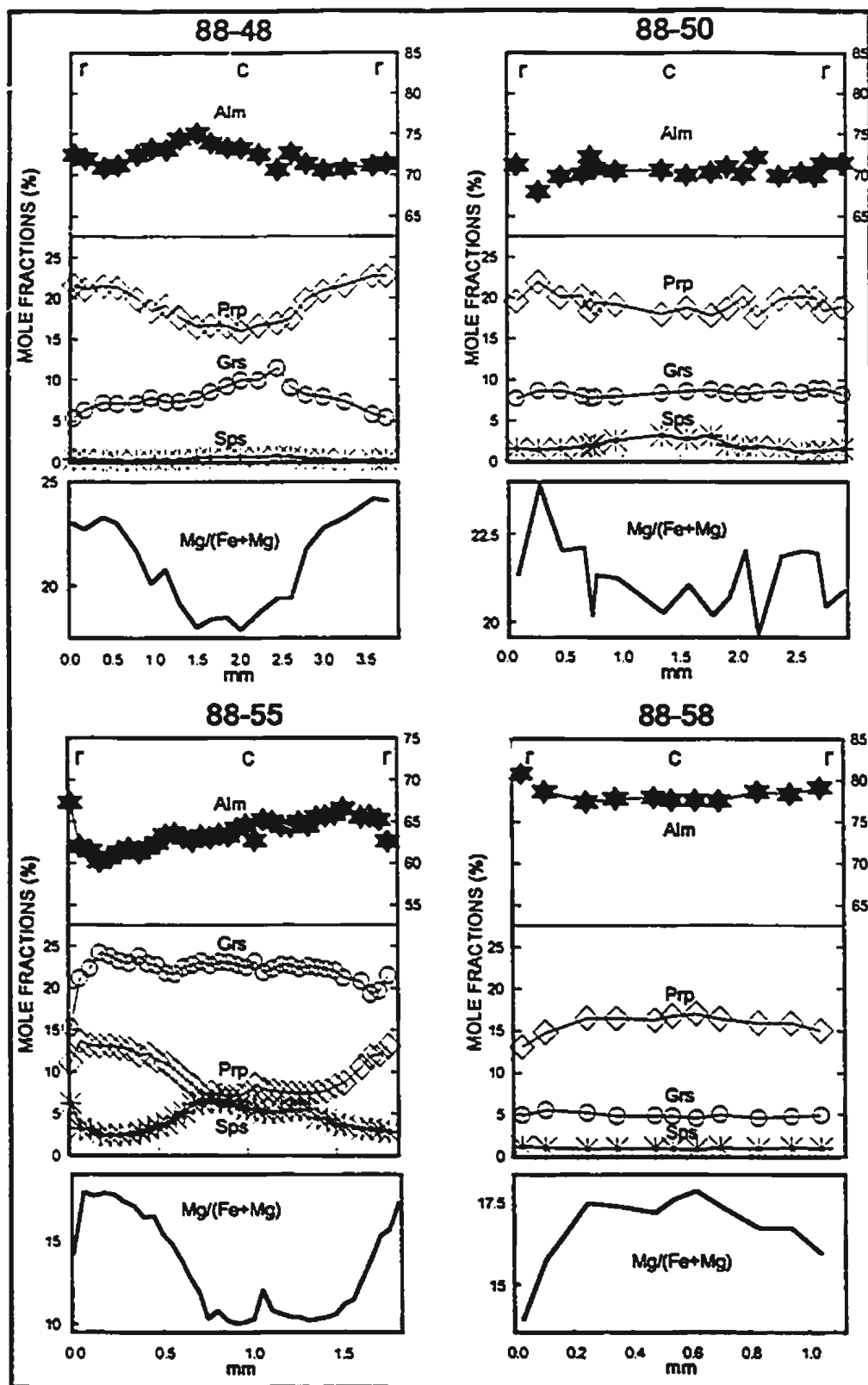


Fig. F2 Chemical profiles through garnets, continued

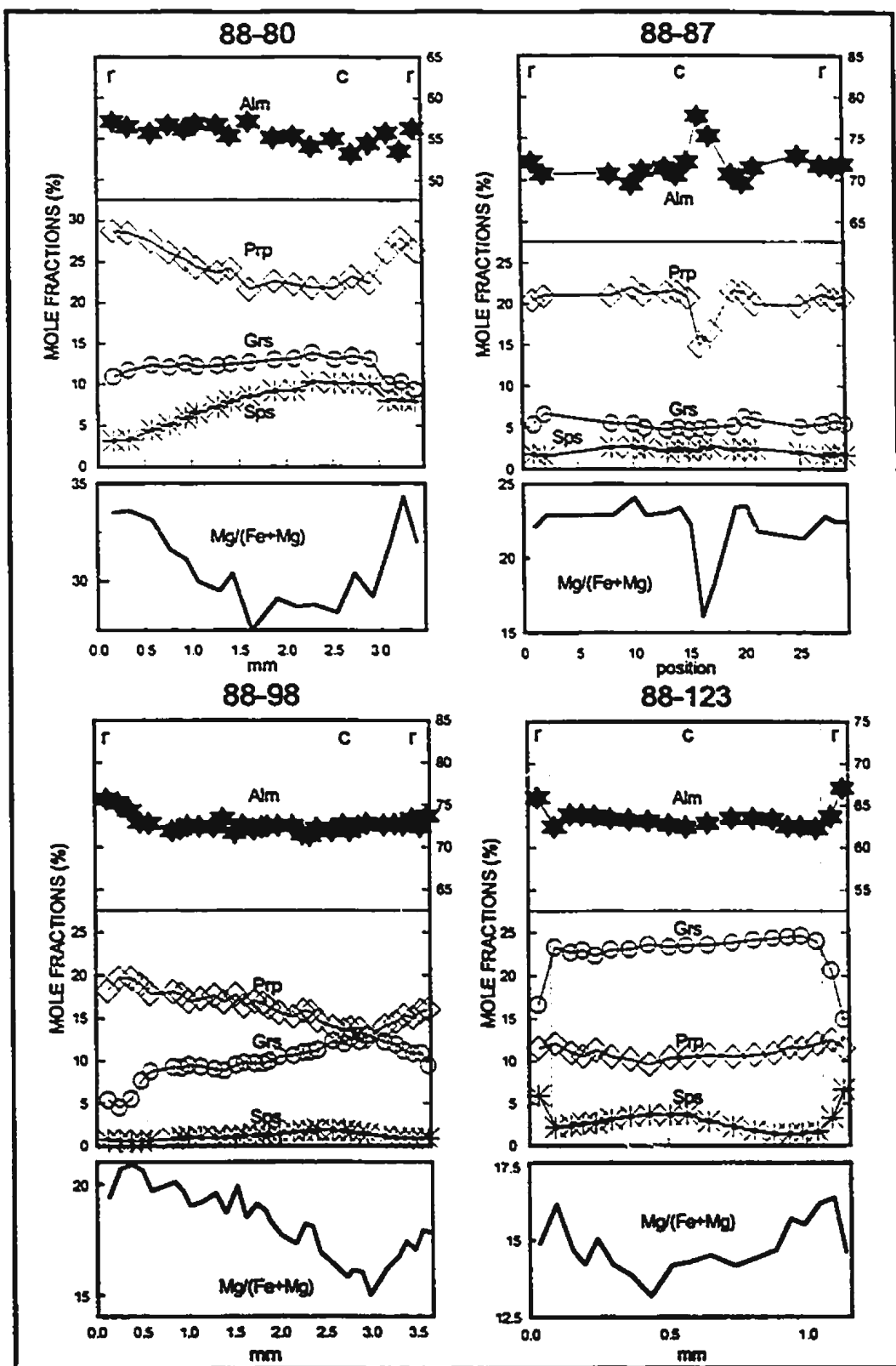


Fig. F2 Chemical profiles through garnets, continued

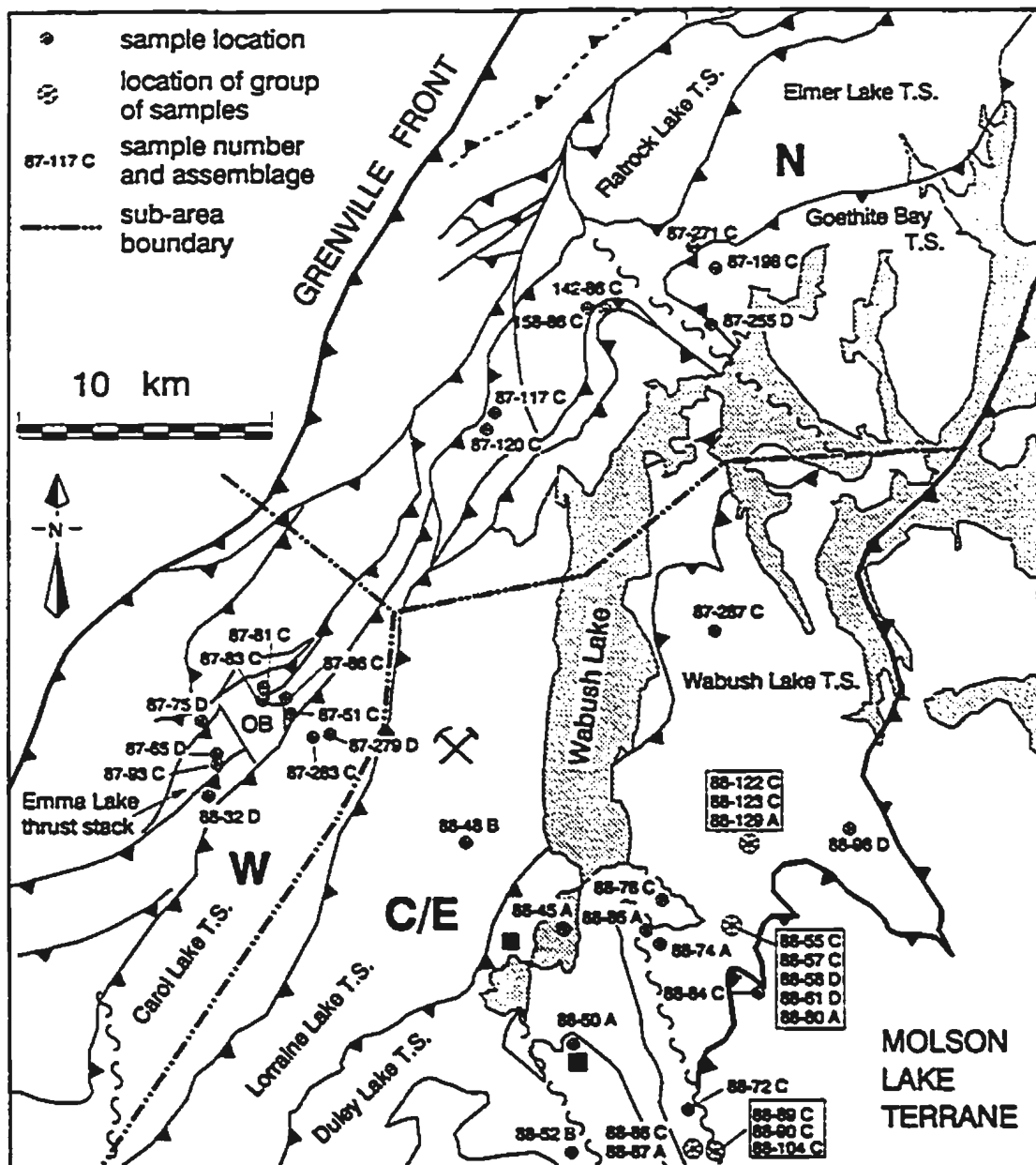


Fig. F.3 Location map for samples used for thermobarometry. Sample numbers in boxes indicate that several samples were taken from one outcrop or several closely spaced outcrops. The figure also shows the subdivision of the map into three sub-areas as well as the names of the thrust sheets mentioned in Section 7.3. C/E = central/eastern area, N = northern area, W = western area. The characters (A to D) after the sample numbers indicate mineral assemblages:



## APPENDIX G

### ELECTRON MICROPROBE ANALYTICAL PROCEDURES

With the exception of garnet profiles for samples 88-50 and 88-87, all mineral chemistry analyses were performed on a JEOL 733 wavelength dispersive electron microprobe at Dalhousie University, Halifax, using LiF, PET and TAP analysing crystals. Operating conditions were a 10 nA specimen current, 15 kV accelerating potential, beam width of 10 $\mu$  and 40 seconds counting time to a maximum of one standard deviation of the total counts for the standard. Data were computed using the Tracor Northern ZAF correction method. Synthetic and natural minerals of known composition were used as standards. Most of the core-rim analyses in garnet and the analyses of biotite, muscovite and plagioclase were taken as the average of two to three separate analyses. In each thin section two or three garnet/matrix pairs were analysed. For garnet profiles, each point of the profile represents a single analysis. A calculation of analytical errors for the microprobe at Dalhousie follows below.

Garnet profiles 88-50 and 88-87 were obtained using a JEOL JXA-50A wavelength dispersive electron microprobe at Memorial University, with LiF, PET and RAP analysing crystals. The garnets were analysed using a 22 nA specimen current, 15 kV accelerating potential, a beam width of 10 $\mu$  and 30 seconds counting time to a maximum of 60,000 counts. Data were corrected according to the Bence and Albee (1968) method. For these garnet profiles only Si, Al, Fe, Mn, Mg and Ca were analysed.

### ANALYTICAL STATISTICS

During microprobe sessions the equipment was calibrated using minerals with known compositions. The analyses of these standards were used to estimate the precision and accuracy of the microprobe. Tables G.1 and G.2 show the results of approximately 30 analyses of a garnet (K GNT) and a Kaersutitic amphibole (KK), performed on the JEOL 733 at Dalhousie University. Most of the major constituent

elements have a standard deviation which is within 2% of the measured average. Repeated analyses of each unknown would have improved the margin of error. The averages are well within one standard deviation of the actual composition, except for Fe, which for both standards is 0.3 weight % oxide too low. The effect of this will cancel out in the Grt-Bt thermometer which depends on Fe-Mg ratios of the two minerals.

**Table G.1 Statistics of analyses of K GNT**

oxide	average*	standard deviation	actual** composition
SiO <sub>2</sub>	41.46	0.34	41.45
TiO <sub>2</sub>	0.44	0.03	0.51
Al <sub>2</sub> O <sub>3</sub>	23.44	0.28	23.50
FeO***	10.42	0.20	10.74
MnO	0.31	0.03	0.33
MgO	18.54	0.41	18.51
CaO	5.23	0.06	5.09

based on 30 analyses

**Table G.2 Statistics of analyses of KK amphibole**

oxide	average*	standard deviation	actual** composition
SiO <sub>2</sub>	40.31	0.40	40.37
TiO <sub>2</sub>	4.73	0.08	4.72
Al <sub>2</sub> O <sub>3</sub>	14.34	0.30	14.25
FeO***	10.57	0.28	10.91
MgO	12.72	0.28	12.80
CaO	10.29	0.14	10.30
Na <sub>2</sub> O	2.58	0.15	2.60
K <sub>2</sub> O	2.04	0.06	2.04

based on 35 analyses

\* oxide weight percentages

\*\* Composition data from Dalhousie University, Department of Geology, Electron Microprobe sample collection.

\*\*\* All iron as Fe<sup>2+</sup>

## APPENDIX H

### THERMODYNAMICS AND CALIBRATIONS OF THE APPLIED THERMOBAROMETERS

Calculation of metamorphic pressures and temperatures from an assemblage of minerals in equilibrium is based on the positioning of a reaction curve in a petrogenetic grid, using thermodynamic and compositional data from the phases involved in the reaction. Thermometers are reactions involving the exchange of similar atoms (Mg and Fe in case of the Grt-Bt thermometer) between two or more sites in one or two minerals. Differences in volume between end-members of the geothermometer assemblages are minor, which makes them virtually independent of pressure (low  $\Delta V$ , steep slope in P-T space). The location of these reaction curves is mainly temperature dependent (high  $\Delta H$ ).

Geobarometer reactions are net transfer reactions which are pressure sensitive because of the difference in volume (large  $\Delta V$ ) between reactants and products in the reaction. They have a shallow slope in a P-T diagram. Wood and Fraser (1977) give a review of the basic thermodynamic principles of geothermometry and geobarometry (see also Essene, 1982, 1989).

The equilibrium condition for solid-solid reactions can be written as:

$$\Delta G_{rxn} = \Delta G + RT \ln K = \Delta H - T \Delta S + (P - 1) \Delta V + RT \ln K = 0$$

(at P and T of interest)

where  $\Delta G_{rxn}$  = change in free energy of the reaction,  $\Delta G$  = free energy at standard state,  $\Delta H$  = enthalpy,  $\Delta S$  = entropy and  $\Delta V$  = volume change of the reaction, R = gas constant, T = temperature in °K, P = pressure in bar and K = reaction constant. This is based on the assumption that  $\Delta V$  is independent of P and T, and that  $\Delta H$  and  $\Delta S$  are independent of T.

This equation can be rewritten for the calculation of equilibrium pressures or temperatures:

$$P = \frac{-\Delta H + T\Delta S - RT \ln K}{\Delta V} + 1 \quad (\text{H1})$$

$$T = \frac{-\Delta H - (P - 1)\Delta V}{R \ln K - \Delta S} \quad (\text{H2})$$

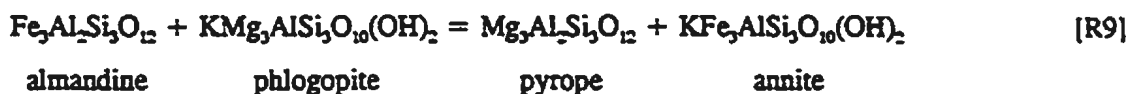
Solution of these equations requires that enthalpy, entropy and volume change of the reaction are known, as well as the concentrations or activities of the end-members in the solid solutions in case of ideal or non-ideal mixing models respectively. Calculation of the equilibrium constant  $K$  from compositions and activities fixes the position of the reaction curve in P-T space.

Tables H.1 and H.2 at the end of the appendix give the thermodynamic data used here. Expressions for calculating  $P$  and  $T$  are found by substitution of values found in Tables H.1 and H.2 into equations (H1) and (H2).

A justification for the choice of thermometers and barometers is given in the main text of Chapter 7. A group of thermometers and barometers have been calibrated by Hodges and Crowley (1985) based on a dataset of natural mineral assemblages for which the pressures and temperatures were calculated using the Hodges and Spear (1984) Grt-Bt thermometer and the Hodges and Royden (1984) calibration of the Grt-Als-Pl-Qtz barometer. These barometers and thermometers together form a set which should give consistent results in different pelitic mineral assemblages. The activity models were used as provided by Hodges and Crowley (1985). Significant deviations from ideal behaviour in mixing of garnet end-members is assumed only for the pyrope-grossular binary. All Margules parameters, except  $W_{\text{grt-pyr}}$ , are thus assumed to be zero, following Ganguly and Kennedy (1974). A detailed evaluation of the activity models is beyond the scope of this thesis. All expressions and thermodynamic data given in this appendix are in calories.

## GARNET - BIOTITE GEOTHERMOMETER

The garnet biotite thermometer is based on the reaction:



which involves exchange of Mg and Fe between garnet and biotite. It has been calibrated empirically by Thompson (1976) and Goldman and Albee (1977) and experimentally by Ferry and Spear (1978) and Perchuk and Lavrant'eva (1983). Many other calibrations exist using different thermodynamic data sets or activity models (see reviews by Essene, 1982, 1989). The calibrations used in this thesis are by Ferry and Spear (1978), based on ideal mixing, and from Hodges and Spear (1982) (identical to the calibration used by Hodges and Crowley, 1985), which is based on the same calibration, but uses non-ideal mixing instead. Ferry and Spear (1978) noted that their calibration is suited only for garnets with compositions of  $(\text{Ca}+\text{Mn})/(\text{Ca}+\text{Mn}+\text{Fe}+\text{Mg}) < 0.2$  and for biotites which fall within the compositional range of  $(\text{Al}^{\text{VI}}+\text{Ti})/(\text{Al}^{\text{VI}}+\text{Ti}+\text{Fe}+\text{Mg}) < 0.15$ . Outside these compositional ranges the mixing in the solid solution diverges too much from ideal behaviour, which is why several other calibrations have been published to correct for this non-ideal mixing. The expressions for temperature calculations are:

$$T = \frac{2089 + 9.56P}{\ln K + 0.782} \quad (\text{H3a})$$

(Ferry and Spear, 1978)

$$T = \frac{2089 + 9.56P + 1661 X_{\text{grt}}}{\ln K + 0.782 + 0.755 X_{\text{grt}}} \quad (\text{H3b})$$

(Hodges and Spear, 1982)

with

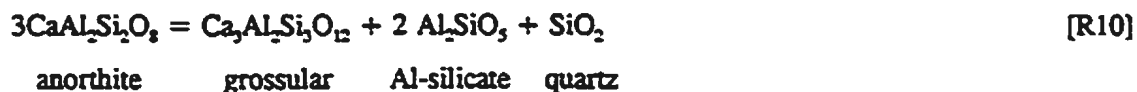
$$K = \frac{(\text{Mg}/\text{Fe})^{\text{grt}}}{(\text{Mg}/\text{Fe})^{\text{bt}}}$$

## GEOBAROMETERS

Three barometers for pelitic rocks were used in the study, each for slightly different mineral assemblages. The first two, Grt-Ky-Qtz-Pl (GASP) and Grt-Ms-Bt-Pl (GMBP), give results that are very compatible. The third barometer, Grt-Bt-Ms-Ky (MABS), for assemblages lacking plagioclase, is less accurate and is mainly given for comparison with the previous two.

### GARNET - ALUMINUM SILICATE - QUARTZ - PLAGIOCLASE

The barometer which has been most widely used for metapelitic rocks is the GASP barometer, based on the net transfer reaction between garnet, plagioclase aluminum silicate and quartz:



which was first calibrated by Ghent (1976) with the assumption of ideal mixing in garnet and plagioclase solid solutions. Subsequent workers refined the calibration using mixing models for non-ideal solid solution of garnet and plagioclase (Ghent et al., 1979; Newton and Haselton, 1981; Hodges and Royden, 1984; Koziol and Newton, 1988; Powell and Holland, 1988). Since in the study area kyanite is the only stable alumino-silicate (with the exception of one sample which does not have the appropriate assemblage for application of this barometer), only the reaction involving kyanite will be considered here. The calibration used here is that of Hodges and Royden (1984), which is based on Newton and Haselton's (1981) calibration with the grossular activity model from Hodges and Spear (1982). Activity expressions are given in Table H.2. The expression for pressure calculation is:

$$P = \frac{-13352 + 36.709T - RT \ln K}{\Delta V} + 1 \quad (\text{H4})$$

(kyanite as stable alumino-silicate)

with

$$K = \frac{\alpha_{an}^3}{\alpha_{grs}}$$

The change in partial molar volume for the reaction is dependent on the garnet composition and has to be calculated separately for each pressure determination. Newton and Haselton (1981) gave the following expressions for calculation of the volume change:

$$\Delta V_{\text{reaction}} = V_{\text{grs}} + 2V_{\text{Ky}} + V_{\text{Qtz}} - 3V_{\text{an}} = 22.688 + 2 \times 44.09 + V_{\text{grs}} - 320.37$$

$$V_{\text{grs}} = \frac{X_{\text{prp}} \cdot V_{\text{grs-prp}} + X_{\text{alm}} \cdot V_{\text{grs-alm}}}{X_{\text{prp}} + X_{\text{alm}}}$$

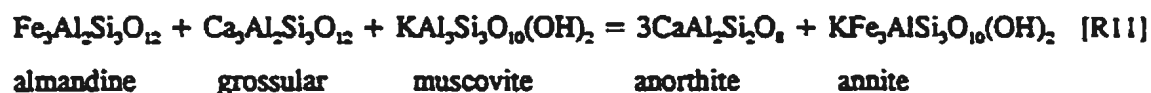
$$V_{\text{grs-prp}} = 125.24 + 0.512(1 - X_{\text{grs}})^2 - 0.418 \left( 1 + \frac{(0.06 - X_{\text{grs}})(1 - X_{\text{grs}})}{0.006889} \right) \cdot \exp\left(\frac{-(0.06 - X_{\text{grs}})^2}{0.013778}\right)$$

$$V_{\text{grs-alm}} = 125.24 + 1.482(1 - X_{\text{grs}})^2 - 0.48 \left( 1 + \frac{(0.086 - X_{\text{grs}})(1 - X_{\text{grs}})}{0.004356} \right) \cdot \exp\left(\frac{-(0.086 - X_{\text{grs}})^2}{0.008712}\right)$$

Combination of the above equations results in a quite lengthy expression which is not shown here.

### PLAGIOCLASE - BIOTITE - GARNET - MUSCOVITE

For mineral assemblages which lack alumino-silicates, Ghent and Stout (1981) calibrated a barometer based on the reaction (GMPB):



and its Mg counterpart involving prp and phl instead of alm and ann. The barometer was originally based on an empirical calibration assuming ideal mixing (Ghent and Stout, 1981). Several new calibrations have been published based on larger data bases and different mixing models for garnet and plagioclase (Hodges and Crowley, 1985;

Powell and Holland, 1988; Stowell, 1989; Hoisch, 1990). For this study the calibration of Hodges and Crowley (1985) was chosen. It was empirically calibrated based on pressures calculated with the GASP barometer. Compared to the Ghent and Stout (1981) calibration, the one used here underestimates  $P$  at lower pressures ( $P < 7$  kbar) and overestimates  $P$  at higher pressures ( $P > 7$  kbar). Activity models for garnet, plagioclase and muscovite are given in table H.2. The expression for pressure calculation is:

$$P = \frac{-16722 + 38.956T - RT \ln K}{1.802} + 1 \quad (\text{H5})$$

with

$$K = \frac{\alpha_{an}^3 \cdot \alpha_{ann}}{\alpha_{alm} \cdot \alpha_{grs} \cdot \alpha_{ms}}$$

Since the activity for muscovite in white mica is pressure dependent (Table H.2) a pressure term has to be extracted from the right hand side of the expression. As a result the final expression for  $P$  is quite lengthy and not shown here.

### MUSCOVITE - GARNET - BIOTITE - ALUMINUM SILICATE

In metapelitic mineral assemblages which lack plagioclase the MABK geobarometer based on the reaction:



can be used. For this reaction there is also another version which involves Mg instead of Fe. The large uncertainty in the thermodynamic data and the small  $\Delta V$  make it an unreliable barometer with a calculated error of up to 18 kbar for certain compositions (Hodges and Crowley, 1985; Essene, 1989). Several calibrations of the MABK barometer are available (Spear and Selverstone, 1983; Robinson, 1983; Hodges and Crowley, 1985; Holdaway et al., 1988). The one used here is that of Hodges and Crowley (1985).

$$P = \frac{-6415 + 5.48T - RT \ln K}{0.225} + 1 \quad (\text{H6})$$

with

$$K = \frac{\alpha_{ann}}{\alpha_{alm} \cdot \alpha_{ms}}$$

Because of the pressure dependence of the activity of muscovite in white mica, the final expression for P is quite lengthy.

Table H.1 Thermodynamic data

Reaction	$\Delta H$ (Cal)	$\Delta S$ (Cal/mol °K)	$\Delta V$ (Cal/bar)
R1	12454	4.662	0.057
R2*	13352	36.709	**
R3	16722	38.955	1.802
R4*	6415	5.480	0.225

\* with kyanite as aluminosilicate

\*\* dependent on garnet composition

Data from Hodges and Crowley (1985)

Table H.2 Activity - composition relations

$$a_{alm} = \left\{ X_{alm} \cdot \exp\left(\frac{(1.5T - 3300) \cdot (X_{prp} \cdot X_{grs})}{RT}\right) \right\}^3$$

$$a_{prp} = \left\{ X_{prp} \cdot \exp\left(\frac{(3300 - 1.5T) \cdot (X_{grs}^2 + X_{alm} \cdot X_{grs} + X_{grs} \cdot X_{sps})}{RT}\right) \right\}^3$$

$$a_{grs} = \left\{ X_{grs} \cdot \exp\left(\frac{(3300 - 1.5T) \cdot (X_{prp}^2 + X_{alm} \cdot X_{prp} + X_{prp} \cdot X_{sps})}{RT}\right) \right\}^3$$

$$a_{ann} = X_{ann} \cdot \exp\left(\frac{610.34}{T} - 0.3837\right)$$

$$a_{ms} = (X_{K,ms} \cdot X_{Al,ms}^2) \cdot \exp\left(\frac{(X_{Na,ms} \cdot X_{Al,ms}^2) \cdot (W_{ms} + 2X_{K,ms} \cdot X_{Al,ms}^2 (W_{pg} - W_{ms}))}{RT}\right)$$

$$a_{ann} = X_{ann}^3$$

$$a_{phl} = X_{phl}^3$$

$X_{alm}$  = Fe/(Fe + Mg + Mn + Ca) in garnet

$X_{prp}$  = Mg/(Fe + Mg + Mn + Ca) in garnet

$X_{grs}$  = Ca/(Fe + Mg + Mn + Ca) in garnet

$X_{sps}$  = Mn/(Fe + Mg + Mn + Ca) in garnet

$X_{ann}$  = Ca/(Ca + Na + K) in plagioclase

$X_{K,ms}$  = K/(Ca + Na + K) in muscovite

$X_{Na,ms}$  = Na/(Ca + Na + K) in muscovite

$X_{Al,ms}$  = Al<sup>VI</sup>/(Fe + Mg + Mn + Ti + Al<sup>VI</sup>) in muscovite

$X_{ann}$  = Fe/(Fe + Mg + Ti + Al<sup>VI</sup>) in biotite

$X_{phl}$  = Mg/(Fe + Mg + Ti + Al<sup>VI</sup>) in biotite

$W_{pg}$  = 2923.1 + 0.1590P + 0.1698T

$W_{ms}$  = 4650.1 + 0.1090P + 0.3954T

R = 1.9871 cal/mole °K

T in °K

P in bar

Data from Hodges and Crowley (1985)

## APPENDIX I

### MICROPROBE ANALYSES AND MINERAL CHEMISTRY

#### ELECTRON MICROPROBE ANALYSES

Tables I.1 to I.4 contain the electron microprobe analyses that were used for geothermobarometry in Chapter 7. Sample locations are shown in Figure F.3. The analyses are grouped by mineral (Garnet, biotite, muscovite and plagioclase) and are numbered by year of collection (for 1986 the format is sample number - year, eg. 142-86, for all others the year precedes the number, eg. 87-51 for sample 51 in 1987). The analyses are ordered firstly by years, then by sample number. The code used in the line labelled 'grain' gives the number of a garnet (abbreviated ga) in a thin section containing several garnet grains, r = for garnet rim analysis or matrix mineral in contact with a garnet rim, c = garnet core analysis or matrix mineral that was used for the calculation of P or T in the garnet core, i = inclusion in garnet or garnet analysis near an inclusion, h = a garnet analysis halfway between core and rim, mat = a matrix mineral at a distance from all garnets in a section. All iron is given as Fe<sup>2+</sup>.

Table I.1 Garnet analyses

SAMPLE GRAIN	142-86 ga3 r1	142-86 ga3 c2	158-86 ga2 r1	158-86 ga2 c2	87-51 ga2 r1	87-51 ga2 c2	87-65 ga1 r1	87-65 ga1 c2	87-75 ga2 r1	87-75 ga2 c2	87-81 ga2 h3	87-81 ga2 r1
SiO <sub>2</sub>	36.72	36.88	36.90	36.66	36.61	36.35	36.76	37.13	36.57	36.19	36.76	36.87
TiO <sub>2</sub>	0.04	0.06	0.13	0.11	0.10	0.09	0.09	0.08	0.07	0.10	0.07	0.07
Al <sub>2</sub> O <sub>3</sub>	20.71	20.40	20.69	20.78	21.00	20.58	21.03	20.60	20.87	20.67	20.76	20.70
Cr <sub>2</sub> O <sub>3</sub>	0.00	0.00	0.00	0.00	0.00	0.00	0.00	0.00	0.00	0.00	0.00	0.06
FeO	30.86	29.91	27.05	27.57	26.89	23.47	26.95	27.48	34.89	33.43	27.84	30.21
MnO	3.14	3.97	5.11	6.01	6.76	10.60	5.74	5.89	1.22	2.70	5.53	2.70
MgO	2.18	1.75	2.31	2.27	1.66	1.26	1.32	1.39	0.74	0.67	1.67	1.84
CaO	6.28	6.91	7.10	5.91	7.06	7.08	7.64	7.18	6.48	5.88	6.82	6.83
Na <sub>2</sub> O	0.03	0.00	0.00	0.00	0.04	0.07	0.00	0.00	0.00	0.00	0.00	0.00
K <sub>2</sub> O	0.00	0.00	0.01	0.00	0.00	0.00	0.00	0.01	0.05	0.01	0.00	0.00
TOTAL	99.96	99.88	99.29	99.32	100.12	99.50	99.52	99.76	100.89	99.65	99.45	99.28
Cations per 12 oxygen												
Si	2.97	2.98	2.98	2.97	2.95	2.96	2.97	3.00	2.96	2.96	2.98	2.99
Ti	0.00	0.00	0.01	0.01	0.01	0.01	0.01	0.00	0.00	0.01	0.00	0.00
Al	1.97	1.95	1.97	1.99	2.00	1.98	2.00	1.96	1.99	1.99	1.98	1.98
Cr	0.00	0.00	0.00	0.00	0.00	0.00	0.00	0.00	0.00	0.00	0.00	0.00
Fe <sup>2+</sup>	2.08	2.02	1.83	1.87	1.81	1.60	1.82	1.86	2.36	2.29	1.89	2.05
Mn	0.21	0.27	0.35	0.41	0.46	0.73	0.39	0.40	0.08	0.19	0.38	0.19
Mg	0.26	0.21	0.28	0.27	0.20	0.15	0.16	0.17	0.09	0.08	0.20	0.22
Ca	0.54	0.60	0.61	0.51	0.61	0.62	0.66	0.62	0.56	0.52	0.59	0.59
Na	0.00	0.00	0.00	0.00	0.01	0.01	0.00	0.00	0.00	0.00	0.00	0.00
K	0.00	0.00	0.00	0.00	0.00	0.00	0.00	0.00	0.01	0.00	0.00	0.00
Total	8.05	8.04	8.03	8.03	8.05	8.05	8.02	8.02	8.05	8.04	8.03	8.02
Xalm	67.13	65.16	59.53	60.90	58.79	51.56	60.02	60.90	76.27	74.47	61.65	67.17
Xpyr	8.45	6.79	9.06	8.93	6.47	4.93	5.24	5.49	2.88	2.66	6.59	7.29
Xgro	17.50	19.29	20.02	16.72	19.78	19.93	21.80	20.39	18.15	16.78	19.35	19.46
Xspe	6.92	8.76	11.39	13.44	14.97	23.58	12.95	13.22	2.70	6.09	12.40	6.08
Mg/(Mg+Fe)	0.112	0.094	0.132	0.128	0.099	0.087	0.080	0.083	0.036	0.034	0.097	0.098

Table I.1 Gemet analyses (continued)

SAMPLE	87-81	87-83	87-83	87-86	87-86	87-86	87-86	87-93	87-93	87-94	87-94	87-94
GRAIN	ga1 c2	ga2 r1	ga2 c2	ga2 r1	ga2 c2	ga4 r1	ga4 c2	ga1 r1	ga1 c4	ga1 r1	ga1 r3	ga1 c5
SiO <sub>2</sub>	36.89	36.66	36.65	36.98	37.00	36.44	36.90	36.45	36.19	36.67	36.94	36.37
TiO <sub>2</sub>	0.00	0.06	0.06	0.07	0.07	0.05	0.08	0.03	0.08	0.04	0.04	0.12
Al <sub>2</sub> O <sub>3</sub>	20.45	20.75	20.70	20.99	20.94	20.74	20.70	20.48	20.74	20.03	20.85	20.88
Cr <sub>2</sub> O <sub>3</sub>	0.00	0.00	0.00	0.00	0.00	0.00	0.00	0.00	0.00	0.00	0.00	0.00
FeO	25.38	29.33	28.82	28.79	27.97	29.50	24.76	33.31	29.16	35.03	34.66	33.44
MnO	9.03	3.99	4.89	4.67	6.13	4.84	10.38	2.17	7.73	1.49	1.51	2.84
MgO	1.36	1.77	1.73	1.85	1.74	1.88	1.30	1.19	0.70	1.05	1.00	0.95
CaO	6.37	6.63	6.46	6.42	6.05	6.00	5.16	5.42	5.20	5.02	5.20	5.41
Na <sub>2</sub> O	0.00	0.02	0.00	0.00	0.00	0.00	0.00	0.00	0.00	0.00	0.00	0.00
K <sub>2</sub> O	0.00	0.00	0.00	0.03	0.00	0.01	0.00	0.01	0.00	0.01	0.01	0.00
TOTAL	99.48	99.21	99.31	99.80	99.90	99.46	99.26	99.06	99.79	99.34	100.21	100.01
Cations per 12 oxygen												
Si	3.00	2.98	2.98	2.98	2.98	2.96	3.00	2.99	2.96	3.01	2.99	2.96
Ti	0.00	0.00	0.00	0.00	0.00	0.00	0.00	0.00	0.00	0.00	0.00	0.01
Al	1.96	1.99	1.98	1.99	1.99	1.99	1.99	1.98	2.00	1.94	1.99	2.00
Cr	0.00	0.00	0.00	0.00	0.00	0.00	0.00	0.00	0.00	0.00	0.00	0.00
Fe <sup>2+</sup>	1.72	1.99	1.96	1.94	1.89	2.01	1.69	2.28	1.99	2.40	2.35	2.28
Mn	0.62	0.27	0.34	0.32	0.42	0.33	0.71	0.15	0.54	0.10	0.10	0.20
Mg	0.16	0.21	0.21	0.22	0.21	0.23	0.16	0.15	0.09	0.13	0.12	0.12
Ca	0.55	0.58	0.56	0.55	0.52	0.52	0.45	0.48	0.46	0.44	0.45	0.47
Na	0.00	0.00	0.00	0.00	0.00	0.00	0.00	0.00	0.00	0.00	0.00	0.00
K	0.00	0.00	0.00	0.00	0.00	0.00	0.00	0.00	0.00	0.00	0.00	0.00
Total	8.02	8.03	8.03	8.02	8.02	8.04	8.00	8.02	8.04	8.02	8.01	8.03
Xalm	66.26	65.15	63.86	63.92	62.11	64.92	56.06	74.73	64.94	78.12	77.65	74.41
Xpyr	5.37	7.01	6.83	7.32	6.89	7.37	5.24	4.76	2.78	4.17	3.99	3.77
Xgro	18.09	18.87	18.34	18.26	17.21	16.92	14.94	15.58	14.84	14.34	14.93	15.42
Xspe	20.27	8.98	10.97	10.50	13.79	10.79	23.76	4.93	17.44	3.37	3.43	6.40
Mg/(Mg+Fe)	0.087	0.097	0.097	0.103	0.100	0.102	0.086	0.060	0.041	0.051	0.049	0.048

Table I.1 Gemet analyses (continued)

SAMPLE GRAIN	87-117 ga2 r1	87-117 ga2 c2	87-117 ga2 c3	87-120 ga2 r1	87-120 ga2 c2	87-198A ga1 r1	87-198A ga1 c3	87-255b ga2 c1	87-255b ga2 r4	88-271 GA1 1r	88-271 GA1 4c	87-279 ga1 r1
SiO <sub>2</sub>	36.35	37.26	36.82	36.33	36.49	36.63	36.50	36.73	36.81	39.37	38.34	37.34
TiO <sub>2</sub>	0.03	0.02	0.03	0.05	0.03	0.20	0.19	0.08	0.07	0.03	0.04	0.07
Al <sub>2</sub> O <sub>3</sub>	20.98	20.95	20.63	21.03	20.92	20.70	20.90	21.30	21.39	20.49	20.34	20.93
Cr <sub>2</sub> O <sub>3</sub>	0.00	0.00	0.00	0.00	0.00	0.13	0.11	0.11	0.15	0.00	0.00	0.00
FeO	33.22	33.85	34.60	35.16	38.87	32.32	31.88	36.56	37.15	28.13	34.14	28.33
MnO	0.39	0.22	1.26	0.28	0.06	1.34	2.33	1.18	0.64	5.01	1.02	3.29
MgO	1.41	1.85	1.16	1.73	2.34	1.96	1.84	2.63	3.06	0.98	1.55	2.40
CaO	6.60	6.83	6.77	6.59	2.08	6.74	6.01	0.85	0.54	6.80	4.76	6.73
Na <sub>2</sub> O	0.00	0.00	0.00	0.00	0.00	0.09	0.14	0.09	0.07	0.05	0.05	0.00
K <sub>2</sub> O	0.01	0.00	0.00	0.02	0.01	0.00	0.00	0.00	0.00	0.01	0.00	0.01
TOTAL	98.99	99.98	100.27	100.18	100.60	99.11	99.90	99.51	99.88	100.87	100.24	99.10
Cations per 12 oxygen												
Si	2.96	3.00	2.98	2.94	2.96	2.98	2.95	2.98	2.97	3.12	3.08	3.01
Ti	0.00	0.00	0.00	0.00	0.00	0.01	0.01	0.00	0.00	0.00	0.00	0.00
Al	2.02	1.99	1.97	2.01	2.00	1.98	1.99	2.04	2.04	1.91	1.92	1.99
Cr	0.00	0.00	0.00	0.00	0.00	0.01	0.01	0.01	0.01	0.00	0.00	0.00
Fe <sup>2+</sup>	2.27	2.28	2.34	2.38	2.62	2.20	2.16	2.48	2.51	1.86	2.29	1.91
Mn	0.03	0.01	0.09	0.02	0.00	0.09	0.16	0.08	0.04	0.34	0.07	0.22
Mg	0.17	0.22	0.14	0.21	0.28	0.24	0.22	0.32	0.37	0.12	0.19	0.29
Ca	0.58	0.50	0.50	0.49	0.18	0.50	0.52	0.07	0.05	0.58	0.41	0.58
Na	0.00	0.00	0.00	0.00	0.00	0.01	0.02	0.01	0.01	0.01	0.01	0.00
K	0.00	0.00	0.00	0.00	0.00	0.00	0.00	0.00	0.00	0.00	0.00	0.00
Total	8.03	8.01	8.03	8.05	8.04	8.02	8.05	8.00	8.00	7.93	7.96	8.00
Xalm	74.51	75.49	76.32	76.95	84.87	72.59	70.50	83.99	84.54	64.43	77.53	63.58
Xpyr	5.84	7.35	4.56	6.75	9.15	7.84	7.25	10.77	12.41	4.00	6.27	9.60
Xgro	18.97	16.66	16.31	15.68	5.85	16.52	17.03	2.50	1.57	19.95	13.85	19.35
Xspe	0.89	0.50	2.81	0.62	0.13	3.05	5.22	2.75	1.48	11.62	2.35	7.48
Mg/(Mg+Fe)	0.070	0.089	0.056	0.081	0.097	0.098	0.093	0.114	0.128	0.058	0.075	0.131

Table I.1 Garnet analyses (continued)

SAMPLE	87-279	87-283	87-283	87-287b	87-287b	88-32	88-32	88-45A	88-45A	88-48	88-48	88-50
GRAIN	ga1 c2	ga1 r1	ga1 c2	ga1 r1	ga1 c2	ga1 r2	ga1 c9	ga4 r1	ga4 c2	ga3 r1	ga3 c2	ga1 r1
SiO <sub>2</sub>	37.16	36.98	36.96	37.93	37.79	36.58	36.75	37.10	37.08	37.84	36.70	36.72
TiO <sub>2</sub>	0.11	0.07	0.18	0.06	0.04	0.05	0.09	0.10	0.09	0.10	0.17	0.08
Al <sub>2</sub> O <sub>3</sub>	20.81	20.84	20.83	21.58	21.90	21.19	21.00	21.60	21.39	21.86	21.48	21.24
Cr <sub>2</sub> O <sub>3</sub>	0.00	0.00	0.00	0.15	0.13	0.06	0.06	0.11	0.13	0.12	0.12	0.10
FeO	25.47	26.27	25.11	27.72	27.58	32.58	32.69	31.63	32.06	33.80	33.53	32.65
MnO	5.58	4.34	6.09	0.98	0.91	2.16	2.63	0.49	0.60	0.13	0.42	0.69
MgO	1.82	1.79	1.60	4.20	5.03	1.68	1.56	4.51	4.82	5.59	3.83	4.40
CaO	8.34	8.65	8.68	7.07	6.93	5.48	6.70	3.30	3.38	1.61	3.45	2.80
Na <sub>2</sub> O	0.00	0.00	0.00	0.07	0.00	0.05	0.03	0.12	0.15	0.10	0.10	0.09
K <sub>2</sub> O	0.00	0.00	0.00	0.00	0.00	0.00	0.00	0.00	0.00	0.00	0.00	0.00
TOTAL	99.39	98.94	99.45	99.77	100.31	99.83	100.51	98.96	99.70	100.95	99.80	98.86
Cations per 12 oxygen												
Si	2.99	2.99	2.98	2.99	2.96	2.96	2.96	2.97	2.96	2.97	2.94	2.96
Ti	0.01	0.00	0.01	0.00	0.00	0.00	0.01	0.01	0.01	0.01	0.01	0.00
Al	1.98	1.99	1.98	2.01	2.02	2.02	2.00	2.04	2.01	2.02	2.03	2.02
Cr	0.00	0.00	0.00	0.01	0.01	0.00	0.00	0.01	0.01	0.01	0.01	0.01
Fe <sup>2+</sup>	1.71	1.78	1.69	1.83	1.81	2.21	2.20	2.12	2.14	2.20	2.25	2.20
Mn	0.38	0.30	0.42	0.07	0.06	0.15	0.18	0.03	0.04	0.01	0.03	0.05
Mg	0.22	0.22	0.19	0.49	0.59	0.20	0.19	0.54	0.57	0.65	0.48	0.54
Ca	0.72	0.75	0.75	0.60	0.58	0.48	0.49	0.28	0.29	0.14	0.30	0.24
Na	0.00	0.00	0.00	0.01	0.00	0.01	0.00	0.02	0.02	0.02	0.02	0.01
K	0.00	0.00	0.00	0.00	0.00	0.00	0.00	0.00	0.00	0.00	0.00	0.00
Total	8.01	8.01	8.02	8.00	8.02	8.03	8.03	8.01	8.04	8.02	8.04	8.03
Xalm	56.54	58.48	55.49	61.24	59.52	72.75	71.95	71.25	70.33	73.43	74.18	72.68
Xpyr	7.20	7.10	8.30	16.54	19.36	6.89	6.12	18.10	18.84	21.77	15.10	17.81
Xgro	23.72	24.66	24.58	20.02	19.15	15.68	16.07	9.52	9.50	4.51	9.78	7.98
Xspe	12.55	9.78	13.63	2.19	1.98	4.89	5.86	1.12	1.33	0.29	0.94	1.56
Mg/(Mg+Fe)	0.113	0.108	0.102	0.213	0.245	0.084	0.078	0.203	0.211	0.229	0.169	0.197

Table I.1 Gemet analyses (continued)

SAMPLE GRAIN	88-50 ga1 c2	88-52b ga2 r1	88-52b ga2 c2	88-55 ga1 r1	88-55 ga1 c3	88-57 ga1 r1	88-57 ga1 c2	88-58 ga1 r1	88-58 ga1 c2	88-61 ga1 r1	88-01 ga1 c2	88-66 ga2 r1
SiO <sub>2</sub>	36.88	37.10	37.17	37.67	37.19	38.13	38.50	37.47	37.17	37.14	37.30	37.31
TiO <sub>2</sub>	0.12	0.07	0.06	0.00	0.00	0.09	0.08	0.07	0.11	0.04	0.05	0.12
Al <sub>2</sub> O <sub>3</sub>	21.33	21.72	21.52	20.96	20.77	22.03	21.81	21.77	21.42	21.32	21.33	20.42
Cr <sub>2</sub> O <sub>3</sub>	0.09	0.10	0.08	0.00	0.00	0.18	0.14	0.08	0.10	0.06	0.04	0.09
FeO	32.38	35.45	34.58	30.57	28.84	26.47	26.63	36.20	35.69	32.20	31.32	24.95
MnO	0.81	0.28	0.63	2.80	3.00	0.70	1.44	0.43	0.41	0.30	0.38	2.07
MgO	4.57	4.56	3.72	2.84	1.80	4.80	5.80	3.83	4.32	4.49	4.97	2.18
CaO	2.87	0.85	2.90	5.42	8.20	7.99	6.01	1.55	1.71	3.38	3.53	11.89
Na <sub>2</sub> O	0.10	0.04	0.08	0.00	0.00	0.07	0.08	0.05	0.05	0.00	0.00	0.09
K <sub>2</sub> O	0.00	0.00	0.00	0.00	0.00	0.00	0.00	0.00	0.00	0.00	0.00	0.00
TOTAL	99.15	100.17	100.64	100.26	99.80	100.47	100.53	101.46	100.98	98.93	98.90	99.72
Cations per 12 oxygen												
Si	2.96	2.96	2.96	3.01	2.99	2.97	2.99	2.96	2.95	2.98	2.98	2.98
Ti	0.01	0.00	0.00	0.00	0.00	0.01	0.00	0.00	0.01	0.00	0.00	0.01
Al	2.02	2.04	2.02	1.97	1.97	2.02	2.00	2.03	2.01	2.02	2.01	1.92
Cr	0.01	0.01	0.01	0.00	0.00	0.01	0.01	0.01	0.01	0.00	0.00	0.01
Fe <sup>2+</sup>	2.17	2.36	2.30	2.04	1.94	1.72	1.73	2.39	2.37	2.16	2.09	1.67
Mn	0.06	0.02	0.04	0.19	0.20	0.05	0.09	0.03	0.03	0.02	0.03	0.18
Mg	0.55	0.54	0.44	0.34	0.22	0.56	0.67	0.45	0.51	0.54	0.59	0.26
Ca	0.25	0.07	0.25	0.46	0.71	0.67	0.50	0.13	0.15	0.29	0.30	1.02
Na	0.02	0.01	0.01	0.00	0.00	0.01	0.01	0.01	0.01	0.00	0.00	0.01
K	0.00	0.00	0.00	0.00	0.00	0.00	0.00	0.00	0.00	0.00	0.00	0.00
Total	8.03	8.02	8.03	8.01	8.03	8.01	8.01	8.02	8.04	8.01	8.01	8.06
Xalm	71.92	78.87	76.06	67.32	63.26	57.58	57.74	79.65	77.60	71.82	69.47	53.34
Xpyr	18.09	18.08	14.58	11.14	7.04	18.61	22.41	15.02	16.74	17.85	19.64	8.31
Xgro	8.17	2.42	8.17	15.29	23.04	22.27	16.69	4.37	4.76	9.66	10.03	32.57
Xspe	1.82	0.63	1.18	6.25	6.66	1.54	3.16	0.96	0.90	0.68	0.85	5.78
Mg/(Mg+Fe)	0.201	0.186	0.161	0.142	0.100	0.244	0.280	0.159	0.177	0.199	0.220	0.135

Table I.1 Garnet analyses (continued)

SAMPLE	88-66	88-72	88-72	88-74A	88-74A	88-76A	88-76A	88-80	88-80	88-85	88-85	88-86
GRAIN	ga2 c2	ga1 c1	ga1 r2	ga1 r1	ga1 c2	ga1 r1	ga1 c2	ga2 c2	ga2 r3	ga2 r1	ga2 l2	ga1 r1
SiO <sub>2</sub>	37.24	37.18	37.37	37.46	37.33	38.48	37.94	37.71	37.96	36.86	37.19	37.62
TiO <sub>2</sub>	0.14	0.13	0.09	0.03	0.03	0.04	0.07	0.11	0.09	0.06	0.07	0.00
Al <sub>2</sub> O <sub>3</sub>	20.42	20.57	20.95	21.71	21.51	21.70	21.77	21.63	21.62	21.20	21.45	20.79
Cr <sub>2</sub> O <sub>3</sub>	0.07	0.07	0.08	0.04	0.05	0.11	0.09	0.07	0.09	0.07	0.08	0.00
FeO	24.85	26.01	26.02	32.75	32.26	24.85	27.31	26.06	26.21	33.20	31.73	33.24
MnO	3.02	2.78	2.30	2.09	1.90	0.79	1.02	4.08	2.44	0.44	0.65	0.66
MgO	2.18	1.52	1.82	4.63	5.19	3.75	3.60	5.95	6.91	4.30	5.01	5.08
CaO	11.62	12.22	12.32	1.40	1.67	11.27	8.69	4.66	4.38	3.26	3.67	2.43
Na <sub>2</sub> O	0.09	0.08	0.05	0.05	0.00	0.00	0.01	0.10	0.08	0.04	0.07	0.00
K <sub>2</sub> O	0.00	0.00	0.00	0.00	0.00	0.00	0.00	0.00	0.00	0.00	0.00	0.00
TOTAL	99.62	100.56	100.80	100.16	99.94	100.99	100.50	100.36	99.78	99.43	99.90	99.82
Cations per 12 oxygen												
Si	2.98	2.96	2.96	2.88	2.97	2.99	2.98	2.96	2.97	2.96	2.95	3.00
Ti	0.01	0.01	0.01	0.00	0.00	0.00	0.00	0.01	0.01	0.00	0.00	0.00
Al	1.93	1.93	1.96	2.03	2.02	1.99	2.01	2.00	1.99	2.01	2.01	1.95
Cr	0.00	0.00	0.01	0.00	0.00	0.01	0.01	0.00	0.01	0.00	0.01	0.00
Fe <sup>2+</sup>	1.66	1.73	1.72	2.18	2.15	1.61	1.79	1.71	1.71	2.23	2.11	2.22
Mn	0.20	0.19	0.15	0.14	0.13	0.05	0.07	0.27	0.16	0.03	0.04	0.04
Mg	0.26	0.18	0.19	0.55	0.62	0.43	0.42	0.69	0.81	0.51	0.59	0.60
Ca	1.00	1.04	1.05	0.12	0.14	0.94	0.73	0.39	0.37	0.28	0.31	0.21
Na	0.01	0.01	0.01	0.01	0.00	0.00	0.00	0.02	0.01	0.01	0.01	0.00
K	0.00	0.00	0.00	0.00	0.00	0.00	0.00	0.00	0.00	0.00	0.00	0.00
Total	8.05	8.07	8.05	8.01	8.02	8.02	8.01	8.04	8.03	8.03	8.04	8.02
Xalm	53.23	55.12	55.34	72.92	70.79	53.13	59.51	55.72	56.24	72.99	68.97	72.14
Xpyr	8.32	5.74	6.14	18.37	20.29	14.29	13.98	22.67	26.42	16.85	19.41	19.65
Xgro	31.89	33.18	33.67	3.99	4.69	30.87	24.26	12.77	12.04	9.18	10.21	6.76
Xspe	6.55	5.97	4.95	4.71	4.22	1.71	2.25	8.84	5.30	0.98	1.42	1.45
Mg/(Mg+Fe)	0.135	0.094	0.100	0.201	0.223	0.212	0.190	0.289	0.320	0.188	0.220	0.214

Table I.1 Garnet analyses (continued)

SAMPLE	88-86	88-87	88-87	88-87	88-87	88-89	88-89	88-90	88-90	88-98	88-98	88-104
GRAIN	ga1 c2	ga2 r4	ga2 c5	ga1 r1	ga1 c2	ga1 r1	ga1 c2	ga2 r1	ga2 c2	ga2 c18	ga2 r3	ga1 r1
SiO <sub>2</sub>	38.12	37.15	36.87	37.32	37.19	37.85	38.04	37.56	37.66	36.85	36.76	38.08
TiO <sub>2</sub>	0.00	0.05	0.06	0.06	0.05	0.07	0.05	0.05	0.00	0.07	0.04	0.09
Al <sub>2</sub> O <sub>3</sub>	20.81	21.17	20.85	21.01	21.30	21.55	22.25	21.78	22.04	21.16	21.52	21.82
Cr <sub>2</sub> O <sub>3</sub>	0.00	0.11	0.09	0.10	0.09	0.04	0.08	0.06	0.08	0.04	0.10	0.03
FeO	32.63	33.38	34.05	33.10	33.30	27.07	25.87	30.23	28.89	32.81	34.73	27.97
MnO	0.49	1.00	1.07	0.75	0.96	0.94	0.84	1.37	1.13	0.76	0.34	1.06
MgO	5.87	4.42	3.81	4.82	4.70	5.86	7.28	5.64	7.05	3.85	4.69	5.18
CaO	2.30	2.29	2.36	2.59	2.10	6.92	6.19	3.95	3.81	3.75	1.80	6.91
Na <sub>2</sub> O	0.00	0.04	0.06	0.05	0.05	0.03	0.03	0.06	0.05	0.04	0.00	0.04
K <sub>2</sub> O	0.00	0.00	0.00	0.00	0.00	0.00	0.00	0.00	0.00	0.00	0.00	0.00
TOTAL	100.22	99.81	99.03	99.79	99.72	100.13	100.63	100.70	100.51	99.33	99.98	101.17
Cations per 12 oxygen												
Si	3.01	2.98	2.97	2.98	2.97	2.95	2.94	2.95	2.94	2.96	2.94	2.96
Ti	0.00	0.00	0.00	0.00	0.00	0.00	0.00	0.00	0.00	0.00	0.00	0.01
Al	1.94	2.00	1.99	1.98	2.01	1.99	2.02	2.01	2.03	2.01	2.03	2.00
Cr	0.00	0.01	0.01	0.01	0.01	0.00	0.00	0.00	0.00	0.00	0.01	0.00
Fe <sup>2+</sup>	2.16	2.24	2.31	2.21	2.23	1.77	1.67	1.98	1.88	2.21	2.32	1.82
Mn	0.03	0.07	0.07	0.05	0.06	0.06	0.05	0.09	0.07	0.05	0.02	0.07
Mg	0.69	0.53	0.46	0.57	0.56	0.68	0.84	0.66	0.82	0.46	0.56	0.60
Ca	0.19	0.20	0.20	0.22	0.18	0.58	0.51	0.33	0.30	0.32	0.15	0.58
Na	0.00	0.01	0.01	0.01	0.01	0.00	0.00	0.01	0.01	0.01	0.00	0.01
K	0.00	0.00	0.00	0.00	0.00	0.00	0.00	0.00	0.00	0.00	0.00	0.00
Total	8.02	8.02	8.03	8.03	8.02	8.05	8.05	8.04	8.05	8.03	8.04	8.04
Xalm	70.12	73.84	75.76	72.32	73.45	57.19	54.32	64.69	61.18	72.52	75.93	59.35
Xpyr	22.48	17.42	15.11	18.77	18.47	22.06	27.24	21.51	26.60	15.16	18.27	19.59
Xgro	6.33	6.49	6.73	7.25	5.93	18.73	16.65	10.83	9.79	10.62	5.04	18.79
Xspe	1.07	2.24	2.41	1.66	2.14	2.01	1.79	2.97	2.42	1.70	0.75	2.28
Mg/(Mg+Fe)	0.243	0.191	0.166	0.206	0.201	0.278	0.334	0.250	0.303	0.173	0.194	0.248

Table 1.1 Garnet analyses (continued)

SAMPLE	88-104	88-112	88-112	88-113	88-113	88-119	88-122	88-122	88-122	88-122	88-123	88-123
GRAIN	ga1 c2	ga1 r1	ga1 c2	ga1 r6	ga1 c8	ga3 c2	ga1 r1	ga1 c3	ga2 r1	ga2 c2	ga1 r1	ga1 c3
SiO <sub>2</sub>	36.88	36.82	37.08	36.31	37.39	37.21	37.75	37.27	37.38	37.40	36.99	37.09
TiO <sub>2</sub>	0.10	0.00	0.06	0.05	0.05	0.18	0.06	0.25	0.06	0.10	0.08	0.11
Al <sub>2</sub> O <sub>3</sub>	21.63	20.26	20.14	20.11	20.06	21.27	21.60	21.33	21.13	21.70	21.15	20.99
Cr <sub>2</sub> O <sub>3</sub>	0.07	0.00	0.00	0.01	0.00	0.14	0.08	0.09	0.08	0.07	0.08	0.07
FeO	26.37	28.60	28.57	28.16	28.24	28.52	29.52	28.94	29.73	28.52	29.12	29.26
MnO	0.94	3.94	3.74	3.70	2.75	1.16	1.70	1.98	3.32	1.37	1.65	1.10
MgO	5.66	1.21	1.26	1.26	1.44	1.93	2.58	1.77	2.23	2.75	2.80	1.97
CaO	6.88	8.70	8.94	9.37	9.49	9.66	7.77	7.97	6.15	8.15	7.71	8.70
Na <sub>2</sub> O	0.06	0.01	0.00	0.00	0.00	0.10	0.00	0.05	0.02	0.01	0.08	0.04
K <sub>2</sub> O	0.00	0.00	0.00	0.00	0.00	0.00	0.00	0.00	0.00	0.00	0.00	0.00
TOTAL	98.61	99.54	99.79	98.97	99.42	100.17	101.06	99.65	100.10	100.07	99.66	99.33
Cations per 12 oxygen												
Si	2.93	2.99	3.00	2.97	3.02	2.96	2.98	2.98	2.99	2.97	2.96	2.98
Ti	0.01	0.00	0.00	0.00	0.00	0.01	0.00	0.02	0.00	0.01	0.00	0.01
Al	2.03	1.94	1.92	1.94	1.91	2.00	2.01	2.01	1.99	2.03	2.00	1.99
Cr	0.00	0.00	0.00	0.00	0.00	0.01	0.00	0.01	0.01	0.00	0.01	0.00
Fe <sup>2+</sup>	1.75	1.94	1.93	1.92	1.91	1.90	1.95	1.94	1.99	1.89	1.95	1.91
Mn	0.06	0.27	0.26	0.26	0.19	0.08	0.11	0.13	0.23	0.09	0.11	0.07
Mg	0.67	0.15	0.15	0.15	0.17	0.23	0.30	0.21	0.27	0.33	0.33	0.24
Ca	0.59	0.76	0.77	0.82	0.82	0.82	0.66	0.68	0.53	0.69	0.66	0.75
Na	0.01	0.00	0.00	0.00	0.00	0.02	0.00	0.01	0.00	0.00	0.01	0.01
K	0.00	0.00	0.00	0.00	0.00	0.00	0.00	0.00	0.00	0.00	0.00	0.00
Total	8.05	8.04	8.04	8.06	8.02	8.03	8.01	7.99	8.01	8.01	8.04	8.02
Xalm	57.05	62.32	62.03	61.01	61.73	62.67	64.46	65.31	66.15	63.03	63.78	64.98
Xpyr	21.82	4.70	4.88	4.86	5.61	7.56	10.04	7.12	8.84	10.83	10.93	7.80
Xgro	19.07	24.29	24.87	26.01	26.58	27.19	21.74	23.04	17.53	23.08	21.63	24.75
Xspe	2.06	8.70	8.22	8.12	6.09	2.58	3.76	4.53	7.48	3.07	3.66	2.47
Mg/(Mg+Fe)	0.277	0.070	0.073	0.074	0.083	0.108	0.135	0.098	0.118	0.147	0.146	0.107

Table I.1 Garnet analyses (continued)

SAMPLE	88-129A	88-129A
GRAIN	ga1 r2	ga1 c3
SiO <sub>2</sub>	38.71	37.60
TiO <sub>2</sub>	0.04	0.14
Al <sub>2</sub> O <sub>3</sub>	21.28	21.26
Cr <sub>2</sub> O <sub>3</sub>	0.07	0.10
FeO	31.53	33.04
MnO	0.44	1.00
MgO	5.82	3.15
CaO	3.11	4.92
Na <sub>2</sub> O	0.04	0.08
K <sub>2</sub> O	0.00	0.00
TOTAL	101.04	101.48

Cations per 12 oxygen

Si	3.02	2.98
Ti	0.00	0.01
Al	1.98	1.98
Cr	0.00	0.01
Fe <sup>2+</sup>	2.06	2.18
Mn	0.03	0.07
Mg	0.88	0.37
Ca	0.26	0.42
Na	0.01	0.01
K	0.00	0.00
Total	8.00	8.02

Xalm	68.05	71.87
Xpyr	22.38	12.21
Xgro	8.60	13.71
Xspe	0.96	2.20
Mg/(Mg+Fe)	0.248	0.145

Table I.2 Biotite analyses

SAMPLE	142-86	158-86	87-61	87-65	87-76	87-81	87-83	87-86	87-86	87-93	87-94	87-94
GRAIN	ga3 r1	ga2 r1	ga2 r1	ga1 r1	ga2 r1	ga2 r1	ga2 r1	ga2 r1	ga4 r1	ga1 r1	ga1 r1	ga1 r3
SiO <sub>2</sub>	35.48	36.43	35.69	35.38	33.83	35.97	36.14	36.15	35.92	35.13	33.72	34.05
TiO <sub>2</sub>	1.64	2.00	1.28	1.57	0.81	1.62	1.41	1.76	1.80	0.12	0.66	0.67
Al <sub>2</sub> O <sub>3</sub>	16.41	18.10	18.00	16.74	17.92	17.57	17.50	17.34	17.42	18.93	17.45	17.80
Cr <sub>2</sub> O <sub>3</sub>	0.00	0.00	0.00	0.00	0.00	0.00	0.00	0.00	0.00	0.00	0.00	0.00
FeO	23.23	17.88	19.02	22.16	27.45	19.78	19.38	18.50	18.93	23.93	26.55	26.66
MnO	0.16	0.16	0.19	0.11	0.14	0.14	0.10	0.07	0.09	0.07	0.09	0.08
MgO	8.36	11.73	10.74	9.35	5.45	10.32	11.08	10.87	11.09	7.60	6.16	6.80
CaO	0.01	0.03	0.04	0.05	0.12	0.00	0.00	0.02	0.04	0.02	0.14	0.14
Na <sub>2</sub> O	0.00	0.07	0.00	0.00	0.00	0.00	0.00	0.00	0.00	0.00	0.01	0.00
K <sub>2</sub> O	9.55	9.27	8.74	9.23	8.97	8.80	8.63	9.12	9.34	8.91	7.82	7.92
TOTAL	94.82	95.67	93.70	94.57	94.69	94.20	94.22	93.83	94.63	94.71	92.61	93.12
Cations per 22 oxygens												
Si	5.55	5.47	5.50	5.51	5.41	5.53	5.54	5.55	5.50	5.48	5.46	5.45
Ti	0.19	0.23	0.15	0.18	0.10	0.19	0.16	0.20	0.21	0.01	0.08	0.08
Al	3.03	3.21	3.27	3.07	3.38	3.18	3.16	3.14	3.14	3.48	3.33	3.36
Cr	0.00	0.00	0.00	0.00	0.00	0.00	0.00	0.00	0.00	0.00	0.00	0.00
Fe <sup>2+</sup>	3.04	2.25	2.45	2.89	3.67	2.54	2.48	2.38	2.42	3.12	3.59	3.43
Mn	0.02	0.02	0.02	0.01	0.02	0.02	0.01	0.01	0.01	0.01	0.01	0.01
Mg	1.95	2.63	2.47	2.17	1.30	2.38	2.53	2.49	2.63	1.77	1.49	1.62
Ca	0.00	0.00	0.01	0.01	0.02	0.00	0.00	0.00	0.01	0.00	0.02	0.02
Na	0.00	0.02	0.00	0.00	0.00	0.00	0.00	0.00	0.00	0.00	0.00	0.00
K	1.91	1.78	1.72	1.83	1.83	1.73	1.69	1.79	1.82	1.77	1.62	1.62
TOTAL	15.70	15.60	15.58	15.68	15.72	15.55	15.57	15.57	15.64	15.65	15.60	15.60
Al <sub>IV</sub>	2.45	2.53	2.50	2.49	2.59	2.47	2.46	2.45	2.50	2.52	2.54	2.55
Al <sub>VI</sub>	0.58	0.68	0.77	0.59	0.79	0.71	0.70	0.70	0.64	0.96	0.79	0.81
Mg/(Mg+Fe)	0.39	0.54	0.50	0.43	0.26	0.48	0.50	0.51	0.51	0.36	0.29	0.32

Table 1.2 Biotite analyses (continued)

SAMPLE	87-117	87-120	87-198A	87-255b	87-271	87-279	87-283	87-287b	88-32	88-45A	88-48	88-50
GRAIN	ga2 r1	ga2 r1	ga1 r1	ga2 r1	ga1 r1	ga1 r1	ga1 r1	ga1 r1	ga1 r2	ga4 r1	ga3 r1	ga1 r1
SiO <sub>2</sub>	34.81	35.43	36.05	35.58	35.73	37.38	36.33	36.11	36.19	36.82	37.19	37.43
TiO <sub>2</sub>	0.13	1.12	1.76	1.28	0.64	1.53	1.71	1.72	1.45	1.62	0.95	1.72
Al <sub>2</sub> O <sub>3</sub>	17.34	18.28	16.97	17.56	17.34	16.83	17.76	17.73	17.59	18.72	19.15	19.31
Cr <sub>2</sub> O <sub>3</sub>	0.00	0.00	0.07	0.06	0.00	0.00	0.00	0.16	0.05	0.09	0.04	0.05
FeO	24.14	22.88	18.62	22.55	22.75	21.08	18.59	16.88	21.04	15.63	14.16	15.93
MnO	0.04	0.00	0.12	0.08	0.13	0.10	0.08	0.05	0.08	0.00	0.00	0.00
MgO	8.40	8.73	11.11	7.83	8.11	10.43	10.61	11.82	9.67	12.48	14.22	13.18
CaO	0.30	0.02	0.02	0.03	0.00	0.15	0.03	0.06	0.02	0.01	0.00	0.00
Na <sub>2</sub> O	0.03	0.09	0.08	0.24	0.11	0.00	0.00	0.28	0.19	0.26	0.36	0.32
K <sub>2</sub> O	7.44	9.43	9.78	9.69	9.01	7.52	9.25	9.16	9.73	7.54	9.06	8.50
TOTAL	92.42	95.98	94.58	94.90	93.72	95.02	94.34	93.78	96.01	93.17	95.13	96.44
Cations per 22 oxygens												
Si	5.52	5.45	5.53	5.54	5.61	5.67	5.55	5.51	5.52	5.55	5.50	5.48
Ti	0.02	0.13	0.20	0.15	0.06	0.17	0.20	0.20	0.17	0.18	0.11	0.19
Al	3.26	3.31	3.07	3.22	3.21	3.01	3.20	3.19	3.16	3.32	3.34	3.33
Cr	0.00	0.00	0.01	0.01	0.00	0.00	0.00	0.02	0.01	0.01	0.00	0.01
Fe <sup>2+</sup>	3.22	2.94	2.39	2.94	2.99	2.67	2.38	2.13	2.68	1.97	1.75	1.95
Mn	0.01	0.00	0.02	0.01	0.02	0.01	0.01	0.01	0.01	0.00	0.00	0.00
Mg	2.00	2.00	2.54	1.82	1.90	2.36	2.42	2.69	2.20	2.80	3.13	2.87
Ca	0.05	0.00	0.00	0.01	0.00	0.02	0.00	0.01	0.00	0.00	0.00	0.00
Na	0.01	0.03	0.02	0.07	0.03	0.00	0.00	0.08	0.06	0.08	0.10	0.09
K	1.51	1.85	1.91	1.93	1.81	1.46	1.80	1.78	1.89	1.45	1.71	1.59
TOTAL	15.59	15.71	15.70	15.69	15.64	15.38	15.56	15.62	15.70	15.36	15.63	15.50
Al <sub>IV</sub>	2.48	2.55	2.47	2.46	2.39	2.33	2.45	2.49	2.48	2.45	2.50	2.52
Al <sub>VI</sub>	0.78	0.76	0.60	0.77	0.83	0.68	0.75	0.70	0.68	0.87	0.83	0.81
Mg/(Mg+Fe)	0.38	0.40	0.52	0.38	0.39	0.47	0.50	0.56	0.55	0.59	0.64	0.60

Table 1.2 Biotite analyses (continued)

SAMPLE	88-52b	88-55	88-57	88-58	88-61	88-66	88-72	88-72	88-74A	88-76A	88-80	88-85
GRAIN	ga2 r1	ga1 r1	ga1 r1	ga1 r1	ga1 r1	ga2 r1	ga1 c1	ga1 r2	ga1 r1	ga1 r1	ga2 r2	ga2 r1
SiO <sub>2</sub>	35.79	36.55	36.92	35.06	36.21	35.21	35.10	35.09	36.31	36.56	37.98	37.29
TiO <sub>2</sub>	2.52	0.06	1.51	2.23	1.73	3.96	3.69	3.47	1.83	2.29	1.13	1.50
Al <sub>2</sub> O <sub>3</sub>	18.36	18.35	17.81	17.62	18.09	14.54	15.98	15.70	17.89	17.30	18.94	18.56
Cr <sub>2</sub> O <sub>3</sub>	0.08	0.00	0.10	0.08	0.06	0.07	0.09	0.10	0.09	0.15	0.09	0.11
FeO	17.31	19.78	16.09	19.41	18.75	21.33	23.10	23.43	17.06	16.53	11.88	14.90
MnO	0.00	0.19	0.15	0.08	0.04	0.20	0.18	0.20	0.07	0.11	0.13	0.01
MgO	11.42	9.87	12.53	10.22	10.40	9.01	7.49	7.54	13.03	11.67	15.43	12.80
CaO	0.02	0.02	0.04	0.05	0.00	0.05	0.08	0.05	0.01	0.03	0.04	0.02
Na <sub>2</sub> O	0.38	0.00	0.22	0.18	0.17	0.09	0.17	0.15	0.38	0.20	0.44	0.35
K <sub>2</sub> O	9.24	9.68	9.56	9.23	9.26	9.53	9.52	9.39	8.33	9.01	8.99	8.10
TOTAL	95.12	94.50	94.93	94.17	94.72	93.99	95.39	95.11	94.99	93.85	95.06	93.66
Cations per 22 oxygens												
Si	5.40	5.61	5.55	5.42	5.52	5.54	5.47	5.50	5.45	5.56	5.55	5.59
Ti	0.29	0.01	0.17	0.26	0.20	0.47	0.43	0.41	0.21	0.26	0.12	0.17
Al	3.27	3.32	3.16	3.21	3.25	2.70	2.94	2.90	3.17	3.10	3.26	3.28
Cr	0.01	0.00	0.01	0.01	0.01	0.01	0.01	0.01	0.01	0.02	0.01	0.01
Fe <sup>2+</sup>	2.19	2.54	2.02	2.51	2.39	2.81	3.01	3.07	2.14	2.10	1.45	1.87
Mn	0.00	0.02	0.02	0.01	0.01	0.03	0.02	0.03	0.01	0.01	0.02	0.00
Mg	2.57	2.26	2.81	2.35	2.36	2.11	1.74	1.76	2.92	2.65	3.36	2.86
Ca	0.00	0.00	0.01	0.01	0.00	0.01	0.01	0.01	0.00	0.00	0.01	0.00
Na	0.11	0.00	0.06	0.05	0.05	0.03	0.05	0.05	0.11	0.06	0.12	0.10
K	1.78	1.90	1.83	1.82	1.80	1.91	1.89	1.88	1.60	1.75	1.68	1.55
TOTAL	15.62	15.67	15.64	15.65	15.58	15.61	15.59	15.60	15.61	15.52	15.59	15.42
Al <sup>IV</sup>	2.60	2.39	2.45	2.58	2.48	2.46	2.53	2.50	2.55	2.44	2.45	2.41
Al <sup>VI</sup>	0.67	0.94	0.71	0.63	0.77	0.24	0.41	0.39	0.62	0.66	0.82	0.86
Mg/(Mg+Fe)	0.54	0.47	0.58	0.48	0.50	0.43	0.37	0.36	0.58	0.56	0.70	0.60

Table 1.2 Biotite analyses (continued)

SAMPLE	88-85	88-86	88-87	88-87	88-87	88-89	88-90	88-98	88-104	88-122	88-122	88-123
GRAIN	ga2 l2	ga1 r1	ga2 r4	ga1 r1	mat	ga1 r1	ga2 r1	ga2 r3	ga1 r1	ga1 r1	ga2 r1	ga1 r1
SiO <sub>2</sub>	36.89	37.01	36.15	35.74	35.98	37.60	37.36	35.76	37.24	34.78	36.33	35.88
TiO <sub>2</sub>	1.44	1.77	2.31	2.43	2.45	1.42	1.02	1.41	1.46	1.34	1.79	2.06
Al <sub>2</sub> O <sub>3</sub>	18.61	19.56	18.24	18.38	18.38	17.85	18.80	18.09	16.87	18.09	18.42	18.20
Cr <sub>2</sub> O <sub>3</sub>	0.05	0.00	0.12	0.09	0.13	0.03	0.05	0.07	0.05	0.07	0.10	0.10
FeO	15.46	16.38	16.10	16.14	16.01	13.73	13.91	19.19	13.43	20.38	18.98	18.60
MnO	0.03	0.02	0.07	0.05	0.06	0.04	0.02	0.05	0.06	0.14	0.12	0.12
MgO	13.33	11.80	11.74	11.50	11.35	15.44	14.75	10.62	15.31	10.48	10.36	10.48
CaO	0.01	0.03	0.00	0.03	0.03	0.02	0.02	0.02	0.04	0.00	0.02	0.04
Na <sub>2</sub> O	0.20	0.28	0.32	0.28	0.30	0.30	0.15	0.25	0.40	0.17	0.18	0.22
K <sub>2</sub> O	8.28	8.73	8.74	9.02	8.75	9.11	8.80	8.37	8.74	8.74	9.53	9.51
TOTAL	94.31	95.58	93.79	93.64	93.43	95.54	94.88	93.84	93.60	94.18	95.83	95.21

Cations per 22 oxygens

Si	5.51	5.48	5.48	5.44	5.48	5.53	5.52	5.49	5.59	5.38	5.48	5.45
Ti	0.16	0.20	0.26	0.28	0.28	0.16	0.11	0.16	0.16	0.16	0.20	0.24
Al	3.28	3.42	3.26	3.30	3.30	3.09	3.27	3.28	2.98	3.30	3.28	3.26
Cr	0.01	0.00	0.01	0.01	0.02	0.00	0.01	0.01	0.01	0.01	0.01	0.01
Fe <sup>2+</sup>	1.93	2.03	2.04	2.06	2.04	1.69	1.72	2.47	1.68	2.64	2.40	2.36
Mn	0.00	0.00	0.01	0.01	0.01	0.00	0.00	0.01	0.01	0.02	0.02	0.02
Mg	2.97	2.61	2.65	2.61	2.57	3.38	3.25	2.43	3.42	2.42	2.33	2.37
Ca	0.00	0.00	0.00	0.00	0.00	0.00	0.00	0.00	0.01	0.00	0.00	0.01
Na	0.06	0.08	0.09	0.08	0.09	0.09	0.04	0.07	0.12	0.05	0.05	0.06
K	1.58	1.65	1.69	1.75	1.70	1.71	1.68	1.64	1.67	1.73	1.84	1.84
TOTAL	15.50	15.47	15.51	15.54	15.48	15.66	15.58	15.56	15.65	15.70	15.61	15.63

Al <sub>A</sub>	2.49	2.52	2.52	2.56	2.52	2.47	2.48	2.51	2.41	2.62	2.52	2.55
Al <sub>B</sub>	0.79	0.90	0.74	0.74	0.77	0.62	0.79	0.77	0.57	0.68	0.76	0.71
Mg/(Mg+Fe)	0.61	0.56	0.57	0.56	0.56	0.67	0.65	0.50	0.67	0.48	0.49	0.50

Table 1.2 Biotite analyses (continued)

SAMPLE	88-129A
GRAIN	ga1 r2
SiO <sub>2</sub>	36.51
TiO <sub>2</sub>	3.37
Al <sub>2</sub> O <sub>3</sub>	18.69
Cr <sub>2</sub> O <sub>3</sub>	0.08
FeO	14.20
MnO	0.04
MgO	11.74
CaO	0.00
Na <sub>2</sub> O	0.11
K <sub>2</sub> O	10.21
<b>TOTAL</b>	<b>94.95</b>

Cations per 22 oxygen:

Si	5.45
Ti	0.38
Al	3.29
Cr	0.01
Fe <sup>2+</sup>	1.77
Mn	0.01
Mg	2.61
Ca	0.00
Na	0.03
K	1.95
<b>TOTAL</b>	<b>15.51</b>

Al <sub>4</sub>	2.55
Al <sub>6</sub>	0.75
<b>Mg/(Mg+Fe)</b>	<b>0.60</b>

Table I.3 Muscovite analyses

SAMPLE	158-86	87-51	87-81	87-83	87-86	87-86	87-117	87-283	87-287b	88-45A	88-50	88-52b
GRAIN	ga2 1r	ga4 1r	ga2 1r	ga1 1r	ga1 1r	ga4 1r	ga1 1r	ga2 1r				
SiO <sub>2</sub>	47.27	46.27	46.33	48.10	49.03	49.55	48.48	49.08	47.67	47.41	45.72	46.77
TiO <sub>2</sub>	0.66	0.45	0.36	0.29	0.45	0.42	0.00	0.32	1.00	0.65	0.73	0.82
Al <sub>2</sub> O <sub>3</sub>	34.65	35.84	35.82	35.20	34.11	34.10	34.86	34.10	30.01	35.51	35.59	34.59
Cr <sub>2</sub> O <sub>3</sub>	0.00	0.00	0.00	0.00	0.00	0.00	0.00	0.00	0.13	0.01	0.00	0.03
FeO	2.00	1.90	2.04	2.21	1.57	1.71	2.03	1.76	2.85	0.94	1.07	1.26
MnO	0.01	0.01	0.00	0.00	0.00	0.00	0.00	0.00	0.01	0.00	0.00	0.00
MgO	1.72	1.44	1.20	1.33	1.33	1.32	1.05	1.34	1.92	0.87	0.95	1.02
CaO	0.00	0.00	0.00	0.00	0.01	0.01	0.01	0.01	0.02	0.00	0.00	0.00
Na <sub>2</sub> O	0.43	0.43	0.28	0.73	0.55	0.66	0.76	0.50	0.73	1.63	1.50	1.21
K <sub>2</sub> O	9.03	7.57	7.83	7.26	9.16	8.98	9.49	9.94	9.96	8.62	8.55	9.64
TOTAL	95.76	93.91	93.86	95.12	96.21	96.76	96.68	97.05	94.30	95.64	94.11	95.34
Cations per 22 oxygen												
Si	6.22	6.15	6.17	6.30	6.39	6.42	6.32	6.38	6.46	6.22	6.11	6.20
Ti	0.07	0.04	0.04	0.03	0.04	0.04	0.00	0.03	0.10	0.06	0.07	0.08
Al	5.37	5.61	5.62	5.43	5.24	5.21	5.36	5.23	4.79	5.49	5.60	5.41
Cr	0.00	0.00	0.00	0.00	0.00	0.00	0.00	0.00	0.01	0.00	0.00	0.00
Fe <sup>2+</sup>	0.22	0.21	0.23	0.24	0.17	0.19	0.22	0.19	0.32	0.10	0.12	0.14
Mn	0.00	0.00	0.00	0.00	0.00	0.00	0.00	0.00	0.00	0.00	0.00	0.00
Mg	0.34	0.29	0.24	0.26	0.26	0.25	0.20	0.26	0.39	0.17	0.19	0.20
Ca	0.00	0.00	0.00	0.00	0.00	0.00	0.00	0.00	0.00	0.00	0.00	0.00
Na	0.11	0.11	0.07	0.19	0.14	0.17	0.19	0.13	0.19	0.41	0.39	0.31
K	1.52	1.28	1.33	1.21	1.52	1.48	1.58	1.65	1.72	1.44	1.46	1.63
Total	13.84	13.70	13.69	13.66	13.77	13.76	13.88	13.86	13.99	13.90	13.94	13.98
Al <sup>IV</sup>	1.78	1.85	1.83	1.70	1.61	1.58	1.68	1.62	1.54	1.78	1.89	1.80
Al <sup>VI</sup>	3.59	3.76	3.79	3.73	3.64	3.63	3.68	3.61	3.25	3.71	3.71	3.61
K/K+Na	0.93	0.92	0.95	0.87	0.92	0.90	0.89	0.93	0.90	0.78	0.79	0.84
Na/Na+K	0.07	0.08	0.05	0.13	0.08	0.10	0.11	0.07	0.10	0.22	0.21	0.16

Table I.3 Muscovite analyses (continued)

SAMPLE	88-55	88-74A	88-80	88-85	88-85	88-86	88-87	88-87	88-122	88-122	88-123	88-129A
GRAIN	ga1 1r	ga1 1r	ga2 2r	ga2 1r	ga2 2l	ga1 1r	ga2 4r	ga1 1r	ga1 1r	ga2 1r	ga1 1r	ga1 2r
SiO <sub>2</sub>	50.48	46.65	46.31	47.55	47.10	46.96	46.54	46.74	45.97	47.44	46.61	48.80
TiO <sub>2</sub>	0.38	0.55	0.41	0.80	0.87	0.67	0.74	0.78	0.34	0.39	0.48	0.06
Al <sub>2</sub> O <sub>3</sub>	31.48	33.65	35.06	33.69	34.49	35.24	34.00	33.38	32.88	33.10	33.41	33.85
Cr <sub>2</sub> O <sub>3</sub>	0.00	0.04	0.08	0.01	0.02	0.00	0.03	0.05	0.04	0.00	0.00	0.00
FeO	2.57	2.56	1.79	1.16	1.13	1.25	1.20	1.41	1.95	2.04	1.83	1.51
MnO	0.00	0.00	0.00	0.00	0.00	0.00	0.00	0.01	0.00	0.00	0.01	0.00
MgO	1.70	0.97	0.78	1.21	1.00	1.11	1.03	1.31	1.30	1.38	1.29	1.66
CaO	0.00	0.00	0.04	0.00	0.02	0.01	0.01	0.00	0.00	0.00	0.00	0.00
Na <sub>2</sub> O	0.18	1.69	2.06	1.42	1.59	0.94	1.15	0.97	0.48	0.51	0.64	0.25
K <sub>2</sub> O	10.49	8.65	8.02	8.70	8.46	9.24	9.21	9.59	10.34	10.33	10.39	10.72
TOTAL	97.28	94.76	94.63	94.66	94.67	95.42	93.91	94.25	93.31	95.19	94.66	96.85

Cations per 22 oxygen

Si	6.58	6.24	6.17	6.32	6.25	6.20	6.25	6.27	6.27	6.33	6.26	6.38
Ti	0.04	0.06	0.04	0.08	0.09	0.07	0.07	0.08	0.03	0.04	0.05	0.01
Al	4.84	5.31	5.51	5.28	5.39	5.48	5.38	5.28	5.29	5.21	5.29	5.21
Cr	0.00	0.00	0.01	0.00	0.00	0.00	0.00	0.01	0.00	0.00	0.00	0.00
Fe <sup>2+</sup>	0.28	0.29	0.20	0.13	0.13	0.14	0.13	0.16	0.22	0.23	0.21	0.17
Mn	0.00	0.00	0.00	0.00	0.00	0.00	0.00	0.00	0.00	0.00	0.00	0.00
Mg	0.33	0.19	0.15	0.24	0.20	0.22	0.21	0.26	0.26	0.27	0.26	0.32
Ca	0.00	0.00	0.01	0.00	0.00	0.00	0.00	0.00	0.00	0.00	0.00	0.00
Na	0.05	0.44	0.53	0.37	0.41	0.24	0.30	0.25	0.13	0.13	0.17	0.06
K	1.74	1.48	1.36	1.47	1.43	1.56	1.58	1.64	1.80	1.76	1.78	1.79
Total	13.86	14.00	13.98	13.88	13.89	13.90	13.92	13.95	14.01	13.97	14.02	13.94
Al <sup>IV</sup>	1.42	1.76	1.83	1.68	1.75	1.80	1.75	1.73	1.73	1.67	1.74	1.62
Al <sup>VI</sup>	3.42	3.55	3.68	3.59	3.64	3.68	3.63	3.55	3.56	3.54	3.56	3.59
K/K+Na	0.97	0.77	0.72	0.80	0.78	0.87	0.84	0.87	0.93	0.93	0.91	0.97
Na/Na+K	0.03	0.23	0.28	0.20	0.22	0.13	0.16	0.13	0.07	0.07	0.09	0.03

Table 1.4 Plagioclase analyses

SAMPLE GRAIN	158-86 ga2 1r	87-61 ga2 1r	87-81 ga2 1r	87-83 ga2 1r	87-86 ga2 1r	87-86 ga4 1r	87-117 ga2 1r	87-283 ga1 1r	87-207b ga1 1r	88-45A ga4 1r	88-50 ga1 1r	88-65 ga1 1r
SiO <sub>2</sub>	62.84	61.80	63.23	63.39	64.14	63.45	65.56	63.86	60.75	62.93	62.65	62.93
TiO <sub>2</sub>	0.00	0.00	0.00	0.00	0.00	0.00	0.00	0.00	0.02	0.00	0.00	0.00
Al <sub>2</sub> O <sub>3</sub>	24.72	24.46	23.66	22.97	23.04	23.24	22.66	22.43	24.40	23.45	24.44	23.40
Cr <sub>2</sub> O <sub>3</sub>	0.00	0.00	0.00	0.00	0.00	0.00	0.00	0.00	0.02	0.00	0.00	0.00
FeO	0.11	0.50	0.44	0.50	0.12	0.06	0.07	0.17	0.06	0.00	0.02	0.08
MnO	0.01	0.00	0.00	0.00	0.00	0.00	0.00	0.00	0.00	0.00	0.00	0.00
MgO	0.00	0.00	0.01	0.00	0.00	0.00	0.00	0.00	0.02	0.00	0.00	0.00
CaO	5.24	5.00	4.54	4.09	4.45	4.56	3.88	4.36	6.36	4.88	5.54	5.15
Na <sub>2</sub> O	7.26	7.85	8.45	9.03	7.51	8.45	8.19	9.40	7.75	8.23	8.24	8.94
K <sub>2</sub> O	0.05	0.10	0.10	0.08	0.09	0.07	0.07	0.03	0.03	0.00	0.00	0.18
TOTAL	100.23	99.71	100.43	100.06	99.35	99.83	100.43	100.25	99.40	99.49	100.89	100.68
Cations per 8 oxygen												
Si	2.76	2.74	2.78	2.80	2.83	2.80	2.86	2.82	2.71	2.79	2.75	2.77
Ti	0.00	0.00	0.00	0.00	0.00	0.00	0.00	0.00	0.00	0.00	0.00	0.00
Al	1.28	1.28	1.23	1.20	1.20	1.21	1.17	1.17	1.28	1.23	1.26	1.22
Cr	0.00	0.00	0.00	0.00	0.00	0.00	0.00	0.00	0.00	0.00	0.00	0.00
Fe <sup>2+</sup>	0.00	0.02	0.02	0.02	0.00	0.00	0.00	0.01	0.00	0.00	0.00	0.00
Mn	0.00	0.00	0.00	0.00	0.00	0.00	0.00	0.00	0.00	0.00	0.00	0.00
Mg	0.00	0.00	0.00	0.00	0.00	0.00	0.00	0.00	0.00	0.00	0.00	0.00
Ca	0.25	0.24	0.21	0.19	0.21	0.22	0.18	0.21	0.30	0.23	0.26	0.24
Na	0.82	0.68	0.72	0.77	0.64	0.72	0.69	0.80	0.67	0.71	0.70	0.76
K	0.00	0.01	0.01	0.00	0.01	0.00	0.00	0.00	0.00	0.00	0.00	0.01
Total	4.91	4.96	4.97	4.99	4.89	4.96	4.91	5.00	4.98	4.95	4.97	5.01
X <sub>alb</sub>	0.71	0.74	0.77	0.80	0.75	0.77	0.79	0.79	0.69	0.75	0.73	0.75
X <sub>an</sub>	0.28	0.26	0.23	0.20	0.25	0.23	0.21	0.20	0.31	0.25	0.27	0.24

Table I.4 Plagioclase analyses (continued)

SAMPLE	88-74A	88-74A	88-76A	88-80	88-86	88-87	88-87	88-122	88-122	88-123
GRAIN	ga1 1r	ga1 1c	ga1 1r	ga2 1r	ga1 1r	ga2 4r	ga1 1r	ga1 1r	ga2 1r	ga1 1r
SiO <sub>2</sub>	64.80	65.87	62.36	63.24	64.69	62.92	63.36	61.67	61.32	61.72
TiO <sub>2</sub>	0.04	0.00	0.00	0.04	0.00	0.01	0.01	0.00	0.00	0.00
Al <sub>2</sub> O <sub>3</sub>	21.83	21.44	23.86	22.68	22.74	22.51	22.22	23.94	24.42	23.77
Cr <sub>2</sub> O <sub>3</sub>	0.01	0.01	0.00	0.00	0.00	0.00	0.00	0.01	0.00	0.01
FeO	0.12	0.12	0.03	0.25	0.03	0.15	0.08	0.09	0.24	0.11
MnO	0.00	0.00	0.00	0.02	0.00	0.00	0.00	0.00	0.00	0.00
MgO	0.01	0.01	0.00	0.02	0.00	0.00	0.00	0.00	0.00	0.00
CaO	3.02	2.45	5.18	4.11	4.10	4.10	3.75	5.57	5.74	5.40
Na <sub>2</sub> O	9.64	10.58	8.31	9.43	8.79	9.10	8.97	8.00	7.90	8.19
K <sub>2</sub> O	0.00	0.00	0.00	0.00	0.08	0.00	0.00	0.00	0.00	0.00
<b>TOTAL</b>	<b>99.47</b>	<b>100.48</b>	<b>99.74</b>	<b>99.79</b>	<b>100.43</b>	<b>98.78</b>	<b>98.39</b>	<b>99.28</b>	<b>99.62</b>	<b>99.20</b>
<b>Cations per 8 oxygen</b>										
Si	2.86	2.88	2.76	2.80	2.83	2.81	2.83	2.75	2.73	2.76
Ti	0.00	0.00	0.00	0.00	0.00	0.00	0.00	0.00	0.00	0.00
Al	1.14	1.11	1.25	1.19	1.17	1.19	1.17	1.26	1.28	1.25
Cr	0.00	0.00	0.00	0.00	0.00	0.00	0.00	0.00	0.00	0.00
Fe <sup>2+</sup>	0.00	0.00	0.00	0.01	0.00	0.01	0.00	0.00	0.01	0.00
Mn	0.00	0.00	0.00	0.00	0.00	0.00	0.00	0.00	0.00	0.00
Mg	0.00	0.00	0.00	0.00	0.00	0.00	0.00	0.00	0.00	0.00
Ca	0.14	0.11	0.25	0.20	0.19	0.20	0.18	0.27	0.27	0.26
Na	0.83	0.90	0.71	0.81	0.75	0.79	0.78	0.69	0.68	0.71
K	0.00	0.00	0.00	0.00	0.00	0.00	0.00	0.00	0.00	0.00
<b>Total</b>	<b>4.98</b>	<b>5.01</b>	<b>4.97</b>	<b>5.01</b>	<b>4.95</b>	<b>4.99</b>	<b>4.97</b>	<b>4.97</b>	<b>4.97</b>	<b>4.98</b>
X <sub>alb</sub>	0.85	0.89	0.74	0.81	0.79	0.80	0.81	0.72	0.71	0.73
X <sub>an</sub>	0.15	0.11	0.26	0.19	0.20	0.20	0.19	0.28	0.29	0.27

## MINERAL CHEMISTRY

The samples used for geothermobarometry have been subdivided into four different groups. Three groups represent the quartzo-feldspathic rocks in the three sub-areas defined in Chapter 7 (north, west and central/east, Fig. F.3 in Appendix F, or Fig. 7.6), the fourth group contains the mafic rocks of the central/eastern sub-area (garnet-amphibolites of the McKay River Formation and mafic inclusions in the Atikamagen Formation). The northern and western sub-areas contain rocks of the upper greenschist to lower amphibolite facies. The rocks from the central/eastern sub-area (including the mafic rocks in the fourth group) are of the amphibolite facies. The minerals considered here are those analyzed for geothermobarometry: garnet, biotite, muscovite and plagioclase. In figures I.1 to I.4 the compositions of these minerals have been plotted, representing all analyses performed for the project, including those that were not used in the final database as presented in the first part of this appendix.

### GARNET

In Figure I.1 compositions of garnets are shown in four diagrams, in which analyses from garnet cores and rims have been separated (in a and b). Garnets are plotted in terms of their end members, in both Ca-Mg-Fe and Mn-Mg-Fe triangular plots, in the left and right of the diagram respectively. All garnets are rich in almandine. The garnets in the low grade areas, near O'Brien Lake and the northern sub-area, as well as garnets from the mafic rocks are poor in Mg, the latter relatively rich in Ca. The low grade garnets have the highest Mn content, whereas those from the metapelites in the Wabush Lake thrust sheet have a very low Mn content, and are enriched in Mg. A comparison of core and rim analyses shows that there is a strong trend of Mn decrease from core to rim. In the Ca-Mg-Fe triangles no obvious trend is present.

Of these garnets a majority falls outside the range of compositions used for calibration of the Ferry and Spear (1978) thermometer.  $X_{Ca} + X_{Mn}$  should be below 0.2, but often exceeds this value, especially in the low grade areas because of the relatively high  $X_{Mn}$ . However, Hodges and Royden (1984) and Schreurs (1985) have

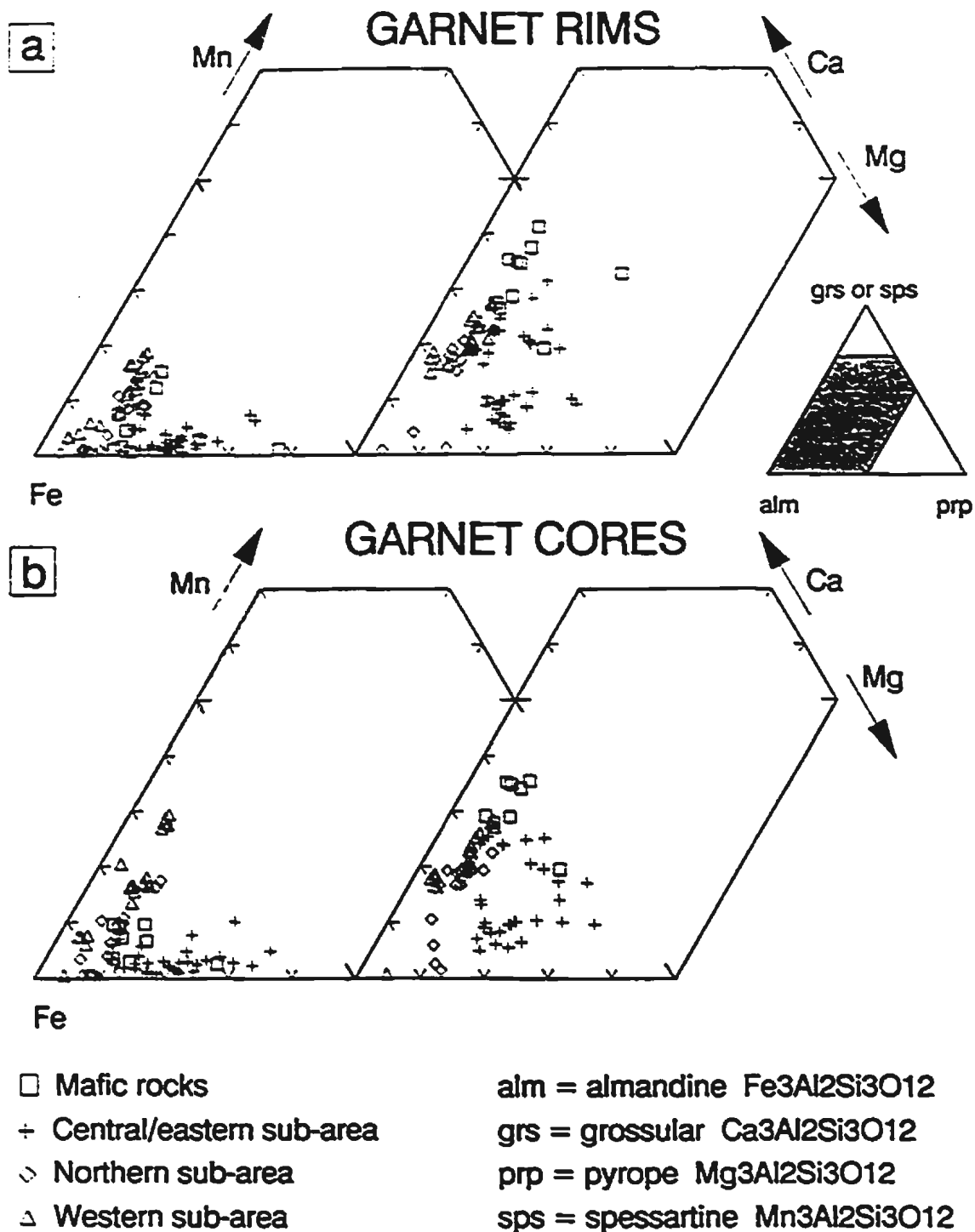
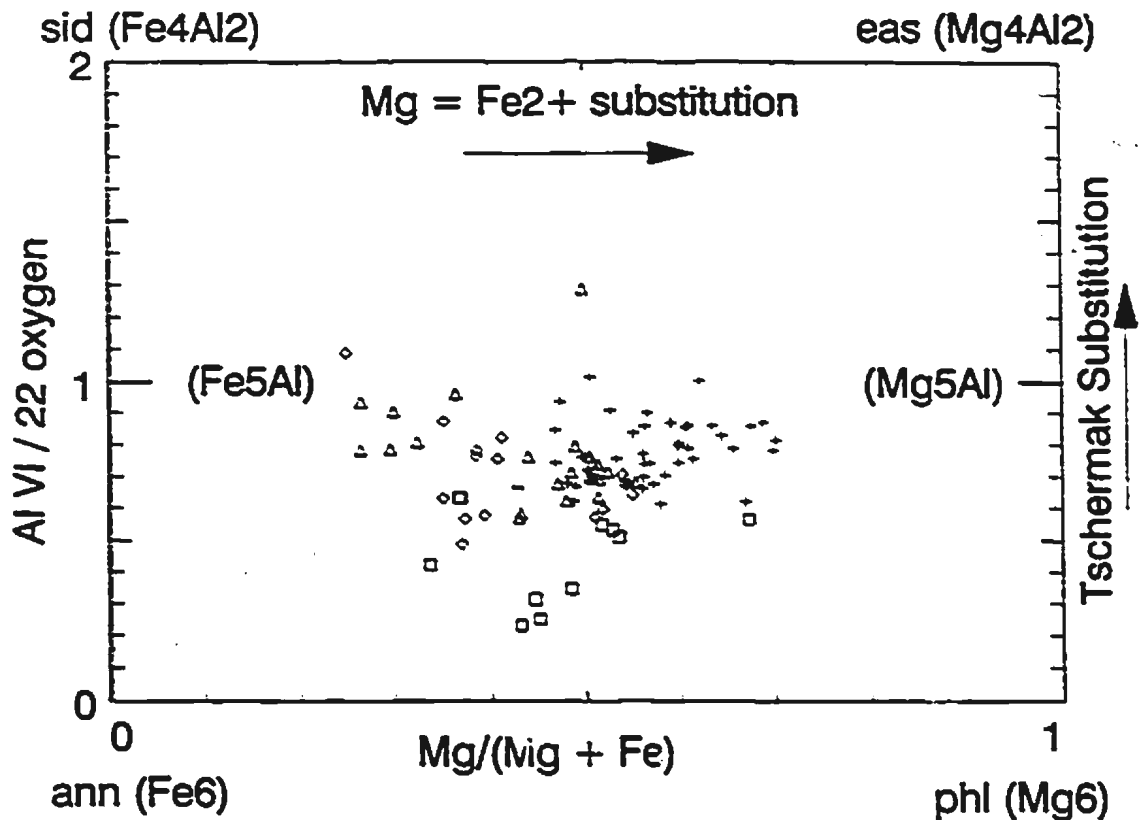


**Fig. 1.1** Partial triangular diagrams of the compositions of the garnets used for geothermobarometry, separated for core and rim analyses. The data are annotated separately for the three sub areas defined in Appendix F, Figure F.3 and for garnets in mafic rocks.



- Mafic rocks
- ◇ Northern sub-area
- Central/Eastern sub-area
- △ Western sub-area

ann = annite  $K_2(Fe_6)(Al_2Si_6O_{20})(OH)_4$

phl = phlogopite  $K_2(Mg_6)(Al_2Si_6O_{20})(OH)_4$

sid = siderophyllite  $K_2(Fe_4Al_2)(Al_2Si_6O_{20})(OH)_4$

eas = eastonite  $K_2(Mg_4Al_2)(Al_2Si_6O_{20})(OH)_4$

Fig 1.2 Composition diagram of the biotites used for geothermobarometry.

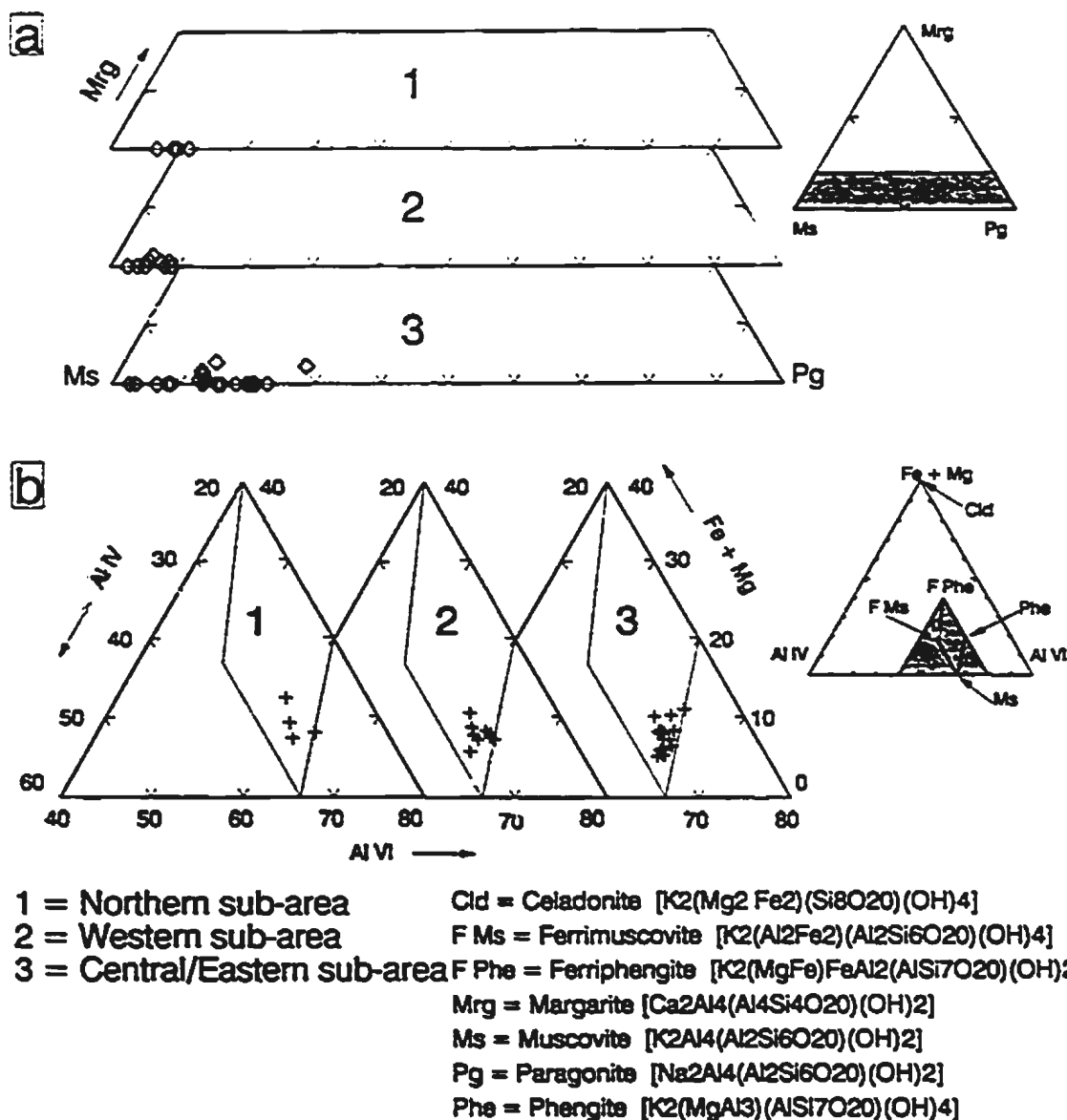
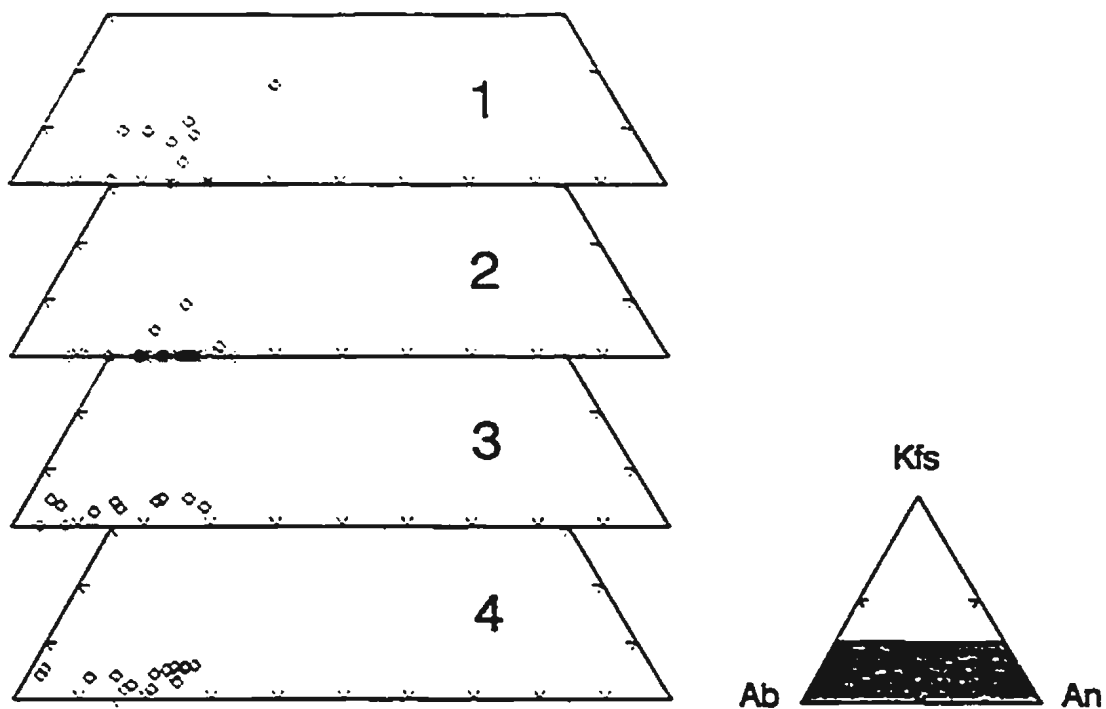


Fig. 1.3 Composition diagram of the white micas used for geothermobarometry. The micas are plotted with respect to the occupation of the alkali site in a) and with respect to the occupation of the tetrahedral and octahedral sites in b). The data are separated in the two figures for the three sub-areas, defined in Appendix F, Figure F.3.



1 = Mafic rocks

2 = Central/Eastern sub-area

3 = Northern sub-area

4 = Western sub-area

Kfs = K-Feldspar  $\text{KAlSi}_3\text{O}_8$

Ab = Albite  $\text{NaAlSi}_3\text{O}_8$

An = Anorthite  $\text{CaAl}_2\text{Si}_2\text{O}_8$

**Fig. 1.4** Partial triangular diagrams of the composition of plagioclase used for geothermobarometry. The data are separated for the three sub-areas, defined in Appendix F, Figure F.3. and for mafic rocks.

shown that the spessartine and grossular contents in garnet do not significantly influence the Fe-Mg exchange between garnet and biotite. Temperatures calculated from garnets with  $X_{Mn} + X_{Ca}$  up to 0.44 used in this study fall within the range of those calculated from garnets with compositions within the range proposed by Ferry and Spear (1978). The upper limit of  $X_{Mn} = 0.25$  in garnets, as proposed by Hodges and Crowley (1985) for their calibration of the barometers used in this study, is not reached in any of the garnets.

## BIOTITE

Biotite compositions have been plotted in Figure I.2 showing the major compositional variations with respect to the four end members annite, phlogopite, siderophyllite and eastonite. The two axes of the diagram represent the substitutions in the octahedral sites of  $Mg = Fe^{2+}$  and the Tschermak substitution  $(Mg, Fe^{2+})Si^{IV} = Al^VI Al^{IV}$ . The distribution of compositions is in accordance with that described by Guidotti (1984) for different rock types. The main variation with respect to the Tschermak substitution lies between  $0.2 < Al^{VI} < 1.0$ . This substitution is weakest in the mafic rocks. The low grade metapelites contain biotites in which  $Mg/(Mg + Fe)$  ranges from 0.25 to 0.55, with biotites from the higher grade metapelites ranging from 0.5 to 0.7. Another important variation in biotite composition is the substitution of Ti in the octahedral sites. In most of the pelitic rocks the Ti in biotite falls within the range of 0.15 to 0.30 Ti per 6 octahedral sites. In the mafic rocks Ti values are higher, ranging between 0.4 and 0.6. With respect to the Ferry and Spear (1978) Gnt-Bt thermometer, the restriction of  $(Al^{VI} + Ti)/(Al^{VI} + Ti + Fe + Mg) < 0.15$  is not met in a fairly large portion of the biotites. Only biotites with compositions within or close to this range were used for thermometry. However, the biotites falling outside the proposed range yielded temperatures similar to those that did meet the requirements. This indicates that the Ferry and Spear (1978) thermometer can be extrapolated outside the range of compositions of biotite that was used for their experiments. All biotites from pelitic rocks fall well within the limits set by Hodges and Crowley (1985) for activity calculations of 20 mole %  $Al^{VI}$  or 5 mole % Ti in the octahedral sites.

## WHITE MICA

Figure I.3 contains all white mica analyses. Three diagrams are presented in figures a and b for data from the three sub-areas separately. No white mica analyses were performed for the mafic rocks.

Figure I.3.a shows the compositions in the  $\text{NaAlO}_2$  -  $\text{KAlO}_2$  -  $\text{CaAl}_2\text{O}_4$  -  $\text{Al}_2\text{O}_3$  -  $\text{SiO}_2$  -  $\text{H}_2\text{O}$  system. With respect to the three end members margarite, muscovite and paragonite, all analyzed white micas have a composition close to the muscovite end member. None of the other end members was encountered in the study. The higher paragonite content in the higher grade area (plot #3) is caused by the narrowing of the muscovite-paragonite immiscibility gap at higher temperatures (Guidotti, 1984).

Apart from the Ms-Pg binary, the Tschermak substitution (or celadonite substitution) in muscovite,  $(\text{Mg,Fe}^{2+})\text{Si} = \text{Al}^{\text{VI}}\text{Al}^{\text{IV}}$ , must also be considered. However, because no distinction is made in the analyses between  $\text{Fe}^{2+}$  and  $\text{Fe}^{3+}$ , the  $\text{Fe}^{3+} = \text{Al}^{\text{VI}}$  substitution cannot be separated from the Tschermak substitution. Figure I.3.b lumps ferric and ferrous iron together and therefore does not distinguish between the two substitutions. The data are plotted following the approach of Guidotti (1984) and show the celadonite component in muscovite. For all three areas the compositions of the white micas lie in between the muscovite and phengite field, fairly close to the ideal muscovite composition.

## PLAGIOCLASE

Plagioclase analyses are presented in Figure I.4. The majority of the plagioclase compositions lies in the range of An10 to An30 (oligoclase). No peristerite gap has been recorded, a continuous range of compositions seems to exist, perhaps due to sub-microscopic exsolution. The majority of the plagioclases from the high grade central/eastern area has a somewhat higher XAn than those from the lower grade western and northern areas. Plagioclases with XCa < 0.18 (approximately) used for barometric computations yielded unrealistically high pressures. Data from these plagioclases were not used in the study. This means that the majority of the samples from the western area could not be used for barometry, in spite of the fact that they contained otherwise suitable assemblages.

# GEOLOGICAL MAP OF THE GRENVILLE P IN SOUTHWESTERN LABRADOR

Compiled by Jeroen A.M. van Gool  
Memorial University of Newfoundland  
1992

## LEGEND

### MOLSON LAKE TERRANE

#### MIDDLE PROTEROZOIC



SHABOGAMO INTRUSIVE SUITE *Coronitic metagabbro and amphibolite*



TRANS LABRADOR BATHOLITH *Foliated granitoids*

0



### GAGNON TERRANE AND FORELAND

#### UNKNOWN AGE



MICHEL LAKE PLUTON *Foliated tonalite to granodiorite*

#### MIDDLE PROTEROZOIC



SHABOGAMO INTRUSIVE SUITE *Coronitic metagabbro and amphibolite*

#### LOWER PROTEROZOIC (Knob Lake Group)



MENIHEK FORMATION *Mica schist or slate, commonly graphite bearing*



SOKOMAN FORMATION (a) *Silicate, carbonate and minor oxide banded iron formation;*  
(b) *oxide banded iron formation*



WISHART FORMATION *White, coarse-grained, crystalline quartzite and minor metapelite*



MCKAY RIVER FORMATION *Volcaniclastic greenschist or amphibolite*



DENAUT FORMATION *Dolomitic marble*



ATTIKAMAGEN FORMATION *Quartzo-feldspathic mica schist, locally garnet, kyanite  
or staurolite bearing; migmatitic in southeast of map area*

#### ARCHEAN

67°00'

66°45'

PROVINCE

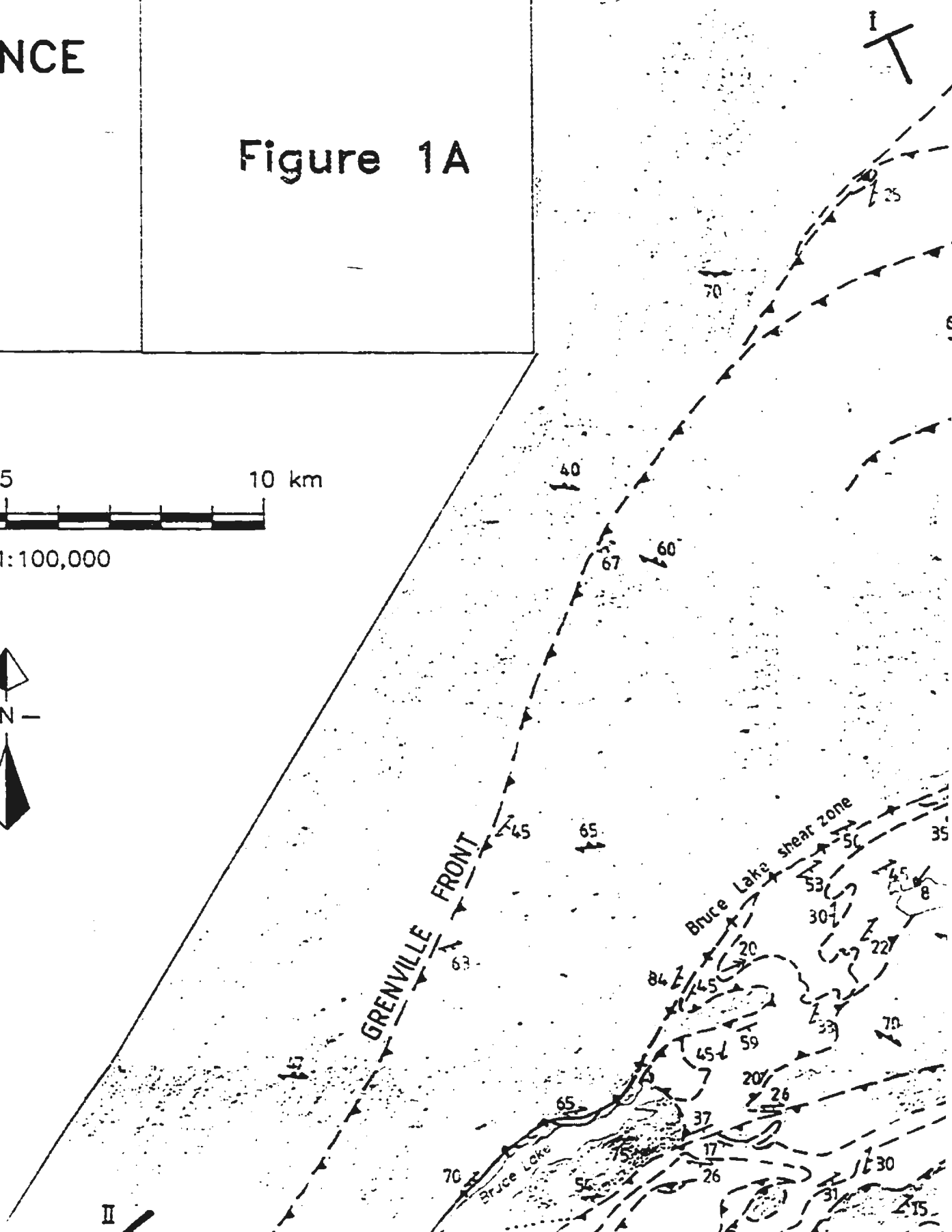
Figure 1A

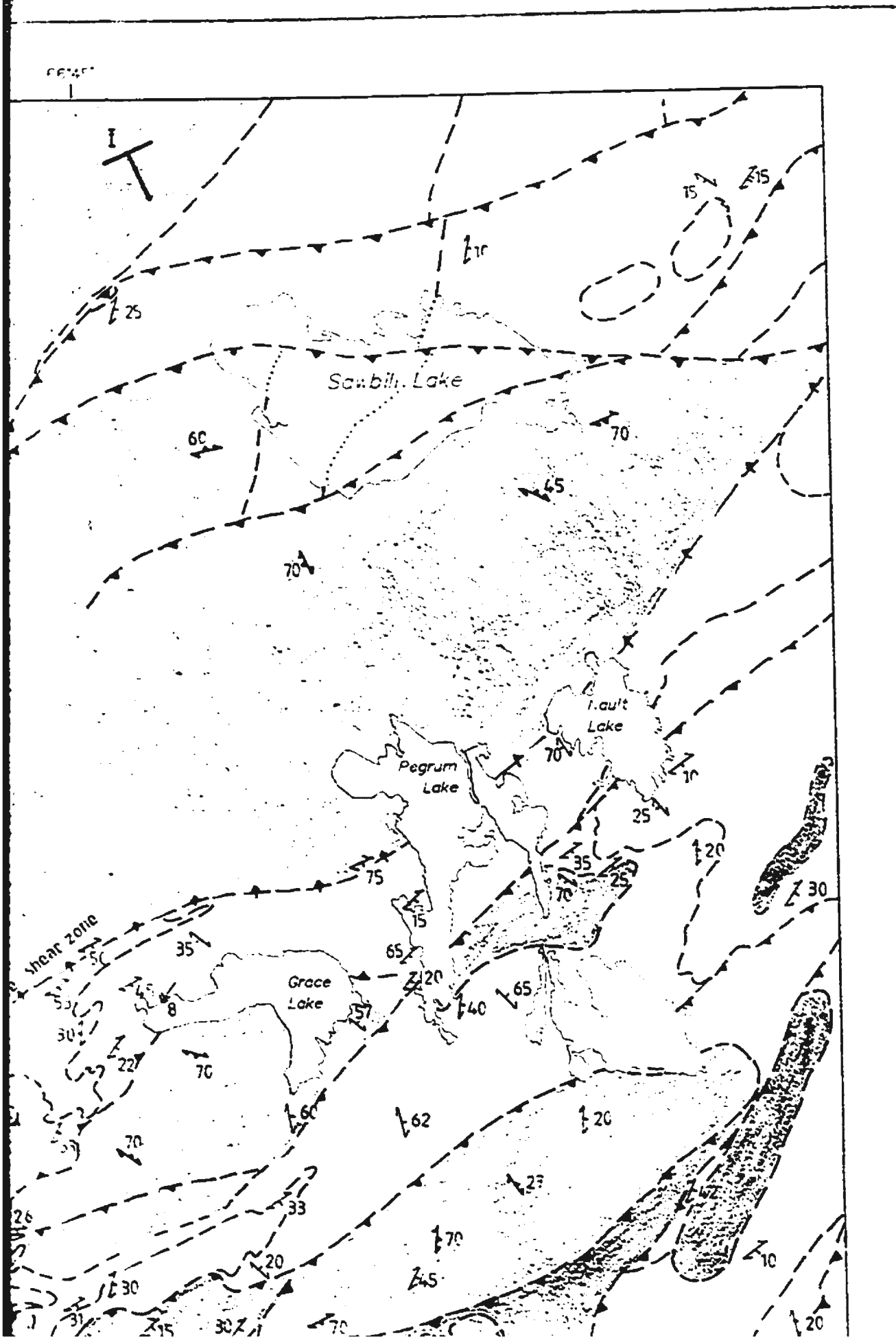
F

5

10 km

scale 1:100,000





Vertical text on the right edge of the page, possibly a page number or reference code.

# ARCHEAN



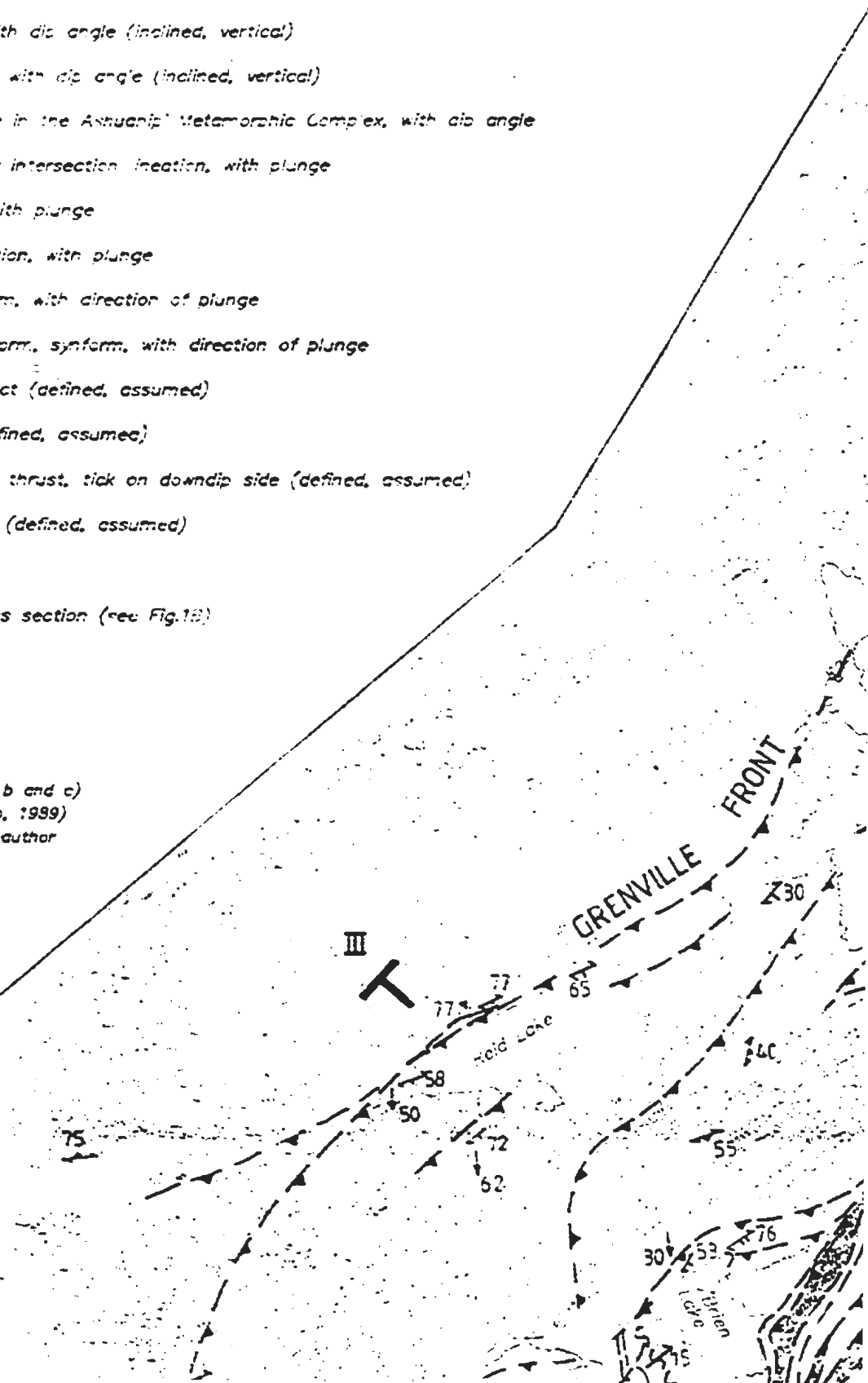
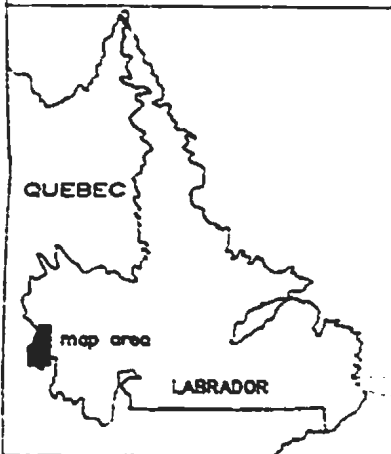
ASHUANUPI METAMORPHIC COMPLEX (a) Coarse grained, two-pyroxene banded gneiss or migmatite, locally finer grained amphibolite, intruded by coarse-grained granite; (b) Locally intensely reworked in the Gagnon terrane

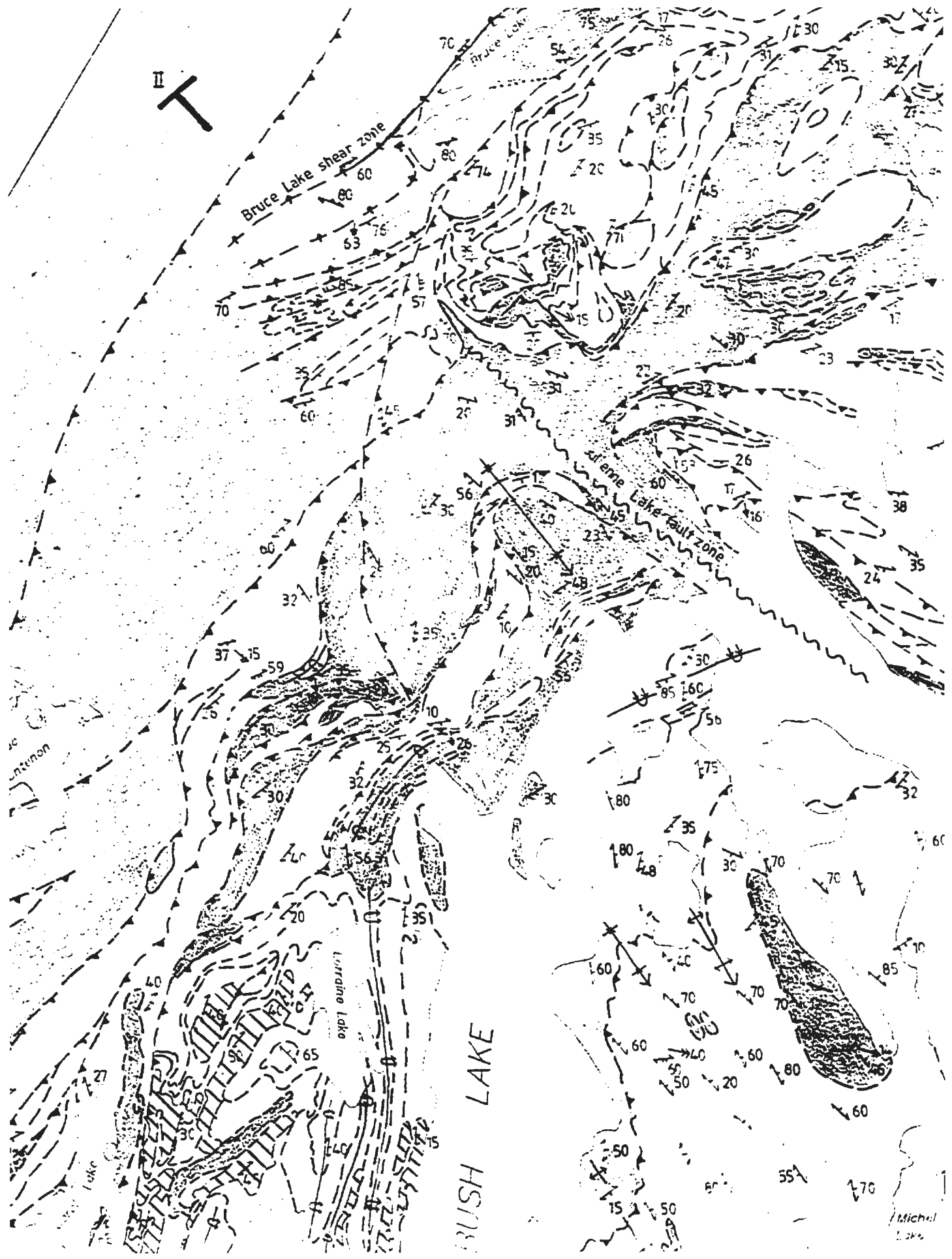
53715

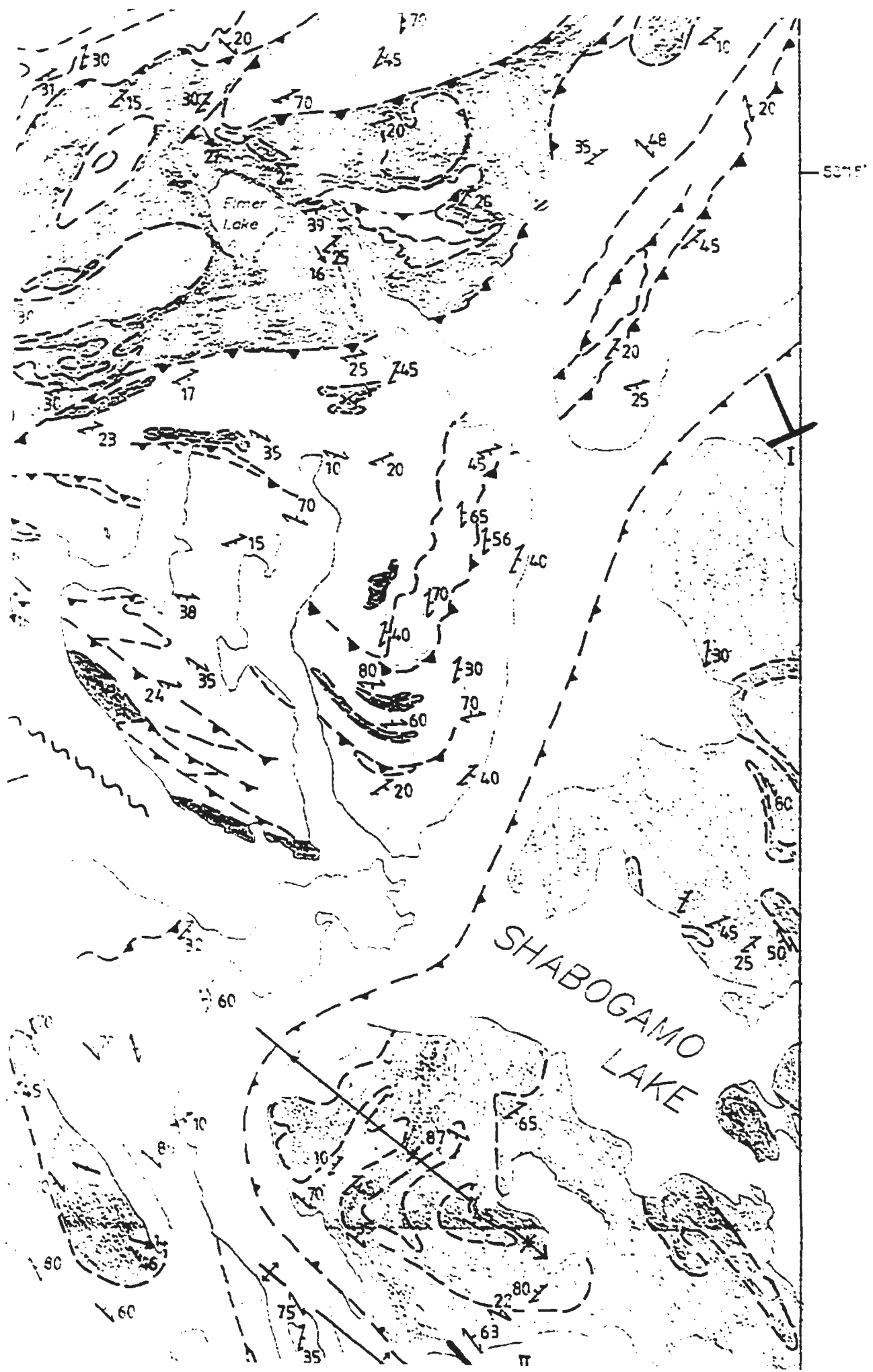
## SYMBOLS

- Bedding, with dip angle (inclined, vertical, overturned)
- S<sub>1</sub> foliation, with dip angle (inclined, vertical)
- S<sub>2</sub> axial plane, with dip angle (inclined, vertical)
- Orissic banding in the Ashuanipi Metamorphic Complex, with dip angle
- F<sub>1</sub> fold axis or intersection lineation, with plunge
- F<sub>2</sub> fold axis, with plunge
- Elongation lineation, with plunge
- Antiform, synform, with direction of plunge
- Overturned antiform, synform, with direction of plunge
- Geological contact (defined, assumed)
- Thrust fault (defined, assumed)
- Overturned back thrust, tick on downdip side (defined, assumed)
- Strike-slip fault (defined, assumed)
- Shear zone
- Location of cross section (see Fig.16)

COMPILED FROM:  
Fahrig (1967), Rivers (1995a, b and c)  
van Gool et al. (1987b, 1988b, 1989)  
and unpublished work by the author  
(see Appendix A)



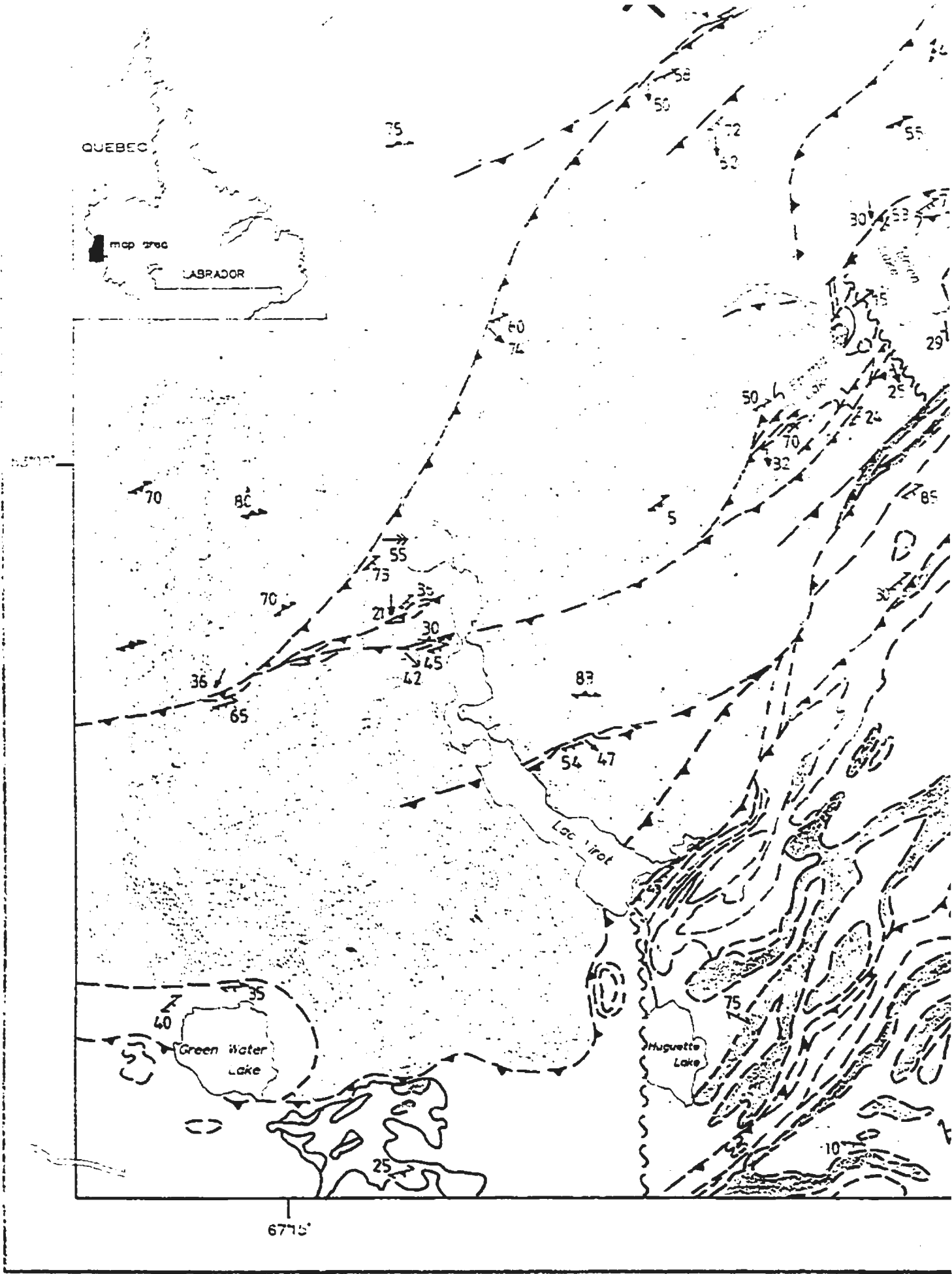




QUEBEC

mcp 2700

LABRADOR



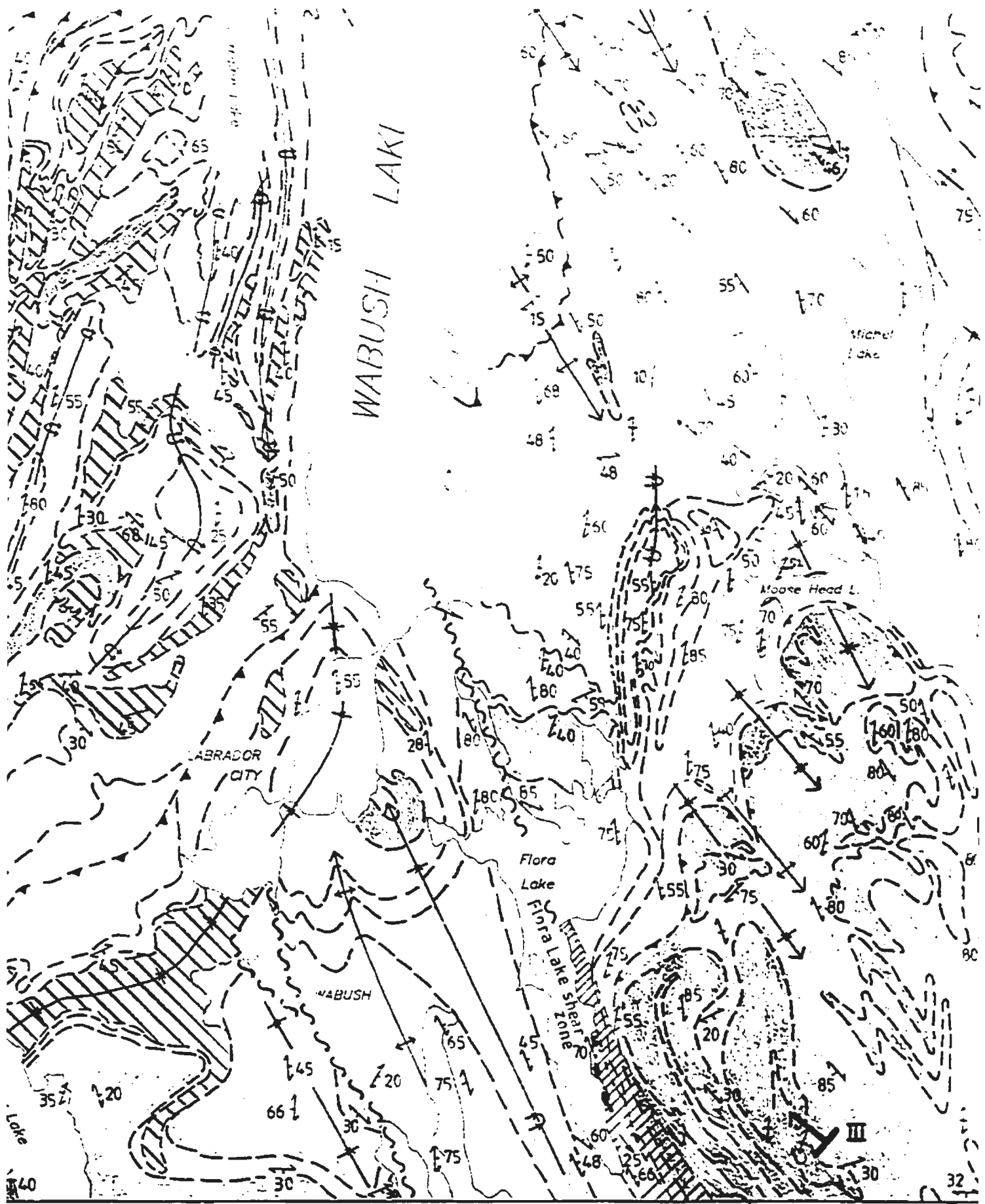
67°15'



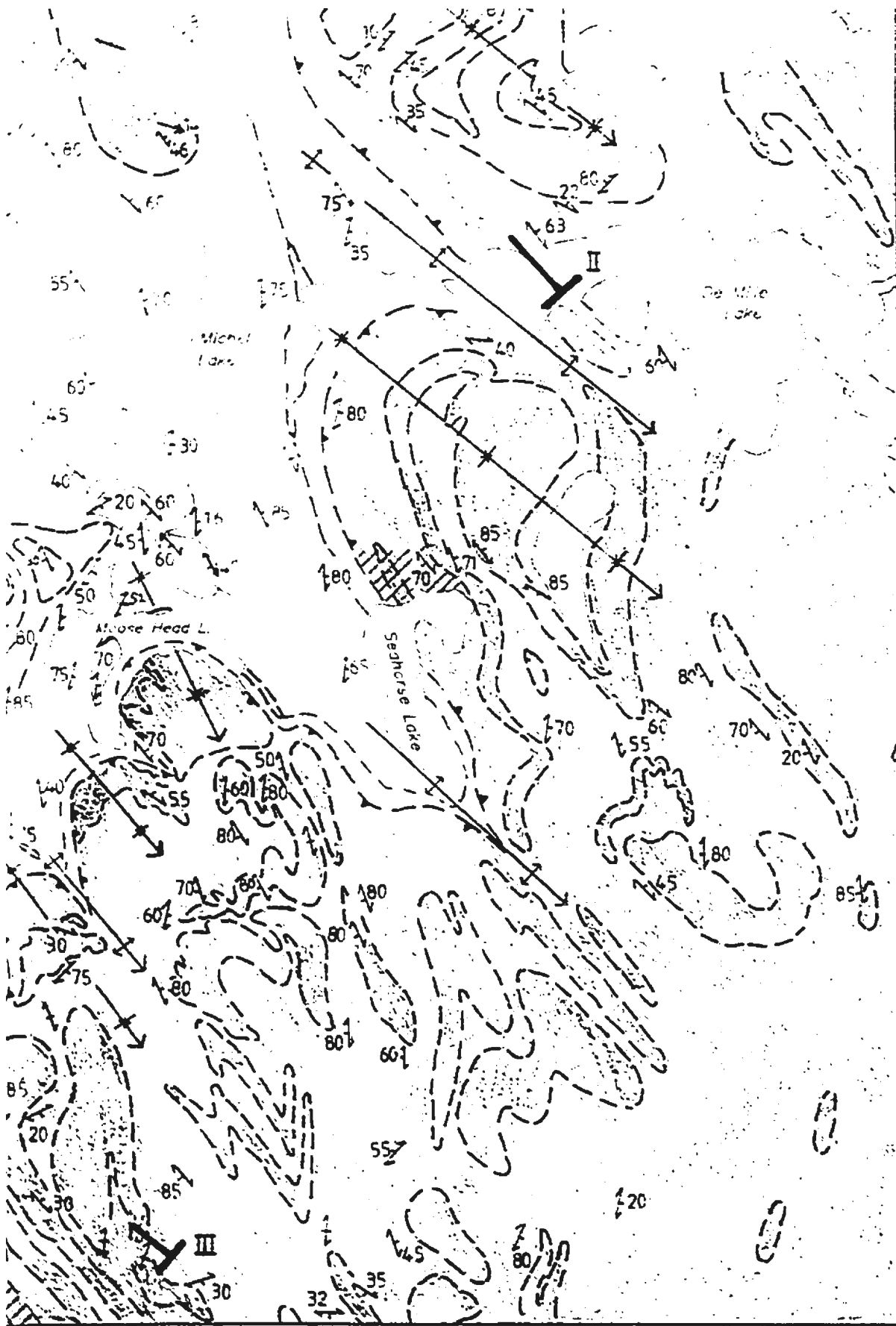
5715'

6700'

# WABUSH LAKE



66'45"



66°45'

# CROSS SECTIONS THROUGH GAGNON TERRANE, SOUTHWESTERN LABRADOR

Jeroen A.M. van Gool  
Memorial University of Newfoundland  
1992

## Figure 1B

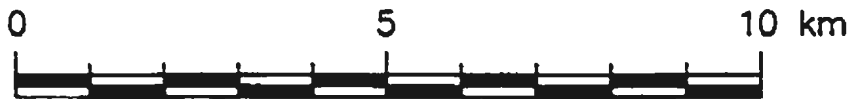
Locations of the sections are shown in Figure 1A.

BLSZ = Bruce Lake shear zone

FLSZ = Flora Lake shear zone

GF = Grenville Front

Note that the cross-sections show greater detail than the associated map (Fig. 1A). Major structures and lithological boundaries are coincident in map and sections, but small structures and details of the distribution of units, both observed and interpreted, are added to the cross sections.



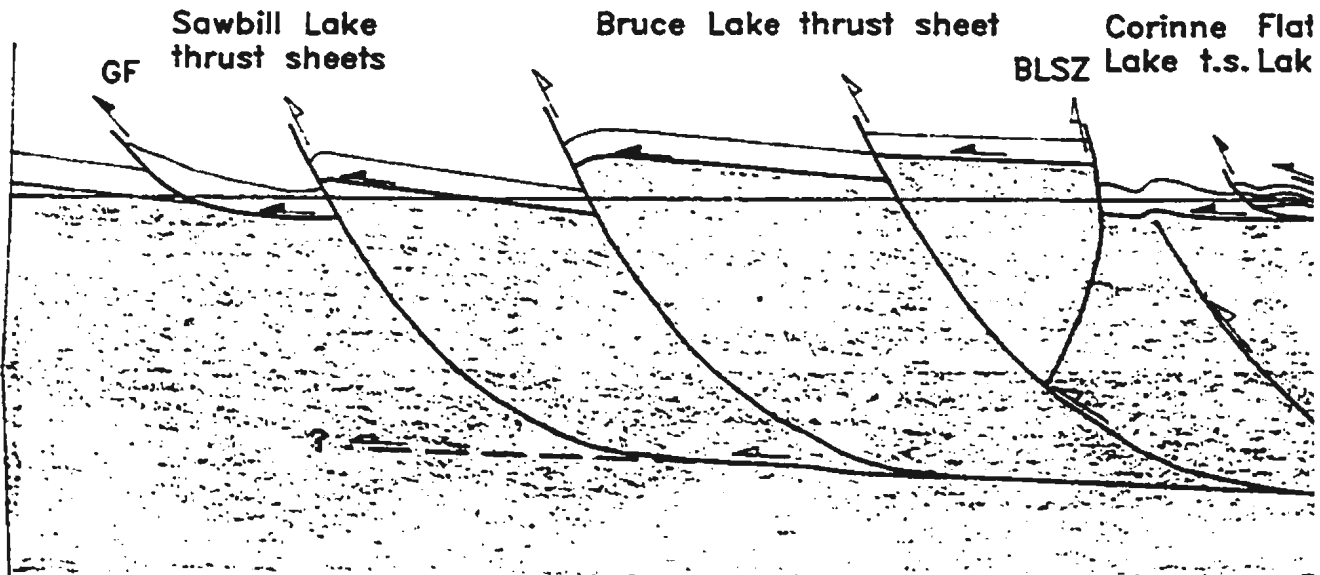
scale 1:100,000

vertical scale = horizontal scale

## SYMBOLS

-  Geological contact
-  Thrust fault, upper
-  Thrust fault, lower
-  Strike-slip shear zone

NW



# SECTIONS THROUGH GAGNON TERRANE, SOUTHWESTERN LABRADOR

Jeroen A.M. van Gool

Memorial University of Newfoundland

1992

## Figure 1B

Sections are shown in Figure 1A.  
Bruce Lake shear zone  
Tara Lake shear zone  
= Grenville Front

Note that the cross-sections show greater detail than the associated map (Fig. 1A). Major structures and lithological boundaries are coincident in map and sections, but small structures and details of the distribution of units, both observed and interpreted, are added to the cross sections.

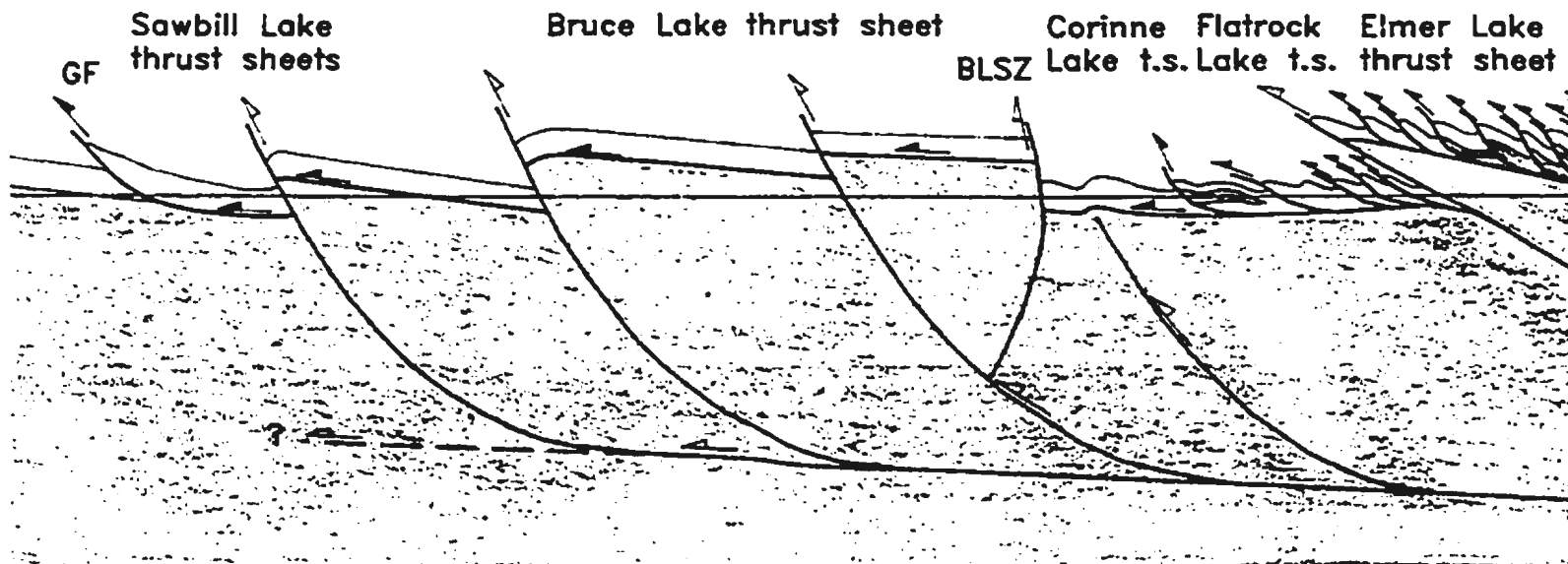
### SYMBOLS



scale 1:100,000

vertical scale = horizontal scale

-  Geological contact
-  Thrust fault, upper system or undefined
-  Thrust fault, lower system
-  Strike-slip shear zone



# LEGEND

## MOLSON LAKE TERRANE

### MIDDLE PROTEROZOIC

-  SHABOGAMO INTRUSIVE SUITE *Coronitic metagabbro and amphibolite*
-  TRANS LABRADOR BATHOLITH *Foliated granitoids*

## GAGNON TERRANE AND FORELAND

### MIDDLE PROTEROZOIC

-  SHABOGAMO INTRUSIVE SUITE *Coronitic metagabbro and amphibolite*

### LOWER PROTEROZOIC (Knob Lake Group)

-  MENIHEK FORMATION *Mica schist or slate, commonly graphite bearing*
-  SOKOMAN FORMATION *Silicate, carbonate and oxide banded iron formation*
-  WISHART FORMATION *White, coarse-grained, crystalline quartzite and minor metap*
-  DENAULT FORMATION *Dolomitic marble*
-  ATTIKAMAGEN FORMATION *Quartzo-feldspathic mica schist, locally garnet, kyanite or staurolite bearing; migmatitic in southeast of map area*

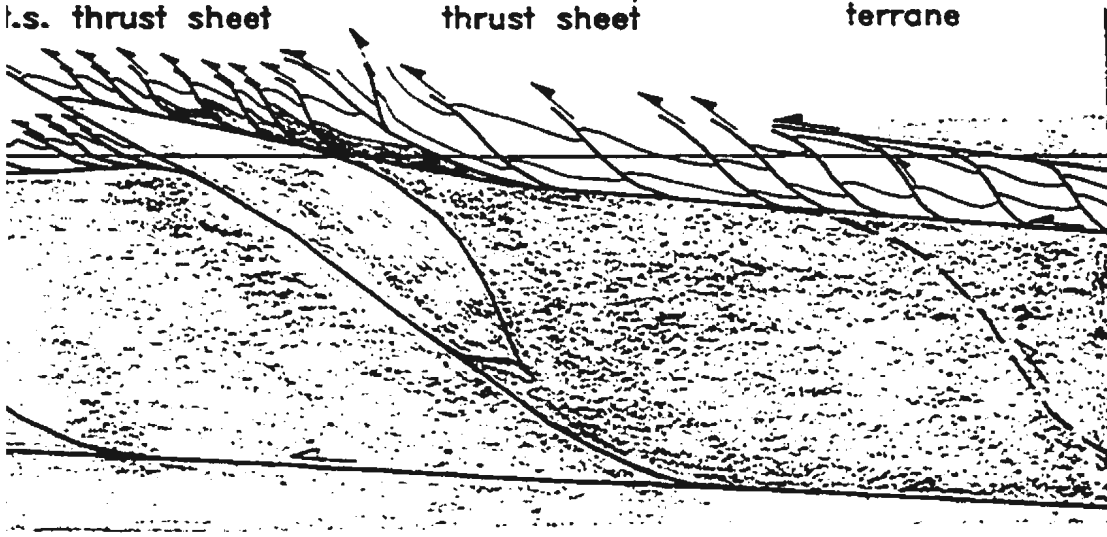
### ARCHEAN

-  ASHUANIPI METAMORPHIC COMPLEX (a) *Coarse grained, two-pyroxene banded gneiss; migmatite, locally finer grained amphibolite, intruded by coarse-grained granite; (b) Locally intensely reworked in the Gagnon terrane*

sk Elmer Lake  
t.s. thrust sheet

Goethite Bay  
thrust sheet

Molson Lake  
terrane



# LEGEND

## MOLSON LAKE TERRANE

### MIDDLE PROTEROZOIC

-  SHABOGAMO INTRUSIVE SUITE *Coronitic metagabbro and amphibolite*
-  TRANS LABRADOR BATHOLITH *Foliated granitoids*

## GAGNON TERRANE AND FORELAND

### MIDDLE PROTEROZOIC

-  SHABOGAMO INTRUSIVE SUITE *Coronitic metagabbro and amphibolite*

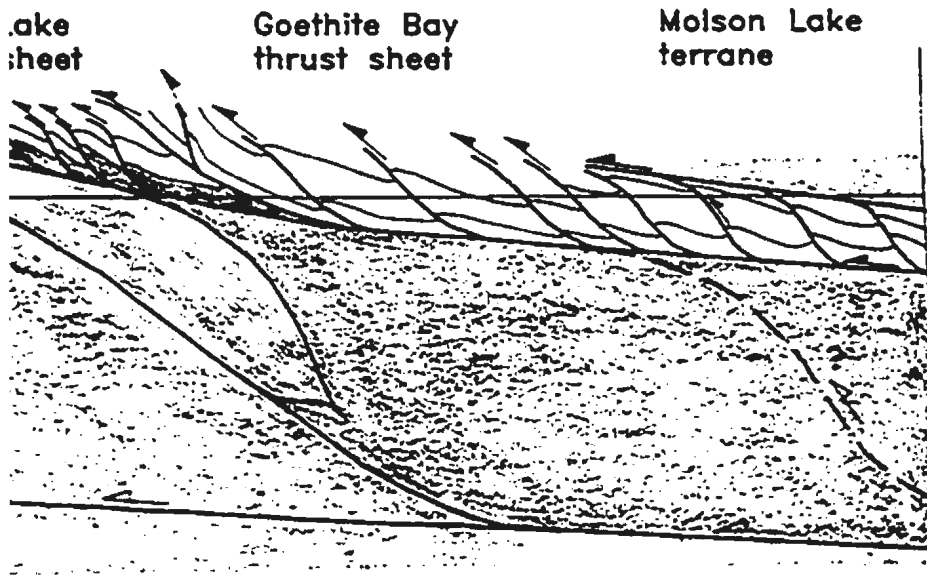
### LOWER PROTEROZOIC (Knob Lake Group)

-  MENIHEK FORMATION *Mica schist or slate, commonly graphite bearing*
-  SOKOMAN FORMATION *Silicate, carbonate and oxide banded iron formation*
-  WISHART FORMATION *White, coarse-grained, crystalline quartzite and minor metapelite*
-  DENAULT FORMATION *Dolomitic marble*
-  ATTIKAMAGEN FORMATION *Quartzo-feldspathic mica schist, locally garnet, kyanite or staurolite bearing; migmatitic in southeast of map area*

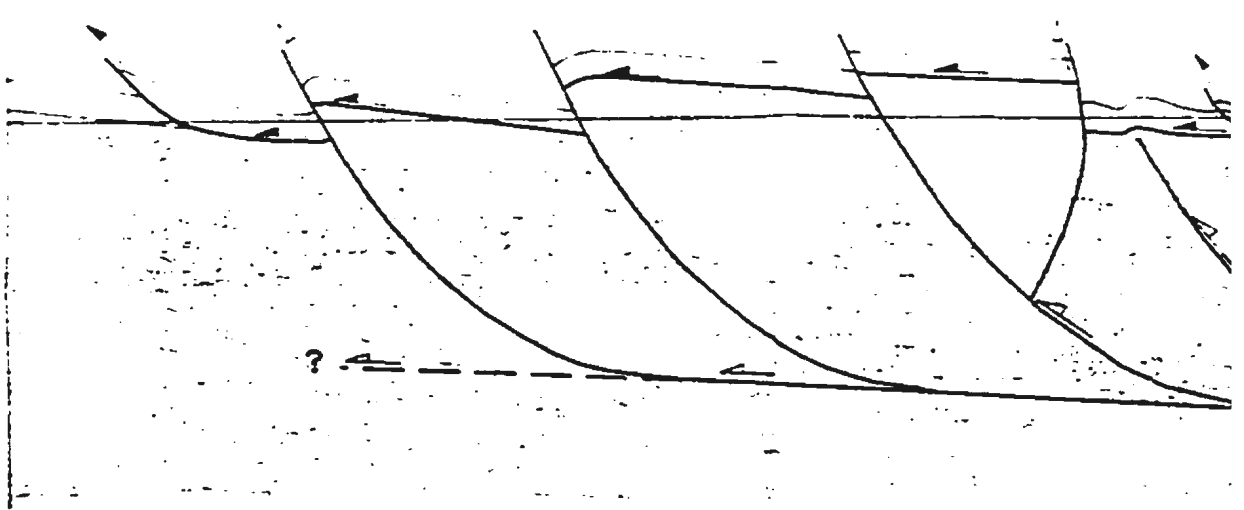
### ARCHEAN

-  ASHUANIPI METAMORPHIC COMPLEX *(a) Coarse grained, two-pyroxene banded gneiss or migmatite, locally finer grained amphibolite, intruded by coarse-grained granite; (b) Locally intensely reworked in the Gagnon terrane*

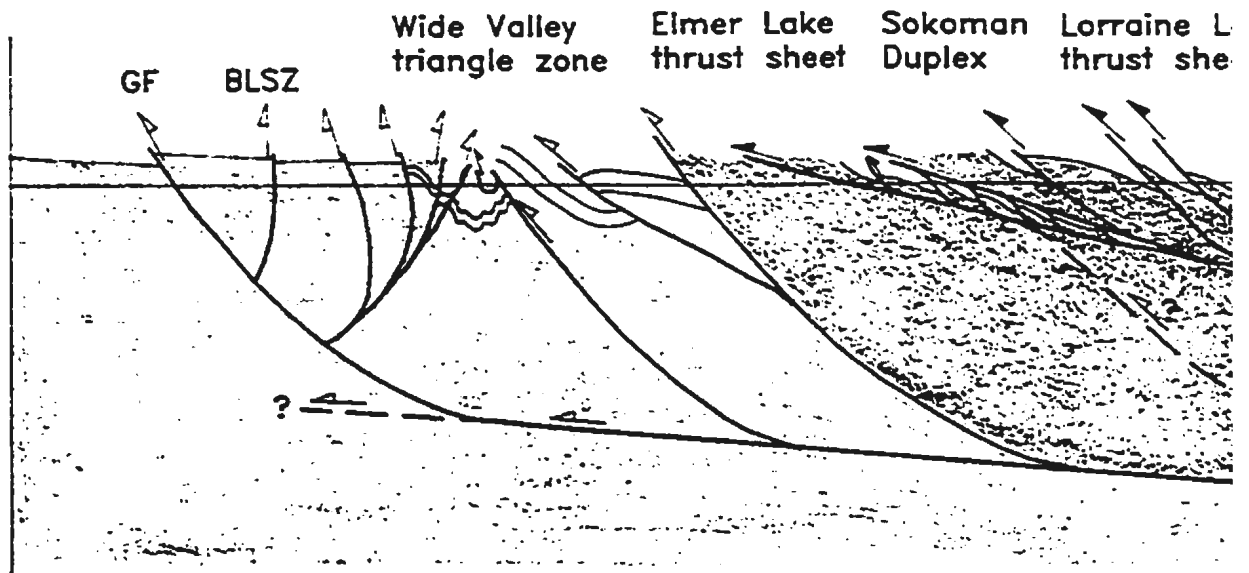
SE



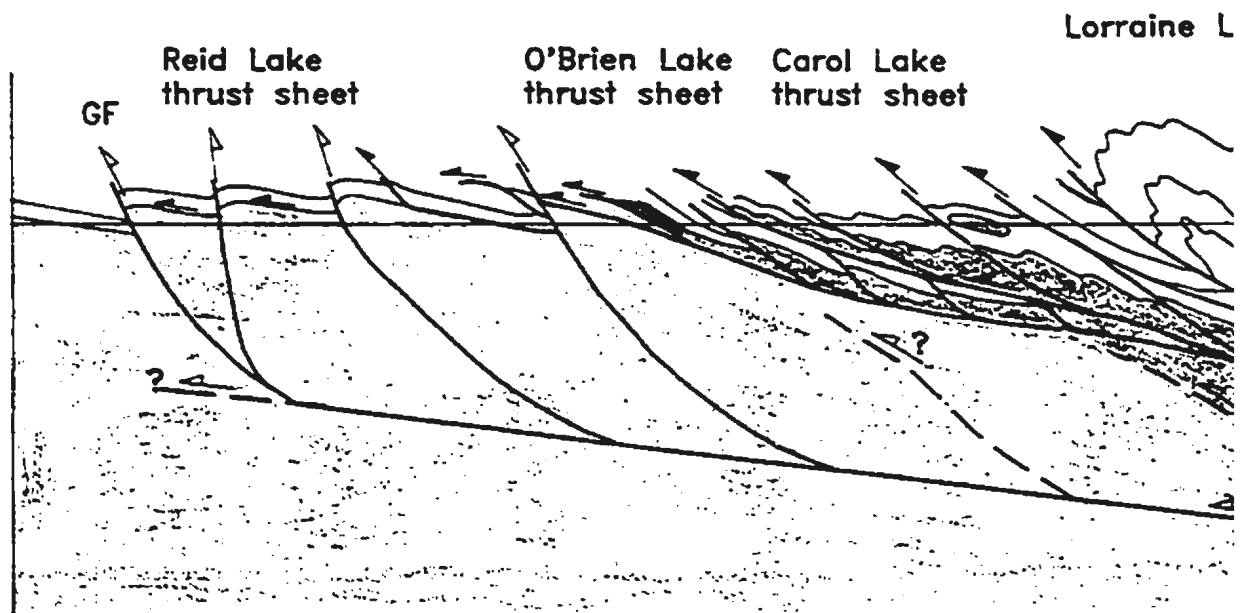
I

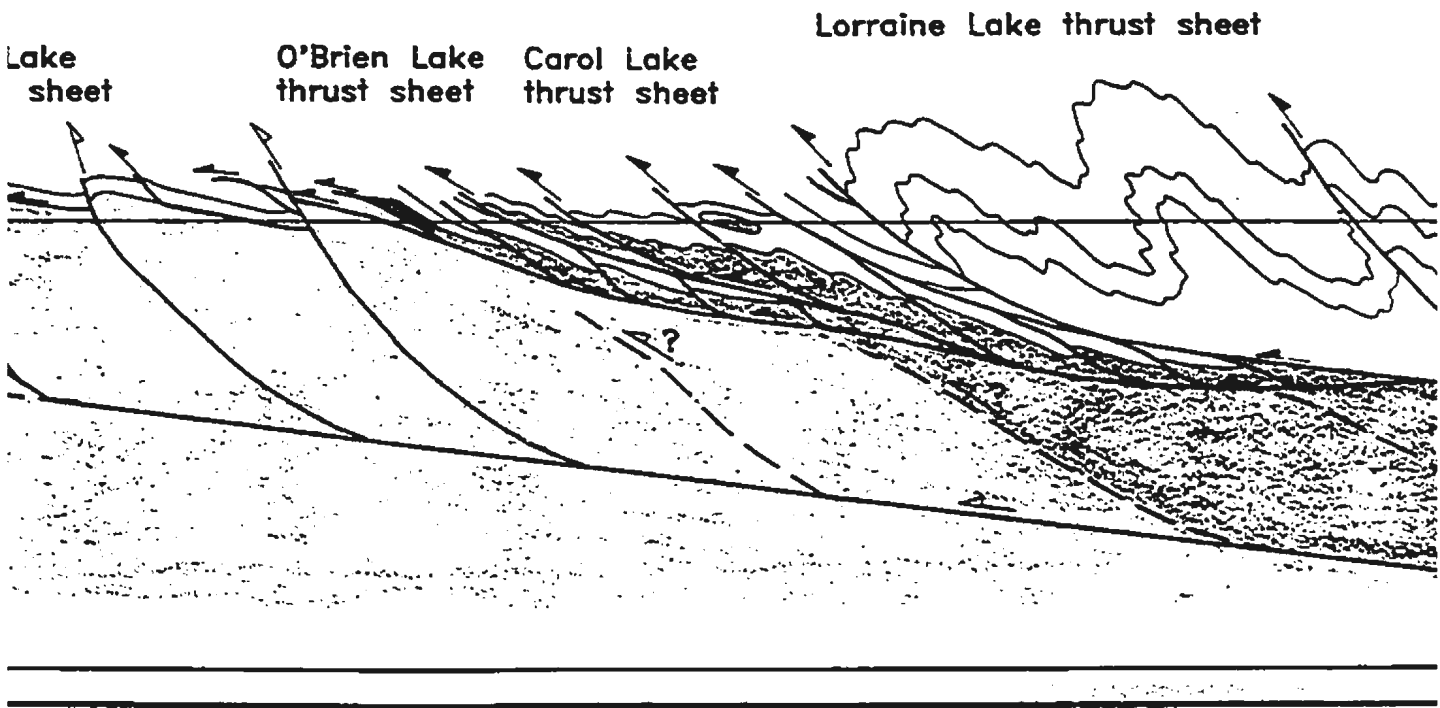
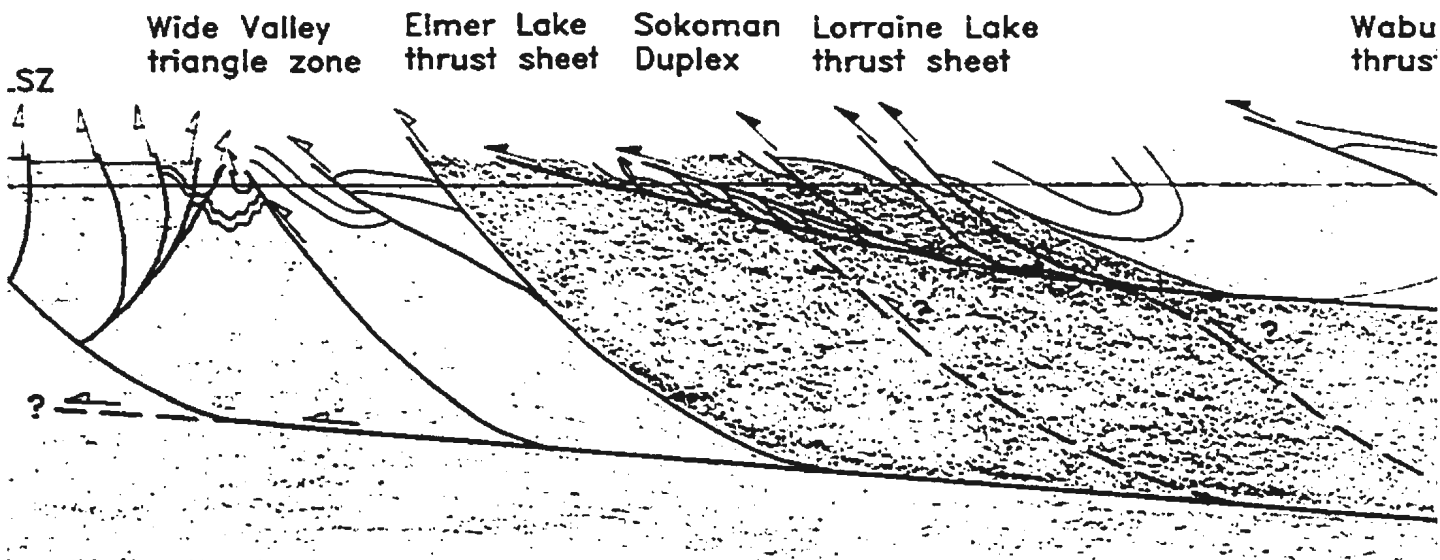
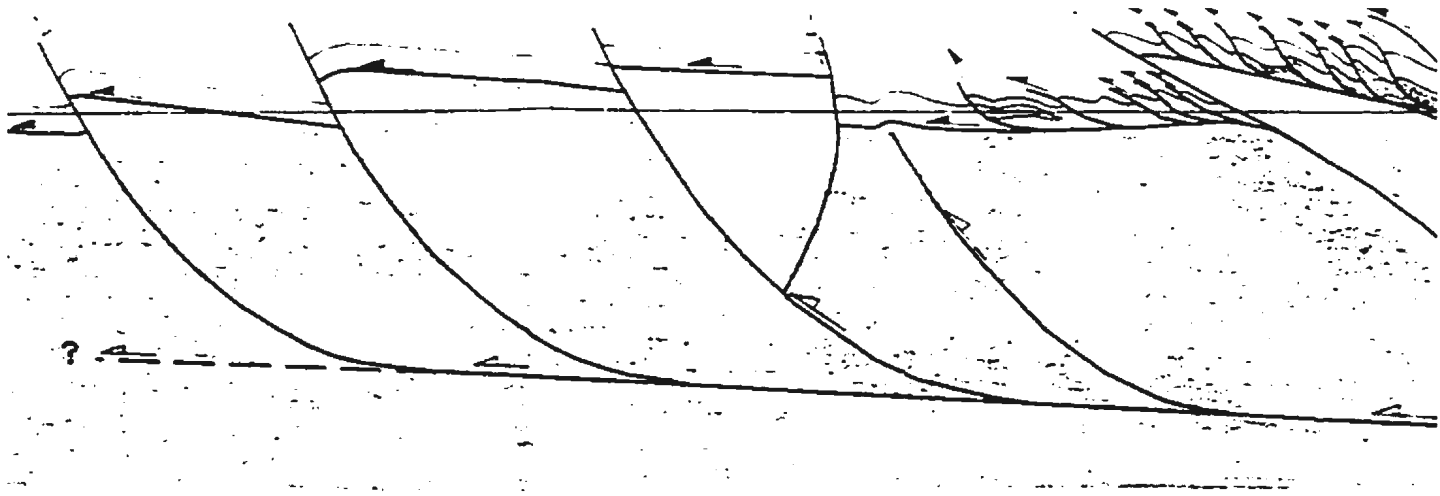


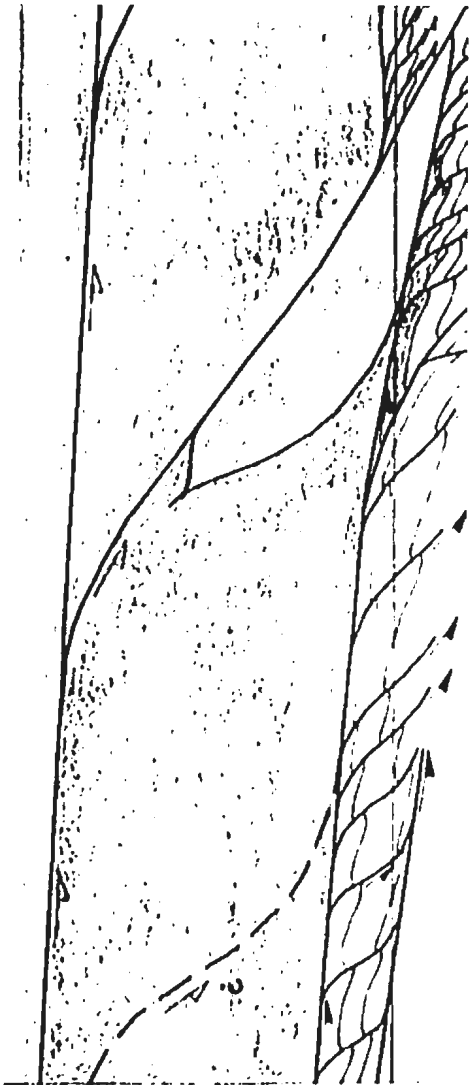
II



III

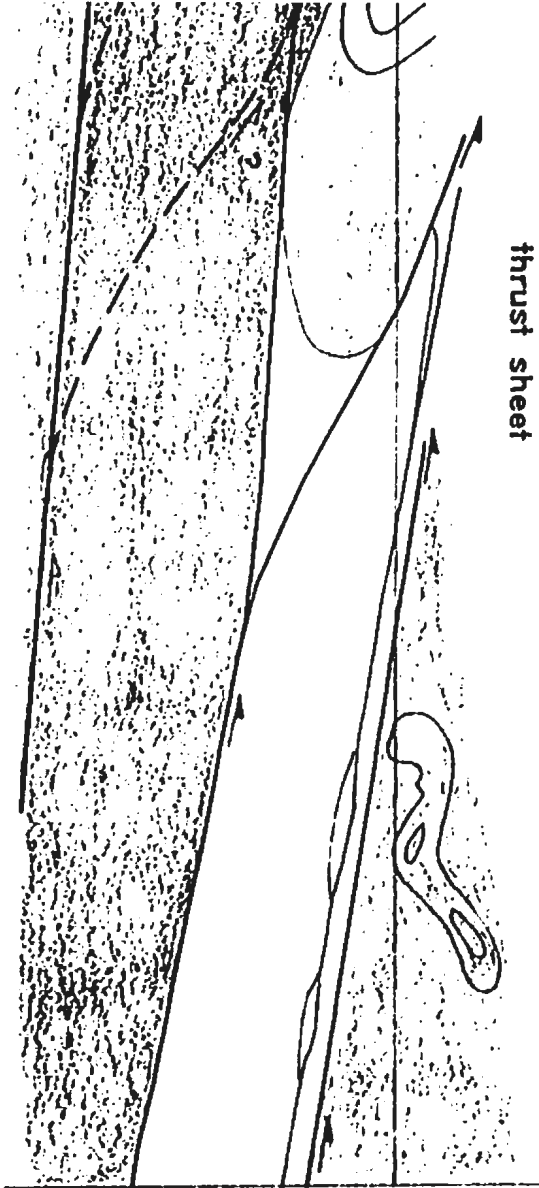






Wabush Lake  
thrust sheet

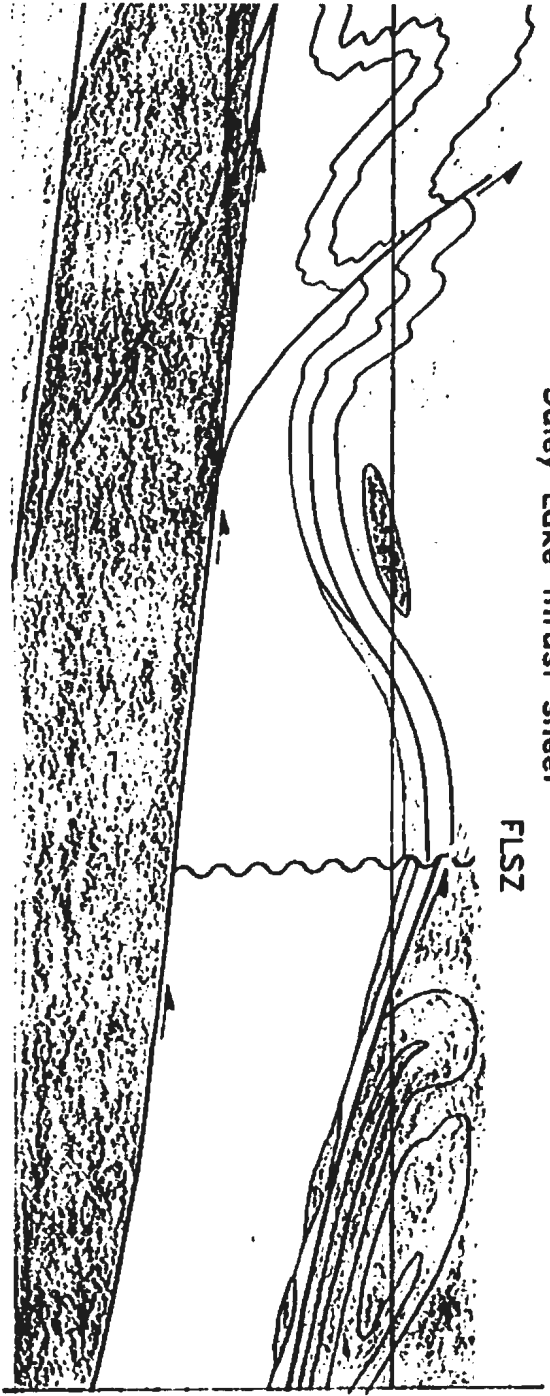
Molson Lake terrane

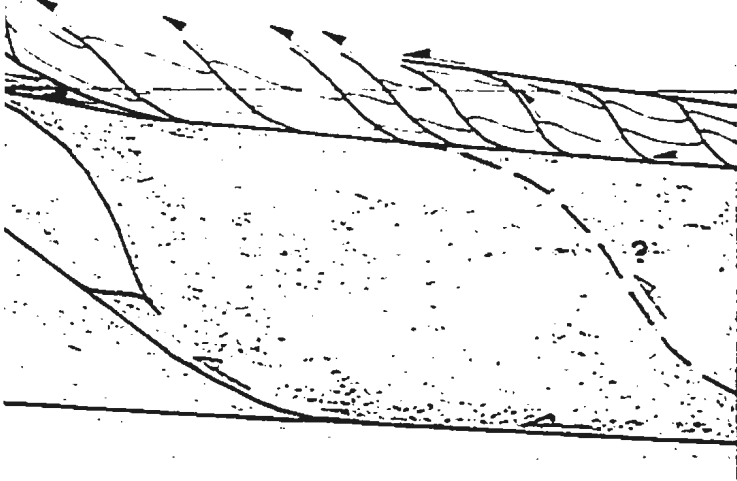


rust sheet

Duley Lake thrust sheet

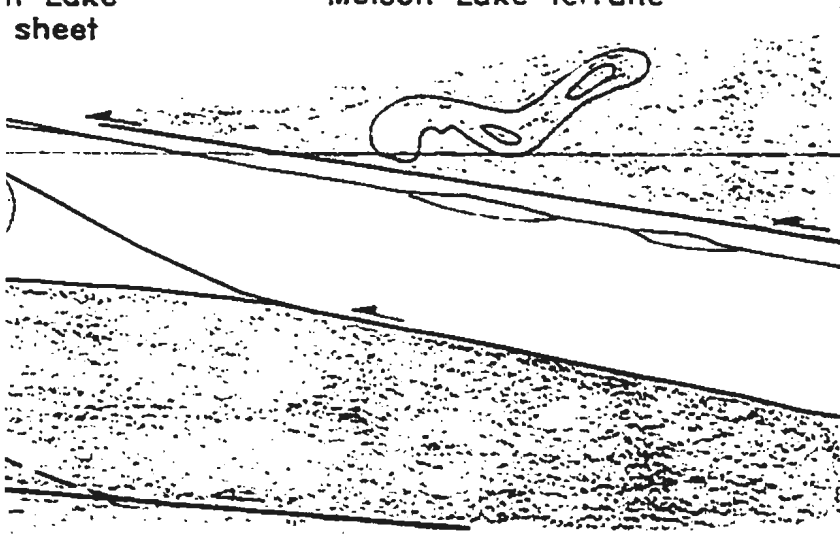
Molson Lake terrane





h Lake sheet

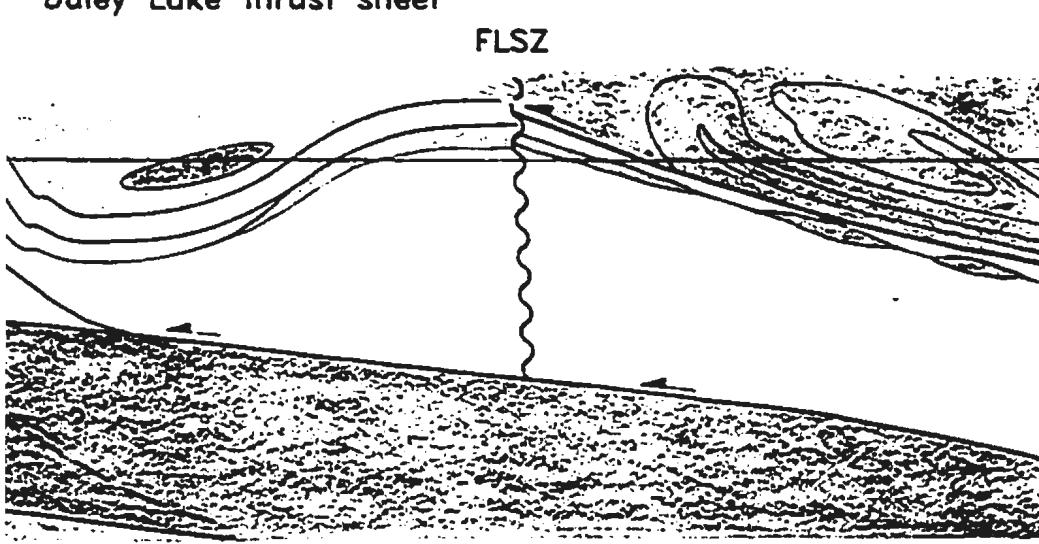
Molson Lake terrane



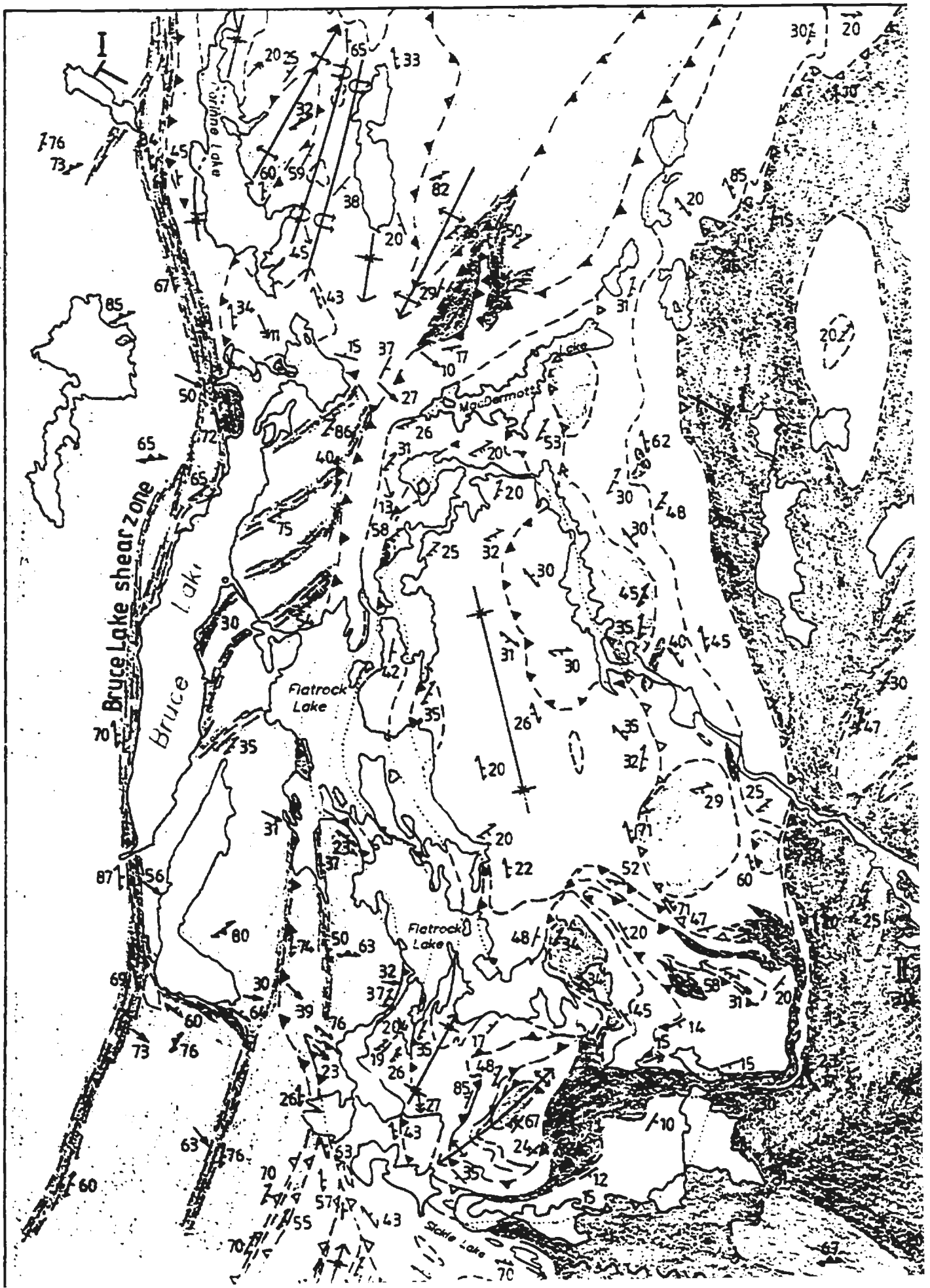
Molson Lake terrane

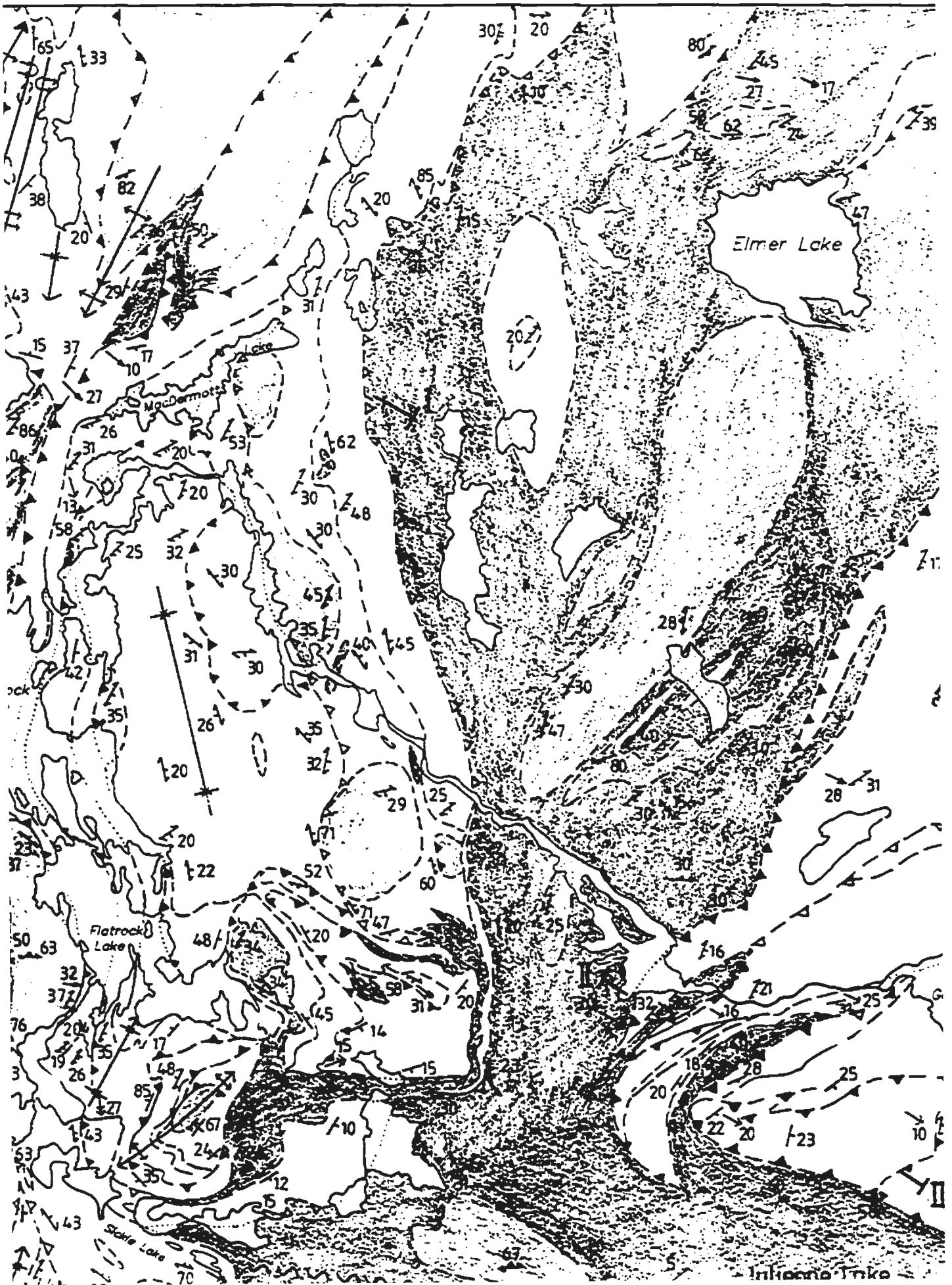
Duley Lake thrust sheet

FLSZ



1 2 3 4 5 6 7 8 9 10 11 12 13 14 15 16 17 18 19 20 21 22 23 24 25 26 27 28 29 30 31 32 33 34 35 36 37 38 39 40 41 42 43 44 45 46 47 48 49 50 51 52 53 54 55 56 57 58 59 60 61 62 63 64 65 66 67 68 69 70 71 72 73 74 75 76 77 78 79 80 81 82 83 84 85 86 87 88 89 90 91 92 93 94 95 96 97 98 99 100

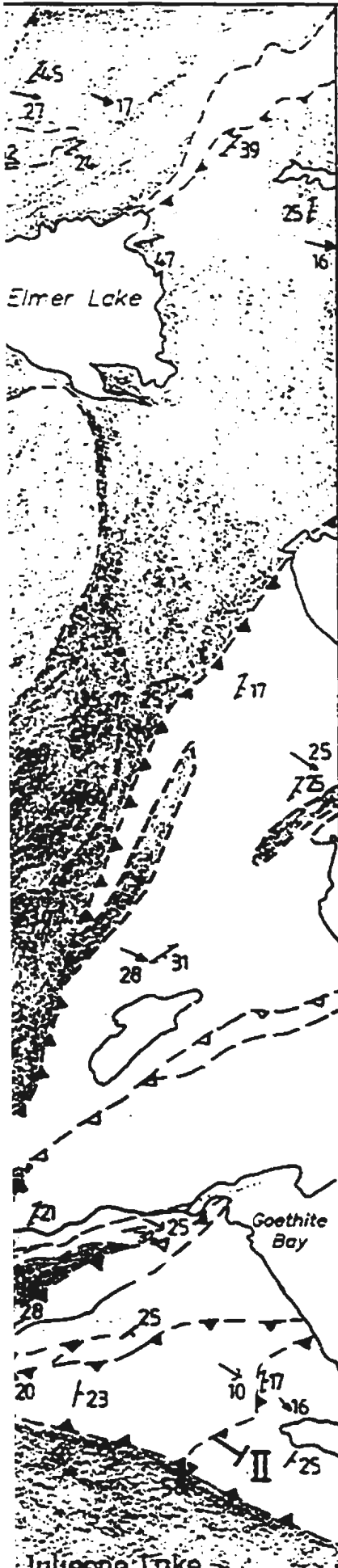




# GEOLOGICAL MAP OF THE BRUCE LAKE AREA IN GAGNON TERRANE, SOUTHWESTERN LABRADOR

Mapping by Jeroen A.M. van Gool  
Memorial University of Newfoundland

1992



## LEGEND

### MIDDLE PROTEROZOIC

 SHABOGAMO INTRUSIVE SUITE *Metagabbro and amphibolite*

### LOWER PROTEROZOIC (KNOB LAKE GROUP)

 MENIHEK FORMATION *Mica-schist or slate, commonly graphite-bearing*

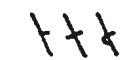
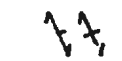
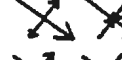
 SOKOMAN FORMATION *Silicate, carbonate, or oxide banded iron formation*

 WSHART FORMATION *White, coarse-grained crystalline quartzite and minor n*

### ARCHEAN

 ASHUANIPI METAMORPHIC COMPLEX (a) *Coarse grained, two-pyroxene banded migmatite, locally finer-grained amphibolite, intruded by coarse granite; (b) Locally intensely reworked in Gagnon Terrane*

## SYMBOLS

-  Bedding (*inclined, vertical, overturned*)
-  S<sub>1</sub> foliation (*inclined, vertical*)
-  S<sub>2</sub> axial plane (*inclined, vertical*)
-  Gneissic banding in the Ashuanipi Metamorphic Complex
-  F<sub>1</sub> fold axis or intersection lineation
-  F<sub>2</sub> fold axis
-  Elongation lineation
-  Antiform, synform, with direction of plunge
-  Overturned antiform, synform, with direction of plunge
-  Geological contact (*defined, assumed*)
-  Thrust fault, upper system or unspecified (*defined, approximate*)
-  Thrust fault, lower system (*defined, approximate*)

# GEOLOGICAL MAP OF THE BRUCE LAKE AREA IN GAGNON TERRANE, SOUTHWESTERN LABRADOR

Mapping by Jeroen A.M. van Gool  
Memorial University of Newfoundland

1992

## LEGEND

### MIDDLE PROTEROZOIC

 SHABOGAMO INTRUSIVE SUITE *Metagabbro and amphibolite*

### LOWER PROTEROZOIC (KNOB LAKE GROUP)

 MENIHEK FORMATION *Mica-schist or slate, commonly graphite-bearing*

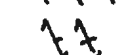
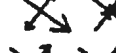
 SOKOMAN FORMATION *Silicate, carbonate, or oxide banded iron formation*

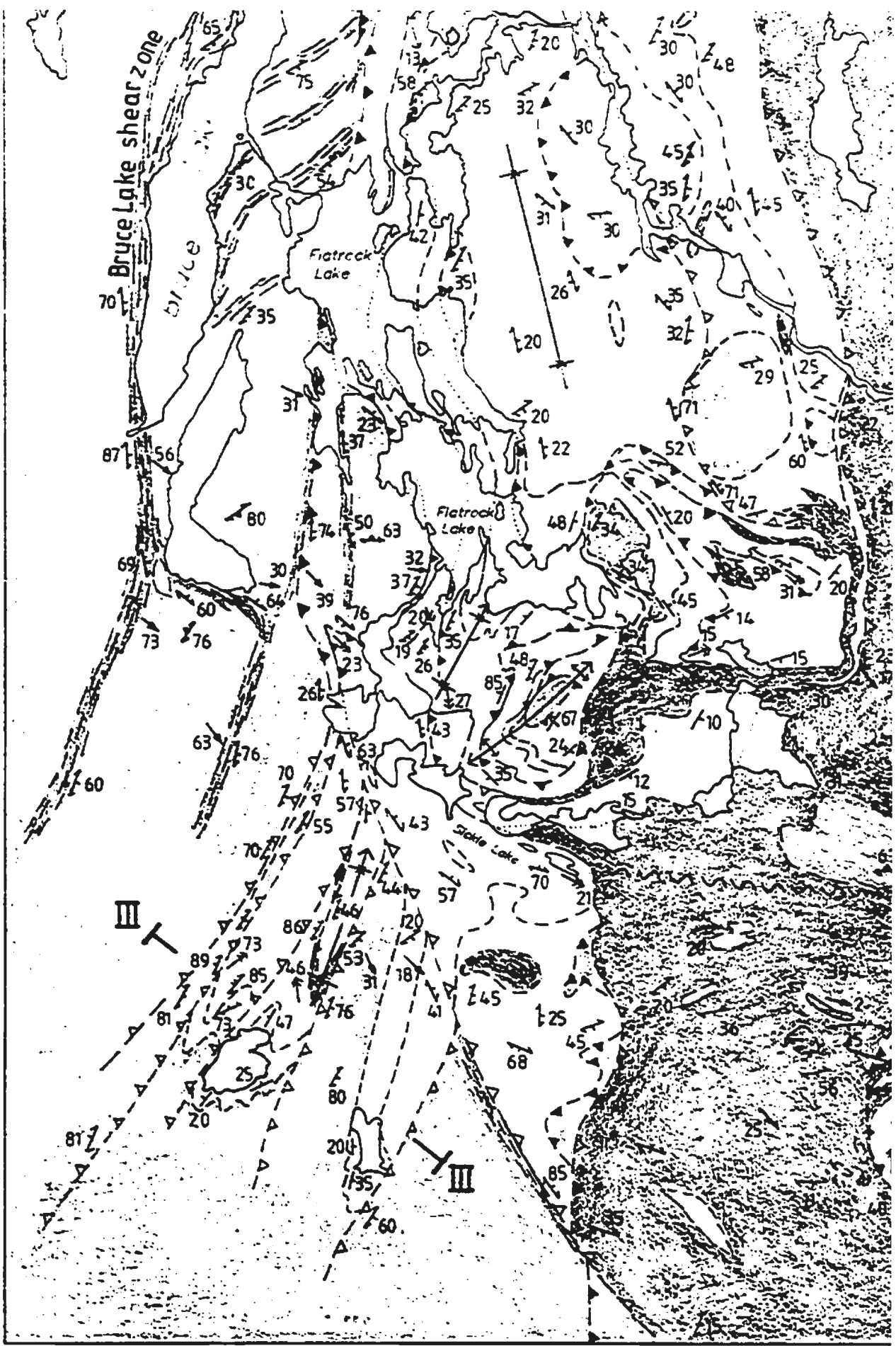
 WISHART FORMATION *White, coarse-grained crystalline quartzite and minor metapelite*

### ARCHEAN

 ASHUANIPI METAMORPHIC COMPLEX (a) *Coarse grained, two-pyroxene banded gneiss or migmatite, locally finer-grained amphibolite, intruded by coarse-grained granite; (b) Locally intensely reworked in Gagnon Terrane*

## SYMBOLS

-  *Bedding (inclined, vertical, overturned)*
-  *S<sub>1</sub> foliation (inclined, vertical)*
-  *S<sub>2</sub> axial plane (inclined, vertical)*
-  *Gneissic banding in the Ashuanipi Metamorphic Complex*
-  *F<sub>1</sub> fold axis or intersection lineation*
-  *F<sub>2</sub> fold axis*
-  *Elongation lineation*
-  *Antiform, synform, with direction of plunge*
-  *Overturned antiform, synform, with direction of plunge*
-  *Geological contact (defined, assumed)*
-  *Thrust fault, upper system or unspecified (defined, approximate)*
-  *Thrust fault, lower system (defined, approximate)*





MIDDLE PROTEROZOIC

 SHABOGAMO INTRUSIVE SUITE *Metagabbro and amphibolite*

LOWER PROTEROZOIC (KNOB LAKE GROUP)

 MENIHEK FORMATION *Mica-schist or slate, commonly graphite-bearing*

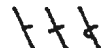
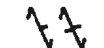
 SOKOMAN FORMATION *Silicate, carbonate, or oxide banded iron formation*

 WSHART FORMATION *White, coarse-grained crystalline quartzite and miner*

ARCHEAN

 ASHUANIPI METAMORPHIC COMPLEX (a) *Coarse grained, two-pyroxene banded migmatite, locally finer-grained amphibolite, intruded by coars granite; (b) Locally intensely reworked in Gagnon Terrane*

SYMBOLS

-  Bedding (inclined, vertical, overturned)
-  S<sub>1</sub> foliation (inclined, vertical)
-  S<sub>2</sub> axial plane (inclined, vertical)
-  Gneissic banding in the Ashuanipi Metamorphic Complex
-  F<sub>1</sub> fold axis or intersection lineation
-  F<sub>2</sub> fold axis
-  Elongation lineation
-  Antiform, synform, with direction of plunge
-  Overturned antiform, synform, with direction of plunge
-  Geological contact (defined, assumed)
-  Thrust fault, upper system or unspecified (defined, approximate)
-  Thrust fault, lower system (defined, approximate)
-  Strike-slip fault (defined, assumed)
-  Mylonitic foliation in the Ashuanipi Metamorphic Complex
-  Location of cross section (see Fig. 5.14)

0 5 km

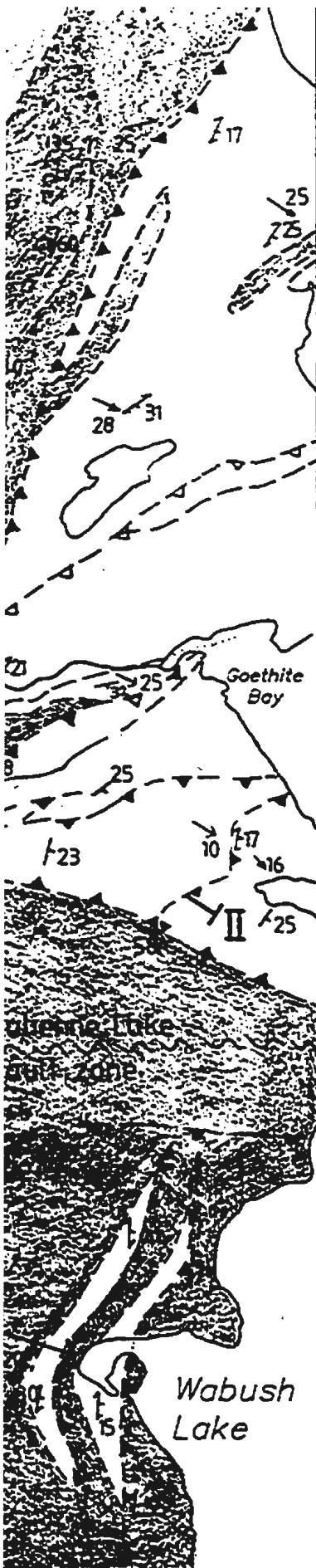


scale 1:50,000



Figure 2

For the location of the map see Figure 5.  
Sources:  
Mapping by the author and Rivers (1980a)



MIDDLE PROTEROZOIC

 SHABOGAMC INTRUSIVE SUITE *Metagabbro and amphibolite*

LOWER PROTEROZOIC (KNOB LAKE GROUP)

 MENIHEK FORMATION *Mica-schist or slate, commonly graphite-bearing*

 SOKOMAN FORMATION *Silicate, carbonate, or oxide banded iron formation*

 WSHART FORMATION *White, coarse-grained crystalline quartzite and minor metapelite*

ARCHEAN

 ASHUANIPI METAMORPHIC COMPLEX (a) *Coarse grained, two-pyroxene banded gneiss or migmatite, locally finer-grained amphibolite, intruded by coarse-grained granite; (b) Locally intensely reworked in Gagnon Terrane*

SYMBOLS

-  Bedding (inclined, vertical, overturned)
-  S<sub>1</sub> foliation (inclined, vertical)
-  S<sub>2</sub> axial plane (inclined, vertical)
-  Gneissic banding in the Ashuanipi Metamorphic Complex
-  F<sub>1</sub> fold axis or intersection lineation
-  F<sub>2</sub> fold axis
-  Elongation lineation
-  Antiform, synform, with direction of plunge
-  Overturned antiform, synform, with direction of plunge
-  Geological contact (defined, assumed)
-  Thrust fault, upper system or unspecified (defined, approximate)
-  Thrust fault, lower system (defined, approximate)
-  Strike-slip fault (defined, assumed)
-  Mylonitic foliation in the Ashuanipi Metamorphic Complex
-  Location of cross section (see Fig. 5.14)

0 5 km



scale 1:50,000

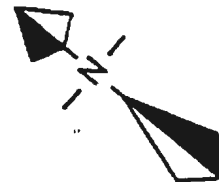


Figure 2

For the location of the map see Figure 5.1  
Sources:  
Mapping by the author and Rivers (1980a and b)

17

25

26

Goethite Bay

17

16

25

bush  
ce



